Integrated numerical modelling of a polyhistory basin, Southern Cantabrian Basin (Palaeozoic, NW-Spain)

INAUGURAL-DISSERTATION
zur
Erlangung der Doktorwürde
der
Naturwissenschaftlich-Mathematischen Gesamtfakultät
der
Ruprecht-Karls-Universität
Heidelberg

vorgelegt von
Dipl. Geol. Zbyněk Veselovský
aus Prag (Tschechische Republik)

Gutachter 1: **Prof. Dr. Thilo Bechstädt**
Geologisch-Paläontologisches Institut, Ruprecht-Karls-Universität,
Im Neunheimer Feld 234, D-69120, Heidelberg, Deutschland

Gutachter 2: **Priv. Doz. Dr. Ulrich Anton Glasmacher**
Max-Planck-Institut für Kernphysik,
Saupfercheckweg 1, D-69117, Heidelberg, Deutschland

Tag der mündlichen Promotionsprüfung: 09. 07. 2004

a) Ich erkläre hiermit, daß ich die vorgelegte Dissertation selbst verfaßt und mich dabei keiner anderen als der von mir ausdrücklich bezeichneten Quellen und Hilfen bedient habe,

b) Ich erkläre hiermit, daß ich keiner anderen Stelle ein Prufüngsverfahren beantragt bzw. die Dissertation in dieser oder anderer Form bereits anderweitig als Prüfungsarbeit verwendet oder einer anderen Fakultät als Dissertation vorgelegt habe.

Heidelberg, den 23. 05. 2004

Embalse de Porma
Summer 2000

Not everything that can be counted counts, and not everything that counts can be counted.

(Albert Einstein)

Mámě,

za můj život...

ACKNOWLEDGEMENTS

Even though it is not possible to mention everyone by name, my thanks go sincerely to all who made the time spent writing this doctoral thesis a wonderful experience.

First of all I would like to thank my first supervisor, Thilo Bechstädt, for allocating the topic of this thesis, his support and speedy revision of the thesis as well as for being instrumental in pointing me in the direction of my next important career step.
My second supervisor, Rainer Zühlke, motivated me even during the hard times. For this, for his supervision, for his revision of my thesis as well as for imparting his knowledge of modelling, I am indebted to him.
I would like to thank Uli Glasmacher for rushing to my aid with regard to his report and advisory opinion.
I am obliged to the DFG (German Research Foundation) and the IPP for funding my travel and material costs.
Thanks go to all who have helped me to complete and improve this thesis.
To Jürgen Adam for his invaluable help in the area of balanced cross-sections and Scott Bowman for his "fly-in" help from the U.S. and explanations of Philomania.
My thanks also go to Covadonga Brime Laca, Gabi Gutiérrez-Alonso, Jenaro García-Alcalde, Martin Keller, C.F. Winkler Prins, Laurence Warr and Michael Amler for their help in Spain and a wealth of valuable advice during the initial stages of the thesis.
I am grateful to Naomi Wilson for correcting my English (which must have been incredibly boring for a non-geologist), as well as for her patience and all her help during this time.
Special thanks go to Birgit, Axel und Michael for improving my overarm throw and for the time spent working in close proximity, for their motivation, discussions and most of all, simply for bearing with me.
Many thanks go to Marta and Fernando for their warm southern European friendship.
Rike, Utz, Jochen, Kai, Peter, Fabio, Kevin and the gang from Marburg and Darmstadt for the unforgettable time spent together in Spain (¡un Don Ramón, por favor!).
To everyone in the Geological-Palaeontological Institute for their forthcoming help with my everyday problems, to Marianne for proof-reading my German and Klaus for his scanning expertise.
To the assistants Lena and Christian for their help with all the work I did not want to do myself.
Thanks also to the "mensa crew" (Anja, Asher, Christina, Francis, Frank, Gesine, Guy, Heiko, Jana, Jens, Jule, Margarita, Roswitha and special guests) for entertaining and educational discussions.
I also thank everyone (especially Thomas and Bonsai) who made me coffee and kept my mind stimulated.
Thanks to my flatmate Carsten for putting up with me in mosquito paradise.
In addition, I would like to thank the families Mayo and Martínez-Álvarez from Villamanín as well as the crew of the bar Nagasaki for their unlimited hospitality and friendship.
Last but not least to my mother, who was always there when needed, and who sadly could not live to see the end of my work.
Finally thanks go to everyone who helped me and who I haven't mentioned here.

CONTENTS

ABSTRACT

ZUSAMMENFASSUNG

RESUMEN

LIST OF ABBREVIATIONS

CHAPTER 1: INTRODUCTION **1**

CHAPTER 2: GEOLOGICAL SETTING **3**

2.1 European Variscan Belt and Orogeny **3**
2.2 Iberian Variscides **3**
2.2.1 Chronology of Variscan deformation *3*
2.2.2 Narcea Antiform and the West Asturian-Leonese Zone *8*
2.2.3 Formation of the Ibero-Armorican Arc *8*
2.3 Palaeogeographical evolution of NW-Iberia **11**
2.3.1 Neoproterozoic/Cambrian *11*
2.3.2 The Avalonia controversy *14*
2.3.3 Ordovician *14*
2.3.4 The Armorica controversy *15*
2.3.5 Silurian *16*
2.3.6 Devonian *16*
2.3.7 Consolidation of the Variscan Orogen *17*
2.3.8 Carboniferous *18*
2.3.9 Post-Variscan *18*
2.4 Cantabrian Zone **19**
2.4.1 Deformation and subdivision *19*
2.4.2 Metamorphism and palaeo-temperature conditions *20*
2.4.3 Structural settings *20*
2.4.4 Stratigraphy *22*

CHAPTER 3: BALANCED CROSS-SECTIONS **47**

3.1 Historical development **47**
3.2 Development and mechanisms of fold-and-thrust belts **47**
3.3 Standard balancing techniques **48**
3.4 Computer based interpretation techniques **49**
3.5 Restrictions **50**
3.6 Bernesga Transect **50**
3.6.1 Location and limits of the transect *50*
3.6.2. Structural domains *51*
3.6.3 Constructional methods of deformed transects *53*
3.6.4 Partitioning of the Bernesga Transect *58*

3.6.5. Balancing of the Bernesga transect *60*
3.6.6 Shortening values of the Southern Cantabrian Basin *62*

CHAPTER 4: SEQUENCE STRATIGRAPHY **65**

4.1 Constraints for the present model **65**
4.2 Stratigraphic gaps and transgression/regression cycles **65**
4.3 Basin stages **71**

CHAPTER 5: QUANTITATIVE BASIN ANALYSIS **73**

5.1 Introduction **73**
5.2 Factors controlling basin-fill development **73**
5.2.1 Accommodation space *73*
5.2.2 Accumulation rates *74*
5.2.3 Carbonate production rates *74*
5.2.4 Lag time *74*
5.2.5 Time span of observation *74*
5.2.6 Flexural response of the crust to loading *74*
5.3 History of quantitative basin analysis **82**
5.4 Different types of modelling **82**
5.4.1 Tectonic deformation models *82*
5.4.2 Basin fill models *82*
5.4.3 Question of dimension *83*
5.5 2D reverse basin and 2D stratigraphic forward modelling within PHIL/BASIM™ **83**

CHAPTER 6: 2D NUMERICAL REVERSE BASIN MODELLING **85**

6.1 Methods **85**
6.1.1 Flexural response of the crust *85*
6.1.2 Concepts and workflow in PHIL/BASIM™ *85*
6.2 Input parameters **87**
6.2.1 Transect and synthetic sections *87*
6.2.2 Time *89*
6.2.3 Sea-level *90*
6.2.4 Lithologies *90*
6.2.5 Compaction/decompaction *91*
6.2.6 Flexural parameters *92*
6.3 Subsidence components **92**
6.3.1 Thermo-tectonic subsidence *92*
6.3.2 Flexural-induced subsidence *92*
6.3.3 Compaction-induced subsidence *92*
6.4 Constraints **94**
6.5 Numerical and graphical output **94**
6.6 Results **94**
6.6.1 Thermo-tectonic subsidence *95*
6.6.2 Flexural-induced subsidence *97*

6.6.3 Compaction-induced subsidence *98*
6.6.4 Total subsidence *98*

CHAPTER 7: 2D STRATIGRAPHIC FORWARD MODELLING **101**

7.1 Objectives **101**
7.2 Modelling software **101**
7.3 Input data **101**
7.3.1 Time *102*
7.3.2 Space *102*
7.3.3 Tectonic subsidence and sea-level *102*
7.3.4 Flexural response of the crust *102*
7.4 Methods and specifications **102**
7.4.1 Siliciclastic deposition *102*
7.4.2 Carbonate deposition *104*
7.4.3 Pelagic deposition *105*
7.4.4 Depositional gradients *106*
7.4.5 Base-level *106*
7.4.6 Substratum, compaction and physical properties *106*
7.4.7 Erosion *107*
7.5 Simulation workflow **107**
7.6 Constraints **108**
7.7 Numerical and graphical output **108**
7.8 Results **109**
7.8.1 Siliciclastic influx *109*
7.8.2 Carbonate accumulation rates *109*
7.8.3 Carbonate production rates *110*
7.8.4 Predicted lithofacies distribution *111*
7.8.5 Eustatic sea-level fluctuations and depositional gaps *117*
7.8.6 Comparison of outcrop and modelling data *121*
7.9 Error analysis **122**
7.9.1 Dependency of stratigraphic forward models on Te *122*
7.9.2 Dependency of sedimentary development on eustatic sea-level changes *122*
7.9.3 Influence of time step *128*
7.9.4 Thermo-tectonic subsidence rates within the stratigraphic forward modelling *128*

CHAPTER 8: BASIN DEVELOPMENT **131**

8.1 Subsidence development **131**
8.1.1 Implications for sedimentary development of syn-orogenic deposits *135*
8.2 Sedimentation development **135**
8.2.1 Sea-level *136*
8.2.2 Siliciclastic input *136*
8.2.3 Subsidence *136*
8.2.4 Carbonate production *137*
8.2.5 Palaeobathymetric evolution *137*
8.3 Intra-Asturo-Leonesian Facies Line (IALF) **138**
8.4 Development and evolution of the Cantabrian High **139**

CHAPTER 9: CONCLUSIONS **141**

9.1 Structural balancing **141**
9.2 2D numerical reverse basin modelling **141**
9.3 2D stratigraphic forward modelling **142**

REFERENCES **145**

LIST OF FIGURES **161**

LIST OF TABLES **163**

LIST OF ANIMATIONS **164**

LIST OF CROSS-SECTIONS **164**

APPENDIX **165**

Cross-sections **165**
Predicted stratigraphic columns **219**

ABSTRACT

In order to model highly deformed sedimentary basins, structural balancing must be carried out prior to 2D reverse basin and 2D stratigraphic forward modelling. This study investigates the Southern Cantabrian Basin, which is the Variscan foreland fold-and-thrust belt of NW Spain.

Structural balancing offers approximations of pre-deformational, spatial relationships between measured cross-sections. It provides information about minimal basin shortening and Late Devonian basin geometry. Three different structural domains can be distinguished along the synthetic, 18km long Bernesga Transect. The style of structural deformation defines the amount of shortening calculated for each domain. The Pedrosa domain has the highest values of up to 65%, followed by the northern Bodón (41%) and the southern Alba (25%) domains. Thrusting and folding each cause approximately the same amount of shortening. At basin scale, the amount of total shortening of the deformed basin infill is 54% at minimum, excluding small-scale faulting and folding.

2D numerical reverse basin modelling is used to estimate the basin architecture development and to establish thermo-tectonic subsidence rates as initial numerical input for the subsequent 2D stratigraphic forward modelling. Six major subsidence trends within the total subsidence rates and its components (thermo-tectonic, flexural-induced and compaction-induced) can be distinguished between 560Ma and 313Ma. These trends reflect a complex evolution from a rift stage, to a post-rift stage (passive continental margin) and finally to a foreland basin, governed by the approach of the Variscan Orogen in the Lower Carboniferous. The rift stage is characterised by decreasing thermo-tectonic subsidence rates until the Middle Cambrian. The time that follows (Late Cambrian until Late Ordovician) is marked by periods of tectonic quiescence and activity, until the passive continental margin established in the Silurian. The post-rift stage is represented by two second-order encroachment subcycles with durations of 20Ma and 41Ma respectively. They result from subsidence patterns and basinward shifts of regional onlap. Maximum marine flooding was reached during Early Llandoverian. The Variscan foredeep stage is characterised by a highly subsiding depocenter, which moves from S to N in time (present day coordinates). This movement reflects the propagation of the Variscan Orogen, with velocities ranging between 4 and 12km/Ma.

2D stratigraphic forward modelling visualises the predicted depositional history along the synthetic Bernesga Transect and quantifies the physical factors determining deposition. From the latest Neoproterozoic to the Early Ordovician the Southern Cantabrian Basin is dominated by a considerable flux of siliciclastic sediments (2600 to 4600m^2/ka). Following a substantial drop in siliciclastic input by more than 65% at the end of Silurian, significant carbonate production started in the Early Devonian. The Devonian is marked by alternating periods of considerable siliciclastic flux rates (2500 to 4600m^2/ka) and prolific carbonate production. Three Devonian carbonate factories (Abelgas, Santa Lucía and Portilla formations) display decompacted carbonate production rates from 90 to 780m/Ma, each depending on (i) amount of siliciclastic input, (ii) accommodation space available and (iii) palaeogeographic position of the depositional area. The production and destruction of accommodation space is governed by differential thermo-tectonic and flexural-induced subsidence, along with fluctuating eustatic sea-level and sediment flux. Due to increased siliciclastic influx and diminishing accommodation space, the decompacted carbonate production rates of the Portilla Fm. dropped by 81% in comparison to the Santa Lucía Fm.

Keywords: Variscan Orogeny, Cantabrian Zone, foreland basin, fold-and-thrust belt, structural balancing, numerical reverse basin modelling, stratigraphic forward modelling

ZUSAMMENFASSUNG

Numerische 2D Rückwärts- und stratigraphische 2D Vorwärts-Modellierungen in stark deformierten Sedimentbecken erfordern eine vorgeschaltete strukturelle Bilanzierung. Diese Arbeit untersucht das südliche Kantabrische Becken, welches sich im variszischen Vorland Falten- und Überschiebungsgürtel NW-Spaniens befindet.

Strukturelle Bilanzierung liefert Näherungen von räumlichen Beziehungen zwischen gemessenen Profilen vor der tektonischen Deformation und stellt Informationen über die Minimalverkürzung und die spätdevonische Beckenarchitektur zur Verfügung. Entlang des synthetischen, 18km langen Bernesga Transektes können drei strukturelle Einheiten unterteilt werden, deren unterschiedlicher Deformationsstil den Verkürzungsbetrag definieren. Die Pedrosa Einheit erreicht die höchste tektonische Verkürzung von 65%, gefolgt von der Bodón Einheit mit 41% und der Alba Einheit im Süden mit 25%. Die Überschiebungsweiten und interne Faltung verursachen ungefähr die gleiche Verkürzung. Minimale Verkürzung der deformierten Beckenfüllung beträgt im Beckenmaßstab 54%, wobei kleinräumige Falten und Störungen nicht berücksichtigt wurden.

Die numerische 2D Rückwärtsmodellierung wird verwendet, um die Entwicklung der Beckenarchitektur abzuschätzen sowie thermo-tektonische Subsidenzraten als initiale Eingabe für die folgende, stratigraphische 2D Vorwärtsmodellierung zu ermitteln. Zwischen 560Ma and 313Ma können innerhalb der totalen Subsidenzraten und ihrer Komponenten (thermo-tektonisch, flexurell- und kompaktions-induziert) sechs bedeutende Subsidenztrends unterschieden werden. Diese Trends spiegeln die komplexe Beckenentwicklung wider, angefangen mit dem Riftstadium, übergehend zum Post-Riftstadium (passiver Kontinentalrand) und schließlich zum Vorlandbecken, gesteuert durch das herannahende variszische Orogen im Unter-Karbon. Das Riftstadium ist durch abnehmende thermo-tektonische Subsidenzraten bis zum Mittel-Kambrium markiert. Die darauf folgende Zeit spiegelt Perioden der tektonischen Ruhe und Aktivität wieder, bis sich im Silur der stabile, passive Kontinentalrand etabliert. Das Post-Riftstadium ist durch zwei 20Ma und 41Ma lange „Encroachment"-Subzyklen vertreten, charakterisiert durch Subsidenzmuster und die beckenwärtige Verschiebung des regionalen „Onlap". Maximale marine Überflutung wird während des frühen Llandovery erreicht. Stark absinkende Depozentren, die in der Zeit vom Süden nach Norden migrieren (Bezug auf das heutige Koordinatensystem), kennzeichnen das variszische Vorlandbeckenstadium. Diese Bewegungen spiegeln das Voranschreiten des variszischen Orogens wieder, welches mit Geschwindigkeiten von 4 bis 12km/Ma erfolgt.

Die stratigraphische 2D Vorwärtsmodellierung visualisiert die Ablagerungsgeschichte entlang des synthetischen Bernesga Transektes und quantifiziert physikalische Steuerungsfaktoren, welche die Ablagerung beeinflussen. Vom spätesten Neoproterozoikum bis in das frühe Ordovizium wird das südliche Kantabrische Becken von hohen siliziklastischen Sedimentfluxraten (2600 bis 4600m2/ka) dominiert. Nach einem beträchtlichen Abfall des siliziklastischen Eintrags um mehr als 65% Ende des Silur, begann Anfang Devon die Karbonatproduktion im bedeutenden Umfang. Das Devon wird durch wechselnde Etappen hohen siliziklastischen Eintrags (Raten von 2500 to 4600m2/ka) und effektiver Karbonatproduktion charakterisiert. Drei Phasen devonischer Karbonatsedimentation (Abelgas-, Santa Lucía- und Portilla-Fm.) zeigen dekompaktierte Karbonatproduktionsraten von 90 bis 780m/Ma, abhängig von (i) der Menge an siliziklastischem Eintrag, (ii) vorhandenem Akkommodationsraum und (iii) der paläogeographischen Position des Ablagerungsgebietes. Die Schaffung und Zerstörung des Akkommodationsraumes wird dabei von differentieller thermo-tektonischer und flexurell-induzierter Subsidenz zusammen mit eustatischen Meeresspiegelschwankungen und Sedimenteintrag gesteuert. Aufgrund des erhöhten siliziklastischen Eintrags und des abnehmenden Akkommodationsraumes zur Zeit der Portilla-Fm. gehen dekompaktierte Karbonatproduktionsraten im Vergleich zur Santa Lucía-Fm. um 81% zurück.

Schlüsselwörter: Variszische Orogenese, Kantabrische Zone, Vorlandbecken, Falten- und Überschiebungsgürtel, strukturelle Bilanzierung, numerische Rückwärtsmodellierung, stratigraphische Vorwärtsmodellierung

RESUMEN

Para poder realizar modelos de cuencas sedimentarias altamente deformadas una reconstrucción estructural por medio de cortes balanceados debe ser llevada a cabo antes de aplicar los métodos de modelado en 2 dimensiones (i) numérico regresivo de cuenca (2D numerical reverse basin modelling) y (ii) estratigráfico progresivo (2D stratigraphic forward modelling). Este estudio se centra en la Cuenca Cantábrica Sur, que constituye la cadena de antepaís de cabalgamiento-plegamiento dentro del orógeno Varisco en el Noroeste de España.

La reconstrucción estructural por medio de cortes balanceados proporciona una aproximación a las relaciones espaciales entre las secciones medidas en este estudio. Además, ofrece información acerca del acortamiento mínimo experimentado por la cuenca estudiada y sobre su geometría en el Devónico Superior. Se pueden distinguir tres dominios estructurales a lo largo del corte compuesto "Bernesga", de 18km de longitud, definiendo el estilo estructural de la deformación en cada dominio la cantidad de acortamiento calculado. El dominio de Pedrosa tiene los valores más altos de acortamiento, hasta un 65%, seguido por el de Bodón (41%) y el de Alba (25%), situados al norte y al sur de éste, respectivamente. Los procesos de cabalgamiento y plegamiento causan aproximadamente el mismo acortamiento. A escala de la cuenca, el acortamiento tectónico total alcanza un mínimo del 54%, excluyendo pliegues y cabalgamientos de pequeña escala.

El método de modelado numérico regresivo de cuenca en 2D se utiliza para estimar el desarrollo de la arquitectura de la cuenca y para establecer promedios de subsidencia termo-tectónica que son necesarios inicialmente para el posterior modelado estratigráfico progresivo en 2D. Hasta seis modalidades de subsidencia, dentro de los valores totales y de sus componentes (termo-tectónico, inducido por flexión e inducido por compactación), pueden ser distinguidas entre los 560Ma y los 313Ma. Estas modalidades reflejan una evolución compleja de la cuenca, que comienza en un estadio de rift, para pasar a un estadio post-rift (margen continental pasivo) y finalizar en una cuenca de antepaís controlada por el avance del orógeno Varisco en el Carbonífero Inferior. El estadio de rift está caracterizado por promedios de subsidencia decrecientes que alcanzan hasta el Cámbrico Medio. El intervalo temporal siguiente (desde el Cámbrico Superior hasta el Ordovícico Superior) está caracterizado por ser un período de relativa calma y actividad tectónica, hasta el establecimiento del margen continental pasivo en el Silúrico. La fase post-rift se distingue por la presencia de dos sub-ciclos de solapamiento con una duración de 20Ma y 41Ma. Estos sub-ciclos son el resultado de variaciones en los patrones de subsidencia y desplazamientos hacia el frente de cuenca del solapamiento regional. Los niveles más altos de profundidad del mar se alcanzaron en el Llandovery temprano. La fase de cuenca de frente orogénico está caracterizada por un depocentro con alta subsidencia, el cual, considerando siempre la disposición actual de la cuenca, se desplazó de Sur a Norte con el tiempo. Este movimiento refleja la velocidad de propagación del orógeno Varisco, cuyo promedio oscila entre 4 y 12km/Ma.

El método de modelado estratigráfico progresivo en 2D permite visualizar la historia deposicional inferida a lo largo del corte compuesto "Bernesga" y cuantificar los factores físicos que controlan la sedimentación. Desde el Precámbrico Superior tardío hasta el Ordovícico Inferior temprano la Cuenca Cantábrica Sur está dominada por un flujo considerable de sedimentos siliciclásticos (2600 a 4200m^2/ka). Después de una caída substancial de dicho flujo al final del período Silúrico, de más del 65%, se inició una producción significativa de carbonatos en el Devónico Inferior. El Devónico está marcado por períodos alternativos de considerable flujo de material siliciclástico (promedios de 2500 a 4600m^2/ka) y otros de abundante producción de carbonatos. Las tres "fábricas" devónicas de carbonatos son las formaciones de Abelgas, Santa Lucía y Portilla. Éstas presentan promedios decompactados de formación de carbonatos que alcanzan desde los 90 a los 780m/Ma, dependiendo de (i) la cantidad de material siliciclástico entrante, (ii) el espacio de acomodación disponible y (iii) la posición paleogeográfica del área deposicional. La generación y destrucción del espacio de acomodación está controladas por el diferencial de la subsidencia termo-tectónica y de la subsidencia inducida por flexión, además de por las variaciones eustáticas en el nivel del mar y en el flujo de sedimentos. Debido a un incremento en el

flujo siliciclástico y a una disminución en el espacio de acomodación, los promedios decompactados de producción de carbonatos en la formación Portilla cayeron en un 81% en comparación a los de la formación Santa Lucía.

Palabras clave: Orogenia Varisca, Zona Cantábrica, cuenca de antepaís, cinturón de cabalgamiento-plegamiento, reconstrucción estructural mediante cortes balanceados, modelado numérico regresivo de cuenca, modelado estratigráfico progresivo.

LIST OF ABBREVIATIONS

μm/a =	micron per year
°C =	degree Celsius
2D/3D =	two/three dimensional
a =	year
ACD =	aragonite compensation depths
approx. =	approximately
CCD =	calcite compensation depths
cm =	centimetre
cm/a =	centimetre per year
CZ =	Cantabrian Zone
E =	east
Fm. =	formation
Gpa =	gigapascal
GPS =	Global Positioning System
H =	Hiatus/stratigraphic gap
HCS =	hummocky-cross-stratification
IALF =	Intra-Asturo-Leonesian Facies Line
ITGE =	Instituto Tecnológico GeoMinero de España
ka =	1000 years
kg/km^3 =	kilogram per cubic kilometre
km =	kilometre
km/Ma =	kilometre per million years
m =	metre
m/Ma =	metres per million years
m^2/ka =	square metres per 1000 years
Ma =	million years
Mb. =	member
N =	north
Nm =	Newton metre
RC =	regression cycle
S =	south
TC =	transgression cycle
Te =	effective elastic thickness
W =	west
WALZ =	West Asturian-Leonese Zone

CHAPTER 1: INTRODUCTION

Sedimentary basins contain most natural resources such as oil, gas, coal or water. Dimensions in time and space range from tens to hundreds of millions of years and cover thousands of cubic kilometres. Models of sedimentary basins tend to be qualitative in nature, raising difficulties in evaluating and quantifying primary control factors and their interactions. Many sedimentary environments comprise complex, small-scale geometries with abrupt lateral and vertical changes of depositional parameters, which cannot be analysed by static, qualitative models. In recent years, the development of numerical basin modelling software has provided a powerful tool for improving the comprehension of long-term basin evolution, and for determining the suitability of modelling for exploration purposes (Lawrence et al. 1990, Kendall et al. 1991, Flemings & Grotzinger 1996, Kendall & Senn 1998, Whitaker et al. 1999, Bowman & Vail 1999, Paola 2000).

In order to carry out basin modelling in a tectonically complex region such as the Cantabrian Zone (see Fig. 2.1 and 2.17), a multidisciplinary approach of detailed fieldwork, structural balancing, subsidence and stratigraphic modelling is required (see Fig. 1.2). Structural balancing has to be implemented before modelling can begin. It reconstructs the basin architecture prior to late Palaeozoic deformation and offers estimations on basin shortening and spatial relationships between the measured vertical sections. The combined dynamic approach of 2D reverse basin and subsequent 2D stratigraphic forward modelling is an effective tool for analysing geological processes in time. The temporal and spatial development of petrophysical and sedimentary parameters are estimated based on the complete basin fill between the top of the rheological basement (560Ma) and the time of maximum burial depths (34Ma). 2D reverse basin modelling is a prerequisite for 2D stratigraphic forward modelling, and analyses the quantitative basin architecture development. Numerical results are estimations of total subsidence rates and its components (thermo-tectonic, flexural-induced and compaction-induced subsidence rates). The 2D stratigraphic forward modelling simulates the shelf-basin development and quantifies the physical factors, which determine deposi-

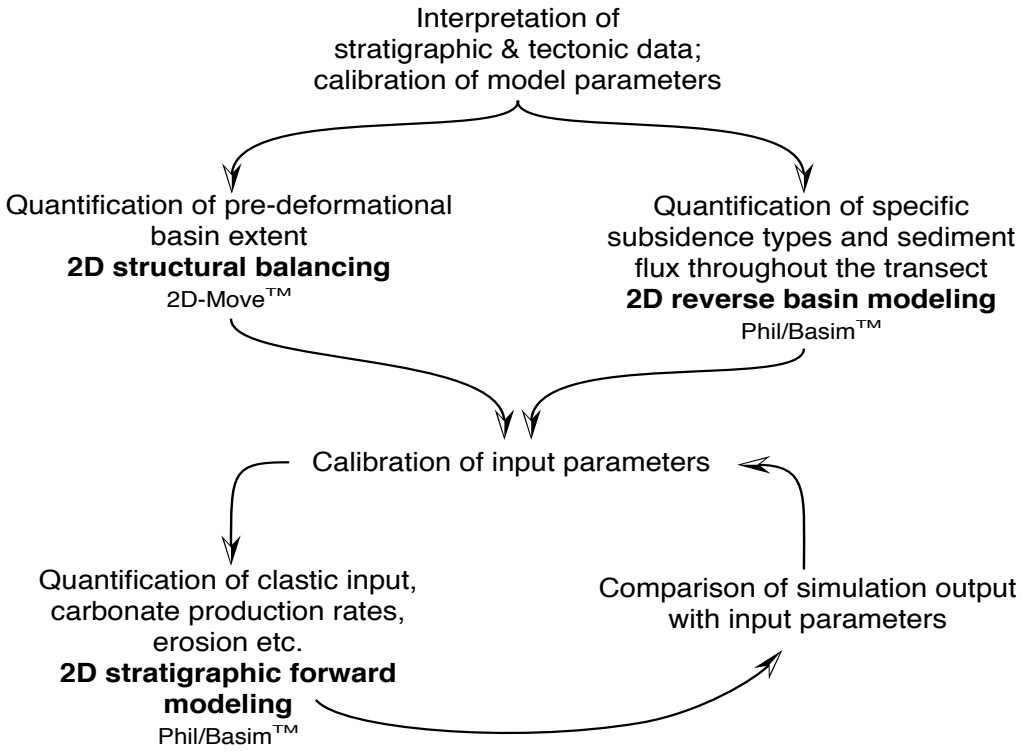

Fig.1.2. Workflow of the modelling study comprising structural balancing, 2D reverse basin modelling and 2D stratigraphic forward modelling. The circle indicates an iterative approach of simulation runs, which are repeatedly compared with present day geologic information in order to recalibrate input parameters and achieve best fit to nature.

tion. The final results enable the reconstruction of the sedimentation history of this highly tectonised Variscan foreland fold-and-thrust belt.

The Pre-Variscan evolution of the Iberian Peninsula has been a topic of numerous publications (Dallmeyer & Martínez-García 1990, Aramburu & Bastida 1995, Gibbons & Moreno 2002 and references herein). Despite the abundance of published data there is still a considerable lack of information about the Southern Cantabrian Basin comprising:

- Balanced structural model covering the whole basin
- Model of the basin architecture in time
- Flexural reverse basin modelling
- Model of basin development based on quantitative subsidence analysis, sediment influx, erosion and sea-level changes
- Stratigraphic forward model of the sedimentation and erosion parameters
- Synthetic numerical model of the basin development

CHAPTER 2: GEOLOGICAL SETTING

2.1 European Variscan Belt and Orogeny

The European Variscan Belt is a continent-scale oroclinal bend (Weil et al. 2001), and extends for almost 4000km from southern Spain to the Carpathian Mountains (Fig. 2.1 A). It is a broad sinuous belt, in some areas more than 900km wide, which developed by convergence and collision of the main continents Laurentia/Baltica and Gondwana, as well as several allochthonous terranes, following the closure of at least three oceanic basins (Matte 1991, discussion in Chapter 2.3). According to Franke (1992), the Variscan collisional belt formed during the Late Devonian between 360 and 380Ma. The collision was accompanied by high-pressure metamorphism and lasted until approximately 280Ma (Fernández-Suárez et al. 2000 a). Plate convergence continued for 100Ma, and resulted in turning the Variscan belt into an Alpine-type orogen (Cloetingh & Burov 1996). According to these authors the thickness of the Variscan crust is remarkably constant, with a value of approximately 30km. The Variscan belt of Western Europe is an example of an orogenic belt lacking exposures of cratonic igneous or metamorphic basement (Fernández-Suárez et al. 2000 a).

2.2 Iberian Variscides

The Iberian part of the Variscan Belt shows a prominent bend in the west, called the Ibero-Armorican or Asturian Arc (Matte 1991, Bastida & Aller 1992, Pérez Estaún et al. 1994, Ábalos et al. 2002). The Iberian Massif represents the south-western part of the Variscan Belt, which is subdivided into five zones based on metamorphic, structural and paleogeographic differences that reflect varying deformation styles (Lotze 1945, Julivert et al. 1972). From NE to SW these are the Cantabrian, West Asturian-Leonese, Central Iberian (including the Galicia Trás-os-Montes Zone), Ossa Morena and South Portuguese zones (Fig. 2.1). They mirror the bilateral symmetry of the Variscan Orogen, allowing a comparison of the two external zones (Cantabrian and the South Portuguese zones) and the internal zones (West Asturian-Leonese, Central Iberian, Ossa Morena; Julivert 1981, Warr 2000). High metamorphic rocks and granitoids are restricted to the internal zones (Fernández-Suárez et al. 2000 a, b). The NW sectors of the Iberian Massif include far-travelled allochthonous terranes of variable provenance and origin (Arenas et al. 1986).

2.2.1 Chronology of Variscan deformation

Dallmeyer et al. (1997) gives a concise overview and absolute age information of the geotectonic evolution, occurrence of igneous rocks, tectonic events and metamorphic evolution for the Iberian zones (see Fig. 2.2).

Cooling ages, obtained for obduction-related amphiboles in the Morais Ophiolite (Central Iberian Zone), show deformation and related syn-orogenic deposition in the innermost zone starting in roughly mid-Devonian times (Dallmeyer & Gil Ibarguchi 1990, Quesada 1991). Combined 40Ar/39Ar dating, X-ray diffraction and electron microprobe analyses constrained the diachronic evolution of main tectonothermal events across the northern Iberian Massif (Dallmeyer et al. 1997). These data are summarised in Fig. 2.3. The latter authors established three diachronous deformation phases, which represent local responses to regional shortening and which migrated eastward with time. The first metamorphic and deformational episode started in the Late Silurian/Early Devonian in the Galicia-Trás-os-Montes Zone and reached the Central Iberian Zone in early Late Devonian. The West Asturian-Leonese Zone was reached in the Tournaisian. In the Cantabrian Zone the Namurian (approx. 322Ma) marked the onset of thrust tectonics and the emplacement of thrust sheets in the westernmost part of the zone as well as the deposition of first flysch turbidites (Olleros Fm., see Chapter 2.4.4 for further detail) from the West Asturian-Leonese Zone. The eastward migration of thrust movements in the Cantabrian Zone is noticeable up until the second deformation episode. This episode displays a similar diachronous character to the previous episode (Fig. 2.3), with older ages in the west (Middle Devonian in the Galicia-Trás-os-Montes Zone) getting younger towards the Cantabrian Zone in the east (Westphalian to Stephanian). A later deformational phase is assumed to have reached the Cantabrian Zone in the Early Permian. Dallmeyer et al. (1997) quantitatively estimated an

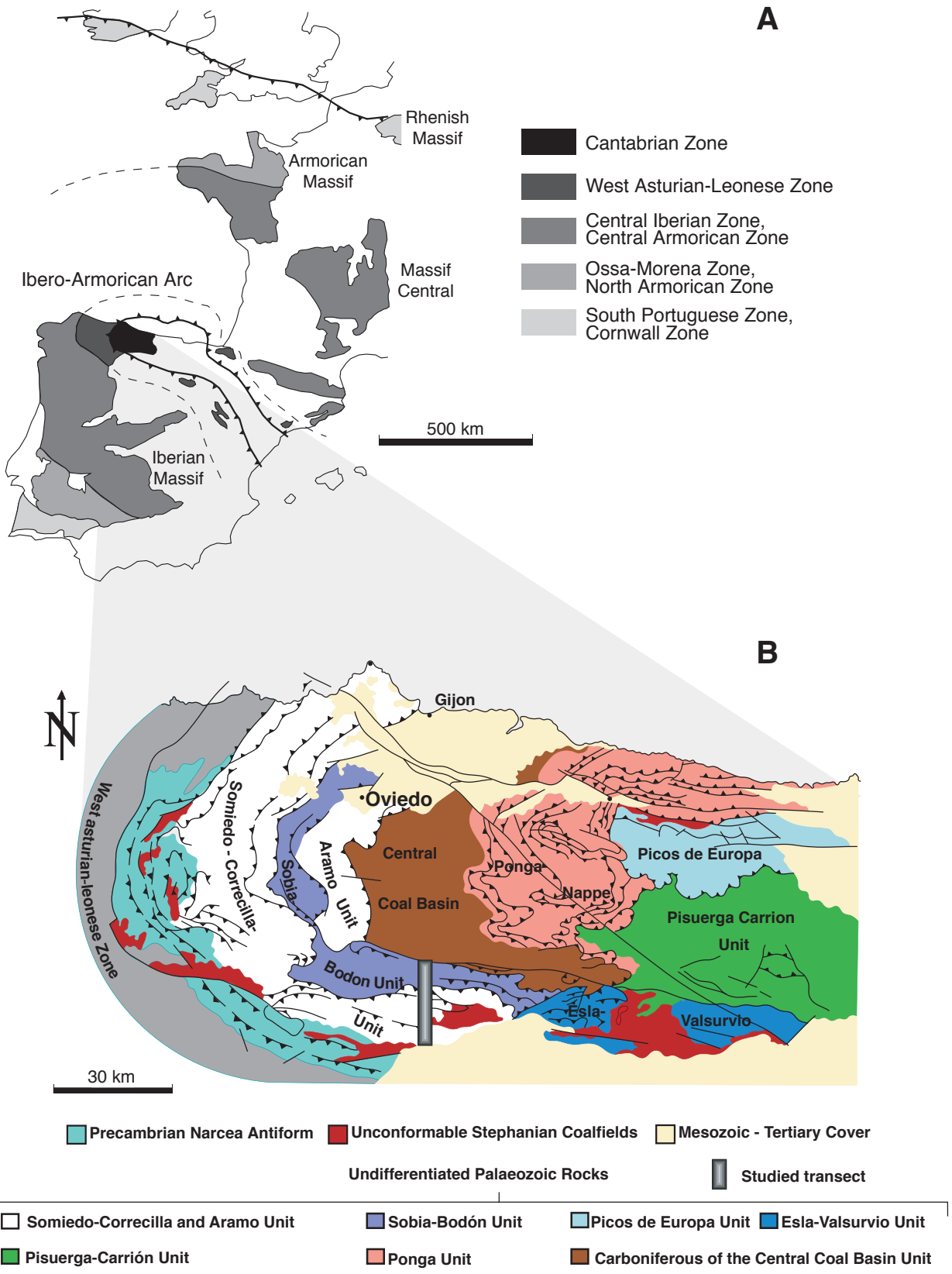

Fig. 2.1.
A: Tectonic zonation of the outcropping Variscan Belt in Western Europe (after Dallmeyer et al. 1997). The Ibero-Armorican Arc is schematically indicated in the west.
B: Subdivision of the Cantabrian Zone in its tectonic units (after Julivert 1971 and Pérez-Estaún et al. 1988). The Bernesga Transect is marked by the shaded bar.

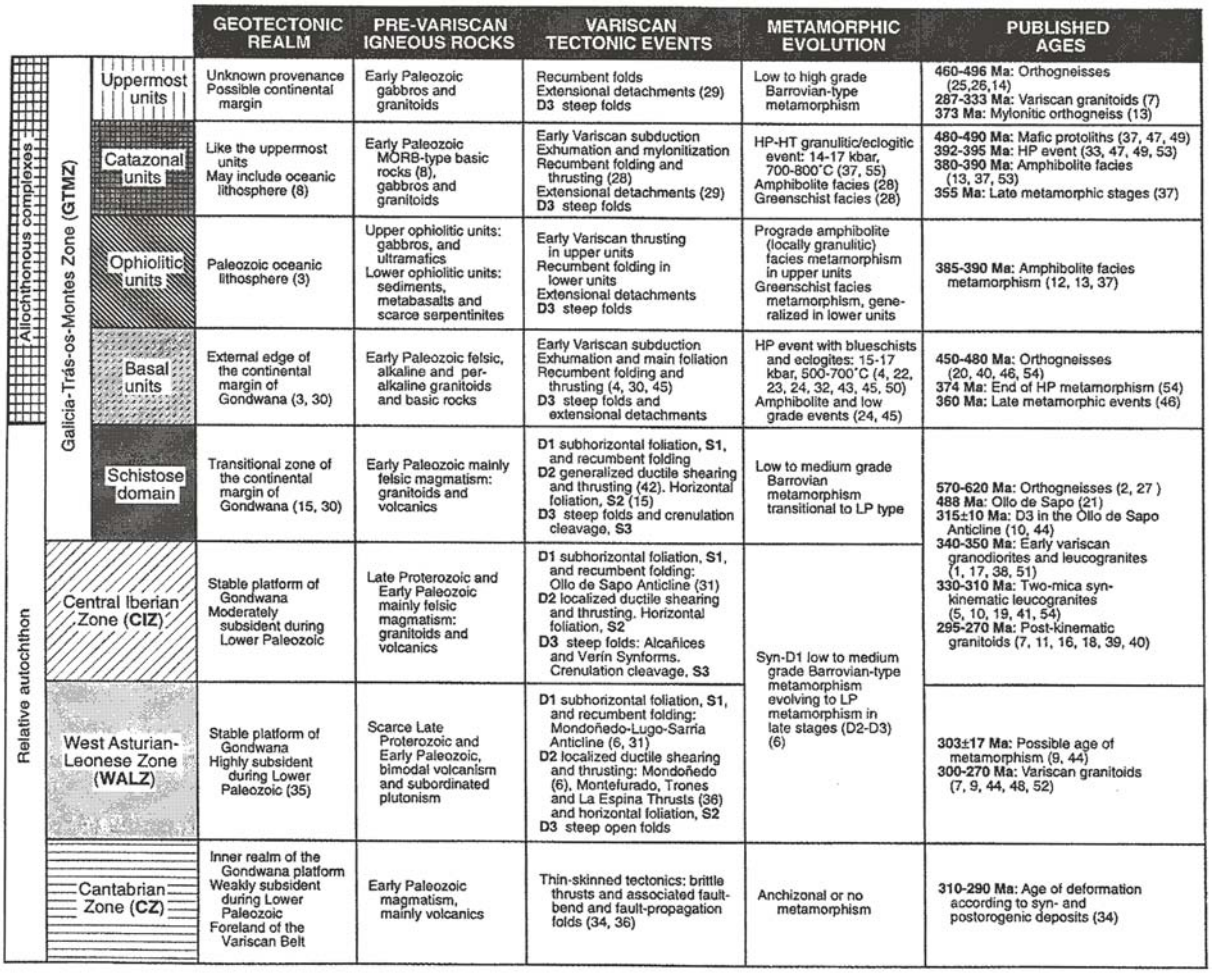

Fig. 2.2. Geotectonic and metamorphic evolution of the Iberian Variscan Orogen. The internal units are situated towards the bottom, the external towards the top of the figure (Dallmeyer et al. 1997).

average propagation rate of the orogenic front as being 5km/Ma, taking into account a hypothetical orogenic shortening of 50 to 75%. This reflects an average convergence rate of 1 to 2cm/a.

According to Frankenfeld (1982) clastic supplies to the Cantabrian Zone increasingly derived from the Central Iberian area from Late Frasnian times onward. This assumption is based on 1-5m thick conglomerate beds within the Nocedo Fm. (see Chapter 2.4.4), composed of exotic clasts (amphibolites, pegmatites, radiolarites, metamorphic quartzites). Frankenfeld presumed, that these clasts came from a zone between Cabo Ortegal (NW coast of Biscay) and Bragança (North Portugal), as this is the only area with outcropping amphibolites. However, although the provenance of these clasts remains unidentified, there are several arguments, which question the theory that Variscan deformation in the Cantabrian Zone can be traced back to Late Frasnian times:

- The Nocedo Fm. (382-373Ma) as well as all preceding clastics were shed from the core of the Cantabrian Zone. More than 50Ma later, the Olleros Fm. (see Chapter 2.4.4) is the first unit that undoubtedly contained sediments derived from the inner part of the Variscan Orogen. It is unlikely that a single thin conglomerate pulse was delivered from the west, being followed by 50Ma of southward-directed transport and pelagic carbonate sedimentation (Alba Fm., 25Ma duration). One would expect, in contrast, an increase of clast delivery from this new source in the west, as the orogen propagated by approx. 5km/Ma (Dallmeyer et al. 1997, see above).
- During the Frasnian the first deformation episode reached the Central Iberian Zone (Dallmeyer et al. 1997, Fig. 2.3). Taking mean shortening values of the Variscan Orogen into consideration (50 to

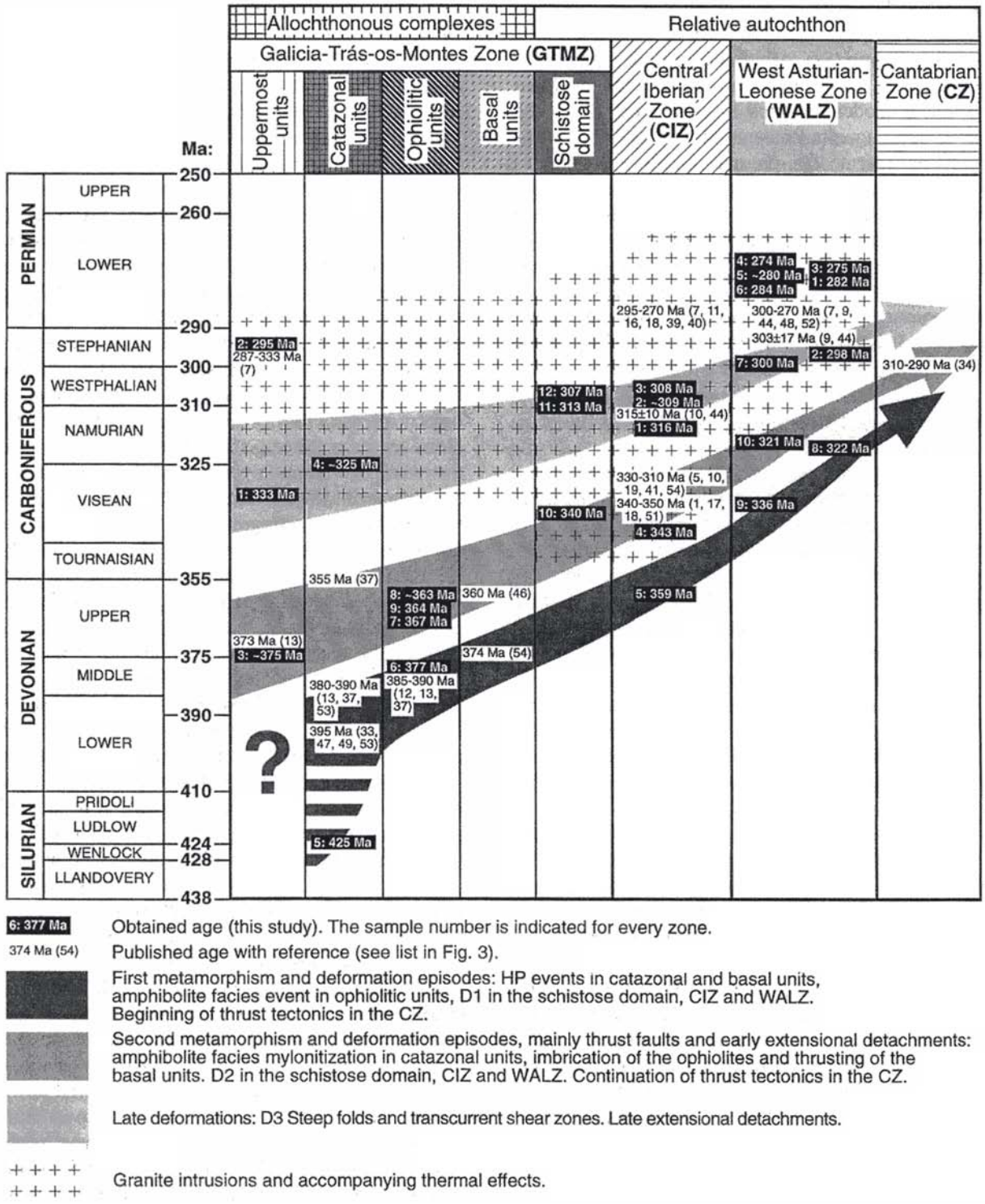

Fig. 2.3. Space/time diagram, showing the diachronism of the main tectonothermal events across the NW Iberian Massif (Dallmeyer et al. 1997). Ages are based on 40Ar/39Ar measurements. The time scale differs slightly from that used in the present study. The zones are placed in their original relative positions with external units of the orogen plotted to the right of the figure.

75% according to Dallmeyer et al. 1997), the uplifted and eroded region would be about 450km away. Such a long transport, if possible, would result in fine-grained material and not in conglomerates with clasts of up to 20cm in diameter (reported by Van Loevezijn 1986). One would also expect mainly quartz components

- To enable a transport over such a long distance, Frankenfeld (1982) argued that there must have been subsidence of at least several hundred meters

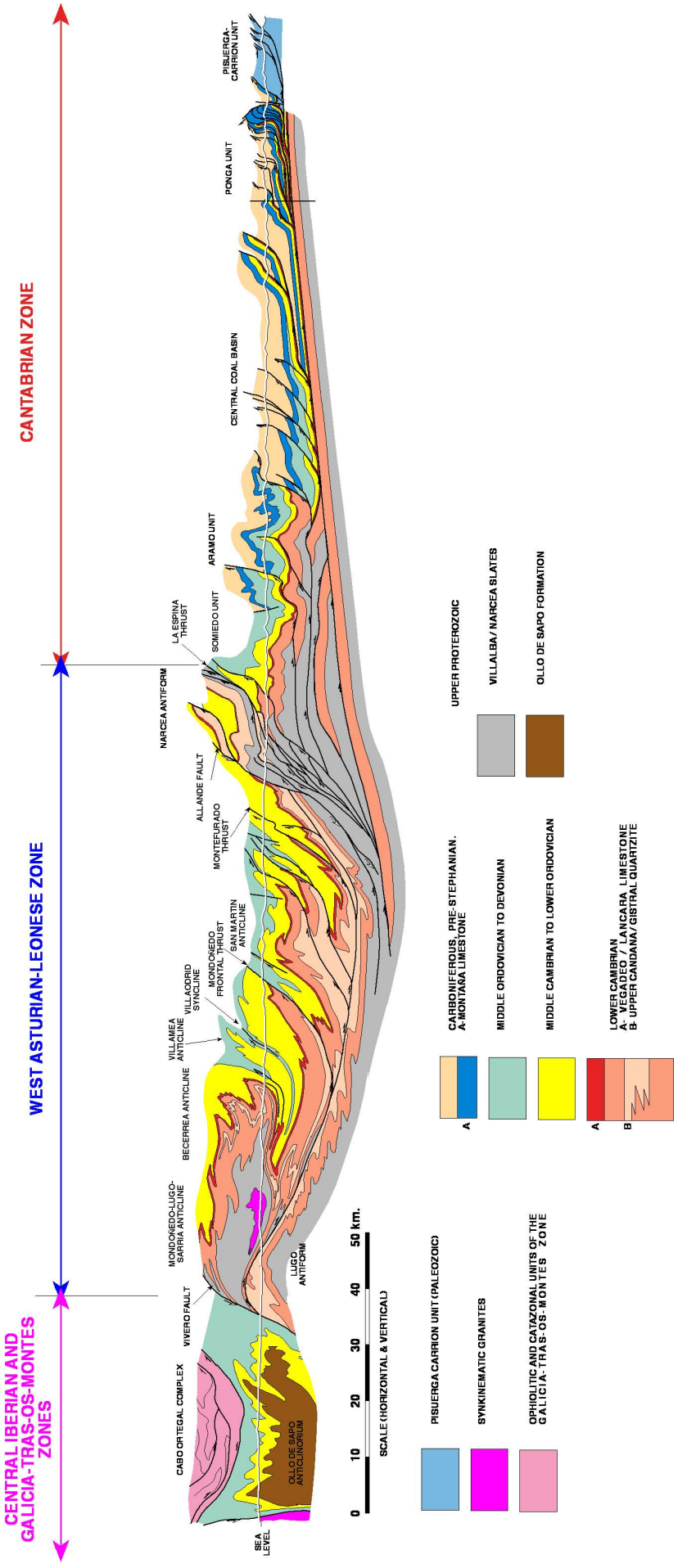

Fig. 2.4. Geological cross-section through the Central Iberian, West Asturian-Leonese and Cantabrian Zones (Pérez-Estaún et al. 1991). The thick Early Palaeozoic succession of the West Asturian-Leonese Zone was thrusted onto the Cantabrian Zone. The border between these zones is represented by the Narcea Antiform. The Cantabrian Zone is dominated by syn-orogenic Carboniferous deposits. To the west the Cabo Ortegal Complex and the Ollo de Sapo Anticline marks the central part of the Variscan Orogen of the Iberian peninsula.

for the conglomerates to be deposited. However, the water depths were much shallower, proven by the underlying Nocedo silt and sandstones, which indicate lower-shoreface depths.

- Van Loevezijn (1988) doubts that the clasts were shed from the west, interpreting their colour as a hydrothermal feature. Making his conclusions based on the facies patterns and palaeo-current directions, the author interprets the provenance of Famennian sediments from N to NE. This seems to be corroborated by the distribution of clast sizes, showing the highest values (up to 20cm) close to the IALF (northernmost occurrence of the conglomerates), rapidly decreasing towards the south (Van Loevezijn 1986).

2.2.2 Narcea Antiform and the West Asturian-Leonese Zone

Neoproterozoic rocks of the Narcea antiformal stack delimit the Cantabrian Zone from the West Asturian-Leonese Zone (Fig. 2.1 and 2.4). The whole antiform was thrust onto the Palaeozoic rocks of the Cantabrian Zone (Julivert & Marcos, 1973, Pérez-Estaún & Bastida, 1990, Pérez-Estaún et al. 1994). It is composed of metapelites and metapsamites, primarily with turbiditic facies as well as volcanoclastic and less frequently volcanic rocks. Together with the Neoproterozoic pelites and greywackes of the Lugo Dome in the West Asturian-Leonese Zone and outcrops in the Central Iberian Zone it represents the oldest rocks exposed in NW Iberia (Fig. 2.4; Fernández-Suárez et al. 2000 b). The age and nature of the underlying basement is uncertain. The West Asturian-Leonese Zone represents the easternmost internal zone of the Iberian Massif, or in other words, the transition between the foreland areas (Cantabrian Zone in the east) and the hinterland (Central Iberian Zone to the west). It is characterised by an Upper Proterozoic flyschoid series unconformably overlain by a thick pre-orogenic Palaeozoic succession comprising 5,000 to 10,000 meters of sediment. (Marcos 1973, Julivert 1981, Pérez-Estaún et al. 1990, Bastida & Aller 1992, Fernández-Suárez et al. 2000 b). The tectonothermal evolution is similar to that of the Central Iberian Zone (see Fig. 2.2 and 2.3). In comparison to the adjacent zones, the West Asturian-Leonese Zone experienced more subsidence during the extensional phase. Volcanism and plutonism are present but scarce and increases towards the west (Dallmeyer et al. 1997, Fernández-Suárez et al. 1998).

2.2.3 Formation of the Ibero-Armorican Arc

The Ibero-Armorican arc is one of the most pronounced features of the European Variscan fold belt (Fig. 2.1). It can be traced in the western Variscan Orogen through France (Brittany) into northern Spain (Kollmeier et al. 2000). In its core the highly curved Cantabria-Asturias Arc consists of the Cantabrian Zone of northern Spain. It is characterised by foreland-directed concavity with inward-facing structures (Hirth et al. 1992). The western boundary of the arc is the Narcea antiform (see above). The structural trend varies by about 180° around the arc. There are several theories regarding the origin and development of the arc. The first structural interpretation was by de Sitter (1962), who proposed two deformation phases. Julivert (1971) and Julivert & Marcos (1973) demonstrated that the Cantabria-Asturias Arc was a primary, pre-orogenic feature and has undergone secondary tightening and development of radial folds during the Variscan orogeny. Studies of kinematic indicators and thrust sheet emplacement mechanisms supported this theory with slight modifications regarding the location of the rotation centre (Julivert & Arboleya 1984, 1986; Pérez-Estaún et al. 1988). Pérez-Estaún et al. (1988) described a continuous deformation of progressive rotational thrust displacements propagating from west to east (Fig. 2.5). A second theory examines the syn-orogenic indentation of a rigid block with the resulting curvature of the arc. This rigid block could have originated from a unique microplate (Riding 1974, Matte & Ribeiro 1975, Lorenz & Nichols 1984) or from a Gondwanan promontory (Bachtadse & Van der Voo 1986, Martínez-Catalán 1990). More recent palaeo-magnetic studies, in which the declination deviation followed the shape of the arc, indicated a secondary nature of at least half of the present curvature, proving it to be an orocline (Bonhommet et al. 1981, Perroud & Bonhommet 1981, Perroud 1986, Hirth et al. 1992, Parés et al. 1994, Stewart 1995, Van der Voo et al. 1997). Palaeomagnetic investigations by Parés et al. (1994) point to a late tightening of a partially curved (ca. 50%) fold-thrust belt, leaving the amount of prior

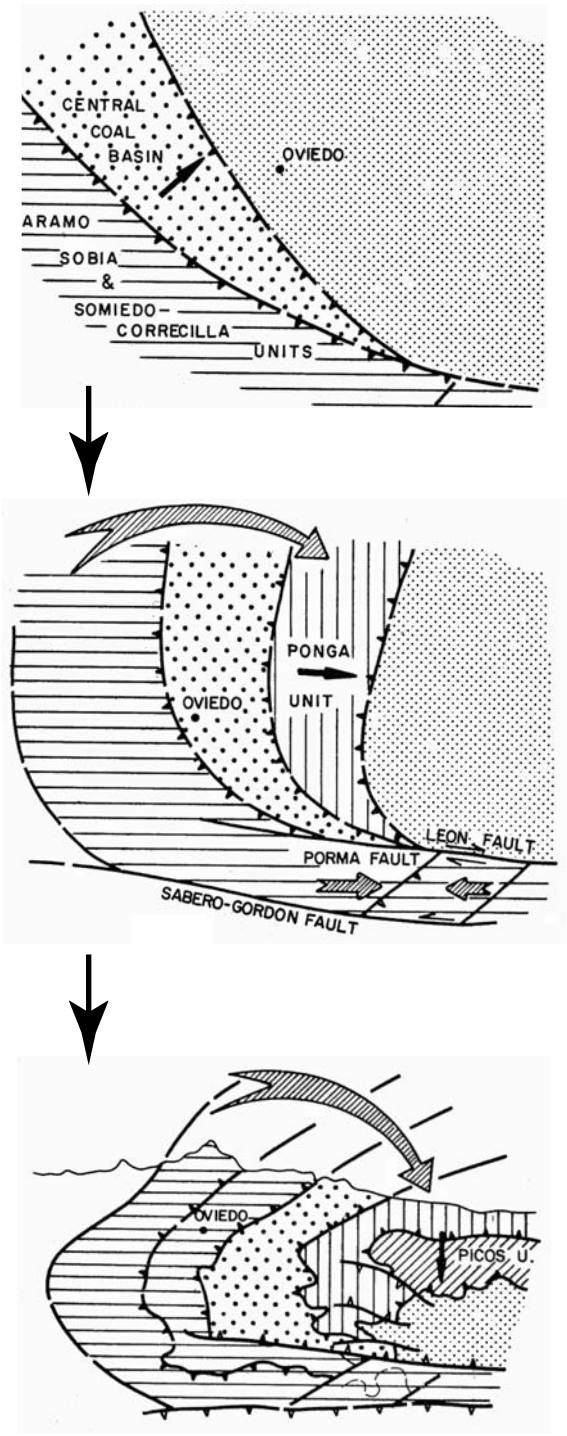

Fig. 2.5. Continuous deformation of progressive rotational thrust displacement propagating from west to east as proposed by Pérez-Estaún et al. 1988.

structural rotations unknown.

Also based on palaeo-magnetic data, Weil et al. (2000, 2001, 2003) describe three folding phases (Fig. 2.6). The authors assume that the present-day curved geometry was caused by the interference of original north-south trending structures (first and second folding phase) with a third superimposed folding phase. The older folding phases were dated as Namurian to Stephanian, whereas the younger phase was of Early Permian age. Consequently, the overall shortening direction changed from E-W in the Carboniferous to N-S in the Permian (in present-day coordinates). The Cantabrian Zone is described as an orocline, indicating oroclinal bending around a vertical axis in the Late Stephanian to Early Permian (Weil et al. 2000, 2001, 2003, Gutiérrez-Alonso et al. 2004). The orocline theory was introduced by Carey (Carey 1955). The theory of Weil et al. (2000, 2001) is supported by the analysis of calcite twinning (Kollmeier et al. 2000). Kollmeier et al. attributes the east-west compression to the collision between the Ebro-Aquitaine massif and the Laurussian margin, followed by a greater, north-directed collision of Gondwana with Laurussia.

The intrusion of most plutons in the Cantabrian, West Asturian-Leonese and northern Central Iberian Zones occurred in a short time span between approx. 295 and 285Ma (Fig. 2.15), indicating post-tectonic extension (Fernández-Suárez et al. 2000 b). This post tectonic magmatic event started 10-15Ma earlier in the most internal zones of the Variscan belt. In order to explain such a voluminous orogen-wide magmatic event, Fernández-Suárez et al. (2000 b) and Gutiérrez-Alonso et al. (2004) propose that delamination of the lithosphere acted as a triggering mechanism. The lithospheric mantle thickened below the inner arc and thinned below the outer arc simultaneously (Fig. 2.7; Gutiérrez-Alonso et al. 2004). This mass imbalance of lithospheric mantle caused a gravitational instability and resulted in the delamination of the lithospheric root (Fig. 2.8). Gutiérrez-Alonso et al. (2004) propose orogen-scale lower crustal melting, widespread magmatism, low pressure-high temperature metamorphism and fluid flow (see also Gasparrini et al. 2003) and coeval mineralization as evidence for the final decoupling of crust and lithospheric mantle. According to these authors delamination may have started between 319 and 310Ma under the Central Iberian Zone (50Ma after the main collision event) and reached its culmination between 300 and 290Ma beneath the entire belt.

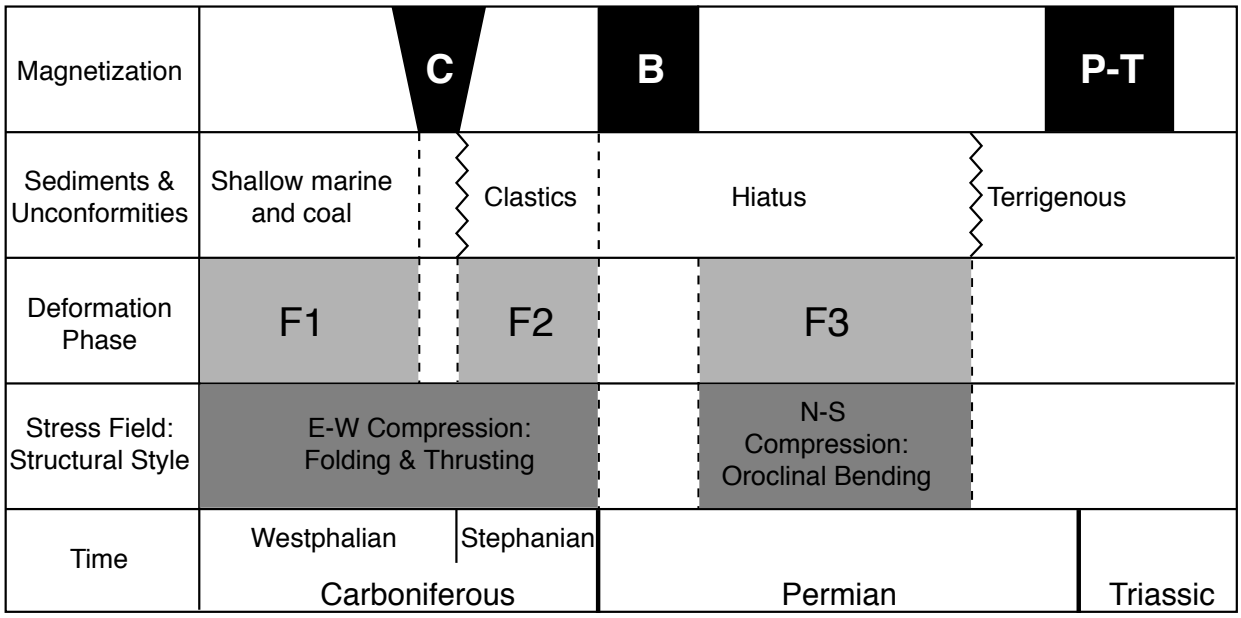

Fig. 2.6. The Variscan deformation history of the Cantabrian-Asturias Arc according to Weil et al. (2000, 2001). The deformation is represented by three deformation phases (F1, F2 and F3), their accompanying stress field, sedimentary history and recorded remagnetisation (C-Late Carboniferous; B-Early Permian; P-T-Permo-Triassic). Zigzag lines mark unconformities.

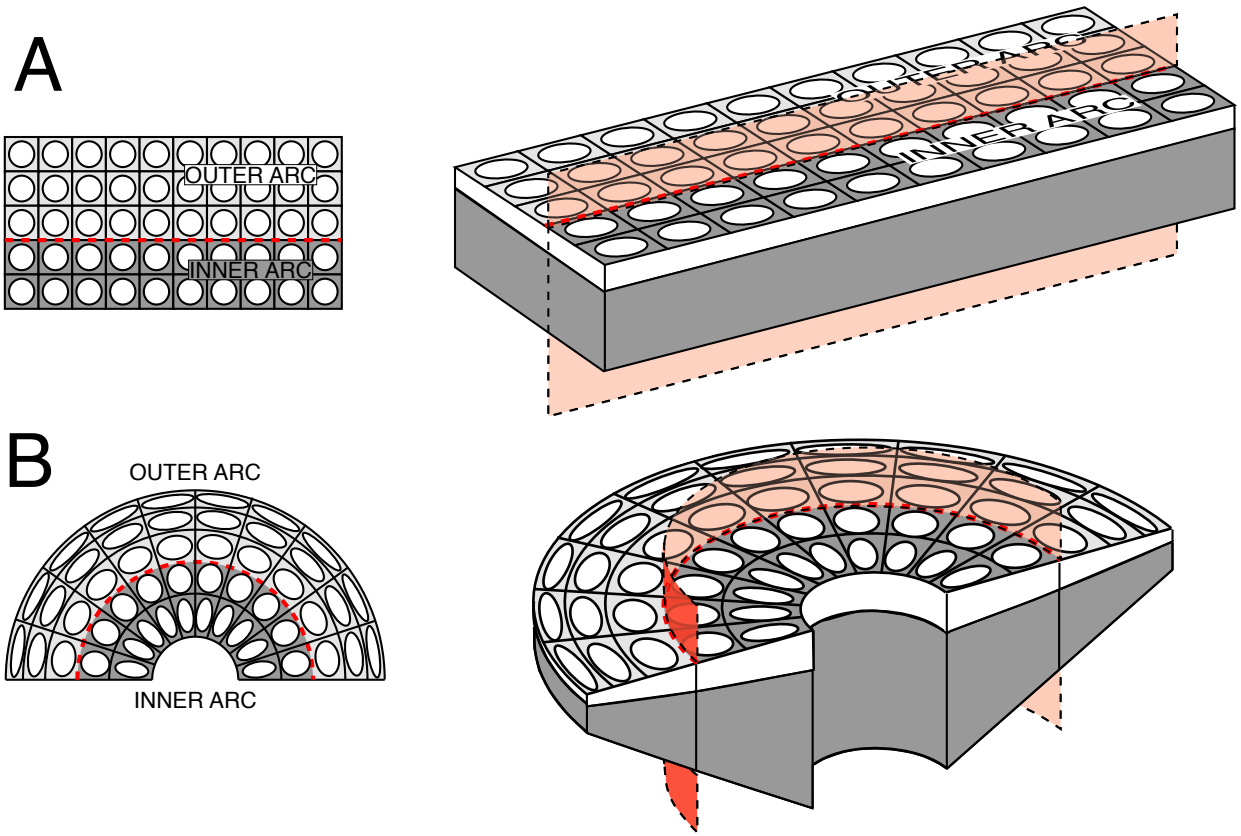

Fig. 2.7. Effect of lithospheric bending around a vertical axis and the resulting tangential longitudinal strain (Gutiérrez-Alonso et al. 2004). Note arc-parallel shortening of strain ellipses and thickening of the mantle lithosphere in the inner arc and arc-parallel stretching of strain ellipses and mantle lithosphere thinning in the outer arc (**A**: plan view; **B**: block diagram).

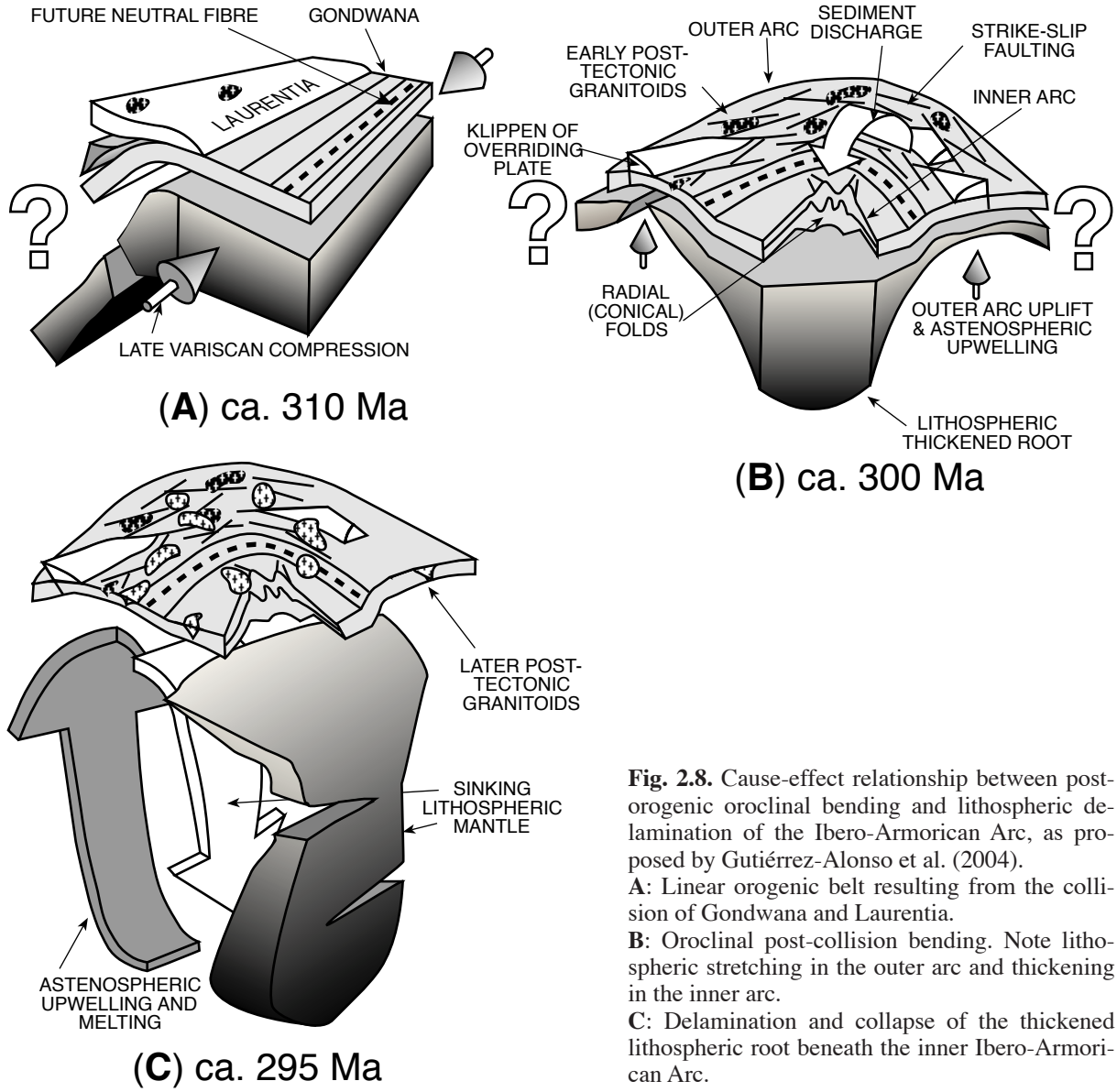

Fig. 2.8. Cause-effect relationship between post-orogenic oroclinal bending and lithospheric delamination of the Ibero-Armorican Arc, as proposed by Gutiérrez-Alonso et al. (2004).
A: Linear orogenic belt resulting from the collision of Gondwana and Laurentia.
B: Oroclinal post-collision bending. Note lithospheric stretching in the outer arc and thickening in the inner arc.
C: Delamination and collapse of the thickened lithospheric root beneath the inner Ibero-Armorican Arc.

2.3 Palaeogeographical evolution of NW-Iberia

2.3.1 Neoproterozoic/Cambrian

A complex cratonic Neoproterozoic basement of variable age and composition existed in the European Variscides as indicated by U-Pb analysis (Fernández-Suárez et al. 2000 a, 2002 a, b, Gutiérrez-Alonso et al. 2003). Fig. 2.9 shows the Neoproterozoic terrane assemblage that developed on an active Gondwanan margin.

Around 600Ma, extensional tectonic was coupled with magmatism and molasse sedimentation. The presence of a marked angular unconformity between the Mora and Herrería formations (Latest Vendian/Cambrian, see Fig. 2.10) has been controversially discussed in literature (see Valladares et al. 2002 for a compilation of data):

(i) For several authors (Marcos 1973, Pérez Estaún 1978, San José et al. 1990), the presence of the angular unconformity is evidence of compressive deformation during the Cadomian (Pan-African) orogeny.

(ii) Valladares et al. (2002) propose that erosion of the orogen combined with a renewed extensional event caused the development of the unconformity.

According to Fernández-Suárez et al. (2002 a, b) and Gutiérrez-Alonso et al. (2003) the area comprised the Cadomian-Avalonian magmatic arc (West Avalonian terrane) and associated back arc basins (NW Iberia and NE Bohemia) situated closer to the Gondwanan margin (Fig. 2.9). This peripheral arc was related to an oblique subduction event on the

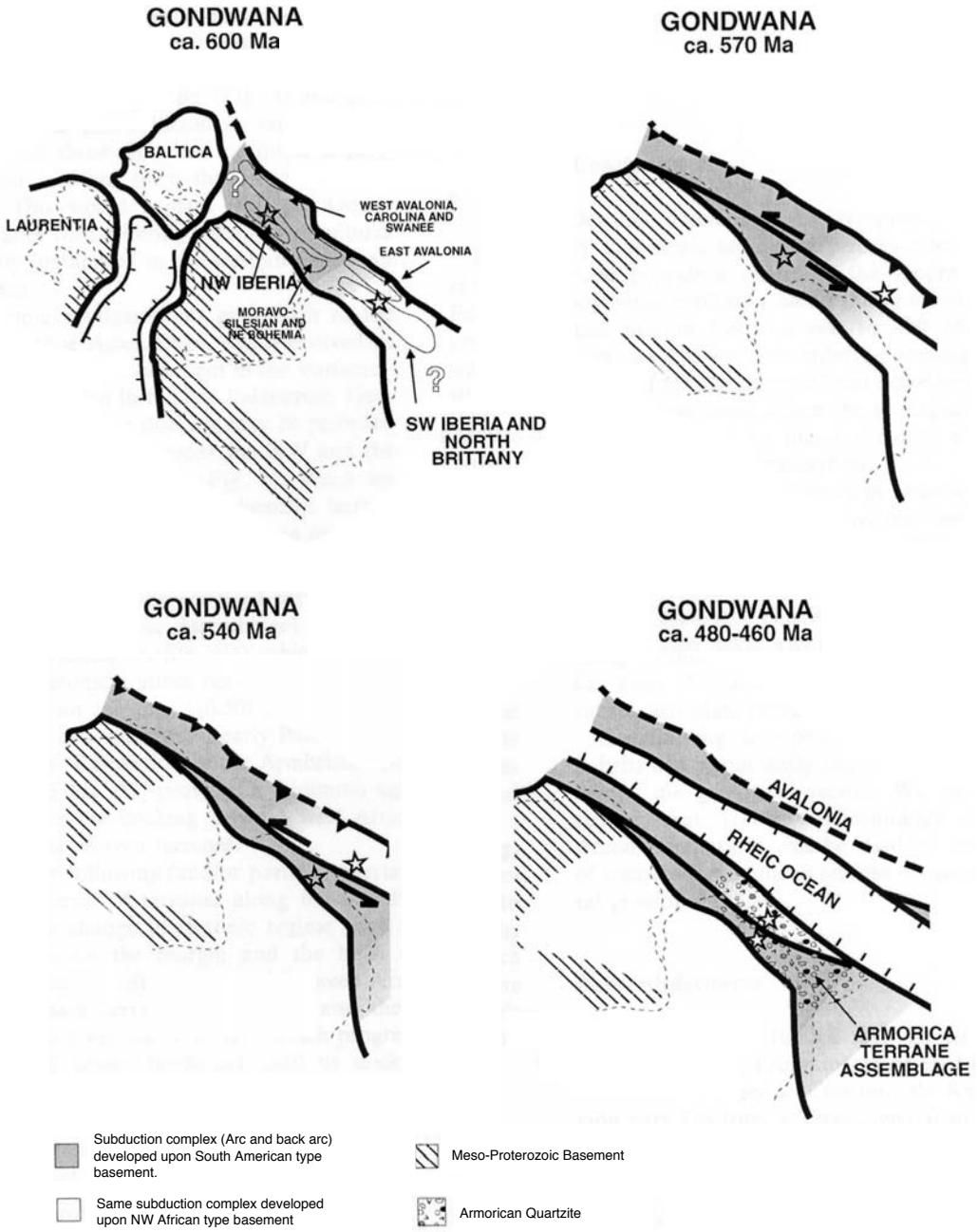

Fig. 2.9. Neoproterozoic terrane distribution and Early Palaeozoic plate-tectonic evolution along the northern Gondwanan margin (600 to 460Ma). Asterisks represent the location of NW Iberia and SW Iberia/Brittany (modified according to Fernández-Suárez et al. (2002 a) and Gutiérrez-Alonso et al. (2003)).

margin of Gondwana (Fig. 2.11). Thick Neoproterozoic sediments were deposited in these back arc basins, derived mainly from the arc (Murphy & Nance 1991) or both the main arc edifice and the margin of Gondwana (Fernández-Suárez et al. 2000 b).

A new controversy arises about the Neoproterozoic position of the various terranes:

(i) Some authors (Nance & Murphy 1996, Martínez Catalán et al. 1997) place Cadomia, Iberia and parts of East Avalonia adjacent to the West African craton. This palaeogeographic position seems to be corroborated by palaeomagnetical and geological evidence, indicating that Iberia and other terranes were located close to NW Africa (Armorican realm of Tait et al. 1997, Robardet 2000).

(ii) In contrast, Fernández-Suárez et al. (2000 a, 2002 a, b) and Gutiérrez-Alonso et al. (2003) argue that NW Iberia was located in a peri-Amazonian position, closer to West Avalonia, Florida and Carolina (South American craton signature), and only SW

Fig. 2.10. Angular unconformity between the Neoproterozoic Mora Fm. and the Herrería Fm. at Irede de Luna (see Chapter 2.4.4 for further details).Hammer for scale (30cm). Courtesy of T. Angerer.

Iberia was situated close to the West African craton (NW African craton signature). They suggest a tectonic transfer (strike slip activity along major transform faults parallel to the Gondwanan margin) prior to the opening of the Rheic Ocean (Fig. 2.9). This strike slip motion moved NW Iberia from an Amazonian realm closer to the West African margin, forming the Armorican terrane. In this way the authors explain why peri-Gondwanan terranes with differing basement signatures have the same Ordovician zircon provenance (Armorican quartzite; see Fig. 2.9).

Subduction and arc-related magmatism continued until about 560Ma (Fernández-Suárez et al. 1998, 2000 a). At that time the arc and back-arc basin developed as a result of crustal thinning (Fig. 2.11) and enhanced melting of the lower crust (main subduction stage approx. 650-570Ma). The lack of widespread deformation or significant crustal thickening suggests that the subduction was not terminated by a final continent-continent collision (Fernández-Suárez et al. 2000 a, 2002 a, b). This seems to be supported by further extension of the back-arc basin, the drift of the Avalonia micro-continent and the resulting opening of the Rheic Ocean (Fig. 2.11; Martínez Catalán et al. 1997, Fernández-Suárez et al. 1998, 2000 b, 2002 a, b). According to Robardet et al. (1990) the Rheic Ocean (Mid-European Ocean) opened in the late Middle or early Late Cambrian. Gutiérrez-Alonso et al. (2003) dated this event between approx. 520-530Ma (age of the youngest detrital zircon in the Cambrian arkose) and 460-470Ma (depositional age of the Armorican quartzite). On both sides of the Rheic Ocean two platforms developed: the Iberian-Armorican platform and the Meguma platform (Fernández-Suárez

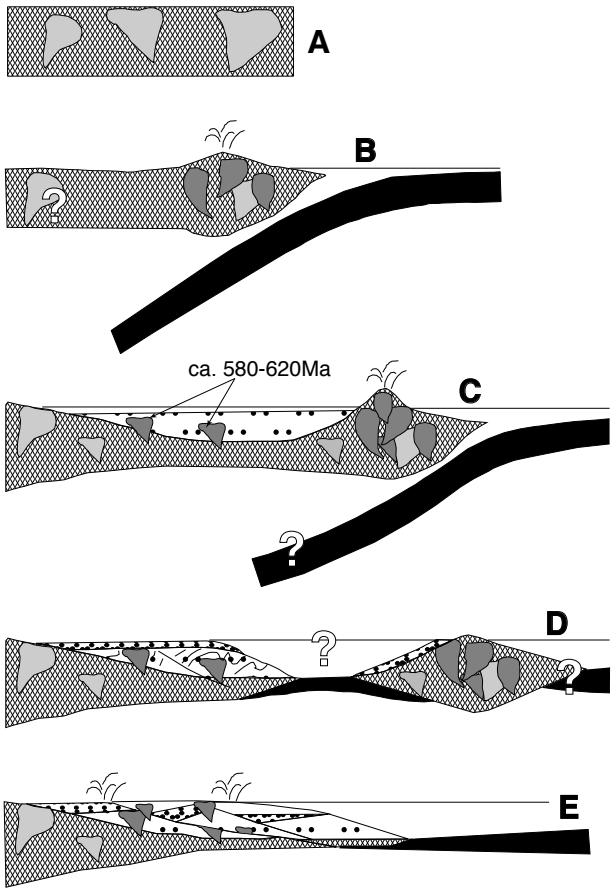

Fig. 2.11. Geological evolution of NW Iberia during the Proterozoic to Early Palaeozoic after Fernández-Suárez et al. (2000 b). **A**: Pre-Neoproterozoic cratonic basement; **B**: Cadomian-Avalonian early magmatic arc (ca. 800-650Ma); **C**: Cadomian-Avalonian back-arc (ca. 640?-560Ma); **D**: Undocking of Avalonia - birth of the Rheic Ocean (ca. 550Ma); **E**: Ollo de Sapo magmatic event (ca. 470Ma).

et al. 1998, 2002 b). Important tectonic activity is recorded at the western Gondwana margin as early as in the late Early Cambrian, increasing towards the Early-Middle Cambrian transition (Bechstädt et al. 1988, Bechstädt & Boni 1989, Russo & Bechstädt 1994, Álvaro et al. 2000 a, b). The mostly terrigenous sediments in the Cantabrian Zone at this time point to rifting processes and an extensional regime (Marcos 1973, Pérez-Estaún 1990, Álvaro et al. 2000 a, b).

2.3.2 The Avalonia controversy

In contrast to the relatively well-founded information regarding the Gondwana and Laurentia/Baltica cratons, there is a great amount of controversy surrounding the palaeogeographic position and significance of microcontinents such as Avalonia and Armorica (Carls 1988, Paris & Robardet 1990, Scotese & McKerrow 1990, Tait at al. 1997, Robardet 2000, 2002, Robardet et al. 2001, Scotese 2004):

(i) According to Tait et al. (1997) and Fernández-Suárez et al. (2002 a, b), Avalonia progressively drifted from Gondwana and Armorica starting in the Llanvirn, and it docked on Baltica during the Silurian. This is indicated by calc-alkaline volcanism and the development of endemic faunas. These authors propose that the Tornquist Sea was located north of Avalonia, separating it from Baltica, wheras the Rheic Ocean was in the south of this microcontinent and the Iapetus Ocean in the west (according to present coordiantes). Crowley et al. (2000) support this idea and propose that the Iapetus Ocean and the Tornquist Sea were narrowed by a northward migration of Avalonia in the Caradoc.

(ii) In contrast, some authors doubt the existence of an isolated terrane Avalonia and the Tornquist Sea (Paris & Robardet 1990). Faunal affinities seem to support Avalonia as the western promontory of Baltica at least since the Middle Cambrian times (Paris & Robardet 1990).

2.3.3 Ordovician

Faunal analyses show a clear separation of three major continental blocks with marine shelf areas (Gondwana, Baltica and Laurentia) located in distinct latitudes (Fig. 2.12) and separated by the Iapetus and Rheic Oceans (Paris & Robardet 1990, Scotese & Barrett 1990, Witzke 1990, Robardet 2000, 2002 and references). Whereas Laurentia remained in tropical latitudes throughout the Ordovician (Paris & Robardet 1990, McKerrow at al. 1991), Gondwana was situated at peri-polar latitudes and Baltica at intermediate to high palaeolatitudes (Torsvik et al. 1992, Crowley et al. 2000).

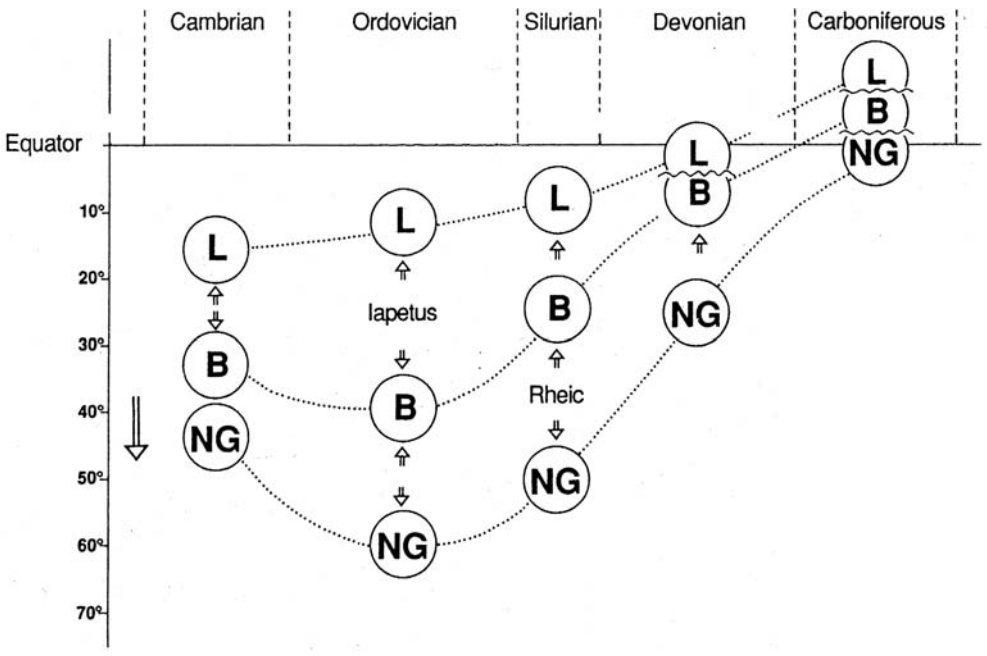

Fig. 2.12. Relative movements of North Gondwana (NG), Baltica (B) and Laurentia (L) from the Cambrian to the Carboniferous. Wavy lines indicate continental collisions (Paris & Robardet 1990).

Baltica drifted northwards reaching more temperate palaeolatitudes at the end of Ordovician, subsequently closing the Iapetus Ocean. The absence of carbonates on the shallow platforms indicates a position at high latitudes (45°-50° according to Paris & Robardet 1990, 65°-75° according to Tait et al. 1997). Palaeomagnetic data from Iberia (Van der Voo 1993) corroborates a high-latitude position during the Ordovician.

The presence of several prominent hiati within the Ordovician succession was interpreted as echoes of "Sardic movements" in the shelf-to-basin transitional zone (Gutiérrez-Marco et al. 2002). Thinning and further fragmentation of the northern Gondwanan margin advanced until the Ordovician, when it was marked by extensive bimodal rift-related magmatism, reaching from the Central Iberian Zone to France, Corsica and Sardinia (Crowley et al. 2000 and references herein). In the Central Iberian Zone this magmatism was marked by the Ollo de Sapo event (Fig. 2.11; Dallmeyer et al. 1997: 460-490Ma; Fernández-Suárez et al. 1998: 465-520Ma). According to Crowley et al. (2000) this alkaline and peri-alkaline granites resulted from the fractionation of mantle-derived melts in a proto-rift zone.

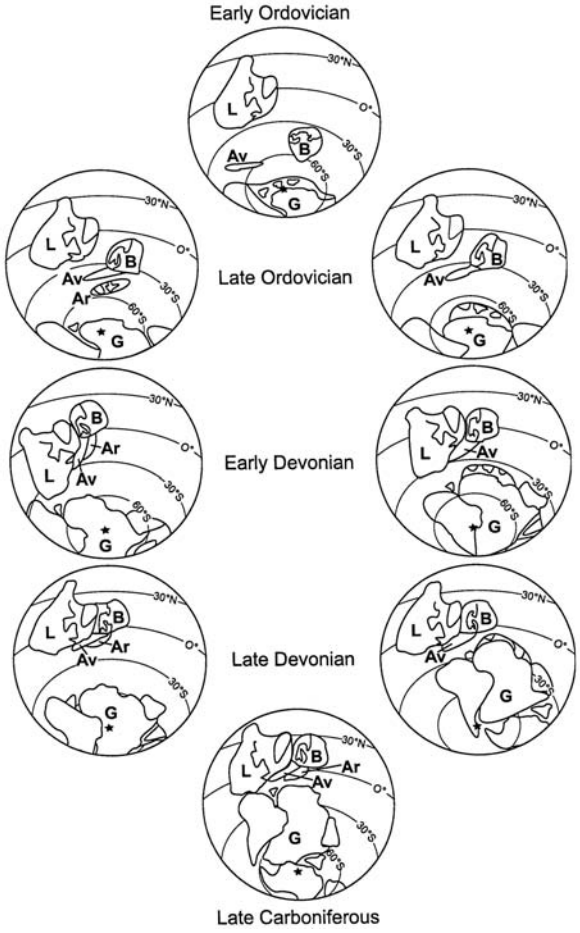

Fig. 2.13. Comparison of palaeogeographical models of the Early Ordovician through Late Carboniferous based on (**A**) palaeomagnetic data (left; Tait 1999 and Tait et al. 2000) and (**B**) on palaeoclimatic and palaeobiogeographical data (right; Paris & Robardet 1990, Robardet et al. 1990, Paris 1998).
Ar-Armorika; Av-Avalonia; B-Baltica; G-Gondwana; L-Laurentia. According to Robardet (2003).

2.3.4 The Armorica controversy

Similar to the case of Avalonia, considerable controversy surrounds the Armorican terrane and the Tornquist Sea (Carls 1988, Paris & Robardet 1990, Robardet et al. 1990, Trench & Torsvik 1991, Tait et al. 1997, Tait 1999, Robardet 2000, 2002, Robardet et al. 2001). The two opposed models are summarised in Fig. 2.13.

(i) The palaeomagnetic community favours the existence of an Armorican microplate (Iberian, Armorican and Bohemian Massifs, Matte 2001) or Armorican Terrane Assemblage (Tait et al. 1997, 2000, Crowley et al. 2000) as an Early Palaeozoic amalgamation of several tectonostratigraphic terranes with similar drift histories (Trench & Torsvik 1991, Tait et al. 1997, Crowley et al. 2000). The Armorican Terrane Assemblage, according to Crowley et al. (2000), remained adjacent to the northern flank of Gondwana at least until Arenigian. Between Llanvirnian and Caradocian it became detached from Gondwana and drifted rapidly to the north. In doing so, it fragmented and numerous narrow seaways developed between the fragments (Anderle et al. 1995, Franke et al. 1995).

(ii) However, from Early Ordovician to the Devonian, close faunal affinities (at species level) between northern Gondwana and the Ibero-Armorican realm contradict the existence of a broad Prototethys Ocean (3000km during Early Devonian according to Tait 1999) separating benthic faunal assemblages (Carls 1988, Paris & Robardet 1990, Robardet et al. 1990, 2001, Robardet 2000). Paris & Robardet (1990) propose that a large embayment called the South Armorican Ocean existed in addition to the Iapetus and Rheic oceans. It separated the Central Iberian and the Mid-North Armorican domains from the Cantabrian Mountains and Aquitaine, but never acted as a significant faunal barrier.

Gutiérrez-Marco et al. (2002) and Robardet (2002, 2003) stress close sedimentary and palaeobiogeographical affinities between North Gondwana and Iberia/Armorica, rejecting all Armorican microplate theories cited above. Robardet (2002, 2003) states that no wide ocean ever separated North Gondwana's Southern Europe from stable Gondwana during the Palaeozoic and that no wide ocean ever existed within the North Gondwanan region.

2.3.5 Silurian

After the Late Ordovician glaciation a major eustatic transgression immersed large parts of North Gondwana (Late Llandovery - Paris & Robardet 1990, Tait et al. 1997). The general outline of the Silurian areas was not significantly different from the Ordovician configuration. Baltica/Avalonia drifted to the north, subsequently narrowing the Iapetus Ocean (Fig. 2.12, Paris & Robardet 1990, Crowley et al. 2000). Others suggest that Baltica and Alvalonia collided in the Late Ordovician/Early Silurian prior to the polyphase collision of Baltica and Laurentia in the time range Late Llandovery to Early Devonian (McKerrow er al. 1991, Tait et al. 1997, 2000). North Gondwana was characterised by the deposition of graptolitic black shales. This type of deposition lasted longer in the distal north-eastern regions such as South Iberia or Sardinia (Paris & Robardet 1990, Oczlon 1992). Due to the differing opinions (see above), there are two contradicting models:

(i) Robardet (2000, 2002) and Robardet et al. (2001) highlight the "faunal barrier" function of the Rheic Ocean throughout the Silurian until the earliest Devonian and the position of the Iberian Peninsula within the proximal shelf of the North Gondwanan province (Fig. 2.13, Robardet & Gutíerrez-Marco 2002).

(ii) In contrast to this opinion, Tait et al. (1997) recognise a narrowing or complete closure of the Rheic Ocean between Armorica and the northern continents in the Late Silurian / Early Devonian. They base this theory on faunal affinities and palaeomagnetical data. However, the palaeomagnetic information for Silurian deposits is not clearly diagnostic as most of the measurements were influenced by later remagnetisation (Van der Voo 1993).

Thus the latitudinal position of Iberia can only be estimated as intermediate between approx. 50° S (latest Ordovician) and approx. 35° S (Early Devonian) (Robardet & Gutíerrez-Marco 2002).

2.3.6 Devonian

In the north, the final stages of the diachronous collision between Laurentia and Baltica/Avalonia led to the birth of the Old Red Continent by Lower Devonian times (Fig. 2.13). Laurentia and Baltica were located at an equatorial position (Fig. 2.12, Paris & Robardet 1990). As already mentioned earlier in this chapter palaeontological data contradicts palaeomagnetic results:

(i) Palaeogeographic reconstructions suggest the closure of all oceans separating Laurentia, Baltica, Avalonia and Armorica by Middle Devonian times and the definitive formation of the Old Red Continent in the Late Devonian (McKerrow et al. 1991, Torsvik et al. 1992, Tait et al. 1997, Crowley et al. 2000). Palaeomagnetic data supports the theory that a broad ocean separated Armorica from Northern Gondwana (Johnson & Tarling 1985, Tarling 1985, Tait et al. 1997).

(ii) However, benthic faunal and floral affinities between the Armorican Massif, Iberian Peninsula and the western Algerian Sahara even at species level do not support the presence of such a broad ocean (Carls 1988, Martínez-Catalán 1990, Paris & Robardet 1990, Robardet et al. 1990, 2001, Robardet 2000, 2002). Robardet et al. (1990) suggest the presence of numerous more or less isolated continental blocks located along the northern margin of Gondwana in order to explain the presence of different sedimentary and faunal domains in SW Europe during the Early Palaeozoic.

According to Paris & Robardet (1990) and Oczlon (1992) the Ibero-Armorican region was still situated on the North Gondwanan shelf located in warmer regions at 30°-35° in Early Devonian times. This is documented by the development of carbonate-terrigenous sediments in the Armorican Massif and the Iberian Peninsula. In the Middle Devonian Gondwana drifted to a tropical position (see also Fig. 2.12), allowing important reef development (Santa Lucía and Portilla formations, Chapter 2.4.4). First palaeontological and palaeobiogeographical evidence for affinities between North Gondwanan regions and the southern margin of Laurussia are reported from the Pragian/Emsian onward (Robardet

2000, 2002, Robardet et al. 2001). These affinities increased during the Emsian and Middle Devonian, indicating that the closure of the Rheic Ocean was progressing.

2.3.7 Consolidation of the Variscan Orogen

The period surrounding the final consolidation of the Variscan orogen was a time of large-scale shearing with the opening of small oceanic basins by transpression (Matte 1991, Quesada 1991). Palaeomagnetic data has demonstrated large-scale differential rotations and deformation throughout the belt (Johnson & Tarling 1985, Hirt et al. 1992, Tait et al. 1997). The global consolidation of the orogen is displayed in Fig. 2.14. Franke & Engel (1986) and Oczlon (1992) already postulated the onset of a convergence by late Devonian (Frasnian/Famennian), marked by flysch and greywacke deposition throughout the entire Variscan Belt. In the Late Devonian the northern margin of Gondwana is interpreted as being an active continental margin in response to the southward-directed subduction of the Rheic

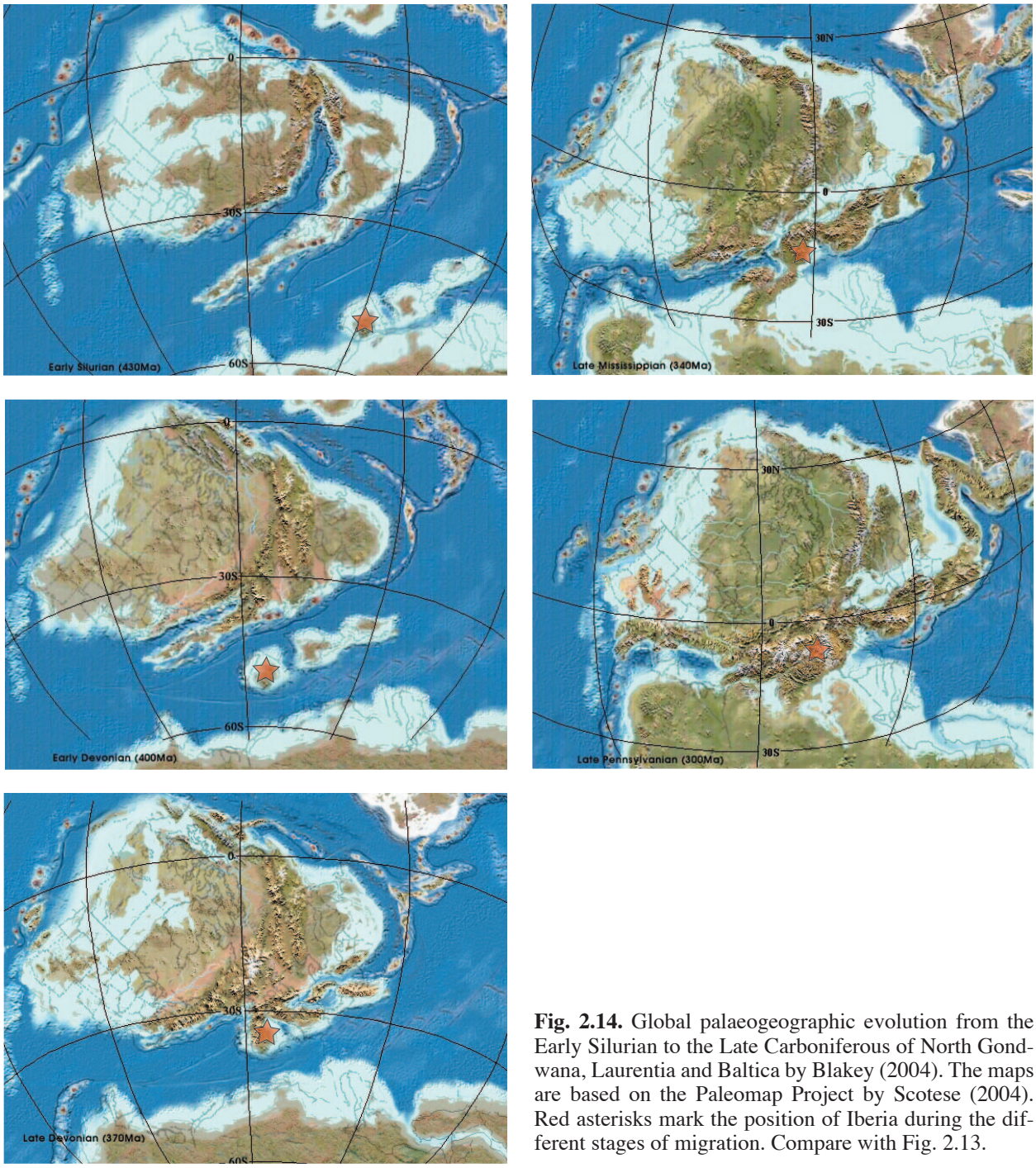

Fig. 2.14. Global palaeogeographic evolution from the Early Silurian to the Late Carboniferous of North Gondwana, Laurentia and Baltica by Blakey (2004). The maps are based on the Paleomap Project by Scotese (2004). Red asterisks mark the position of Iberia during the different stages of migration. Compare with Fig. 2.13.

Ocean (Oczlon 1992). Palaeomagnetic data points to the closure of the ocean separating the Old Red Continent and Gondwana by the Late Devonian and the initiation of the collision in the Early Carboniferous (Tait et al. 1997). In the western part of the Iberian Peninsula (Cabo Ortegal, Ordenes etc.) high-pressure metamorphic rocks and ophiolites point to a westward subduction (according to the present coordinate system) from 380-370Ma ago (Martínez Catalán et al. 1997, see also Fig. 2.15). These ophiolitic nappes were stacked during the closure of the Rheic Ocean and mark the suture (Dallmeyer et al. 1997). After the closure of the Rheic Ocean the outer edge of Gondwana was also subducted, deducting the subduction direction from the metamorphic gradient (Martínez Catalán et al. 1997). The migration of metamorphic stages across the orogen is consistent with the migration of syntectonic granitoids in time (Fernández-Suárez et al. 2000 b). The underthrusting of continental material subsequently proceeded (375-365Ma), causing intracontinental deformation that progressed towards the more external parts of the orogen in time (Fig. 2.15, also compare Chapter 2.2.1). However according to Fernández-Suárez et al. (2000 b) there is no record of significant magmatic activity related to this stage in the autochthon of NW Iberia.

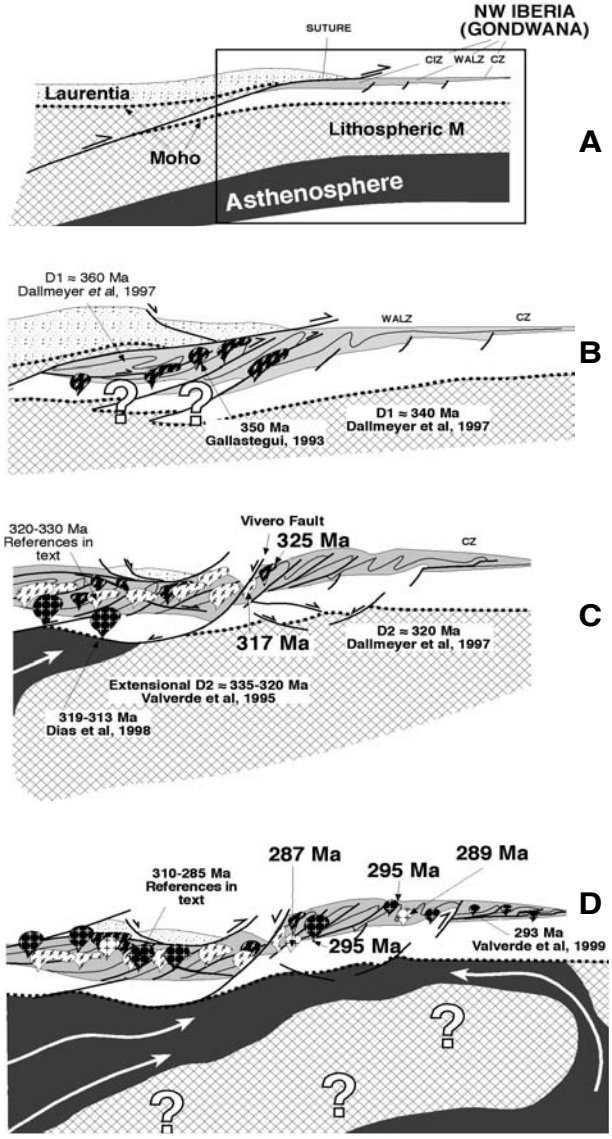

Fig. 2.15. Tectonic evolution of the NW Iberian Variscan Belt according to Fernández-Suárez (2000 b). **A**: pre-tectonic association; **B & C**: syn-tectonic associations; **D**: post-tectonic association. Geochronologic information is based on U-Pb measurements of NW Iberian granitoids.

2.3.8 Carboniferous

The position of the Iberian Peninsula in Lower Carboniferous is little constrained (Amler 2000). Johnson & Tarling (1985) place Iberia as part of a terrane approx. 20° south of the equator relatively near to the southern margin of Laurussia. Others believe it was located closer to the northern border of Gondwana (Scotese et al. 1979, Paris & Robardet 1990). Johnson & Tarling (1985) and Tarling (1985) imply that Brittany (southern border of Laurasia) and Spain (Armorica) collided in the Lower Carboniferous and ultimately converged with Gondwana in the Upper Carboniferous.

The eastward diachronous progradation of the Variscan deformation in NW Iberia was described in Chapter 2.2.1. Various Variscan deformational phases (see Pérez-Estaún et al. 1991, Dallmeyer et al. 1997) represent local responses to regional shortening. Average propagation rates of approx. 5km/Ma were proposed by Dallmeyer et al. (1997) who compared isotopic ages of different areas. These propagation velocities are supported by migrating intrusion ages recorded by Fernández-Suárez et al. (2000 b). The Variscan deformation in the Cantabrian Zone lasted until 290Ma (Martínez Catalán et al. 1997, Dallmeyer et al. 1997). Further evolution of the Ibero-Armorican Arc was described in Chapter 2.2.3.

2.3.9 Post-Variscan

A rifting episode gave rise to the development of a Permo-Triassic basin development (Martínez García et al. 1983, Leprvrier & Martínez García

1990). During the Early-Middle Jurassic and Early Cretaceous an extensional event was instrumental in opening the Atlantic Ocean and the Bay of Biscay (García-Mondejar 1989, Verhoef & Srivastava 1989). During the Cenozoic Alpine Orogeny the Variscan basement and an undetached Mesozoic cover were uplifted to create the Cantabrian Mountains (Pulgar et al. 1995). See Alonso et al. (1995) for further details regarding the Alpidic Orogeny in the region.

2.4 Cantabrian Zone

The Cantabrian Zone represents the core of the Ibero-Armorican Arc (Fig. 2.1), representing the easterly-directed Variscan foreland fold-and-thrust belt (also called the Cantabria-Asturias Arc). The geology of the region is well documented on maps (scale 1:50,000) of the Instituto Tecnológico GeoMinero de España (Lobato et al. 1984, Matas & Rodríguez Fernández 1984, Suárez Rodríguez et al. 1990, Alonso et al. 1991 and others) and older maps, mostly contributed by geologists from Leiden (Savage & Boschma 1980 and others).

2.4.1 Deformation and subdivision

Several E-directed thrust units were emplaced during Carboniferous times and show a rather tight arcuate trend with its concavity towards the foreland (Julivert 1971, Weil et al. 2000). As indicated by the syn-orogenic and post-orogenic deposits, the orogenic wave reached the Cantabrian Zone in the Late Carboniferous time (Pérez-Estaún et al. 1988, Quesada 1991). Dallmeyer et al. (1997) estimated the age of deformation within the Cantabrian Zone as ranging between 310 and 290Ma (see also Chapter 2.2.1 and Fig. 2.3). It can be subdivided into several domains and units as displayed in Fig. 2.1. The Somiedo-Correcilla Unit (Fold nappe belt after Julivert 1971) marks the first occurrence of unmetamorphosed Palaeozoic sedimentary units east of the basement core of the Narcea Antiform (Gutiérrez-Alonso 1996). The eastward continuing deformation (toward the foreland) produced the Sobia-Bodón and Aramo units (Fig. 2.16), the Central Coal Basin (Aller & Gallastegui 1995), Ponga Unit (Alvarez-Marrón 1995), and the more easterly Picos de Europa and Pisuerga-Carrión provinces (Pérez-Estaún & Bastida 1990). The westernmost Cantabrian unit (Somiedo Thrust Sheet) was emplaced during the early Westphalian (Dallmeyer et al. 1997). The more external structures were emplaced during lower Stephanian (Pérez-Estaún et al. 1988), which implies a time span of approx. 15-20Ma for the emplacement of all units (Dallmeyer et al. 1997). The formation and evolution of the Ibero-Armorican Arc

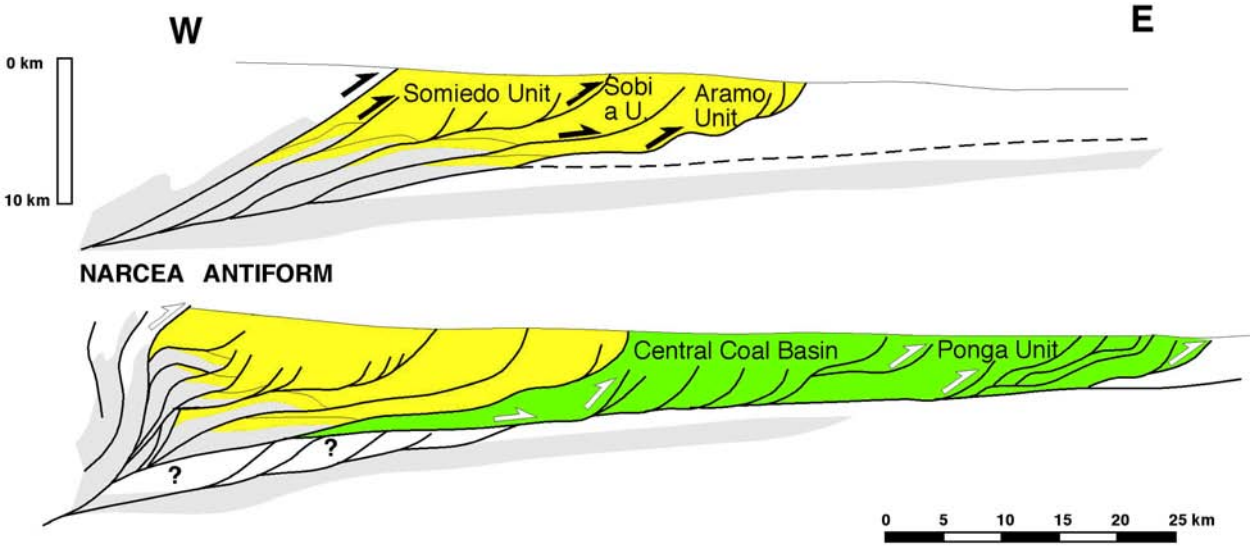

Fig. 2.16. Sketch of the continuing foreland-directed deformation. First the Somiedo, Sobia and Aramo units were produced (upper picture), followed by the subsequent formation of the Central Coal Basin and Ponga units (lower picture). Grey tones mark the Precambrian Narcea-Antiform (after Pérez-Estaún & Bastida 1990).

was already described in Chapter 2.2.3.

Julivert (1971) and Julivert & Marcos (1973) described two main Variscan deformation phases in the Cantabrian Zone: (i) the first was caused by east-west compression (in present-day coordinates), causing thrust initiation related to the formation of longitudinal folds, characterised by horizontal fold axes and steep axial surfaces parallel to the curvature of the arc; (ii) the second phase is marked by a radial set of folds with steep fold axes and is associated with the final tightening of the Cantabria-Asturias Arc.

Alpine deformation reactivated many Variscan structures, resulting in further compression with steepened thrusts and faults and increased structural shortening (see also Fig. 2.18). Thus, the present-day structural setting gives only a partial and distorted picture of the Variscan Belt prior to the oroclinal bending (Ábalos et al. 2002, Robardet 2002). However, the structural situation with sub-vertical dipping cross-sections in every single thrust sheet offers good information about the Southern Cantabrian Basin.

2.4.2 Metamorphism and palaeo-temperature conditions

The Cantabrian Zone was deformed at shallow crustal levels without significant metamorphism. Penetrative cleavage developed only locally and is interpreted as being generally of pressure-solution origin (Hirth et al. 1992, García López et al. 1997, Bastida et al. 1999). The cleavage does not display any relationship to compressional structures (Aller et al. 1987). Palaeo-temperature estimates based on conodont alteration index (CAI) and illite crystallinity (IC) values indicate anchizonal conditions with maximum temperatures of 150°-250°C only in the lower part of the Somiedo Unit (Raven & van der Pluijm 1986, Bastida et al. 1999). Values obtained by calcite twinning analysis (Kollmeier et al. 2000) point to temperatures ≤200°C. Further to the north diagenetic conditions become dominant (Correcillas Unit, La Sobia-Bodón Unit). The highest metamorphic overprint with epizonal values were experienced by rocks situated near the León Line fault system and the Narcea-Antiform. Anchizonal conditions prevailed in the Central Coal Basin and some of the Stephanian basins (Keller & Krumm 1993, García-López et al. 1999, Frings 2002, Ayllón 2003)

2.4.3 Structural settings

The Cantabrian Zone is a zone of closely related thrusts that are geometrically, kinematically and mechanically linked, and is, according to the nomenclature of McClay (1992), a thrust system. The

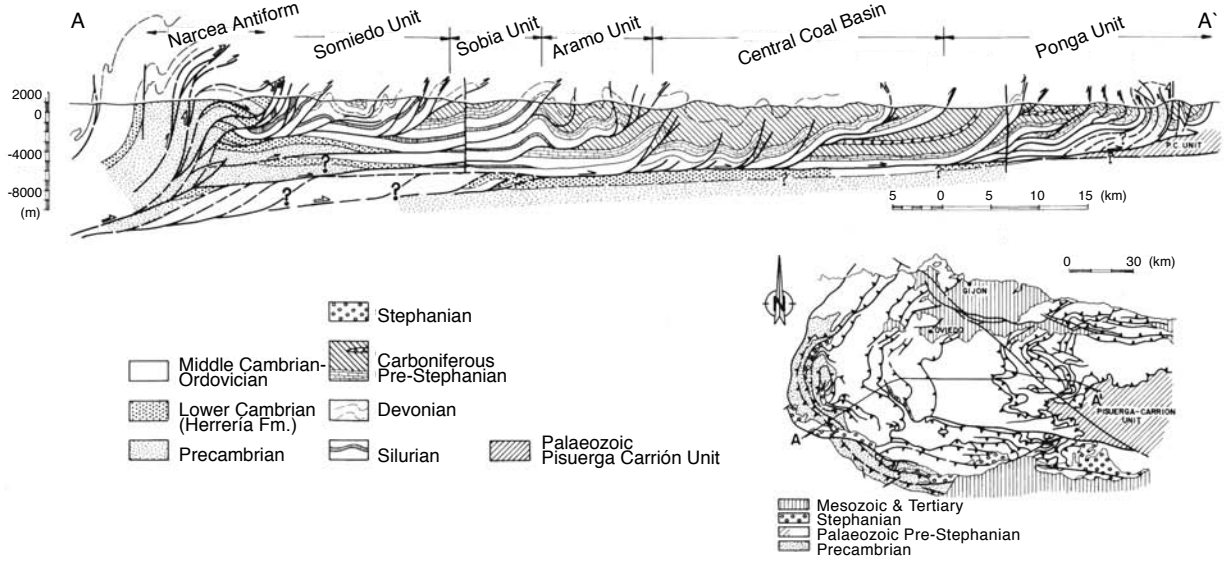

Fig. 2.17. Detailed geological cross-section through the Cantabrian Zone (after Pérez-Estaún et al. 1995). Note the thin-skinned deformational style and the thrusting of the Narcea Antiform on the Cantabrian Zone. See Fig. 2.4 for the extension of the cross-section to the west.

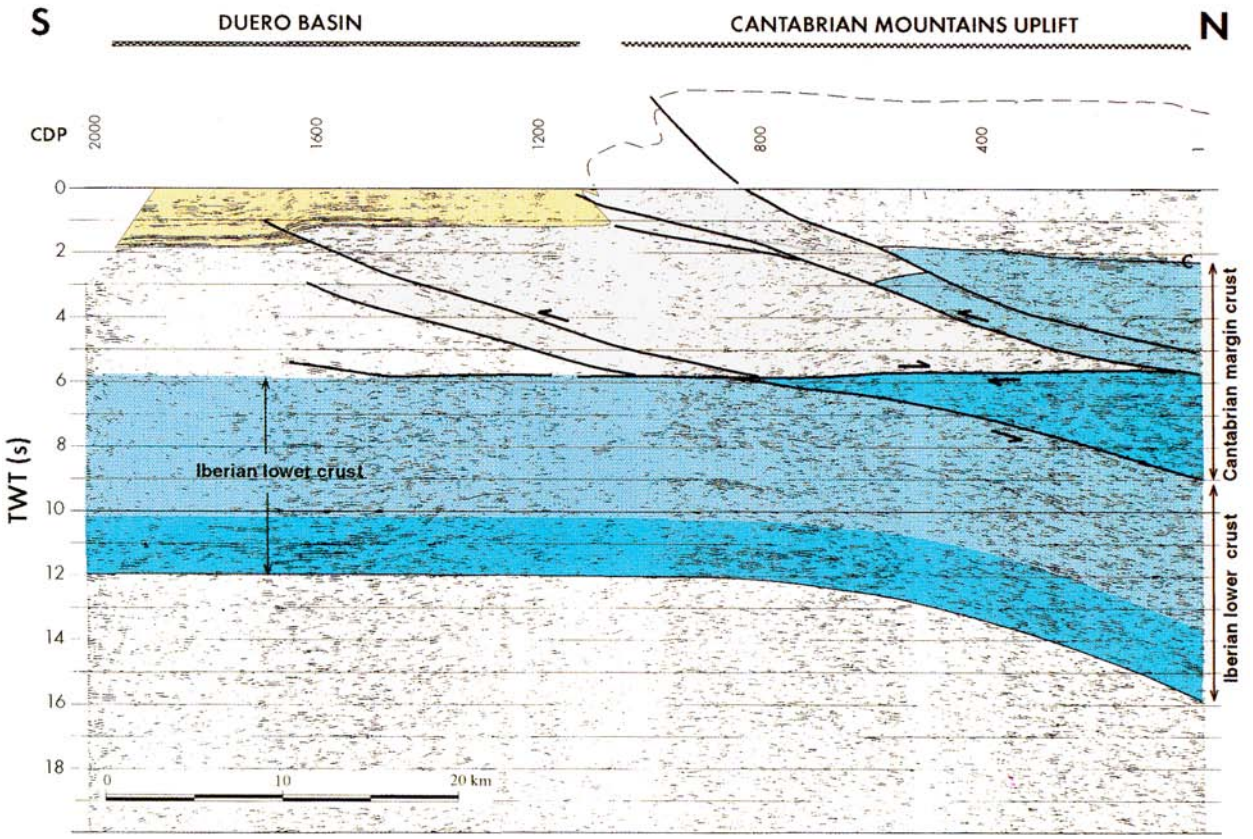

Fig. 2.18. Deep crustal section across the ESCI-N2 transect showing the Alpine duplication of the lower crust under the Cantabrian Mountains. Reflector C shows the subvertical décollement of the Palaeozoic succession. The Duero Basin (yellow colour) is displayed by well-defined reflectors in the sub-surface (Pulgar et al. 1995).

basin architecture of the southern arm of the Cantabria-Asturias arc is characterised by thin-skinned tectonics (Fig. 2.17), with its main detachment horizon located at the base of the Láncara Fm. (Early Cambrian) and some minor décollements within higher stratigraphic horizons (Julivert 1971, Pérez Estaún et al. 1988). Deep seismic reflection profiles (ESCI-N1 and ESCI-N2; Estudio Sísmico de la Corteza Ibérica Norte = Seismic Study of the North Iberian Crust) show a subhorizontal to gently dipping reflective band corresponding to the Cantabrian Zone detachment (Fig. 2.18), with a dip close to 3° toward the west and south (Pérez-Estaún et al. 1988, 1994, 1995, Pulgar et al. 1995). In the northern part of the region there is an additional prominent detachment within the Precambrian Herrería formation.

The Palaeozoic succession was strongly deformed during Variscan times by a set of imbricate thrusts and cogenetic folds, as well as by late, high-angle faults (Ábalos et al. 2002). The structural pattern of the Cantabrian Zone results from interference between thrust sheets, arcuate folds and older radial folds cross-cutting the first fold set (Julivert 1971, Julivert & Marcos 1973). According to Alonso (1987) and Pérez-Estaún et al. (1988) the first fold set was at least partially caused by the development of duplexes and antiformal stacks. Kollmeier et al. (2000) also identified two fold sets. Early longitudinal folds running tangential to the arc are overprinted by a cross-cutting radial fold set. The deformation was subsequently hindered by hanging-wall ramp anticlines, duplexes and antiformal stacks (see Chapter 3). Consequently the existing folds were tightened and the thrust sheets began to fold (Hirt et al. 1992). These new folds generally overprinted the existing structures and were, therefore, longitudinal in relation to older folds and thrusts. The radial folds superposed on the above structures are defined most clearly in the core of the Asturian arc and vanish towards its outer peripheries (Hirth et al. 1992).

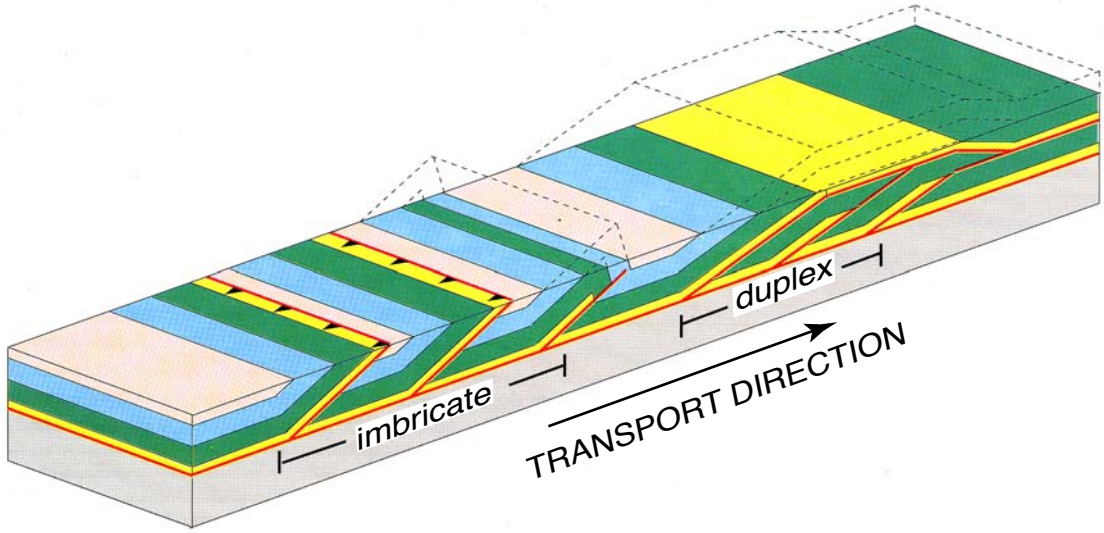

Fig. 2.19. Typical structural features of the Iberian fold and thrust belt. The block diagram shows different thrust associations in the form of imbricate thrust sheets and duplexes. Note the transport direction from left to right (after Alonso & Pulgar 1995).

In the Southern Cantabrian Zone, a "piggy-back thrust" mechanism (see Chapter 3.6.3 and Fig. 3.1) shows a forward-breaking sequence of individual thrust sheets as well as basal accretion within the Herrería Fm. Geometries are characterized by overlapping ramp anticlines, curved ramps, imbricated systems, duplexes and anticlinal stacks. These are typical features caused by increased basal friction (Fig. 2.19; Mitra 1986, Nieuwland et al. 2000). The high basal friction theory (see Chapter 3) is supported by comparing thrust sheet length and displacement width, and is in concordance with sandbox experiments carried out by Nieuwland et al. (2000). The resulting thrust-sheet geometry is that of a series of individual ramp anticlines (according to the terminology of McClay 1992). The structural framework of the Southern Cantabrian Mountains can be divided into three domains. These (Bodón, Pedrosa and Alba domains) are described in detail in Chapter 3.6.2.

Several out-of-sequence faults with unknown displacement factors and characteristics are present in the region (see Chapter 3.6). The most prominent of these is the León Line fault system (Chapter 3.6.1 and Fig. 3.5) extending E-W for about 150km. The main fault has a steep dip and has caused extensive brecciation and small scale faulting. Julivert (1968) interprets first movements along this fault system to have occurred in the Late Westphalian, as a result of the structural development of the Central Coal Basin and Ponga units. Some authors suggest an initial sinistral strike-slip movement, being reactivated during later structural movements of possibly Permian age as reverse faults (Marcos 1968, Julivert et al. 1971, Marcos et al. 1979, Heward & Reading 1980). Pulgar et al. (1999) suggest the possibility of a subsequent reactivation during the Alpidic Orogeny.

2.4.4 Stratigraphy

Compared to the West Asturian-Leonese Zone containing about 11km of sediment, the Cantabrian Zone shows a much thinner Lower Palaeozoic sedimentary succession, with a thickness of only three kilometres (Marcos, 1973, Julivert 1981, Pérez-Estaún et al. 1990, Bastida & Aller 1992).

The general lithologic subdivision of the Palaeozoic succession in the Cantabrian Zone comprises two parts (Fig. 2.20):

1. Pre-Carboniferous sediments which were deposited on a clastic-carbonate shelf, thickening towards the convex part of the arc;
2. Carboniferous succession, which marks a major change in sedimentation, indicating the beginning of the Variscan Orogeny and a change from syntectonic to post-tectonic conditions (Marcos & Pulgar 1982).

A stratigraphic chart of the Southern Cantabrian Ba-

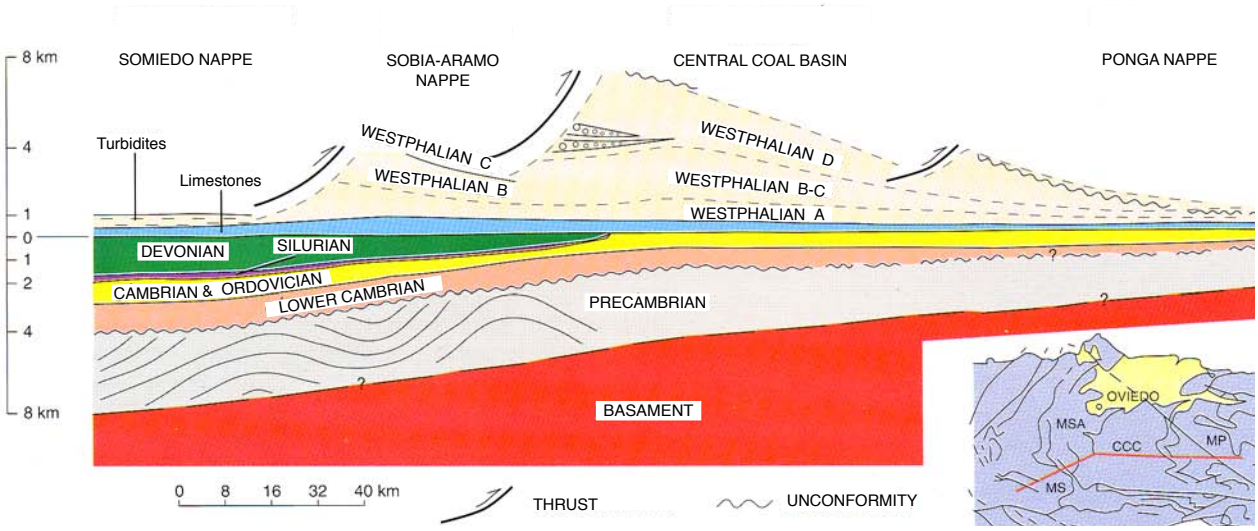

Fig. 2.20. Stratigraphic section through the Cantabrian Zone (Marcos & Pulgar 1982, Alonso & Pulgar 1995). The lower part represents the pre-orogenic succession (Cambrian to Devonian). The upper part shows the evolution of syn-orogenic Carboniferous sediments with implied Variscan thrusts.

sin is shown in Fig. 2.21. The Precambrian to Silurian sedimentary succession is dominated by siliciclastic sediments (Herrería, Oville, Barrios, Formigoso, San Pedro formations) and several long-term hiati. The only exemptions are the Lower Cambrian carbonates of the Láncara Fm. From the deposition of the Silurian San Pedro Fm. onward, the influence of an elevated area in the northeast (Cantabrian High) became visible, with the development of thicker basinal successions to the southwest (Fig. 2.20 and 2.21) and onlap towards the northeast. During the Devonian, an alternating deposition of carbonates (Abelgas, Santa Lucía, Portilla formations) and siliciclastics (Esla, Huergas, Nocedo, Fueyo formations) evolved. Each period of carbonate growth, producing major reefs, was followed by a succession of clastic material and a new phase of carbonate deposition. However, the end of the Givetian marked the demise of the Devonian reefs, manifested in the Frasnian event (García-Alcalde 1998, García-Alcalde et al. 2002). Subsequently, the whole Cantabrian Zone was covered by siliciclastics (Ermita Fm.) and condensed carbonates of the Alba Fm. until the Early Namurian. Thick synorogenic turbidites (Olleros Fm.), initiated in the Sepukhovian, mark the onset of the Variscan orogenic phase in the Cantabrian Zone (see Chapter 2.2.1). Large carbonate platforms developed (Barcaliente, Valdeteja formations), which were subsequently covered by terrigenous sediments from the approaching Variscan Orogen (San Emiliano Fm.). The thickness of the mainly shallow marine Palaeozoic succession ranges between 3800m and 5000m. Isolated intra-montaneous basins with mostly continental deposits formed in the Stephanian due to renewed tensional tectonics (Fig. 2.1). The following Permian and Mesozoic/Cenozoic succession in the Cantabrian Zone was mostly eroded (if present at all) and cannot be reconstructed. Thicknesses stated in the following text are indicative only for the area investigated (see Fig. 3.5).

MORA FM.

This formation represents the oldest outcropping rocks in the region. Lotze (1956) first named these Precambrian rocks the "Pizarras del Narcea." In 1961 Sitter defined the Mora Fm. Liñán et al. (2002) and Valladares at al. (2002) integrate all Neoproterozoic deposits into the Narcea Group.

Type locality: Close to the village of Mora de Luna (Sitter 1961), ITGE Map 129 "La Robla" (Matas & Rodríguez Fernández 1984).

Thickness: There is no complete section available; Pérez-Estaún (1978) presumes a thickness of 1500-1700m.

Lithology: Shales, siltstones, fine sandstones, micro-conglomerates, greywackes (Staalduinen 1973, Barba & Fernández 1990). See Fig. 2.10.

Depositional environment: Martin Parra (1989) interprets the sediments to be submarine fan depos-

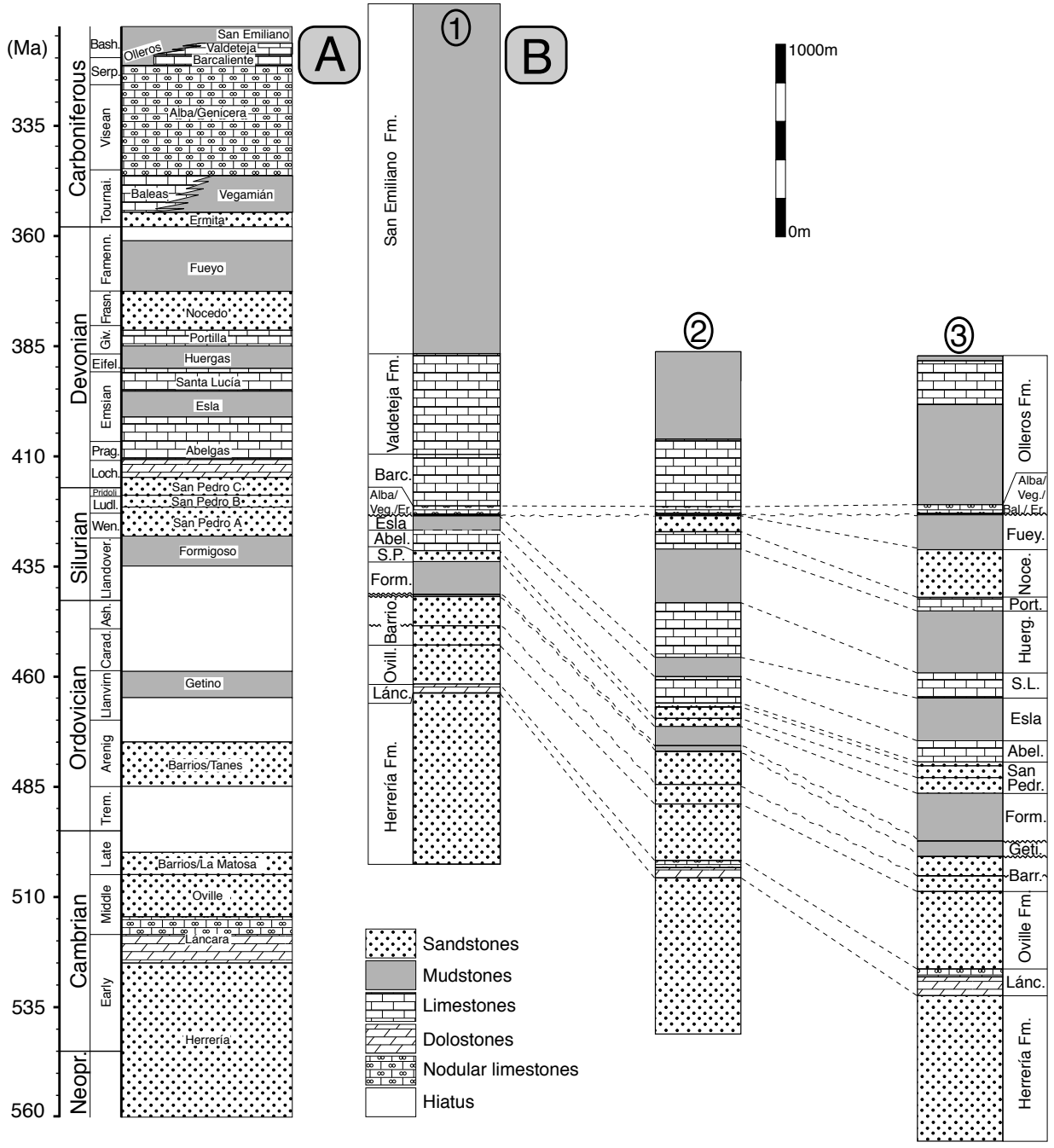

Fig. 2.21.
A: Stratigraphic chart of the Southern Cantabrian Mountains showing formation names in the stratigraphic columns. Absolute ages are taken from the German Stratigraphic Commission (2002). Stratigraphic gaps are indicated by white fields.
B: Three selected synthetic stratigraphic sections along the Bernesga Transect.
No. 1: Proximal section at km 7 (northern part of the transect)
No. 2: Section at km 42
No. 3: Distal section at km 54 (southern part of the transect)
Note the wedge-shaped pattern of the Ordovician to Devonian formation thicknesses, increasing basinwards to the south. Due to the depositional/erosional hiatus in the northern section, most of the Devonian formations are missing. Hiati are marked by wavy lines.

its in mid-fan to lower-fan positions. Palaeo-current indicators imply sedimentation from NE, NW and NNW.
Age: The age within the Precambrian has not been determined conclusively.

HERRERÍA FM.
The Herrería Fm. overlies the Mora Fm. with a clear angular unconformity (Fig. 2.10). Comte (1938) first introduced the name "Areniscas de la Herrería."
Type locality: Approx. one kilometre north of Cerecedo in the Porma Valley (Comte 1959), ITGE Map 104 "Boñar" (Lobato et al. 1984).
Thickness: Evers (1967) and Aramburu (1992) measured the formation in the area of Los Barrios de Luna with an overall thickness of 700-900m.
Lithology: The Herrería Fm. was divided into three members: (i) lower member with conglomerates, sandstones, sandy limestones; (ii) middle member composed of mainly coarse sandstones, micro-conglomerates (Fig. 2.22) and (iii) upper member with alternating sandstones and shales as well as dolomite lenses (Oele 1964, Evers 1967, Staalduinen 1973, Aramburu et al. 1992, Aramburu & García Ramos 1993).
Depositional environment: The angular unconformity was interpreted as the result of Cadomian tectonism (Ábalos et al. 2002, Fig. 2.10). The Herrería Fm. was deposited in a deltaic environment (Rupke 1965, Bosch 1969, Savage & Boschma 1980) or within a shallow marine setting (Comte 1959, Oele 1964, Rupke 1965, Evers 1967, Sjerp 1967, Vilas Minondo 1971, Savage & Boschma 1980). Some authors interpret the sediments as being deposits of braided rivers (Rupke 1965, Bosch 1969, Meer Mohr et al. 1981) and intertidal coastal environments (Leyva et al. 1984, Aramburu et al. 1992). Oele (1964) measured a transport direction from N to S. In the uppermost part of the formation black pyritic shales and marls indicate shallow seas with restricted circulation after a sharp decrease in clastic supply (Evers 1967).
Age: Late Precambrian (Vendian) - Early Cambrian Relative ages of the upper part are determined on the basis of trilobites and ichnofossils (Sdzuy 1967, Bosch 1969, Meer Mohr 1969, Truyols 1969, Vidal et al. 1999). Liñán et al. (1993) place the base of the Herrería Fm. at the Precambrian-Cambrian boundary whereas Aramburu et al. (1992) propose an Ediacarian age.

LÁNCARA FM.
The Láncara Fm. transitionally overlies the Herrería Fm. and represents the oldest formation composed mostly by carbonates in the region. Its former name, as given by Comte in 1937 was "Calcaires de Láncara."
Type locality: The type locality of Comte (1937) in the vicinity of Láncara de Luna is now flooded by the artificial reservoir Los Barrios de Luna. Therefore Zamarreño (1972) proposed three additional reference sections: Los Barrios de Luna (Somiedo-Correcillas Unit), Arintero (Bodón thrust sheet) and Carangas (Ponga thrust sheet). ITGE Map 102 "Los Barrios de Luna" (Suárez Rodríguez et al. 1990).
Thickness: Varies between 32m (Evers 1967), 48m (Hinsch 1997) in the Forcada Unit and 95m (Evers 1967) and 137m (Leyva et al. 1984) in the Alba syncline.
Lithology: Different authors have divided the Láncara Fm. into either two or three members. The lithologic distribution of the formation is complex, which results in some members missing in different areas. A good overview is given by Barba & Fernández (1990, 1991). Zamarreño (1972) described the following subdivision: (i) lower member composed of dolomites and limestones with birdseye structures; (ii) upper member with glauconitic biomicrites and red nodular limestones. According to Álvaro et al. (2000 b) the contact between both members represents an erosive discontinuity in some areas. Evers (1967) describes three members, dividing the lower member of Zamarreño into well-layered dolomites at the base and fine to coarse-grained limestones on top.
Depositional environment: The lower member was deposited in supratidal (birdseye structures), intertidal (stromatolithes) and subtidal (oolithes) environments. Aramburu et al. (1992) interprets a homoclinal ramp setting. All authors agree with a deeper setting (shallow neritic to bathyal) of the upper member (Oele 1964, Evers 1967, Bosch 1969, Zamarreño 1972, Aramburu et al. 1992, present work) starting with a transgressive glauconite layer. This transgressive surface is well documented in the section west of Barrios de Luna. According to

the definition of Schlager (1981), the Láncara Fm. represents a typical drowned platform. Álvaro et al. (2000 b) give a sequence-stratigraphic interpretation of this formation in the Esla Nappe.

Age: Upper Early Cambrian - Lower Middle Cambrian

Trilobites point to a diachronous age, both for the top and the base of the formation (Sdzuy 1961, Zamareño 1972, Liñán et al. 1993, 2002).

OVILLE FM.

The Oville Fm. was formally introduced by Comte (1937).

Type locality: South of the village Oville (Comte 1937), ITGE Map 104 "Boñar" (Lobato et al. 1984).

Thickness: The thickness increases from north (170m) to south (400m).

Lithology: The Oville Fm. shows a gradual transition from the underlying Láncara Fm. It is composed of trilobite-rich shales and siltstones with an increasing content of sand towards the top of the formation. The white quartz-rich sandstones contain a high percentage of glauconite, which was used to distinguish the Oville Fm. from the overlying Barrios Fm. (Bosch 1969). Aramburu & García Ramos (1993) distinguish three members within this region: (i) Genestosa Mb. (trilobite-rich, greenish shales and siltstones, calcareous nodules); (ii) Adrados Mb. (intercalated shales, siltstones and sandstones, highly bioturbated, coarsening and thickening upwards, abundant ichnofossils); (iii) La Barca Mb. (intercalated sandstones and siltstones, to the top pure, white sandstones).

Depositional environment: Oele (1964) proposed shallow marine conditions and prograding deltaic systems. Gietelink (1973) identified a complex system of interfingering shoreface and beach deposits, as well as tide-dominated, destructive delta systems. Aramburu et al. (1992) proposed a braid to braidplain delta, changing to external platform conditions below the wave-base (Genestosa Mb.) and later to internal platform conditions (Adrados Mb.). The La Barca Mb. corresponds to littoral environments influenced by periodic sheet floods. All deposits had a source area located in the NNE.

Age: Middle Cambrian

Ages of all members are diachronous, indicated by trilobites and palynomorphs (Barrois 1882, Lotze 1961, Sdzuy 1961, 1968, Zamarreño & Julivert 1967, Liñán et al. 1993).

BARRIOS FM.

The Barrios Fm. represents a thick pile of siliciclastic sediments, forming prominent, well visible ridges in the region (Fig. 2.23). The formation was formally defined by Comte (1937).

Type locality: Barrios de Luna (Comte 1937), ITGE Map 102 "Los Barrios de Luna" (Suárez Rodríguez et al. 1990).

Thickness: Thicknesses increase from the western part of the Cantabrian Zone (>700m) to the inner part of the arc (>1000m). In the area of the Cantabrian High the formation may decrease to some tens of meters or disappear completely due to extensive erosion in this area.

Lithology: Transition from the Oville Fm. is gradual, and therefore difficult to localise. Aramburu et al. (1992) distinguishes three members within the Barrios formation: (i) La Matosa Mb. (white quartz-rich sandstones with volcanic intercalations, very common ichnofossils, erosive top); (ii) Ligüeria Mb. (conglomerates and sandstones, only present in the eastern part of the Cantabrian Zone and absent in the research area); (iii) Tanes Mb. (whitish to pinkish quartz-rich sandstones). The Tanes and the La Matosa members are separated by a long-term hiatus in the area of research (Aramburu & García Ramos 1988, Truyols et al. 1990, Aramburu et al. 1992). However, due to the similar facies of the La Matosa and Tanes members, the separating unconformity is not always obvious (see Chapter 4.2 for discussion).

Depositional environment: Present-day outcrops of the Barrios quartz sandstone, widely known as Armorican quartzite, occur in Iberia, Armorican and Bohemian Massifs, Corsica, Turkey and several realms of North and West Africa (Fernández-Suárez et al. 2002 b). The Barrios Fm. has been deposited in a braid to braid-plain delta environment with marine influence on an extensive shallow continental platform (Aramburu & García Ramos 1993). The Tanes Mb. represents fluvial to coastal and shallow marine deposits. Palaeocurrent analysis and facies distribu-

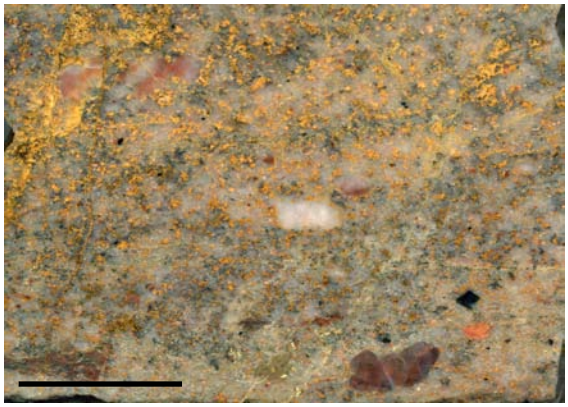

Fig. 2.22. Polished slab of the Herrería Fm. showing a micro-conglomerate composed mostly of well-rounded quartz components. Scale 2cm.

Fig. 2.23. "Embalse de Luna" north of the village Barrios de Luna. The dam wall was built along the course of the Barrios Fm., which forms prominent ridges in the region. The Barrios Fm. consists of quartz-rich, well-sorted sandstones.

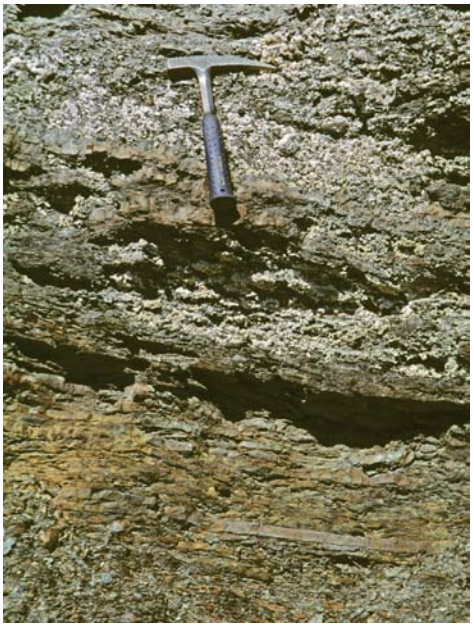

Fig. 2.24. Efflorescence of pyrite-bearing black shales and siltstones (Formigoso Fm.) north of the village Barrios de Luna. Hammer for scale (30cm).

Fig. 2.25. Abundant ripple marks characterise shallow marine sandstones of the San Pedro Fm. in the Bernesga Valley (north of the village La Vid). Hammer for scale (30cm).

Fig. 2.26. Desiccation polygons in the Mb. A of the San Pedro Fm. Coin (2cm) for scale.

Fig. 2.27. Thrust within the San Pedro Fm., displacing shaly to sandy sediments onto massive ironstones. Scale 1m.

tion point to sediment transport from the core of the Ibero-Armorican arc, according to the present coordinate system from north to south.

Age: Middle-Cambrian - earliest Arenig

This formation was mainly dated by *Cruziana* ichnofossils and acritarchs (Aramburu et al. 1992). The base was dated as Middle-Cambrian with some uncertainty as to its isochronity (Julivert & Truyols 1983). The top of the Tanes Mb. is assigned to the uppermost Arenig (Aramburu 1987, Gutierrez Marco & Rodriguez 1987). The Cambrian/Ordovician boundary is situated in a non-continuous succession (Aramburu & García Ramos 1988, Aramburu et al. 1992).

GETINO FM./CAPAS DE GETINO

The sediments of this age were briefly described by several authors, drawing a new lithostratigraphic unit ("transitional beds" of Bosch 1969) or including them in the lower part of the Silurian Formigoso Fm. (Evers 1967 and Vilas Minondo 1971). However, Aramburu (1989) proposed the Getino Fm., comprising sediments between the Barrios and Formigoso formations. Aramburu et al. (1992) preferred to use an informal name, "Capas de Getino."

Type locality: Near the village of Getino (Aramburu 1989); ITGE Map 103 "La Pola de Gordón" (Alonso et al. 1991)

Thickness: The thickness decreases from north to south. 8.9m was measured in the Gayo unit (Evers 1967), 10.5m in the Correcillas unit (Sarmiento et al. 1994) and 79m at the southern branch of the Alba syncline (Aramburu et al. 1992, Gutierrez-Marco et al. 1996).

Lithology: Above the erosive contact with the Barrios Fm. there are brecciated sandstones, glauconitic sandstones and red and green shales. In the Alba syncline (on the road to Portilla de Luna) there are limestones and marls outcropping at the top of the formation (Gutierrez-Marco et al. 1996, this work). Evers (1967) describes a sharp undulating boundary between the Barrios Fm. and the overlaying black shales, proposing a nonconformity marked by the concentration of well-rounded, white quartz pebbles.

Depositional environment: The presence of glauconite, ferruginous sediments and intense bioturbation indicates a marine environment reaching coastal to inner ramp depths. Aramburu (1989) postulates condensed sedimentation with several sedimentary hiati and subaerial exposure towards the top of the formation. According to Gutierrez-Marco et al. (1996) the limestones at the top imply open platform conditions. Investigations for this study support marine conditions of the limestones with no indication of subaerial exposure.

Age: Middle-Ordovician

The age was a subject of controversial discussion by numerous authors. Sarmiento et al. (1994) and Aramburu et al. (1992) suggest a Middle to Late Ordovician age, whereas Aramburu (pers. com. 2003) states that the base of the formation starts in the Llanvirnian. Truyols & Julivert (1983) and Suarez de Centi et al. (1989) documented a huge stratigraphic gap reaching up to the Early Llandovery. Thus the Ordovician/Silurian boundary is located within an important hiatus. Continuous sedimentation from the Ordovician to Devonian took place only in the region of Cabo de Peñas.

FORMIGOSO FM.

Type locality: Formigoso Valley SE of Villamanín de la Tercia (Comte 1937); ITGE Map 103 "La Pola de Gordón" (Alonso et al. 1991)

Thickness: The distribution of thicknesses varies, being high in the northernmost part of the Bernesga Transect (170m, Los Chabanos section in the Appendix), dropping to 84m in the Gayo Unit (north of Getino) and increasing again southward (247m on the southern branch of the Alba syncline).

Lithology: Black to dark grey graptolitic shales (Fig. 2.24) with thin intercalated silt and fine-grained sandstone beds towards the top. The formation shows coarsening and thickening upwards successions, well visible in the Caldas de Luna sections (CL-W, CL-E). The base of the formation is located on top of a large stratigraphic gap, whereas contact with the overlaying San Pedro formations is gradual. Kegel (1929) distinguishes two members: (i) Pizarras del Bernesga (black shales with abundant graptolites) and (ii) Capas de Villasimpliz (black shales/siltstones with intercalated sandstone beds).

Depositional environment: During this time the depositional environment shows open marine to offshore conditions in the lower part, becoming shallower towards the top. Suarez de Centi (1988) and

Barba & Fernández (1991) report the occurrence of hummocky cross-stratification in thicker sandstone beds, revealing depositional conditions between wave and storm wave base to the top of the formation. Shallow water environment with little circulation and a lack of oxygen were proposed as the cause of black shales (Evers 1967). Anoxic conditions prevailing over North Gondwana were probably caused by persisting stratification of seawater (lower cool waters resulting from the melting of ice-sheets). According to Paris & Robardet (1990) these conditions do not necessarily indicate very deep-water environments. Nevertheless, the lower part of the Formigos Fm. is assumed to be sedimented in depths of up to 150m, whereas the upper part has sedimentation depths of less than 80m, being deposited above the storm wave base.

Age: Middle to Late Llandovery

Abundant graptolites were dated by Kegel (1929), Comte (1959), Truyols et al. (1982) and others. Ichnofossils were identified by Suarez de Centi et al. (1989). Further information about Silurian fossils is summed up in Robardet & Gutíerrez-Marco (2002).

SAN PEDRO FM.

Type locality: Near San Pedro de Luna (Comte 1937), ITGE Map 102 "Los Barrios de Luna" (Suárez Rodríguez et al. 1990)

As in the case of the Láncara Fm., the type locality is now drowned in the artificial lake Embalse de Luna. Therefore Evers (1967) used additional sections between Villasimpliz and La Vid in the Bernesga Valley as reference sections, ITGE Map 103 "La Pola de Gordón" (Alonso et al. 1991).

Thickness: The thickness increases from the north (56m in the Millaró section) to the south (162m in the Olleros section).

Lithology: According to Bosch (1969) and Suarez de Centi et al. (1989) first iron-oolithic sandstones mark the border to the underlying Formigoso Fm. The formation was divided into two (Cramer 1964, Rupke 1965, Evers 1967) or three members (Bosch 1969, Staalduinen 1973, Suarez de Centi et al. 1989): (i) Mb. A is composed of thick-bedded, brownish to reddish sandstones intercalated with thick iron-oolithic beds (Fig. 2.27); abundant ripple marks and desiccation polygons (Fig. 2.25 and 2.26); (ii) Mb. B shows variable lithology of bioturbated reddish to greenish silt to sandstones intercalated with dark grey and green shale lenses; (iii) Mb. C displays well-bedded, yellowish to whitish, quartz-sandstones. In the north (Puertos de Pajares and La Cubilla), Bosch (1969) describes the coarsest sandstones with abundant volcanic material. Transition to the Abelgas Fm. is gradual, as visible in the La Vid section (see Appendix).

Depositional environment: Cross-bedded sandstones with ripple-marks (see Fig. 2.25) and sections Millaró, Aralla in the Appendix), mudstone-chips, iron-ooids and abundant ichnofossils are interpreted as deposits of a shallow epicontinental platform, situated near the coast (Evers 1967, Vilas Minondo 1971, Krans 1982, Suarez de Centi et al. 1989, present work). Indicative ichnofossils point to a gradual transition from coastal/shoreface environments to a platform in a more distal position (Suarez de Centi et al. 1989). Sanchez de la Torre et al. (1984) suggest a more open marine environment further to the west. Abundant iron originated from subaerial weathering of basic, volcanic material (Van den Bosch 1969, Suarez de Centi et al. 1989). The iron oxide content of 7.3% is fairly low and the intensive colour in the field is mainly caused by the low fraction ($< 6.3\mu$) of the iron minerals (Führer 1982). The carriers of the colour are hematite, goethite and chamosite. Mb. B displays a deeper depositional environment (lower shoreface) in comparison to Mb. A, whereas Mb. C reaches litoral to upper shoreface depths again. With increasing terrigenous input (Late Silurian and Early Devonian) Robardet & Gutiérrez-Marco (2002) place the depositional area within the inner proximal part of the North Gondwanan shelf in a high energy, storm influenced near-shore environment with a warm and dry climate (García-Alcalde et al. 2002).

Age: Wenlockian - Lochkovian

Some age-indicative ichnofossils were dated by Suarez de Centi et al. (1989). The Silurian/Devonian boundary is situated in the uppermost 25 to 50m of the formation (Truyols et al. 1974, Suarez de Centi et al. 1989, Aramburu et al. 1992) respectively 13 to 15m of the formation (Richardson et al. 2000, 2001). In the La Vid section (Bernesga Valley) the San Pedro Fm. seems to be entirely Silurian (Priewalder 1997). Richardson (2001) reports the

absence of Wenlockian fossils in some sections and the diachronousity of the San Pedro boundaries.

ABELGAS FM. (LA VID GROUP)

Together with the Esla Fm., the Abelgas Fm. forms the La Vid Group (Keller 1988). Formally these formations were designated as members of the La Vid Fm. ("Schistes et calcaires de la Vid" Comte 1937; Brouwer 1964, Evers 1967, Bosch 1969, Vilas Minondo 1971, Staalduinen 1973, García-Alcalde et al. 1979 and Leweke 1983). In recent Spanish literature the La Vid Group is divided in four formations according to Vera de la Puente (1989): Dolomías de Felmín and Calizas de La Pedrosa are the equivalent to the Abelgas Fm. whereas the Pizarras de Valporquero and Calizas de Coladilla are the Esla Fm. equivalent.

Type locality: East of the village La Vid (Comte 1937), ITGE Map 103 "La Pola de Gordón" (Alonso et al. 1991). See Fig. 2.28.

Thickness: 98m (Valporquero section) to 229m (La Pola de Gordón section)

Lithology: The Abelgas Fm. consists of several units and members (see Keller 1988 and Keller & Grötsch 1990 for detail). The denomination of these members however does not follow standard stratigraphic rules, as name-giving localities and type sections have only partly been established. These are therefore partly informal stratigraphic units. The succession is as follows (from base to top):

-Alternating shales, silt/sandstones and greyish to yellowish dolomites and limestones (Transition Unit). The Transition Unit marks the transition from the San Pedro Fm. to the Abelgas Fm., well visible in the La Vid typus locality (see section La Vid in the Appendix; meters 273 to 285 along section).

• Skeletal grainstones and packstones, wackestones, black shales (Lumajo Mb.), does not crop out in any of measured sections.

• Early diagenetic dolomites with microbial mats, mudcracks, ripples, birdseyes, intraformational breccias and gypsum-pseudomorphs (Dolomite Mb.). Crops out e.g. on top of the Transition Unit in section La Vid (Fig. 2.29) or in section Felmin.

• Thin-bedded, dark greyish limestones (mud to packstones) (Wavy Limestone Mb.) cropping out above the Dolomite Mb. in section La Vid (Fig. 2.30) and Felmin.

• Intercalated fossiliferous, argillaceous limestones, marlstones (2.31) and dark shales (Limestone Marlstone Mb.).

• Fossiliferous grain to packstones with shale intercalations (Millaró Limestone Mb.), named after the locality Millaró (see Appendix).

Depending on the position along transect, the Dolomite, Lumajo and Wavy Limestone "members" replace each other. The same accounts for the Limestone Marlstone and the Millaró Limestone "members."

Depositional environment: Vera de la Puente (1989) interprets the succession to represent an epicontinental ramp with conditions ranging from carbonate tidal flats to deep ramp settings. According to Keller & Grötsch (1990) the succession was deposited on an open marine carbonate ramp, extending from coastal sabkha to offshore pelagic environments. Sabkha conditions were characterised by microbial mats, LLH-stromatolites, mudcracks and tepee structures.

Age: Lochkovian - Middle Emsian

Brachiopods were mostly used for dating, as they represent the most abundant fossil group.

ESLA FM. (LA VID GROUP)

The Esla Fm. is composed of the Shale Unit and two intercalated marlstone/limestone members (Sagüera and Villayandre members, Keller 1988). The formation has formally been described as a member of the La Vid Fm. (Evers 1967 and others, see above).

Type locality: East of the village La Vid (Comte 1937), ITGE Map 103 "La Pola de Gordón" (Alonso et al. 1991). See Fig. 2.28.

Thickness: 65m (Genicera section) to 243m (La Vid section)

Lithology: The Shale Unit (middle member, Evers 1967; Pizarras de Valporquero, Vera de la Puente 1989) is composed of greenish-brown shales with several crinoidal limestone lenses to layers (Fig. 2.32). The base and the top are gradual. The Sagüera and Villayandre members are highly fossiliferous with crinoidal grainstones and marls. The top of the Villayandre Mb. (Calizas de Coladilla, Vera de la Puente 1989) is based on the change of colour from pinkish (Esla Fm.) to grey (Santa Lucía Fm.) crinoidal limestones due to the diminishing influence of terrigenous mud.

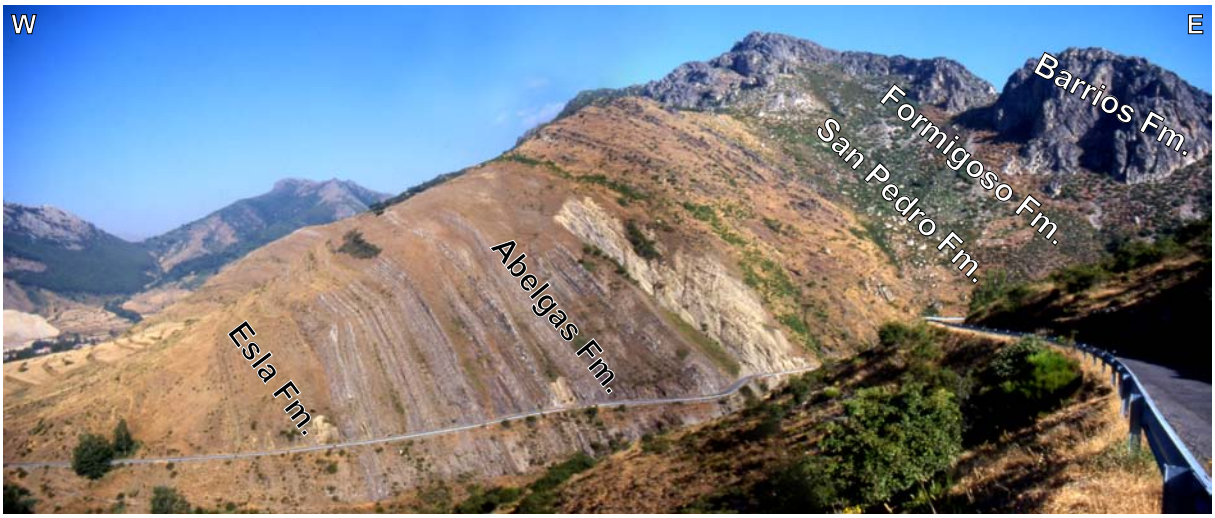

Fig. 2.28. Type locality of the La Vid Group east of the village La Vid. The overturned beds (older formations to the east) of the Abelgas Fm. show a clear cyclicity.

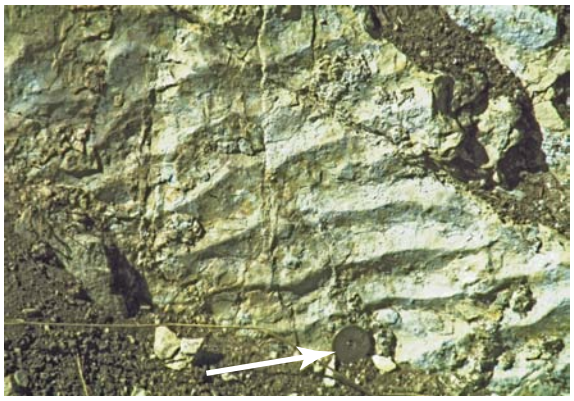

Fig. 2.29. Symmetric wave ripples in the Dolomite Mb. of the Abelgas Fm. west of the village Felmin. Coin (2cm) for scale (arrow).

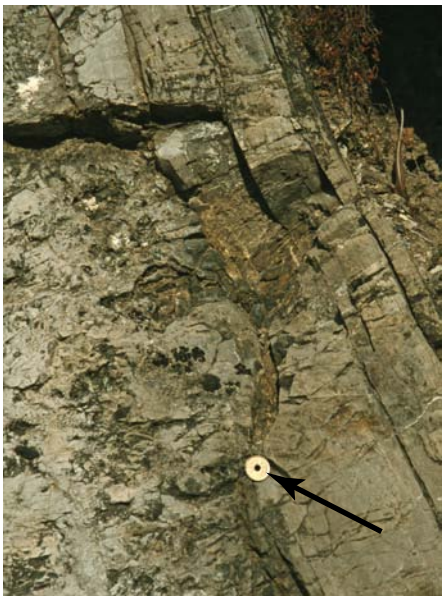

Fig. 2.30. Erosional tempestite-scour in the Abelgas Fm. (La Vid section). Top to the left. Coin (2cm) for scale (arrow).

Fig. 2.31. Thin section from the upper part of the Abelgas Fm. (Limestone Marlstone Mb. in the La Vid section). The packstone to grainstone show a geopetal fabric within a brachiopod shell, partly filled with carbonate mud partly with calcite. Scale 1cm.

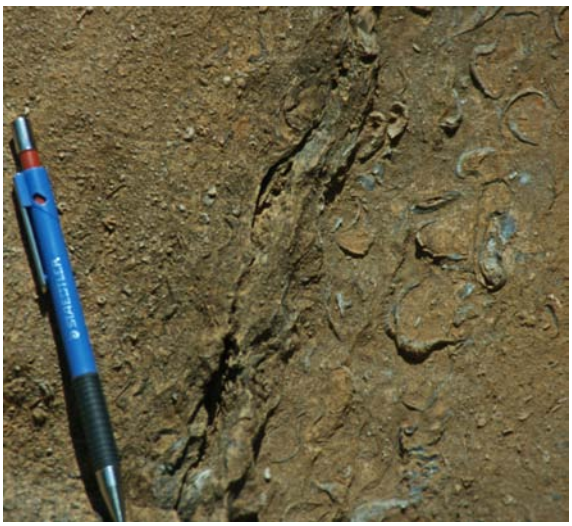

Fig. 2.32. Coquina composed of brachiopods and crinoidal stems, intercalated in the shales of the Esla Fm. (Los Chabanos section). Pencil (15cm) for scale.

Depositional environment: The Shale Unit was deposited below the fair weather wave base, caused by a rapid relative sea-level rise (Keller & Grötsch 1990). According to García-Alcalde et al. (2002) deposition dropped below the storm wave base, located in calm and quiet conditions far from the coast and influenced by hurricanes. According to these authors the grainstone members represent submarine swells. Barba & Fernández (1990) specify a deep ramp, which evolves to shallower conditions with calcarenitic ridges and tidal channels. The ramp was influenced by episodic storms, which produced thick brachiopod coquinas (see Fig. 2.32). The source area for most of the Devonian siliciclastic sediments in this region was the western prolongation of the Cantabro-Ebroian Massif (sensu Carls 1983, 1988), now covered by sediments from the Central Coal Basin, Ponga and Picos de Europa zones (García-Alcalde 2002).
Age: Middle to Late Emsian

SANTA LUCÍA FM.
The Santa Lucía Fm. forms prominent ridges in the area, as it is situated between the less resistant Esla and Huergas formations.
Type locality: Between the villages of Santa Lucía and Vega de Gordón ("Calcaires de Santa Lucía," Comte 1937), ITGE Map 103 "La Pola de Gordón" (Alonso et al. 1991). See Fig. 2.33.
Thickness: 130m (Olleros section) to 280m (Beberino section)
Lithology: The transition from the Esla Fm. is gradual, being indicated only by a change of colour in the crinoidal coarse grainstones (see above). The formation was subdivided into five members by Bosch (1969) or three main facies groups by Coo et al. (1971), Coo (1974) and Méndez Bedía (1976). Three different depositional environments correspond to different depositional areas within the Southern Cantabrian Basin. Next to the Cantabrian High a peritidal lagoon developed (argillaceous, laminated, micritic, pelloidal limestones with mudcracks, birds-eyes and evaporites, Fig. 2.35 and 2.37), followed by a reef belt (massive boundstones built of corals and stromatoporoids, Fig. 2.34 and 2.36) and fore-reef deposits (well-bedded bioclastic limestones, bioturbated marls and reddish bioclastic limestones). The Santa Lucía Fm. is very rich in fossils, comprising stromatoporoids, corals, bryozoans, echinoderms, brachiopods, bivalves etc. (Fig. 2.34 and 2.36). Méndez-Bedia et al. (1994) recorded biostromes composed of branching tabulate coral and associations of different organisms with stromatoporoids, as well as stromatoporoid bioherms. Reef evolution can be described e.g. along the Luna lake outcrops (GPS coordinates N 42°52.158´ and W 005°51.902´), where abundant stromatoporoids consolidate the highly mobile, underlaying crinoidal grainstones, prior to branching tabulate corals can start to develop. The corals completely replace the stromatoporoids upsection, before they appear together towards the top of the reefal edifice.
Depositional environment: The facies arrangement results in the following depositional subdivision: proximal zone with intertidal to supratidal sediments (lagoon-facies); intermediate zone with reefal structures (reef facies) and an external zone on a high-energy open marine platform (fore-reef-facies). Buggisch et al. (1982) distinguishes six facies zones from north to south: (1) lagoon, (2) alternation of lagoon and non-reef sediments, (3) alternation of reef and lagoon, (4) barrier reef zone, (5) reef and non-reef limestones and (6) non-reef sediments. Peritidal facies is situated towards the concavity of the Asturian Arc, while the sublittoral, open marine facies can be found to the W and S of the Cantabrian Zone. Reef development suggests the absence of a continuous reef barrier (see Fig. 2.33) rimming the platform (Méndez-Bedia et al. 1994). However most of the bioherms must have been situated close to the platform margin and developed under different conditions as indicated by different organism associations. At the top of the formation the influence of siliciclastic input becomes evident (Fig. 2.38).
Age: Late Emsian to earliest Eifelian
Stratigraphic gaps, based on the occurrence of assumed palaeokarst features on top of the Santa Lucía Fm. near Sagüera (southern limb of the Alba syncline) and cited by Buggisch et al. (1982), are placed in doubt by the present author (see Chapter 4 for discussion) and García-Alcalde et al. (2002). García-Alcalde (1995, 1996) and García-Alcalde et al. (2000, 2002) summarised data pertaining to biostratigraphically useful fossils in the Cantabrian Zone.

Fig. 2.33. Type locality of the Santa Lucía Fm. east of the village Santa Lucía. Note the massive reefal edifice to the left (arrow). The street to the right marks the transition with the shaly Huergas Fm.

Fig. 2.34. Abundant silicified corals of the Santa Lucía Fm. in the lower part of the Beberino section. Scale 20cm.

Fig. 2.35. Desiccation cracks are an abundant feature in the lagoonal deposits of the Santa Lucía Fm. (Valporquero section, see Appendix). Scale 20cm.

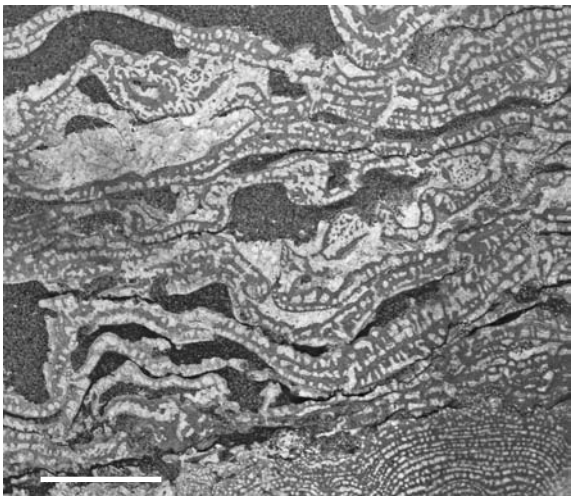

Fig. 2.36. Thin section of a stromatoporoid boundstone of the Santa Lucía Fm. (section Santa Lucía). The position of the sample is at metre 256 along section (see Appendix). Scale 1cm.

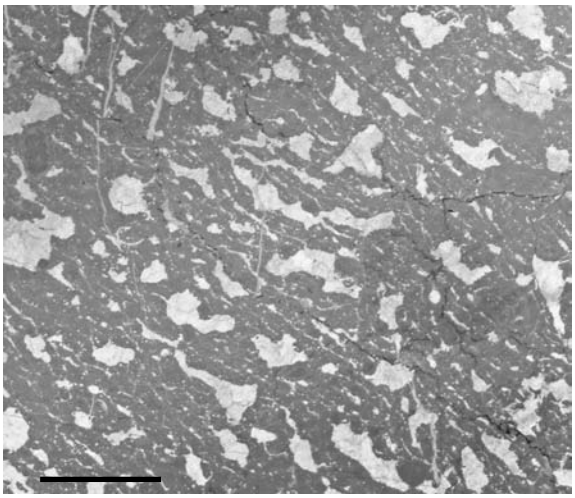

Fig. 2.37. Thin section of a mudstone with abundant birds-eye structures from the lagoonal section of the Santa Lucía Fm. near Valporquero. The position of the sample is at metre 176 along section (see Appendix). Scale 1cm.

HUERGAS FM.

The Huergas Fm. is usually covered by vegetation, forming wide valleys between the calcareous, competent Santa Lucía and Portilla formations.

Type locality: Near the village Huergas de Gordón ("Areniscas y Pizarras de Huergas," Comte 1959), ITGE Map 103 "La Pola de Gordón" (Alonso et al. 1991).

Thickness: 31m (Valporquero section) to 300m (Huergas section)

Lithology: Lithology is highly variable in the region, comprising highly bioturbated greyish to greenish shales and siltstones interbedded with greenish to brownish sandstones. In some outcrops (section Bebberino, see Appendix), the middle part of the formation contains higher proportions of coarser, sandy material whereas the lower and the upper parts are shale dominated. According to García Ramos (1978) the succession is composed of several fining and coarsening upward sequences with frequent cross-stratification and ichnofossils. Evers (1967) distinguishes three members that contain ferruginous sandstones in the lower part of the formation.

Depositional environment: In section Beberino and Huergas, the Huergas Fm. overlies the Santa Lucía Fm. with a clear drowning unconformity. García-Ramos (1978) depicts a platform setting with the provenance of siliciclastic material from NE. The platform was affected by currents and waves, which created numerous coarse-grained shoals with fine sediment accumulated in between. The sediments show strong bioturbation, pointing to a well-oxygenated sea floor. The platform was also influenced by tempestites. Reijers (1973) assumes prodelta and delta slope environments. García-Alcalde (2002) interprets the variety of depositional environments as marine and transitional settings linked to large south-sloping deltas.

Age: Early Eifelian - Early Givetian

Due to the unsuitable facies development for conodonts (García-Alcalde et al. 2000), the conodonts of the overlaying Portilla Fm. were used to determine the upper boundary of the Huergas Fm. García-Alcalde & Soto (1999) found evidence of the Kacák-*otomari* Event (global transgressive event at the top of the Eifelian with important faunal changes in the pelagic realm) in the centre of the Huergas Fm.

PORTILLA FM.

The Portilla Fm. records the return to reefal conditions in the Cantabrian Zone.

Type locality: Right bank of the Arroyo de la Portilla NW of Matallana-Estación (Comte 1936), ITGE Map 103 "La Pola de Gordón" (Alonso et al. 1991)

Thickness: 58m (Huergas section) to 90m (Beberino section)

Lithology: The formation is morphologically subdivided into two resistant limestone members, separated by a less resistant middle member, not present in every outcrop (Fig. 2.39 and 4.1). The latter is composed of sandy limestones to calcareous sandstones, containing well-developed ooidal grainstones in some sections (see Fig. 2.40 and 2.42). Numerous authors split the formation into three (Comte 1936, Mohanti 1972, Raven 1983, Fernández et al. 1997) or four members (Bosch 1969, Reijers 1972, 1973, Reijers & Ten Have 1983). Evidence from this study supports the subdivision into three members: (i) lower member (crinoidal and bryozoan, argillaceous grainstones, gradual base, to the top development of biostromes); (ii) middle member (sandstones, shales, detritic limestones, oolith, in some outcrops erosive base) and (iii) upper member (thick-bedded biostromal and biohermal limestones alternating with crinoidal-bryozoan grainstones or siliciclastics; Fig. 2.43). Méndez-Bedia et al. (1994) characterise biostromes of branching tabulate corals, which can be associated with other organisms and different stromatoporoid, alveolitid and phillipsastreid biostromes and bioherms (Fig. 4.1). In the Mirantes de Luna section red bands of cross-bedded *Thamnopora* grainstones reach thicknesses up to 11m (Fig. 2.41).

Depositional environment: Reijers (1972, 1985) classifies a reef-rimmed platform geometry, composed of (i) lagoonal backreef facies belt; (ii) reef tract with bistromal and biohermal limestones and (iii) fore-reef facies belt distally grading to deeper-water marls and shales. This general model assuming a reef barrier rimming a platform with back-reef facies and fore-reef facies has found broad agreement (Reijers 1972, 1984, 1985, Mohanti 1973, Reijers et al. 1984, Frankenfeld 1981, Raven 1983). By contrast, Méndez-Bedia et al. (1994) and Fernández et al. (1997) introduced a different model based on (i) small isolated bioherms which did not

Fig. 2.38. Thin section of a crinoidal grainstone at the top of the Santa Lucía Fm. (metre 311 in section Santa Lucía). The onset of terrigenous sedimentation is marked by the orange colour of the grainstone. Scale 1cm.

Fig. 2.39. Section of the Portilla Fm. north of the village of La Pola de Gordón. The three members are clearly visible, with a sandy middle member (separated by dotted lines). See Fig. 2.40 for detail indicated by the arrow.

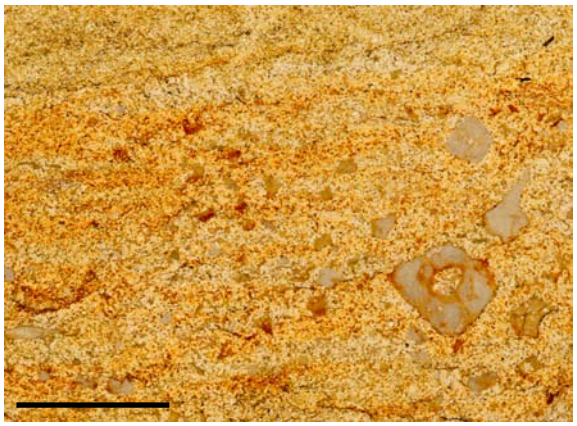

Fig. 2.40. Thin section of the middle Portilla member composed of fine sandstones with crinoidal debris. The location of this sample is marked by an arrow in Fig. 2.39. Scale 1cm.

Fig. 2.41. Highly fossiliferous limestones of the Portilla Fm. south of Mirantes de Luna. Intervals of up to 11m in thickness are composed of fragments of stromatoporoids and *Thamnopora* corals. Hammer for scale.

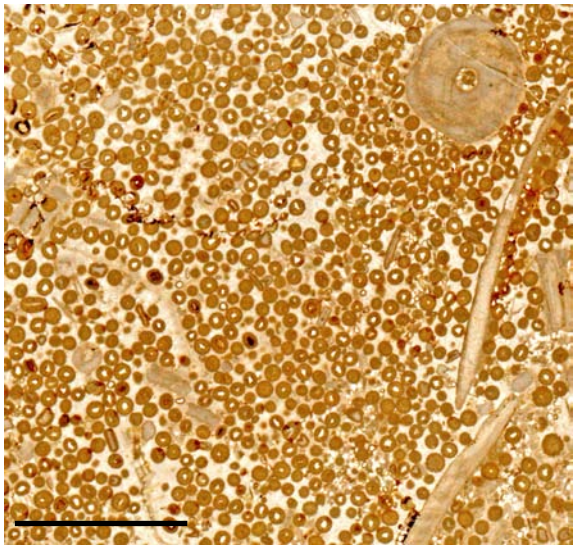

Fig. 2.42. Thin section of the middle Portilla member composed of ooidal grainstone with bioclastic components (west of Mallo de Luna). Scale 1cm.

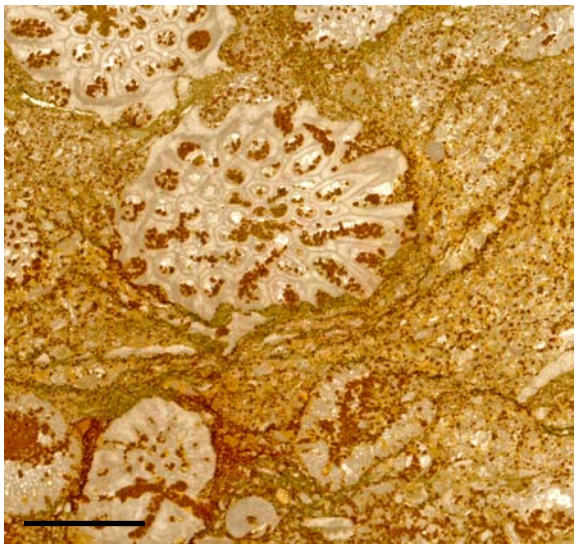

Fig. 2.43. Thin section of the lower Portilla Fm. in its type section (south of Matallana de Torio), showing the high siliciclastic content of the limestones. Scale 1cm.

form a continuous reef barrier, (ii) rare occurrence of a complete reef development succession, (iii) no widespread occurrence of sheltered back-reef facies. According to these authors, the Portilla Fm. was deposited in a shallow-water, lagoon to shelf environment on a carbonate ramp, where small isolated bioherms were able to develop on tectonic (?) highs within the inner ramp setting. Nevertheless the facies associations are very similar to that of the Santa Lucía Fm. Present investigations and modelling results show a close connection of reefal development towards the Intra-Asturo-Leonesian Facies Line (see Chapter 8.3). This fact was also partly visible during the development of the Santa Lucía Fm. (see Chapter 7 for further details).

Age: Middle to Late Givetian

NOCEDO FM.

Due to the similarities of Late Devonian siliciclastic and the difficulties of establishing formation boundaries, Julivert et al. (1968) introduced the expression "Areniscas del Devónico Superior" to denote the amalgamation of the Nocedo, Fueyo and Ermita formations. However this "unification" was, proposed by a structural geologist; in terms of sedimentology, these clastic units should be separated. The Nocedo Fm. occurs only in the southern part of the Southern Cantabrian Basin.

Type locality: Near the village Nocedo ("Grès de Nocedo", Comte 1959), ITGE Map 103 "La Pola de Gordón" (Alonso et al. 1991)

Thickness: 45m (La Pola de Gordón section) to 428m (Huergas section). The striking difference in thickness within a very short distance was interpreted in terms of a syn-sedimentary normal fault (Intra-Asturo-Leonese Facies Line sensu Raven 1983, See Fig. 3.5 and Chapter 8.3).

Lithology: Uniform sandstones and siltstones dominate the succession, interrupted by several biostromal horizons in some areas (Valdoré and Crémenes limestones). Loevezijn (1983) and Loevezijn & Raven (1983) subdivided the formation into two members.

Lower member (Gordón Mb.; Mb. A): bioturbated shales/siltstones passing into well-sorted quartzsandstones coarsening upward, cross-bedded, reddish crinoidal grainstones (Fig.2.44) with numerous hardgrounds marked by haematitic crusts and abundant brachiopods. Herringbone cross-stratification is common at the top of the Gordón Mb. (Fig. 2.45) and section Huergas in the appendix: meters 208.4 to 212.9 along section).

Upper member (Millar Mb.; Mb. B): occurs only south of the IALF; coarsening upward, shales and siltstones with intercalated conglomerates at the top. These conglomerates are composed of exotic clasts (pegmatites, radiolarites, metamorphic quartzites) of unknown origin (see discussion in Chapter 2.2.1 and Fig. 2.46).

Depositional environment: The formation is deposited in two regressive cycles, representing the two members of the formation. Depending on the position along the transect, the depositional environment comprises middle to outer shelf areas, nearshore coastal settings influenced by strong, longshore drift and protected lagoon areas (Loevezijn & Raven 1983). The uniform, well-sorted sandstones of the lower part of the succession point to a upper shoreface deposition above fair weather wave base. During times of limited sand supply, limestone deposition created carbonate platforms, which were killed by a renewed siliciclastic pulse. Large-scale current ripples indicate transport directions towards SW (210°-240°). The uppermost carbonate part of the Gordón Mb. represents a condensed succession with numerous hiati marked by common hardgrounds.

Age: Frasnian, based on conodont data (García Alcalde et al. 1979, Raven 1983, Loevezijn 1986, 1988).

FUEYO FM.

The Fueyo Fm. was included in the Nocedo Fm. by numerous authors (Evers 1967, Bosch 1969, Loevezijn & Raven 1983). However, Vilas Minondo (1971) and Raven (1983) suggested separating the Fueyo and the Nocedo formations because of a hiatus between them. As in the case of the Millar Mb. of the Nocedo Fm., the Fueyo Fm was deposited only south of the IALF.

Type locality: Near the village of Nocedo, ("Schistes de Fueyo", Comte 1959) ITGE Map 103 "La Pola de Gordón" (Alonso et al. 1991).

Thickness: 108m (Huergas section) to 180m (Olleros section)

Lithology: Dark, nodular shales alternating with

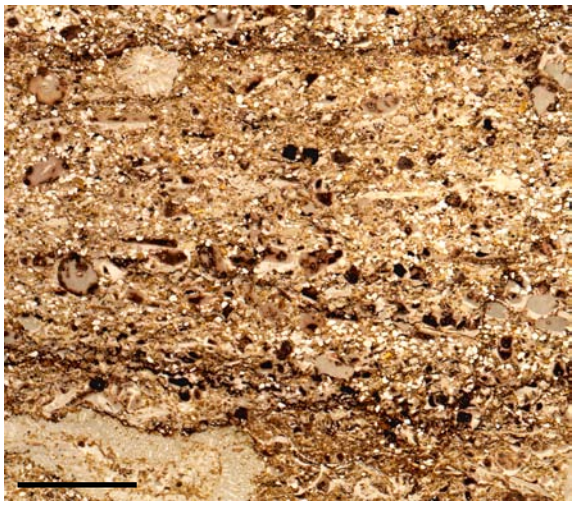

Fig. 2.44. Thin section of the Nocedo Fm. (uppermost Gordón Mb.) in the Huergas section (metre 200.5) showing thick deposits of sandy bioclastic grainstones. Scale 1cm.

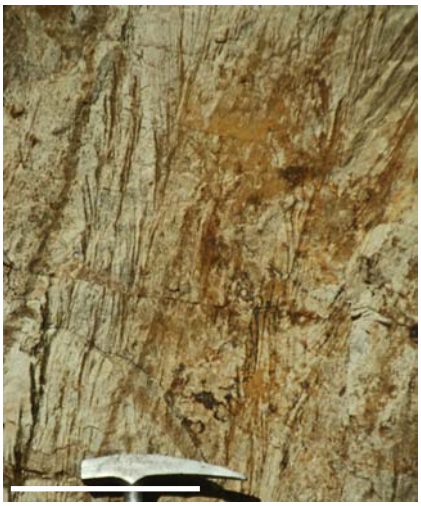

Fig. 2.45. The top of the Gordón Mb. (Nocedo Fm.) is composed of quartz sandstones with abundant herringbone cross-stratification. Scale 20cm .

Fig. 2.46. The top of the Millar Mb. (Nocedo Fm.) shows conglomerates composed of exotic clasts and unknown origin. Coin (2cm, arrow) for scale. Location near Santiago de las Villas.

Fig. 2.47. Dark shales alternating with well-sorted siltstones characterise the Fueyo Fm. (north of Piedrasecha). Hammer for scale (30cm).

Fig. 2.48. The Ermita Fm. south of Llomberas displays large-scale cross-bedded sandstones (top left). The outcrop is approx. 10m high.

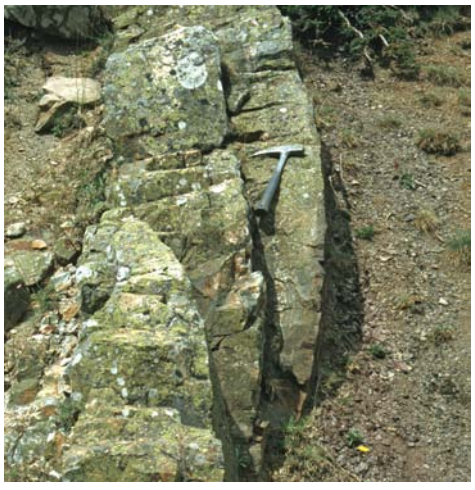

Fig. 2.49. In the Millaró section (metre 231) the Ermita sandstone cuts into the shales of the Esla Fm. and forms multiple crosscutting channels. Hammer for scale (30cm).

well-sorted siltstones and fine-grained sandstones, sandstone channels. Bed thickness varies between several tens of cm and less than one cm and shows abundant fining upward beds (see Fig 2.47 and section Piedrasecha in the appendix). Raven (1983) describes Bouma sequences with units A, C, D and E. Flaser and lenticular bedding is common.

Depositional environment: Barba & Fernández (1990) and García-Ramos & Colmenero (1981) interpret a transgressive setting with the deposition of proximal turbidites and sediments of an external platform/deeper shelf. Slumping structures indicate the presence of a palaeo-slope. García Alcalde et al. (2002) prefer the idea of a sublittoral, open marine platform, formed at the distal part of a deltaic system. In the present work a regression cycle was interpreted, beginning with the Fueyo Fm. and reaching into the lower part of the overlaying Ermita Fm.

Age: Earliest Famennian to Late Famennian based on conodont data (Raven 1983).

ERMITA FM.

Type locality: Near Ermita del Buen Suceso south of Huergas de Gordón ("Grès de l´Ermitage," Comte 1959), ITGE Map 103 "La Pola de Gordón" (Alonso et al. 1991). The name Ermita Fm. was formally introduced by Sjerp (1967). Adrichem Boogaert (1967) proposed a new type section near Camplongo in the northern part of the Bernesga Valley. Brouwer (1962, 1967) introduced the name Aguasalio Fm. for regions where no boundary between Nocedo and Ermita formations can be determined.

Thickness: 3m (Valporquero section) to 65m (Piedrasecha section)

In the southern part of the basin some authors (Bosch 1969, Loevezijn 1983, 1986, Raven 1983) describe a succession composed of badly sorted argillaceous siltstones and sandstones of several tens to a few hundreds of meters in thickness. These authors also record a large erosional hiatus spanning almost the entire Famennian. However, according to García-Alcalde et al. (2000, pers.com. 2003) this hiatus comprises only 1-3Ma. In the present work the greatest thicknesses of the Ermita Fm. are measured south of the IALF (up to 65m). The underlying shales and siltstones are assigned to the Fueyo Fm. North of the IALF the Ermita Fm. is represented as a relatively thin transgressive sandstone unit, several meters thick (see Chapter 4 for discussion).

Lithology: South of the IALF the lower Ermita Fm. is composed mainly of siltstones with some intercalated sandstone beds. North of the IALF only the upper part of the formation is present, which contains well-sorted, medium grained quartz sandstones, polymict conglomerates (Fig. 2.50), thin intercalations of shales and silts, large-scale cross-stratification (Fig. 2.48, section Llomberas in the appendix) and erosive channels (Fig. 2.49, section Millaró in the appendix). In some sections (e.g. Los Chabanos) there are abundant brachiopod moulds in fine-grained sandstones at the top of the succession (Fig. 2.51). In the uppermost part, black mud pebbles are common. To the north the Ermita Fm. rests on progressively older sediments. In the northernmost sections it unconformably overlies the Cambrian Oville Fm. The angle of the unconformity was calculated by Smith (1966) and Raven (1983) showing values of 0.5° to 1.5°. There is also evidence of small-scale intra-formational erosion indicated by fragments of the Vegamián Fm. within the Ermita sandstones (Raven 1983).

Depositional environment: As already discussed, the lower part of the Ermita Fm. was deposited only south of the IALF in continuity of the coarsening upward regression cycle, which started in the Fueyo Fm. (see Chapter 4 for further discussion). The transgressive upper part can be attributed to a high-energy, shallow-water, littoral environment, where siliciclastic sediments were reworked and sorted. Intertidal deposits in the proximal zones in the north pass in shoreface sediments further to the south. The upper part can be subdivided into a lower cross-bedded unit without fossils and an upper unit with abundant brachiopod moulds (see above). The latter represents a marine transgression, which reworked the underlaying strata. Uplift during the initiation of the Variscan Orogeny in the Cantabrian Zone combined with a marked global Early Famennian sea-level fall, resulted in the emergence and peneplanation of the marine platform. According to García-Alcalde et al. (2002) the eroded platform tilted slightly eastward in the Late Famennian, allowing the Ermita Fm. to prograde over increasingly older strata. Thus the base of the Ermita Fm. is slightly diachronous.

Age: Latest Famennian to Early Tournaisian based on brachiopod data (García Alcalde et al. 1979).

BALEAS FM.

The Baleas and the Vegamián formations are highly variable in the region. They replace each other, but also occur together. The Baleas Fm. has often been included in the Ermita Fm. (Evers 1967, Bosch 1969, Raven 1983, Loevezijn 1986).

Type locality: Baleas quarry north of La Pola de Gordón (Wagner 1971), ITGE Map 103 "La Pola de Gordón" (Alonso et al. 1991).

Thickness: 8m (Rocalo section) to 10.5m (La Pola de Gordón section)

Lithology: Whitish to reddish, coarse, crinoidal grainstones with wavy bedding, current ripples and stylolithes. Abundant hardgrounds are often enriched in haematite and indicate condensation (section Beberino in the appendix). Fossil-rich packstones and wackestones are less common and contain crinoids, bryozoans and brachiopods. Few clastic intercalations can be found.

Depositional environment: Shallow water environment above the fair weather wave base. Sanchez de la Torre et al. (1983) noted a low productivity carbonate platform model with abundant high-energy bars and shoals (Baleas Fm.) and deeper, protected areas. The latter represent the depositional environment of the black shales corresponding to the Vegamián Fm.

Age: Early to Middle Tournaisian based on conodonts (Higgins et al. 1964, Adrichem Boogaert 1967, Truyols et al. 1982, Raven 1983, Sanz-López et al. 1998). In some outcrops the base of the Baleas Fm. is situated at the Famennian/Tournaisian boundary (Baleas type section, García-Alcalde & Menéndez Alvarez 1988, Sánchez de Posada et al. 1990).

VEGAMIÁN FM.

Type locality: Comte (1959) introduced this name (Couches de Vegamián). Ginkel (1965) chose the type locality 1km SW of the village Vegamián north of the village Boñar. The Vegamián and the type locality are now drowned in the artificial lake Embalse de Porma. Therefore Evers (1967) designated a new stratotype near the Mirador de Vegamián (Fig. 2.52), ITGE Map 104 "Boñar" (Lobato et al. 1984).

Thickness: 1m (Canseco section) to 10m (Porma section)

Lithology: Black, poorly fossiliferous shales with abundant phosphate, manganese, markasite and chert nodules and radiolarites. Thin siltstone and argillaceous sandstone intercalations, greenish glauconitic shales as well as limestone lenses are common. Basal contact is sharp, possibly erosive whereas the contact with the overlaying Alba Fm. is mostly gradual.

Depositional environment: Adrichem Boogaert (1967) estimated the depositional depth to be approx. 50m, whereas Raven (1983) estimates higher water depths of around 70m. The authors attribute the low oxygen content to restricted water circulation in a depositional environment with low sedimentation rates below the wave base. Poor faunal content in the black shales and the phosphatic nodules point to O_2-depleted, quiet water, associated with an upwelling scenario (Balthasar 2001). Martinez Chacon & Winkler Prins (1993) propose that this is a result of deposition below wave base, whereas Sánchez de la Torre et al. (1983) assume deposition in deeper water on the shelf edge. However, they mention the lack of genuine deep-water fauna, pointing to the possibility of deposition in quite shallow water (mud flats). According to Seibert (1986), the onset of black shale deposition is coupled with subsidence and a eustatic sea-level rise of second order, shifting the deposition of shales to the upper slope regions. The author interprets the facies to represent 50-200m depositional depth.

Age: Middle to Late Tournaisian (Martinez Chacon & Winkler Prins 1993). Higgins (1964), Adrichem Boogaert (1967) and Sánchez de Posada et al. (1990) report Early Visean age for the top of the formation. According to Seibert (1986), the base and top of the formation are diachronous.

ALBA/GENICERA FM.

This formation has been the subject of extensive investigation, as it represents an easily recognisable and laterally uniform marker in the Cantabrian Zone.

Type locality: South of Puente de Alba village in the lower Bernesga Valle ("Griotte de Puente de Alba," Comte 1959), ITGE Map 103 "La Pola de Gordón" (Alonso et al. 1991). The formation was described

by Barrois as early as 1882 ("Mármol Griotte") and named by Ginkel (1965) as Alba Fm. Wagner et al. (1971) renamed the formation Genicera Fm. with a new type locality near the village of Genicera (ITGE Map 104 "Boñar", Lobato et al. (1984)), stating the incompleteness of the original type section. However, this work uses the name Alba Fm., as this was the first formation name to be established.

Thickness: 28m (Huergas section) to 46m (Piedrasecha section)

Lithology: Predominantly red, nodular limestones with frequent stylolithes crop out throughout the Asturian Arc (Fig. 2.53 and 2.54). Wagner et al. (1971) Sanchez de la Torre et al. (1983) and Balthasar (2001) distinguish three members: (i) Gorgera Mb.: reddish shales with intercalated limestone concretions, reddish nodular limestones, bioclastic wackestones/mudstones; (ii) Lavandera Mb.: reddish to greenish, cherty, shales, radiolarites and (iii) Canalón Mb.: well-bedded, reddish, greyish wavy nodular limestones (Fig. 2.55), mudstones to bioclastic wackestones (Fig. 2.58), thin interbedded reddish to greenish shales. Winkler Prins (1968) divided the formation into the Gete, Valdehuesa and La Venta members, whereas Seibert (1986) established a subdivision in five members (A - E). In the Alba syncline the Alba Fm. is overlain by terrigenous sediments of the Olleros Fm. The gradual transition (ca. 20m in the Alba syncline), composed of reddish and greenish shales and marls has been described as "Capas de Olaja" by Wagner et al. (1971), "Entomozoen Schiefer" by Becker et al. (1975) or "Mb. E" of the Alba Fm. by Seibert (1986).

Depositional environment: The Alba Fm. is interpreted as a condensed unit deposited in several hundred metres of water (Sánchez de la Torre et al. 1983, Wendt & Aigner 1985) on a relatively well-oxygenated pelagic platform (Fig. 2.57) with gentle slopes (2.59). During the deposition of the Alba Fm. no significant terrigenous influx occurred in the region. Hemleben & Reuther (1980) suggest that deposition took place during times of tectonic quiescence (Fig. 2.56). The deposits indicate minimal sedimentation rates with only pelagic sedimentation in the Lavandera Mb. and highly condensed sedimentation in the Canalón Mb. Seibert (1986) and Balthasar (2001) note four facies-associations based on sedimentological and faunal differences based on the palaeogeographical position within the basin: (i) swell facies (Agausalio facies), (ii) slope facies (Genicera facies), (iii) basinal facies (Redilluera facies) and (iv) steeper fore-slope facies (Cardaño facies). High faunal diversity at the base of the Alba Fm. points to a rapid transgressive succession causing a transition to stable, oxic conditions also in the formerly euxinic basinal regions (Seibert 1986). The uppermost members are marked by carbonate debris flows and olistostromes (Mb. D) and the transition from oxic to anoxic conditions (Mb. E). In section Piedrasecha (see Appendix) large slumps were observed (Fig. 2.59).

Bathymetry was interpreted by numerous authors (Winkler-Prins 1968, Bosch 1969, Hemleben & Reuther 1980, Raven 1983, Sanchez de la Torre et al. 1983, Seibert 1986, Balthasar 2001 and others). Seibert (1986) identifies shallow shelf (20-60m for the basal member) to basinal open marine environments (100-300m). Faunal indicators point to depths of between 50m and 500m (see Seibert 1986 for details). Balthasar (2001) interprets the Gorgera Mb. as deeper neritic and the Canalón Mb. as upper bathyal, with deposition depths of 300-500m. Parts of the fauna reflect aphotic, cold and dysoxic conditions. The Alba Fm. reflects maximum transgression during the Visean (Colmenero et al. 2002).

Age: Latest Tournaisian to Late Serpukhovian based on conodont, goniatite, trilobite and radiolarite data. The base is highly diachronous (Late Tournaisian to Early Visean) with age decreasing towards deeper depositional areas (Balthasar 2001).

BARCALIENTE FM.

In earlier studies the Barcaliente and the Valdeteja Formations were integrated to the Caliza de Montaña Fm. (Comte 1959, Evers 1967 and others).

Type locality: Arroyo de Barcaliente in the Curueño Valley (Wagner et al. 1971), ITGE Map 104 "Boñar" (Lobato et al. 1984).

Thickness: 180m (Canseco section) to 394m (Carbonera section)

Lithology: The lower part commences with graded, allodapic limestones with slumping structures and chert. Various facies are present towards the top: (i) fine-grained, laminated to well-bedded (Fig. 2.60), dark, bituminous limestones (mudstones, wackestones), (ii) grey, highly bioturbated lime-

Fig. 2.50. In the north of the Bernesga Transect (Millaró section) the base of the Ermita Fm. is composed of iron-rich, polymict conglomerates, indicating a fluvial origin. Scale 5cm.

Fig. 2.51. To the top of the Ermita Fm. well-sorted sandstones with abundant brachiopod moulds indicate a marine transgression. Scale 5cm.

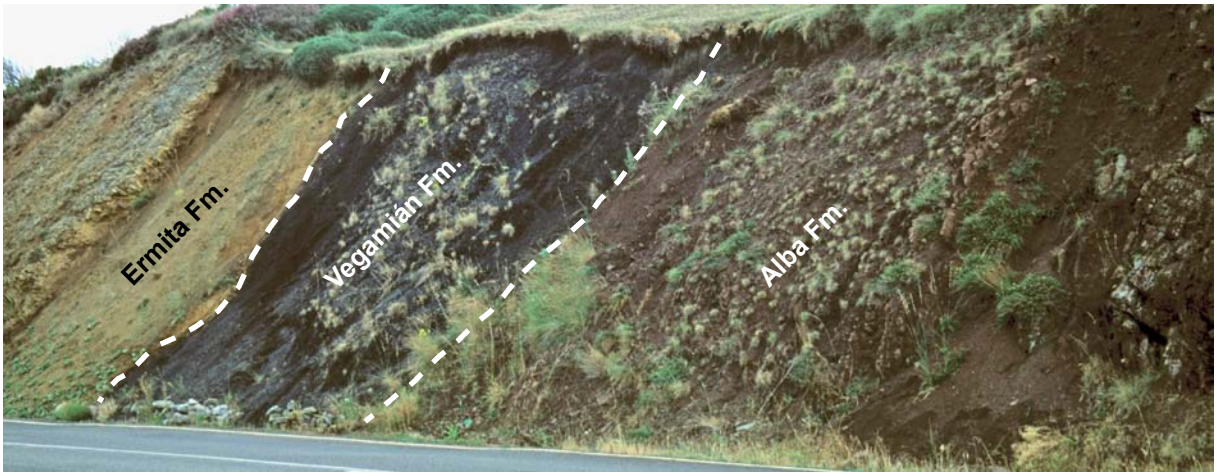

Fig. 2.52. The new stratotype of the Vegamián Fm. at the Mirador de Vegamián (Porma Lake) with the outcropping Ermita, Vegamián and Alba formations.

Fig. 2.53. Nodular limestones of the Alba Fm. in the section Los Chabanos in the north of the Bernesga Valley. The reddish limestones represent a good marker throughout the Cantabrian Zone. Hammer for scale (30cm).

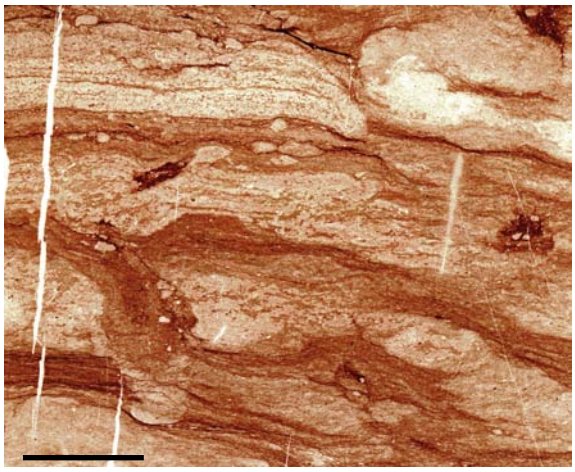

Fig. 2.54. Thin section of the Alba Fm. (Canseco section) with carbonate-rich nodules surrounded by dark red clay-streaks. Scale 1cm.

stones and (iii) limestones with pseudomorphs of anhydrite and gypsum (González Lastra 1978, Hemleben & Reuther 1980, Sánchez de la Torre et al. 1983). The top of the formation shows a poorly sorted, polymict breccia (Porma Breccia, Reuther 1977, Fig. 2.61). Fossil content is generally very low. An epigenetic dolomitisation is common (Gasparrini et al. 2003).

Depositional environment: Hemleben & Reuther (1980) interpret a shallowing upward succession with deposition of distal turbidites in the lower part and shallow marine carbonates towards the top. Where present, ichnofossils indicate anoxic conditions only in deeper parts of the sediment. The palaeobathymetry of the allodapic limestones is assumed to be 100-300m (Hemleben & Reuther 1980). The upper part of the formation was deposited under shallow marine, low-energy conditions marked by small channels, unconformities, stromatolithes and intense bioturbation (Hemleben & Reuther 1980, Balthasar 2001). In contrast, Gonzales Lastra (1978) and Sánchez de la Torre et al. (1983) suggest a shallow marine carbonate platform with low subsidence rates, high evaporation and restricted circulation, which impeded the development of life. The Porma Breccia (Fig. 2.61) is believed to have originated as a result of strong earthquakes on top of the filled basin (Hemleben & Reuther 1980), or by mass flows and/or collapse due to the dissolution of evaporites (Eichmüller 1986, Colmenero et al. 1988). Eichmüller & Seibert (1984) established a model of a stable shallow marine/lagoonal carbonates in the north, bordering to the south and west to a ramp with allodapic limestones and finally deeper marine shaly deposits (Capas de Olaja). Wagner & Winkler Prins (1999) describe a marked surface of subaerial exposure and karstification to the top of the formation.

Age: Late Serpukhovian to Earliest Bashkirian

OLLEROS FM.

The Olleros Fm. crops out in the south of the Bernesga Transect (Alba syncline). The terminology surrounding this formation was a matter of debate, as it represents a very heterogeneous sediment succession. It has been described as "Facies Culm" (Sitter 1962, Rupke 1965), "Facies Flysch" (Evers 1967) or the basal member of the Cuevas Fm. (Boschma & Staalduinen 1969, Staalduinen 1973).

Type locality: Arroyo de San Martín near the village Olleros de Alba (Wagner et al. 1971), ITGE Map 129 "La Robla" (Matas & Rodríguez Fernández 1984).

Thickness: Only minimum thickness can be calculated, as the top is always eroded. According to Wagner et al. (1971) 740m for the whole succession above the Alba Fm. Sanchez de la Torre et al. (1983) calculated 518m for the lower turbiditic member.

Lithology: Sanchez de la Torre et al. (1983) distinguish three members: (i) alternating shale and sandstone beds with some intercalated micro-conglomerate beds, siderite nodules, Bouma sequences Tc-e and Tb-e, to the top highly bioturbated and brecciated; (ii) black, highly deformed limestone lenses and thick beds variable in thickness and occurrence crop out in the middle part. The facies is very similar to the Barcaliente Fm. described above, and (iii) shales and conglomerates, pebbly mudstones, intercalated black limestones and sandstones with Bouma sequences Tc-e and Tb-e.

Depositional environment: According to Sanchez de la Torre et al. (1983) and Colmenero et al. (2002) this formation records the onset of terrigenous supply derived from an elevated area in the SW to S, in the opposite direction to the Devonian transport direction. In contrast to the shallow marine carbonate platform (Barcaliente Fm.), the Olleros Fm. represents foredeep deposits of turbiditic origin (Fig. 2.62). The intercalated thick limestones were referred to as Barcaliente Fm. (Wagner et al. 1971) and interpreted by Sanchez de la Torre et al. (1983) as deeper marine, low-energy deposits with debrisflows on top (breccias), situated between thick turbiditic deposits. The occurrence of sandy beds in the shales indicates an increase of depositional energy and sedimentation rates.

In the Pedroso syncline, turbiditic sediments (106m) with the same lithologic appearance and provenance as the Olleros Fm. appear on the top of the Barcaliente Fm.

Age: Late Serpukhovian to earliest Bashkirian; the Olleros Fm. is time equivalent to the Barcaliente Fm. and the lower part of the Valdeteja Fm. (Colmenero et al. 2002).

Fig. 2.55. Polished slab of the Alba Fm. (Rocalo section). This figure demonstrates that the carbonate-rich nodules occur both isolated and in layers with nodular surfaces. Scale 10cm.

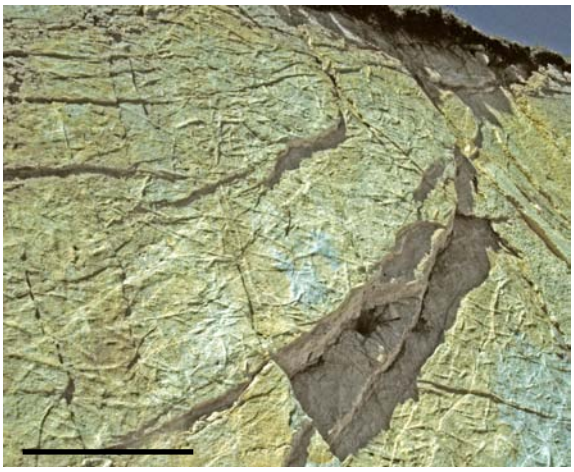

Fig. 2.57. Well-oxygenated substrate conditions in the upper Alba Fm. is marked by intense bioturbation in the Los Chabanos section. Scale 1m.

Fig. 2.59. In the southern part of the Bernesga Transect (Piedrasecha section) large slump folds are developed on top of the Alba Fm. indicating a palaeogradient of the depositional surface. Hammer for scale (30cm).

Fig. 2.56. Bedding plane of the Alba Fm. covered with articulated crinoid stems up to one metre long, (SE of Genicera). Scale 40cm.

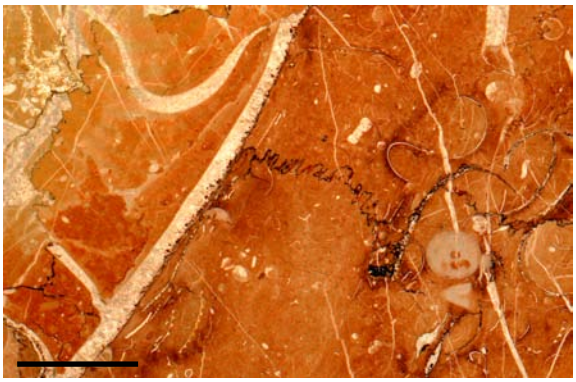

Fig. 2.58. Red bioclastic wacke to packstone with abundant ammonoid shells in the La Braña section (Alba Fm.). Scale 1cm.

Fig. 2.60. The Barcaliente Fm. (Carbonera section, see Appendix) is composed of uniformly bedded dark limestone beds.

VALDETEJA FM.

Type locality: Near the village of Valdeteja (Wagner et al. 1971), ITGE Map 104 "Boñar" (Lobato et al. 1984).

Thickness: 0m to 520m (Valporquero section)

Lithology: Light grey massive limestones, intercalated bedded to lenticular marlstones and limestones, microbial boundstones, mudstones to bioclastic grainstones, ooliths, oncolithes and calcareous breccias. Beside the Barcaliente Fm., the Valdeteja Fm. represents the most dolomitised formation in the Cantabrian Zone (Gasparrini et al. 2003).

Depositional environment: The Valdeteja Fm. was interpreted as a raised carbonate platform, with distinguishable platform top, platform margin, steep slope and basin facies (Eichmüller 1985, 1986, Bahamonde et al. 1997, Kenter et al. 2002). According to Fernández (1993), the Valdeteja platform in the Fold and Nappe province grew on submarine highs produced by the incipient emplacement of new thrust units (blind thrusts). The author distinguishes five vertically stacked platforms, separated by discontinuities which point to an unstable setting close to the orogen. In the northern part of the Cantabrian Zone, the Valdeteja platform consists of strongly prograding strata, which are separated by subaerial exposure, followed by platform flooding (Della Porta 2003, 2004). The platform interfingers with terrigenous sediments of the Olleros and San Emiliano formations (Fig. 2.63). The isochronous deposition of deeper water terrigenous sediments (Olleros & San Emiliano formations) and the growth of shallow water carbonate platforms (Barcaliente & Valdeteja formations) have been interpreted as indicative of the synorogenic scheme of an orogenic foredeep (Colmenero et al. 2002).

Age: Earliest Bashkirian to Middle Bashkirian

The base of the formation is isochronous whereas the top is strongly diachronous (Lobato et al. 1984).

SAN EMILIANO FM.

Type locality: Near the village San Emiliano (Brouwer & Ginkel 1964), ITGE Map 102 "Los Barrios de Luna" (Suárez Rodríguez et al. 1990).

Thickness: 1250m to 1800m according to Barba & Fernández (1990) and Dallmeyer & Martinez-García (1990). The top of the formation is always cut by thrusts.

Lithology: The formation was studied by numerous authors (Moore 1971, Bowman 1979, 1982, Riding 1979, Truyols & Sánchez de Posada 1983, Fernández 1993, Ginkel & Villa 1996 and others) and divided into three members: (i) Pinos Mb. (shales with interbedded turbiditic sandstones, abundant calcareous breccias and olistoliths, Fig. 2.64 and 2.65); (ii) La Majúa Mb. (alternating shales and sandstones with coal seams and limestone bands of varying thickness) and (iii) Candemuela Mb. (coal-bearing sandstone-mudstone alternations, limestone, and rare coal seams). At the base of the Villamanín beds (sensu Truyols & Sánchez de Posada 1983) the "Caliza masiva" represents an up to 250m thick limestone intercalation, containing numerous *Donezella* mounds (Riding 1979).

Depositional environment: The Pinos member was interpreted as basinal and slope deposits, overlain by coastal, shallow water sediments of minor prograding deltas (La Majúa Mb.) and deltaic environment influenced by shallow marine and alluvial deposits (Candemuela Mb.) (Bowman 1982, Fernández 1993). The Villamanín beds are time-equivalent to the Candemuela Mb., reflecting a more distal setting with mainly siliciclastic shelf sediments and some carbonate platforms (Colmenero et al. 2002). The formation received sediments from two different areas: (i) calcareous debris flows, turbidites and olistoliths from the carbonate Valdeteja platform at its external margin and (ii) terrigenous material from proximal sources to the S and W (Bowman 1982, Fernández 1993).

Age: Middle to Late Bashkirian

STEPHANIAN SUCCESSIONS

In some areas Precambrian to Carboniferous sediments of the Southern Cantabrian Basin are unconformably overlain by intermontane, coal-basin successions of Stephanian age (La Magdalena, Sabero and Ciñera-Matallana basins for instance, Figs. 2.1 and 3.4). The basins are thought to have formed during late Variscan tectonism, linked with reactivated pre-existing thrusts and wrench faults (Colmenero et al. 2002). It is not evident whether the isolated outcrops represent a number of small basins or are remnants of a single large basin. The continental basin-fill (Fig. 2.66) extends from 1500m to 3000m and is divided into numerous formations (from base to top: San Francisco, Pastora, Cascajo, Roquera,

Fig. 2.61. The top of the Barcaliente Fm. shows the poorly sorted, polymict Porma Breccia, attributed to strong earthquakes on top of the filled basin (Hemleben & Reuther 1980). Scale 20cm.

Fig. 2.63. North of Cármenes the Valdeteja carbonate platform is covered by the shally/sandy San Emiliano Fm., which contains numerous carbonate horizons.

Fig. 2.65. Detail of a fining-upward calci-turbiditic bed of the San Emiliano Fm. For the location see arrow in Fig. 2.64. Scale 20cm .

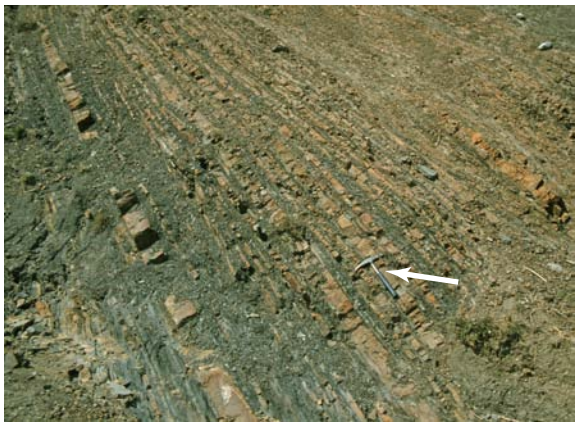

Fig. 2.62. The turbiditic Olleros Fm. marks the onset of syn-orogenic sedimentation in the Southern Cantabrian Basin. Hammer for scale (30cm, see arrow).

Fig. 2.64. South of the village Villanueva de la Tercía (Bernesga Valley) the San Emiliano Fm. is composed of dark turbiditic successions. Arrow indicates close-up in Fig. 2.65. Scale 1m.

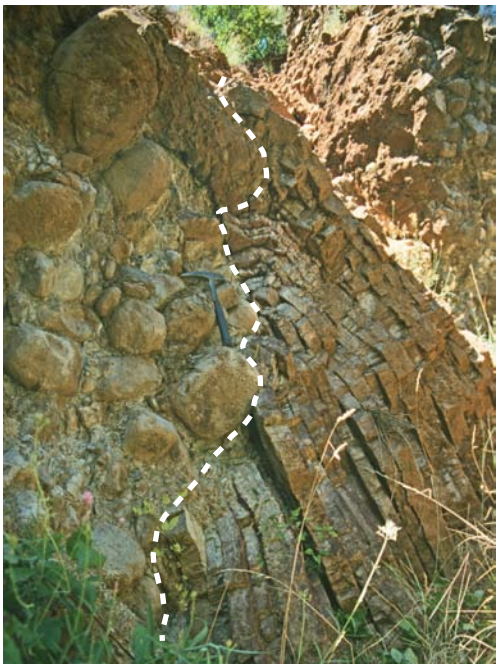

Fig. 2.66. In the La Pola de Gordón section Stephanian conglomerates erosively overlie the Baleas and Alba formations.. Hammer for scale (30cm).

San José, Bienvenidas, Matallana). The succession developed in a fining-upward succession in an alluvial fan-like environment (Heward 1978b, Colmenero et al. 1996). The basins have been interpreted as pull-apart basins (Nijman & Savage 1989, Villegas 1996).

MESO AND CENOZOIC

To the east of the region, Permian to Tertiary deposits crop out. In the south, the Palaeozoic sediments are covered by the Cretaceous and Tertiary basin-fill of the Duero Basin (see Fig. 3.5). It is unclear as to whether sediments of this age also covered parts of the Southern Cantabrian Basin and were eroded later, or if the sediments were restricted to the Duero Basin. The Cretaceous is represented by the Utrillas/Voznuevo Fm. (Evers 1967, Leyva et al. 1984, Barba & Fernández 1991) with fluvial siliciclastics and intertidal carbonates at the top (Boñar Fm. after Evers 1967). The thickness amounts to up to 500m in the region. According to Evers (1967), only the lowermost 50m to 100m of the Palaeogene Vegaquemada Fm. were deposited in the region, thickening to 400m and 600m further to the south. The formation is mostly composed of argillaceous sandstones deposited as alluvial fans. Frings et al. (2004) estimate about 1000m of overburden on top of the Stephanian sediments, based on vitrinite reflectance data and thermal modelling.

CHAPTER 3: BALANCED CROSS-SECTIONS

Stratigraphic modelling of sedimentary basins, which were subject to orogenic processes during late stages of their development, is a delicate matter. Tectonics conceal the basin architecture and the spatial relationships between measured profiles before deformation. Such tectonic settings offer repetitive insights into the evolving stratigraphic succession within each structural unit or thrust sheet. Prior to modelling, all tectonically affected domains have to be adjusted back into their depositional, pre-deformational position ("balancing"), in order to quantify basin shortening and to understand the pre-orogenic basin configuration and architecture. The most commonly used technique is balanced cross-sections (Woodward et al. 1985, 1989, Jamison 1987). A final balanced structural model promotes a better understanding of the geological history.

3.1 Historical development

The principal technique of balanced cross-sections was initially used to determine the depth to décollement/detachment of underlying concentric folds (Chamberlain 1910, 1919). This author already assumed that cross-sectional area is conserved during deformation above a single detachment. He used area balancing for orogenic shortening calculations, presuming plane strain and pure shear deformation. Bucher (1933), Dahlstrom (1969), Woodward et al. (1985, 1989) and many others subsequently applied and improved this technique.

The first truly balanced cross-section was published by Bally et al. in 1966 as a combination of academic curiosity and exploration necessity, as the available seismic data was of much lower quality than today (Woodward et al. 1989). However even today, seismic data and modern processing techniques leave room for interpretation and consequently several possible solutions. In order to limit the set of possible results, Dahlstom (1969) established balancing techniques, which verify the plausibility of each model. He drew up basic rules for the verification of coherence between different structural elements and their extrapolation in the subsurface. Later, these techniques were evolved in terms of fold types and geometries by Jamison (1987).

By reversing Chamberlains depth-to-detachment technique, Gwinn (1970) was the first to evaluate the shortening of an orogenic belt by using area balancing in the Central Appalachians. In the same area Dennison & Woodward (1963) utilised the line-length balancing method not only to calculate orogenic shortening but also to draw palinspastic restorations in order to explain facies relationships. Nowadays exploration companies widely use this approach.

3.2 Development and mechanisms of fold-and-thrust belts

This chapter introduces some important terms and mechanisms, which were used during the structural rasibalancing. The evolution of a peripheral foreland basin begins when an ocean has closed at a destructive plate boundary and the front of the overthrust belt has reached the stretched crust of an existing continental margin (Einsele 2000). Where continents collide, foreland basins develop as a result of downflexing of the overridden plate under the load of the advancing thrust belt (Aigner et al. 1989, Waschbusch & Royden 1992, Watts 1992, Toth et al. 1996, Watts 2001, Garcia-Castellanos 2002, Lin & Watts 2002). The loads of fold-and-thrust belts form a depocentre into which thick sediment successions are deposited (Watts 2001). Foreland basins develop on continental crust not only as a result of the vertical weight of an approaching thrust belt, but also because of the lateral force exerted by plate compression (Einsele 2000, Lin & Watts 2002). These loads can be supracrustal (loads applied during emplacement of thrust sheets) or subcrustal (loads transmitted from the subduction zone itself). The latter are also called buried loads, which can be detected by Bouguer gravity anomalies (Watts 2001).

Convergent orogens such as foreland thrust belts can be visualised in terms of a wedge-shaped prism resting on a rigid slab that is sliding beneath it (Platt 1986). They are dynamic systems with stresses and resulting strains reflecting a dynamic equilibrium (Nieuwland et al. 2000) and begin to form with a critical wedge (Suppe 1985). As the wedge reaches a critical angle, a normal piggy-back sequence of

thrusting, propagating towards the foreland will begin (Fig. 3.1). Younger thrusts develop in front of the old ones, and ride passively on the back of the latest thrust without further internal deformation. The structural style and geometry of a thrust complex strongly depends on basal friction. This in turn is dependent on the resistance of the décollement material. Constant boundary conditions in terms of constant basal friction are essential for the development of a piggy-back thrust belt (Nieuwland et al. 2000).

The subsidence history is controlled by the flexure of the underlying lithosphere (see Chapter 5.2.6) and the step-by-step overthrust process as well as unloading due to subaerial erosion or thrust sheets and changing geothermal gradients (Einsele 2000). Tectonic loads become particularly effective if they reach high elevations above sea-level. Orogenic wedges tend to deform internally until they reach a stable configuration by balancing gravitational and traction forces. In the case of frontal accretion, which lengthens the wedge, internal shortening is required in order to regain a stable geometry. This internal shortening can take the form of late (out-of-sequence) thrusting, backthrusting and folding (Platt 1986). Underplating of sediment or crustal slices thickens the wedge, compensating by means of internal extension. This is expressed by listric normal faults, which can merge downward into zones of horizontal ductile extension (Platt 1986, Nieuwland et al. 2000).

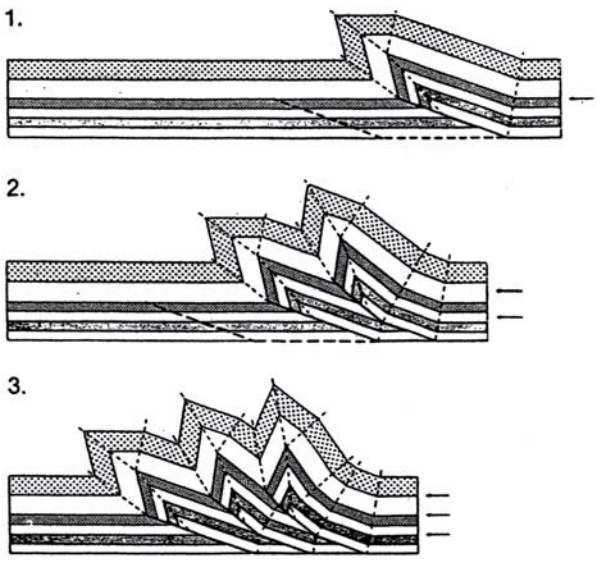

Fig. 3.1. Deformation of a piggy-back thrust mechanism under consideration of fault-propagation-folds (Mitra 1986).

3.3 Standard balancing techniques

Balanced cross-sections are the most commonly utilized geometric constraint for overthrust structures (Jamison 1987). Tectonic structures are mostly the result of heterogeneous deformation built up by three different components. These are the change of volume or form and both translation and rotation related to an external system of coordinates. Each deformation can be described as coordinate-transformation of matter-particles in space. One place cannot be occupied by two particles at the same time. This is the basic strain-compatibility principle during deformation postulated by Ramsay & Huber (1987). In a tectonic coherent body only steady changes of deformation are possible. Discrete changes result in faults. Consequently, balanced cross-sections are the assumption for any quantitative analysis of subsurface structures in brittle deformed rocks.

The viable and admissible balanced cross-section is the central test carried out to determine the consistence of bed lengths, areas or volume. It is a check to assure that the total rock volume remains constant throughout the history of the development of a geologic structure (Jamison 1987). Balancing is only valid if it observes the physical principal of mass-maintenance. Neighbouring tectonic bodies have to retain coherence both in the deformed and undeformed state in order to keep the total volume constant. Geometrically admissible cross-sections are not automatically plausible and cannot be verified in nature. While constructing cross-sections there are generally a number of geometrically plausible solutions, which cannot all be true. The number of solutions depends greatly on the quality of the database. Geometrically not admissible and consequently not balanceable cross-sections are incorrect in a strict sense.

There are three possible methods of balancing cross-sections, which will be discussed in the following section: volume-balancing, equal-area and equal bed length. As volume-balancing addresses 3D calculations, it requires a broad structural database, available only by combining many types of data such as seismic logs and profiles, borehole data etc.

As shown in Fig. 3.2, segment V_1 has been moved due to regional shortening with the norm vector Δx in the direction of the x-axis. The removed segment ΔV_1 is a function of Δx (norm vector of shortening), z_0 (depth to detachment) and y_0 (width of the segment). The primary volume ΔV_1 corresponds to the added volume ΔV_2 after shortening. Because of the above-mentioned constancy of rock-volume, the equation (1) is valid:

$$\Delta V_1 = \Delta V_2 = \Delta x * y_0 * z_0 \qquad (1)$$

However, because complex deformation, like ductile yielding or intrusion of magma, can still not be calculated quantitatively, one has to use simplified assumptions. The equal-area method of Woodward et al. (1985, 1989) reduces 3D-calculation to 2D-area balancing within a cross-section. It requires equal cross-sectional area in both the deformed and restored states. Woodward et al. (1989) refers especially to thrust sheets in which deformation of geological bodies occurs in the form of rotation, translation and simple shear. On account of this, deformation occurs without changes to plains in the cross-section. Cross-sections have to be placed parallel to the strain-direction, analogous to the displacement vectors or perpendicular to the thrust planes. In this case, the mass-maintenance principle is simplified to a geometrical principle of plain conservation within the cross-section. This simplification permits the following equation (see Fig. 3.2):

$$\Delta F_1 = \Delta F_2 = \Delta x * z_0 \qquad (2)$$

The third method uses Dahlstrom´s (1969) fundamental rule of bed lengths. This rule is summarised as a simple test of the geometric validity of a cross-section, which measures bed lengths. These bed lengths must be consistent unless a discontinuity intervenes. Compared with all other methods, this one is the most effective. It predicates on the assumption that deformation neither creates nor destroys rock volume. This permits reassembling of the undeformed state from the deformed state. If the presumption of constant thickness of all beds during the deformation is assumed, the equal-area method can be simplified to the bed-length method (Fig. 3.2). The amount of shortening can be calculated by

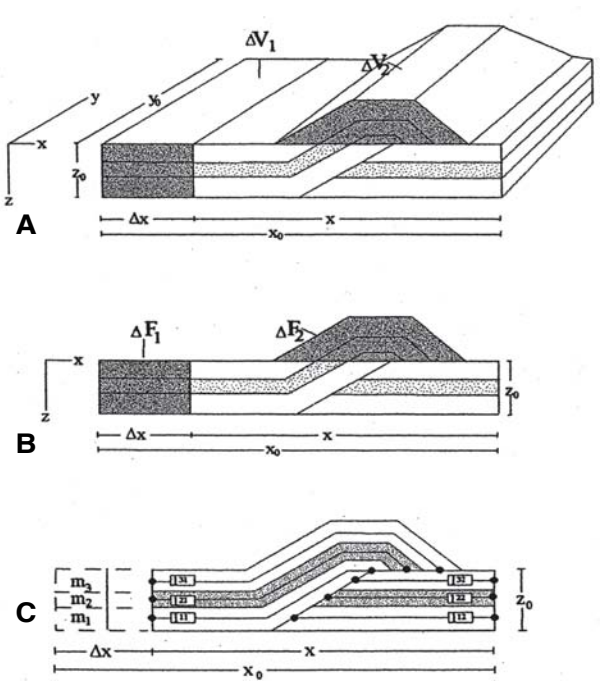

Fig. 3.2. Different balancing methods for regions affected by thrusting (after Linzer 1989):
A: volume-balancing; **B**: equal-area balancing; **C**: equal bed length balancing.

the following equation:

$$\Delta x = x_0 - x \qquad (3)$$

Shortening ε in percent is computed by equation (4):

$$\varepsilon = (x - x_0) / x_0 * 100 \qquad (4)$$

whereby x_0 presents the restored stage and x the deformed one.

3.4 Computer based interpretation techniques

In the last years computer based balancing proved to be very advantageous and became a standard method in exploration geology. Beside the balacing programs Geosec, Locase, Gocad, Stretch, Orogeny or Thrustbelt, 2D-Move (Midland Valley Ltd.) is one of the most popular software programs on the market. 2D-Move™ is a structural analysis and modelling program that allows line-length and area balancing of cross-sections from any tectonic regime. Both structural restorations and forward modelling can be carried out. The program uses different bal-

ancing algorithms, which can be chosen according to different tectonic settings. Properties include decompaction (coupled with burial history and Airy isostasy), depth to basement, line-length and flexural-slip unfolding, restore and others. Kinematic algorithms include incline shear and fault parallel flow. Footwall deformation due to isostatic loading and unloading allows full 2D backstripping of regional sections. 2D-Move™ uses two different approaches in structural restoration. The first, simple technique called "unfolding restoration" ignores the fault geometries. If the scope of work and the database allow the consideration of fault geometry on hangingwall deformation, "move on fault restoration" can be used. Both techniques are able to perform the following procedures:

- remove fault displacement
- remove the effects of erosion
- remove the volume loss attributed to sediment compaction
- remove fault related folds by incline shear, flexural slip or fault parallel flow
- remove folding related to flexural slip

Due to the fact that variable information can be integrated into cross-sections, 2D-Move™ can carry out complex calculations such as the integration of dip values, flexural isostasy, decompaction or depth conversion.

3.5 Restrictions

- Using the presented simplifications only plane strain and simple shear can be used
- Parallel folding with flexural slip between beds is assumed
- Cross-sections have to be placed parallel to the direction of strain analogous to the displacement vectors or perpendicular to the thrust planes
- No movement into or out of the plane of the section can be calculated in the 2D version
- Presumption of minimal volume loss or tectonic compaction for example by means of pressure solution and preservation of line-length during deformation is necessary
- Transects have to contain completely restorable structures
- Only a limited suite of structures can exist in a specific geological environment (Dahlstrom, 1969). In other words, not every geometrical viable model is geologically plausible and can be checked in nature.

On the other hand, the balanced cross-section-method offers reliable quantitative predictions of the subsurface architecture even if there is no seismic data basis, borehole information or sufficient surface data. However, one has to keep in mind, that cross-sections are interpretations of map data and are only as good as the initial information (Woodward et al. 1989).

3.6 Bernesga Transect

The overall geologic situation and generation of the Variscan fold-and-thrust belt has been explained in detail in Chapter 2. The balancing procedure starts with the construction of a deformed section, which follows the thrust rules. Then bed lengths are measured in order to relocate faults in the undeformed state. This simple and straightforward process is more difficult when the section is based only on surface data without observed footwall cutoffs, such as in the present study. Unfortunately only poor data is available from few borehole-logs or seismic sections. In 1995, Pulgar et al. and Pérez-Estaún et al. published deep seismic reflection profiles called ESCI-N1 and ESCI-N2. The ESCI-N2 profile was traced N-S along the southern slope of the Cantabrian Mountains about 70km to the east of the Bernesga transect (see Fig. 2.18). Unfortunately, only limited data could be used in the present work as the seismic profiles focus on the deep crustal structure and do not resolve shallow crustal floors.

3.6.1 Location and limits of the transect

The Bernesga Transect is situated along the rivers Torio and Bernesga, on the southern slope of the Cantabrian Mountains (Fig. 3.3). Both rivers arise in the peaks of the Cantabrian Mountains in the region of Puerto Piedrafita and Pajares and run approximately in a N-S direction. South of La Robla, the river Bernesga enters the Duero plain situated around León, capital of the province León.

The Bernesga Transect has been chosen for this study because of its highly suitable outcrops and suitable orientation in regard to the overall tectonic transport direction in the region. Fig. 3.4 shows

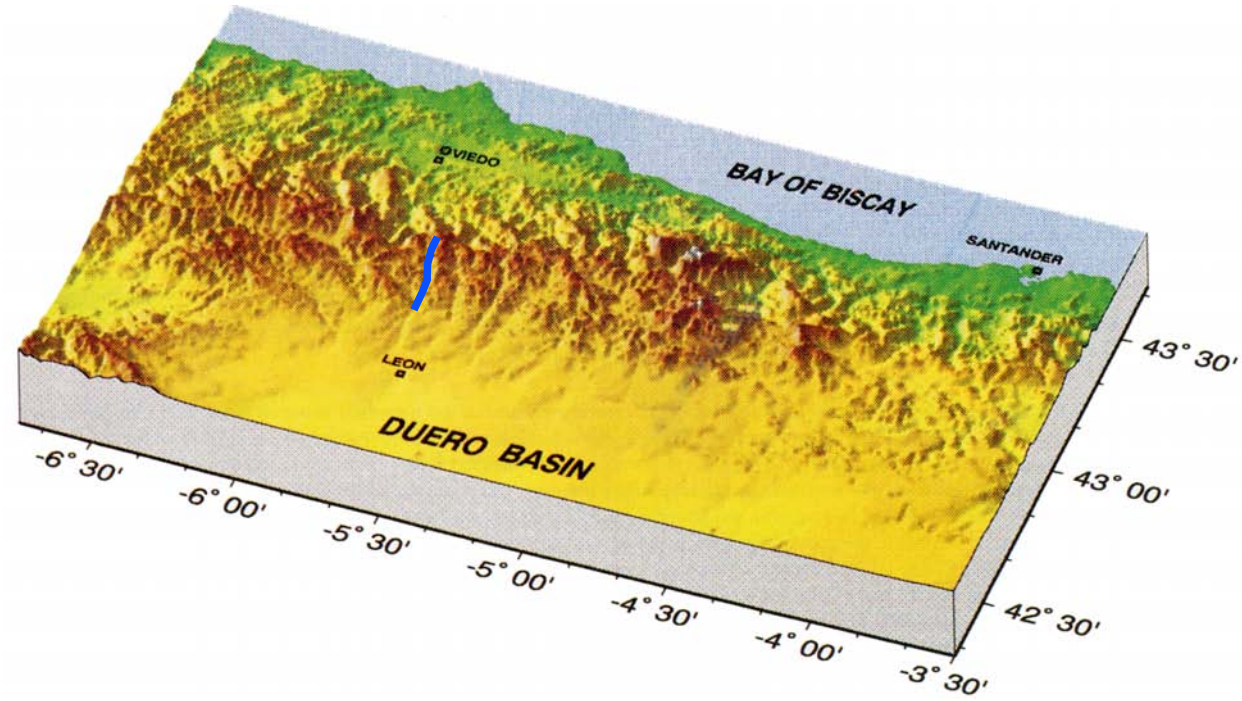

Fig. 3.3. Location of the Bernesga Transect (blue line) on the southern slope of the Cantabrian Mountains. 3D topographic diagram taken from Pulgar et al. (1995).

the geological map of the Bernesga region. As mentioned above, inherent to the method of cross-section balancing is the assumption that the line of section is parallel to the direction of thrust movement (see Chapter 3.3). As the thrusts and nappes of the Southern Cantabrians Mountains have been transported to the north (according to the present coordinate system) only transects situated approximately in a N-S direction are balanceable. For balancing purposes and due to tectonic difficulties, which will be discussed in Chapter 3.6.4, the Bernesga Transect was split in two parts. Therefore the term transect is utilised here, and not cross-section as is used in Chapter 3.3 where theoretical methods of balancing cross-sections were explained. The Bernesga Transect was split along the thrust plane delimiting the Correcillas Nappe in the north from the Aralla-Rozo Nappe in the south (see Fig. 3.4).

Although the stratigraphic model considers the whole area between the Central Coal Basin in the north and the Duero Basin in the south (see Fig. 3.5 and Chapter 7), the structural model is restricted by different structural limits. Both in the north and south E-W trending out-of-sequence faults form the boundary of the Bernesga Transect. In the north the approximately 150km long León Line fault system cross-cuts the Bernesga transect. It is still poorly understood and thus a matter of discussion. It is associated with a broad zone of brecciation and fracturing (tens of meters wide) and cuts through the whole Paleozoic stack. The León Line thrust system cross-cuts the Bodón Nappe south of the village of Pontedo, adjoining the stratigraphic level of the Formigoso Fm. (at the northern side of the fault) and Barcaliente Fm. (at the southern side of the fault). In the south, the Southern Border Thrust (Staalduinen 1973) thrusts the Paleozioc succession over Mesozoic sediments of the Duero Basin (Figs. 3.4 and 3.5), indicative of Alpidic movements. The León Line fault system as well as the Southern Border Thrust are out-of-sequence thusts with unknown displacement factors and characteristics. Therefore no structural balancing was performed north of the León Line fault system and south of the Southern Border Thrust.

The position of both parts of the Bernesga transect can be seen in Fig. 3.4.

3.6.2. Structural domains

According to the overall structural framework, this part of the Cantabrian Zone can be divided into three domains. From north to south these are the Bodón,

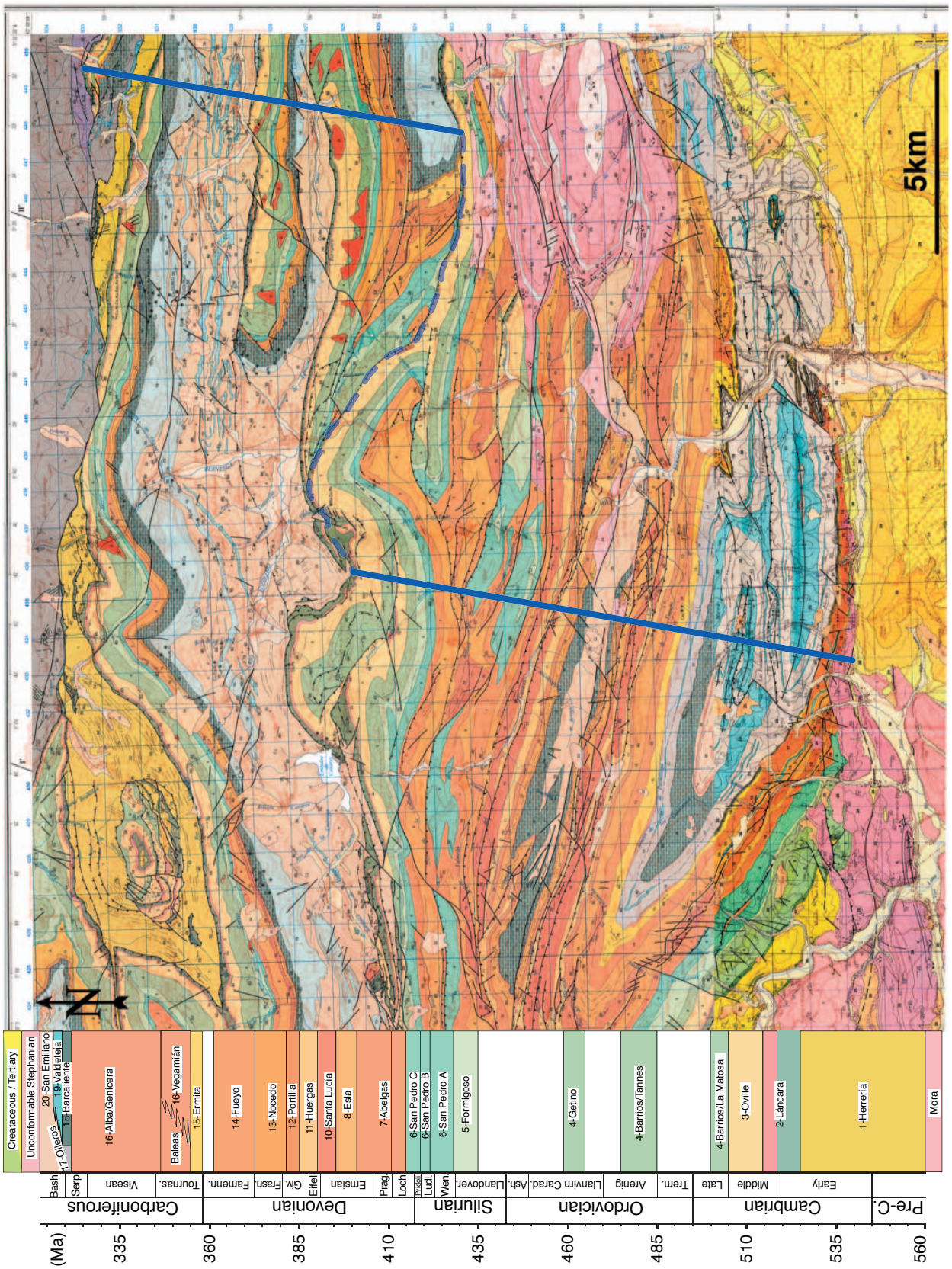

Fig. 3.4. Geological map of the Bernesga region. The position of the Bernesga Transect is marked by a blue line. The split of the transect is displayed by a blue dashed line. The different colours on the southern part of the map result from the use of a second map (northern part: Alonso et al. 1991; southern part: Matas & Rodríguez Fernández 1984).

Pedrosa and Alba domains (see also Weil et al. 2001 and Fig. 3.5). These domains as well as most of the thrust sheets are limited by steep dipping or overturned thrusts and have the following characteristics:

1. *The Bodón domain* in the north comprises the Bodón, Gayo and Correcilla nappes. To the north it is bound by the León Line fault system and shows three large open folds in the scale of kilometres (see Fig. 3.5 and 3.15A). This unit displays not only the already mentioned basal detachment at the base of the Láncara Fm. (see Chapter 2.4.3), but also a second detachment in the Herrería Fm. Alonso & Suárez Rodríguez (1991) assumes staircase geometry of this thrust, admitting problems in tracing the course in this area. The thrust surface has been folded west of the Bernesga transect, being well exposed in the Cueto Negro antiform (Fig. 3.4).
2. *The Pedrosa domain* is characterized by multiple overthrust sheets in form of an imbricated thrust system. The unit is composed of the Aralla-Rozo Nappe and the Pedroso Syncline, which is in fact the northern part of the Abelgas-Bregón Nappe (see Fig. 3.5 and 3.15A). The basal detachment is situated on the base of the Láncara Fm. It is not surprising that the imbricated thrust system shows the highest rate of shortening within the transect (see Chapter 3.6.6).
3. *The Alba domain*, representing the southern part of the Abelgas-Bregón Nappe, is composed by large synformal structures (see Fig. 3.5 and 3.15A). In the southernmost part of the Bernesga transect, the Southern Border Thrust marks the delineation of the Duero basin. Paleozoic sediments of the Southern Cantabrian Basin have been thrusted over the Mesozoic basin infill of this basin. The large, open Alba Syncline (Fig. 3.6) has suffered the least amount of shortening within the transect. Despite this fact, small-scale faulting and folding is very common but have not been considered within the balancing process.

Figs. 3.7 to 3.12 display a wide range of folds present in the Southern Cantabrian Zone, comprising among others large synclines, recumbent, irregular, lobate, concentric, kink and chevron folds.

3.6.3 Constructional methods of deformed transects

The structural framework was acquired using data sets derived from literature and augmented by fieldwork collected for this study. In addition aerial photographs and geological maps represented an important database for the present work. Mainly the maps of Savage & Boschma (1980), Lobato et al. (1984), Matas & Rodríguez Fernández (1984), Suárez Rodríguez et al. (1990) and Alonso et al. (1991) have been used for this study. Only major structural elements were taken into account. Small-scale faulting and folding, even though abundant in many locations, goes beyond this study and was neglected.

Depth to detachment method

There are several techniques required for the construction and following restoration of cross-sections. As mentioned in Chapters 3.1 and 3.3 Chamberlain (1910) and Woodward et al. (1985) postulated the fundamental depth to detachment rule. This step was not necessary in the present study. In the Southern Cantabrian Mountains the main detachment horizon is defined by the outcropping main thrusts, situated at the base of the Lancára Fm. (see Chapter 2.4.3 for detail) and subordinate the Herrería Fm. This knowledge permits the use of "regionals" in order to calculate the depth of major detachments. Regionals are stratigraphic thickness data not involved in thrust related structures (McClay 1992), which allow us to determine the local depth of a main detachment. The known stratigraphic thicknesses between a specified datum and the main detachment can be placed in synclines (within the fold axis plane) or undeformed parts of the section, where the specific datum crops out. The depth of main detachment can then be projected in the subsurface.

Stratigraphic separation diagrams

In case of problematical thrust characteristics, stratigraphic separation diagrams (Woodward et al. 1989) were used in order to analyse and localise ramps and flats. Stratigraphic separation diagrams are a quantitative way to evaluate how far thrusts travel in a particular stratigraphic horizon. For this purpose, the

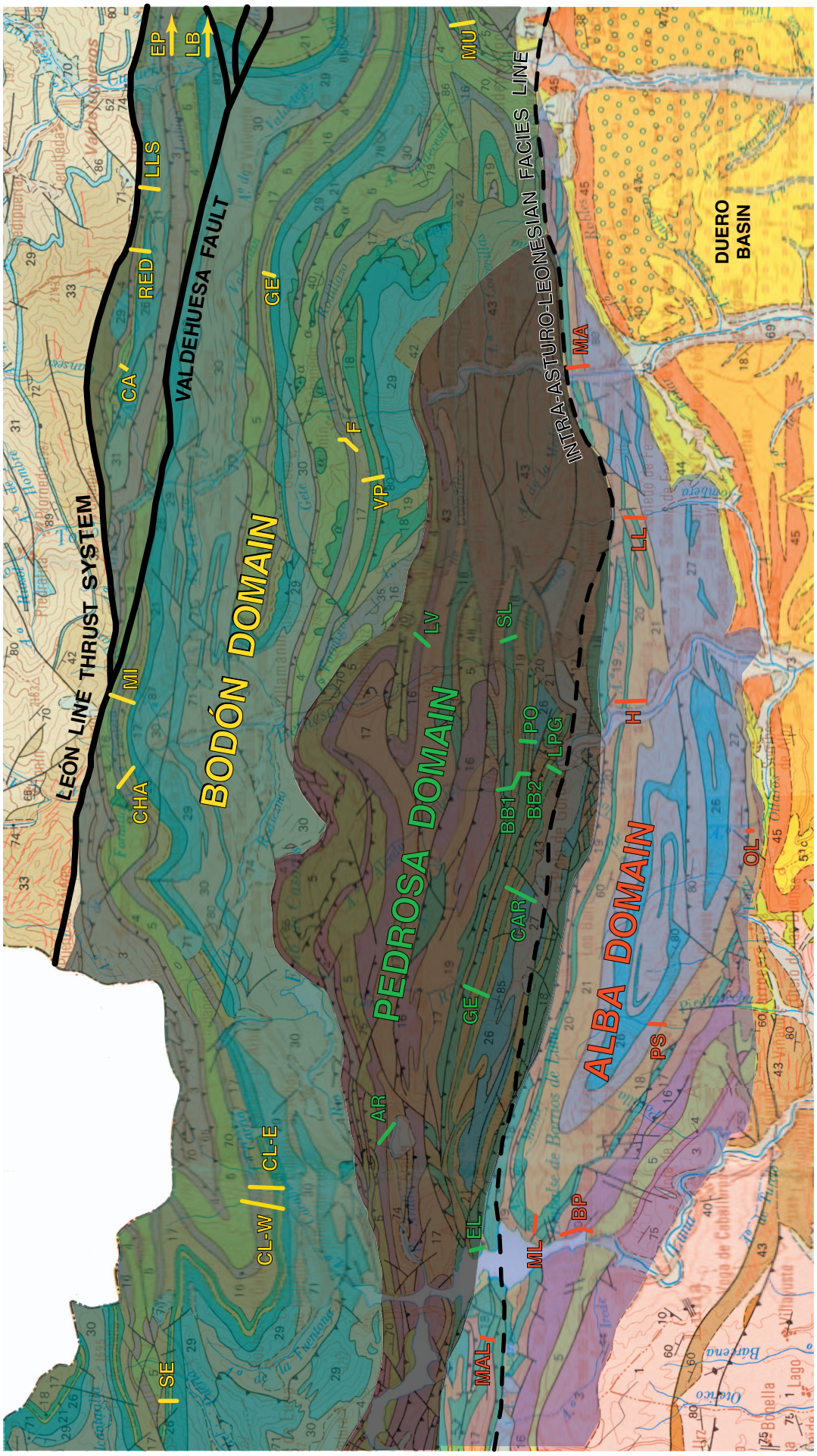

Fig. 3.5. Map of the three main structural domains (Bodón, Pedrosa and Alba) of the Southern Cantabrian Basin. The locations of the measured cross-sections and their abbreviations are shown each in the colour of the particular domain. Note the position of the Duero Basin (in the south), León Line thrust system (in the north) and the Intra-Asturo-Leonesian facies line (IALF). See Appendix for the plotted cross-sections. Geologic map after Suárez et al. (1994).

Fig. 3.6. The large open Alba Syncline is characterised by the least amount of deformation in the Southern Cantabrian Basin. View from the village Mallo de Luna, facing east.

hangingwall stratigraphic unit is plotted geographically against the footwall stratigraphic unit. A stratigraphic separation diagram is located perpendicular to the transport direction in order to show lateral ramps or along the transport direction to distinguish frontal ramps. This method was used to estimate the ramp angle of the footwall and the transport range of the hangingwall.

Basal detachment

One of the main features of the Bernesga Transect is the basal detachment at the base of the Láncara Fm. (see Chapter 2.4.3). The basal detachment is visible as a continuous subhorizontal band in the deep seismic reflection profile ESCI-N2 (Fig. 2.18; Pulgar et al. 1995). At a distance of 20km north of the Mesozoic Duero basin (Millaró section in the north of the Bernesga Transect), the band is situated at 1.8 s two-way-time. In the Millaró section the proportion of siliciclastic (2405m) to carbonates (1056m) is 2.3:1. Under consideration of average travel times at depths between 1000 and 3000m (siliciclastics: 3000 m/s; carbonates: 4000 m/s) and the ratio mentioned above, the detachment is situated at a depth of approx. 3000m. Together with a 2.5° to 3° detachment dip-angle to the south (consistent with Pérez-Estaún et al. 1988, 1994, 1995, Pulgar et al. 1995), this corresponds with the projected regionals in the Valporquero and Alba synclines (see Fig. 3.15A).

Folds and thrusts

The common occurrence of thrusts (Fig. 2.27) in this region suggests a genetic coherence of fold-development and thrusting. Major thrusts in the Cantabrian Zone show an Appalachian style geometry (Pérez-Estaún et al. 1994). During the projection of structural data in the subsurface, estimated fold mechanisms have to be examined for their geologic suitability and potentiality to obtain a balanceable result. Not all fold types represent balanceable structures. For example, concentric folds (Fig. 3.10) formed under brittle conditions suffer serious space problems. On the other hand, not every geologic setting allows the occurrence of every fold type. As early as 1934, Rich proposed the concept of generating rootless folds by translating hanging-

Fig. 3.7. South-vergent, asymmetric Montuerto Syncline south of Nocedo de Curueño. The large fold-structure has a curved axis dipping steeply to the west. According to Potent (2000) it developed in a polyphase deformation process. The dark rocks in the foreground represent the Barrios Fm. (quartz sandstones), whereas the light grey limestones in the back are part of the Santa Lucía Fm.

Fig. 3.8. Large-scale, recumbent folds within the Santa Lucía Fm. outcropping NE of the village Corecillas. The axial plains are flat-lying to horizontal. Overturned limbs show a tight, asymmetric pattern.

Fig. 3.9. Large-scale folds in the centre of the Alba Syncline. The irregular, lobate folds show ptygmatic forms with large amplitudes to the wavelength ratio.

Fig. 3.10. South of Llombera this concentric fold crops out. It is composed of highly fossiliferous limestones and marls of the Portilla Fm. and shows a steeply dipping fold axial plane. Scale approx. one metre.

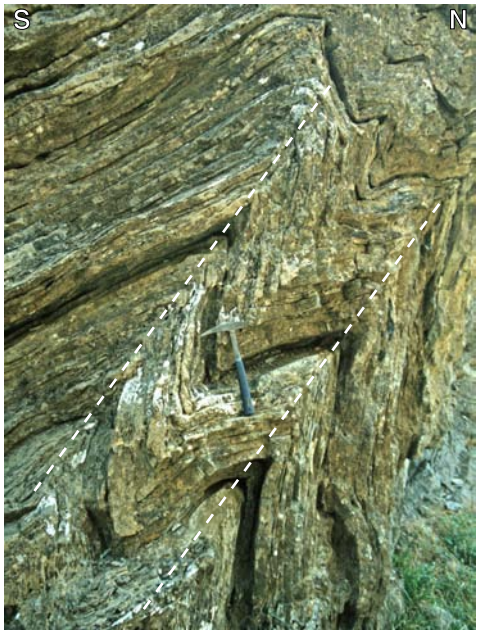

Fig. 3.11. North-vergent kink folds (chevron fold) with flexural slip movement along pelite horizons. The outcrop is located on the southern limb of the Alba Syncline, north of the village Piedrasecha. Hammer for scale (30cm).

Fig. 3.12. NE of the village Caldas de Luna this variable folding in the Alba Fm. is caused by flexural flow. Note white carbonate mineralization infilling the dilation vug in the hinge (arrow). Hammer for scale (30cm).

wall block up a thrust with a staircase thrust trajectory. Since then, the staircase or stair-step trajectories have been the accepted geometry for all thrust belts and were used to produce balanced cross-sections (Cooper & Trayner 1986). The characteristic flat-ramp-flat geometry is produced by a long bedding-parallel décollement, separated by a shorter high-angle fault segment cutting across the bedding to a higher level bedding-parallel décollement (Elliott & Johnson 1980, McClay 1992). Basically there are three different thrust fold-types (Jamison 1987): (i) detachment folds; (ii) fault-bend folds and (iii) fault-propagation folds. Detachment folds develop above a bedding parallel detachment without the presence of ramps and require a ductile décollement layer in order to fill the newly generated space at the base of the fold (McClay 1992). As ramp segments are clearly visible in the field, this fold type can be precluded. Both fault-propagation folds and fault-bend folds are characteristic for the architectural style of thrust-belts (Jamison 1987). They can be distinguished on the basis of the position of the fold and the hanging wall truncation relative to the ramp (Suppe 1983, Jamison 1987). Fault-bend folds were used in the construction of the transect, as this fold type is the only possible solution for observed geometry of the tectonic suite of the region (Fig. 3.13). They are a typical feature in thrust-belts and develop as the hangingwall of a thrust is transported through a ramp region on the thrust surface (Jamison 1987). A tight anticline (aperture angle of 95°) north of Rodillazo (IGME Map 104 "Boñar", Lobato et al. 1984) is a prominent example of a fault-bend fold (Potent 2000).

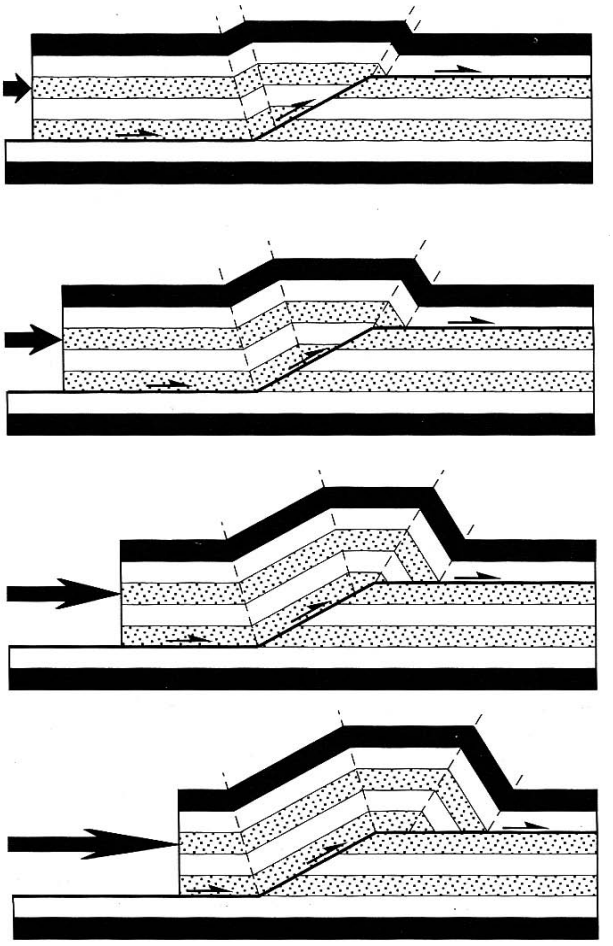

Fig. 3.13. Growth model for the development of fault-bend folds (McClay 1992).

Duplexes

Duplexes are a common feature in thrust belts and together with blind imbricates the most widely used way to fill volumes at depth when the surface geology limits the number of exposed thrusts (Woodward et al. 1989). By definition they are an array of thrust horses bounded by a floor thrust at the base and by a roof thrust at the top (McClay 1992). According to Mitra (1986) there is a threefold classification: (i) independent ramp anticlines and hinterland sloping duplexes; (ii) true duplexes and (iii) overlapping ramp anticlines. The independent ramp anticlines show a much greater spacing between the thrusts than the displacement on the individual thrust. They occur mostly in similar lengths and distances to each other, also visible in sand box models (pers. com. Adam 2001). Overlapping ramp anticlines show partial or total overlapping crests of successive ramp anticlines. A system of completely overlapping ramp anticlines can develop to an antiformal stack as in case of the Cueto Negro NW of Villamanín de la Tercia (see Figs. 3.4 and 3.14).

Deformation mechanisms

Two deformation mechanisms are well visible in the deformed transect. The "piggy-back thrust" mechanism shows a forward-breaking sequence of the individual thrust-sheets with the chronology running from south to north (Fig. 3.1 and 3.15A). Basal accretion within the Herrería Fm. is exposed in the Cueto Negro antiformal stack and in the subsurface as two duplexes south of pin line P3 and P8 (Fig. 3.14 and 3.15A). Basal accretion occurred af-

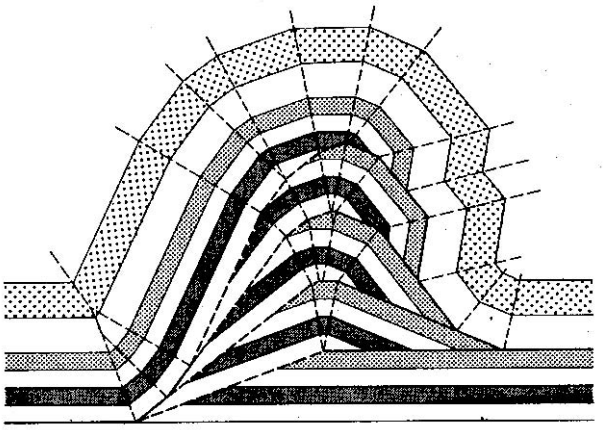

Fig. 3.14. Geometry of an antiformal stack as a possible model for the Cueto Negro Antiform (after Mitra 1986 and Woodward et al. 1989).

ter frontal accretion, with a resulting deformation of the basal detachment at the base of the Láncara Fm. Potent (2000) proposed three other deformation phases for the Southern Cantabrian Mountains. These have not been determined in this study. However, there are several indications for further deformation phases as out-of-sequence faults (León Line thrust system, Sabero-Gordón line, Alba Syncline backthrust), overthrusting of the Palaeozoic sediments on the Cretaceous Duero basin (Southern Border Thrust) and the steepening and overturning of many Variscan thrusts.

3.6.4 Partitioning of the Bernesga Transect

As mentioned in Chapter 3.3 and 3.5, movements out of or into the transect plain cannot be balanced or calculated by 2D balancing programs. Transport of material out of the transect plain is difficult to quantify and has to be restored before the construction of the cross-section. Later, during processing, such movements are geometrically not restorable, providing incorrect results within the balanced cross-section. Consequently, structures that perform this kind of movement have to be avoided. One type of such structures are lateral ramps. An example is well visible south of Villamanín de la Tercía, where the Correcillas Unit pinches out between the Gayo and Aralla-Rozo Units (Fig. 3.4 and 3.5). Therefore the Bernesga Transect was split along the trend of the Rozo thrust into a northern and a southern part, passing the lateral ramp. Relating to the northern part of the transect, the southern part was displaced 12km to the west (see Fig. 3.4). Very similar geometries of the adjacent ramps allowed highly accurate geometrical joining of both parts following the balancing process (see Chapter 3.6.5).

Northern part

The northern part contains, from north to south, the Forcada and the Bodón nappes of the Sobia-Bodón Unit and the Gayo and Corecillas nappes of the Somiedo-Correcillas Unit (see Fig. 3.4 and 3.15A). It is located in NNE-SSW direction, parallel to the transport direction of the main thrusts. The Central Coal Field (Cuenca Carbonífera Central) marks the northern limit of the Forcada Nappe and also the transect (N 42°59.175´; W 005°32.648´). The southern limit of the northern part of the Bernesga Transect is indicated by the thrust contact of the Correcillas and the Aralla-Rozo Nappe, southeast of the village Valporquero de Torío (N 42°53.783´; W 005°33.112´).

The León Line thrust system discussed earlier intersects the Bodón and the Forcada thrusts. The sense of motion and displacement width is not yet clarified (see discussion in Chapter 3.6.1), but here it is interpreted as a steep north-dipping fault. Due to this problem, the northernmost structural unit of the Southern Cantabrian Basin, the Forcada Nappe, was not balanced. To the north of the León Line the Bodón Unit is limited by the Herrería Fm. The northernmost part of the constructed transect interprets a subsurface Herrería overlapping ramp anticline cut by the León Line. This assumption can be reinforced by the presence of a large tectonic window approx. 20km to the west. This antiformal stack is composed of numerous repetitions of Precambrian to Ordovician formations (Herrería, Láncara, Oville, Barrios formations), called the Cueto Negro Antiform (Marcos 1968, Alonso & Suárez-Rodríguez 1991, see also Fig. 3.4). The Herrería Fm. can be traced along the main strike direction (W-E) to the position of the Bernesga transect, where it represents a higher tectonic floor of the antiformal stack. Further to the south there is an independent ramp anticline, which deformed the basal detachment at the base of the Láncara Fm. (Fig. 3.15A). This ramp anticline has been interpreted in the subsurface to account for the formation of the Valporquero Syncline (showed by pin line P3 in Fig. 3.15A). As al-

ready discussed (see Chapter 3.6.3) these independent ramp anticlines form a more or less symmetrical pattern, which can be evidenced in the deformed Bernesga Transect. The southern part of the transect displays another independent ramp anticline (south of the Pedroso Syncline, pin line P8) at a distance of approx. 8km to the south. The large Herrería antiformal stack is found within the same distance to the north, cut by the León Line.

North of the Gayo thrust (see Fig. 3.4) the sediments of the San Emiliano Fm. (see Chapter 2.4.4 for lithologic description) show strong internal deformation. This internal folding has been left out in the present tectonic model, since the complex deformation style would demand detailed structural studies. The Valporquero Syncline within the Correcillas Nappe has been interpreted controversially within different publications. Earlier studies of mainly Dutch geologists (Evers 1967, Staalduinen 1973, Savage & Boschma 1980) assume a syncline without any further deformation. More recent studies (Alonso et al. 1991) the Valporquero Syncline shows a large thrust in the northern limb between the Alba and Huergas formations. However the outcrop in the village Valporquero (on the road to the Cueva de Valporquero, N 42°54.516´; W 005°33.638´) covering the transition from the Santa Lucía, Huergas and Alba formations as well as additional data from surrounding outcrops allow an advanced interpretation. There is a low angle shift in the dip (8°-10°) within the Alba Fm. southeast of Valporquero, indicating the presence of a minor fault. No evidence of a major thrust could be found, as drawn between the Huergas and Alba formation in the map of Alonso et al. (1991). Therefore only a minor fault has been interpreted in the present study, which has not been taken into consideration during the balancing of the transect

Southern part

The Bernesga Transect was split and shifted 12km to the west (Fig. 3.4). Firstly due to the fact that Stephanian sediments of the Sabero-Gordón Basin cover the eastern part of the working area (south of the Valporquero Syncline). And secondly, because the lateral ramp south of Villamanín de la Tercia was avoided during the restoration process as explained in the previous chapter.

The southern part experienced greatly differing internal deformation from north to south. The imbricated thrust system in the north shows the highest level of shortening within the whole transect, whereas the wide open fold of the Alba Syncline only experienced a minor amount of deformation (Fig. 3.15A). According to McClay (1992) an imbricate thrust system is a closely related branching array of overlapping thrusts. They were formed by duplexes, which eroded the leading branch line. In contrast to the Bodón Unit, the stratigraphic succession of the single thrust sheets is heavily reduced here (see Fig. 3.4 and 3.15A). The basal thrust is interpreted as having changed its level by up-stepping from the base of the Láncara Fm. to the upper part of the Barrios Fm. and the Abelgas and Esla formations, respectively. Therefore, the now-missing upper layers must have been transported further to the north and eroded later (pers. com. Adam 2001).

The high number of thrusts and complex faults north of the Pedroso Syncline and especially within the anticline between the Pedroso and Alba synclines had to be reduced while balancing. Thus the constructed cross-section of this part of the Bernesga transect is only a simplification of the present geological setting. The reason for the formation of the tight Pedroso Syncline is, as in the case of the Valporquero Syncline, an independent ramp anticline in the subsurface. The relationship between the independent ramp anticlines is explained in the previous chapter. On the southern border of the transect, the Devonian Portilla Fm. is thrust over the steeply dipping Cretaceous sediments (Southern Border Thrust). This southward displacement originated a big monoclinal fold overturning the Palaeozoic and Meso/Cenozoic sediments and was interpreted on the basis of seismic data as an Alpine north-dipping reverse fault cutting deep into the basement (Alonso et al. 1995, Pulgar et al. 1995, Fig. 2.18). The Cantabrian Mountains represent the hanging wall of this fault, moving to the south over the footwall of the Duero basin. Associated with the Southern Border Thrust there is a well developed out-of-sequence back-thrust cropping out 2.3km further to the north (pers. com. Adam 2001). As explained in Chapter 3.2, orogenic wedges tend to deform internally until they reach a stable configuration by balancing gravitational and traction forces. Regaining stable geometry requires internal shortening, expressed as

late (out-of-sequence) thrusting, backthrusting and folding (Platt 1986).

3.6.5. Balancing of the Bernesga transect

Pin lines

Restorable cross-sections should contain a completely restorable structure (see Chapter 3.5) with the undeformed hinterland and foreland. For this study this is not the case. The undeformed hinterland in the south is covered by Cretaceous and Tertiary rocks of the Duero Basin, whereas in the north the León Line cross-cuts the transect (see discussion in Chapter 3.6.1 and Fig. 2.1). Consequentially pin lines had to be set. Pin lines are lines perpendicular to bedding (assumed to be the major sliding surfaces) in both deformed and undeformed states (Woodward et al. 1985). Following Dahlstroms (1969) rules pin lines must be placed along planes of no slip, like axial planes of major synclines or planes perpendicular to the regional dip of undisturbed beds. Good examples of pin lines placed parallel to the axial planes of synclines are the pin lines P3 and P8 in Fig. 3.15A. True pin lines are the starting point for measuring bed length in every discrete unit. However, it is not always possible to set true pin lines. In the present geologic setting all hanging wall cutoffs are eroded. If no syncline or anticline is present in a specific thrust sheet to place a true pin line, local pin lines had to be used. The best way to achieve this is to place a local pin line in the trailing edge of each thrust sheet and restore the sheets as isolated blocks (Woodward et al. 1989). In the present transect there are several thrust sheets indicating this problem. The four imbricated thrust sheets of the Aralla-Rozo and Abelgas-Bregón nappes in the north of the southern part of the transect (see Fig. 3.4) can only be restored with local pin lines (pin lines P4 to P7 in Fig. 3.15A). Woodward et al. (1989) state that local pin lines located in the centre of homoclinal sheets do not present locations of no or minimal slip between the planes, as required by Dahlstrom (1969). Nevertheless, they represent the best solution for dealing with this problem. By using local pin lines parallel to each other, we can make the assumption that they represent lines across which bedding plane shear was approximately the same. This method was used to place pins P4 to P7 (Fig. 3.15A). As already discussed, only the area between pin lines P1 and P9 has been restored and is marked by saturated colours in Fig. 3.15A.

Balancing procedure

Due to the incomplete structure (see Chapter 3.6.1) the Bodón and the Abelgas-Bregón nappes were only balanced partially. The Gayo, Corecillas and Aralla-Rozo nappes have been restored completely. The balanced Bernesga Transect is shown in Fig. 3.15B.

As mentioned in Chapter 3.3, the present work used the line length method for balancing purposes. Because of the different structural styles, the three domains (see Chapter 3.6.2) were balanced separately and stitched along the common ramps. In a first step the different nappes have been balanced manually and later verified using the structural balancing program 2D-Move™ (see Chapter 3.4). Construction of the deformed section and its balancing was accomplished simultaneously in an iterative way by using sets of intermediate templates.

Ramp geometries and angles result from balanced bed-lengths. Fault-bend folds show ramp angles between 10° and 40° (Boyer & Elliott 1982, Suppe 1983, Jamison 1987, McClay 1992, Nieuwland et al. 2000). In the present model the ramp angles range between 17° and 25° (Fig. 3.15B). The ramps break through from south to north with an angle increasing towards the top. This listric trend could have been caused by diminishing overburden to the top of the sequence (Potent 2000) or by high basal friction at the décollement (Nieuwland et al. 2000). However Cooper & Trayner (1986) state that progressive steepening of the thrusts may have been created as a result of insufficient bed length due to ductile deformation. Ductile deformation such as layer parallel shortening can reduce bed length and result in an underestimation of the undeformed state. The only solution to this problem would be to incorporate strain data into the balanced section and to consider the time relationships between ductile strain and brittle thrusting (Cooper & Trayner 1986). Unfortunately, no strain information was available for this study. To minimise this problem, competent beds, which have suffered the least amount of ductile deformation, were chosen for bed length balancing. Due to steepening and overturning of the thrusts during later deformation, hangingwall truncations are not always located in foreland direction of the ramps.

The lowermost horizon of the Herrería Fm. was deformed by basal accretion (see Chapter 3.6.3) and was not taken into consideration within the balanc-

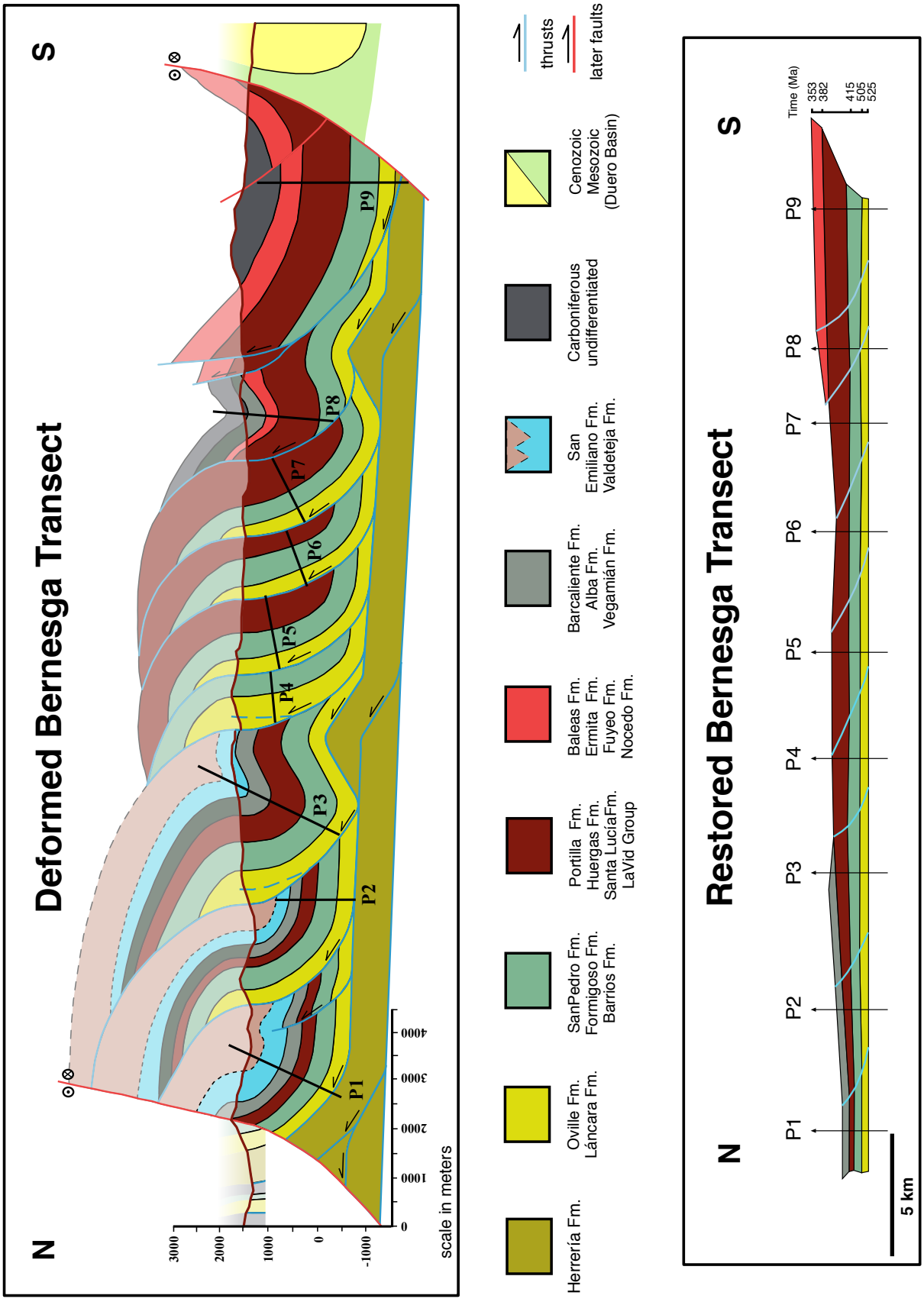

Fig. 3.15. Structural balancing of the Bernesga Transect. The upper picture shows the deformed state, whereas the lower picture visualises the restored transect. Note the different scales of the upper and lower figures. For graphical reasons, different formations were grouped into units with identical colours. The result of structural balancing is an undeformed, largely horizontal stack of sedimentary formations of varying thickness. The topographic feature of the Cantabrian High is only characterised by the diminishing thickness of Devonian formations (red brown colour) towards the north.

ing procedure. Due to an unknown structure and geometry (no high-resolution seismics is available), the duplexes and the antiformal stack in the north have been displayed only schematically.

There is no consistent sedimentary stack along the entire balanced transect. In some younger nappes, the staircase thrusting removed the upper part of the sediments, which were transported further to the north and eroded later (pers. com. Adam 2001). Thus no single reference datum could be used for all nappes. For areas between pin line P1 and P7, the top of the Oville Fm. was chosen as the reference datum, as it occurs in each of these nappes, including the imbricated thrust system of the Aralla-Rozo Nappe. The top of the Portilla Fm. was chosen for the southernmost pin lines (P8 and P9), because the top of the Oville Fm. only partly intersects pin line P8. Due to thickness variations and the interfingering of the uppermost units (Valdeteja and San Emiliano formations), these were not balanced. Additionally the top of the San Emiliano Fm. is never exposed in the region, as it is always cut by thrusts. For visual clarity reasons, formations were grouped into four groups, designated with specific colours (see Fig. 3.15).

Within the deformed transect, intersections between reference horizons (top Oville and Portilla formations) and pin lines were projected perpendicularly onto a horizontal datum. Thus, not only the internal deformation of the unique nappes is calculated, but also the overthrusting distance between two neighbouring nappes. However, displacement widths were calculated independently for every unique nappe by measuring the distance between the foowall and hangingwall cut-off points along the different thrust surfaces. This workflow is in alignment with the 2D-Move™ "unfolding restoration" algorithms (see Chapter 3.4). Due to problems of the software version handling steep to overturned thrusts, fault geometries were not examined using the "move on fault restoration" tool.

The result of the balancing process is an undeformed, horizontal stack of beds with varying thicknesses, formed during sedimentation (see Fig. 3.15B). After being balanced, the sediments do not reflect any syndepositional topographic features, such as the Cantabrian High. This topographic high is characterized only by the diminishing sediment thicknesses to the north since the Silurian times, well visible in the brown horizon of the Devonian formations. All pin lines show the expected vertical position after balancing.

3.6.6 Shortening values of the Southern Cantabrian Basin

As already stated, this schematic balancing procedure provides only minimum shortening values for the Bernesga transect. Values may vary and increase if out of plane deformation and small scale internal folding and faulting are taken into consideration. The effective shortening might therefore be considerably higher.

The length of the constructed, deformed transect totals to 17.91km, whereas in the restored state the length increases to 38.58km (both distances measured between pin lines P1 and P9) resulting in a shortening distance of 20.67km. Employing the equation (4) minimal shortening of the Bernesga Transect amounts to 54%. Detailed calculations for the individual nappes are displayed in Table 3.1.

In terms of minimal shortening of the three domains (see Chapter 3.6.2), the Pedrosa Domain displays the highest values, reaching 65%, followed by the Bodón (41%) and Alba (25%) domains. Areas north of pin line P1 and south of pin line P9 are not taken into account for the calculation. Only the Bodón and Correcillas nappes, as well as the, comparably slightly deformed Alba Syncline show lower values in proportion to the total shortening of the transect. As expected, the highest shortening values are displayed by the imbricated thrust system north of the Pedroso Syncline (up to 78%), showing minimal shortening to be 23% to 45% higher than average.

Regarding the Forcada Nappe in the north of the Bernesga transect which was not balanced, values greater then 70% (comparable to the Gayo Unit) can be estimated, as the León Line fault system and other residual faults point to a significantly higher internal deformation. It can be reasonably assumed that the area between the pin line P9 and the Southern Border thrust will range from around 20% to 25%, considering the backthrust on the southern limb of the Alba syncline and the simplifications mentioned above.

The minimal shortening estimated in this study ranges between the values suggested by Julivert

	Bodón Domain	Pedrosa Dom.	Alba Domain
Minimal shortening	41 %	65 %	25 %
Displacement widths	1,61 - 1,76km	1,02 - 1,40km	0,31 - 0,63km

Table 3.1. Values for the minimal shortening and displacement widths along the transect. See Chapter 3.6.6 for an explanation and Figure 3.15 for the constructed and balanced transect.

& Arboleya (1984), who proposed 40-50% shortening for the Cantabrian Zone and Oczlon (1992) and Ábalos et al. (2002), presuming 70-80%. On one side, Oczlon (1992) and Ábalos et al. (2002) consider the whole Cantabrian Zone (Narcea Antiform to the Pisuerga-Carrión Domain, see Fig. 2.1). The tectonic shortening in the inner part of the Variscan Orogen is expected to be significantly higher. On the other side, as already mentioned, the values obtained by this work for the Southern Cantabrian Basin do not consider internal and out of plane deformation. Potent (2000) assumes 60% shortening, balancing a 6.3km long cross-section of the highly deformed Montuerto syncline (Curueño valley).

Displacement widths reflect the structural differences between the three different domains (see Table 3.1). With regard to the timing of the Variscan thrusting, the youngest nappes (Alba domain; pin lines 9 & 8) show the lowest displacement widths (0.63km and 0.31km) along transect. The imbricated thrust system of the Pedroso domain (pin lines 7, 6, 5, 4) possesses uniform values of 1.02km to 1.40km, whereas the Bodón domain (pin lines 2 & 3) features the highest values (1.76km and 1.61km). Values for the northernmost nappe (pin line 1) are not significant, as the León Line thrust system conceals the cut-off lines. Increasing displacement widths to the north can be explained by the later deformation phases, steepening the thrusts by a southward-vectored compression regime. The overall shortening caused by displacement along the thrusts totals 9.21km. This value corresponds to 48% of the total minimal shortening (folding plus thrusting). In other words, thrusting and folding cause approximately the same amount of shortening along the Bernesga Transect.

CHAPTER 4: SEQUENCE STRATIGRAPHY

Sequence stratigraphy is used in order to obtain an accommodation model based on a chronostratigraphic framework for a specific basin fill. It subdivides the basin fill into genetic packages bounded by unconformities and their correlative conformities (Emery & Myers 1996). The resulting subdivision can be used for correlating cross-sections and, particularly in exploration, as a tool for predicting facies distribution.

The concept of sequence stratigraphy is based upon the studies of Sloss (1962, 1963) and was introduced and developed by numerous authors such as Vail et al. (1977), Posamentier et al. (1988), Posamentier & Vail (1988), Sarg (1988), van Wagoner et al. (1988, 1990) and others. It first gained access to basin modelling through the work of Jervey (1988). Van Wagoner et al. (1988) give a concise overview of the fundamentals of sequence stratigraphy.

In contrast to the first sequence stratigraphic concepts, ongoing work stressed the importance of previously underestimated attributes such as (i) the influence of sediment supply on the accommodation space development (Thorne & Swift 1991, Posamentier & James 1993, Schlager 1993), (ii) the importance of compaction-induced and flexural-induced subsidence (Cloetingh 1988, Reynolds et al. 1991, Steckler et al. 1993) or (iii) the combined influence of total subsidence and eustatic sea-level changes on the accommodation space development (Jordan & Flemings 1991, Reynolds et al. 1991, Steckler et al. 1993, Bowman & Vail 1999).

Depending on the data available and the time-span investigated there are different hierarchies of cycles. Duval et al. (1998) described four main hierarchies of stratigraphic cycles, dependent on their duration. Cycles within different cycle-orders are controlled by distinct factors, such as tectono-eustasy, rate of tectonic subsidence, glacio-eustasy or autocyclic processes. However, many of these factors are still a matter of debate (Cloetingh 1988, Miall 1986 and many others), especially during greenhouse climates.

4.1 Constraints for the present model

Chapters 2 and 3 illustrated the complex structural setting of the Cantabrian fold-and-thrust belt. Even though the spatial relationships between measured cross-sections were reconstructed by structural balancing (see Chapter 3.6.6), the outcropping geological record of the Southern Cantabrian Basin remains restricted. The Variscan fold-and-thrust belt offers repetitive slices through the basin in every thrust sheet rather than a continuous section along the whole course of the basin. Consequently, there is a lack of sufficiently high-resolution information for a temporal and spatial sequence stratigraphic interpretation. The following data cannot be gathered in the field:

(i) Stacking patterns, (ii) coastal onlap and (iii) stratal geometries and terminations. Additionally, neither seismic sections with reasonable seismostratigraphic resolution, nor well data are available. In comparison to sequence stratigraphic studies based primarily on well information, low-resolution seismic information and the long time-span of the Southern Cantabrian Basin evolution, only second order transgression/regression cycles (3-50Ma) were investigated in this study.

4.2 Stratigraphic gaps and transgression/regression cycles

The basin is separated by several major unconformities. However, even though there is no doubt about the presence of these hiati, their duration cannot be estimated with sufficient precision. The time-interval of the stratigraphic gaps ranges between a minimum of 3Ma (Hiatus 5) and a maximum of 24Ma (Hiatus 3). In the following, only major hiati in the region are listed (see Fig. 2.21 and 8.1).

The basin architecture experienced a polyphase development during the evolution of the Southern Cantabrian Basin. The sedimentary fill of the basin is divided into second-order cycles (3-50Ma) following the hierarchical concept of cycles proposed by Duval et al. (1993). Second-order cycles represent transgression/regression cycles caused by changes in the rate of tectonic subsidence in the ba-

sin, or rate of uplift in the sediment source terrane (Emery & Myers 1996).

The overview of parameters for the Southern Cantabrian Basin development are summarised in Fig. 8.1. The oldest unconformity is the angular unconformity between the Mora and Herrería formations. Its origin is still a matter of debate (see Chapter 2.3 and Figure 2.10). However, as the Mora Fm. marks the rheological basement for the present model, this unconformity is not investigated in the present work.

TC 1

Starting with the Herrería Fm., the facies development in the southern part of the Bernesga Transect points to a long-term transgression cycle with a fining upward development from the lower member (conglomerates, sandstones, sandy limestones), passing the sandy middle member and finally reaching slightly deeper marine deposits (sandstones, shales, dolomite lenses) in the upper member. This so-called "Cambrian transgression" (Vail et al. 1991, Liñán et al. 2002) has been described as a long-lived global event marking the beginning of a transgressive phase of the first major Phanerozoic flooding cycle. This major transgression cycle is interrupted by three relative sea-level drops recorded in the Lower Cambrian of Iberia (Córdoba, Cerro del Hierro and Daroca regressions, see below). See Liñán et al. (2002) for further detail. There is no information available about thickness variations along the Bernesga Transect. The formation crops out only in the southernmost and northernmost part of the basin and is always cut by thrusts in the north. However, further to the west, Aramburu et al. (1992) reports an increase in thickness from south to north.

RC 1

The transition to the Láncara Fm. is gradual. The lower member (shallow marine carbonates) of the Láncara Fm. can be defined as a regression cycle, with a prograding shallow marine platform. This regression has been called "Daroca regression" by Liñán et al. (2002). The discontinuity separating the lower from the upper member of the Láncara Fm. represents an important transgressive surface. An erosive contact is developed in the Esla nappe (Álvaro et al. 2000 b).

TC 2

The transgressive surface marks the beginning of the transgression cycle TC 2, which can be correlated to other neighbouring platforms of the Mediterranean region (Bechstädt & Boni 1989, 1994; Álvaro & Vennin 1996, 1997; Álvaro et al. 1999). It is characterised by glauconitic pellets and reworked material from underlaying beds (Álvaro et al. 2000 b). A second discontinuity is located at the base of red nodular limestones and intercalated shales. These nodular limestones with a more open marine fauna (Álvaro et al. 2000 b) are a good marker throughout the entire region and indicate a rapid deepening of the depositional environment. According to Bechstädt et al. (1988), Bechstädt & Boni (1989), Aramburu et al. (1992) and Russo & Bechstädt (1994) this discontinuity marks a slightly diachronous, tectonic breakdown of the Cambrian carbonate platforms from Northern Spain to Sardinia and Montagne Noire. The TC 2 probably reaches into the lowermost shales of the Oville Fm.

RC 2

High siliciclastic input of the Oville Fm. initiates the RC 2. The regressive pattern of the Oville Fm. is documented by a coarsening upward succession of the rapidly prograding deltaic system. The progradation is also reflected in the diachronity of the formation and its members (Barrois 1882, Lotze 1961, Sdzuy 1961, 1968, Zamarreño & Julivert 1967, Liñán et al. 1993). RC 2 continues with the deposition of the La Matosa Mb. (Barrios Fm.). The coarsening upward trend persists in this member, and ends with the development of the first subaerial, erosive hiatus at its top. Both the Láncara and the Oville formations reach their greatest thicknesses in the southern part of the transect.

Hiatus 1 (~15Ma)

The La Matosa and Tanes members of the Barrios Fm. are separated by a major erosional unconformity (500-485Ma; Late Cambrian to top Tremadocian). However, similar facies of the members often conceals the exact position of the unconformity.

TC 3

In contrast to the La Matosa Mb., the Tanes Mb. of the Barrios Fm. becomes finer to the top and is

interpreted as a transgressive succession. Both the base of the Tanes Mb. and its top are limited by a hiatus (Hiatus 2). The members of the Barrios Fm. have a relatively consistent thickness across the whole transect.

Hiatus 2 (~10Ma)
The Tanes Mb. of the Barrios Fm. is separated from the Capas de Getino by another major unconformity (475-465Ma; Middle Arenigian to Middle Llanvirnian). As the Capas de Getino are only represented by a few outcrops (e.g. Portilla de Luna) and contain little fossil content, the true duration of this hiatus is uncertain (see below).

RC 4
The time period that follows is concealed due to poor biostratigraphic information and only a few outcrops. The overlaying Capas de Getino are described by numerous authors (Aramburu et al. 1992, Sarmiento et al. 1994, Gutiérrez-Marco et al. 1996) mostly from the southern part of the region. Additionally Aramburu et al. (1996) reports Middle-Ordovician sediments from the Barrios de Luna section as being deposited during the time interval of Hiatus 2. The duration of the stratigraphic gaps before and after the deposition of the Capas de Getino may consequently overestimate the true extent of the hiati at least in the southernmost part of the Bernesga Transect. The maximum duration can be assumed for the northern part of the transect. The facies development of the Capas de Getino shows a shallowing upward tendency of condensed sediments. In the Portilla de Luna section alternating black shales and sandstones are toped by fossiliferous limestones. The following Hiatus 3 with a duration of estimated 24Ma separates the Capas de Getino from the Formigoso Fm. The contact is sharp but not necessarily erosive. It is more likely - at least in the distal part of the basin - that condensed sedimentation of the Capas de Getino lasted much longer than generally assumed, being interrupted by numerous minor hiati. In terms of 2nd order cycles the Capas de Getino represent a regressive cycle of uncertain duration. The greatest thicknesses are recorded in the southernmost part near Portilla de Luna (79m), whereas in the northern cross-sections (e.g. Getino) only a few meters were deposited between the Barrios Fm. and the Formigoso Fm.

Hiatus 3 (~24Ma)
The largest stratigraphic gap is assumed to exist between the Capas de Getino and the Formigoso Fm. (459-435Ma; Caradocian to Middle Llandovery). The duration of this correlative unconformity might be considerably shorter in the distal parts of the basin, as indicated by new discoveries of age-indicative fossils (Aramburu & García Ramos 1993, Aramburu et al. 1996, see below).

RC 5
After a rapid deepening of the whole region, sedimentation of black graptolitic shales (Formigoso Fm.) started above a transgressive surface. The Formigoso Fm. shows a shallowing and coarsening upward succession deposited in a regressive cycle. The succession is well visible in the Bernesga valley starting with black graptolitic shales (Bernesga Mb.) deposited in an offshore position. Towards the top (Villasimpliz Mb.), alternating shales and sandstones with abundant hummocky cross stratification and ripples point to deposition above the storm wave base in lower shoreface depths. RC5 also includes Member A of the San Pedro Fm. which conformably overlays the Formigoso Fm. Richardson (2001) reports the absence of Wenlockian fossils in some sections, implying a stratigraphic gap between the two formations. However, the contact between the formations is gradual, making it difficult to locate the boundary. The top of Member A marks maximum regression and is topped by a transgressive surface (base Mb. B). The Formigoso Fm. has a major depocenter in the northern part of the Bernesga transect (Millaró section), a sharply diminished thickness in the Getino section, which continuously thickens to the south. By comparison, the San Pedro Fm. diminishes from 165m in the Olleros section to 56m in the Millaró section (see Fig. 3.5 for the geographical position of the sections).

TC 6
Member B of the San Pedro Fm. was deposited in a slightly deeper environment than Member A as indicated by decreasing grain-size, the loss of shallow-water sedimentary structures and iron-oolites as well as the occurrence of hummocky-cross-stratification. Towards the north, Members B and C are reduced in thickness until they completely disappear in the proximal sections as a result of erosion

(e.g. Millaró, Los Chabanos). In Millaró, dolomites of the Abelgas Fm. are situated on top of the lower part of Member A, which indicates that Member A was also affected by erosion (see section Millaró in the appendix).

RC 6

Due to erosion in the proximal sections, TC 6 and RC 6 are based on information from distal areas (southern branch of the Alba syncline), where Member B and C of the San Pedro Fm. are preserved. Member C (sandy, coastal deposits) is interpreted as having been deposited during a regression cycle, which passes in an erosional unconformity in proximal sections. This marks maximum regression and maximum basinward shift of coastal onlap. It has to be mentioned that poor biostratigraphic information makes it difficult to estimate the true time-spans of the San Pedro Fm. members.

Hiatus 4 (~equivalent to upper RC 5 – RC6)

The San Pedro Fm. contains an intra-formational, erosional hiatus in the proximal part of the Bernesga Transect. In the northern sections the Abelgas Fm. rests erosively on the lower part of Member A (San Pedro Fm.), whereas in distal sections (e.g. Barrios de Luna) the San Pedro Fm. succession seems to be complete. Thus, the duration of the hiatus increases in a northern, proximal direction. However, the exact duration is hard to estimate, as the facies of the San Pedro Fm. contains only spores, acritarchs and Chitinozoa for dating (Richardson et al. 2000, 2001). A major fall in eustatic-sea level occurred at the Ludlow/Pridoli boundary (see Fig. 7.9) and might be responsible for erosion in proximal areas.

TC 7

With the onset of the Abelgas Fm. the whole area was flooded. This indicates the start of a new transgression cycle. As already mentioned, the Abelgas Fm. onlaps on progressively older sediments to the north, as the underlying San Pedro Fm. was partially removed by erosion. The Transition Unit, Lumajo Mb. and the lower part of the Dolomite Mb. were deposited above the transgressive surface.

RC 7

Going by the conodont dating by Keller & Grötsch (1990), the upper part of the supra/intertidal Dolomite Mb. progrades over deeper marine sediments of the Lumajo and Wavy Limestone members. This marks a new short-term regression cycle.

TC 8

TC 8 commences with a transgressive surface at the base of the Millaró Mb. The deepening of the depositional environment continued in the entire region with the deposition of the Esla Fm. and its dark offshore shales.

RC 8

At the top of the Esla Fm. the Villayandre Mb., composed of shallowing upward marls and crinoidal grainstones, points to the onset of a new regression cycle. The transition from the Esla Fm. to the Santa Lucía Fm. is based on the diminishing influence of terrigenous mud. The coastal onlap migrated basinward and was situated at approx. km 12 along the transect during the onset of the Santa Lucía Fm. The biggest depocenter of the Santa Lucía Fm. is clearly situated around the type locality near the village of Santa Lucía with diminishing thicknesses to the north and to the south. The reefal facies is generally thicker than the fore-reef and lagoonal facies (see also Chapter 2.4.4).

RC 9

A drowning unconformity developed on top of the Santa Lucía Fm., visible for example in the Beberino section (see Appendix). As this unconformity is equivalent to the 2nd order maximum flooding surface, a new regressive cycle begins. The transgressive cycle is located within the drowning unconformity. The contact between the Santa Lucía and Huergas formations is interpreted as an omission surface by Buggisch et al. (1982). These authors propose that an important palaeokarst surface developed near Sagüera at the southern branch of the Alba Syncline. However, the lack of any characteristic palaeokarst indicators (such as red clay deposits, relict sediments etc.) and the palaeo-geo-

graphic position of this outcrop at the deeper, distal part of the shelf, tend to support the presence of a thrust contact, as proposed by Rodriguez Fernandez (1989).

The Huergas Fm. probably contains a higher-order regressive cycle in the middle of the formation, composed of coarser material than the underlying and overlying parts. However limited outcrop conditions prevent further interpretation.

The RC 9 continues with the Portilla Fm., which is characterised by two episodes of reef formation and separated by a siliciclastic to ooidal middle part. Consequently the formation can be divided into several higher-order T-R-cycles (see also Fernández et al. 1997). However, due to the short duration of deposition (approx. 3Ma), the formation is interpreted as one single regression cycle. Coastal onlap shifted 20km basinward, being situated at approx. km 32 along the transect.

The position of reefal edifices is associated with the course of the IALF. This feature was already present during Santa Lucía times, but becomes obvious during the deposition of the Portilla Fm. It was interpreted by Reijers (1972, 1974) as hinge line movements between the shelf and the basin, providing a suitable position for reef growth along the hinge line. Consequently, these movements already started during the deposition of the Santa Lucía Fm.

In the Beberino section (see Figure 4.1 and Appendix) a huge wavy contact between the Portilla and the Nocedo formations is present. These channel-like features are 3-8m deep and were interpreted as palaeokarst features by numerous authors (Van Staalduinen 1973, Herbig & Buggisch 1984). However, as in case of the outcrop in Sagüera (see above), no characteristic palaeokarst indicators (such as red

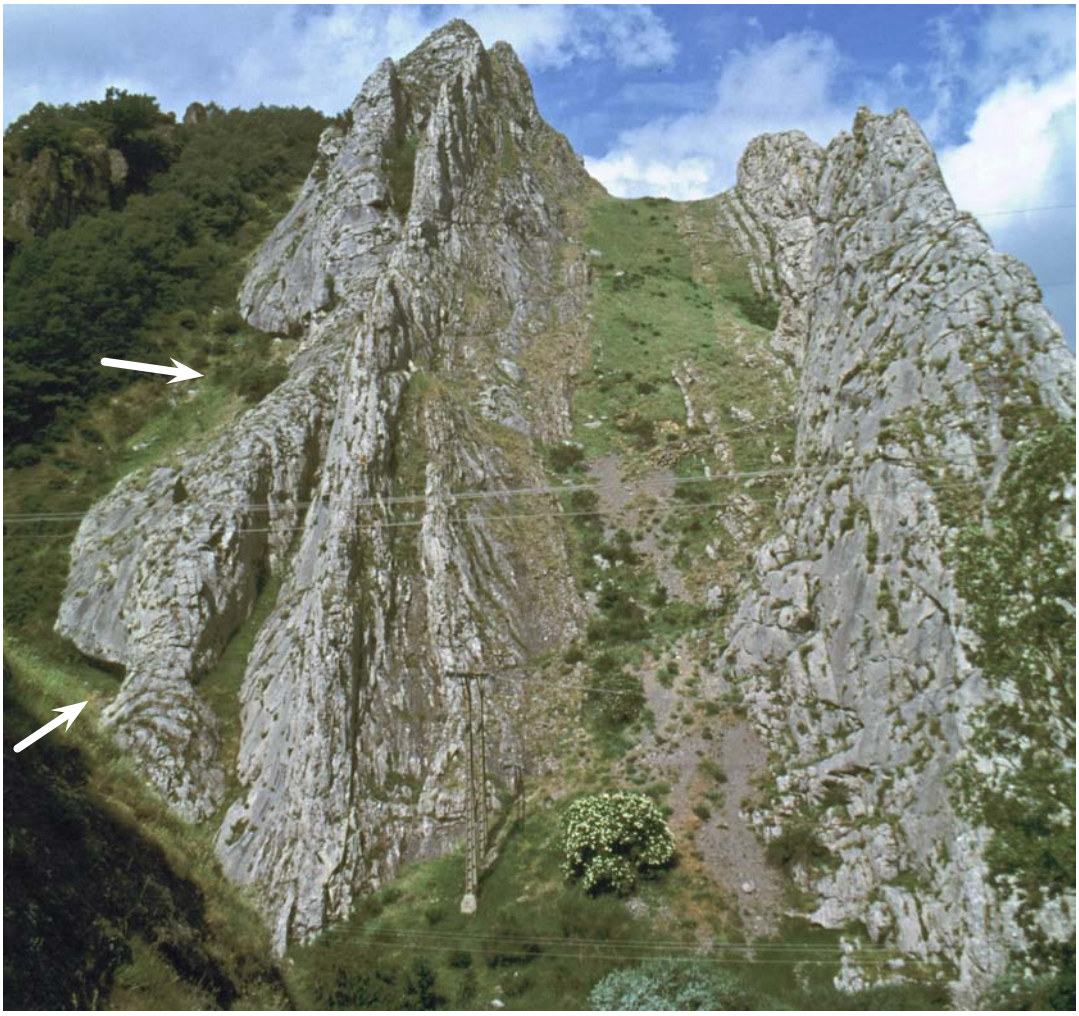

Fig. 4.1. The Beberino section showing the three members of the Portilla Fm. The channel-structures to the left (shown by arrows) of the outcrop are caused by submarine erosion of semi-lithified material or represent submarine dunes composed of crinoidal debris.

clay deposits, relict sediments etc.) are present. Additionally the smooth wavy surface is very atypical of karstification surfaces. The isolated occurrence of only one section (approx. 250m) also contradicts the palaeokarst theory. The presence of reefal buildups can be excluded, as the mounds are solely composed of coarse, sandy crinoidal grainstones. In the present work the interpretation offered by Frankenfeld (1981) is preferred, proposing submarine erosion of semi-lithified material. Alternatively the wavy contact may represent a number of submarine dunes, composed of crinoidal debris.

RC 10

The RC 10 cycle can, for example, be observed in the Huergas section (see Appendix). It covers the Gordón Mb. of the Nocedo Fm., deposited in a coarsening upward succession. Shales and siltstones are gradually replaced by argillaceous sandstones and clean sandstones. Towards the top of the member these sandstones are cross-bedded and topped by several tens of meters of cross-bedded crinoidal grainstones. The latter was interpreted as a transgressive unit, based on sections from the Esla region (Van Loevezijn 1986). However, as no information is available from this area in the present work and the carbonate unit is overlain by clean littoral sandstones with abundant herring-bone cross-stratification (Huergas section), it is included in RC 10. However, it might represent a higher order transgression cycle within RC 10. By comparison with RC 9, coastal onlap shifted only slightly basinward. The depocenter of this cycle was situated south of the IALF (see Fig. 3.5), indicating a major change of basin architecture.

RC 11

The RC 11 can only be recognised south of the IALF and comprises the Millar Mb. of the Nocedo Fm. The regressive pattern is also documented by a strong basinward shift of coastal onlap by 12km, now situated at km 44 along the transect. As already mentioned, the basin architecture changed, comprising a highly subsiding southern part and a relatively stable northern part. Sediments transported from a source area in the north bypassed the proximal part of the transect and filled the ensuing accommodation space in the south. The cycle commences with shales and siltstones deposited below the storm-wave base changing to intercalated siltstones and sandstones. It is topped by polymict conglomerates with clasts of up to 20cm in diameter. Consequently a single coarsening upward succession is documented. As already mentioned in Chapter 2.4.4, these conglomerates are composed of exotic clasts (pegmatites, radiolarites, metamorphic quartzites) of uncertain origin (see Chapter 2.2.1 for discussion).

RC 12

RC 12 can also only be observed south of the IALF, showing a similar basin configuration to that of RC 11. RC 12 consists of the Fueyo Fm. and the lower part of the Ermita Fm. The Fueyo Fm. starts with the deposition of shales and intercalated siltstones deposited in an offshore setting. In the Piedrasecha section, abundant fining upward beds indicate a turbiditic origin. This is in concordance with Raven (1983) who described Bouma sequences (A, C, D and E) from the Fueyo Fm. The amount of sand increases towards the top. The lower part of the Ermita Fm. occurs only above the Fueyo Fm. and is absent north of the IALF, where an area of non-deposition persisted. It is composed of siltstones with an increasing number of sandstone beds. Both formations form a single coarsening upward cycle developed south of the IALF.

Hiatus 5 (~1-3Ma)

The shortest, but most prominent hiatus is situated within the Ermita Fm. It is an erosional, angular unconformity covering the latest Famennian (361-358Ma). Towards the north, the upper part of the Ermita Fm. unconformably overlays increasingly older strata. In the most proximal sections (e.g. Llamazares, Redilluera) the Ermita Fm. lies unconformably above the Oville Fm., resulting in a hiatus lasting nearly 150Ma. Consequently, in the proximal sections all hiati stated above converge in one single erosional unconformity. The angle of the unconformity shows values of 0.5° to 1.5° (Smith 1965, Raven 1983).

Thus, the lower part of the Ermita Fm. may be attributed rather to the underlying Fueyo Fm. than to an overlying formation, which would then be split by an angular unconformity.

TC 13

The upper part of the Ermita Fm. marks the onset of a transgressive cycle situated above an erosional hiatus (see above). TC 13 commences with the deposition of medium to coarse-grained sandstones and conglomerates (see Fig. 2.50), with abundant large-scale cross-bedding and erosive channels (see Fig. 2.48 and 2.49). These sediments are interpreted as littoral deposits with possible fluvial influence and cover the entire Southern Cantabrian Basin. The following marine encroachment is evident in the uppermost part of the Ermita Fm. with abundant brachiopod moulds (e.g. Los Chabanos section, Fig. 2.51). The carbonate Baleas Fm. was deposited as shoals and bars above the fair weather wave base. Black shales of the Vegamián Fm. accumulated in more protected and deeper-marine areas. In the southern part of the transect depositional depths reached up to 150m. Finally, condensed sediments of the Alba Fm. (red nodular limestones, intercalated shales, radiolarites) show the highest depositional depths, reaching water depths of up to 300m. These sediments consequently mark the maximum transgression in the basin.

4.3 Basin stages

The rift phase is indicated by a main rifting period during the Early-Middle Cambrian times (Marcos 1973, Bechstädt et al. 1988, Bechstädt & Boni 1989, Pérez-Estaún 1990, Russo & Bechstädt 1994, Álvaro et al. 2000 a, b, Valladares et al. 2002). See Chapter 2.3.1 and Fig. 8.1 for further detail.

The Late Cambrian to Late Ordovician is characterised by several indicators for tectonic activity:

(i) Widespread discontinuities are reported within the Láncara Fm. (see TC2) by Bechstädt et al. (1988), Bechstädt & Boni (1989), Aramburu et al. (1992) and Russo & Bechstädt (1994) from Northern Spain to Sardinia and Montagne Noire.

(ii) Long-term stratigraphic gaps (Hiatus 1 to 3, see above and Fig. 2.21, 8.1) persist in the Cantabrian Zone and Sardic movements are active across the entire northern margin of Gondwana (Gutíerez-Marco et al. 2002).

(iii) Widespread rift-related volcanism is active in Iberia (Ollo de Sapo event, see Chapter 2.3.3), France, Corsica and Sardinia (Dallmeyer et al. 1997, Fernández-Suárez et al. 1998, Crowley et al. 2000, Gutíerez-Marco et al. 2002).

It is likely that the northern Gondwanan shelf is unstable and a site of fragmentation and extension for a long period of time. Periods of quiescence (e.g. the sedimentation of the Oville Fm.) are followed by widespread tectonic activity.

The tectonically quiet, passive continental margin becomes evident when black shales of the Formigoso Fm. are deposited during the Llandoverian. This post-rift stage lasts until the onset of the Variscan Orogeny (Variscan foredeep stage in Fig. 8.1) in the Lower Carboniferous (322Ma).

CHAPTER 5: QUANTITATIVE BASIN ANALYSIS

5.1 Introduction

A sedimentary basin is the result of the sum of all geologic, geophysical and geochemical processes having acted on its component parts during its entire geologic history (Poelchau et al. 1997). Over the past number of decades, geologic investigations have progressed considerably, providing a huge volume of new data. Methods of gaining detailed information about basins have also improved significantly. Computer simulations, employing algorithms that describe the complex interaction of the processes mentioned, can be used to improve our understanding of what controls sedimentary evolution (Aigner et al. 1989). The significance of simulations of sedimentary basins is that, although they may not provide a unique answer to what caused a particular sediment geometry or relationship, they can be used to test hypotheses. These might involve the effects of eustatic change, tectonic movement, and changes in the rates of sedimentation by providing geometries to match outcrops, well log cross sections, and seismic lines (Kendall et al. 1991). Depending on the financial budget, complex data acquisition methods can be used, such as 3D seismic data from reflection and/or refraction sections, well logs, gravity measurements, etc. combined with traditional lithofacial and palaeontological, cross-sectional information. These expensive data acquisition techniques are primarily employed by the oil industry.

5.2 Factors controlling basin-fill development

The Southern Cantabrian Basin is filled by a mixed siliciclastic and carbonate succession. Factors, controlling the basin development partly affect types of deposits, while others affect only one of these. The characteristics and architecture of both sedimentation environments, clastics and carbonates, are influenced by:

(i) Accommodation space development (see below)
(ii) rates and distribution of tectonic subsidence
(iii) rates and distribution of the flexural response of the lithosphere
(iv) compaction of the basement (if compactable) and the sediment itself
(v) extent and geometry of the basin
(vi) antecedent topography and bathymetry
(vii) climate.

Siliciclastic environments are in addition highly dependent on:

(i) Sediment supply from outer sources, influenced by rates of erosion, denudation and characteristics of land areas delivering terrigenous sediments
(ii) rates of sediment flux in the basin.

Carbonate systems are primarily influenced by:

(i) In-situ biogenic production rates
(ii) rates of redistribution
(iii) the impedance of carbonate growth by terrigenous influx.

The depth and distance-dependent functions for light, salinity, temperature, nutrients and oxygen concentration have been discussed in many publications. Light is the dominating factor on carbonate production (Bosscher & Schlager 1992), other factors like lateral sediment transport and accumulation is far less important in this environment. Schlager (1993) attributes changes in platform architecture to changes in accommodation and sediment supply. He investigates different types of carbonate factories and their productivity potential throughout the Phanerozoic (Schlager 2000, 2003). In the overhelming majority of environments, the amount of sediment supply is very important, being it clastic input (Thorne & Swift 1991) or redeposited carbonate sediment and in-situ carbonate production (Schlager 1993). Sediment accumulation volumes (see below) are controlled by the ratio of accommodation to sediment supply (Tinker 1998). Despite of the accommodation space, accumulation rates and lag time are the factors that most influence the geometry and facies of a simulated geological succession (Enos 1991).

5.2.1 Accommodation space

Accommodation space is defined as the amount of space available for sediment accumulation (see below). Accommodation space can be described as a function of eustatic sea-level fluctuations and total subsidence (see Chapter 6.3).

5.2.2 Accumulation rates

Evaluating carbonate accumulation rates is the first step in quantifying the growth potential of a carbonate system. Accumulation rates are the net result of sediment input and in situ production (for carbonate environments) less export through bypass or removal by erosion. The evaluation is particularly possible in shallow-water carbonate environments, where carbonates are produced in-situ within the depositional setting. Accumulation rates depend on depositional environment, symmetry of a basin, climate, tectonic setting, preservation potential, depositional gradients and the time increment being modelled (Enos 1991). An additional problem in the carbonate realm is the dissolution of carbonate matter. Accumulation rates are mostly calculated in 1D at a specific locality and normally given as compacted values. If the sediment supply/production of a system is bigger than the 1D accommodation space for this locality, the accumulation rates at this locality are governed by the accommodation space development and not by the production potential of the organisms. Nearby localities might receive, however, exported carbonate material from this locality, which is often not considered.

5.2.3 Carbonate production rates

Accumulation rates should not be confused with the growth potential of carbonate systems, representing the maximum production potential for a specific sedimentation environment. Production rates calculated in the present model are decompacted values in 2D, indicating the vertical accumulation together with sediment export and bypass. In the carbonate realm, sediment input from outside sources is often negligible compared with in situ production rates, which are of far higher importance (except for the slope and basin margin). On the other hand there are carbonate realms such as tidal flats, where transport controls the sedimentation and in situ production is negligible. In fact all other values are accumulation rates giving only approximate values for production.

5.2.4 Lag time

Lag time is defined as the period of time a carbonate factory needs to reach its full potential after its inundation. Carbonate accumulation lags to a relative rate of sea-level rise, resulting in a deepening succession (Read et al. 1986). Schlager (1981) describes the function of time/production potential. However, Enos (1991) proposes, that lag time is rather a depth dependent parameter (lag depth), governed by a physical basis such as the wave base. The corresponding time would thus be defined by the rate of change in relative sea-level, as a function of eustasy, subsidence, compaction and accumulation rate.

5.2.5 Time span of observation

The observation span has a major impact on calculated sedimentation rates. Schlager (2000) plotted sedimentation rates against the period of observation for many different sedimentary settings. Sedimentation rates of all carbonate and of most siliciclastic systems decrease with the increasing length of the observation span. This is due to periods of non, or reduced deposition (or even erosion) within a given interval. Consequently, we cannot compare short-term events such as the growth rates of modern corals, measured in the tens to thousand-year domain, with the long-term deposition rates of ancient deposits averaging millions of years. It is in the nature of geology that there are exceptions, such as the very stable conditions of the abyssal and bathyal realms.

5.2.6 Flexural response of the crust to loading

Lithosphere, adjacent to local or regional loads such as water, ice, sediment accumulation or approaching orogens, reacts by downwarping in order to reach an isostatic and flexural equilibrium. The greater the loads and/or the time of loading, the more significant the flexural response is. The time required to reach equilibrium depends on the rheological properties of the lithosphere (Einsele 2000, Stüwe 2000). Flexure results from vertical forces, horizontal forces and torques in any combination and effects the elastic upper part of the lithosphere, which retains elastic stresses over geological time scales (Allen & Allen 1990). Primarily, a rapid downwarped flexural depression appears around the load. This vertical deflection decreases sinusoidally away from the load (Einsele 2000). Further away from this dell an upwarped peripheral bulge or forebulge develops (Fig. 5.1). The mass balance equa-

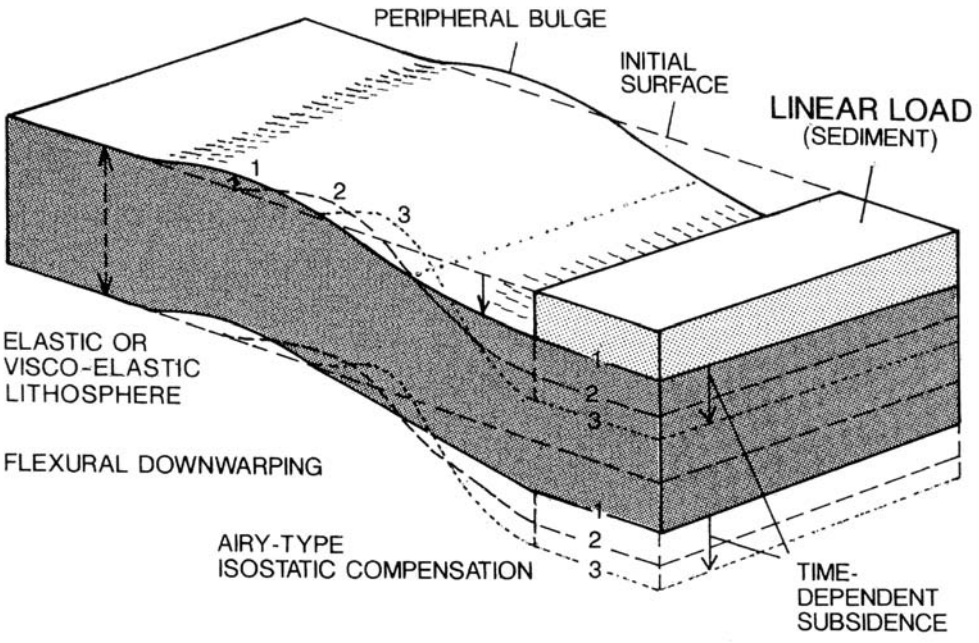

Fig. 5.1. Flexural response of the lithosphere adjacent to wide linear loads, such as orogenic fronts. The subsidence is rapid in the initial stage (1), followed by slow subsidence (2) until an ultimate isostatic equilibrium is reached (3). Also note the migration of the peripheral bulge towards the load (Einsele 2000).

tion normally reflects the mass of displaced material with the applied load. Secondarily, if the load remains in place, a deeper central depression forms together with a narrower basin by means of uplift and progressive movement of the forebulge towards the applied load. The volume of the basin does not depend on the rigidity of the plate (Stüwe 2000).

Flexural rigidity and effective elastic thickness (Te)

The static deformation of the lithosphere can be explained as flexure of a thin competent elastic or visco-elastic plate overlying a viscous fluid (asthenosphere) (Waschbusch & Royden 1992, Watts 1992, Cloetingh & Burov 1996, Einsele 2000, Watts 2001, Turcotte & Schubert 2002). The different properties of the plate (elastic, plastic etc.) control its deflection (Burov & Diament 1995). Modelling 2D-bending of plates is also referred as cylindrical bending because the plate forms a segment of a cylinder (Turcotte & Schubert 2002).

The parameter that characterises the apparent strength of the lithosphere is the flexural rigidity D, which is commonly expressed through the effective or equivalent elastic thickness (Te) of the lithosphere (Burov & Diament 1995, 1996, Cloetingh & Burov 1996, Einsele 2000, Stüwe 2000). Te is not a physical thickness, but can be used to estimate lithospheric strength expressed in response to loading by topography and subsurface loads (Burov & Diament 1996). It provides important information about the history, mechanical and thermal state of the lithosphere, rheological properties and allows comparisons between different plates and the detection of thermal events. For mathematic explanations and comparisons see Stüwe (2000), Watts (2001) or Turcotte & Schubert (2002).

Oceanic lithosphere

Variations of Te for oceanic plates depend on the period of time the lithosphere needs to cool from an initially melted stage to its present thermal state, called thermal age (Watts et al. 1992, Burov & Diament 1996). Te is defined by the following equation:

$$T_e = \left(12D\left(\frac{1-v^2}{E}\right)\right)^{-3} \qquad (5)$$

D - flexural rigidity; E - Young's modulus; v - Poisson's ratio.

Variations in E and v may lead to a 10-20% scatter in estimates of Te (Burov & Diament 1995). Burov & Diament (1995, 1996) assume a 20-25% un-

certainty for the accuracy of most data on Te. Crustal heterogeneities may cause significant (Burov et al. 1998: 40%; pers. com. Zoetemeijer 2003: 70%) local reductions of lithospheric strength. Oceanic lithosphere responds to longterm (>10^6 years) geological loads as an elastic plate that increases its strength with age (Watts 1992, Burov & Diament 1996, Cloetingh & Burov 1996, Einsele 2000, Maggi et al. 2000). The effective elastic thickness (Te) for oceanic lithosphere is marked by a specified isotherm, which defines the base of the mechanical lithosphere. This isotherm is still a matter of debate and authors have obtained values ranging from between 400°C and 900°C:

(i) Watts 1992, McKenzie & Fairhead 1997, Einsele 2000: ***450°C***

(ii) Burov & Diament 1996, Cloetingh & Burov 1996: ***400-600°C***

(iii) Stockmal et al. 1986: ***750°C***

(iv) Ranalli 1994: ***900°C***.

However, more than 75% of all estimated Te of the oceanic lithosphere plot within the range of the 300-600°C isotherm (Fig. 5.2). Deviations of this age/Te dependence have been explained by local thermal anomalies or flexural stress (Cloetingh & Burov 1996) whereas some authors (Stüwe 2000) doubt the relevancy of any isotherm. The average Te for oceanic lithosphere is in the order of 20-30km (Watts 2001), which is approximately 25-50% of the seismic thickness, with most values at about 40%.

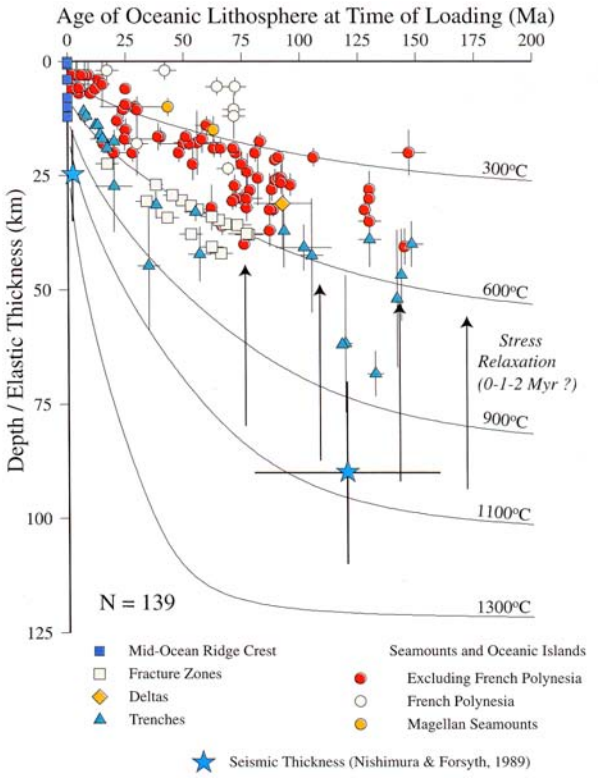

Fig. 5.2. Plot of effective elastic thickness (Te) against the age of oceanic lithosphere at time of loading in Ma. Note that more than 75% of all estimates plot in the range of 300-600°C isotherms (Watts 2001).

Continental lithosphere

Continental lithosphere is more complex, due to specific geological or physical boundaries, multiple deformation, structural inhomogeneities and igneous events (Waschbusch & Royden 1992, Watts 1992, Burov & Diament 1995, Cloetingh & Burov 1996). The major difference between the rheological structures of the continental and oceanic lithospheres is the 4-5 times thicker, heterogeneous continental crust (normally 35-40km; Cloetingh & Burov 1996) and its complex evolution. Continents are characterised by loads of a far longer duration than those in oceans, but the geometry of these loads is often unknown (Watts 2001). Fig. 5.3 shows the dependency of Te on the age of the continental lithosphere at the time of loading. Because of tectonic erosion, denudation, rifting and orogenesis the surface loads are either not well preserved or removed/added in continental areas. Burov & Diament (1992, 1995, 1996) and Cloetingh & Burov (1996) suggest that Te in continents not only depends on parameters such as thermal structure (geotherm age), but also on mineral composition and geometry of the plate and the strength reduction caused by mechanical decoupling of the upper-crust and the mantle lithosphere. Mechanical decoupling of the upper crust and mantle lithosphere lead to a significant reduction in Te. Thus, Te of continental lithosphere does not correspond to any geotherm (Burov & Diament 1996, Cloetingh & Burov 1996 and Burov et al. 1998). Fig. 5.4 points out the strong Te-dependence on crustal thickness. Mechanical decoupling between crustal and mantle lithosphere, and consequential strong Te reduction, occur mostly in the case of a thick (>35km) and sufficiently hot crust at Moho depth (Burov & Diament 1996, Cloetingh & Burov 1996). With a thin and cold crust (at Moho depth) no decoupling occurs and the strong lithosphere behaves mechanically in the same way as the oceanic lithosphere. The Te of a thermally young

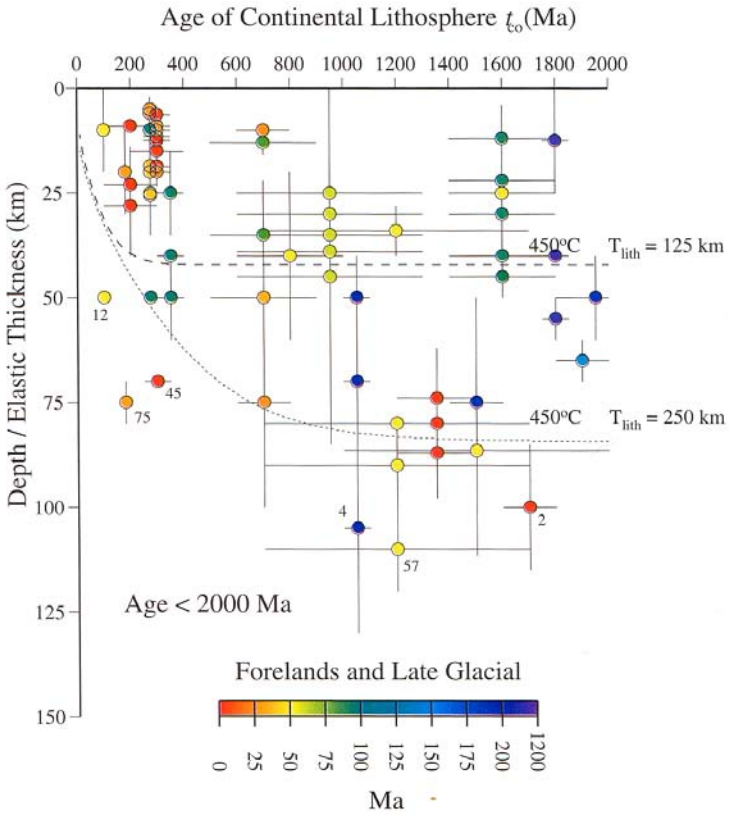

Fig. 5.3. Plot of effective elastic thickness (Te) against the age of continental lithosphere at time of loading in Ma (Watts 2001). Note the wide range of values in comparison to the Te of oceanic lithosphere (Figure 5.2). A better fit to the 450°C isotherm (Karner et al. 1983) was not possible, not with a 250km thick thermal lithosphere, nor with 125km thickness.

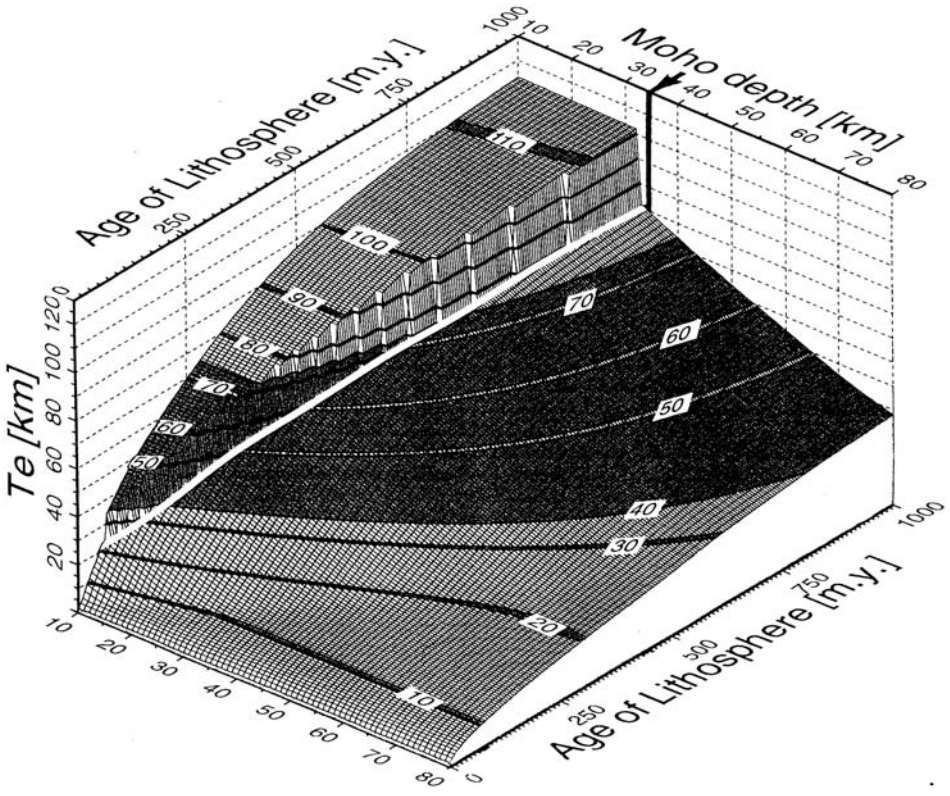

Fig. 5.4. Dependency of Te, thermal age of the lithosphere and Moho-depth/crustal thickness (Burov & Diament 1996). This diagram allows estimations of Te from thermal age and crustal thickness. The white line represents a critical crustal thickness with decoupled regime (reduced Te) below the line and coupled regime above the line.

continental lithosphere is mainly controlled by the crustal strength, whereas the Te of older lithosphere is roughly equal to the thickness of the mechanical mantle. A critical crustal thickness (old lithosphere 35±5km; young lithosphere 15-20km) defines the boundary between the coupled and decoupled state. Thus most continents (75%) are decoupled (Burov & Diament 1996). However, few authors (for example, Doucoure et al. 1996) assume an association between continental Te and the 600°C isotherm.

Despite the wide range of values ranging between 0km and 134km (Watts 2001), Te in the continents has a bimodal distribution with a primary peak at 10-20km and a secondary peak at 80-90km (Watts 1992). High values can be explained as being due to the association with cratons and they reflect low temperature gradients that have been inferred for these regions (Watts 1992, Burov & Diament 1995). The origin of lower values is still not fully understood (Burov & Diament 1995, Garcia-Castellanos et al. 2002). Several suggestions have been proposed as solutions to this problem, such as viscous relaxation of stresses during flexure, mechanical decoupling between crust and mantle, plastic yielding in the lithosphere during its bending, presence of a compressional tectonic force during bending or additional heating of the lithosphere. However some authors (McKenzie & Fairhead 1997, Maggi et al. 2000) are not convinced that the Te of continental lithosphere exceeds 25km. They propose that there is a close link between Te and the thickness of the seismogenic crust and a weak mantle beneath the continents rather than a weak lower crust between a relatively strong upper crust and mantle.

Te-estimations of continental lithosphere

Te of continental lithosphere can be estimated by several observations such as the external loads or the plate deflection caused by these loads. These parameters can be gained from estimations of Moho geometries, Free air and Bouguer anomalies, thermal flux, bathymetry, spectral analysis, earthquake focal depths, 2D forward mechanical modelling or the correlation between topography and gravity anomalies (Burov & Diament 1996, Cloetingh & Burov 1996, McKenzie & Fairhead 1997, Burov et al. 1998, Maggi et al. 2000, Watts 2001). An important additional factor that may influence any Te assumptions is the use of the present day geotherm.

Actual values for foreland basins vary widely. Some forelands are associated with low values of 5-15km (Apennines, Dinarides, Taiwan: Kruse & Royden 1994, Lin & Watts, 2002) while others are associated with intermediate values of 40-55km (Tarim: Lyon-Caen & Molnar 1984) or values as high as 50-70km (Appalachians: Stewart & Watts 1997). Low levels of flexural rigidity will produce narrow and deep basins, whereas high values are associated with wide, shallow basins. This fact suggests that the tectonic setting may be a significant factor determining the Te of continental lithosphere.

Einsele (2000) expects the densities of the underlying viscous mantle material and the overlying water body and/or sediments to be the most important factors controlling the bending of the crust. Some authors (for example Stockmal et al. 1986) suggest the size of load to be the driving factor on the development of foreland basins. If the load becomes too big and loads the plate to its limit, the plate may break rather than flex. This has been proposed as an explanation for rather strange observations in Taiwan (Lin & Watts 2002). However the discrepancy between the seismogenic layer (mostly 25km thick; peak at 10-15km) and continental Te (0-120km, no peak) has still not been explained (Watts 2001).

There are several mechanisms increasing or decreasing Te. Ongoing orogeny decreases the strength (Te) of the lithosphere underlying the orogenic belt. On the other hand, plate unloading due to erosion or postglacial rebound will increase Te. Thus Te reflects an ongoing dynamic balance between the topography, plate-boundary forces, and lithospheric structure (Burov & Diament 1995). The age of the lithosphere is important in this context. Tectonic stress of 200-500Mpa may decrease the Te of a 400Ma old lithosphere by 15-20%, but for lithosphere younger than 200Ma this decrease may be as large as 30% for the same level of stress (Cloetingh & Burov 1996).

Cantabrian Zone

Although Europe's lithosphere constitutes one of the best-investigated areas in the world, there are many uncertainties when it comes to estimating lithosphere strengths for a particular region. In order to compare Te of investigated regions with the

Cantabrian Zone, the plate age and the load age for each increment have to be estimated. Unfortunately, these ages are uncertain in many cases. Rock ages only reflect the age of the last thermal event and, in addition, the duration of a loading event is often long (Watts 2001). It is therefore difficult to determine the precise plate and load age.

The geologic history of Iberia reflects a wide spectrum of plate configurations (see Chapter 2.3). After a Precambrian/Cambrian rifting and drifting stage, the area remained at the passive continental margin of Gondwana for a long period of time and subsequently involved in the convergence and collision of Gondwana and Laurussia. These different paleogeographic positions require corresponding Te-values for each lithosphere composition. For this model the absence of a substantial difference between the mechanical behaviour of very old Precambrian lithosphere and middle-aged Variscan lithosphere (Cloetingh & Burov 1996) is of great significance. It suggests a minor temperature control on Te variations after approximately 400Ma. Continental Te in foreland basins displays values between 0km and 120km (Watts 2001). Extensional basin settings such as continental rift valleys or passive continental margins generally show lower continental Te values within the range 3-60km (Watts 2001).

The actual average Te of European continental lithosphere is in the order of 20-30km (Fig. 5.5) but before the Variscan orogeny Te might have been much

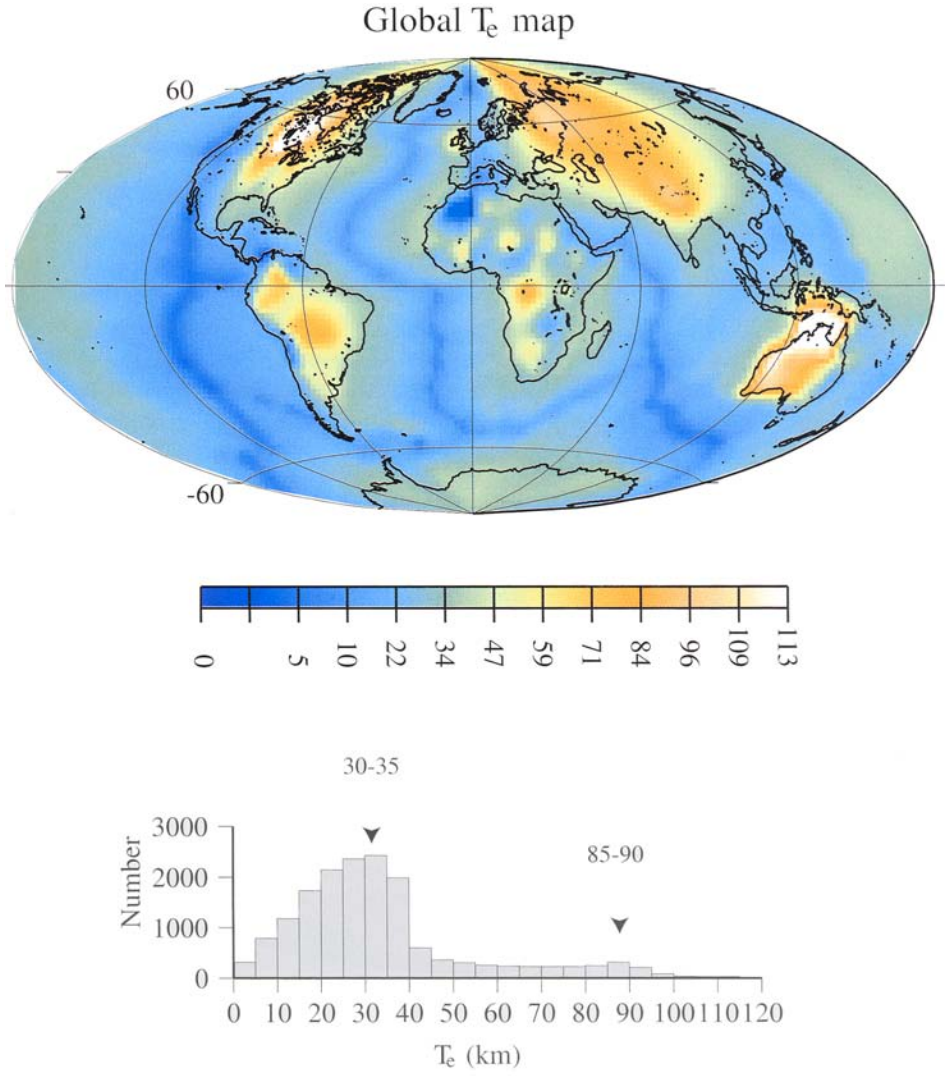

Fig.5.5. Map of global distribution of effective elastic thickness (Te). The oceanic Te is determined by the 450°C isotherm. Contours on continents are based on coherence results (Watts 2001). The lower diagram shows the bipolar distribution of continental Te with a major peak at 30-35km and a minor peak at 85-90km. Note the present day Te distribution of passive continental margins with Te values ranging between 10 and 70km.

stronger. According to Zoetemeijer (pers. com. 2003), Te might have been around 50-100km, comparable to a North American type of lithosphere. The depth of the Moho in the Southern Cantarian Mountains has been well established in 1997 (Santanach 1997). According to the deep seismic reflection survey ESCI-N, the characteristics of the Cantabrian basement at lower-crustal levels and the thin-skinned structure is similar to the Appalachian Foreland (Pérez-Estaún et al. 1994). According to Turcotte & Schubert (2002) this would result in Te of 54km. However, García-Castellanos (2002) classifies the Te values of most of the modern foreland basins in a relatively narrow range of 15 to 40km.

In Fig. 5.6 different flexural-induced subsidence values, obtained from 2D reverse basin modelling, was plotted along the Bernesga transect at 389Ma and 317Ma. Colored lines represent effective elastic thicknesses (Te) ranging from 10km to 100km. There is a similar trend with low trajectory gradients for Te values higher than 30km. Very low Te values (<20km) are represented by higher gradients of flexural induced subsidence due to the low rigidity of the lithosphere. Only at these values a reversal of the dip towards a fictive forebulge is visible. However, the wavelength for stiffer plates is not long enough to show a forebulge within the length of the Bernesga Transect. According to Stüwe (2000), common lithospheric rigidities ranging from 10^{22} to 10^{24}Nm, show wavelengths of 100 to 200km.

The Te-values can be estimated using Fig. 5.4 This figure shows the maximum initial (preflexural) Te on the thermal age and crustal thickness (for the mathematical explanation see Burov & Diament 1995, 1996). For young lithosphere (<250Ma) there is almost no effect on Te due to the depth of Moho. Older lithosphere is strongly dependent on its age and Moho depth with regard to the Te development. Thus there are two values which have to be estimated for any Te calculations (i) age of lithosphere and (ii) moho depth.

(i) Age of lithosphere:

In areas where cratonic basement is not exposed (i.e. Variscan belt of Western Europe, see Chapter 2.1), constraints on the age and nature of older basement can be determined by the presence of inherited zircons in magmatic rocks, detrital zircons in sedimentary rocks, and by neodymium isotopic studies (Fernández-Suárez et al. 2000 a, 2002 a, b, Gutiérrez-Alonso et al. 2003). Zircon ages reflect numerous Proterozoic events (2500-2800Ma, 1800-2200Ma, 900-1300Ma, 550-800Ma) indicating the presence of a pre-Neoproterozoic basement (Fernández-Suárez et al. 2002 a, b). The present study commences in the latest Neoproterozoic (560Ma), when this basement had already undergone distinctive thermal overprints (see also Chapter 2.3). At the end of the Neoproterozoic, the northern active margin of Gondwana was the scene of subduction (Fernández-Suárez et al. 1998). During this period, a prominent change in tectonic regime (compression/extension) resulted in further stretching of the back-arc basin and the birth of the Rheic Ocean (Martínez Catalán et al. 1997, Fernández-Suárez et al. 1998, 2000 b, 2002 a, b). Thus for the beginning of the numerical model, a Meso/Neoproterozoic crust with a Neoproterozoic filling of the back-arc basin has to be assumed. Fernández-Suárez et al. (1998) presume that mantle upwelling and upper-mantle to lower-crustal melting in a progressively thinning lithosphere were the factors that triggered this magmatic event. With the formation of the Rheic Ocean, the active margin of Gondwana evolved to a passive margin environment. However, there are signs of crustal thinning and magmatism in Iberia until the deposition of the Armorican quartzite.

(ii) Moho depth:

While the Rheic Ocean was opening, the Moho was only a few kilometres deep. However, throughout the passive margin stage an average crustal thickness of 30-35km can be assumed on the base of present examples. The development of a passive continental margin and Moho depth in time has been a subject of discussion (see Chapter 2.3). The importance of secular cooling, which would lead to a descent of Moho is not very well constrained. According to Watts (1992) and Lin & Watts (2002) a developing foreland inherits the Te-structure of the underlying margin. Therefore no additional adjustments to Te or to the depth of Moho are made for the beginning of the Variscan orogeny.

Te estimations for the Southern Cantabrian Basin

Te for the stretched crust and creation of oceanic crust was estimated to be 5-15km according to the mid-values for rifting areas (Watts 2001). This time-

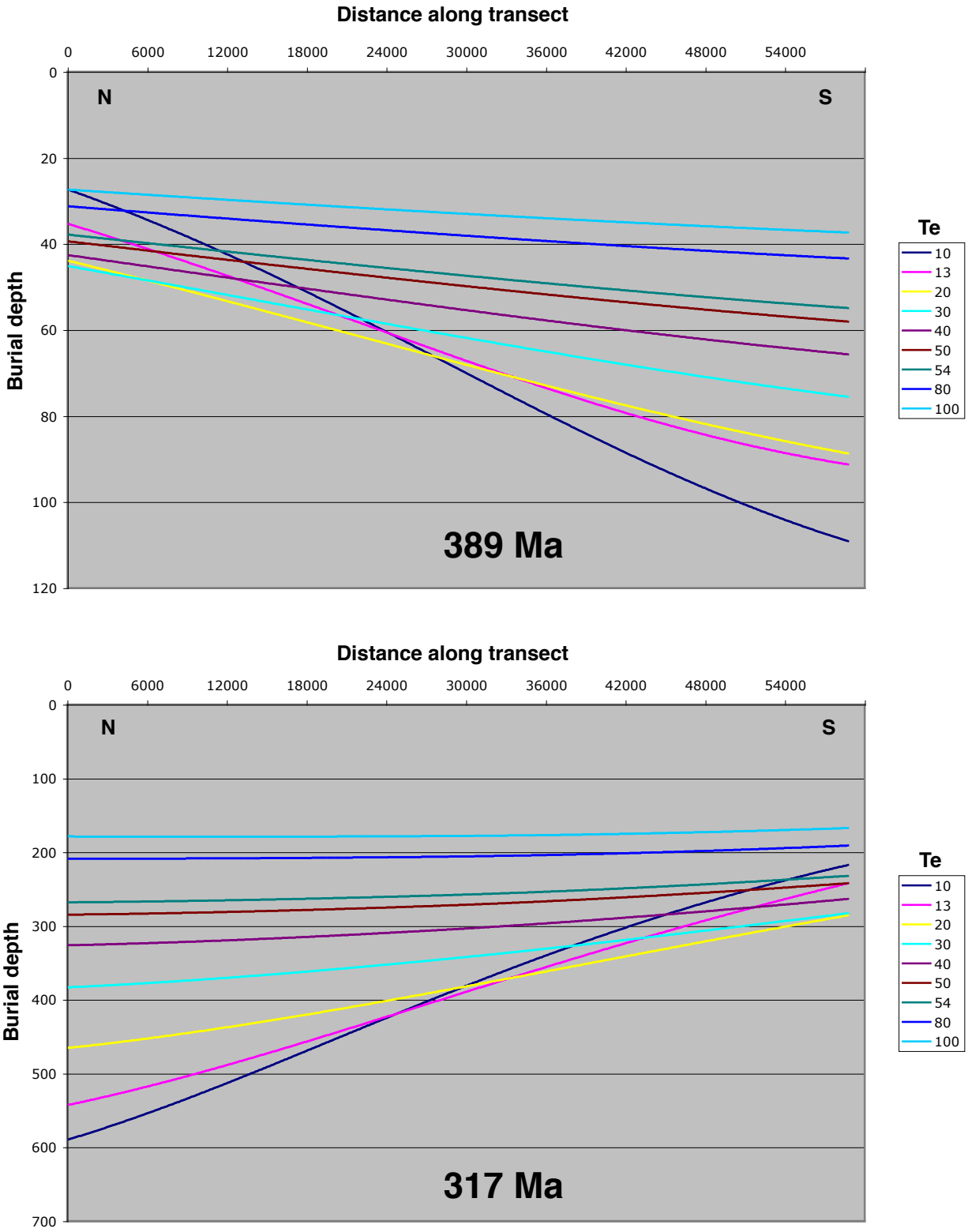

Fig. 5.6. Flexural-induced subsidence rates for two time increments (389Ma and 317Ma) dependent on different Te values ranging from 10 to 100. Note similar behaviour for Te values 30-100km. The length of the transect is generally too short for the development of a fore bulge. However, Te values <20 show a trend towards a reverse dip and the development of a fictive fore bulge. Compare Figure 6.2 for the basin architecture of the time increments.

span lasted from the Precambrian to the Early Cambrian. However the magmatic event in the Ordovician points to further extension of the continental margin. Estimations can only be made concerning the further development of Te on the passive margin of Gondwana. Te values for passive margins vary from 5 to 60km with a peak between 10-30km (Watts 2001 and references). However, a problem with most of the estimates is, that they represent the average response of the lithosphere to sediment loading. They do not refer to a particular crustal type (e.g., stretched continental crust) or age since rifting (Lin & Watts 2002). In this work a slight increase of Te in time has been adopted for the development of the passive continental margin. In respect to the length of the present transect (54km) there are significant differences in the flexure of the continental plate only where Te values are less than 20km (see Fig. 5.6.). A linear increase of Te from 10 to 60km has been applied for Late Ordovician to Early Carboniferous for 2D stratigraphic forward modelling. As 2D reverse basin modelling only allows one value for the entire time modelled, a mean value of 35km has been chosen.

5.3 History of quantitative basin analysis

In 1962 Sloss proposed the first modern stratigraphic model, suitable as a basis for quantitative modelling. The first modern-style dynamic model of basin filling is the one of evaporite sedimentation by Briggs & Pollack in 1967. In 1978 a number of publications incorporate a broad variety of quantitative models for: (i) basin subsidence on viscoelastic lithosphere (Beaumont 1978), (ii) alluvial architecture (Leeder 1978), (iii) thermal subsidence following extension (McKenzie 1978), (iv) river-channel width for channels with active sediment transport (Parker 1978) and (v) the relationship between shoreline and sea-level influenced by tectonic subsidence (Pitman 1978). Further development, well summarised by Paola (2000), passed "rigid-lid" models with a fixed horizontal sediment surface and went on to "geometric models" (see definition below) with prespecified geometries assigned to surfaces associated with various environments. Dynamic models (see definition below) mark the present state of modelling sedimentary systems and of basin analysis (Aigner et al. 1989, Allen & Allen 1990, Cross 1990, Franseen et al. 1991, Boscher & Schlager 1992, Flemings & Grotzinger 1996, Kendall et al. 1991, Liu et al. 1998, Harbaugh et al. 1999, Bowman & Vail 1999, Burgess et al. 2001, Csato & Kendall 2002 and others). A concise overwiew of the advantages and disadvantages of existing stratigraphic computer programmes is given in Bowman & Vail (1999).

5.4 Different types of modelling

In the following, examples will be given only of models related to the topic of the present work - basin modelling. Regardless of the model's specification, there are four types of models applied in basin studies: tectonic deformation models, basin-fill models, groundwater fluid-flow models and thermal-history models (Poelchau et al. 1997). The present survey only covers the first two models.

5.4.1 Tectonic deformation models

Many basins are structurally complex, because they have been affected by tectonics during or after sedimentation. Structural balancing offers information about relationships between single tectonic units, former lateral extent (amount of basin shortening) as well as architecture of the basin and spatial relationships between measured cross-sections before orogenic movements. Chapter 3 deals in detail with structurally balanced cross-sections.

5.4.2 Basin fill models

Analysis of basin fill comprises qualitative and quantitative models. The majority of publications deal with qualitative basin models. Controlling factors and quantitative values are poorly evaluated and the interaction between different controlling factors is generally loosely constrained or inadequately defined.

Quantitative basin analysis by means of numerical modelling analyses changes of controlling parameters, which govern the development of a sedimentary basin in time. The parameters comprise: (i) subsidence rates (total, thermo-tectonic, compaction-induced and flexural-induced) and uplift, (ii) porosity and density, (iii) palaeobathymetry, (iv) sedimentation and erosion rates, (v) facies distribution, (vi)

initial bathymetry and (vii) crustal parameters (effective elastic thickness, density etc.). These models reconstruct basin history, establishing patterns in changes of the controlling parameters.

Einsele (2000) and Paola (2000) distinguish between two groups of basin filling models on the basis of the sediment surface: (i) Geometric models with a surface with predetermined geometry and balanced sedimentation and subsidence rates. The simplest type is a "rigid-lid" model with a fixed horizontal surface. (ii) Dynamic models taking into account sediment transport and deposition rates. The resulting model reflects lateral changes to different processes in time (creation/destruction of accommodation space, sediment input, erosion), which can modify the basin geometry.

Dynamic models, such as in the present study, use a combined approach of deterministic reverse basin and stochastic forward simulations in order to analyse the geological development in time (see below). The spatial and temporal development of petrophysical and sedimentary parameters is investigated from the deposition of the oldest sediment in the basin to the present-day state. The main aim of stochastic computer models is to compare present day outcrop-data with virtual results, and to determine the complex interactions of controlling factors in an iterative process. Such investigations also provide a powerful tool for geological predictions in areas with a poor geological record (Paola 2000).

5.4.3 Question of dimension

1D models, focused on the simulation of sequences by vertical accretion, generally ignore lateral transport (Read et al. 1986). However, this essentially rules out the possible existence of autocyclic sequences that are controlled by lateral sediment progradation (Ginsburg 1971). Nevertheless, one-dimensional models offer an effective, fast tool for simple basin analysis.

In a 2D model a second, horizontal dimension is added parallel to the mean transport direction. This method displays the most common case in basin modelling, as it represents the best compromise between a reasonably accurate sedimentological approach and acceptable computing time (see Chapter 7).

3D models require a high-level of software and hardware as well as an excellent database. Some geological conditions require a 3D-approach such as combined lateral and transversal sediment transport, basins with multiple interacting source points or highly three-dimensional subsidence (Paola 2000). There are some auspicious solutions available, such as REPRO (Hüssner et al. 1997), DIONISOS (Granjeon & Joseph 1999) or CARBONATE 3D (Warlich et al. 2002). However, many depositional systems include too many complexities to be adequately modelled with existing 3D software.

5.5 2D reverse basin and 2D stratigraphic forward modelling within PHIL/BASIM™

The combination of reverse basin (Chapter 6) and stratigraphic forward modelling (Chapter 7) in the present study allows the development of a more rigorous genetic basin development model. This approach is particularly successful at evaluating and demonstrating conceptual models, since parameters can be easily varied, isolated and investigated. In a procedural loop, data from forward modelling can be used to control and modify reverse modelling results, as it considers sedimentary parameters and has a superior spatial and temporal resolution (see Fig. 5.7). Modelling for this study was accomplished using the PHIL/BASIM™ (PetroDynamics Inc., Houston) programme package with its two basic components: PHIL™ Utility (Uppc 020220) for 2D reverse basin modelling and PHIL™ 1.5 (1.5 v. 030404) for 2D stratigraphic forward modelling. Bowman & Vail (1999) published the fundamental algorithms implemented in the stratigraphic simulator. Numerical modelling with PHIL/BASIM™ permits the quantitative analysis of key controls in basin development including their temporal and spatial variations. The program comprises a comprehensive set of sedimentation and deformation algorithms that model:

- Tectonic history (subsidence and uplift)
- Sea-level history
- Palaeoenvironmental parameters/proxies
- Crustal response due to flexural loading of sediment and water loads
- Compaction of sediment
- Traction of siliciclastic sediment in fluvial and coastal settings

- Dispersion of suspension load in marine settings
- Gravity-flow sedimentation (slope failure, turbidites)
- Production and redistribution of carbonate sediment
- Erosion (subaerial, shoreline)

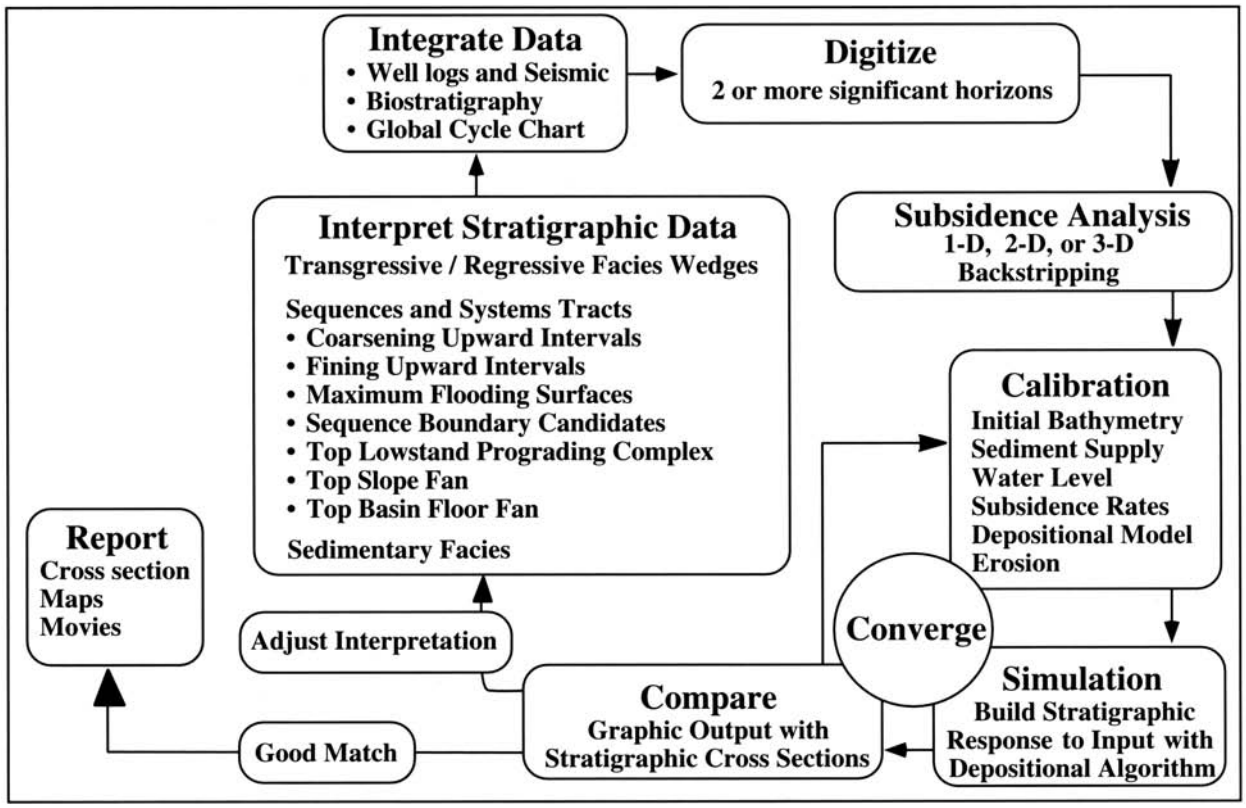

Fig. 5.7. Workflow of the PHIL/BASIM™ modelling procedure as described in Chapter 5.5 (after Bowman & Vail 1999). Note that the data for this study does not contain seismic profiles or well logs.

CHAPTER 6: 2D NUMERICAL REVERSE BASIN MODELLING

2D numerical reverse basin modelling not only serves to obtain quantitative thermo-tectonic subsidence rates as an initial numerical input for 2D stratigraphic forward modelling (Chapter 7.3.3). Flexural 2D reverse modelling also analyses the development of basin architecture in consideration of lithofacies, incremental compaction, sea-level changes and flexural loading of the crust. These parameters influence the long-term evolution of accommodation space in time. In the Cantabrian Basin, the evolution of thermo-tectonic subsidence rates in time reflect different lithospheric configurations prior, during and after the Variscan orogeny.

6.1 Methods

Reverse basin modelling determines the burial history of a basin, a technique introduced by Watts & Ryan (1976), Steckler & Watts (1978) and Turcotte & Schubert (1982). Leeder (1999) distinguishes between tectonic, thermal and load-induced bending subsidence types assembling total subsidence. In this concept the backstripping procedure calculates and removes the effect of sediment loading and compaction from the basement subsidence, as well as changing palaeo-bathymetry and eustatic sea-level variations, enabling the quantification of tectonic subsidence (Sachsenhofer et al. 1997, Einsele 2000, Watts 2001). By restoring sediment thickness at the time of deposition, taking into account compaction and water depth changes, and then isostatically unloading it, it is possible to determine the depth at which the basement would be in the absence of water and sediment loading (Watts 2001). This technique has proved to be an adequate method for analysing stratigraphic data in the form of well logs, seismic reflection profiles and, as in the present study, geological cross-sections (Fig. 6.1). Taking the lithospheric behaviour into account, subsidence or uplift of a particular sedimentary basin is determined by several factors:

- Thinning/thickening of the lithosphere caused by extension/compression
- Upwelling of mantle material due to crustal thinning
- Changes in lithosphere density
- Isostatic uplift/subsidence in response to erosion/sedimentation, flexural loads

6.1.1 Flexural response of the crust

Computer simulations on passive margins and foreland basins demonstrated the important impact of flexural response to sediment/water loading and compaction (Flemings & Jordan 1989, Reynolds et al. 1991). The flexural response of the crust can become very prominent, especially for greater loads and extended duration of loading (Einsele 2000, Stüwe 2000).

There are two main types of isostatic adjustment: Airy and flexure. The Airy type adjustment includes a "backstripping equation" (see Watts 2001, equation 7.9), which allows tectonic subsidence to be determined directly from stratigraphic data. This equation can be divided into three individual parts.

(i) Water-depth: depth of deposition of each stratigraphic unit

(ii) Sediment loading: deformation of the crust and mantle by sediment loads with particular thickness and density

(iii) Water-loading: global sea-level changes (for discussion on sea-level curves see Chapter 6.2.3 and 7.8.5)

Flexural reverse modelling computes the flexure due to total sediment load and subtracts the resulting flexure from the observed thickness in order to obtain tectonic subsidence or uplift (Watts 2001). The effects of palaeo-bathymetry and sea-level changes are taken into account. Because this approach is two-dimensional, it requires information about the spatial variation of the strength of the underlying lithosphere. Dependent on the effective elastic thickness of the lithosphere flexural bending can have a significant influence on the model (Fig. 5.6; see Chapter 5.2.6 for detailed discussion).

6.1.2 Concepts and workflow in PHIL/BASIM™

2D reverse basin modelling follows a sequence stratigraphic concept, which considers the creation/destruction of accommodation space and its infill as the principal determinant on sedimentary systems and basins (Zühlke et al. 2004). Accommodation space development is constrained by subsidence/uplift, eustatic sea-level changes and the compaction

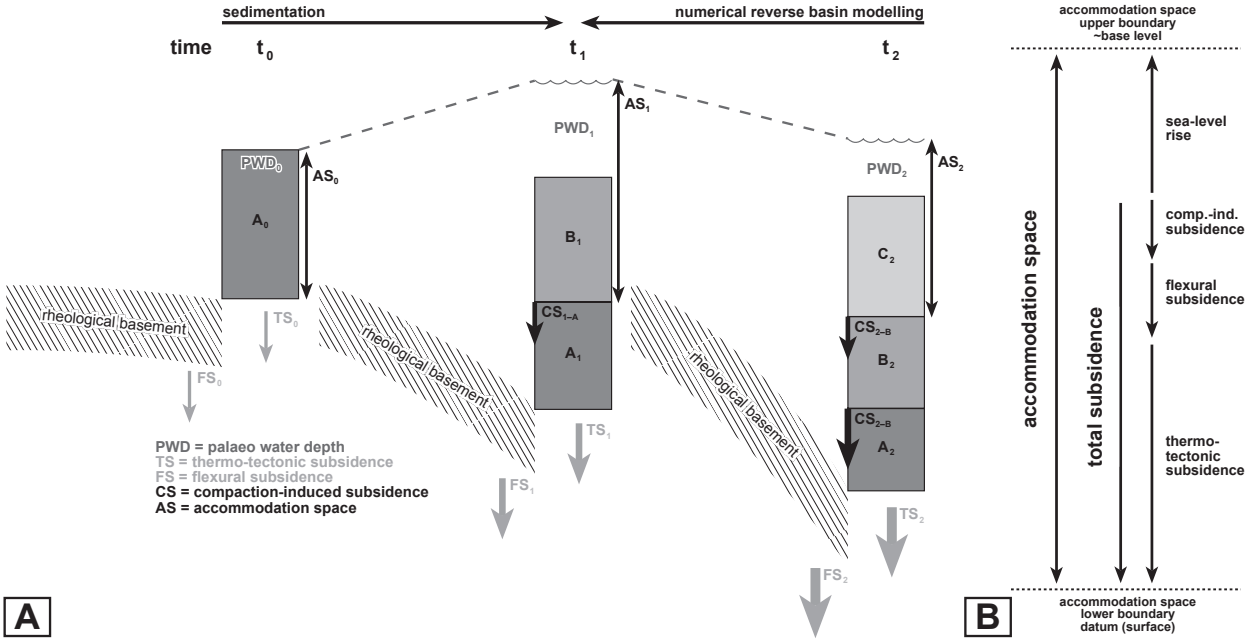

Fig. 6.1. Genetic components of accommodation-oriented 2D reverse basin modelling, comprising (i) accommodation, (ii) sea-level changes, (iii) sediment influx and (iv) subsidence components. Total subsidence includes thermo-tectonic, flexural and compaction-induced subsidence.
A: Deposition of stratigraphic units (sediment flux) is marked by letters A to C, the development in time from left to right by letters t_0 to t_2. Vectors of tectonic subsidence (TS) and flexural-induced subsidence (FS) are marked by arrows below the stratigraphic columns and the rheological basement respectively (thick arrow: high subsidence; thin arrow: low subsidence). Accommodation space (AS) increases from t_0 to t_1 by an increase in TS_1 and FS_1, rising palaeo-water depth (PWD_1) and compaction-induced subsidence of unit A ($CS_{1\text{-}A}$). In contrast to AS_1, the accommodation space decreases during t_2 due to falling PWD_2, although TS_2, FS_2 and $CS_{2\text{-}A}$ increase additionally amplified by the compaction-induced subsidence of unit B ($CS_{2\text{-}B}$). The rheological basement is only influenced by thermo-tectonic and flexural-induced subsidence.
Note that reverse basin modelling works in the opposite temporal direction to sedimentation (arrows to the top of the figure).
B: Norm-vectors show the components of total subsidence and accommodation space. This condition shows the situation for the highest possible increase in AS with rising sea-level and positive subsidence.

in the buried sedimentary infill. Subsidence/uplift can be caused by a number of forces, such as flexural response to loading/unloading (by sediment, water or any additional load) or thermal changes. The algorithms for the backstripping analysis within PHIL/BASIM™ are acquired from a dynamic deformation model of Sawyer & Harry (1991). The flexural response of the crust to loading or unloading by deposition and erosion of sediment and sea-level changes is calculated using a homogeneous elastic plate over a liquid half-space solution (Turcotte & Schubert 1982). The PHIL/BASIM™ algorithms assume several given factors within the flexural calculation (Bowman & Vail 1999). First, all sedimentation is distributed equally, perpendicular to the cross section, within the flexural wavelength of the model. The flexural response occurs within the time increment of the model. According to Bowman & Vail (1999) these assumptions are good approximations for passive margins and models with time increments larger than 1ka. The authors published algorithms for calculation of the flexural response of the crust to loading/unloading by deposition/erosion of sediment and sea-level changes. Compaction of sediments is taken into account. For simplification purposes, mechanical, non-reversible compaction is assumed, without any chemical alteration or diagenesis of the sediment. Deflection across the transect w(x) is calculated using the following equation (Bowman & Vail 1999):

$$w(x) = \frac{V_0\ \alpha^3}{8\ D}\ e^{-x/\alpha}\left(\cos\frac{x}{\alpha} + \sin\frac{x}{\alpha}\right) \qquad (6)$$

x - distance from load; V_0 - line load applied at x=0; D - flexural rigidity of the bending plate.

Flexural rigidity D is calculated by:

$$D = \frac{\alpha^4 g\,(\rho_m - \rho_w)}{4} \qquad (7)$$

ρm - mantle density; ρw - water density; g - gravitational constant.

Effective thickness of the lithosphere h is than calculated with equation (8):

$$h = \sqrt[3]{\frac{12\,D\,(1-n^2)}{E}} \qquad (8)$$

E - Young´s modulus constant at 70Gpa; n - Poisson´s ratio constant at 0.25.

PHIL/BASIM™ calculates changes in bathymetry by evaluating fluctuations of sediment (sedimentation/erosion) and water loads (sea-level changes) during each time increment. During the procedure, all time layers are incrementally removed, starting with the time of maximum burial depth and continuing until the top of the rheological basement is reached (see Fig. 6.1). After a specific time layer has been removed, the next underlying layer is adjusted according to the predefined palaeobathymetric depth. All older layers are decompacted with predefined compaction parameters. This procedure is repeated for each time increment, calculating the sediment flux and different subsidence rates, removing the effects of palaeobathymetric changes, flexural loading, compaction and eustatic sea-level changes. Numerical results are quantitative approximations for thermo-tectonic, flexural-induced, compaction-induced, and total subsidence rates, as well as sediment flux throughout the basin in time. They represent the fundamental basis for the stratigraphic forward modelling.

6.2 Input parameters

Data gathered in the field include biostratigraphic and lithostratigraphic information, thicknesses, large-scale geometries, characteristic surfaces and structural measurements. This information was derived from cross-sections and outcrops that were projected into the modelled transect. Due to the complex structural character of the investigation area, thrust planes were used as projection lines. The distances between the cross-sections prior to Variscan orogeny have been obtained by means of the structural balancing procedure mentioned earlier. Table 6.1 shows the input parameters for 2D reverse basin modelling.

6.2.1 Transect and synthetic sections

Detailed fieldwork provided 36 synthetic sections (see Appendix) located along a NNE-SSW striking transect in the León province in Spain (see Figs. 3.4 and 3.5). Within the synthetic sections, lateral thickness variations, lithology, burial depth, facies and unconformities have been considered in order to obtain sufficient information in seismic scale for the reconstruction of basin development (see Fig. 6.2). The distances between the cross-sections prior to the

Time-layer dependent parameters	Time-layer independent parameters
Thickness	Mantle density
Absolute Age	Eustatic sea-level fluctuations
Palaeobathymetry	
Compaction parameters Initial porosity Compaction rate Compaction rate limit	
Flexural parameters Te (eff. el. thickness) External projection taper limit	

Table 6.1. Input parameters for 2D numerical reverse basin modelling.

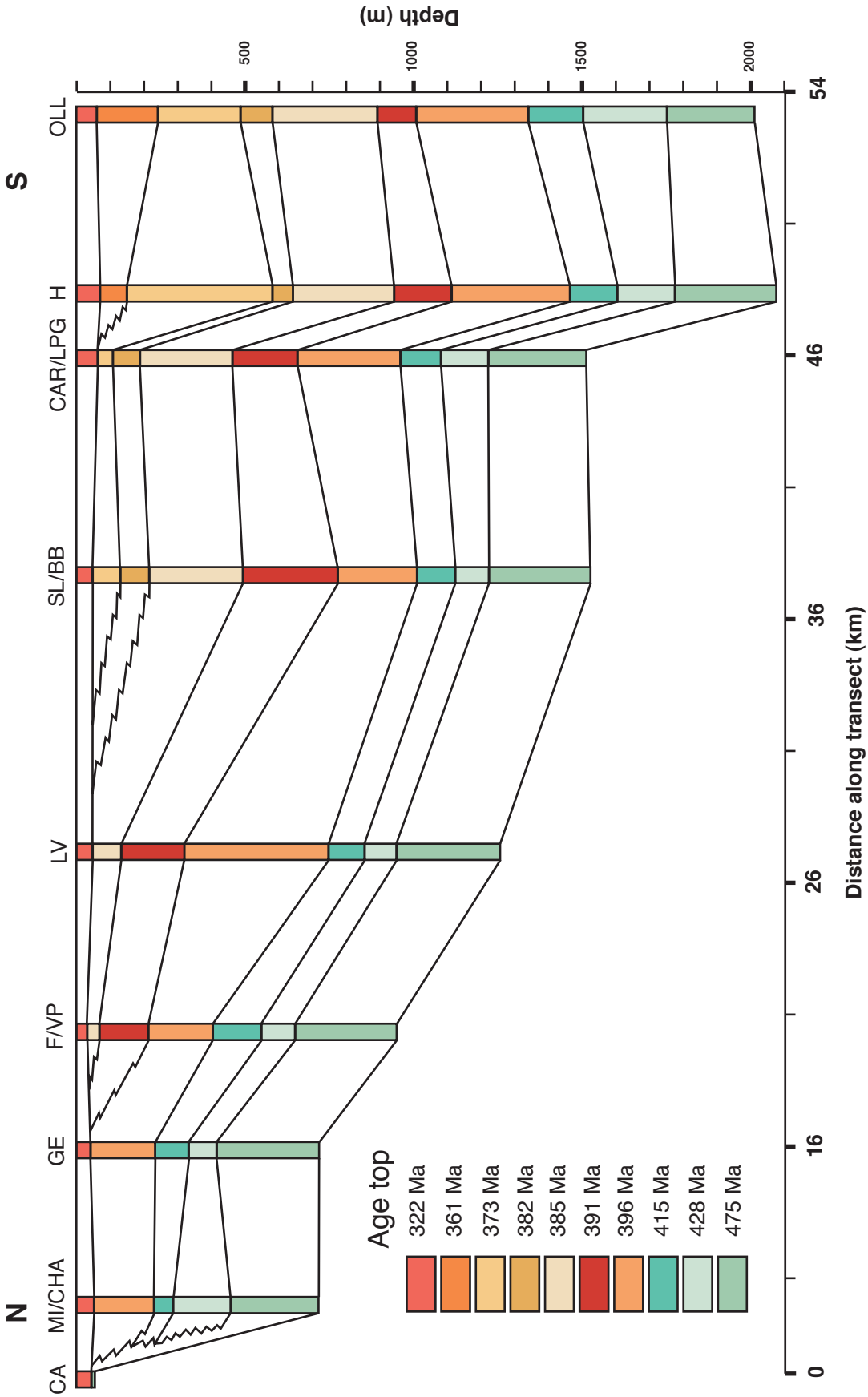

Fig. 6.2. Basin architecture along the Bernesga Transect according to 9 selected synthetic cross-sections. The cross-sections were levelled up to the marker horizon of the Alba Fm. (322Ma) and do not contain syn-orogenic formations. Note the restriction of deposition to the south with decreasing age of the formations. The distances between the cross-sections were corrected by structural balancing (see Chapter 3).

Variscan orogeny have been obtained by the structural balancing procedure (see Chapter 3 for further detail). Changes in palaeowater depth strongly influence the quantification of tectonic subsidence and therefore had to be evaluated. Eroded successions could not be restored for the Southern Cantabrian Basin. All details are displayed within the synthetic sections and tables in the appendix.

6.2.2 Time

The basin fill was subdivided by 35 time layers, based on the biostratigraphic framework available (Evers 1967, Bosch 1969, Higgins & Wagner-Gentis 1982, García-Alcalde et al. 1985, 2000, García-López 1986, Barba & Fernández 1991, Aramburu et al. 1992, 1996, García-Alcalde 1994, 1996 and many others). For each time-line at every location along the transect data including absolute age, burial depth, palaeobathymetry were gathered. The youngest time-line (Cenozoic, 34Ma) marks the period of maximum burial depth of the basin, supported by new fission track dating (pers. com. Carrière 2004). From this point of time, thicknesses of subsequently older time layers were incrementally added until reaching the top of basement in the Precambrian (560Ma). The plot of these time lines (Fig. 6.3) show the basin architecture with Variscan deformation removed. Absolute ages for stage boundaries have been taken from the German Stratigraphic Commission (2002). This timetable is based on Gradstein et al. (1994; Cretaceous), Berggren et al. (1995, Tertiary), Tucker & McKerrow (1995; Ordovician, Cambrian), Menning (1995, 2001; Permian), Menning et al. (2000; Carboniferous), Pálfy et al. (2000; Jurassic) and Weddige (2001; Devonian). Depending on the presence of indicative fossils,

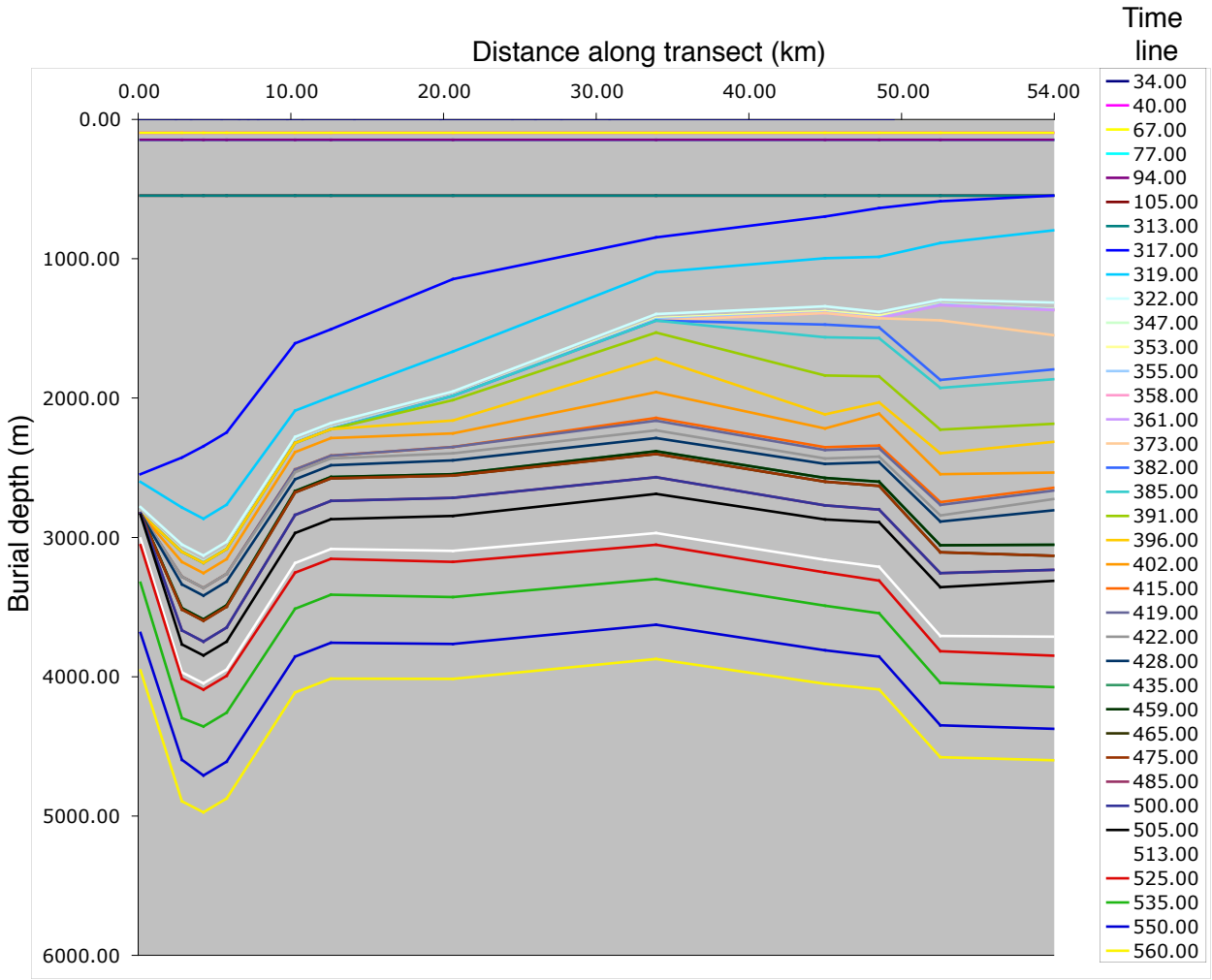

Fig. 6.3. Burial depth of time lines at the time of maximum burial (34Ma). Note the marked change in basin architecture with the deposition of the syn-orogenic succession starting at 322Ma (compare with Fig. 6.2). The extent of the transect is based upon structural balancing.

time resolution reaches stage level. For information about the radiometric age dating methods used, see German Stratigraphic Commission (2002) and references herein.

6.2.3 Sea-level

For the Quaternary, the sea-level curves are estimated precisely by the combination of glacial ice volume with $\delta^{18}O$ content of pelagic foraminifers. Unfortunately, this method is only applicable throughout the Cenozoic (Enos 1991). For the Meso and Paleozoic, sequence stratigraphic studies provided data, which were incorporated in sea-level curves (Vail et al. 1977, Haq et al. 1987). However, the detail of such sea-level curves decrease with increasing age of the rocks investigated. This method has been criticized by some authors (Miall 1986, Burton et al. 1987, Gradstein et al. 1988, Matthews 1988). There is no general agreement on the magnitude of ancient sea-level changes (Watts 2001). The published sea-level curves for the entire Phanerozoic (Vail et al. 1977, Hallam 1984, Haq et al. 1987) show significant discrepancies and do not match the detailed curves published for single series (Johnson et al. 1985, Ross & Ross 1985, 1988, 1996, Heckel 1986, Crowley & Baum 1991, Johnson & McKerrow 1991, Witzke & Bunker 1996, 1997 and others). Therefore, a synthetic curve was established for this study based on:

0-70Ma: Mitchum et al. 1991 (Haq et al. 1987)
70-160Ma: Kendall et al. 1992 (Haq et al. 1987)
160-256Ma: Haq et al. 1987
255-355Ma: Ross & Ross 1988
355-410Ma: Johnson et al. 1985 & Dennison 1985
410-438Ma: Ross & Ross 1996
435-540Ma: Ross & Ross 1988
540-560Ma: Vail et al. 1977

The synthetic sea-level curve is plotted in Fig. 6.4. Only second order changes of eustatic sea-level were considered, because sea-level changes of higher magnitude are poorly constrained throughout the Palaeozoic. Palaeo-water depths were estimated from facies analysis and faunal assemblages.

6.2.4 Lithologies

PHIL/BASIM™ uses 11 siliciclastic and 8 carbonatic/evaporitic lithologies with definable bulk rock density, initial porosity, compaction rate parame-

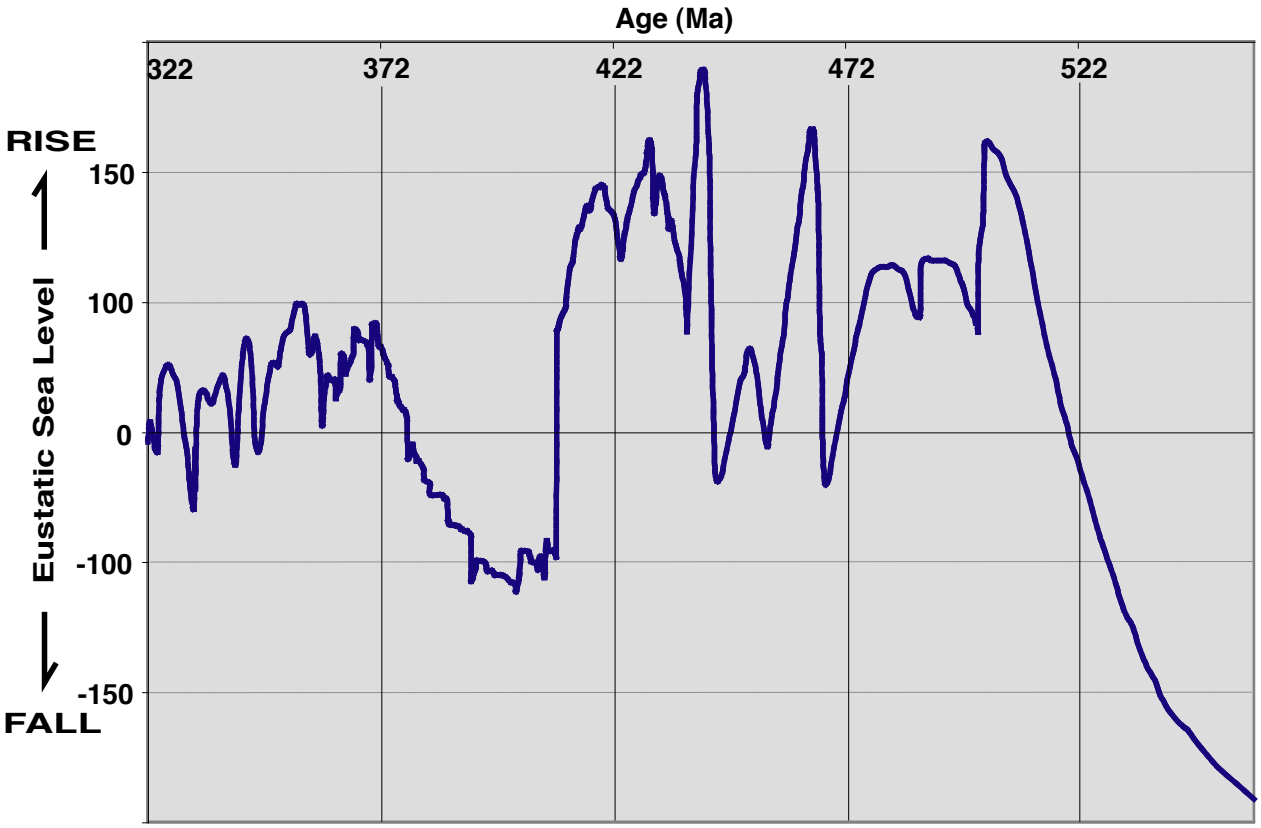

Fig. 6.4. Composed eustatic sea-level curve for the Southern Cantabrian Basin. See text for further detail.

Lithology	Density (kg/m^3)	Initial Porosity (ϕ_0)	Compaction Rate (r_c)
Coarse sand to cobbles	2650	0.40	0.0001
Quartz silt size	2650	0.30	0.001
Quartz sand/clay	2650	0.40	0.002
Quartz silt/clay	2650	0.45	0.003
Interbedded quartz/silt	2650	0.50	0.0005
Interbedded silt/clay	2750	0.50	0.002
Marine mud	2750	0.50	0.003
Clay	2750	0.50	0.003
Silt/coal	2450	0.60	0.008
Clay/coal	2300	0.85	0.009
Coal	2000	0.92	0.01
Cemented carbonate	2800	0.45	0.0001
Carbonate fine grainstone	2800	0.60	0.001
Carbonate coarse grainstone	2800	0.70	0.0005
Carbonate boundstone	2800	0.60	0.002
Micrite	2800	0.70	0.004
Algal laminates	2800	0.60	0.0005
Dolomite	2900	0.40	0.0001
Gypsum	2330	0.10	0.00001

Table 6.2. List of lithologies and compaction parameters used in the present study.

ter and maximum depth of compaction (Table 6.2). Together with burial depth, these values control the compaction of all time layers. For the Bernesga Transect a mean initial porosity war required for the 2D reverse basin modelling. It has been calculated by estimating the percentage of different lithologies proportional to their thickness within a specific cross-section. These percentages were combined with assumed initial porosities for the specific lithologies (Table 6.2) and calculated for three cross-sections in a proximal (Millaró section), intermediate (Valporquero section) and distal (Huergas section) position. The average initial porosity for the Bernesga Trasect amounts to 46.5%. See following chapter for details.

6.2.5 Compaction/decompaction

The numerical modelling includes incremental decompaction of the succession in each time layer. Decompaction is calculated using empirical porosity/depth relations for specific lithologies. The thickness of a particular layer at time of deposition h_{s1} can be calculated by the following equation (Einsele 2000, Stüwe 2000):

$$h_{sl} = \left(\frac{1-n_p}{1-n_1}\right) * h_{sp} \qquad (9)$$

h_{s1} - original thickness; h_{sp} - present thickness; n_p - present mean porosity; n_1 - initial mean porosity
Appropriate porosity-depth curves and values were taken from Goldhammer (1997), Welte et al. (1997) and Bowman & Vail (1999) and used for mean porosity estimations. These calculations were made in order to check and refine the results of computer simulations. PHIL™ incorporates sediment compaction as a function of burial depth (Bowman&Vail 1999). The burial depth related porosity $\phi(z)$, which is dependent on the lithology, was estimated according to the following equation:

$$\phi(z) = \frac{\phi_0}{1 + z * r_c} \qquad (10)$$

ϕ - porosity; z - depth in m; ϕ_0 - initial porosity; r_c - compaction coefficient

During each time-step, PHIL/BASIM™ calculates textural porosities within each cell according to its depth and lithology from the top to the bottom of the series. According to the loss of porosity for a time interval, the thickness is decreased equally and the horizon depths are adjusted. Diagenetic trends can be considered by adjusting the compaction coefficient (r_c in Eq. 9). Sediment compaction is assumed under normal pressures, with the option of overpressured basin conditions (where compaction is delayed) resulting in thicker sections with lower densities.

6.2.6 Flexural parameters

There are three user-defined parameters, which influence the flexural loading:

- Effective elastic thickness (Te)
- Mantle density
- Taper limit (approximately three times the flexural wavelength)

The dependency on Te for flexural behaviour of the crust has been discussed in Chapter 5.2.6. For the 2D reverse modelling a mean Te-value of 35km was chosen. The mantle density amounts to 3340 kg/km^3 (see Bowman & Vail 1999 for discussion). Due to the relatively short Bernesga Transect changes of taper limit did not show any changes on the results.

6.3 Subsidence components

Total subsidence comprises three genetic components: thermo-tectonic, flexural-induced and compaction-induced subsidence. Time-distance rates throughout this thesis are given in m/Ma (= mm/1000a = μm/a). This unit has been introduced by Fischer (1969) as Bubnoff-unit.

6.3.1 Thermo-tectonic subsidence

Basin subsidence is caused by downwarping of the basin floor due to thermo-tectonic forces, such as crustal extension and cooling (McKenzie 1978, Steckler & Watts 1978, Watts et al. 1982, Sachsenhofer et al. 1997, Watts 2001, Turcotte 2002). Thus the thermo-tectonic subsidence rates depend on the spreading rate and time or distance of the spreading centre (Enos 1991). For interior basins, intra-plate stress is the main factor causing subsidence. At the beginning of basin formation, tectonic subsidence often surpasses sedimentation. In later stages of basin evolution, subsidence may also be actively driven by an increasing sediment load (Einsele 2000).

6.3.2 Flexural-induced subsidence

Loads applied to an elastic plate cause bending in order to reach isostatic equilibrium (Waschbusch & Royden 1992, Watts 1992, Cloetingh & Burov 1996, Einsele 2000, Watts 2001, Turcotte & Schubert 2002). The bending depends on many different parameters such as the effective lithospheric thickness, the time of applied load, the external projection taper limit or mantle density (see Chapter 6.2.6). Loads can vary across a broad spectrum, covering tectonic loading from adjacent mountain belts (foreland basins), single thrusts, growing reefs/carbonate platforms or any other kind of sediment (clastic depocenter in a delta for instance) and water loads causing subsidence due to isostatic compensation. This kind of subsidence has also been called isostatic subsidence (Enos 1991). The flexural response of the lithosphere to external loads is discussed controversially within the scientific community (compare Chapter 5.2.6).

6.3.3 Compaction-induced subsidence

Depending on initial porosities, cementation, grain size, degree of grain-support, sorting within the sediment and compaction rate and its limit, compaction-induced subsidence can account for a large percentage of total subsidence. The initial porosity/burial depth relationship, assumed during modelling, is shown in Fig. 6.5. It primarily reflects an exponential decline in porosity with depth. However, only the change of bulk volume and not a change in porosity determines the amount subsidence (Enos 1991). The change of bulk volume and not a change in porosity determines the amount subsidence (Enos 1991). This clarifies the need to take into account not only the loss of porosity by physical compaction, but also by cementation. Thus porosity curves converted to bulk volume loss may exaggerate the level of compaction, while production of secondary porosity by dissolution at depth may lead to underestimations of compaction (Enos 1991). As already mentioned, cementation during burial of a specific lithology, causing a “slower than normal” compaction, can be partly considered in the software, adjust-

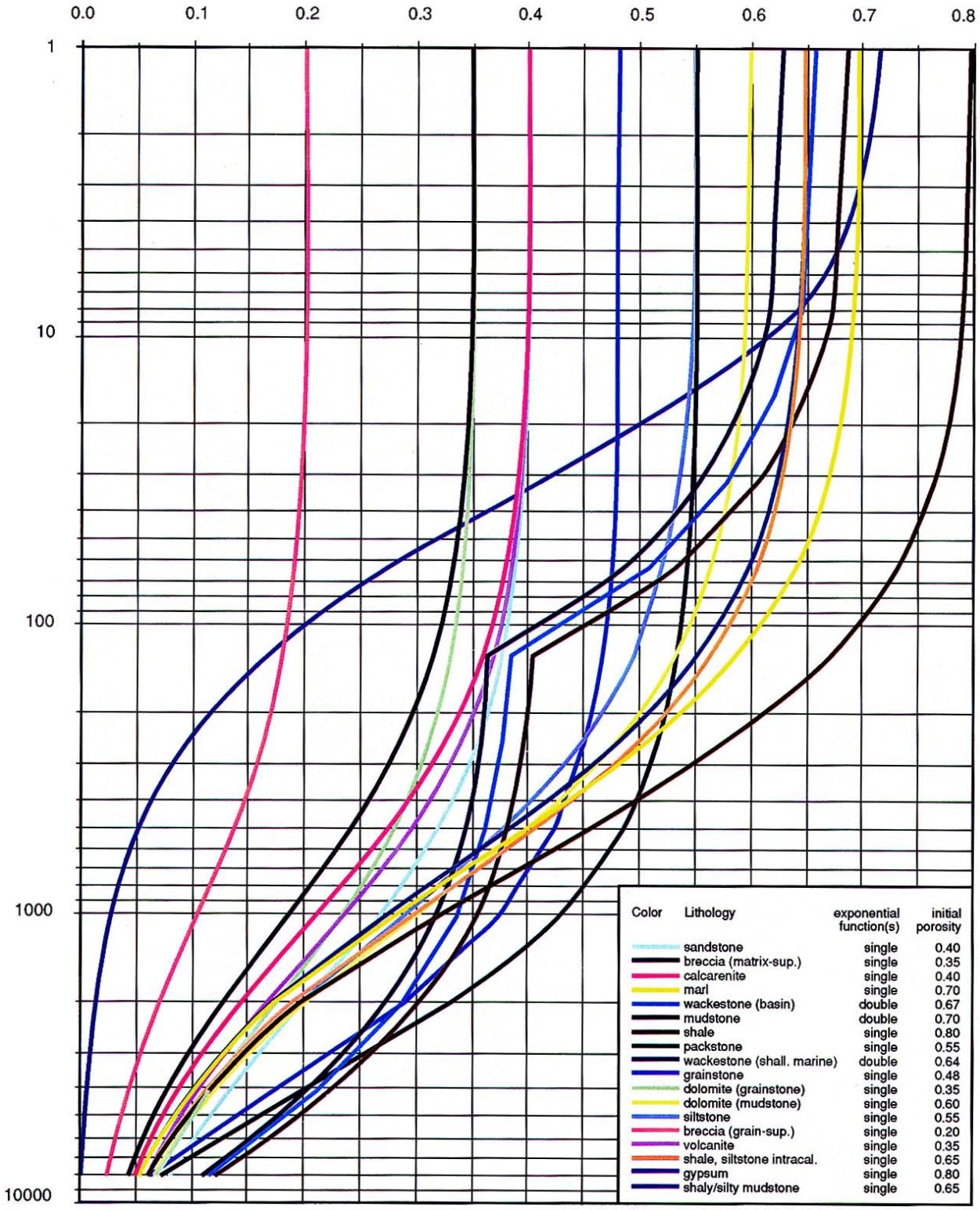

Fig. 6.5. Porosity versus burial depth for the most common lithologies. Note the logarithmical scale for burial depth. Data composed from Goldhammer (1997) and Welte et al. (1997).

ing the compaction coefficient (see Chapter 6.2.5). However, such a cementation event, for instance in carbonates, adds material, so that the original thickness during sedimentation would be overestimated. On the other hand, pressure-solution might remove material. Anderson & Franseen (1991) estimated the compaction of reef carbonates due to pressure solution at depth to be 30%. Compaction can additionally be retarded by the generation of overpressure in fast accumulating fine-grained sediments.

This can be taken into consideration in the modelling program. Differential compaction-induced subsidence could occur, for example, when a platform progrades over compactable basinal facies.

6.4 Constraints

There are several major and minor constraints, making the model less accurate:

- The time information is often not sufficiently precise. During the sedimentation history of the Southern Cantabrian Basin only a few volcanoclastics (within the Oville, Barrios, San Pedro formations) were deposited in the area, and these have not yet been radiometrically dated (Gutiérrez-Alonso 2003, pers. comm.). Biostratigraphic data are often much less precisely dated chronostratigraphically than needed for the model. Starting the model in the Precambrian causes additional uncertainties due to a lack of biostratigraphic data. Any attempts to increase the time resolution using the current data would result in linear time-interpolations and consequently in arguable models.
- Linear space interpolation is a basic method in 2D numerical reverse modelling. For all time-increments, both subsidence/uplift rates and sediment supply are interpolated between the locations along transect. This is especially problematic if the palaeogeography is complex (e.g. reef-basin topography instead of ramps). Consequently, the more cross-section within one transect can be incorporated the lower are the interpolated distances, increasing the accuracy of the model.
- Flexural behaviour of the crust is highly dependent on the effective elastic thickness (Te) of the lithosphere (see Chapter 5.2.6 for discussion). Average values for Te during the reverse basin modelling cause uncertainties within the flexural-induced subsidence results.
- Initial porosities and compaction parameters for standard lithologies have been used. They are based on particle size, matrix/grain-support and mud/shale content. Coefficients for carbonate and siliciclastic lithologies incorporate different compactional behavior with increasing burial depths (see Chapter 6.2.5). However, each time-increment incorporates information for only one specific lithology. Consequently neither facies changes, nor diagenetic processes effective for one lithology in one formation can be considered within the backstripping procedure of the software used.

6.5 Numerical and graphical output

Besides numerical interpretations, several graphical approaches have been applied in order to display the results of the 2D numerical reverse basin modelling. First graphic captures of selected time lines visualise the development of the depositional and structural characteristics in time (Fig. 6.6). Displaying all time-lines would go beyond the scope of a printed version, thus the most prominent changes have been selected. The whole evolution of the Southern Cantabrian Basin is displayed as a QuickTime™ time-series animation (see file "Movie_1.mov"). Spectrograms are used in order to display three variables in a 2D-plot. The y-axis of the plot represents the time-development of the basin whereas the distance along transect is plotted on the x-axis. Differential subsidence rates can be visualised with a specific colour code. Thus the development of subsidence rates can be easily observed in time and space (Fig. 6.7A total subsidence, 6.7B tectonic subsidence, 6.7C flexure-induced subsidence, 6.7D compaction-induced subsidence).

6.6 Results

Time lines younger than 313Ma are based on projected data (see Chapter 2.4.4) as they do not outcrop in the investigation area. Thus these time layers show a layer-cake geometry (Fig. 6.3) due to missing information about provenance, lithofacies distribution or thickness variations. Consequently the information in terms of subsidence development along transect is trivial and will not be further considered. Nevertheless, the information about the overburden is important for the compaction/decompaction development of the underlaying strata. Between 560Ma and 313Ma six major subsidence trends can be determined (Fig. 6.8). Values for all trends and all subsidence components, as well as their absolute ages, are summarised in Table 6.3. Positive values indicate subsidence, negative values uplift.

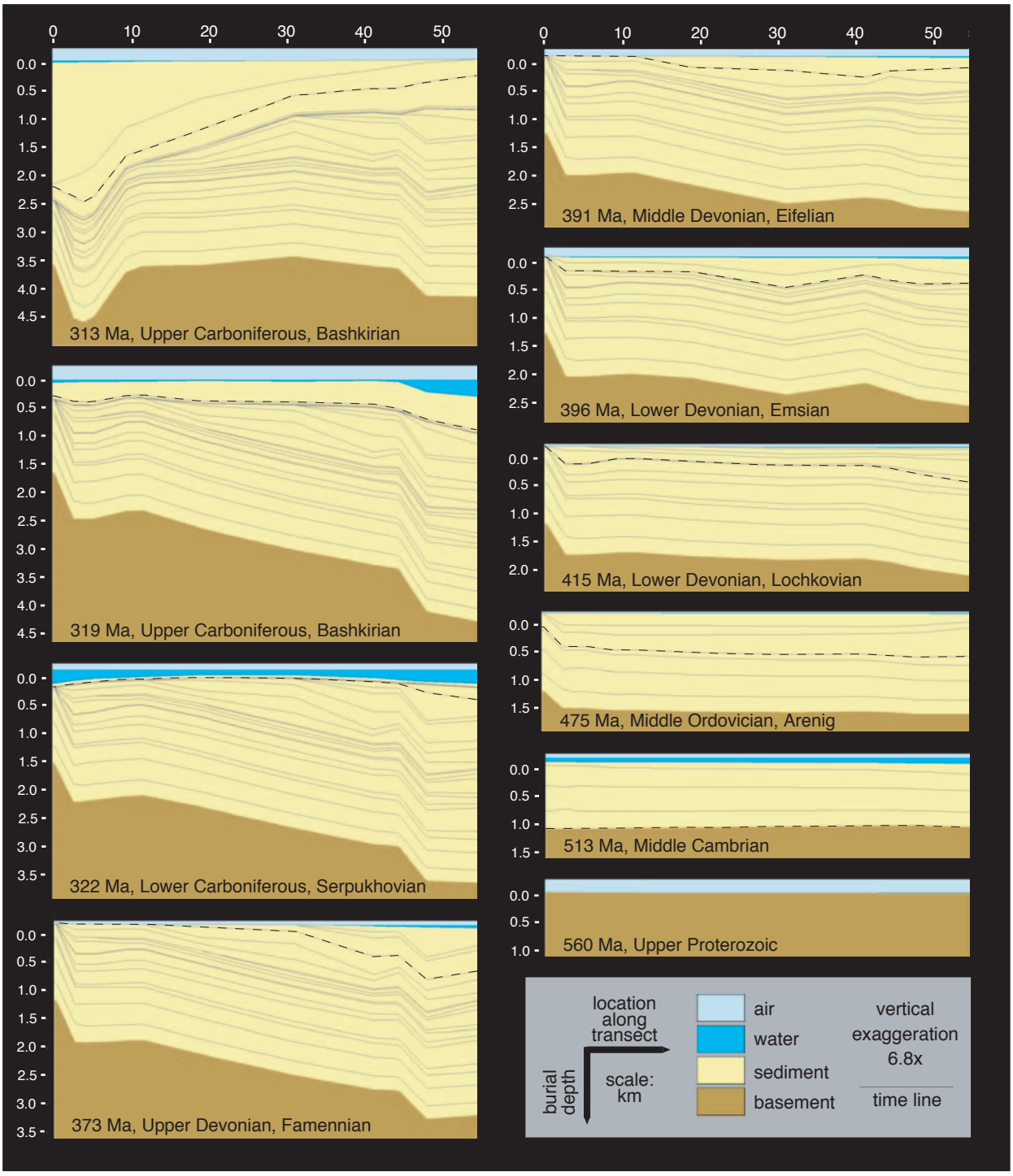

Fig. 6.6. 2D reverse basin modelling displayed as plots of selected time lines. They visualise the development of depositional and structural architecture from Late Proterozoic to Late Carboniferous. The top of an increment is marked by a dashed line in the plot that follows.

6.6.1 Thermo-tectonic subsidence

The thermo-tectonic subsidence rates range from -156 to 432m/Ma over the entire modelling period (see Fig. 6.7B).

The first subsidence trend (560-505Ma, Fig. 6.8 and Table 6.3) is indicated by slightly elevated values with mean rates of 16m/Ma. The spatial pattern is uniform, with higher values (up to 34m/Ma) in the northern part of the transect (km 6). Within the first four time increments (560-513Ma) a trend can be observed showing thermo-tectonic subsidence values diminished in time by 40%.

The second trend (505-435Ma) is marked by alternating increments of slight subsidence (up to

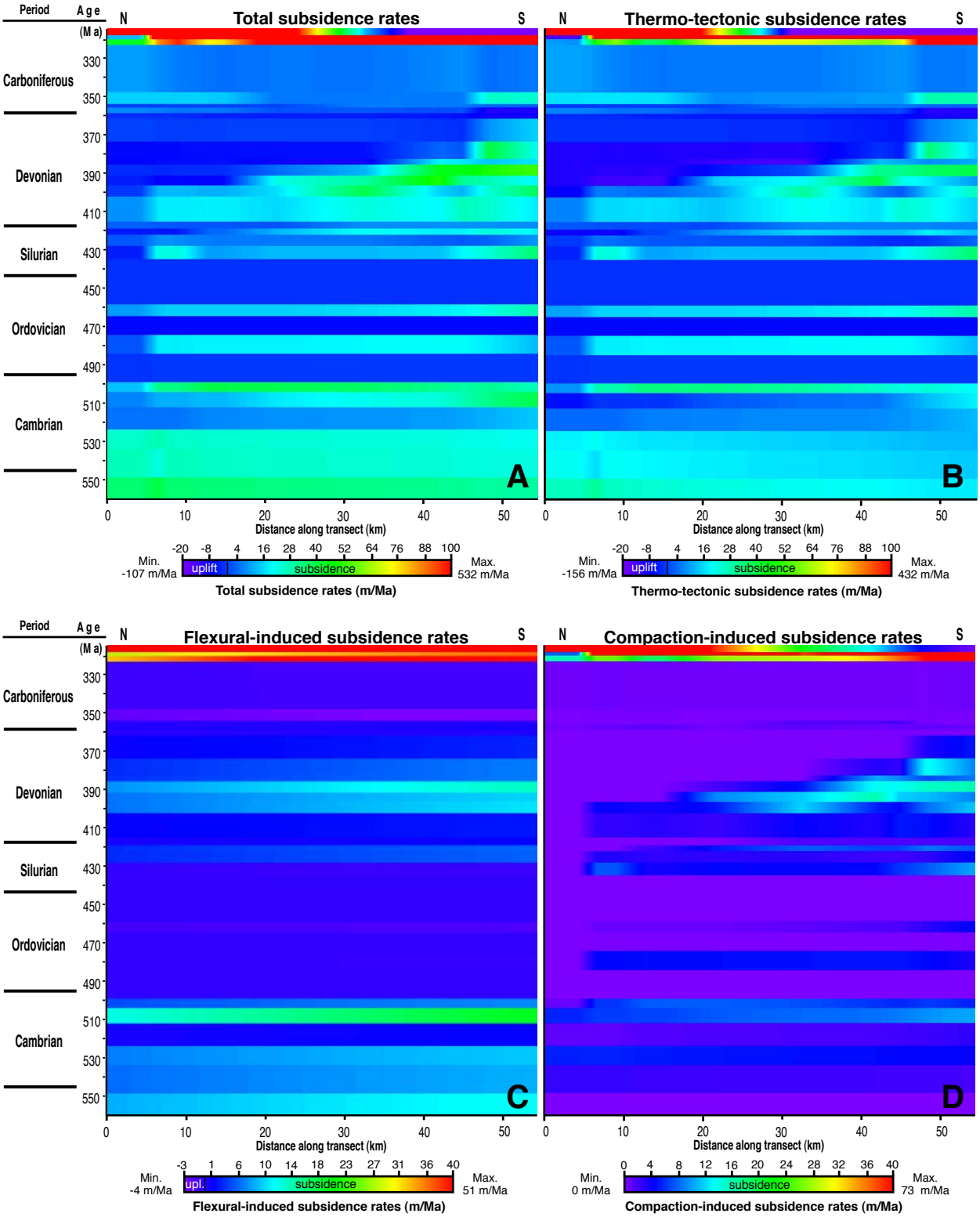

Fig. 6.7. Spectrogram plots of total subsidence rates (**A**) and its specific components (thermo-tectonic (**B**), flexural-induced (**C**) and compaction-induced (**D**)). The y-axis of each figure represents the time-development of the basin in Ma, whereas the distance along the transect is plotted on the x-axis. Differential subsidence rates are visualised with specific colour codes, with the spectrum cut in order to highlight medium-range values (see colour-bars at the bottom of each graph). Therefore maximum and minimum values are given for each plot. Detailed maximum, minimum and mean values for all trends are stated in Table 6.3.

30m/Ma) to very slight uplift (maximum uplift -6m/Ma). The distribution of values is uniform, with decreasing values to the north and to the south. Three 10 to 24Ma long hiati subdivide the sedimentary record (see Fig. 2.21, 6.8 and discussion about the accuracy of the hiati in Chapter 4.2).

The third trend (435-415Ma) indicates the first inhomogeneity in spatial distribution of subsidence rates. Its first time increment (Formigoso Fm.; 435-428Ma) shows two local subsidence maxima (km 7 and km 54 with values up to 35m/Ma), whereas the subsequent increments (San Pedro Fm.; 428-415Ma) are characterised by the development of an uplifted area (Cantabrian block) of no deposition (up to -8m/Ma) in the north. This structural high propagates in time to the south (Mb. B of the San Pedro Fm.; 422-415Ma), restricting the areas of deposition to the south.

The pattern vanishes at the beginning of the fourth trend (415-361Ma). The Esla Fm. (402-396Ma) shows a marked subsidence peak at km 32 along transect. However, the subsiding areas start to become restricted once again towards the south from the deposition of the Santa Lucía Fm. onwards (396-391Ma). Maximum subsidence rates (40m/Ma) are reached during the deposition of the Santa Lucía Fm. The uplifted areas (up to -13m/Ma) extend to km 47 at the time of the Fuyeo Fm. (373-361Ma). This wedge-shaped pattern is well visible in the spectral plot in Fig. 6.7B.

The fifth trend (361-322Ma) commences with a short hiatus (3Ma) and an alteration of thin carbonate and siliciclastic formations. The wedge-shaped pattern vanishes in the uppermost Devonian, switching to fairly uniform subsidence rates (up to 28m/Ma). The most important feature of this trend is the deposition of the condensed Alba Fm. (347-322Ma), representing 25Ma of uniform subsidence and low sedimentation rates along the transect.

In contrast to these uniform conditions, the sixth trend (322-313Ma) is characterised by highly subsiding areas (up to 432m/Ma), with neighbouring regions of strong uplift (up to -156m/Ma). During time increment 317Ma, highest values of 241m/Ma are displayed at km 43 along transect. Throughout time increment 313Ma, the pattern shows a maximum subsidence restricted to the northernmost part of the Bernesga transect (up to 432m/Ma at km 0), whereas the southern part has been strongly uplifted (-156m/Ma). Thus, within the three time increments of this trend, the subsiding depocentres migrate from the southernmost to the northernmost part of the Bernesga Transect (see Fig. 6.8). See Chapter 8.1 for the calculation of propagation rates along the transect.

6.6.2 Flexural-induced subsidence

This subsidence component does not mirror all six subsidence trends reflected in thermo-tectonic subsidence (Fig. 6.7C). The first trend (560-505Ma) is

	(Ma) / (m/Ma)	Trend 1	Trend 2	Trend 3	Trend 4	Trend 5	Trend 6
		560-500	500-435	435-415	415-361	361-322	322-313
Total	min	7	-6	-4	-10	-9	-107
	max	50	33	45	70	25	532
	mean	28	6	13	15	4	175
Thermo-tectonic	min	-6	-6	-8	-13	-10	-156
	max	34	30	35	40	28	432
	mean	16	5	7	5	4	98
Flexural-induced	min	1	-1	-1	2	-4	28
	max	20	0	6	14	1	51
	mean	8	0	2	6	0	41
Compaction-induced	min	0	0	0	0	0	0
	max	10	5	10	16	2	73
	mean	4	1	3	4	0	36

Table 6.3. Trends of total subsidence rates and its specific components (thermo-tectonic, flexural-induced and compaction-induced) for the time interval from 560Ma to 313Ma. Spectral plots are shown in Figure 6.7. See text for further explanations.

well developed with values of up to 20m/Ma. The carbonates of the Láncara Fm. (525-513Ma) display no augmented flexural-induced subsidence, which increases again during the subsequent Oville and Barrios formations (513-500Ma). The second (505-435Ma) and third trends (435-415Ma) are reflected by minimal flexural values (mean values of 0 to 2m/Ma). The fourth trend (415-361Ma) shows higher subsidence in the southern part of the transect, caused by the bending of the lithosphere due to sediment loading in the basinal area. In the fifth trend (361-322Ma) no subsidence to slight uplift uniformly occur along transect. The sixth trend (322-313Ma) commences with high values in the south and lower values in the north. The flexural-induced subsidence has a comparatively minor impact on the total subsidence development with mean proportions of 10-25% on the total subsidence. The flexural-induced values depend to a great extent on the sediment thickness and the palaeobathymetry. However, due to the low specific gravity of water in comparison to sediment, only higher water depth cause major flexural response of the crust.

6.6.3 Compaction-induced subsidence

The end of the first trend (560-505Ma) shows a slight uniform compaction-induced subsidence (max. 10m/Ma; Fig. 6.7D). During the second trend (505-435Ma) this subsidence component is negligible. In comparison to the second, the third (435-415Ma) and fourth trends (415-361Ma) are fairly well developed, displaying the wedge-shaped pattern of the thermo-tectonic subsidence results. Higher compaction-induced subsidence rates are also due to the highly compactable black shales of the Formigoso Fm. and the sediment deposited south of the Cantabrian High. Hardly any compaction-induced subsidence is visible during the fifth trend (361-322Ma). The sixth trend (322-313Ma) fully corresponds to the thermo-tectonic results, showing highly subsiding regions (up to 73m/Ma) migrating northwards in time. The proportion of the compaction-induced subsidence is slightly lower but in the same order as the flexural-induced subsidence. Compaction-induced subsidence is very prominent during times of high sedimentation rates, as for example during the deposition of the San Emiliano or Olleros formations. In general, therefore, compaction-induced subsidence mirrors the accommodation space, provided by thermotectonic and flexural-induced.

6.6.4 Total subsidence

Total subsidence represents the sum of thermo-tectonic, flexural-induced and compaction-induced subsidence. The subsidence values over the whole model period range from -107 to 532m/Ma. As the thermo-tectonic subsidence is the dominating component of the total subsidence, and its percentages range usually around 35% and 100% of total subsidence, both show fairly identical patterns (see Fig. 6.7A). During times of high sedimentation rates (e.g. first and sixth subsidence trends) compaction of deposited sediment and its load cause considerable increase of the subsidence values, reaching 25-40% of total subsidence rates.

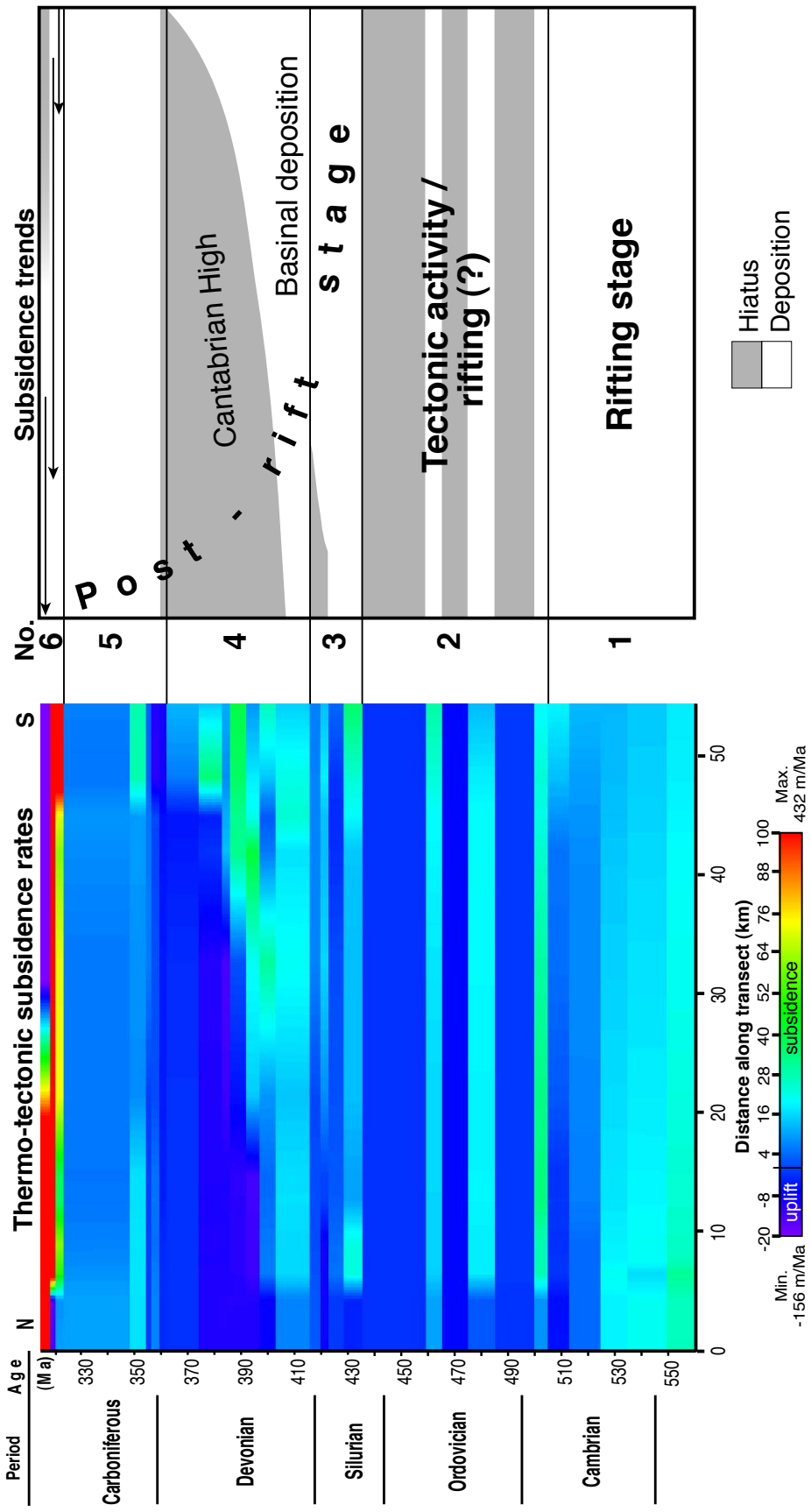

Fig. 6.8. The left part is extracted from Figure 6.7B. showing thermo-tectonic subsidence rates for the time between 560 Ma and 313 Ma. The right side indicates the specific numbers of subsidence trends (see text for further detail) as well as the development stages of the Southern Cantabrian Basin. Trend 6 at the top of the figure represents the Variscan foredeep stage, with arrows indicating movements of highly subsiding depocentres in time.

CHAPTER 7: 2D STRATIGRAPHIC FORWARD MODELLING

7.1 Objectives

Stratigraphic forward modelling was applied to simulate basin development, and to quantify the physical factors determining deposition. This study focuses on the evaluation and quantification of internal and external parameters governing deposition, e.g. sediment transport, in-situ carbonate production, erosion and compaction. Within the stratigraphic forward simulations with PHIL/BASIM™ (Petro-Dynamics Inc., Houston), these parameters can be numerically modelled and visualised independently in order to determine the primary factors and develop a quantitative geologic model for testing and modifying existing qualitative models. The simulation results also account for subsidence and uplift, flexural loading and eustatic sea-level changes. This method offers minimum/maximum models of sedimentary geometries and lithofacies distribution in time and space, predicting lithostratigraphic information in areas between outcrops. Consequently, it provides an opportunity to reconstruct and visualise seismic scale geometries in a tectonically highly disturbed basin (after structural modelling has been applied, see Chapter 3), where only slices of the basin filling crop out, as is the case in the Southern Cantabrian Basin. Further results comprise predictions of data between measured outcrops, such as:

(i) Distribution of lithofacies and depositional environments
(ii) Distribution of lithophysical parameters (density, porosity)
(iii) Distribution of palaeo-water depth
(iv) Information about depositional systems

Sedimentary systems are composed of a large number of processes, which control the filling and development of a specific basin. The interaction of these processes is highly complex and goes beyond the scope of any computer simulation program. Consequently the PHIL/BASIM™ modelling software simulates key processes in basin evolution and its results.

7.2 Modelling software

Over the last fifteen years there have been several computer-based quantitative approaches which simulate the stratigraphic record (Tetzlaf & Harbaugh 1989, Aigner et al. 1990, Lawrence et al.1990, Demicco et al. 1991, Jordan & Flemmings 1991, Kendal et al. 1991, Read et al. 1991, Boscher & Schlager 1993, Bosence et al. 1994, Eberli et al. 1994, Flemmings & Grotzinger 1996, Nordlund 1996, Hüssner et al. 1997, Wendebough & Harbaugh 1997, Liu et al. 1998, Bowman & Vail 1999, Granjeon & Joseph 1999, Warrlich et al. 2002 and others). Although PHIL/BASIM™ is only one modelling software package among many, it considers the most complete bundle of processes in comparison with the mostly two-dimensional stratigraphy computer models (see Bowman & Vail 1999). Due to large data volumes and intensive computing processes, most simulations handle only a few specific aspects. Some models do not include both siliciclastic and carbonate sedimentation, and are therefore suitable only for a small number of sedimentary basins. There are many examples of close interaction during the evolution of sedimentary basins such as high sedimentation rates influencing flexural and compaction-induced compaction, with a major impact on the accommodation space development and the resulting facies distribution. Consequently, an adequate sedimentation model must correctly respond to all reasonable tectonic, water level, and sediment-supply conditions (Bowman & Vail 1999). It must respond to short and long-term processes which both influence the sedimentation processes in specific ways. Stratigraphic modelling is the only means of building plausible quantitative models, based on tested and/or empirically derived algorithms. Because many secondary parameters cannot be measured in fossil depositional systems quantitative stratigraphic models usually rely on stochastic simulations.

7.3 Input data

For this study, 36 sections were measured in the field, in terms of lithofacies, lateral thickness variations, large-scale geometries, biostratigraphic data

and characteristic surfaces (see Chapter 6.2.1 and Figs. 6.2 and 6.3). Field data was digitised and interpolated into the synthetic Bernesga Transect according to tectonic restrictions (see Chapter 3.5) in order to obtain sufficient information for reconstructing the basin development in seismic scale.

7.3.1 Time

All variables are set at the start of the model and can be varied for each time-step. Time steps may vary between 1a and 2Ma. A constant time-step of 500ka was chosen for this study. This is a reasonable simplification at basin scale and the long simulation time of 238Ma. For the simulation time from 560Ma to 322Ma the model comprises 476 layers. Carbonate deposition uses an independent time increment of 21ka in order to adequately reflect the sensitivity of carbonate production systems to, for example, relative sea-level changes.

7.3.2 Space

The 54km long synthetic Bernesga Transect (Fig. 3.3 and 3.4) is divided into user-defined evenly spaced cells. Each cell is influenced by processes, which are active throughout the entire basin (for example thermo-tectonic subsidence) or only derived from surrounding cells, such as limited sediment supply transported by traction from a neighbouring cell. The spatial resolution of the transect has a significant influence on the final basin-infill model. The cell spacing width of 250 meters was chosen for the present study as a reasonable compromise between resolution and computing time.

7.3.3 Tectonic subsidence and sea-level

Tectonic subsidence rates vary spatially and temporally. Numerical data has been calculated within 2D reverse basin modelling (see Chapter 6.6). As the total and tectonic subsidence rates vary along the transect, differential changes in accommodation space along the shelf/basin transition exist. The sea-level within PHIL/BASIM™ can be defined in terms of sinusoidal or saw-tooth cycles with an adjustable period, amplitude and phase, or a digitised water level history. A composed eustatic sea-level curve was used, identical to the curve utilised in the 2D reverse basin modelling (see Fig. 6.4 and Chapter 6.2.3). No additional superimposed cycles were added to the composed sea-level curve.

7.3.4 Flexural response of the crust

The importance of flexural response to sediment loading was discussed by numerous authors (see discussion in Chapter 5.2.6). The effective elastic thickness (Te) of the lithosphere in the present region of study changes through time, because the lithospheric plate experienced a broad variety of settings (see Chapter 2.3). Te for stretched crust and creation of oceanic crust has been estimated to be 5-15km according to the mid-values for rifting areas (Watts 2001). This time span lasted from the Precambrian up to the Early Cambrian. A linear increase of Te from 10 to 60km was applied for the time from Late Ordovician to Early Carboniferous (see Chapter 5.2.6 for discussion).

7.4 Methods and specifications

7.4.1 Siliciclastic deposition

Within PHIL/BASIM™ siliciclastic material is defined as erosional product, user-defined constant, cyclic input or digital sediment influx history. It is transported and redistributed by traction and suspension processes, slumping and gravity-flow processes. The user can define the percentage of material transported by traction, the percentage of sand fraction and age/supply rates. The siliciclastic sediment supply is given in m^2/ka as it represents the filling of a two-dimensional area in a two-dimensional model (see below).

Traction

Traction is one of the processes, which transports sediment into the basin and shapes the siliciclastic depositional profile. In contrast to suspension, it moves sediment along the sediment surface. Table 7.1 shows the user-defined variables which influence the traction algorithm. The values utilised for the present study are compared with published data.

The depth of the offlap break depends on the strength of the prevailing winds as it mostly corresponds to the fair-weather wave base (5-20m). The rollover width describes the transition between the shoreface and depositional front. The coastal-plain width and gradient control the geometry of the coastal plain. The depositional profile can be split into unique segments and is defined and subdivided into fluvial plain, coastal plain and shoreface

	Range Bowman & Vail 1999	Range Southern Cantabrian Basin
Traction variables		
Width of coastal plain (km)	0 - 200	30 - 35
Siliciclastic rollover width (km)	1 - 5	3
Depth of offlap break (m)	10 - 20	10
Traction fraction (%)	0 - 100	10 - 90
Sand fraction (%)	0 - 100	0 - 70
Suspension variables		
Width of the mixing layer (m)	1 - 200	50 - 80
Dispersion distance (km)	5 - 100	15 - 60

Table 7.1. List of adjustable variables for siliciclastic depositional environments. The values used for the Southern Cantabrian Mountains are compared with published data by Bowman & Vail (1999).

(Fig. 7.1). The traction process within the simulation is a consequence of several consecutive steps. If space is available below base-level at a specific location, the volume of sediment required to fill this space is removed from the sediment supply. After the space has been filled to base-level, the depositional interface progrades one cell spacing basinward. This process (filling of available space below base-level, progradation etc.) repeats until the volume of sediment transported by traction is exhausted for a specific time increment. Siliciclastic input suppresses carbonate productivity when a user-designated threshold is reached.

Suspension

Suspended sediment is injected into the marine environment and settles as a function of the mixing volume within a hypopycnal inflow (Bowman & Vail 1999). This process is influenced by two user-defined variables: (i) Width of mixing layer and (ii) dispersion distance (Table 7.1).

The width of the fluvial-marine mixing contact, where the sediment-loaded fluvial stream is inject-

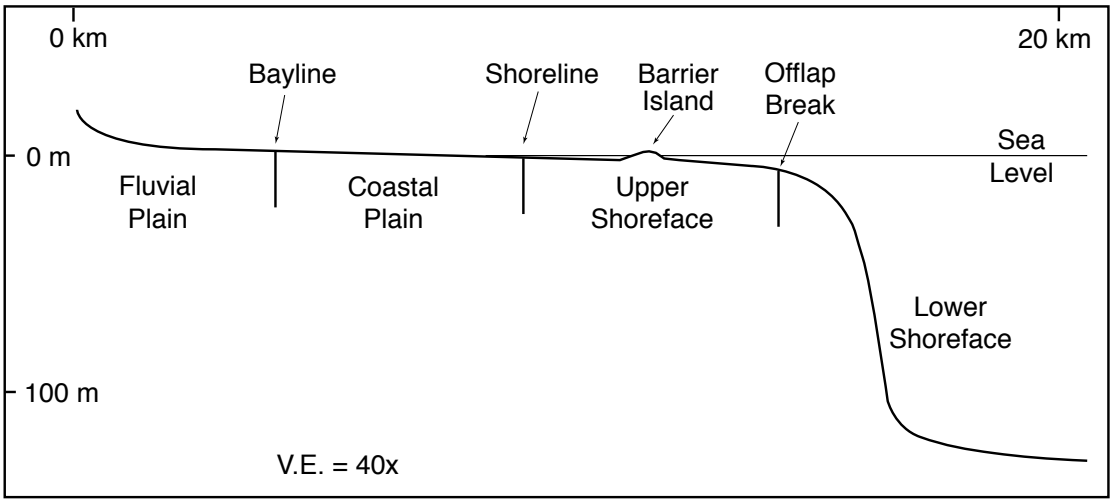

Fig. 7.1. Siliciclastic depositional profile within the 2D stratigraphic forward modelling with PHIL/BASIM™ and its subdivision into specific segments. See Chapter 7.4.1 for details.

ed into the marine water column, can reach 200m. The dispersion distance describes the greatest distance of transported sediment by suspension, which can range between 5 and 100km (Bowman & Vail 1999).

PHIL/BASIM™ uses an empirically derived function (11) for suspension deposition:

$$T(x) = \frac{V_w V_s}{50000\ C_d} \qquad (11)$$

T - thickness of sediment deposited in a cell; V_w - volume of water the sediment has passed through to reach that cell; V_s - volume of sediment that reaches this cell; C_d - dispersion distance constant (the distance in km the injected stream extends into the marine setting).

V_w is defined by

$$V_w = V_p + V_x \qquad (12)$$

V_p - total volume of water encountered in previous cells; V_x - volume of water in the mixing cell.

V_x is calculated by

$$V_x = MC \qquad (13)$$

M - depth of the mixing column (in meters); C - cell spacing (in meters).

The amount of sedimented material out of suspension is proportional to the sediment supply and the volume of water with which it has mixed. Above the fair-weather wave base no suspended sediment can be deposited.

7.4.2 Carbonate deposition

The thickness of a sediment column at a specific cell within the simulation is represented by simultaneously acting carbonate production and subsequent redistribution (Bosscher & Schlager 1993). Within the stratigraphic simulation the following carbonate depositional systems can be simulated: (i) sabkha/ supratidal coastal plain, (ii) tidal flat, (iii) lagoon, (iv) back reef, (v) fore reef, (vi) slope and (vii) basin. For all depositional environments maximum inclination can be adjusted in time.

In nature the carbonate factory is divided into specific, water-depth dependent segments. PHIL/ BASIM™ appropriates this fact by dividing the depositional profile into four water-dependent functions:

(i) Coarse-grained traction-load material production within a
- Laterally unrestricted factory
- Laterally restricted shelf-margin factory

(ii) Fine-grained suspension-load production within a
- Unrestricted fine-grained factory
- Pelagic factory

Table 7.2 summarises the maximum and minimum production rates for the four carbonate factories within the present study. All carbonate factories produce material as a function of water depth and turbidity. The adjustable productivity function (see Fig. 7.2) is a normal distribution curve with a specified width and maximum production at a specified bathymetry (Bowman & Vail 1999). The dominant influence of light on reef growth (Boscher & Schlager 1992) is incorporated in this carbonate production curve. The production values for a cell during a specific time increment (P_{depth}) is defined by

Coarse-grained unrestricted	
Maximum growth rate (m/Ma)	90 - 710
Depth of maximum growth (m)	2 - 8
Width of the depth function (m)	10 - 12
Coarse-grained restricted (shelf-margin)	
Maximum growth rate (m/Ma)	20 - 780
Depth of maximum growth (m)	3 - 8
Width of the depth function (m)	5 - 7
Width of the distance function (km)	1
Fine-grained unresticted	
Maximum growth rate (m/Ma)	10 - 290
Depth of maximum growth (m)	8 - 10
Suspension distance (km)	15
Maximum suspension depth (m)	15
Pelagic	
Maximum growth rate (m/Ma)	25 - 43
Siliciclastic damping limit (m/Ma)	100

Table 7.2. Table of maximum and minimum carbonate production rates for the four water-depth dependent production functions used in the present study. Only Devonian values for the Abelgas, Santa Lucía and Portilla formations are considered.

the following equation:

$$P_{depth} = M\ t\ R \exp\left(\frac{-(B - D_{mp})^2}{W^2}\right) \qquad (14)$$

M - maximum production rate (m/Ma); T - time (Ma); R - siliciclastic reduction factor (see below); B - bathymetry (m); D_{mp} - maximum production bathymetry (m); W - width of the production function (m).

The reduction of carbonate productivity through siliciclastic sedimentation (siliciclastic reduction factor R from equation above) is expressed by the following equation:

$$R = 1 - \sqrt{\frac{S}{C}} \qquad (15)$$

C - rate limit of siliciclastic sedimentation (m/Ma) above which no carbonate production is possible; S - siliciclastic sedimentation rate and suspended sediment flux for the specific cell (m/Ma).

In Table 7.3 user defined carbonate variables utilised in this study are compared with published data by Bowman & Vail (1999). The simulation distinguishes between regions of high/low productivity and high/low preservation potential and distributes sediment according to these given parameters. Consequently sediment input is different at each position along the transect, as in-situ carbonate production and redistribution of sediment vary.

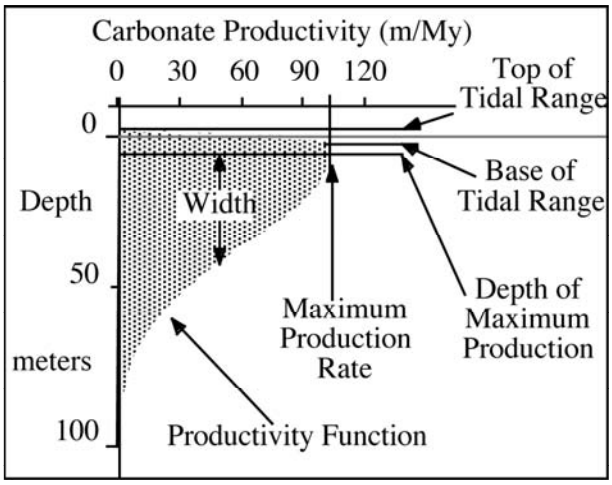

Fig. 7.2. Carbonate productivity function for stratigraphic forward modelling. The user can adjust the curve by defining the width of the production function, depth of maximum production and maximum production rate. Consequently the shape of the curve can change during the simulation. The upper limit is defined by the top of the tidal range (Bowman & Vail 1999).

7.4.3 Pelagic deposition

Organically derived pelagic sediment is produced as a function of bathymetry:

$$P = M\ T\ \left(1 - \frac{1}{\exp(0.1\ B)}\right) \qquad (16)$$

P - production of a specific cell during a time increment (m/Ma); M - maximum pelagic production rate (m/Ma); T - time (Ma); B - bathymetry (m).

	Range Bowman & Vail 1999	Range Southern Cantabrian Basin
Tidal range (m)	0 - 15	3
Carbonate rollover width (km)	0.5 - 3	0.8
Depth of fairweather wavebase (m)	?	10
Density of the mantle (kg/m^3)	3200 - 3400	3340
Density of water (kg/m^3)	1030	1030
Eff-elastic thickness (km)	1 - 65	15 - 60

Table 7.3. List of adjustable variables for carbonate depositional environments and physical variables. The values used for the Southern Cantabrian Mountains are compared with published data by Bowman & Vail (1999).

Pelagic sedimentation occurs at depths below the offlap break. Position of the CCD and ACD are not relevant, as the depositional environment of the Southern Cantabrian Basin never reached that depth.

7.4.4 Depositional gradients

PHIL/BASIM™ offers the possibility of adjusting the gradients of many different depositional environments such as fluvial, coastal plain, shoreface and depositional front gradients. All gradients measure elevation loss per distance travelled, and are unit independent ratios (meter:meter). The gradient difference between the continental and marine environments is two or three orders of magnitude (Bowman & Vail 1999). Jervey (1988) assumes that this difference alone is capable of producing the costal onlap associated with base-level changes. Table 7.4 compares the ranges of gradients used in the present study with data published by Bowman & Vail (1999).

7.4.5 Base-level

Base-level is a theoretical surface that determines whether a surface is undergoing deposition or erosion (Wheeler 1964). The position of base-level is closely linked to the intersection of water level and the depositional interface (Bowman & Vail 1999). The base-level is defined by the depositional environment:

(i) Non-marine setting:
- Siliciclastic sediment: coastal plain, stream profile
- Carbonate sediments: upper tidal range

(ii) Marine setting:
- Above the fair-weather wave base for traction-load and suspended-load deposition
- Basinward at the offlap break
- Basinward of the offlap break by gravity-flow processes

If sediment fills the space below base-level, the depositional profile migrates basinward by one cell spacing. The sedimentation is strongly influenced by the movements of base-level surface through time. This surface is controlled by the relative sea-level and the rates of sediment supply and total subsidence. Deposition occurs only if the depositional interface is below base-level and accommodation space is available, otherwise erosion can occur.

7.4.6 Substratum, compaction and physical properties

The substratum compacts as sediment is deposited from above. Thick compactable substrata result in considerable compaction subsidence (see Chapter 6.3.3 and 6.6.3). Sediment compaction is calculated as a function of burial depths (see Chapter 6.2.5). Eleven siliciclastic and eight carbonate lithologies,

	Range Bowman & Vail 1999	Range Southern Cantabrian Basin
Fluvial plain gradient	0.001 - 0.00001	0.001 - 0.0009
Coastal plain gradient	0.0 - 0.00001	0.00001 - 0.00008
Shoreface gradient	0.01 - 0.001	0.008 - 0.0009
Depositional front gradient	0.1 - 0.01	0.08 - 0.008
Tidal flat gradient	0.0001 - 0.0006	0.0001
Backreef gradient	0.1 - 0.001	0.007
Foreslope gradient	0.01 - 1.1	0.077

Table 7.4. List of depositional gradients for the siliciclastic and carbonate environments. The values used for the Southern Cantabrian Mountains are compared with published data by Bowman & Vail (1999).

each with specific density, initial porosity and compaction rate constant are applied (see Table 6.2). The generation of overpressure can occur by rapidly accumulating muddy sediments followed by tight lithologies, which do not allow a release of hydrostatic pressure. The consequent retardation of compaction is considered within this simulation. The distribution of porosity in the cross section is determined by the lithofacies and maximum burial depth of the interval. The distribution of physical properties, such as permeability and density is derived from porosity and lithology (Bowman & Vail 1999). They can form the basis for synthetic seismic sections.

7.4.7 Erosion

There are two types of erosion considered within the modelling: subaerial and submarine erosion. They are subdivided into four mechanisms:

(i) Shoreface erosion produced by wave-energy
(ii) Non-marine channel-incision
(iii) Surface bevelling
(iv) Bottom-current transport

Subaerial erosion removes material from exposed regions, changing the shape of the eroded area and adding the eroded sediment to the clastic sediment supply, which is redeposited in adjacent areas. The base of the erosive profile is defined by the storm-weather wave base. Bowman & Vail (1999) introduced the following equation for surface bevelling as a function of the average surface gradient on either side of a particular cell.

$$S = E\,T\,\frac{R_r + R_l}{2\,C} \qquad (17)$$

S - amount of sediment eroded (m); E - erosion rate (m/Ma); T - time increment (Ma); R_r and R_l - differences in relief between the cell of interest and the cells on the right and left (m); C - cell spacing (m). Fig. 7.3 displays the user defined variables controlling erosion processes. Submarine erosion redistributes sediment material, smoothing submerged areas. Erosion by waves, slumps and slides can affect large regions and remove huge quantities of sediment. Erosion by marine currents is simulated by the "marine current smoothing width." The slope is tested for stability in each time increment, taking a user-defined angle of slope stability into consideration.

7.5 Simulation workflow

Sedimentation along basin margins includes mixed carbonate-siliciclastic depositional systems with determining depositional algorithms. The model generates each stratal or time-line by means of a series

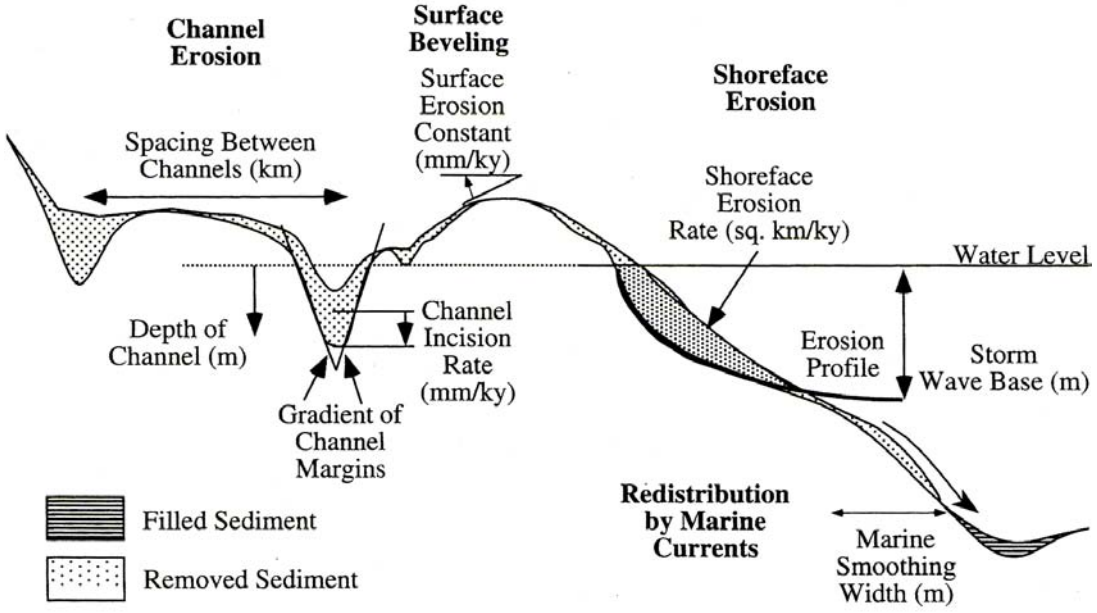

Fig. 7.3. Sketch showing the variables that control erosion processes during stratigraphic modelling with PHIL/BASIM™.

of steps (Bowman & Vail 1999):

- Adjustment of the profile for tectonic and sea-level specifications, location of the intersection between the sea-level and the profile.
- Calculation of the flexural response of the crust to a change in water column and sediment load deposited in the previous time-step.
- Adjustment of the depths of the horizons for compaction as a function of depth and sediment type.
- Modification of the profile by erosion where it lies above the base-level of erosion.
- Addition of the eroded siliciclastic sediment to the siliciclastic sediment supply and of eroded carbonate sediment to the excess carbonate sediment supply for redistribution. A compilation of erosion rates has been published by Enos (1991).
- Basinward progradation of a depositional profile until the traction load portion of the siliciclastic sediment supply is exhausted. The siliciclastic deposition algorithm models traction processes with the prograding clinoform, and deposition of suspension load by injection and mixing within the marine water column.
- Production of carbonate sediment as a function of the bathymetry, position on the margin, and distribution of siliciclastic sediment. The excess production is removed and redistributed first in the lagoon and then in the basin below a prograding clinoform. Suspended carbonate sediment is transported offshore in the water column and deposited by settling.
- Deposition of pelagic sediment as a function of water depth in marine settings.
- Removal of the deposited sediment with slopes greater than a defined limit of stability above a fault scarp. Basinward sediment transport by slumping and turbidites, basin-floor fan deposition, submarine canyon and channel-overbank fan formation.

At the end of each time-step a time-line is recorded in the transect. This procedure is repeated for every time-step and cell of the model.

7.6 Constraints

- No out-of-plane sediment transport. All processes working in the third dimension such as sediment transport out of or into the cross-section plane or channel incision can only be predicted to a limited extent
- Limited bio/chronostratigraphic resolution in the early Palaeozoic
- No climatic and/or hydrodynamic simulation, except for abrasion and reworking above wave base (traction, suspension).
- Palaeoenvironmental parameters are indirectly considered by evaporation rates, tidal depth, shoreline erosion etc.
- Non-uniqueness of results. Different combinations of input parameters can lead to the same modelling results. Numerical models are geological assessed. Minimum/maximum models limit the range of possible parameter configurations.
- Unsolved biotic interactions. No simulation is capable of modelling the complex interactions within the carbonate factory and siliciclastic environments with sufficient accuracy. The unique interplay between organisms, water conditions such as bathymetry, salinity or nutrient content and climate in time depends on a large number of variables. Each simulation must make a compromise between a sufficient quantity of variable parameters, determinable variables and an acceptable simulation runtime. For example, the type of terrigenous sediment suppressing carbonate productivity is not taken into account, although organisms usually tolerate accumulation of coarse sediment better than of mud. Additionally different genera tolerate terrigenous input in different ways. Considering the high percentage of mud and continuing carbonate production in many rocks, the tolerance of carbonate organisms to mud is probably higher than generally noted (Enos 1991). In nature the type of substrate also influences the ability of organisms to colonise an area. A sandy, unstable and shifting ground will only be suitable for a few pioneer faunas, etc.

7.7 Numerical and graphical output

The evolution of the basin architecture can be visualised by means of a time-series animation, whereas the numerical results can be plotted as cross sections, stratigraphic columns or chronostratigraphic

plots:

(i) The lithostratigraphic evolution of the Southern Cantabrian Basin for the whole simulation duration is best visible in the QuickTime™ time-series animation (see file "Movie_2.mov").

(ii) A series of lithostratigraphic plots illustrate the predicted distribution of facies along the transect, as well as the development of sediment geometries before the onset of the Variscan deformation (Fig. 7.4). In the same way physical properties such as porosity, density or permeability are plotted in time along the transect.

(iii) A palaeobathymetry figure plots the bathymetry at the time of deposition (Fig. 7.5A).

(iv) A chronostratigraphic diagram plots the thickness of each horizontal interval according to its position along the cross section. The thickness of the interval is represented by the height of the interval for each cell. Depositional depths (palaeobathymetry) are plotted in relation to time (Fig. 7.5B).

(v) Stratigraphic columns can be drawn for each cell and compared with cross-sections in order to calibrate the forward simulation to real-world basin fill data (Fig. 7.6 and 7.7). The interval may be filled with lithofacies, systems tract, or palaeobathymetric information of the interval. Stratal patterns corresponding to lithofacies boundaries are expressed in the weathering profile. Missing time intervals are represented by arrows, the widths of these are proportional to the amount of time missing.

(vi) The relative sea-level figure plots the given sea-level and tectonic histories, with the resulting total subsidence, and relative change of sea-level history (sum of total subsidence and sea-level changes), through time (Fig. 7.8). The relative sea-level curve varies for different locations along the transect, due to different rates of tectonic subsidence.

7.8 Results

Basin fill development is mainly controlled by two major parameters: accommodation and sediment supply/production (see Chapter 5.2). For case of comparison, relative changes in 2D influx/production may be focus on (instead of absolute rates).

7.8.1 Siliciclastic influx

Changes in sediment input and sea-level fluctuations are plotted in Fig. 7.9. From the uppermost Neoproterozoic to the Early Ordovician the area was dominated by a high flux of siliciclastic sediments interrupted by several long-term hiati and the deposition of a thin carbonate succession (Láncara Fm., 525-513Ma). The sedimentation rates fluctuated around 3200m²/ka during Herrería time. The siliciclastic flux increased slightly from the deposition of the Oville Fm. (4000m²/ka) to the La Matosa Mb. of the Barrios Fm. (4600m²/ka) and diminished again to 2600m²/ka (Tannes Mb.). In the southern part of the transect, the Getino Fm. represents a thin, mixed siliciclastic/carbonate succession with very low sediment flux (400m²/ka) and condensed character. During Silurian times only siliciclastic material was deposited. The deeper water dark shales and siltstones of the Formigoso Fm. indicate quiet depositional environments with very low sedimentation rates (600m²/ka). This pattern changes considerably with the onset of shallow water coarse-grained San Pedro sandstones and iron oolithes. During this time, flux rates increased to 1800m²/ka, diminishing towards the top of the formation by 60% (600m²/ka). The Devonian is characterised by an alternating deposition of siliciclastics and carbonates, with highly variable clastic sediment supply (770m²/ka up to 4000m²/ka; see Fig. 7.9). Periods of clean carbonate deposition (Abelgas, Santa Lucía, Portilla formations) were disrupted by shaly deposits of the Esla Fm. (700 to 1000m²/ka) and the high sedimentation rates of the shaly to sandy Huergas Fm. (3800 to 4000m²/ka). The alternating periods of siliciclastic and carbonate deposition reflect the complex interplay between total subsidence, sediment input and eustatic sea-level fluctuations. After the last period of large reefal development in the Southern Cantabrian Basin (Portilla Fm.) siliciclastic sedimentation dominated until the Early Carboniferous. Siliciclastic flux increased slightly during the deposition of the Nocedo Fm. (1800 to 2200m²/ka), decreasing again throughout the Fueyo (770m²/ka), Ermita (210m²/ka) and Vegamián times (20m²/ka).

7.8.2 Carbonate accumulation rates

Compacted accumulation rates were used for the quantitative comparison of the Cantabrian carbon-

ate factories with data taken from literature. These rates are the most common and easiest way of making quantitative estimates. Decompacted values of the formations investigated and the comparison to the compacted values are calculated for information purposes in Table 7.5. Fig. 7.10 shows a compilation of compacted accumulation rates of carbonate systems for the Devonian, Carboniferous and Cenozoic. Only rates with a time span of observation between 2 and 20Ma were plotted, corresponding to the time spans of the Cantabrian carbonate formations. Schlager (2000) stressed that the sedimentation rates of all carbonate systems decrease with an increasing time span of observation. This is due to periods of non, or reduced deposition within a given interval (see discussion in Chapter 5.2.5). Decompacted rates for the three Devonian carbonate formations reach values 20 to 39% higher than compacted values (see Table 7.5). Compacted accumulation rates of the Santa Lucía Fm. (26 to 56m/Ma) achieve values slightly lower than values printed for comparison (Fig. 7.10). The values increase from the northernmost occurrence of this formation (km 15 along transect) to the south, reaching a peak at km 42 (56m/Ma). Further to the south the values diminish by nearly 54% reaching 26m/Ma in the southernmost part of the transect. Portilla (19 to 30m/Ma) and Abelgas (8 to 18m/Ma) formations show considerably lower rates. Maximum accumulation rates within the Portilla Fm. are reached at km 42 along the transect, at the same position as in the case of the Santa Lucía Fm. The peak value of the Abelgas Fm. is located slightly further to the south at km 45.

7.8.3 Carbonate production rates

Values for carbonate production as well as carbonate accommodation are given in m/Ma. The first carbonate deposits in the Southern Cantabrian Basin are those of the Láncara Fm. The lower member, composed of shallow marine limestones and dolomites (see Chapter 2.4.4), displays carbonate production rates of 15 to 32m/Ma. A major transgression flooded this shallow marine environment, resulting in the deposition of biomicrites and red nodular limestones (upper member). The carbonate production rates mirror this marked change towards a deep-water condensed environment, diminishing

Table 7.5. Comparison of compacted and decompacted accumulation rates for the three Devonian carbonate factories. The difference is calculated in % and shows 25% to 39% higher rates for decompacted values.

Cross-section	Mi/Cha	Genicera	F/VP	LV	PO/BB/SL	Geras/LPG	Huergas	Olleros deAlba
Accumulation rates (compacted) in m/Ma								
Portilla Formation	0.00	0.00	0.00	0.00	29.83	25.67	19.33	23.60
Santa Lucía Formation	0.00	0.00	29.16	37.00	56.04	37.44	34.00	26.00
Abelgas Formation	8.15	9.62	7.54	14.23	10.38	17.62	15.38	8.46
Accumulation rates (decompacted) in m/Ma								
Portilla Formation	0.00	0.00	0.00	0.00	37.21	32.85	25.79	30.34
Santa Lucía Formation	0.00	0.00	36.40	46.55	71.29	49.38	45.01	34.75
Abelgas Formation	11.14	12.72	10.12	18.26	13.79	22.52	20.69	11.79
Difference in %								
Portilla Formation	0.00	0.00	0.00	0.00	124.74	127.99	133.42	128.58
Santa Lucía Formation	0.00	0.00	124.81	125.81	127.21	131.89	132.37	133.66
Abelgas Formation	136.65	132.28	134.19	128.29	132.78	127.83	134.46	139.37

	Abelgas Formation	Santa Lucía Formation	Portilla Formation
Coarse-grained unrestricted	90 - 230	100 - 710	130
Coarse-grained restricted	20 - 50	100 - 780	150
Fine-grained unresticted	10	290	50
Pelagic	25 - 30	36 - 43	31

Table 7.6. Compilation of maximum and minimum carbonate production rates for the three Devonian carbonate formation. See Chapter 7.8.3 for details.

significantly by an order of magnitude (0.5 to 4.5m/Ma). After the deposition of the Láncara Fm. it took nearly 100Ma before environmental conditions suitable for the development of a carbonate factory were re-established.

The Devonian is one of the most significant maxima of reefal carbonate production in the Phanerozoic (Kiessling et al. 2000). In the Southern Cantabrian Basin three important carbonate producing intervals occur within the Devonian. These are the Abelgas Fm. (415-402Ma), Santa Lucía Fm. (396-391Ma) and Portilla Fm. (385-382Ma). These three Cantabrian carbonate factories show very different production rates (Table 7.6). The oldest, Abelgas Fm. (415-402Ma), has the lowest carbonate production rates (10 to 90m/Ma) increasing towards the top of the succession by more than 100% (50 to 230m/Ma). Following the shaly deposits of the Esla Fm. (402-396Ma), the significant reefs of the Santa Lucía Fm. developed. They represent the highest production rates in the entire simulation interval. However, the development of carbonate production rates shows peak values only in the middle part of the succession (290 to 780m/Ma). The lower and the upper parts of the succession display significantly lower levels of carbonate production, ranging between 100 and 290m/Ma. The carbonate sedimentation is once again followed by high siliciclastic sediment influx (4000m^2/ka, Fig. 7.9) from the Huergas Fm. (391-385Ma). The carbonate factory managed to re-appear again in the form of the Portilla Fm., but was not capable of reaching the productivity boasted by the Santa Lucía factory. The renewed carbonate conditions display significantly lower carbonate production rates of 50 to 150m/Ma (Table 7.6). Thick siliciclastic depositions of the Nocedo (382-373Ma), Fueyo (373-361Ma) and Ermita formations (358-355Ma) interrupted the carbonate production for a considerably long period of time. Due to the fact that the thin (up to 10.5m in the La Pola de Gordón section) Baleas Fm. was deposited at the same time as the Vegamián and Ermita formations, estimations on carbonate production rates were not possible within the simulation. In addition, numerous hardgrounds within the coarse-grained, bioclastic carbonates point to several minor hiati within the formation, making more detailed estimations on carbonate productivity difficult. The facies of the Alba Fm. is comparable to the upper member of the Láncara Fm., being composed of red nodular limestones, radiolarites and shales. The carbonate production of the pelagic factory shows comparable rates of 5m/Ma.

7.8.4 Predicted lithofacies distribution

Stratigraphic forward modelling offers unique possibilities for predicting the lithofacies distribution between information points, such as measured cross-sections in the present study. Within the Southern Cantabrian Basin this represents the only means of gaining stratigraphic data, where structural complications inhibit further investigations. The evolution of lithostratigraphic distribution in time is documented as a time-series animation in the file "Movie_2.mov". The animation comprises the evolution of the basin for the time span between the top of the basement (560Ma) and the top of the Alba Fm. (322Ma) before the onset of Variscan deformation in the Cantabrian Zone (see Chapter 2.2.1). As mentioned in Chapter 7.3.1 the time step is 500ka with a total of 476 time lines. 3D isometric plots of the depositional area within the animation have been chosen in order to highlight the progradational and retrogradational patterns of facies belts. Fig. 7.4 plots the lithofacies distribution for five selected time lines (513, 511, 391, 373 and 322Ma).

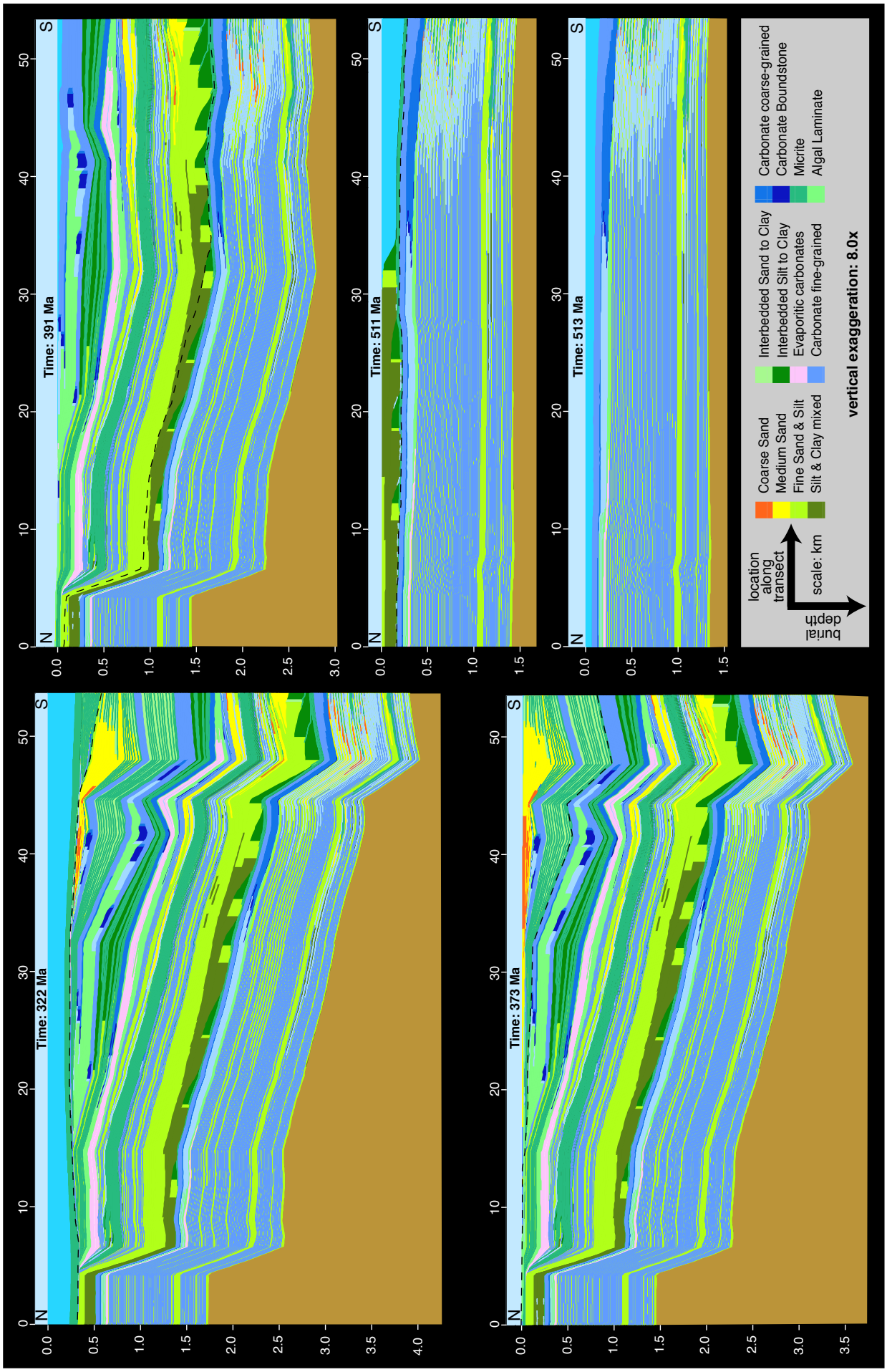
Time: 391 Ma
Time: 511 Ma
Time: 513 Ma
Time: 322 Ma
Time: 373 Ma
N
S
location along transect
scale: km
burial depth
Coarse Sand
Medium Sand
Fine Sand & Silt
Silt & Clay mixed
Interbedded Sand to Clay
Interbedded Silt to Clay
Evaporitic carbonates
Carbonate fine-grained
Carbonate coarse-grained
Carbonate Boundstone
Micrite
Algal Laminate
vertical exaggeration: 8.0x

Fig. 7.4. Plots of selected time lines showing the predicted lithologic distribution along the Bernesga Transect before the onset of Variscan deformation. The top of an increment is marked by a dashed line in the plot that follows. 513Ma: Top Láncara Formation; 511Ma: Oville Formation; 391Ma: Top Santa Lucía Formation; 373Ma: Top Nocedo Formation; 322Ma: Top Alba Formation.

Thick siliciclastic deposits of the Herrería Fm. (Chapter 2.4.4) display a uniform distribution of sandy to silty material across the transect. South of km 47, coarse-grained sandstones show retrogradational and progradational patterns (Fig. 7.4). Palaeobathymetric information is plotted in Fig. 7.5 and displays continental to intertidal depositional depths increasing slightly basinwards.

The Láncara Fm. is composed of algal laminates, supratidal and intertidal fine-grained carbonates in its lower part (Fig. 7.4). A rising eustatic sea-level (see Fig. 7.8) causes a progradation of facies belts (km 32 to 37) and a low-order transgressive surface, above which pelagic nodular limestones were deposited in depths of 70 to 150m.

The onset of high siliciclastic flux rates in the Oville Fm. (4000m^2/ka, Fig. 7.9) results in a rapid progradation of a deltaic system. During progradation of the foresets, compaction of underlying strata is clearly visible in the animation (Movie_2.mov). The deposition of finer, deeper water siliciclastics in the lower part and coarser material under shallow water conditions in the upper part of the formation causes the development of a coarsening upward and shallowing upward pattern within this time period. The subsidence along the transect is uniform throughout the deposition of the Herrería to Oville Fm., being slightly influenced by compaction-induced subsidence.

The subsequent Barrios Fm. is a uniformly composed, litoral, fine-grained sandstone succession with some medium to coarse-grained intercalations. The animation and the chronostratigraphic plot (Fig. 7.5B) show two major hiati (15 and 10Ma), marked by a slight uplift and subsequent erosion of parts of the deposits.

The deposition of the Capas de Getino Fm. is characterised by a combination of siliciclastic and carbonate deposition. These somewhat condensed sediments are partly eroded and redistributed during the subsequent significant stratigraphic gap (24Ma, See Chapter 4.2 for discussion).

Increased subsidence and a rising eustatic sea-level produce sufficient space for the deposition of the Formigoso Fm. (Fig. 7.5). This formation is dominated by uniform dark shales with intercalated siltstones, showing coarser material to the top (Fig. 7.4 and Chapter 2.4.4).

A strong increase in sediment input (600 to 1800m^2/ka, Fig. 7.9) initiates the sedimentation of the San Pedro Fm. The continental to intertidal medium-grained sandstones of the basal member are uniformly deposited across the transect. Slight uplift and subsequent erosion of the northern part of the transect restricts the deposition of the upper part of the formation (Members B and C) to the southern areas.

The basin remains in shallow water conditions, but the siliciclastic input has ceased (Fig. 7.9). This enables supratidal sabkha deposits from the Abelgas Fm. (Chapter 2.4.4) to spread across the basin. In a deepening upward succession these deposits are followed by deeper water limestones, which are covered by the shales of the Esla Fm. The shelf experiences a differential subsidence during this time as can be clearly seen in the animation, This results in two thickness maxima at km 33 and 54 (Fig. 7.4).

The renewed onset of carbonate production (see above) results in the deposition of coarse-grained bioclastic carbonates and a subsequent progradation of prominent boundstone edifices. These thick bodies cause major compaction of the underlying material, producing a jagged pattern within the plots. A supratidal lagoon develops landward from the reefs, marked by light greenish colours (algal laminate). However, the lack of accommodation space in the northern areas impedes any deposition north of kilometer 15 during the Santa Lucía time.

Strong subsidence in the southern areas and high siliciclastic sedimentation rates (up to 4000m^2/ka) allows the accumulation of thick intercalated shales and sandstones in the Huergas Fm.

The subsequent carbonate Portilla Fm. is restricted to the area south of km 33. The reefal development here is less prominent than the development of the reefs of the Santa Lucía Fm., but they grow at about the same position along the Bernesga Transect (approx. km 42, Table 7.6, Chapter 7.8.2 and 8).

The Nocedo Fm. has the same spatial restrictions as

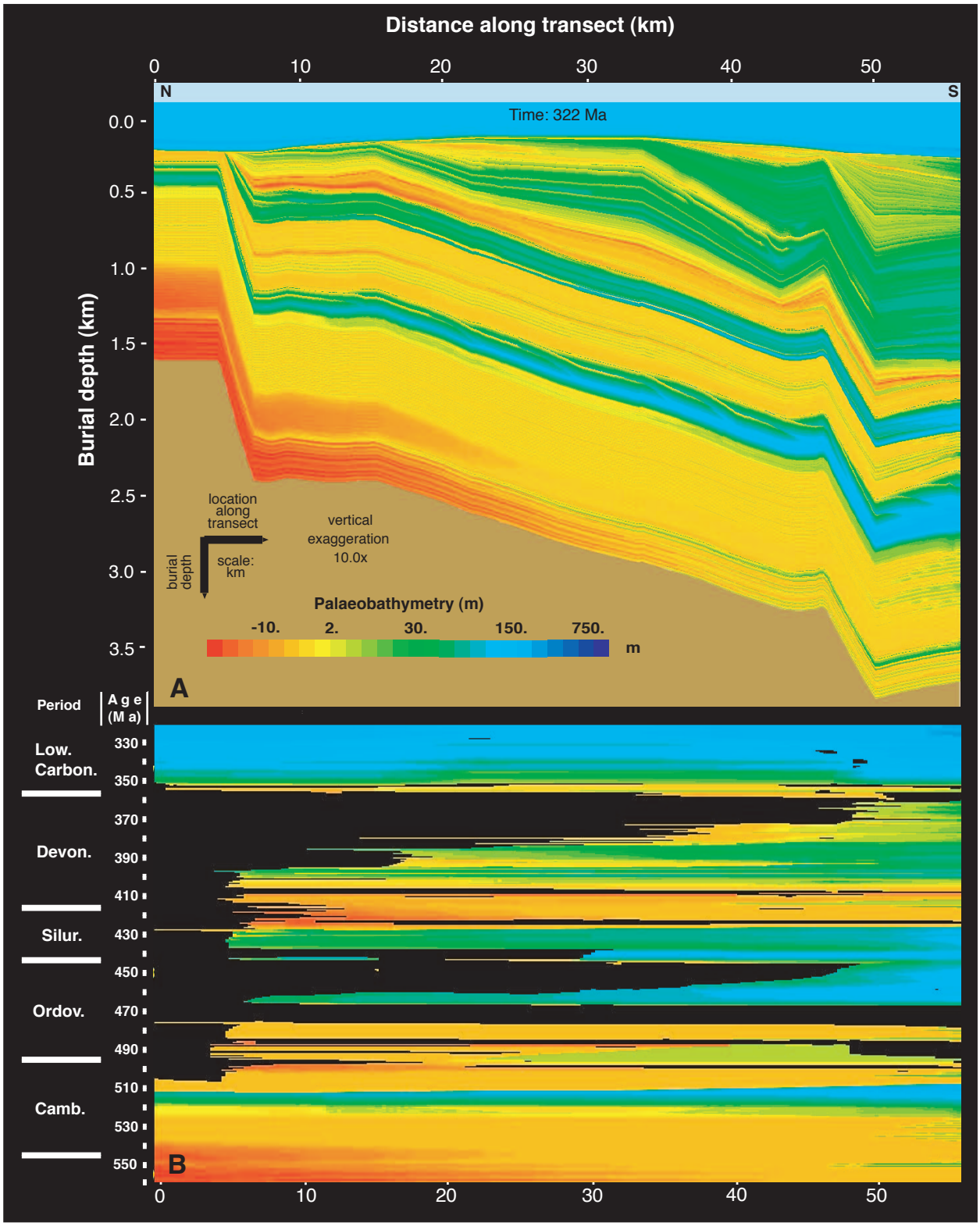

Fig. 7.5.
A: Depositional depths (palaeobathymetry) of sediments along the Bernesga Transect. The youngest sediments represent the top of the Alba Formation (322Ma). Note the predominance of shallow marine settings throughout the basin development.
B: Chronostratigraphic plot for the time 560Ma to 322Ma. Depositional depths (palaeobathymetry) are plotted in relation to time. Areas of non-deposition (hiati) are coded in black. See the pronounced backstepping of depositional areas and expansion of the uplifted region to the south in the Devonian.

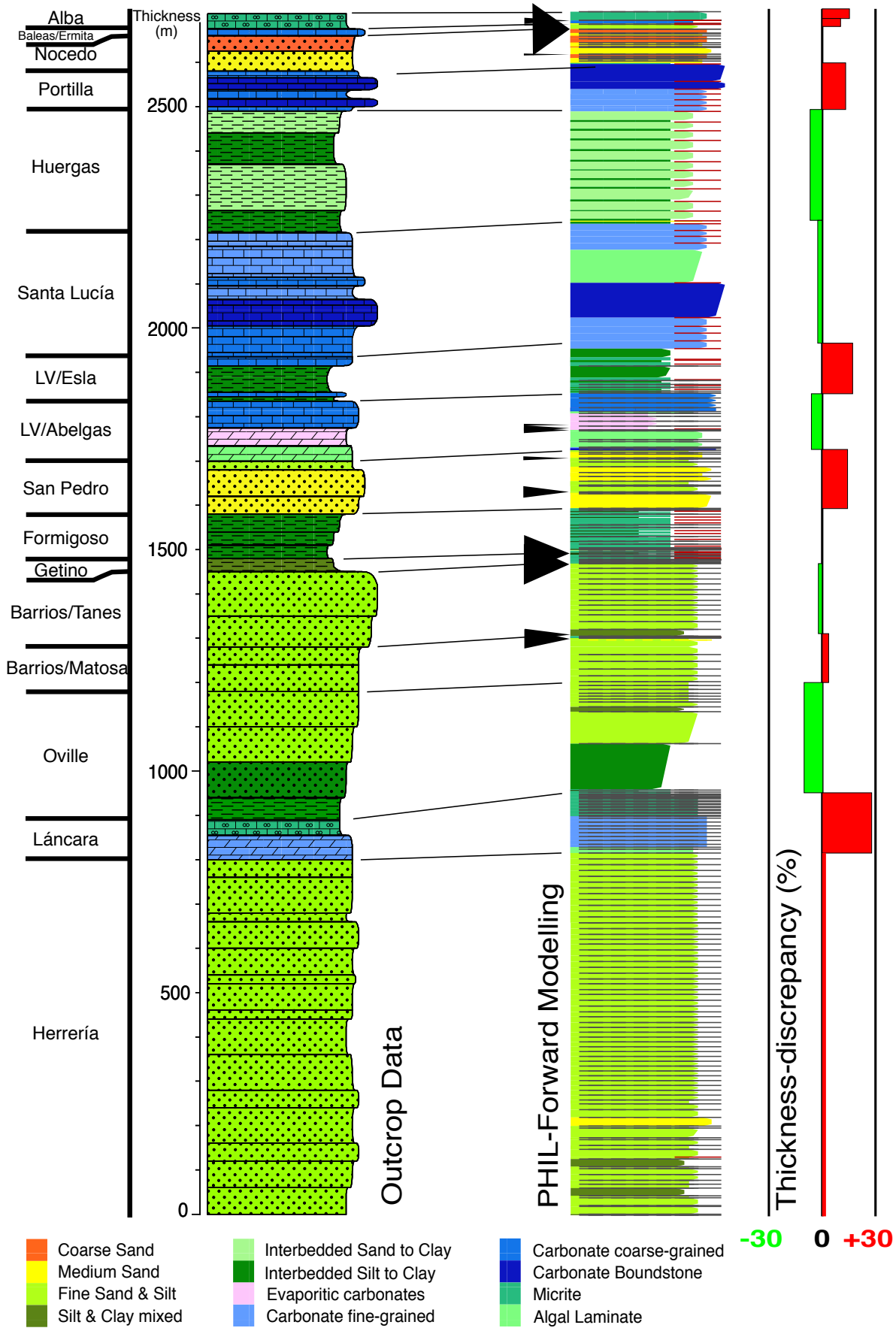

Fig. 7.6. Comparison of outcrop data (simplified stratigraphic section) and synthetic cross-section (output forward stratigraphic modelling) at an identical position along the transect (km 42). Black arrows indicate times of non-deposition and/or erosion. They are proportional to the hiatus time span. Mean values for thickness discrepancy range between 5% and 12%. See Figure 2.21 for absolute ages of the formations.

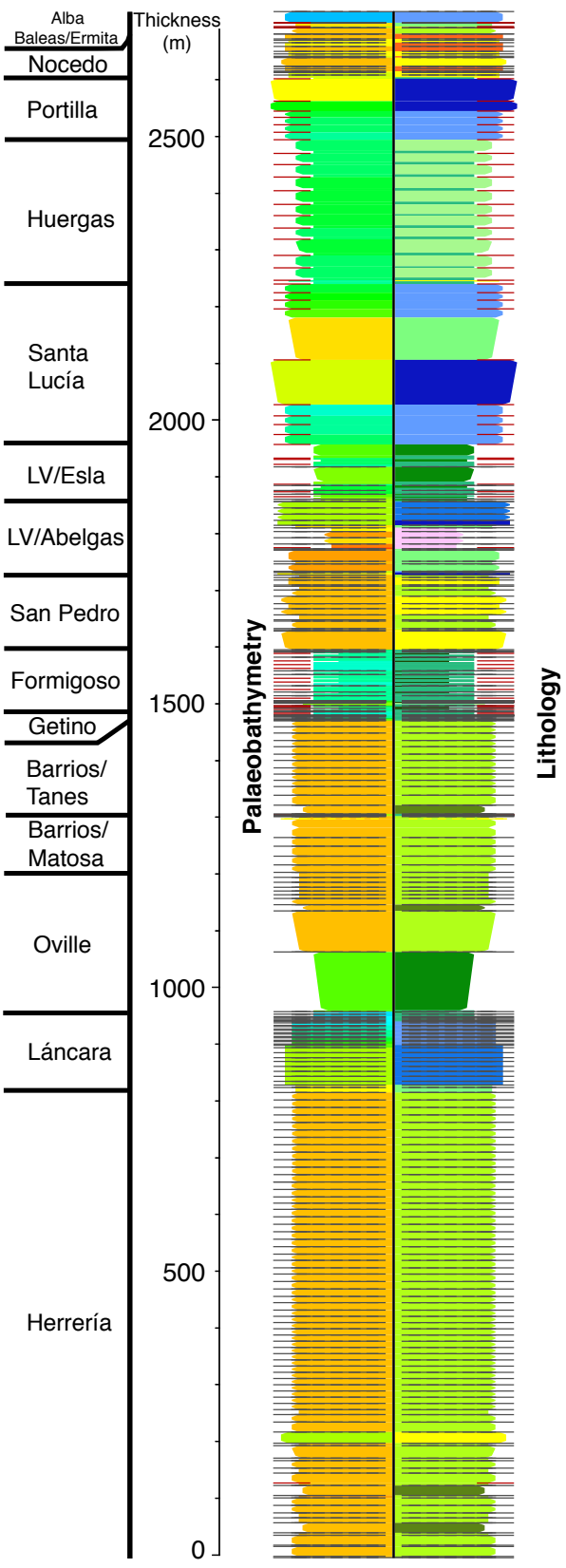

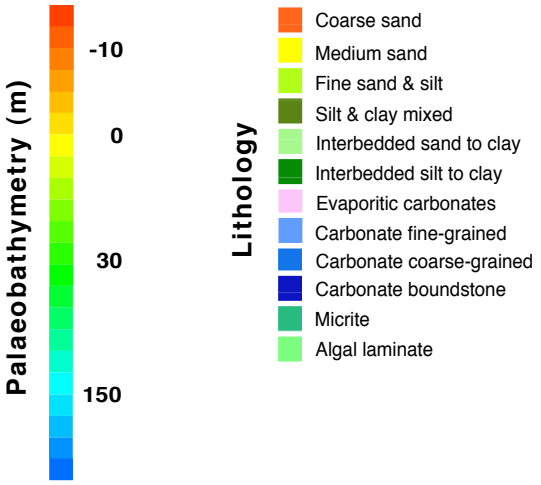

Fig. 7.7. Predicted stratigraphic column with combined lithologic and palaeobathymetric information. The position of the column is the same (km 42 along the Bernesga Transect) as in Fig. 7.6. Note the different keys for the different columns.

the Portilla Fm. however, it shows a very remarkable thickness distribution. Relatively thin (60-80m), coarse-grained sandstones are deposited between kilometer 35 and 46 (Fig. 7.4). At km 45 strong subsidence creates a trough, which is filled by a thick succession (up to 430m) of uniform sandstones. This succession thins towards the distal parts of the basin by 43%.

The shales and siltstones of the Fueyo Fm. are restricted only to the area of the thick trough of the previous formation (south of km 46). During the deposition of the Nocedo and Fueyo formations, the northernmost part of the Bernesga Transect experiences a slight uplift, whereas the middle part remains stable. During the following hiatus the whole transect is considerable uplifted and affected by erosion. This uplift is stronger in the northern areas (see "Movie_2.mov").

The shallow-water Ermita and Baleas formations are deposited over the flattened area. However, due to the minor thickness of these two formations (3 to 10m), they are not visible with the resolution used for the present study, and do not allow detailed facies estimates.

The depositional environment subsequently experiences significant deepening accompanied by the deposition of black shales of the Vegamián Fm. and red nodular limestones of the Alba formation (Chapter 2.4.4). The subsidence is fairly uniform with slightly higher values to both the north and south. This causes a shallower area in the middle of the Bernesga Transect with slightly thinner deposits. The palaeobathymetry of the Alba Fm. ranges from a water depth of 100 to 300m (Fig. 7.5 A). Predict-

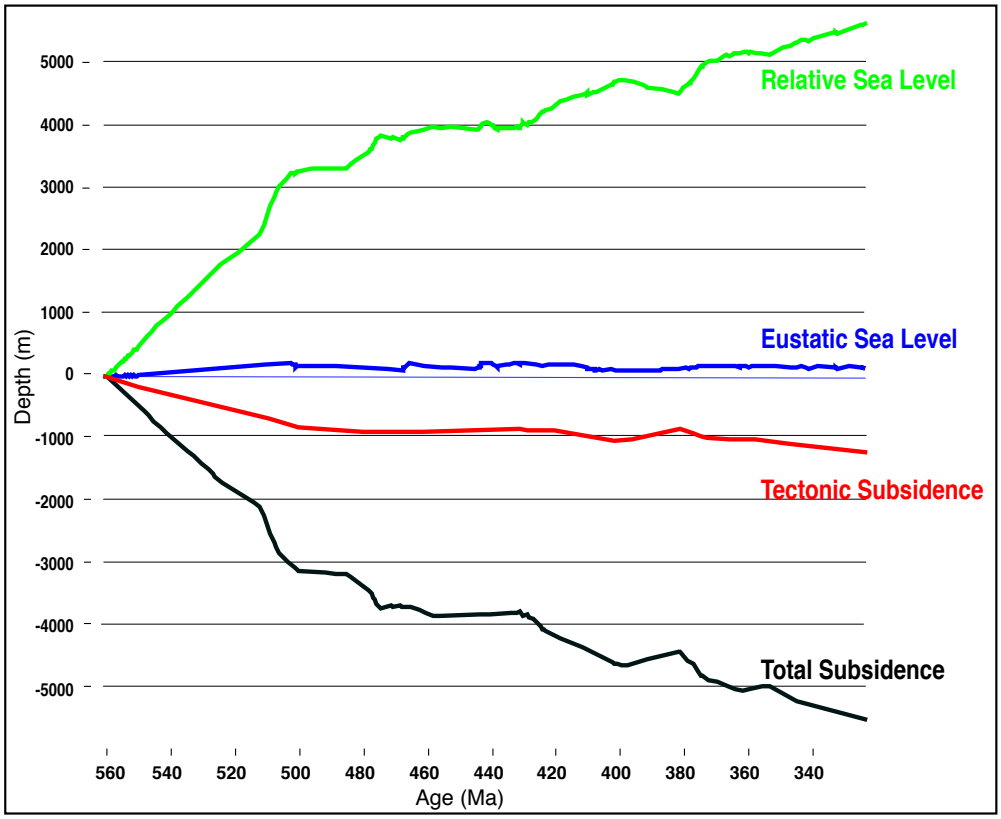

Fig. 7.8. Relative sea-level changes, tectonic and total subsidence calculated during the stratigraphic forward modelling at the offlap break. See Chapters 6.2.3 and 7.3.3 for details on the eustatic sea-level curve. Note that the offlap break was not static during the simulation.

ed porosity and density distribution along the Bernesga Transect is plotted in Figs. 7.11 and 7.12. As expected, both physical parameters are strongly dependent on the burial depth and type of lithofacies distribution (see Chapter 7.4.6). In other areas, such plots are highly important for exploration on hydrocarbons.

7.8.5 Eustatic sea-level fluctuations and depositional gaps

2D stratigraphic modelling using the composed eustatic sea-level curve (see Chapter 6.2.3, 7.3.3 and Fig. 6.4) was not able to match the geologic patterns observed in the Southern Cantabrian Basin. High amplitudes of main eustatic peaks, for example in the Late Cambrian, Middle Ordovician and Early Silurian to Early Devonian, caused unreliable results (see below). Multiple simulation runs tested the eustatic sea-level curve for differentially changed thermo-tectonic subsidence rates as well as for altered siliciclastic sediment flux rates and carbonate production rates. All attempts ended in unrealistic features, such as incorrect water depths during deposition, unrealistically high sediment thicknesses, non-observed erosional gaps, exaggerated bathymetric trends along the Bernesga Transect or non-fitting facies patterns. As the only realistic solution, amplitudes of the composed eustatic sea-level curve were reduced by 1.5 to 21% with a mean value of 9%, while the overall track was preserved (see Fig. 7.13). By using the modified eustatic sea-level curve only minor changes needed to be made to thermo-tectonic subsidence rates in comparison to 2D reverse basin modelling results. This is an important result of this study.

Major falls in the eustatic sea-level correlate well with the occurrence of stratigraphic gaps (Fig. 7.9). The first major sea-level fall (approx. 70m) in the Late Cambrian matches the initiation of the first major hiatus (500 to 485Ma) in the Southern Cantabrian Basin. Fig. 7.5 B shows the plot of depositional water depth in relation to time. Black areas signify times of non-deposition (hiati). However, the first hiatus is not well shown in the figure. This is due to the fact that sediment was eroded and redistributed along the transect during this time period.

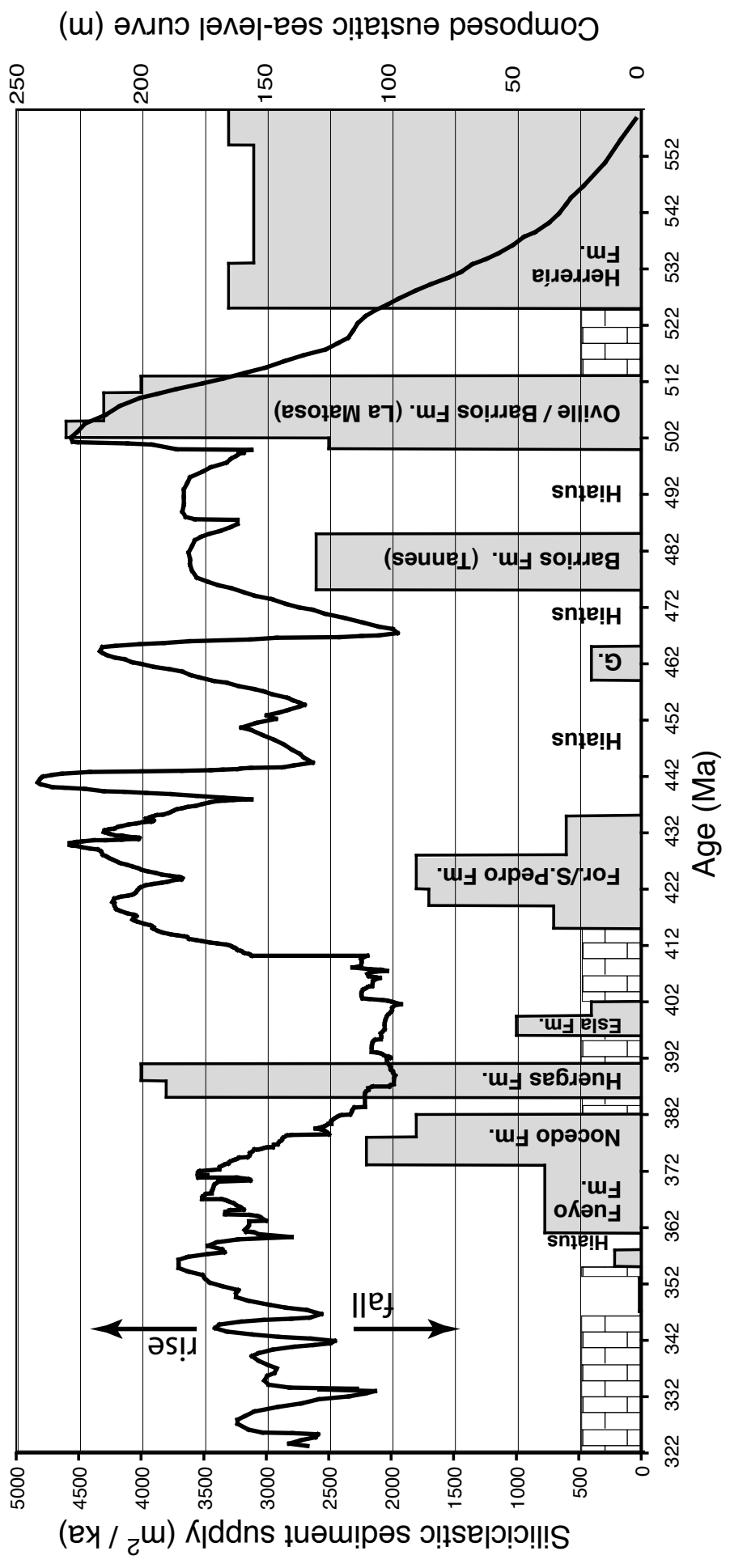

Fig. 7.9. Siliciclastic flux, carbonate deposition, stratigraphic gaps and sea-level changes for the Bernesga Transect. Shaded areas represent siliciclastic sediment supply in time. Values are given in square meters per 10,000 years, as they represent the supply for a two-dimensional transect and do not fill a three-dimensional space. Eustatic sea-level fluctuations are plotted as a solid line. See text for references. Times of carbonate deposition are marked with a brick-signature in order to distinguish them from the hiati. The height of the column does not signify the amount of carbonate production. Note the good fit btween major eustatic sea-level falls and hiati during the following time spans: 500-485Ma, 475-465Ma, 459-435Ma and 361-358Ma. The position of the hiati within the stratigraphic record is given in Fig. 2.21.

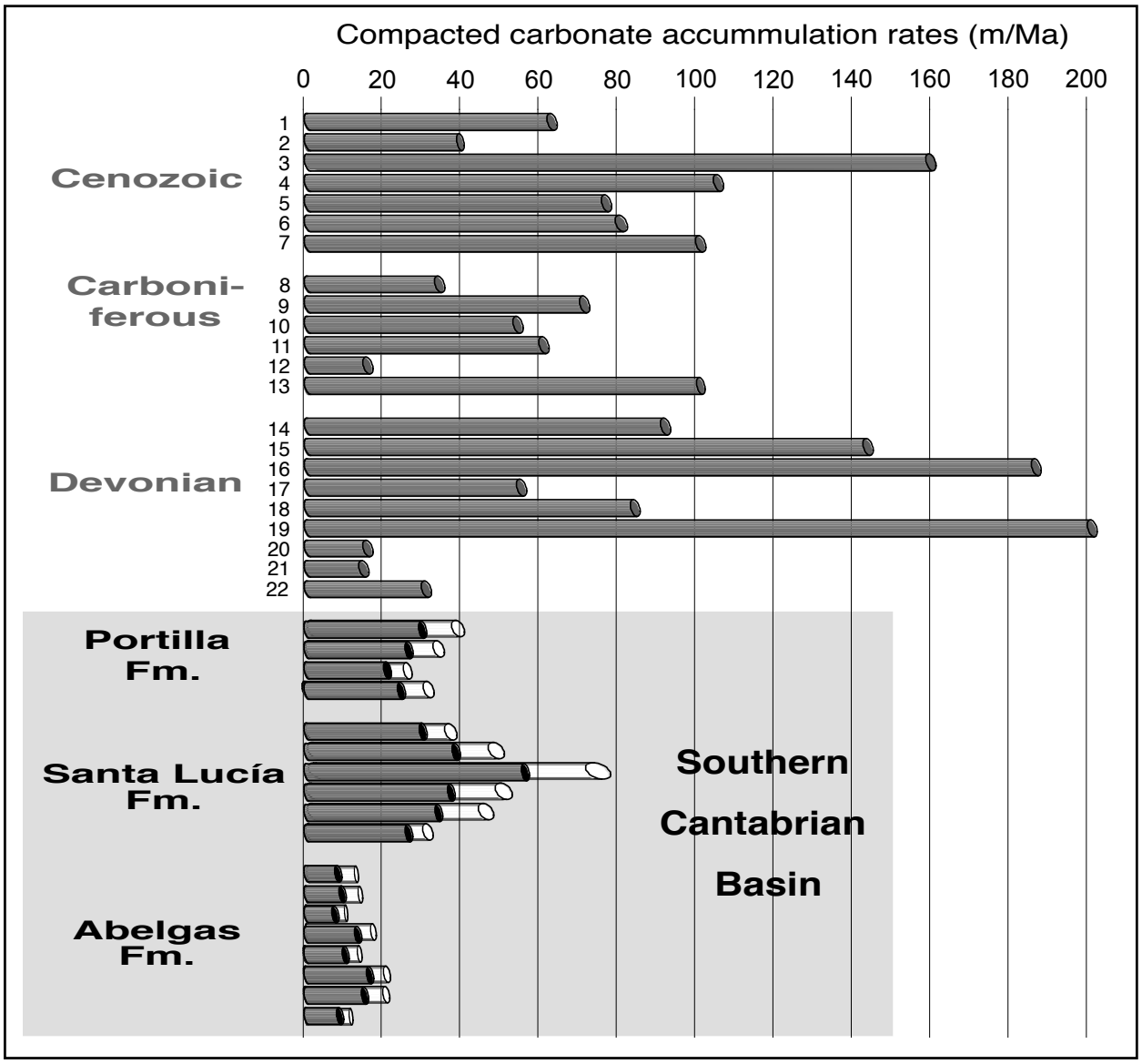

Fig. 7.10. Compacted carbonate accumulation rates for the Devonian, Carboniferous and Cenozoic, as well as for the three Devonian carbonate formations of the Southern Cantabrian Basin (Abelgas, Santa Lucía and Portilla formations). Decompacted carbonate accumulation rates of the Cantabrian formations are plotted in white bars. Data outside the Cantabrian Mountains has been put together from the following authors: (1) Chevalier 1973; (2) Frost 1981; (3) Terry & Williams 1969; (4-7) Enos 1991; (8) Parkinson 1957; (9) Lees 1961; (10) Rose 1976; (11-13) Enos 1991; (14) Walls et al. 1979; (15) Playford 1980; (16) Krebs 1974; (17) Muir et al. 1985; (18, 19) Burchette 1981; (20-22) Enos 1991.

Thus PHIL/BASIM™ records sediment movement from one cell to another, which is defined as deposition. The second hiatus (475 to 465Ma) developed after the onset of the second major fall in sea-level (approx. 80m) starting at 477Ma (Fig. 7.9). From 464Ma to 455Ma the eustatic sea-level fell by approx. 80m, coinciding with the largest hiatus in the evolution of the Southern Cantabrian Basin (459 to 435Ma). However, a major rise in sea-level by approx. 105m (peak at 441Ma) and subsequent fall by approx. 80m is not recorded in the development of the stratigraphic gap. The extent of this hiatus and the stratigraphic record of the Capas de Getino Fm. are poorly constrained and vary between outcrops (see Chapter 4.2 for discussion). Late Ordovician is missing in the majority of outcrops. Consequently, the continuous sedimentation plotted in the southern part of the Bernesga Transect (see Fig. 7.5B) is arguable, partly caused by the erosion/redistribution problem mentioned above. Also the youngest hiatus (361 to 358Ma) coincides with a fall in eustatic sea-level, even though this fall is smaller (approx. 25m)

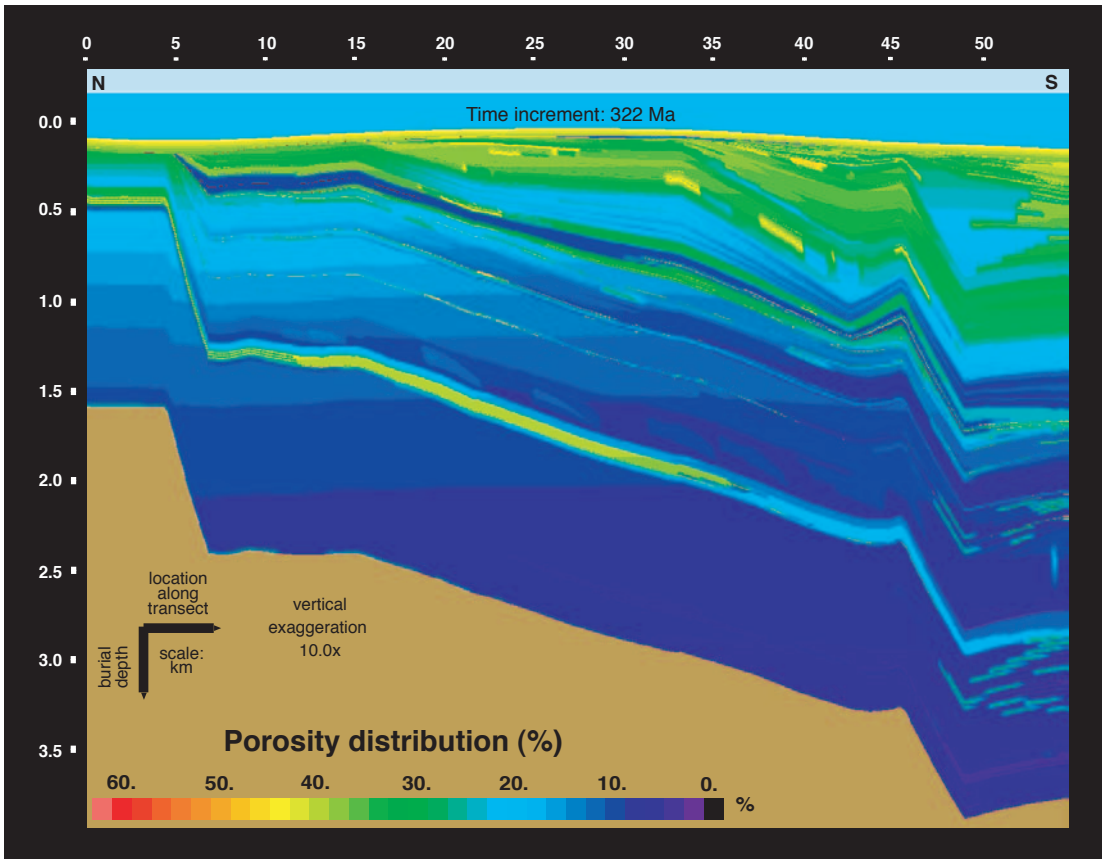

Fig. 7.11. Porosity distribution along the Bernesga Transect for the entire simulation time from 560Ma to 322Ma. Note the relationship between lithofacies, porosity loss and increasing burial depth.

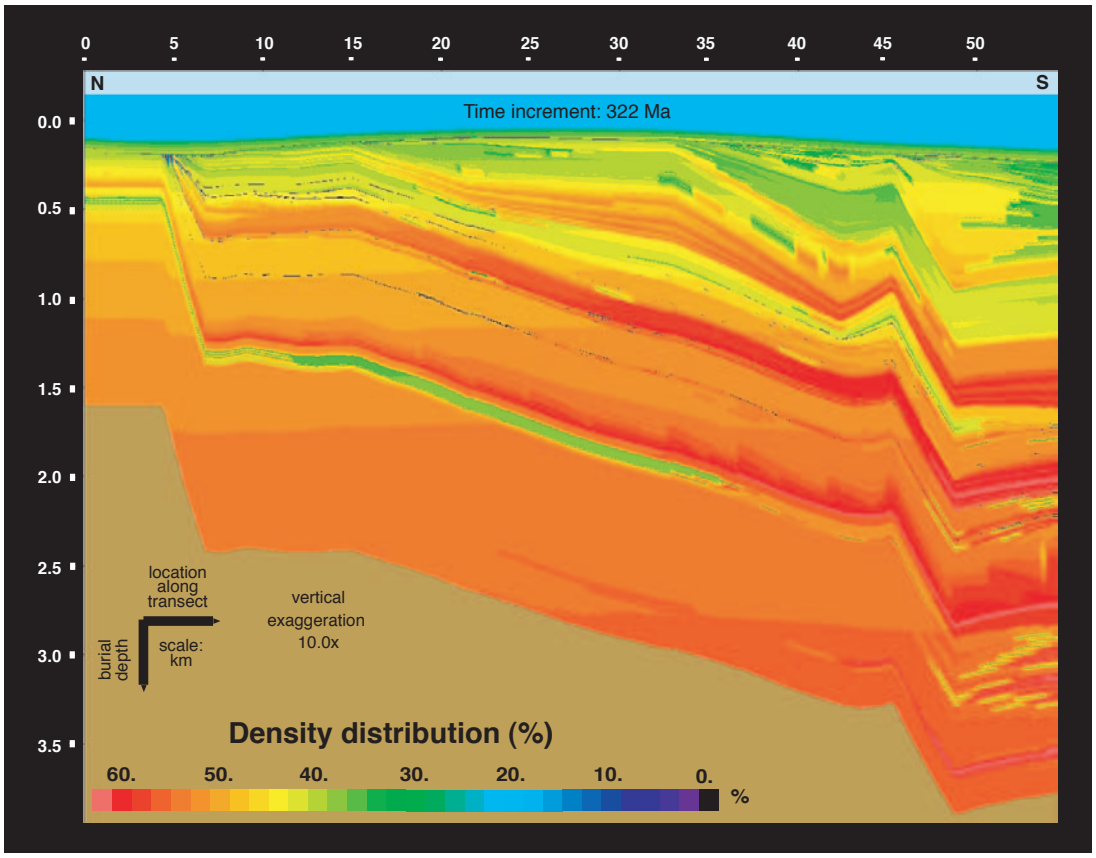

Fig. 7.12. Density distribution along the Bernesga Transect for the entire simulation time from 560Ma to 322Ma. Note the increase of density with burial depth and the dependency on lithofacies distribution (compare Figure 7.4.).

to the previous fall. Concluding, it can be said that each stratigraphic gap occurs in combination with a fall of the eustatic sea-curve (2nd order) used for this model (see Fig. 7.9).

7.8.6 Comparison of outcrop and modelling data

One of the most important tools for comparing real world data with forward modelling output are synthetic cross-sections. Synthetic cross-sections are virtual slices through the predicted lithofacies distribution plot drawn at arbitrary positions along the transect. They offer detailed information on 1D lithofacies development, cyclicity, compacted thicknesses of discrete formations, palaeobathymetric evolution, hiati, etc (see Figs. 7.6 and 7.7).

For comparison, a representative synthetic cross-section was chosen at km 42 along the Bernesga Transect, representing the position of the Santa Lucía/Rocalo/La Pola de Gordón sections in the Bernesga Valley (see Fig. 3.4). A reasonable detailed comparison for the Herrería Fm. is not possible, as this formation only crops out in the southernmost and northernmost areas of the transect. Data from these areas was projected onto the transect and shows a uniform siliciclastic succession with a thickness-discrepancy between outcrop and modelling data of 2% (see Fig. 7.6). The subsequent Láncara Fm. reflects fairly well a progression from shallow marine carbonates/dolomites to deeper marine, micritic nodular limestones. However, condensed deposition causes difficulties in the model, resulting in the highest thickness-discrepancy of the entire simulation (28%). This might be due to not well-established chronostratigraphic age constraints for this formation. The coarsening and shallowing upward trend within the Oville Fm. can be seen clearly in the synthetic cross-section, displaying up to 10% lower thicknesses. Facies and thickness development of the coastal to shallow-marine Barrios and sub-tidal Capas de Getino formations match the field observations. Black arrows indicate times of non-deposition and their widths are proportional to the hiatus time span. However, the true duration of the first hiatus is underestimated, as explained in the

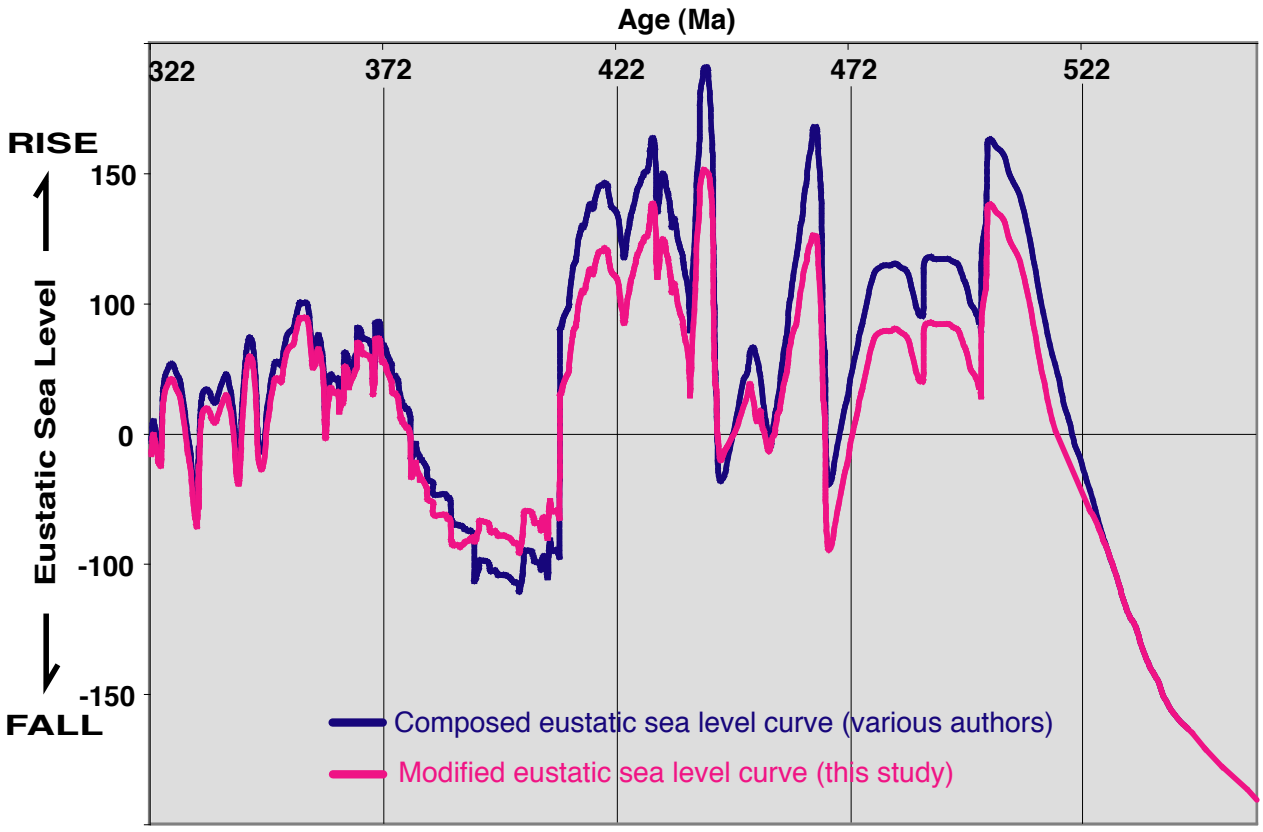

Fig. 7.13. Composed eustatic curve from Fig. 6.4 (blue line) and the modified curve (red line) as a result of multiple stratigraphic forward simulations (see Chapter 7.8.5 for further details). Note the identical shape of the curves and the diminished amplitudes of eustatic sea-level fluctuations in the modified curve. Amplitudes of the composed eustatic sea-level curve were reduced by 1.5 to 21% with a mean value of 9%.

previous chapter. The change from the shaly/silty Formigoso Fm. to the coarse-grained sandstones of the San Pedro Fm. was modelled with a 0% to 14% thickness discrepancy. Two minor hiati reflect littoral conditions in the San Pedro Fm., with wave ripples, channels and cross-bedding. Three additional small-scale hiati within the carbonatic Abelgas Fm., together with the formation of algal laminates and evaporitic carbonates, show continuing inter- to supratidal conditions (with a thickness discrepancy amounting to 6%). The deepening of the depositional area can be seen in the palaeobathymetric plot (Fig. 7.5 A). The intercalated siliciclastics of the Huergas Fm. and the renewed onset of carbonate production (Santa Lucía Fm.) clearly match, with thickness differences of 2% to 17%. Within this carbonate interval, the carbonate boundstone signature represents the position and the thickness of the main reefal edifice. A poor geologic outcrop record of the Huergas Fm. along the Bernesga Transect restricts the adequate comparison of this time interval. During the short time (3Ma) of the Portilla Fm. a new boundstone unit developed. Possibly due to the relatively large time step of 500ka (Chapter 7.3.1), the middle argillaceous to sandy part of the Portilla Fm. was underestimated in its thickness. The overlaying siliciclastics represent the Nocedo and possibly the Ermita Fm. These formations are difficult to differentiate due to insufficient biostratigraphic data. The Ermita Fm. at this location was probably replaced by the relatively thick Baleas Fm. (up to 10m), which has similar depositional environments. Nevertheless, these middle to coarse-grained sandstones and grainstones (thickness discrepancy 0% to 10%) as well as the erosional hiatus are well constrained in the modelling results. The pelagic-condensed Alba Fm. is the last formation in this model with a higher thickness difference of 15%.

This representative example shows both the advantages and the problems of simulations with PHIL/BASIM™. Shallow-water carbonates have a large number of adjustable parameters and can be modelled with a high level of accuracy. In contrast, condensed deeper-water deposits like the Láncara and Alba formations show the highest thickness discrepancies. In summary, the output of 2D stratigraphic forward modelling closely reflects the lithofacies, architecture and palaeobathymetric evolution of the Southern Cantabrian Basin. Mean values for thickness discrepancies range between 5% and 12%. Of course, fine-tuning of parameters for such periods might have decreased this mismatch at the end. One of the problematic factors is, for instance, the evaluation of time, because chronostratigraphic data is not very well constrained in the Paleozoic. However, because different parameter combinations might give similar results, it is unclear, if after such a fine-tuning the reliability of the model would really be closer to nature.

7.9 Error analysis

7.9.1 Dependency of stratigraphic forward models on Te

As discussed in Chapter 5.2.6 and 7.3.4, effective elastic thickness (Te) has a major impact on basin development. In order to differentiate between the influence on lithofacies and palaeobathymetric distribution, several simulations were run with varying Te-values. Fig. 7.14 shows three simulation runs for the time span 560Ma to 322Ma and the following Te-values: (i) constant 15 (A); (ii) 15-30 (B) and (iii) 15-60 (C).

Adjustment C was used for the present study. Lower Te-values result in a stronger bending of the lithosphere, enabling higher subsidence of the southern part of the Bernesga Transect. The deepest position of the basement (at km 50) in model A is situated 700-800m deeper than in model C. As expected, the arrangement of deeper palaeobathymetric values can be seen clearly for lower Te-values and distal areas of the transect. These palaeobathymetric differences (deeper values for lower Te) shift in time to intermediate and proximal areas. The values for sediment thicknesses in model A are only slightly higher than in model B and C, probably caused by a sediment bypass due to higher depositional gradients.

7.9.2 Dependency of sedimentary development on eustatic sea-level changes

Several simulations were run to test how eustatic sea-level changes influence the sedimentary succession of the Southern Cantabrian Basin. First, to get a rough estimate, the whole model was simulated with sea-level fluctuations switched off.

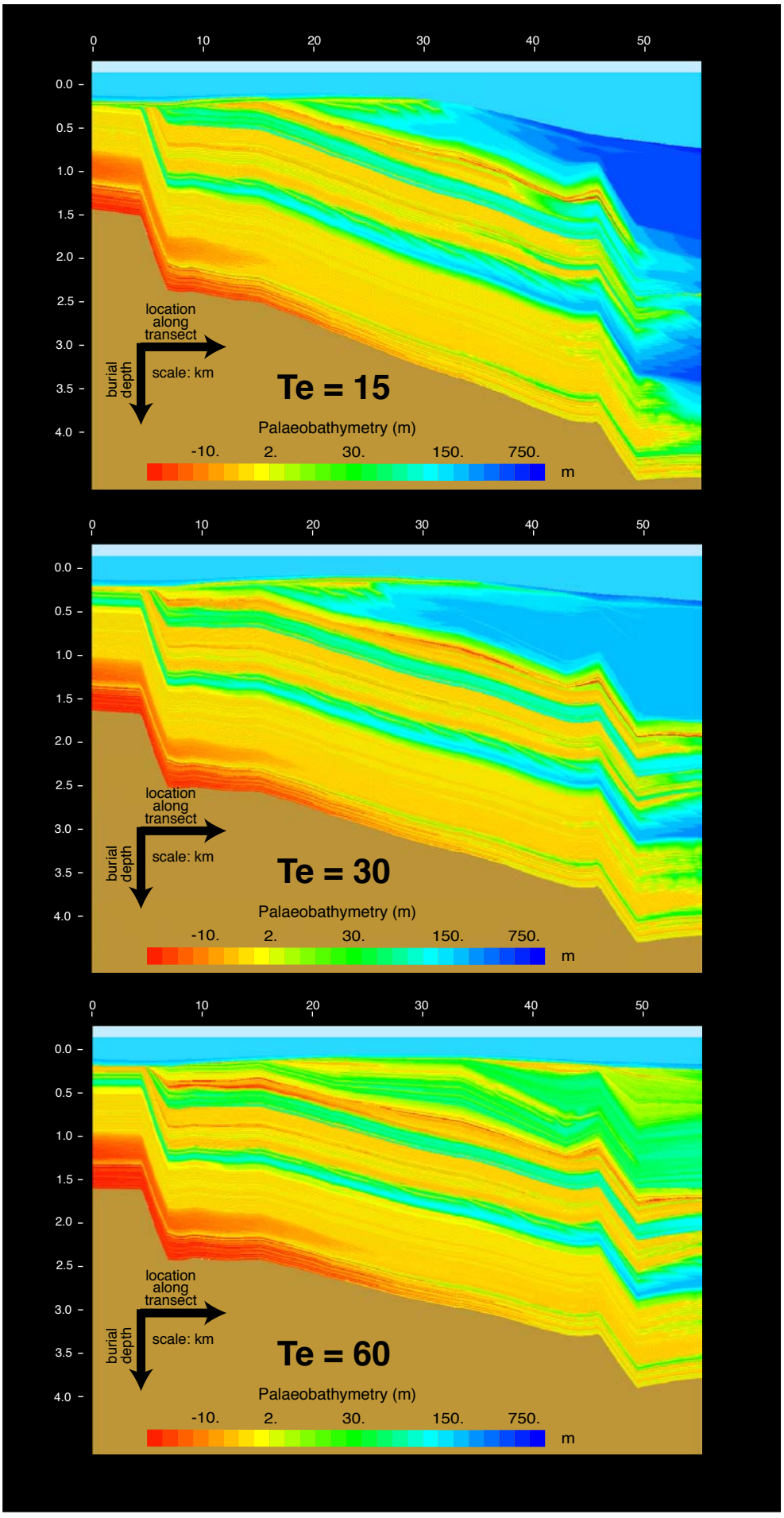

Fig. 7.14. Comparison of palaeobathymetry distribution along the Bernesga Transect (560-322Ma simulation time span) for three different effective elastic thickness adjustments (Te). Note the increase of water depth in distal areas for low lithospheric rigidities (Te=15). See Chapter 7.9.1 for more details.

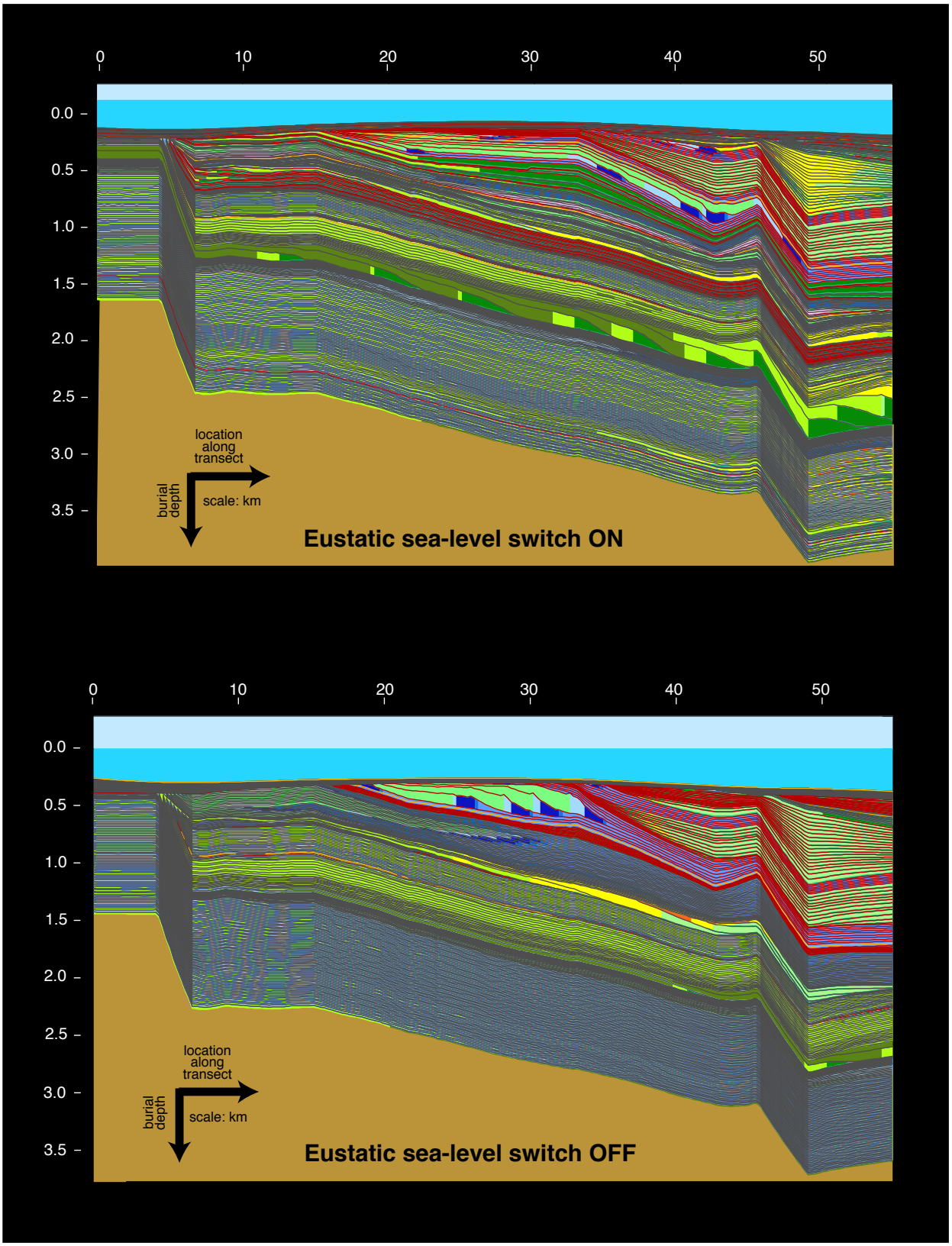

Fig. 7.15. Different lithofacies and thickness distributions due to eustatic sea-level fluctuations being switched off (lower figure). The original simulation with eustatic sea-level switched on is shown in the upper picture for comparison. Note the different position of sea level and different palaeobathymetry for the last time increment (322Ma). The simulation comprises the entire time period from 560 to 322Ma. On the next page, the same figures without stratal lines are plotted for comparison and better visibility of facies distribution. See Chapter 7.9.2 for details and Fig. 7.4 for the lithology key.

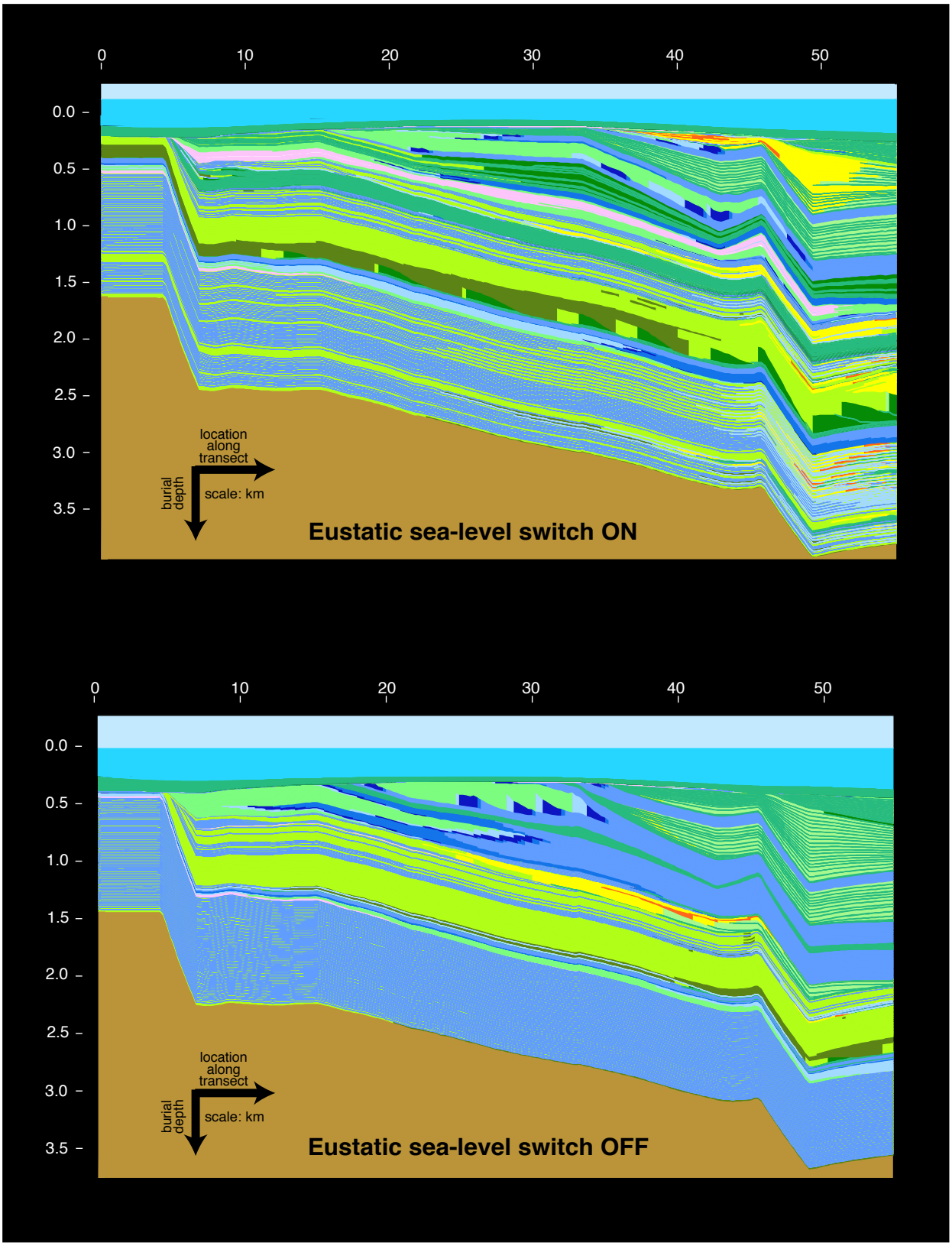

Fig. 7.15. Continued from page 124.

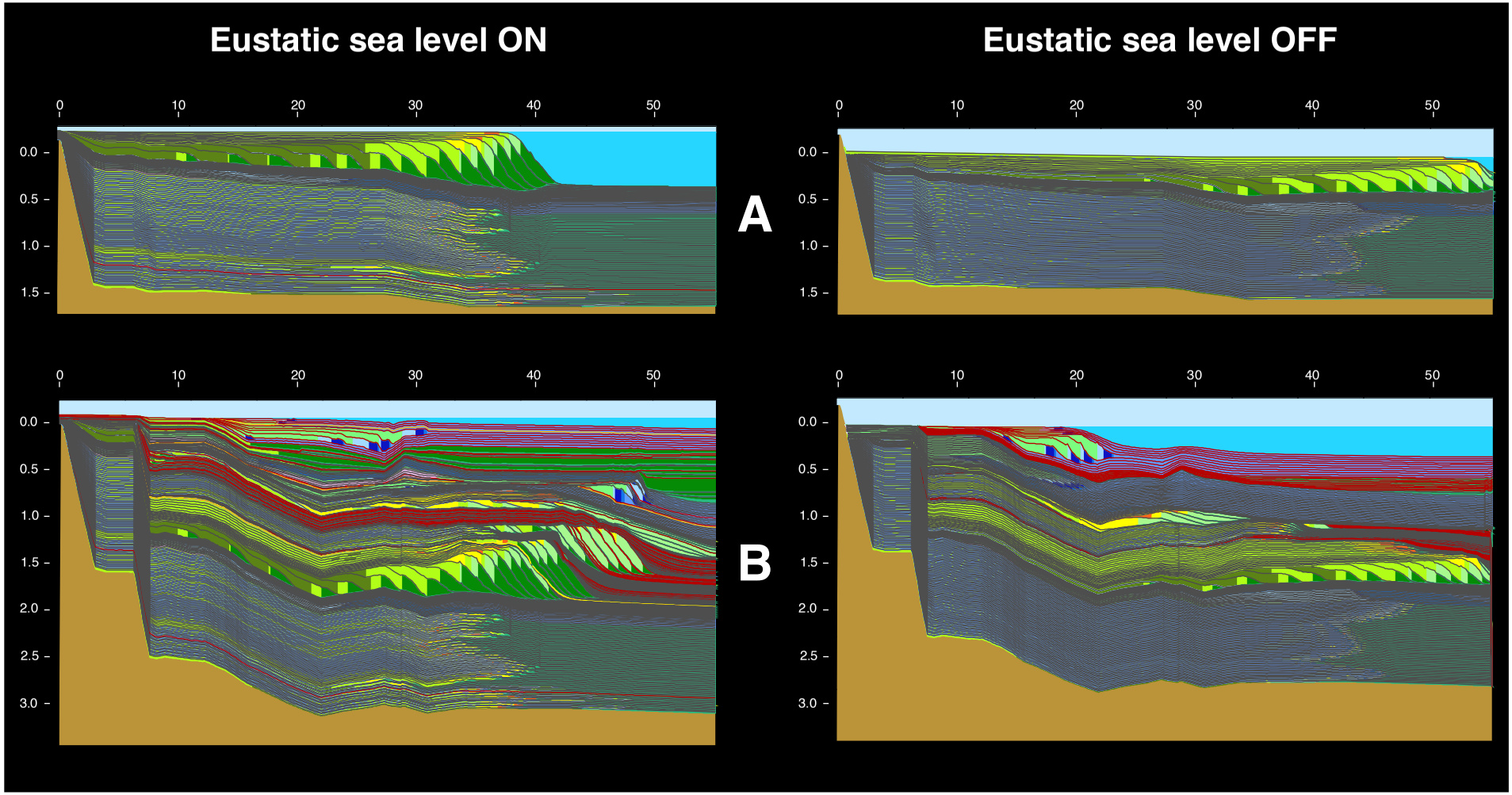

Fig. 7.16. Comparison of the dependency on eustatic sea-level fluctuations. The right side of the figure represents simulations with sea level switched off. See Figure 7.4. for the lithology key.
A: Simulation run untill the top of the Oville Fm. (505Ma). Note the position of sea level. Missing sea-level rise in the right figure causes a rapid progradation of the Oville Fm. with flat foresets.
B: Simulation run untill the top of the Santa Lucía Fm. (391Ma). With sea level switched off the Santa Lucía Fm. is not able to keep up with higher water depths caused by differential development of underlying strata.
C: See next page.

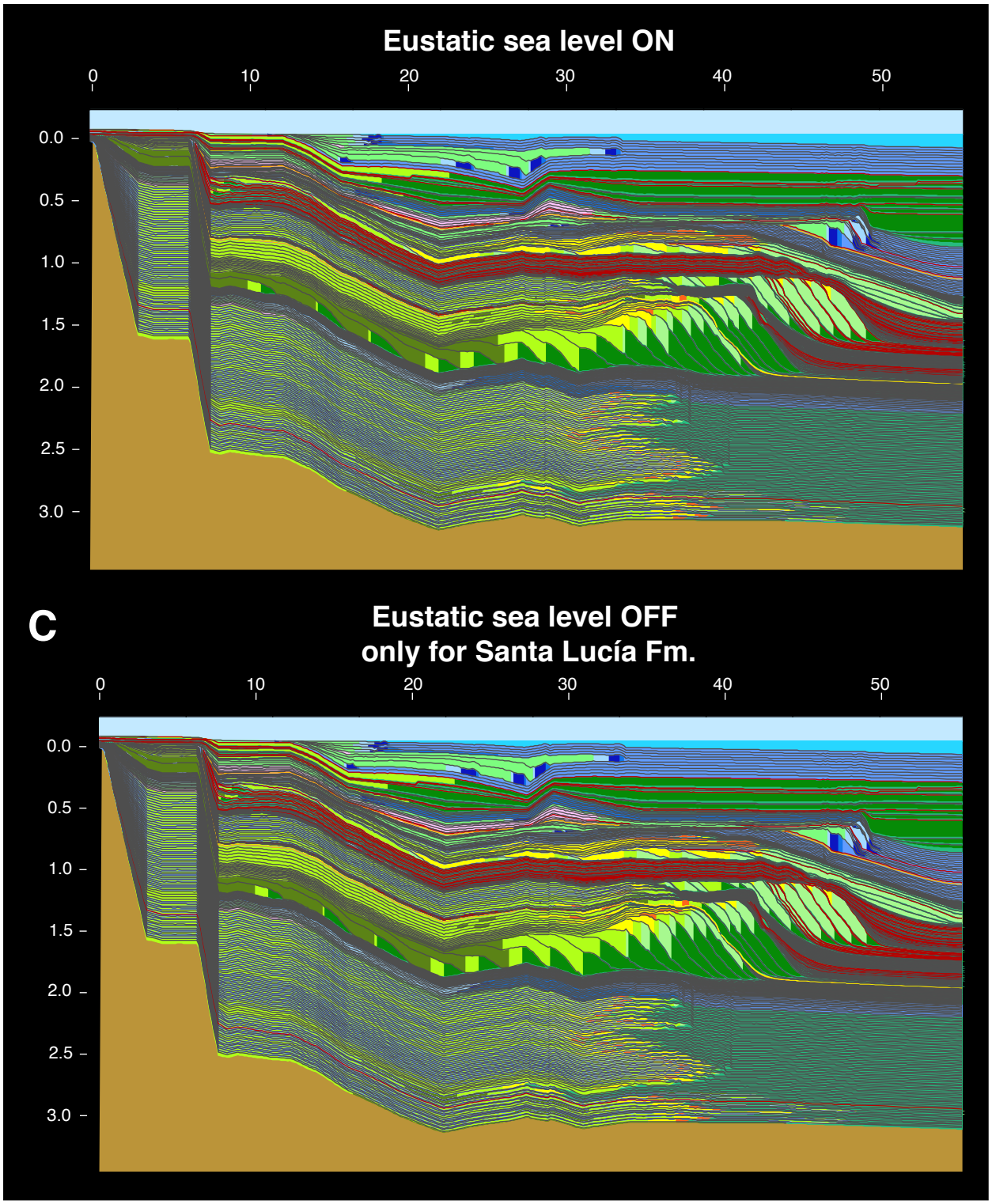

Fig. 7.16. Continuation from page 126.
C: The sea level was switched off only during the deposition of the Santa Lucía Fm. (396-391Ma) to receive an identical initial depositional surface. There are no differences visible for the sedimentation of the formation with and without sea-level fluctuations.

In Fig. 7.15, this simulation run shows strong deviations in lithofacies distribution and type. In particular, various depositional gradients in the Oville (7.16A) and Santa Lucía (7.16B) formations differ strongly from the simulation with a fluctuating sea-level. In the case of the Oville Fm. a strongly rising eustatic sea-level (Fig. 7.13) causes the deposition of high angle foresets in a prograding delta setting. With sea-level switched off, the same amount of siliciclastic influx favours a much faster progra-

dation and deposition of flat foresets, due to limited accommodation space. During the simulation of the Santa Lucía Fm. the carbonate factory responds distinctly to higher water depth in the south of the Bernesga Transect, caused by thin deposits of the San Pedro and Esla formations. The Santa Lucía Fm. shows steeper fore-reef gradients during progradation and subsequent backstepping at the end of the time increment. The palaeobathymetric distribution (not displayed here) shows exaggeratedly high palaeo-water depths in the proximal areas and low values in the distal part of the transect. As expected, the complete lack of eustatic sea-level fluctuation has a major impact on the sedimentary development of a basin. For the Santa Lucía Fm. an additional simulation was run with the purpose of determining the sole response of the carbonate factory to eustatic sea-level fluctuations. The sea-level was switched on for the deposition of the Herrería to Esla Fm. to get an identical initial surface. The sea-level remained static only for the deposition of the Santa Lucía Fm. (396-391Ma). Fig. 7.16C shows no difference between the model with a fluctuating sea-level and the model with sea-level switched off. The result is an identical distribution of lithofacies for both simulation runs. The amplitude of the sea-level changes during this time-period amounts to 10m (Fig. 7.13).

7.9.3 Influence of time step

Fig. 7.17 shows lithofacies plots at time 322Ma for three different time steps: (i) 300ka, (ii) 500ka and (iii) 700ka.

Time step 500ka has been chosen for the present study. The duration of time steps shows a major impact on the evolution of palaeobathymetry, physical properties, and lithofacies. The varying resolution of the model is well displayed in the size of prograding foresets of the Oville Fm. Progradational and retrogradational patterns are better constrained within the short time-step models. Whereas the siliciclastic successions only show minor differences (distribution of coarse-grained sandstones in the Huergas and Nocedo formations), carbonate formations experience major changes in facies distribution. Short time steps (300ka) seem to favour the development of supratidal carbonates and evaporites in the model (Abelgas and Santa Lucía formations). This might be due to the ability of supratidal carbonate factories to keep up with eustatic sea-level fluctuations. Longer time steps cause the deepening and subsequent drowning of these low-productive factories. Models with long time steps (700ka) tend to show a reduction in the thicknesses of boundstone units and to shift their position along the transect (Santa Lucía and Portilla formations). The basinward shift of the main Santa Lucía reefal edifice between the 500ka and the 700ka model amounts to 5-7km. Long time steps impede a carbonate factory's ability to respond correctly to accommodation space fluctuations. Utilising long time steps, a strong eustatic sea-level rise can cause a carbonate factory to drown, whereas it would be able to keep up employing shorter time steps.

7.9.4 Thermo-tectonic subsidence rates within the stratigraphic forward modelling

Thermo-tectonic subsidence rates were derived from the 2D reverse basin modelling (Chapter 6.6.1). However, as the spatial and temporal resolution of the 2D stratigraphic forward modelling is significantly higher, the results from reverse modelling had to be adjusted for some time increments. These subsidence corrections range from -1.14m/Ma to 3.15m/Ma for the whole model. The differences were displayed in a spectral plot, as they vary in time along the Bernesga Transect (Fig. 6.18). The first formation that needed adjustment was the Formigoso Fm. Reverse basin modelling underestimated the subsidence of the distal part (red peak at 435 to 428Ma) by 8.5%. This was also the highest correction required for the whole model. The thermotectonic subsidence in the distal part of the Santa Lucía Fm. was reduced by -1.14m/Ma, to account for the palaeobathymetric information from the field. In conclusion, the results from reverse modelling required only minor modifications and returned good results regarding the development of thermotectonic subsidence rates.

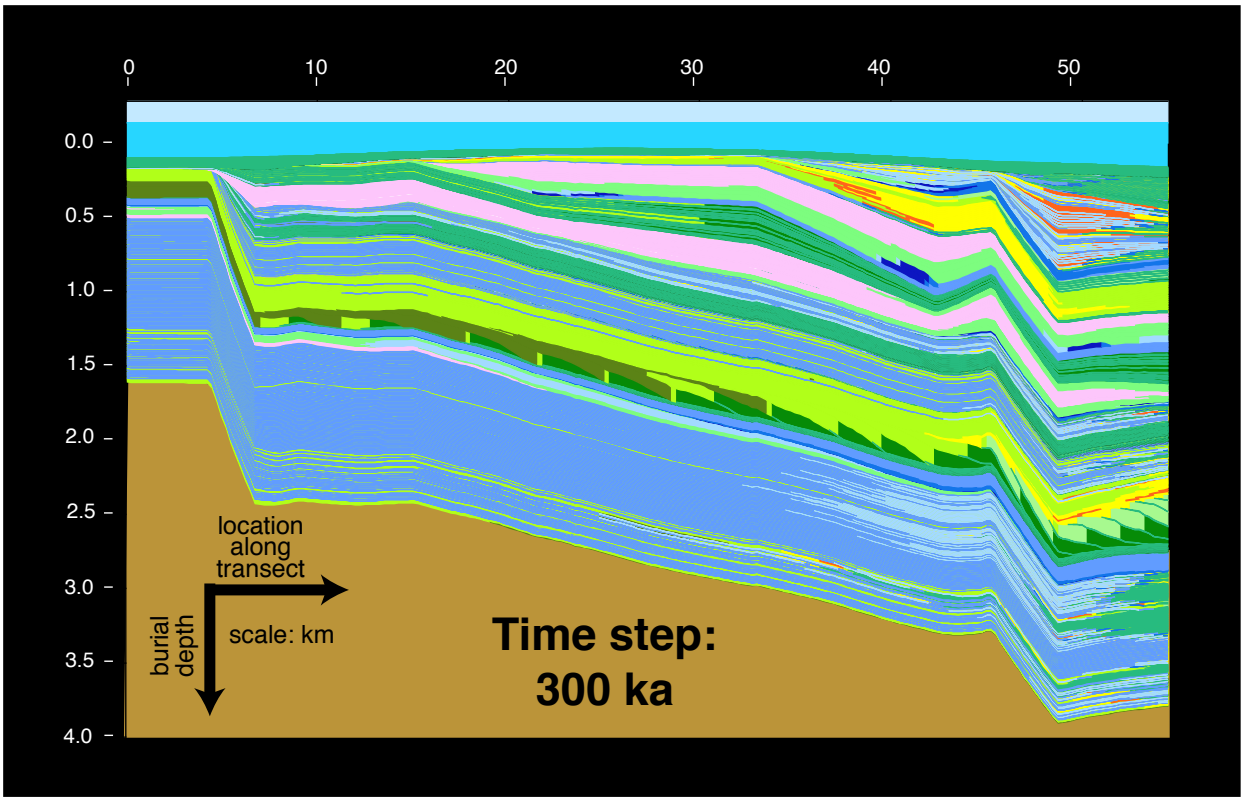

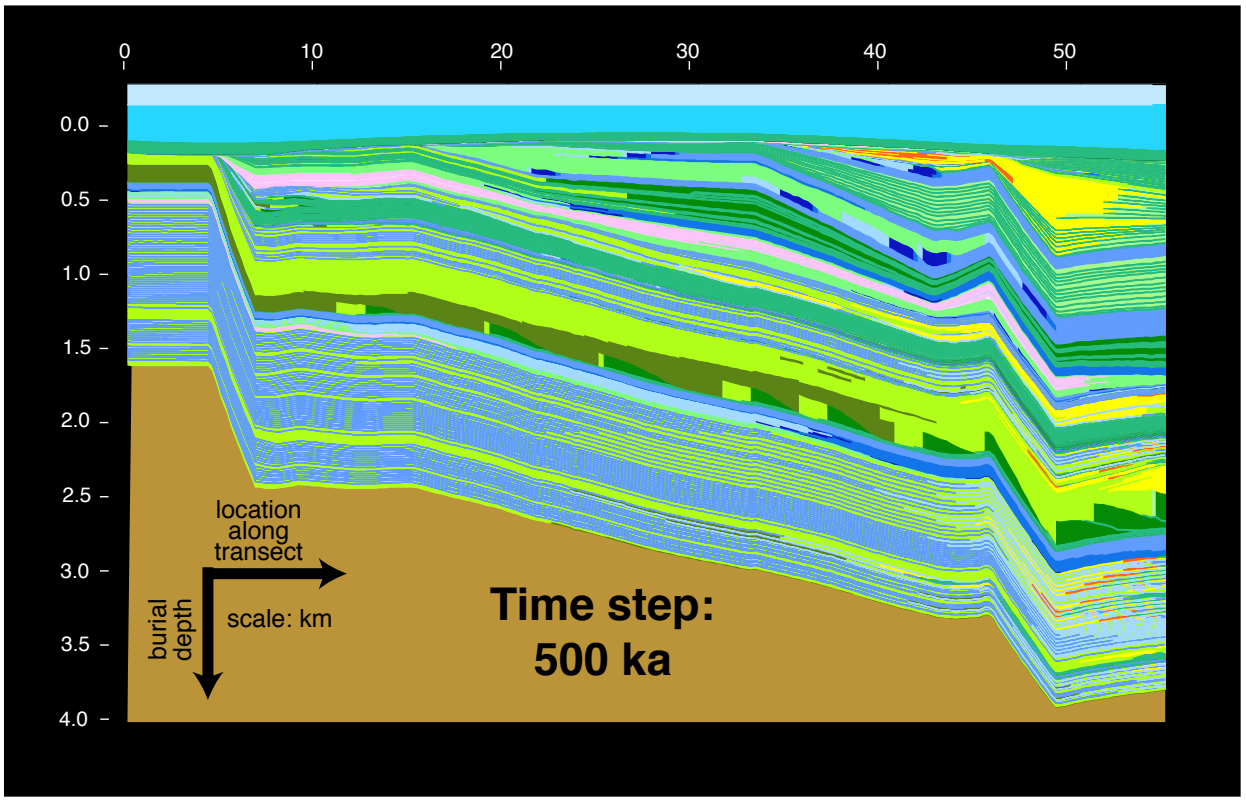

Fig. 7.17. Lithofacies changes due to different time steps (300, 500 and 700ka) used for the simulation from 560-322Ma. See Figure 7.4 for lithology key and Chapter 7.9.3 for further details. A plot with a 700ka time step is shown on the next page.

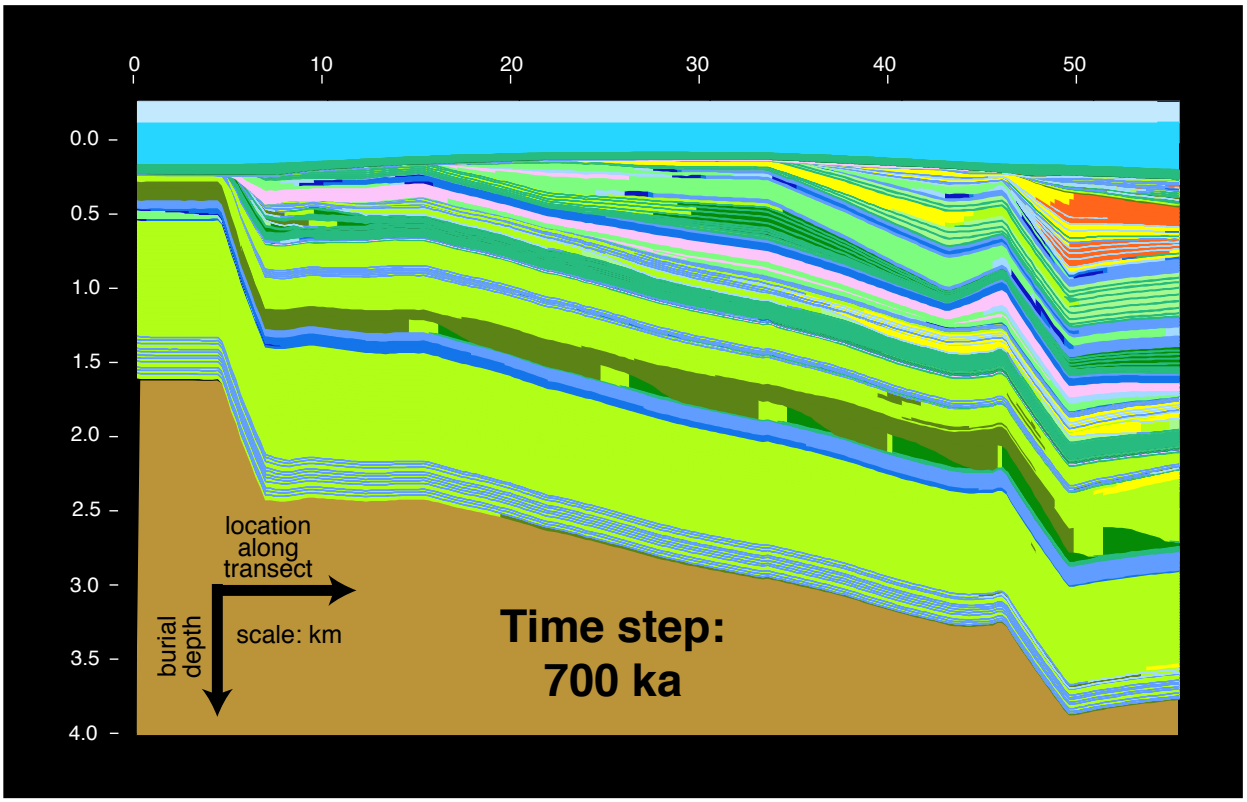

Fig. 7.17. Continued from page 129.

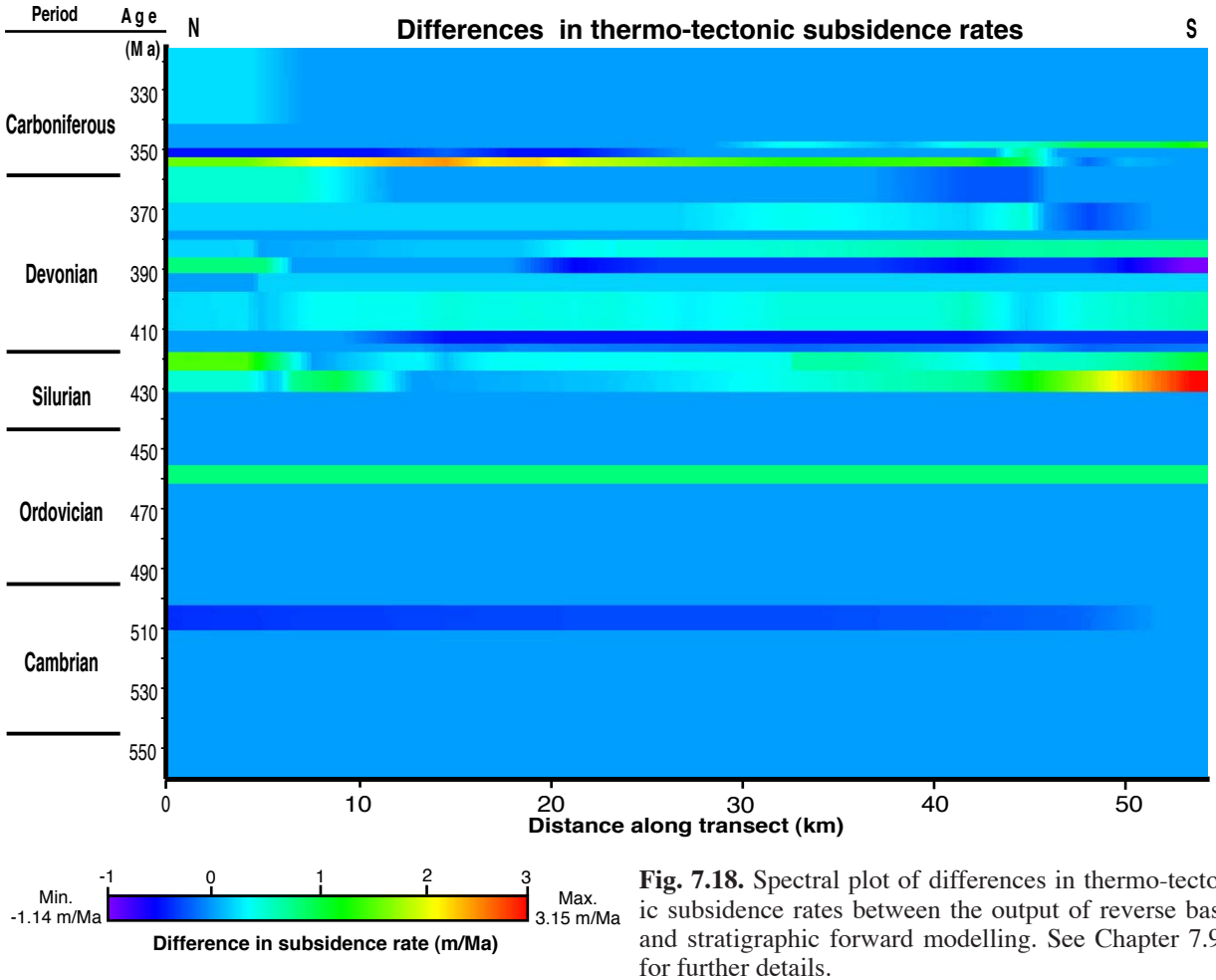

Fig. 7.18. Spectral plot of differences in thermo-tectonic subsidence rates between the output of reverse basin and stratigraphic forward modelling. See Chapter 7.9.4 for further details.

CHAPTER 8: BASIN DEVELOPMENT

The Southern Cantabrian Basin can be referred to as a "polyhistory basin" (Klein 1987) or a "polyphase basin" (Einsele 2000), having experienced major tectonic changes in the course of its development. The overview of parameters for the Southern Cantabrian Basin development is summarised in Fig. 8.1.

8.1 Subsidence development

2D reverse basin modelling results reflect the complex evolution from a rift stage (classification according to Prosser 1993), to a post-rift stage (passive continental margin) and finally to a foreland basin, governed by the approach of the Variscan Orogen in the Early Carboniferous. This evolution (560Ma to 313Ma) is visualised in Figs. 6.7 and 6.8 and shows six major subsidence trends of the total subsidence rates and its components. Numerical results are summarised in Table 6.3. The overall pattern is in accordance with the qualitative, palaeogeographical reconstructions published by Paris & Robardet (1990), Tait et al. (1997), Fernández-Suárez et al. (1998, 2000 a, 2002 a, b), Robardet (2000, 2002) and others. Existing qualitative models are summarised in Fig. 8.2 and 8.3.

First trend

Rifting leads to rapid initial subsidence, which is followed by persistent, exponentially decaying thermal subsidence (Einsele 2000). The pattern of the first subsidence trend (560-505Ma; mean value: 16m/Ma) fits this assumption regarding the development of highest subsidence rates during the early stages of the model (rifting) and declining subsidence rates towards the post-rift stage. However, it is difficult to attribute the time correlation with any precision due to a lack of adequate bio and chronostratigraphic information (in particular during the Precambrian). This could lead to existing data being misinterpreted.

Second trend

The second subsidence trend (505-435Ma) indicates a phase of low subsidence (mean value: 5m/Ma), with minor spatial differences in subsidence rates along the N-S Bernesga transect and several long persisting hiati (10-24Ma). During this trend, terrigenous sedimentation rates (2500-2600m²/ka), derived from 2D stratigraphic forward modelling, decline by 46% compared with the rates at the end of the first trend (4600m²/ka). According to Einsele (2000) this feature is typical for the shift from rifting to drifting stage (immediate post-rift stage according to Prosser 1993). An Early Ordovician (Arenigian) magmatic event in the Central Iberian Zone (Ollo de Sapo event; see Chapter 2.3.3) is marked by alkaline and peralkaline granites. It was interpreted as proto-rift volcanism by Crowley et al. (2000), indicating renewed thinning and further extension of the crust, until the detachment of the Armorican Terrane Assemblage from North Gondwana in the Caradocian. However, this time period is concealed by several long-term hiati in the Cantabrian Zone, which were probably caused by the tectonic movements recorded in the Central Iberian Zone. See Chapter 4 for discussion.

Third and fourth trend

Differential subsidence with an uplifted area in the north (-8m/Ma; Cantabrian High) and higher subsid-

Fig. 8.1. Overview of parameters for the Southern Cantabrian Basin development. The figure is split on the next two pages. Time is indicated in Ma in column I, comprising the term from the top of the rheologic basement (560Ma) to the top of the San Emiliano Fm. (313Ma).
A: Formations and members of the Southern Cantabrian Basin. **B:** Main lithologies for different basin formations (Chapter 2.4.4). **C:** Transgression/regression cycles as determined in Chapter 4.2. **D:** Sediment flux in m²/Ma (siliciclastic flux, shaded area) and m/Ma (decompacted carbonate production rates, brick-pattern), resulting from 2D reverse basin and 2D stratigraphic forward modelling. **E:** Thermo-tectonic subsidence rates along the Bernesga Transect (from north to south) in m/Ma (see Fig. 6.7 for scale and Chapter 6.6 for further detail.) **F:** Subsidence trends for the thermo-tectonic subsidence rates (Fig. 6.8 and Chapter 8.1). **G:** Basin stages defined on the basis of unconformities, basin architecture and 2D reverse basin modelling results (see Chapter 8 and Fig. 6.8). **H:** Composed eustatic sea-level curve with a scale bar in metres (Fig 6.4 and Fig. 7.13)**. I:** Chronostratigraphy according to German Stratigraphic Commision (2002). As stratigraphic forward modelling did not cover the syn-orogenic sediments (322-313Ma), no information is available about siliciclastic sediment flux and T/C cycles during this time-span.

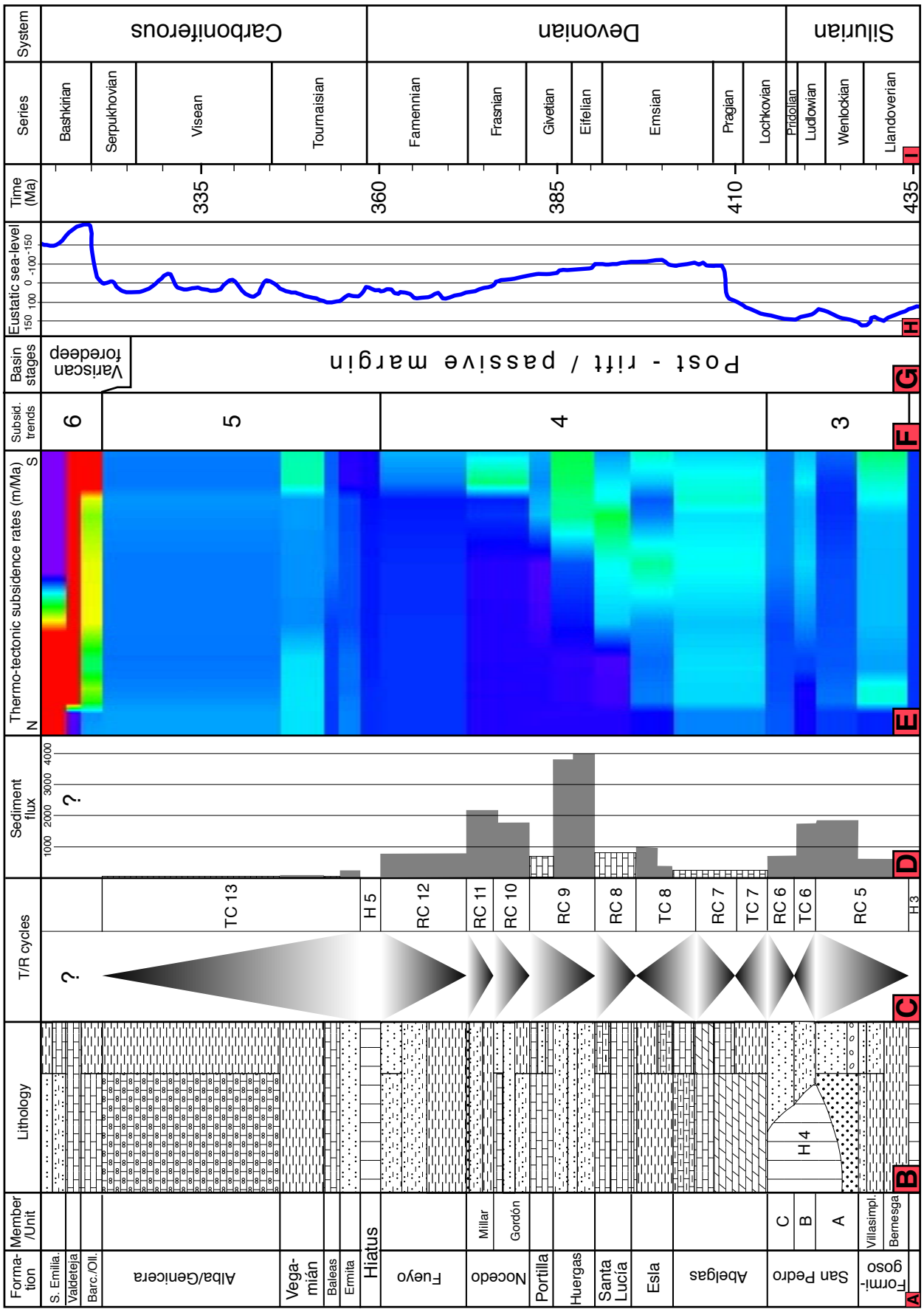
Formation
Member /Unit
Lithology
T/R cycles
Sediment flux
Thermo-tectonic subsidence rates (m/Ma)
Subsid. trends
Basin stages
Eustatic sea-level
Time (Ma)
Series
System
Alba/Genicera
Vega-mián
Baleas
Ermita
Hiatus
Fueyo
Nocedo
Portilla
Huergas
Santa Lucía
Esla
Abelgas
San Pedro
Formi-goso
Millar
Gordón
Villasimpl.
Bernesga
Barc./Oll.
Valdeteja
S. Emilia.
TC 13
H 5
RC 12
RC 11
RC 10
RC 9
RC 8
TC 8
RC 7
TC 7
RC 6
TC 6
RC 5
H 4
H3
Post - rift / passive margin
Variscan foredeep
Bashkirian
Serpukhovian
Visean
Tournaisian
Famennian
Frasnian
Givetian
Eifelian
Emsian
Pragian
Lochkovian
Pridolian
Ludlowian
Wenlockian
Llandoverian
Carboniferous
Devonian
Silurian
335
360
385
410
435
A
B
C
D
E
F
G
H
I

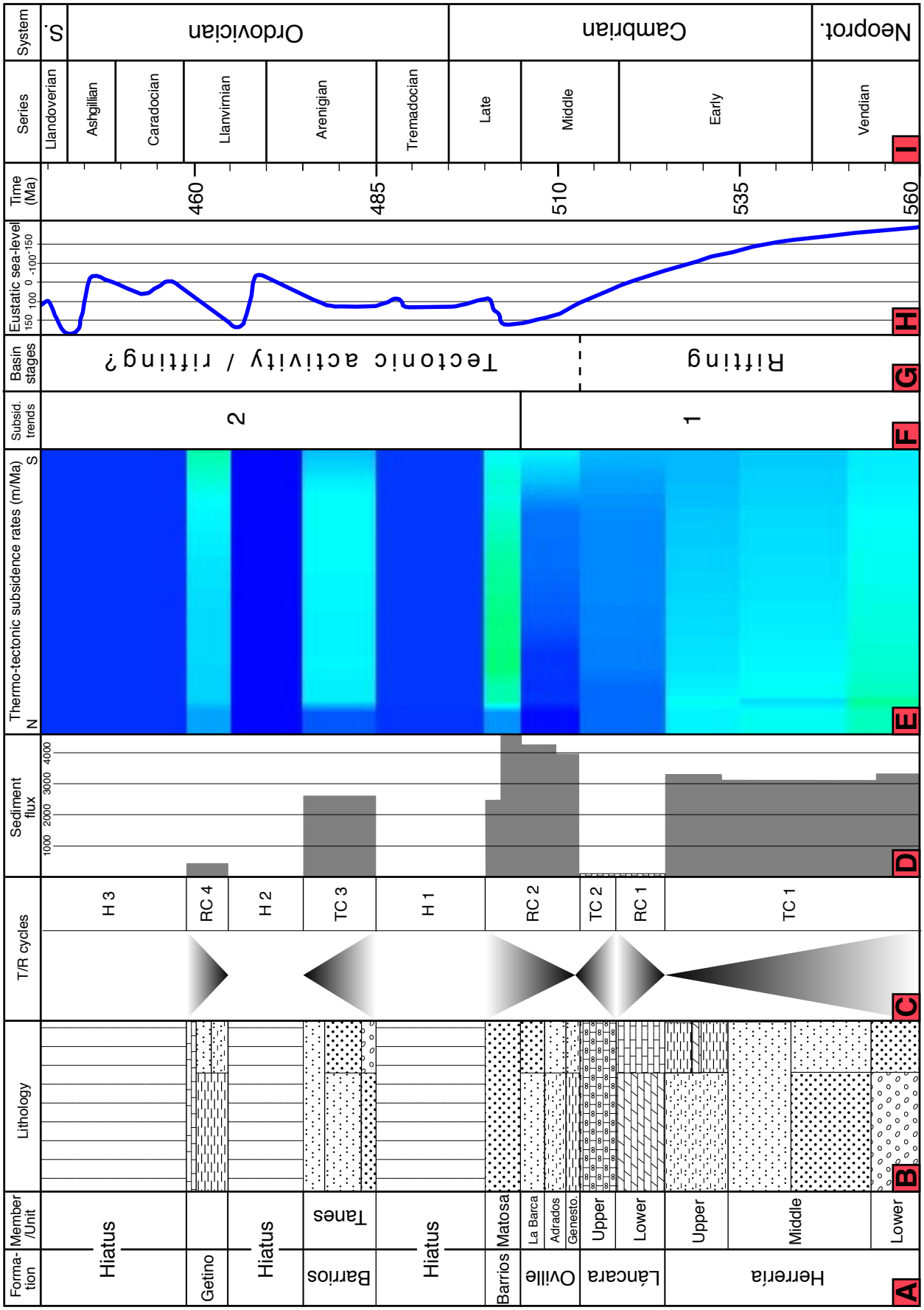
Formation
Member /Unit
Lithology
T/R cycles
Sediment flux
Thermo-tectonic subsidence rates (m/Ma)
N
S
Subsid. trends
Basin stages
Eustatic sea-level
Time (Ma)
Series
System
A
B
C
D
E
F
G
H
I
Hiatus
Getino
Hiatus
Barrios
Tañes
Hiatus
Barrios
Matosa
Oville
La Barca
Adrados
Genesto.
Láncara
Upper
Lower
Herrería
Upper
Middle
Lower
H 3
RC 4
H 2
TC 3
H 1
RC 2
TC 2
RC 1
TC 1
1000
2000
3000
4000
2
1
Tectonic activity / rifting?
Rifting
150
100
0
-100
-150
460
485
510
535
560
Llandoverian
Ashgillian
Caradocian
Llanvirnian
Arenigian
Tremadocian
Late
Middle
Early
Vendian
S.
Ordovician
Cambrian
Neoprot.

ence to the south (up to 35m/Ma) becomes visible in the third trend (435-415Ma), and is reinforced in the fourth trend (415-361Ma; -13 to 40m/Ma). Reverse basin modelling results points to the development of the Cantabrian High as a structural elevated area from the Lludlovian on (Fig. 6.7). In time, the Cantabrian High extends in two pulses (428-415Ma and 415-361Ma) to the south, displacing the regions of main subsidence and deposition basinwards. Consequently the non-depositional/erosional hiatus of the Cantabrian High extends spatially to the south (see Fig. 6.7 and 6.8). Compaction-induced subsidence rates highlight this movement, as compactable sediment is only deposited south of the shifting topographic high. Fig. 7.5A shows the depositional depths (palaeobathymetry) along the Bernesga Transect. As most of the sediments were deposited under shallow-marine conditions, flexure caused by water burden can be ruled out. In a global context this subsidence configuration in the Southern Cantabrian Basin points to the onset of a long-term continental encroachment cycle of first order, with a basinward shift of regional onlap. This concept was proposed by Duval et al. (1998) and is displayed in Fig. 8.4. Two continental encroachment cycles with a duration of greater than 50Ma (1st order) occurred during the Phanerozoic, caused by changes to the ocean basin volume induced by the break-up and subsequent joining of supercontinents (Duval et al. 1998). During the older encroachment cycle (latest Proterozoic to the end of the Permian) the change from a backstepping/transgressive phase to a forestepping/regressive phase, marked by a major downlap surface, took place at 500Ma. After a eustatic highstand during the Ordovician-Silurian and maximum marine transgression at the Ordovician-Silurian boundary, the marine domain gradually retreated from the Silurian to the Permian. Cycles of higher orders were superimposed (2nd to 4th order). Regression-transgression cycles (2nd order; duration 3-50Ma), bound by hiati and associated with 2nd order eustatic cycles, are assumed to be the result of changes in the rate of regional tectonic subsidence and/or changes in the rate of sea-floor spreading (Vail et al. 1984). Not every aspect of this concept is reflected in the Cantabrian Zone. The change from a transgressive to a regressive phase is not visible in the Cantabrian Zone as this time is characterised by numerous hiati (Fig. 7.5B and 7.9) and the tectonic overprint makes seismic scale surfaces unrecognisable. Maximum marine flooding is marked by the black shales of the Formigoso Fm. (see Chapter 2.4.4) with a slightly delayed onset of approx. 8Ma in contrast to the data published by Duval et al. (1998). This might be due to the presence of a major stratigraphic gap during this time and poor biostratigraphic information about the Capas de Getino Fm. Nevertheless, the top of this significant hiatus (435Ma) marks the start of a second order encroachment subcycle. The San Pedro Fm. shows a basinward shift of regional onlap from Mb. A to Mb. B. The subcycle lasts 20Ma and ends at time-line 415Ma. The second and more pronounced basinward displacement of regional onlap (see Fig. 7.4 and 7.5B) commences with the deposition of the Esla Fm. and lasts until the Upper Devonian hiatus (361Ma). The total duration of this second encroachment subcycle amounts to 41Ma. However, there is no marked hiatus separating the two continental encroachment subcycles.

Fifth trend

During the fifth trend (361-322Ma), fluvial/littoral (Ermita Fm., see discussion in Chapter 4.2) to shallow marine sediments (uppermost part of the Ermita Fm. and the Baleas Fm.) were deposited throughout the entire basin above an erosion surface. In deeper marine regions black shales of the Vegamián Fm. were sedimented during the same time period. The Alba Fm. (red nodular limestones and shales) marks the top of the trend, characterised by condensed sedimentation in bathyal depths. During this period, the inner parts of the orogen became already deformed due to the continental collision, causing the development of an active margin (Colmenero et al. 2002, Chapter 2.2.1). The terrigenous input from the evolving mountain range was trapped in an orogenic foredeep, initially situated in the West Asturian-Leonese Zone (see Fig. 2.1) and had not reached the Cantabrian Zone. This is, however, not visible in the field, as the sediments in this foredeep became uplifted, eroded and later filled the younger foredeep of the Cantabrian Zone (Ábalos et al. 2002). This recycling may be the reason, why Cantabrian Carboniferous clastics are poor in indicator minerals.

Sixth trend

The sixth trend (Variscan foredeep stage; 322-313Ma) marks a sharp change in subsidence rate distribution in the uppermost Early Carboniferous and a manifest change in basin evolution. High thermo-tectonic subsidence rates in the southernmost part and moderate rates in the north indicate strong spatial differences along the Bernesga Transect (Fig. 6.7). The younger, southern, highly subsiding depocentres migrate in time to the NE (according to the present coordinate system). They are interpreted as orogenic foredeeps situated in front of the orogenic belt. The movement of the foredeep along the Bernesga Transect indicates the migration of the approaching orogen (see Fig. 6.8). Assuming the dating established by Truyols & Sanchez de Posada (1983) and Dallmeyer et al. (1997), first evidence for the advance of the Variscan Orogen in the examined area became visible in the Middle Namurian A (approx. 322Ma). Dallmeyer et al. (1997) demonstrated that it was possible to date deformation stages in the Cantabrian Zone palaeontologically by syn and post-orogenic sediments.

The NE propagating Variscan deformation was caused as new material was added to its front. The model published by Dallmeyer et al. (1997, see Fig. 2.3) shows that the entire orogenic wedge remained active, locally producing distinct structures at different times. The authors proposed that the orogenic front propagated at an average rate of 5km/Ma. Calculations in the present model highly depend on age information and the amount of basin shortening. Neither the biostratigraphic age (see Chapter 6.4) nor the basin shortening (calculated in Chapter 3.6.6) can be determined with absolute certainty. Values are calculated for both, minimum shortening at 54% and maximum shortening assumed at 80%, which includes also small scale folding and faulting. Consequently the results comprise a minimum (minimum age and shortening) and maximum spread of values (maximum age and shortening). According to these values, the propagation rate of the orogenic front along the Bernesga Transect ranges between 4 and 12km/Ma. However, as the propagation of the orogen occurred slightly oblique to the Bernesga Transect, the true rates may be even higher.

8.1.1 Implications for sedimentary development of syn-orogenic deposits

The upper limit of the 2D stratigraphic forward model is placed at 322Ma, directly before the onset of Variscan deformation in the Cantabrian Zone (see Chapter 2.2.1). The development of the syn-orogenic succession is a matter of further investigations (Dietrich et al. 2003). However, 2D reverse basin modelling results permit some observations on the accommodation space/sedimentation interactions for this time period. The sedimentary record of foreland basins is closely related to the flexural response of the continental lithosphere to orogen loading (Garcia-Castellanos 2002). Prior to the approach of the overthrust belt, the basin is shallow marine (or continental) and slowly subsiding (Einsele 2000, this study). The palaeobathymetric plot (Fig. 7.5A) demonstrates that shallow marine conditions continue throughout the Devonian. With the onset of crustal flexure the basin deepens until terrestrial sediment influx overcomes subsidence. At this turning point the basin reaches its maximum water depth, which leads to flysch deposits (Olleros Fm.). This time increment (322-319Ma) marks the beginning of the sixth subsidence trend, characterised by high tectonic and flexural-induced subsidence rates (see Chapter 6.6). Subsequently, the basin rapidly fills up with shallow-marine carbonates and clastics, deltaic and finally continental sediments (Einsele 2000). In the Southern Cantabrian Basin this pattern is well developed, starting with the Barcaliente platform, which developed in a distal position from the orogen. The shallow-marine Valdeteja platform was subsequently interfingering with basinal siliciclastics and covered by the terrigenous San Emiliano Fm. In a stratigraphic forward model both platforms should display a considerable amount of compaction in the underlying strata, as they prograde over highly compactable basinal sediments. The filling of foreland basins may not only be accentuated by pulses of overthrusting but also by strong changes in sediment accummulation.

8.2 Sedimentation development

2D stratigraphic forward modelling creates a high-resolution synthetic shelf-basin transect (Fig. 7.4

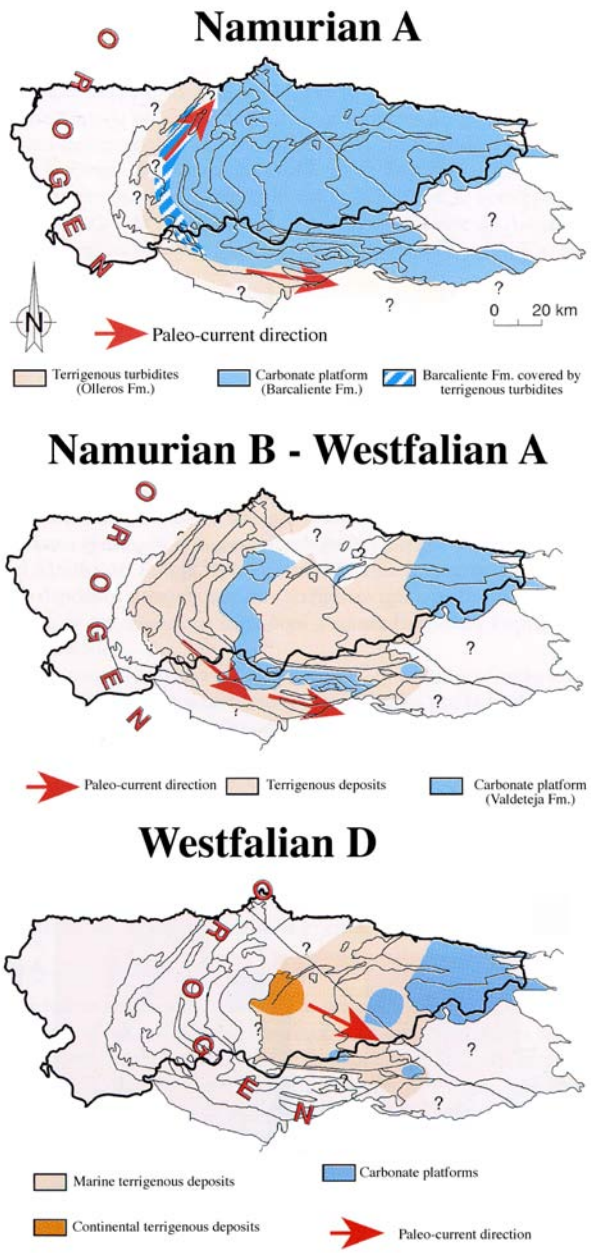

Fig. 8.2. Palaeogeographic evolution of the Cantabrian Zone from the Namurian A through Westphalian D according to Fernández (1995). Note the movement of the orogenic front and its foredeep, marked by terrigenous sediments of the Olleros and San Emiliano formations. See Fig. 8.3 for geologic cross-sections.

and "Movie_2.mov"). In terms of lithofacies distribution, thicknesses, palaeo-water depth and depositional systems, the outcrop data matches the modelling results to a large extent (Fig. 7.6). The dominance of siliciclastic deposition from the Precambrian to the Ordovician is reflected by very high sediment flux rates throughout the basin, ranging between 2500 and 4600m^2/ka (Fig. 7.9). These high sedimentation rates also influenced the total subsidence history by means of flexural loading. Increased flexural-induced subsidence rates created the necessary accommodation space for depositing the thick siliciclastic succession. The siliciclastic succession is interrupted by numerous phases of non-deposition (Fig. 2.21 and 7.5B), which show a good correlation with major falls of eustatic sea-level (Fig. 7.9 and Chapter 7.8.5).

Reef growth is chiefly controlled by numerous, closely related extrinsic controls. These comprise the (i) sea-level, (ii) palaeoclimate, (iii) oceanography, (iv) plate tectonics, (v) nutrients and (vi) tectono-sedimentary setting, which cannot all be simulated within the present model.

8.2.1 Sea-level

In contrast to the rising eustatic sea-level (Emsian to early Famennian, see Fig. 7.13) and a worldwide transgressive trend, the Devonian sediments of the Asturo-Leonese Domain were deposited in a regressive pattern (García-Alcalde et al. 2002). This pattern was caused by the regional tectonic movements of the Cantabrian High and the Intra-Asturo-Leonesian Facies Line (discussed below).

8.2.2 Siliciclastic input

Carbonates in the Abelgas Fm. were able to develop in the Early Devonian because the siliciclastic input dropped to 600m^2/ka at the end of the Silurian. Also during later times strong fluctuations in siliciclastic input were one of the major limiting factors for carbonate growth. The carbonate Santa Lucía (Eifelian) and Portilla (Upper Givetian) formations were drowned by sandy siliciclastics with mean flux rates of 2000 to 3950m^2/ka (Fig. 7.9).

8.2.3 Subsidence

In addition to the influence of siliciclastics on the carbonate factories, carbonate production rates were governed by differential thermo-tectonic and flexural-induced subsidence and their strong impact on the creation and destruction of accommodation space. During the deposition of the Abelgas Fm., low thermo-tectonic (7-24m/Ma) and flexural-induced (1-3m/Ma) subsidence rates together with a falling eustatic sea-level limited the accommodation space available. In the case of the Santa Lucía Fm., high subsidence (up to 40m/Ma) and a slowly

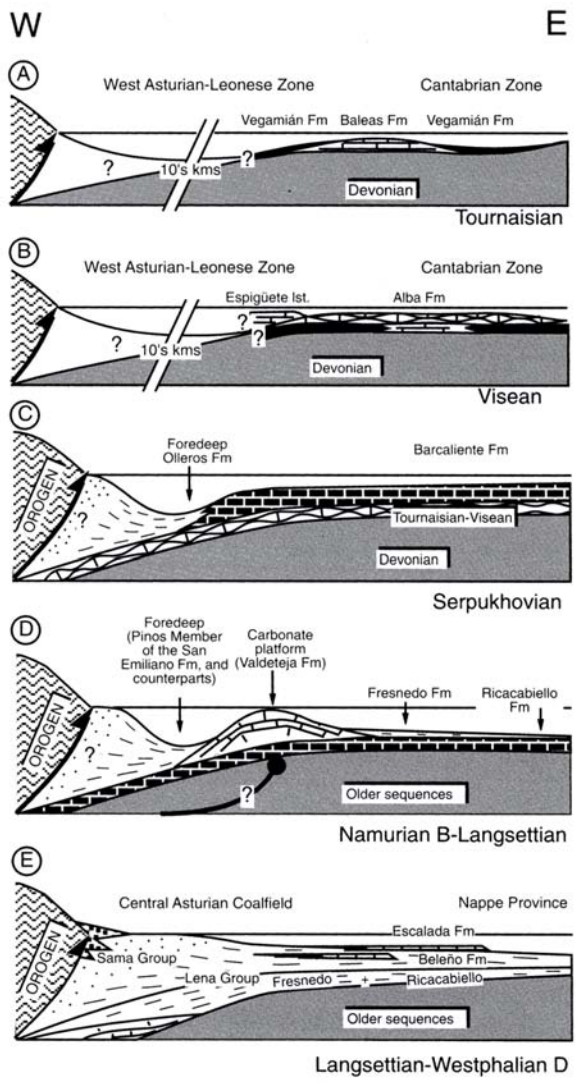

Fig. 8.3. Main stages of the foreland basin evolution in the Cantabrian Zone during the Carboniferous (Colmenero et al. 2002). See Fig. 8.2 for palaeogeographic maps.

rising eustatic sea-level (Johnson et al. 1985, Dennison 1985) offered sufficient accommodation space for basin development (outside the transect) and the growth of a thick carbonate reef succession (up to 356m - decompacted value).

8.2.4 Carbonate production

Based on their great number and dimensions, the Devonian reefs probably produced the largest amount of reefal carbonate in the Phanerozoic (Kiessling et al. 2000). Decompacted carbonate production rates show evidence of a significant increase in production during the Devonian. The values rise from 90m/Ma in the lowermost Gedinnian (Abelgas Fm.) up to 780m/Ma in the Eifelian (Santa Lucía Fm., Table 7.6). The Santa Lucía Fm. marks the first appearance of highly productive reef organisms in the Cantabrian Zone. The quantitative results point to a shift in the sedimentation environment towards tropical conditions adequate for reef growth. This is consistent with the qualitative, palaeogeographic models published by Paris & Robardet (1990) and Oczlon (1992), proposing that Iberia drifted northward during this time period and that the Ibero-Armorican region was located in warmer regions at 30°-35° during the Early Devonian times (see Fig. 2.12). According to the palaeogeographic position, facies distribution and palaeobathymetry, the Devonian reefs of the Cantabrian Zone fit well into the tropical shallow-water carbonate factory proposed by Schlager (2000), being situated in the tropical and subtropical surface waters of the ocean, approximately 30° N and S of the Equator. Carbonate production rates in the Portilla Fm. (Upper Givetian) dropped to 150m/Ma, which is 81% less than in the Eifelian (Table 7.6). This drop is caused by increased terrigenous input suppressing the carbonate productivity and possibly diminished accommodation space during this time. The terrigenous influence during the time period of the Portilla Fm. can be observed in the field. The middle member is often composed of sandy limestones to sandstones (section La Pola de Gordón, see Appendix) and the content of sand increases continuously towards the top of the formation. The carbonate production rates in the Southern Cantabrian Mountains reached their peak close to the Emsian/Eifelian boundary. This is in slight disagreement with the global data published by Kiessling et al. (2000), who claim that the maximum of total production rates was in the Givetian-Frasnian, seen for example in the Canning Basin platforms (Playford et al. 1989).

Compared to the highly productive Devonian carbonate factories, the Lower Carboniferous Alba Fm. is represented by condensed sediments (nodular limestones) with very low carbonate production rates (1.2 to 1.8m/Ma).

8.2.5 Palaeobathymetric evolution

The Southern Cantabrian Basin experienced very low bathymetric fluctuations throughout its history. Apart from the Láncara and Alba Fm. (red nodular limestone) and the black shales of the Formi-

goso and Vegamián formations, the depositional environment was constantly at shallow marine depth (see Fig. 7.5A). Long-persisting morphological basin configuration and the maintenance of shallow marine facies were described as a "balanced basin" (Einsele 2000), where sediment supply and vertical buildup approximately compensates for subsidence. On the other hand, due to the Mesozoic and Cenozoic cover of the Duero Basin and the complex structural situation there is currently no data available to enable an approximation of the true former extent of the Southern Cantabrian Basin. Consequently, long-persisting shallow-marine conditions probably signify that the basin was oversupplied with sediment at some time. In this case the sediment flux throughout the basin may have been underestimated, as an uncertain amount of sediment was transported by high-energy shelf conditions to deeper, sediment-starved regions, which are not visible in the present geological record.

8.3 Intra-Asturo-Leonesian Facies Line (IALF)

Since the Frasnian, the already existent depositional pattern (subsiding basinal areas in the south and low sediment thicknesses in the north) experienced a strong amplification. The Bernesga Transect was split into a large northern area of non-deposition and slight erosion and a strong subsiding southernmost area (south of km 45), the depositional area of the Nocedo (Millár Mb.) and Fueyo formations (Fig. 6.2 and 7.4). This sharp facies and thickness boundary was documented by numerous earlier authors (Evers 1967, Loevezijn 1983 and others) and named the Sabero-Gordón Line after a prominent regional fault zone running in the same direction (Fig. 3.5). However, because this facies line was not only observed in the vicinity of the Sabero Gordón Line, Raven (1983) proposed a new name, the Intra-Asturo-Leonesian Facies Line (IALF). In more recent literature (Alonso et al. 1995) the Sabero Gordón

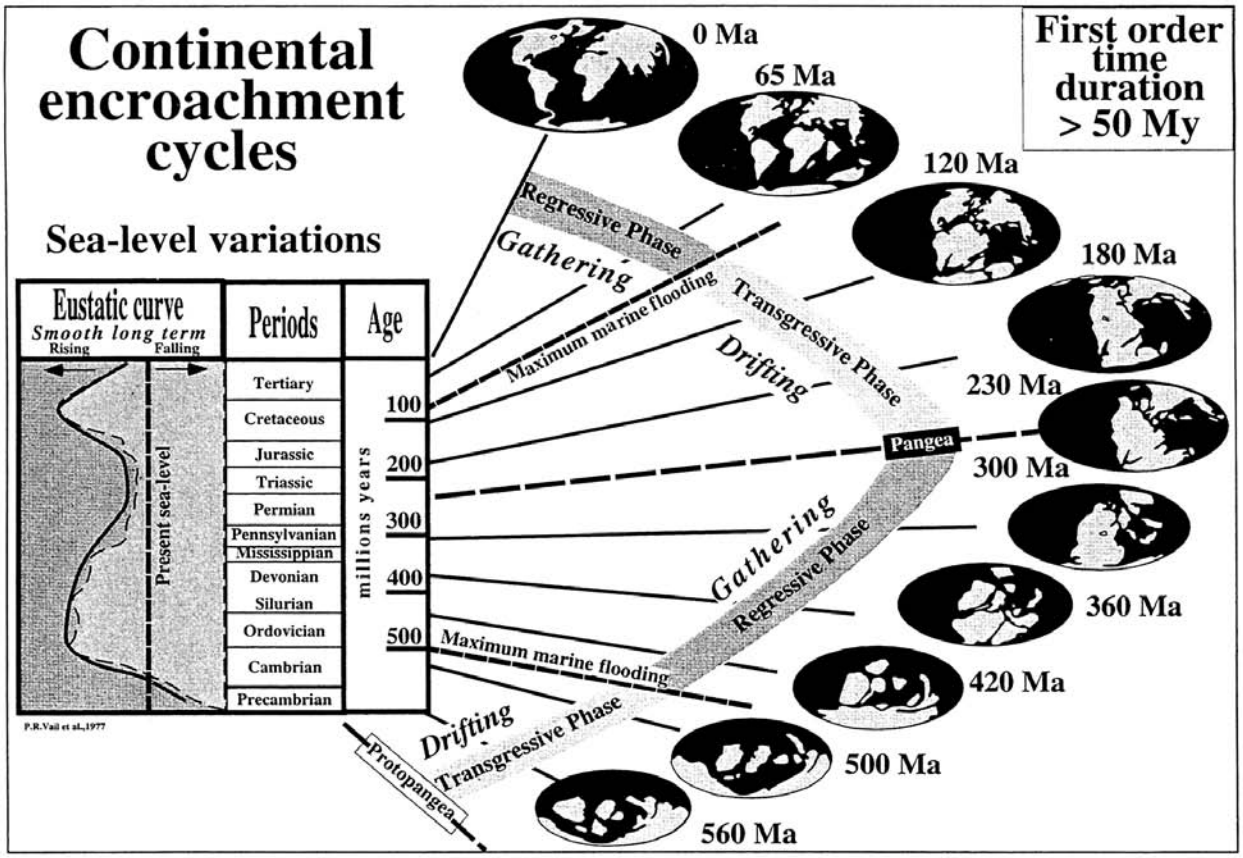

Fig. 8.4. Two Phanerozoic continental encroachment cycles associated with the break-up and gathering of supercontinents (Duval et al. 1998). Each cycle is composed of a transgressive and a regressive phase.

Line was described as an Alpine thrust/fault. In contrast, the results of this study point to the development of a syn-sedimentary fault between km 45 and 47 starting at latest at the beginning of the Late Devonian. The identical position of reefal development during the Santa Lucía and Portilla times at km 42 only a few kilometres north of the IALF, could also indicate its influence on carbonate palaeogeography (Fig. 7.4). To conclude, the present study proposes that a syn-sedimentary fault (IALF) developed at an early stage (from Late Emsian (?) to Late Famennian) and was later partly reactivated during the Alpidic Orogeny (Sabero Gordón Line).

8.4 Development and evolution of the Cantabrian High

The differential development of sediment thicknesses between the southern basinal areas and the northern uplifted region was observed early on by numerous authors. This uplifted region, referred to in the present study as the Cantabrian High (see above), has been given different names including the "Cantabrian Block" (Radig 1962), "Asturian Geanticline" (Adrichem Boogaert 1967), "Asturisches Sandfeld" (Kullmann & Schönenberg 1979, Frankenfeld 1981) and others.

The uplift or lower subsidence of the Cantabrian High has been visible since the deposition of the Barrios Fm. The material deposited on the Cantabrian High was marginally eroded as early as during the Barrios Fm. with various time intervals of non-deposition (see enclosed time series animation "Movie_2.mov"). Important erosional periods in the northern areas were identified during the deposition of the Lower San Pedro Fm., lower Huergas Fm., Nocedo Fm. and a strong pulse during the hiatus between the Fueyo and Ermita formations as well as in the lower part of the Ermita Fm. But even in periods of non-erosion, there was no or only very low accommodation space available in the northern part of the Bernesga Transect. It is not possible that all this erosion occurred during later periods, e.g. the Carboniferous. A single erosional period in the Lower Carboniferous, able to remove a uniformly deposited sediment succession in the northern Cantabrian High, would have required implausibly high erosion rates within a short time period. According to García Alcalde (2000) the Lower Carboniferous hiatus comprises only 1-3Ma. Additional arguments against such a model are the thinning and onlapping features observed during Silurian and Devonian, as mentioned earlier.

CHAPTER 9: CONCLUSIONS

The "epic poem of the Earth" is written in a language that we still do not entirely understand (Paola 2000). However, the multidisciplinary approach applied in this study provides new quantified data for the evolution of the Palaeozoic polyhistory of the Southern Cantabrian Basin and an insight into the complex history of NW Iberia.

Basin modelling in the Variscan fold-and-thrust belt of Northern Iberia requires a threefold methodology. Structural balancing has to be carried out before modelling can begin. The combined dynamic approach of 2D reverse basin followed by 2D stratigraphic forward modelling analyses geological processes in time. 2D modelling was implemented with the PHIL/BASIMTM modelling software package (Bowman & Vail 1999).

9.1 Structural balancing

Structural balancing ("balanced cross-sections") supplies fundamental data about the basin architecture prior to late Palaeozoic deformation and provides estimations on basin shortening and spatial relationships between measured sections. It was applied to the 18km long Bernesga Transect running N-S on the southern slope of the Cantabrian Mountains (see Figs. 3.3 and 3.4 and Chapter 3.6.1 for discussion). Both in the north and south, E-W trending out-of-sequence faults with unknown displacement factors (León Line fault system and Southern Border Thrust) form the boundaries of the transect. According to the overall structural framework, this part of the Cantabrian Zone can be divided into three domains: (i) Bodón, (ii) Pedrosa and (iii) Alba (see Fig. 3.5). These domains show different structural characteristics, which govern the amount of shortening calculated. The least amount of shortening is calculated in the southern Alba domain (25%). This domain is composed of large synformal structures (Fig. 3.6) cut by back-thrusts and faults. The Bodón domain in the north of the transect shows three large open folds on a scale of kilometres (see Fig. 3.15A). The shortening for this domain amounts to 41%. The Pedrosa domain in the middle of the Bernesga Transect suffered most shortening (65%). It is composed of multiple overthrust sheets in the form of an imbricated thrust system (see Table 3.1 for minimum shortening values and displacement widths along the Bernesga Transect).

The overall minimal shortening of the Bernesga Transect, measured between the outer pin lines P1 and P9 (see Fig. 3.15), amounts to 54%. However, taking small-scale faulting and folding into consideration, the shortening values will amount to significantly higher values. The minimal shortening of the transect can be split into the displacement widths between individual thrust sheets and their internal deformation. The ratio of 48% to 52% illustrates that thrusting and folding each cause approximately the same amount of shortening along the Bernesga Transect.

9.2 2D numerical reverse basin modelling

2D numerical reverse modelling analyses the development of basin architecture in consideration of lithofacies, incremental compaction, sea-level changes and flexural loading of the crust. It offers quantitative estimations of total subsidence rates and its components (thermo-tectonic, flexural-induced and compaction-induced subsidence rates). The thermo-tectonic subsidence rates serve as initial numerical input for 2D stratigraphic forward modelling.

Numerical results reflect a complex evolution from a rift stage, to a post-rift stage (passive continental margin) and finally to a foreland basin, governed by the approach of the Variscan Orogen in the Early Carboniferous. This evolution (560Ma to 313Ma) is marked by six major subsidence trends (see Fig. 6.8 and Table 6.3). The first subsidence trend (560-505Ma) displays declining subsidence rates during its course and indicates a shift from a rifting stage to an early drifting stage. The second trend (505-435Ma) is marked by periods of tectonic quiescence and activity, and is concealed by several long-term hiati. These are probably caused by tectonic movements along the northern magin of Gondwana (e.g. Ollo de Sapo event, see Chapter 2.3.3). The stable passive continental margin established in the Silurian. During the third trend (435-415Ma), an uplifted area in the north and increased subsidence to the south becomes visible along the Bernesga Transect.

This pattern is reinforced during the fourth trend (415-361Ma). The uplifted area in the north (Cantabrian High) extends from Lludlovian onwards to the south, displacing regions of main subsidence and deposition basinwards. At the same time the non-depositional/erosional hiatus of the Cantabrian High extends spatially to the south (see Fig. 6.7 and 6.8). This basin configuration points to the onset of a long-term continental encroachment cycle of first order, with a basinward shift of regional onlap (see Chapter 8.1). Maximum marine flooding is marked by the black shales of the Formigoso Fm. The first order encroachment cycle is subdivided in two subcycles of second order. The top of a significant hiatus (435 Ma) marks the onset of the first subcycle. It is characterised by a basinward shift of regional onlap from Mb. A to Mb. B of the San Pedro Fm. and lasts 20Ma. The second and more pronounced encroachment subcycle commences with the deposition of the Esla Fm. (402Ma) and lasts until the Upper Devonian hiatus (361Ma). The basinward displacement of regional onlap is visible in figures 6.4 and 6.6 and lasts 41Ma. Marine transgression over an erosive surface, deepening and condensed sedimentation in bathyal depths characterise the fifth subsidence trend (361-322Ma). The uniform sedimentation throughout the entire basin changes fundamentally in the sixth trend (322-313Ma). High thermotectonic subsidence rates in the southernmost part and moderate rates in the north indicate strong spatial differences along the Bernesga Transect. The southern, highly subsiding depocentres migrate in time to the NE (according to the present coordinate system). They are interpreted as the Variscan orogenic foredeep situated in front of the orogenic belt. The movement of the foredeep along the Bernesga Transect indicates the migration of the approaching Variscan orogen (see Fig. 6.8). By calculating these movements the orogenic propagation velocities can be estimated. The propagation rate of the Variscan orogenic front along the Bernesga Transect ranges from 4 to 12km/Ma depending on the basin shortening estimates (minimum 54%; maximum 80%).

9.3 2D stratigraphic forward modelling

Stratigraphic forward modelling simulates basin development, and quantifies the physical factors determining deposition. It offers minimum/maximum models of sedimentary geometries and lithofacies distribution in time and space, predicting lithostratigraphic information in areas between outcrops.

Numerical results comprise siliciclastic influx rates (Fig. 7.9) and carbonate production rates (Fig. 7.10 and Table 7.6) for the time period modelled (560-322 Ma). From the latest Neoproterozoic to the Early Ordovician the Southern Cantabrian basin is dominated by a considerable flux of siliciclastic sediments (2600 to 4600m^2/ka), interrupted by several long-term hiati and the deposition of a thin carbonate succession of the low-productive Láncara Fm. (15 to 32m/Ma). After the deposition of the Láncara Fm. it takes nearly 100Ma before environmental conditions suitable for the development of a carbonate factory are re-established. During Silurian times only siliciclastic material is deposited with the dark shales and siltstones of the Formigoso Fm. (600m^2/ka) and the shallow-water, coarse-grained San Pedro Fm. (1800m^2/ka). During the deposition of the upper San Pedro members flux rates diminish by more than 65% (600m^2/ka). This, combined with the palaeogeographic position of Iberia (see Chapter 2.3), is primarily responsible for enabling the development of Abelgas Fm. carbonates in the Early Devonian. At this time the productivity of the carbonate factory is rather low (90m/Ma). The highest carbonate production rates are calculated in the Santa Lucía Fm. (290 to 780m/Ma), whereas the Portilla Fm., deposited only 6Ma later, records production rates 81% lower (50 to 150Ma). This drop is caused by increased terrigenous input (see also Fig. 7.9) suppressing the carbonate productivity and diminished accommodation space. Periods of carbonate production are interrupted by high siliciclastic sediment influx (700m^2/ka for the Esla Fm. to 4000m^2/ka for the Huergas Fm.). Siliciclastic sediment input finally impedes any significant carbonate development in the Devonian, starting with the deposition of the Nocedo Fm.

This study demonstrates that reef growth is chiefly governed by numerous, closely-related extrinsic controlling factors. These factors comprise the (i) eustatic sea-level, (ii) total subsidence and (iii) siliciclastic input (see Chapter 8.2.4 for discussion). In addition, an important structural feature of the Southern Cantabrian Basin influences the carbonate

palaeogeography along the transect. The Intra-Asturo-Leonesian Facies Line (IALF) is interpreted as a syn-sedimentary fault situated between kilometres 45 and 47 along the Bernesga Transect (Fig. 7.4). It has been active since the Late Givetian and possibly latest Emsian, corroborated by the locations of the Portilla and Santa Lucía reefs, both only a few kilometres north of the IALF.

REFERENCES

Ábalos, B., Carreras, J., Druguet, E., Escuder Viruete, J., Gómez Pugnaire, T., Lorenzo Alvarez, S., Quesada, C., Rodríguez Fernández, L.R. & Gil-Ibarguchi, J.I. (2002) Variscan and Pre-Variscan tectonics. In: The geology of Spain. (Eds. Gibbons, W. & Moreno, T.), Geological Society, London: 155-183.

Adrichem Boogaert, H.A.van (1967) Devonian and Lower Carboniferous conodonts of the Cantabrian mountains (Spain) and their stratigraphic application. Leidse Geologische Mededelingen, **39**: 129-192.

Aigner, T., Doyle, M., Lawrence, D., Epting, M. & van Vliet, A. (1989) Quantitative modeling of carbonate platforms: some examples. In: Controls on Carbonate Platform and Basin Development. (Ed. Crevello, P.D.), Spec. Publ. Soc. Econ. Paleont. Miner., **44:** 323-338.

Aigner, T., Brandenburg, A., van Vliet, A., Doyle, M., Lawrence, D. & Westrich, J. (1990) Stratigraphic modelling of epicontinental basins; two applications. In: Processes and patterns in epeiric basins. (Eds. Aigner, T. & Dott, R.H.), Sedimentary Geology, **69:** 167-190.

Allen, P.A. & Allen, J.R. (1990) Basin analysis: principles and applications. Blackwell Science: 451 p.

Aller, J., Bastida, F., Brime, C. & Pérez-Estaún, A. (1987) Cleavage and its relation with metamorphic grade in the Cantabrian Zone (Hercynian of NW Spain). Sci. Geol. Bull., **40**: 1-18.

Aller, J. & Gallastegui, J. (1995) Analysis of kilometric scale superposed folding in the Central Coal Basin (Cantabrian Zone, NW Spain). J. Struct. Geol., **17**: 961-969.

Alonso, J.L. (1987) Sequences of thrusts and displacement transfer in the superposed duplexes of the Esla Nappe region (Cantabrian Zone, NW Spain). J. Struct. Geol., **9**(8): 969-983.

Alonso, J.L. & Suárez Rodríguez, A. (1991) Tectónica. In: Memoria del mapa geologico de España, Escala 1:50.000, No.103 (La Pola de Gordón). 2. Seria (MAGNA). ITGE, Madrid**:** 79-88.

Alonso, J.L., Suárez Rodríguez, A., Rodríguez Fernández, L.R., Farias, P. & Villegas, H. (1991) Cartografía del mapa geologico de España, Escala 1:50.000, No.103 (La Pola de Gordón). IGME, Madrid.

Alonso, J.L., Pulgar, J.A. (1995) La estructura de laZona Cántabrica. In: Geología de Asturias (Eds. Aramburu, C & Bastida, F.), Ediciones TREA, S.L., Gijón: 103-112.

Alonso, J.L., Pulgar, J.A., Garcá-Ramos, J.C. & Barba, P. (1995) Tertiary basins and Alpine tectonics in the Cantabrian Mountains (NW Spain). In: Tertiary Basins of Spain. (Eds. Friend, P. &Dabrio, C.)**:** 214-227.

Alvarez-Marrón, J. (1995) Three-dimensional geometry and interference of fault-bend folds: Examples from the Ponga Unit, Variscan Belt, NW Spain. J. Struct. Geol., **17**: 549-560.

Álvaro, J.J. & Vennin, E. (1996) Tectonic control on Cambrian sedimentation in south-western Europe. Ecolg. Geol. Helv., **89**: 935-948.

Álvaro, J.J. & Vennin, E. (1997) Episodic development of Cambrian eocrinoid-sponge meadows in the Iberian Chains (NE Spain). Facies, **37**: 49-64.

Álvaro, J.J., Vizcaino, D. & Vennin, E. (1999) Trilobite diversity patterns in the Middle Cambrian of southwestern Europe: a comparative study. Palaeogeogr. Palaeoclimat. Palaeoecol., **151**: 241-254.

Álvaro, J.J., Rouchy, J., Bechstädt, T., Boucot, A.J., Boyer, S., Debrenne, F., Moreno-Eiris, E., Perejón, A. & Vennin, E. (2000 a) Evaporitic constraints on the southward drifting of the western Gondwana margin during Early Cambrian times. Palaeogeography, Palaeoclimatology, Palaeoecology, **160**: 105-122.

Álvaro, J.J., Vennin, E., Moreno-Eiris, E., Perejón, A. & Bechstädt, T. (2000 b) Sedimentary patterns across the Lower-Middle Cambrian transition in the Elsa nappe (Cantabrian Mountains, northern Spain). Sedimentary Geology, **137**: 43-61.

Amler, M.R.W. (2000) Paläobiographie von Iberia im Karbon. Progr. 70. Jahrestagung der Paläont. Ges., Coburg, Terra Nostra 00/3.

Anderle, H.-J., Franke, W. & Schwab, M. (1995) Stratigraphy. In: Pre-Permian geology of central and eastern Europe. (Eds. Dallmeyer, R.D., Franke, W. & Weber, K.), Springer**:** 99-107.

Anderson, N.L. & Franseen, E.K. (1991) Differential compaction of Winnipegosis reefs - a seismic perspective. Geophysics, **56**(1): 142-147.

Aramburu, C. (1987) Descubrimiento de Graptolitos arenigienses en la escama de Rioseco (Zona Cantábrica, N. De España): Discusión. Cuad. Lab. Xeol. Laxe, **11**: 221-223.

Aramburu, C. & García-Ramos, J.C. (1988) Presencia de la discontinuidad sárdica en la Zona Cantábrica. Geogaceta, **5**: 11-13.

Aramburu, C. (1989) La sedimentación cambro-ordovícica en la Zona Cantábrica (NO de España). PhD Thesis, University of Oviedo.

Aramburu, C., Truyols, J., Arbizu, M., Méndez-Bedía, I., Zamarreño, I., García-Ramos, J.C., Suarez de Centi, C., Valenzuela, M. (1992) El Paleozoico Inferior de la Zona Cantábrica. In: Paleozoico Inferior de Ibero-America, (Eds. Gutiérrez Marco, J.C., Saavedra, J. & Rábano, I.), Univ. of Extremadura, Badajoz: 397-421.

Aramburu, C. & García-Ramos, J.C. (1993) La sedimentación cambroordovícica en la Zona Cantábrica (NO de España). Trabajos de Geologia, **19**: 45-73.

Aramburu, C. & Bastida, F., Eds. (1995) Geología de Asturias. Ediciones TREA, S.L., Gijón: 314 p.

Aramburu, C., Arbizu, M., Gutierrez-Marco, J.C., Mendez-Bedia, I., Rabano, I. & Truyols, J. (1996) Primera identificacion de materiales del Ordovicico Medio en la seccion de Los Barrios de Luna (Zona Cantabrica, noroeste de Espana). Geogaceta, **20**(1): 7-10.

Arenas, R., Gil Ibarguchi, J.I., Gonzáles Lodeiro, F., Klein, E., Martínez Catalán, J.R., Ortega Girones, E., Pablo Maciá, J.G.d. & Peinado, M. (1986) Tectonostratigraphic units in the complexes with mafic and related rocks of the NW of the Iberian Massif. Hercynica, **2**: 87-110.

Ayllón, F. (2003) Mineral, fluid and thermal evolution in veins from late orogenic coal basins of the Cantabrian Zone (Variscan, NW Spain). PhD Thesis, Ruprecht-Karls University, Heidelberg: 183 p.

Bachtadse, V. & Van der Voo, R. (1986) Palaeomagnetic evidence for crustal and thin-skinned rotations in the European Hercynides. Geophys. Res. Lett., **13**: 161-164.

Bahamonde, J.R., Colmenero, J.R. & Vera, C. (1997) Growth and demise of Late Carboniferous carbonate platforms in the eastern Cantabrian Zone, Asturias, nortwestern Spain. Sedimentary Geology, **110**: 99-122.

Bally, A.W., Gordy, P.L. & Stewart, G.A. (1966) Structure, seismic data and orogenic evolution of southern Canadian Rocky Mountains. Bulletin of Canadian Petroleum Geology, **14**: 337-381.

Balthasar, U. (2001) Taxonomy and Palaeoecology of silicified Foraminifera from the Lower Carboniferous Genicera Formation (Cantabrian Mountains, Northern Spain). Diploma thesis, Philipps Universität, Marburg, 58 p.

Barba, P. & Fernández, L.P. (1990) Estratigrafía. In: Memoria del mapa geologico de España, Escala 1:50.000, No.102 (Los Barrios de Luna), 2. Seria (MAGNA). ITGE, Madrid**:** 10-61.

Barba, P. & Fernández, L.P. (1991) Estratigrafía. In: Memoria del mapa geologico de España, Escala 1:50.000, No.103 (La Pola de Gordón), 2. Seria (MAGNA). ITGE, Madrid**:** 10-73.

Barrois, C. (1882) Recherches sur les terrains anciens des Asturies et de la Galice. Mem. Soc. Géol. Nord., **1** (2): 630 p.

Bastida, F. & Aller, J. (1992) Rasgos geológicos generales. In: Geología de Asturias. (Eds. Aramburu, C. & Bastida, F.), Ediciones Trea, S. L.**:** 27-34.

Bastida, F. & Brime, C., García-López, S., Sarmiento, G.N. (1999) Tectono-thermal evolution in a region with thin-skinned tectonics: the western nappes in the Cantabrian Zone (Variscan belt of NW Spain). Int. Journ. Earth Sciences, **88** (1): 38-48.

Beaumont, C. (1978) The evolution of sedimentary basins on a viscoelastic lithosphere: theory and examples. Geophys. J. R. Astronom. soc., **55**: 471-497.

Bechstädt, T., Schledding, T. & Selg, M. (1988) Rise and fall of an isolated, unstable carbonate platform: the Cambrian of southwestern Sardinia. Geol. Rund., **77**: 389-416.

Bechstädt, T. & Boni, M. (1989) Tectonic control on the formation of a carbonate platform: the Cambrian of southwestern Sardinia. Soc. Econ. Paleontol. Mineral., Spec. Publ., **44**: 107-122.

Bechstädt, T. & Boni, M., Eds. (1994) Sedimentological, stratigraphical and ore deposits field guide of the autochthonous Cambro-Ordovician of southwestern Sardinia. Mem. Descrittive Carta Geol. Italia, Serv. Geol. Naz.: 434 p.

Becker, G., Bless, M.J.M. & Kullmann, J. (1975) Oberkarbonische Entomozoen-Schiefer im Kantabrischen Gebirge (Nordspanien). Neues Jahrbuch fuer Geologie und Palaeontologie. Abhandlungen, **150**(1): 92-110.

Berggren, W.A., Kent, D.V., Swisher III, C.C. & Aubry, P.P. (1995) A revised Cenozoic geochronology and chronostratigraph. In: Geochronology, time scales and global stratigraphic correlation. SEPM Spec. Publ., **54:** 129-212.

Blakey, R. (2004) "Plate Tectonics and Continental Drift: Regional Paleogeographic Views of Earth History." http://jan.ucc.nau.edu/~rcb7/nat.html (10.05. 2004).

Bonhommet, N., Cobbold, P.R. & Perroud, H. (1981) Paleomagnetism and cross-folding in a key area of the Asturian arc (Spain). Journal of Geophysical research, 86(B3): 1873-1887.

Bosch, van de W.J. (1969) Geology of the Luna-Sil Region, Cantabrian Mountains (NW Spain). Leidse Geologische Mededelingen, **44**: 137-225.

Boschma, D. & Staalduinen, van C.J. (1969) Mappable units of the Carboniferous in the southern Cantabrian mountains (NW-Spain). Leidse Geologische Mededelingen, **43**: 221-231.

Bosence, D.W.J., Pomar, L., Waltham, D.A. & Lankester, T.H.G. (1994) Computer modeling a Miocene carbonate platform, Mallorca, Spain. AAPG Bulletin, **78**(2): 247-266.

Bosscher, H. & Schlager, W. (1992) Computer simulation of reef growth. Sedimentology, 39: 503-512.

Bosscher, H. & Schlager, W. (1993) Accumulation Rates of Carbonate Platforms. The Journal of Geology, **101**: 345-355.

Boucot, A.J. & Gray, J. (1983) A Palaeozoic Pangea. Science, **222**: 571-581.

Bowman, M.B.J. (1982) The stratigraphy of the San Emiliano formation and its relationship to other Namurian/Westphalian A sequences in the Cantabrian Mts., NW Spain. Trabajos de Geología, **12**: 23-35.

Bowman, S.A. & Vail, P. (1999) Interpreting the stratigraphy of the Baltimore Canyon section, offshore New Jersey with PHIL, a stratigraphic simulator. In: Numerical experiments in stratigraphy: recent advances in stratigraphic and sedimentologic computer simulations. (Eds. Harbaugh, J.W., Watney, W.L., Rankey, E.C., Slingerland, R., Goldstein, R.H. &Franseen, E.K.), SEPM Spec. Publ., **62:** 117-138.

Boyer, S. & Elliott, D. (1982) Thrust systems. Bull. Am. Ass. Petrol. Geol., **66**: 1196-1230.

Briggs, L.I. & Pollack, H.N. (1967) Digital model of evaporite sedimentation. Science, **155**: 453-456.

Brouwer, A. (1962) Deux faciès dans le Dévonien des Montagnes cantabriques méridionales. Breviora Geologica Asturiana, 8: 3-10.

Brouwer, A. & Ginkel, van A.C. (1964) La sucession carbonifère dans la partie méridionale des Mountagnes Cantabriques (Espagne du Nord-Ouest). C. R. V. Congr. Strat. Geol. Carb., Paris.

Brouwer, A. (1967) Devonian of the Cantabrian mountains, northwestern Spain. In: International symposium on the Devonian system, Vol. II**.:** 37-45.

Bucher, W.H. (1933) The Deformation of the Earth´s Crust. Princeton Univ. Press. 518 p.

Buggisch, W., Meiburg, P. & Schumann, D. (1982) Facies, paleogeography, and intra-Devonian stratigraphic gaps of the Asturo-Leonese Basin (Cantabrian Mts./ Spain). In: Subsidenz-Entwicklung im Kantabrischen Variszikum und an passiven Kontinentalraendern der Kreide; Teil 1, Sonderforschungsbereich 53 Tuebingen. (Eds. Kullmann, J., Schoenenberg, R. &Wiedmann), **163:** 212-230.

Burchette, T.P. (1981) European Devonian reefs; a review of current concepts and models. In: European fossil reef models (Ed. Toomey, D.F.). SEPM Spec. Publ., **30**: 85-142.

Burgess, P.M., Wright, V.P. & Emery, D. (2001) Numerical forward modelling of peritidal carbonate parasequence development: implications for outcrop interpretation. Basin Research, **13**(1): 1-16.

Burov, E.B. & Diament, M. (1992) Flexure of the continental lithosphere with multilayered rheology. Geophys. J. Int., **109**: 449-468.

Burov, E.B. & Diament, M. (1995) The effective elastic thickness (Te) of continental lithosphere; what does it really mean? Journal of Geophysical Research, B, Solid Earth and Planets, **100**(3): 3905-3927.

Burov, E.B. & Diament, M. (1996) Isostasy, equivalent elastic thickness, and inelastic rheology of continents and oceans. Geology, **24**(5): 419-422.

Burov, E.B., Jaupart, C. & Mareschal, J. (1998) Large-scale crustal heterogeneities and lithospheric strength in cratons. Earth and Planetary Science Letters, **164**(1-2): 205-219.

Burton, R., Kendall, C.S.C. & Lerche, I. (1987) Out of our depth-on the impossibility of fathoming eustasy from the stratigraphic record. Earth Science Reviews, **24**: 237-277.

Carey, S. (1955) The orocline concept in geotectonics. Royal Society of Tasmania Proceedings, **89**: 255-288.

Carls, P. (1983) La Zona asturoccidental-leonesa en Aragón y el Macizo del Ebro como prolongacíon del Macizo cantábrico. In: Geología de España, Libro Jubilar (Eds. J. M. Ríos. Comba, J.A.), Madrid, IGME. **3:** 11-32.

Carls, P. (1988) The Devonian of Celtiberia (Spain) and Devonian paleogeography of SW Europe. In: Devonian of the world; proceedings of the Second international symposium on the Devonian System; Volume I, Regional syntheses. (Eds. McMillan, N.J., Embry, A.F. &Glan, D.J.), Memoir - Canadian Society of Petroleum Geologists, **14:** 421-466.

Chamberlain, R.T. (1910) The Appalachian folds of Central Pennsylvania. Journal of Geology, **18**: 228-251.

Chamberlain, R.T. (1919) The building of the Colorado Rockies. Journal of Geology, **27**: 225-251.

Chevalier, J.P. (1973) Geomorphology and Geology of Coral Reefs in French Polynesia. Biology and geology of coral reefs, Vol. **1**, Geology 1, Acad. Pres. New York.

Cloetingh, S. (1988) Intraplate stresses: A tectonic cause for third-order cycles in apparent sea-level. In: Sea-level changes: an integrated approach. (Eds. Wilgus, C.K., Hastings, B.S., Kendall, C.G.S.C., Posamentier, H.W., Ross, C.A. & Wagoner, van J.C.), Soc. Econ. Paleont. Min. **42**.

Cloetingh, S. & Burov, E.B. (1996) Thermomechanical structure of European continental lithosphere: constraints from rheological profiles and ETT estimates. Geophys. J. Int., **124**: 695-723.

Colmenero, J.R., Águeda, J.A., Fernández, L.P., Salvador, C.I., Bahamonde, J.R. & Barba, P. (1988) Fan-delta systems related to the Carboniferous Evolution of the Cantabrian Zone, northwestern Spain. In: Fan Deltas: Sedimentology and Tectonics Settings. (Eds. Nemec, W. &Steel, R.J.), Blackie & Son, London: 267-285.

Colmenero, J.R., Bahamonde, J.R. & Barba, P. (1996) Las facies aluviales asociadas a los depósitos de carbón en las cuencas estefanienses de Léon (borde sur de la Cordillera Cantábrica. Cuadernos de Geología Iberíca, **21**: 71-92.

Colmenero, J.R., Fernández, L.P., Moreno, C., Bahamonde, J.R., Barba, P., Heredia, N. & González, F. (2002) Carboniferous. In: The Geology of Spain. (Eds. Gibbons, W. &Moreno, T.), The Geological Society, London**:** 93-116.

Comte, P. (1936) La série dévonienne du Léon (Espagne). C. R. Acad. Sci. Paris, **202**: 237-239.

Comte, P. (1937) La série cambrienne et silurienne du Léon. C. R. Acad. Sci. Paris, **202**: 337-341.

Comte, P. (1938) La sucession lithologique des formations cambriennes du Léon (Espagne). 71ème Congrès Soc. Sav., Nice: 181-183.

Comte, P. (1959) Recherches sur les terrains anciens de la Cordillére Cantabrique. Memorias, **60**, IGME, Madrid.

Coo, de J.C.M., Deelman, J.C. & Baan, D.v.d. (1971) Carbonate facies of the Santa Lucía Formation (Emsian-Couvinian) in León and Asturias, Spain. Geologie en Mijnbouw, **50**(3): 359-365.

Coo, de J.C.M. (1974) Lithostratigraphy of the devonian Santa Lucia limestones in Leon, Spain. Ph.D. thesis, Univ. Est. Leiden: 88 p.

Cooper, M.A. & Trayner, P.M. (1986) Thrust-surface geometry; implications for thrust-belt evolution and section-balancing techniques. In: Thrusting and deformation. (Eds. Platt, J.P., Coward, P., Deramond, P. & Hossack, J.), Jour. Struct. Geol., **8** (3-4): 305-312.

Cramer, F.H. (1964) Some Acritarchs from the San Pedro Formation (Gedinnien) of the Cantabric Mountains in Spain. Bull. Soc. Belge Géol. Paléont. Hydrol., **73**(1): 33-38.

Cross, T.A. (1990) Quantitative dynamic stratigraphy. Prentice Hall, Englewood Cliffs.

Cross, T.A. & Harbaugh, J.W. (1990) Quantitative dynamic stratigraphy; a workshop, a philosophy, a methodology. In: Quantitative dynamic stratigraphy. (Ed. Cross, T.A.), Prentice Hall, Englewood Cliffs**:** 3-20.

Crowley, Q.G., Floyd, P.A., Winchester, J.A., Franke, W. & Holland, J.G. (2000) Early Palaeozoic rift-related magmatism in Variscan Europe: fragmentation of the Armorican Terrane Assemblage. Terra Nova, **12**: 171-180.

Crowley, T.J. & Baum, S.K. (1991) Estimating Carboniferous sea-level fluctuations from Gondwanan ice extent. Geology, **19**: 975-977.

Csato, I. & Kendall, C.G.S.C. (2002) Modeling of stratigraphic architectural patterns in extensional settings towards a conceptual model. Computers & Geosciences, **28**(3): 351-356.

Dahlstrom, C.D.A. (1969) Balanced cross sections. Canadian Journal of Earth Sciences = Journal Canadien des Sciences de la Terre, **6**(4, Part 1): 743-757.

Dallmeyer, R.D. & Gil Ibarguchi, J.I. (1990) Age of amphibolitic metamorphism in the ophiolitic unit of the Morais Allochthon (Portugal); implications for early Hercynian orogenesis in the Iberian Massif. Journal of the Geological Society of London, **147**(5): 873-878.

Dallmeyer, R.D. & Martinez-Garcia, E., Eds. (1990) Pre-Mesozoic geology of Iberia, Springer Verlag.

Dallmeyer, R.D., Martínez-Catalán, J., Arenas, R., Gil Ibarguchi, J.I., Gutiérrez-Alonso, G., Farias, P., Bastida, F. & Aller, J. (1997) Diachronous Variscan tectonothermal activity in the NW Iberian Massif: evidence from 40Ar/39Ar dating of regional fabrics. Tectonophysics, **277**: 307-337.

Della Porta, G., Kenter, J.A.M. & Bahamondet, J.R. (2004) Depositional facies and stratal geometry of an Upper Carboniferous prograding and aggrading high-relief carbonate platform (Cantabrian Mountains, N Spain). Sedimentology, **51**: 267-295.

Demicco, R.V., Spencer, R.J., Waters, B.B. & Cloyd, K.C. (1991) Two-dimensional computer models of a Cambrian carbonate shelf deposit. In: Sedimentary modeling; computer simulations and methods for improved parameter definition. (Eds. Franseen, E.K., Watney, W.L., Kendall, C.G.S.C. & Ross, W.), Bulletin - Kansas, State Geological Survey, **233:** 463-472.

Dennison, J.M. & Woodward, H.P. (1963) Palinspastic maps of central Appalachians. American Association of Petroleum Geologists Bulletin, **47**: 666-80.

Dennison, J.M. (1985) Devonian eustatic fluctuations in Euramerica: Discussion. Geol. Soc. of America Bulletin, **96**: 1595-1597.

Dietrich, B., Bechtädt, T. & Zühlke, R. (2003) Paleozoic Basin Study: Structure, Stratigraphy and Quantitative Modelling in the Southern Cantabrian Mountains, NW-Spain. Conference proceeding: Analogue and nummerical forward modelling of sedimentary systems; from understanding to prediction, Utrecht: p. 23.

Doucoure, C.M., de Wit, M.J. & Mushayandebvu, M.F. (1996) Effective elastic thickness of the continental lithosphere in South Africa. Jour. of Geophys. Research, **101**(B5): 11291-11303.

Duval, D., Cramez, C. & Vail, P. (1993) Types and hierarchy of stratigraphic cycles. Sequence strat. of european basins, CNRS-IFP.: 495 p.

Duval, B.-C., Cramez, C. & Vail, P.-R. (1998) Stratigraphic cycles and major marine source rocks. In: Mesozoic and Cenozoic sequence stratigraphy of European basins. (Eds. De Graciansky, P.C., Hardenbol, J., Thierry, J. & Vail, P.R.), SEPM, **60:** 43-52.

Eberli, G.P., Kendall, C.G.S.C., Moore, P., Whittle, G.L. & Cannon, R. (1994) Testing a seismic interpretation of Great Bahama Bank with a computer simulation. AAPG Bulletin, **78**(6): 981-1004.

Eichmüller, K. (1985) Die Valdeteja Formation: Aufbau und Geschichte einer oberkarbonischen Karbonatplattform (Kantabrisches Gebirge, Nordspanien). Fazies, **13**: 45-154.

Eichmüller, K. (1986) Some Upper Carboniferous, Namurian-Westphalian, lithostratigraphic units in northern Spain; results and implications of an environmental interpretation. Boletin Geologico y Minero, **97**(5): 590-607.

Eichmüller, K. & Seibert, P. (1984) Faziesentwicklung zwischen Tournai und Westfal D im Kantabrischen Gebirge (NW-Spanien). In: Das Iberia Symposium der Deutschen Geologischen Gesellschaft. (Eds. Meiburg, P. & Schumann, D.), Enke, **135 (1):** 163-191.

Einsele, G. (2000) Sedimentary basins, Springer Verlag: 792 p.

Elliott, D. & Johnson, M. (1980) Structural evolution in the northern part of the Moine thrust belt, NW Scotland. Eart Sci., **71**: 69-96.

Emery, D. & Myers, K.J. (1996) Sequence Stratigraphy. Blackwell Science: 297 p.

Enos, P. (1991) Sedimentary parameters for computer modeling. In: Sedimentary modeling; computer simulations and methods for improved parameter definition. (Eds. Franseen, E.K., Watney, W.L., Kendal, C.G.S.C. & Ross, W.), Bulletin - Kansas, State Geological Survey, **233:** 63-99.

Evers, H.J. (1967) Geology of the Leonides between the Bernesga and Porma rivers, Cantabrian mountains (NW Spain). Leidse Geologische Mededelingen, **41**: 83-151.

Fernández, L.P. (1993) La Formación San Emiliano (Carbonífero de la Zona Cantábrica, no. de España): Estratigrafía y extensión lateral. Algunas implicaciones paleogeográficas. Trabajos de Geología, **19**: 97-122.

Fernández, L.P. (1995) El Carbonífero. In: Geología de Asturias (Eds. Aramburu, C. & Bastida, F.), Ediciones TREA, S.L., Gijón: 63-80.

Fernández, L.P., Fernández-Martínez, E., García-Ramos, J.C., Méndez-Bedia, I. & Soto, F. (1997) A sequential approach to the study of reefal facies in the Candás and Portilla Formations (Middle Devonian) of the Cantabrian Zone (NW Spain). Bol. R. Soc. Esp. Hist. Nat. (Sec. Geol.), **92**(1-4): 23-33.

Fernández-Suárez, J., Gutiérrez-Alonso, G., Jenner, G.A. & Jackson, S.E. (1998) Geochronology and geochemistry of the Pola de Allande granitoids (northern Spain): their bearing on the Cadomian-Avalonian evolution of norhtwest Iberia. Can. J. Earth Sci., **35**: 1-15.

Fernández-Suárez, J., Gutiérrez-Alonso, G., Jenner, G.A. & Tubrett, M.N. (1999) Crustal sources in Lower Palaeozoic rocks from NW Iberia: insights from laser ablation U-Pb ages of detrital zircons. Journal of the Geological Society, London, **156**: 1065-1068.

Fernández-Suárez, J., Gutiérrez-Alonso, G., Jenner, G.A. & Tubrett, M.N. (2000 b) New ideas on the Proterozioc-Early Paleozoic evolution of NW Iberia: insights from U-Pb detrital zircon ages. Precambrian Research, **102**: 185-206.

Fernández-Suárez, J., Dunning, G.R., Jenner, G.A. & Gutiérrez-Alonso, G. (2000 a) Variscan collision magmatism and deformation in NW Iberia: constraints from U-Pb geochronology of granitoids. Journal of the Geological Society, London, **157**: 565-576.

Fernández-Suárez, J., Gutiérrez-Alonso, G., Cox, R. & Jenner, G.A. (2002 b) Assembly of the Armorica Microplate: a strike-slip terrane delivery? Evidence from U-Pb Ages of detrital Zircons. Journal of Geology, **110**(5): 619-626.

Fernández-Suárez, J., Gutiérrez-Alonso, G. & Jeffries, T.E. (2002 a) The importance of along-margin terrane transport in northern Gondwana: insights from detrital zircon parentage in Neoproterozoic rocks from Iberia and Britany. Earth and Planetary Science Letters, **204**: 75-88.

Fischer, A.G. (1969) Geological time-distance rates: the Bubnoff unit. Geol. Soc. Am. Bulletin, **80**: 549-552.

Flemings, P.B. & Jordan, T.E. (1989) A synthetic stratigraphic model of foreland basin development. Jour. of Geophys. Research, **94**(B4): 3851-3866.

Flemings, P.B. & Grotzinger, J.P. (1996) STRATA: Freeware for analyzing classic stratigraphic problems. GSA today, **6**(12): 1-7.

Franke, W. (1992) Tectonic evolution of Europe; Phanerozoic structures and events in Central Europe. In: A continent revealed; the European Geotraverse. (Eds. Blundell, D., Freeman, R. & Mueller, S.), Camb. Univ. Press.

Franke, W. & Engel, W. (1986) Synorogenic sedimentation in the Variscan belt of Europe. Bull. Soc. Géol. France, **1**: 25-33.

Franke, W., Dallmeyer, R.D. & Weber, K. (1995) Geodynamic evolution. In: Pre-Permian geology of central and eastern Europe. (Eds. Dallmeyer, R.D., Franke, W. & Weber, K.), Springer**:** 579-593.

Frankenfeld, H. (1981) Krustenbewegung und Faziesentwicklung im Kantabrischen Gebirge (Nordspanien) vom Ende der Devonriffe (Givet/Frasne) bis zum Tournai. Clausthaler Geol. Abh., **39**: 91 p.

Frankenfeld, H. (1982) Das Ende der devonischen Riff-Fazies im nordspanischen Variszikum. In: Subsidenz-Entwicklung im Kantabrischen Variszikum und an passiven Kontinentalraendern der Kreide; Teil 1, Sonderforschungsbereich 53 Tuebingen. (Eds. Kullmann, J., Schoenenberg, R. & Wiedmann, J.), E. Schweizerbart'sche Verlagsbuchhandlung, **163:** 238-241.

Frankenfeld, H. (1984) Deckenbewegungen im Namur des östlichen Kantabrischen Gebirges und die damit verbundenen Vorstellungen über die Paläographie der Namur- und prä-Namur-Schichten. Z. dt. geol. Ges., **135**: 223-241.

Franseen, E.K., Watney, L., Kendall, C.G.S.C. & Ross, W.C. (1991) Sedimentary modelling: computer simulations and methods for improved parameter definition. Kansas Geol. Surv. Bull., **233**.

Frings, K.H. (2002) Palaeotemperature anomalies in late-Variscan coal basins, Ciñera-Matallana basin, Cantabrian Zone, NW Spain. GAEA heidelbergensis, **11**: 128 p.

Frings, K.H., Lutz, R., de Wall, H. & Wall, L.N. (2004) Coalification history of the Stephanian Ciñera-Matallana pull-apart basin, NW Spain: Combining anisotropy of vitrinite reflectance and thermal modelling. Int. J. Earth Sci., **93**: 92-106.

Frost, S.H. (1981) Oligocene reef coral biofacies of the Vicentin, Northeast Italy. In: European fossil reef models (Ed. Toomey, D.F.), SEPM Spec. Publ., **30**: 483-539.

Fuehrer, J. (1982) Die San Pedro-Formation. In: Subsidenz-Entwicklung im Kantabrischen Variszikum und an passiven Kontinentalraendern der Kreide; Teil 1, Sonderforschungsbereich 53 Tuebingen. (Eds. Kullmann, J., Schoenenberg, R. & Wiedmann, J.), E. Schweizerbart'sche Verlagsbuchhandlung, **163:** 173-175.

Garcia Ramos, J.C. (1978) Estudio e interpretacion de las principales facies sedimentarias comprendidas en las formaciones Naranco y Huergas (Devonico medio) en la cordillera Cantabrica. Trabajos de Geologia, Oviedo, **10**: 195-248.

Garcia Ramos, J.C. & Colmenero, J.R. (1981) Evolution sedimentaria y paleogeogafica durante el Devonico en la Cordillera Cantabrica. Conference proceedings, Curso de conferencias sobre el programa internacional de correlacion geologica (PICG), Madrid.

García-Alcalde, J.L. (1994) El Devonico de la rama Astur-Leonesa de la Zona Cantabrica (N de Espana). In: Comunicaciones de las X jornadas de paleontologia. (Ed. Fernandez, L.S.), Sociedad Espanola de Paleontologia, Universidad Complutense de Madrid y Consejo Superior de Investigaciones Cientificas, **10:** 76-80.

García-Alcalde, J.L. (1995) L´evolution paléogéographique pré-varisque de la zone cantabrique septentrionale (Espagne). Rev. Esp. de Paleont., **10**(1): 9-29.

García-Alcalde, J.L. (1996) El Devonico del dominio Astur-Leones en la zona cantabrica (N de Espana). Revista Espanola de Paleontologia, **Special issue**: 58-71.

García-Alcalde, J.L. (1998) Devonian events in northern Spain. Newsl. Stratigr., **36**(2/3): 157-175.

García-Alcalde, J.L., Arbizu, M., García-López, S. & Mende-Bedía, I. (1979) Guide book of the field trip. Meeting of the International Subcomision on Devonian Stratigraphy, Serv. Publ. Univ. de Oviedo: 41 p.

García-Alcalde, J.L., Menendez Alvarez, J.R., Garcia Lopez, S. & Soto, F. (1985) El devonico superior y el carbonifero inferior del sinclinal de Beberino (Pola de Gordon, Leon, NO. de Espana). Dixieme Con-

gres Int. de Stratigraphie et de Geologie du Carbonifere, Madrid. 375-386.

García-Alcalde, J.L. & Menendez Alvarez, J.R. (1988) The Devonian-Carboniferous boundary in the Asturo-Leonese domain (Cantabrian Mountains, NW Spain). In: Devonian-Carboniferous boundary; results of recent studies. (Eds. Flajs, G., Feist, R. & Ziegler, W.), Senckenbergische Naturforschende Gesellschaft, **100:** 21-37.

García-Alcalde, J.L. & Soto, F. (1999) El limite Eifeliense/ Givetiense (Devonico medio) en la Cordillera Cantabrica (N de Espana). Revista Espanola de Paleontologia, **Numero extraordinario**: 43-56.

García-Alcalde, J.L., Truyols-Massoni, J., Pardo-Alonso, V., Bultynick, P. & Carls, P. (2000) Devonian chronostratigraphy of Spain. Cour. Forsch.-Inst. Senckenberg, **225**: 131-144.

García-Alcalde, J.L., Carls, P., Pardo Alonso, M.V., Sanz López, J., Soto, F., Truyols-Massoni, M. & Valenzuela-Ríos, J.I. (2002) Devonian. In: The Geology of Spain. (Eds. Gibbons, W. & Moreno, T.), The Geological Society, London**:** 67-91.

García-Castellanos, D. (2002) Interplay between lithospheric flexure and river transport in foreland basins. Basin Research, **14**: 89-104.

García-Castellanos, D., Fernandez, M. & Torne, M. (2002) Modeling the evolution of the Guadalquivir foreland basin (southern Spain). Tectonics, **21**(3).

García-López, S. (1986) Los conodontos y su aplicacion al estudio de las divisiones cronoestratigraficas mayores del Devonico asturleones (Espana); Parte I, Biostratigrafia. Boletin Geologico y Minero, **97**(3): 271-312.

García-López, S., Brime, C., Bastida, F. & Sarmiento, G. (1997) Simultaneous use of thermal indicators to analyse the transition from diagenesis to metamorphism: an example from the Variscan Belt of northwest Spain. Geol. Mag., **134** (3): 323-334.

García-López, S., Bastida, F., Brime, C., Aller, J., Valín, M.L., Sanz-López, J., Méndez, C. & Menéndez-Álvarez, J. (1999) Los episodos metamórficos de la Zona Cantábrica y su contexto estructural. Trabajos de Geologia, **19**: 177-187.

García-Mondejar, J. (1989) Strike-slip subsidence of the Basque-Cantabrian Basin of Northern Spain and its relationship to Aptian-Albian opening of Bay of Biscay. In: Extensional tectonics and stratigraphy of the North Atlantic margins. (Eds. Tankard, A.J. & Balkwill, H.R.), AAPG Memoir, **46:** 395-409.

Gasparrini, M., Bakker, R., Bechstädt, T. & Boni, M. (2003) Hot dolomites in a Variscan foreland belt; hydrothermal flow in the Cantabrian Zone (NW Spain). Journal of Geochemical Exploration, **78-79**: 501-507.

German Stratigraphic Commision (ed.) (2002) Stratigraphic Table of Germany 2002. Stein, Potsdam.

Gibbons, W. & Moreno, T., Eds. (2002) The Geology of Spain. Geological Society, London: 649 p.

Gietelink, G. (1973) Sedimentology of a linear prograding coastline followed by three high-destructive delta-complexes (Cambro-Ordovician, Cantabrian Mountains, NW Spain). Leidse Geologische Mededelingen, **49**(1): 125-144.

Ginkel, van A.C. (1965) Carboniferous fusulinids from the Cantabrian mountains (Spain). Leidse Geologische Mededelingen, **34**: 1-225.

Ginkel, van A.C. & Villa, E. (1996) Paleontological data of the San Emiliano Formation (Cantabrian Mountains, Spain) and their significance in the carboniferous chronostratigraphy. Geobios, **29**(2): 149-170.

Ginsburg, R.N. (1971) Landward movement of carbonate mud-new model for regressive cycles in carbonates. AAPG Bulletin, **55**(2): 340 p.

Goldhammer, R.K. (1997) Compaction and decompaction algorithms for sedimentary carbonates. Journal of Sedimentary Research, **67**(1): 26-35.

González Lastra, J. (1978) Facies salinas en la Caliza de Montaña (Cordillera Cantábrica). Trabajos de Geología, **10**: 249-265.

Gradstein, F.M., Agterberg, F.P., Aubry, M.P., Berggren, W.A., Flynn, J.J., Hewitt, R., Kent, D.V., Klitgord, K.D., Miller, K.G., Obradovitch, J., Ogg, J.G., Prothero, D.R. & Westerman, G.E.G. (1988) Sea level history. Science, **241**: 599-601.

Gradstein, F.M., Agterberg, F.P., Ogg, J.G., Hardenbol, J., Van Veen, P., Thierry, J. & Huang, Z. (1994) A Mesozoic time scale. J. Geophys. Res., **99**(12): 24,051-24,074.

Granjeon, D. & Joseph, P. (1999) Concepts and applications of a 3-D multiple lithology, diffusive model in stratigraphic modeling. SEPM Spec Publ, **62**: 197-210.

Gutiérrez-Alonso, G. (1996) Strain partitioning in the footwall of the Somiedo Nappe: structural evolution of the Narcea Tectonic Window, NW Spain. Journal of Structural geology, **18**(10): 1217-1229.

Gutiérrez-Alonso, G., Fernández-Suárez, J., Jeffries, T.E., Jenner, G.A., Tubrett, M.N., Cox, R. & Jackson, S.E. (2003) Terrane accretion and dispersal in the northern Gondwana margin. An Early Paleozoic analogue to a long-lived active margin. Tectonophysics, **365**: 221-232.

Gutiérrez-Alonso, G., Fernández-Suárez, J. & Weil, A.B. (2004) Orocline triggered lithospheric delamination. In: Orogenic Curvature. (Eds. Sussman, A.J. & Weil, A.B.), GSA Special Paper. *in press*.

Gutiérrez-Marco, J.C. & Rodríguez, L. (1987) Descubrimiento de graptolitos arenigienses en la Escama de Rioseco (zona Cantábrica, N de España). Cuad. Lab. Xeol. Laxe, **11**: 209-220.

Gutiérrez-Marco, J.C., Aramburu, C., Arbizu, M., Mendez-Bedia, I., Rabano, I. & Villas, E. (1996) Rasgos estratigraficos de la sucesion del Ordovicico Superior en Portilla de Luna (Zona Cantabrica, noroeste de Espana). Geogaceta, **20**(1): 11-14.

Gutiérrez-Marco, J.C., Robardet, M., Rábano, I., Sarmiento, G.N., San José Lancha, M.A. & Herranz Araújo, P. (2002) Ordovician. In: Geology of Spain. (Eds. Gibbons, W. & Moreno, T.), Geological Society, London**:** 31-49.

Gwinn, V.E. (1970) Kinematic patterns and estimates of lateral shortening, Valley and Ridge and Great Valley Provinces, Central Appalachians, south-central Pennsylvania. In: Studies in Appalachian Geology: Central and Southern. Intersciende: 127-146.

Hallam, A. (1984) Pre-Quaternary sea-level changes. Ann. Rev. Earth Planet. Sci., **12**: 205-243.

Haq, B.U., Hardenbol, J. & Vail, P.R. (1987) Chronology of fluctuating sea levels since the Triassic. Science, **235**(4793): 1156-1167.

Harbaugh, J.W., Watney, W.L., Rankey, E.C., Slingerland, R., Goldstein, R.H. & Franseen, E.K. (1999) Numerical experiments in stratigraphy; recent advances in stratigraphic and sedimentologic computer simulations. Spec Publ. SEPM, **62**.

Heckel, P.H. (1986) Sea-level curve for Pennsylvanian eustatic marine transgressive-regressive depositional cycles along midcontinent outcrop belt, North America. Geology, **14**: 330-334.

Hemleben, C. & Reuther, C.D. (1980) Allodapic limestones of the Barcaliente Formation (Namurian A) between Luna and Cea rivers (southern Cantabrian Mountains, Spain). Neues Jahrbuch fuer Geologie und Palaeontologie. Abhandlungen, **159**(2): 225-255.

Herbig, H.G. & Buggisch, W. (1984) Frasnian Limestone Intercalations in the Nocedo Formation of N-León (Cantabrian Mountains/NW-Spain). Z. dt. geol. Ges., **135**: 149-161.

Heward, A.P. (1978b) Alluvial fan sequence and megasequence models: with examples from Westphalian D-Stephanian B coalfields, Northern Spain. In: Fluvial Sedimentology. (Ed. Miall, A.), Canadian Society of Petroleum Geologists, **Memoir 5:** 669-702.

Heward, A.P. & Reading, H.G. (1980) Deposits associated with a Hercynian to late Hercynian continental strike-slip system, Cantabrian Mountains, northern Spain. In: Sedimentation in oblique-slip mobile zones. (Eds. Ballance, P.F. & Reading, H.G.), Spec. Publ. IAS, **4:** 105-125.

Higgins, A.C., Wagner-Gentis, C.H.T. & Wagner, R.H. (1964) Basal Carboniferous Strata in Part of Northern Leon, NW Spain: Stratigraphy, Conodont and Goniatite Faunas. Bull. Soc.Belg.Geol. Paleont. Hydrol., **72**: 205-248.

Higgins, A.C. & T, Wagner-Gentis, C.H.T. (1982) Conodonts, goniatites and the biostratigraphy of the earlier Carboniferous from the Cantabrian mountains, Spain. Paleontology, **25**(2): 313-350.

Hinsch, R. (1997) Kinematische Entwicklung der variszisch angelegten Forcada Einheit, Kantabrisches Gebirge, Nord-Spanien (südliches Arbeitsgebiet). Diploma thesis, Universität Hamburg: 134 p.

Hirth, A., Lowrie, W., Julivert, M. & Arboleya, M. (1992) Paleomagnetic results in support of a model for the origin of the Asturian arc. Tectonophysics, **213**: 321-339.

Hüssner, H., Roessler, J. & Monz, R. (1997) REPRO - a 3D simulation program for reef growth models. Zbl Geol Paläont, **9**(Teil 1): 957-968.

Jamison, W.R. (1987) Geometric analysis of fold development in overthrust terranes. Journal of Structural geology, **9**(2): 207-219.

Johnson, G.A.L. & Tarling, D.H. (1985) Continental convergence and closing seas during the Carboniferous. 10. Congr. Internat. Stratigr. Géol. Carbonifère, Madrid 1983: 163-168.

Johnson, J.G., Klapper, G. & Sandberg, C.A. (1985) Devonian eustatic fluctuations in Euramerica. GSA Bulletin, **96**(5): 567-587.

Johnson, M.E. & McKerrow, W.S. (1991) Sea level and faunal changes during the latest Llandovery and earliest Ludlow (Silurian). Historical Biology, **5**: 153-169.

Jordan, T.E. & Flemmings, P.B. (1991) Large scale stratigraphic architecture, eustatic variation, and unsteady tectonism: a theoretical evaluation. J. Geophys. Res., **96**: 6681-6699.

Jervey, M.T. (1988) Numerical modelling of deposition sequences and their seismic expression. In: Sequences, stratigraphy, sedimentology; surface and subsurface. (Eds. James, D.P. & Leckie, D.A.), Canadian Society of Petroleum Geologists, **15:** 571.

Julivert, M. (1971) Decollement tectonics in the Hercynian Cordillera of Northwest Spain. American Journal of Science, **270**(1): 1-29.

Julivert, M. (1981) A cross-section through the northern Part of the Iberian Massif. Geol. en Mijnbouw, **60**: 107-128.

Julivert, M., Pello, J. & Fernández-García, L. (1968) La estructura del Manto de Somiedo (Cordillero Cantábrica). Trabajos de Geología, **2**: 1-43.

Julivert, M., Fontboté, J.M., Ribeiro, A. & Conde, L.N. (1972) Mapa tectónico de la Península Ibérica y Baleares. Madrid, IGME.

Julivert, M. & Marcos, A. (1973) Superimposed folding under flexural conditions in the Cantabrian zone (Hercynian cordillera, northwest Spain). American Journal of Science, **273**: 353-375.

Julivert, M. & Truyols, J. (1983) El Ordovício en el Macizo Ibérico. In: Libro Jubilar de J. M. Ríos, Geología de España. (Ed. Comba, J.A.), IGME, Madrid, **1**: 192-246.

Julivert, M. & Arboleya, M.L. (1984) An geometrical and kinematical approach to the nappe structure in an arcuate fold belt: the Cantabrian nappes (Hercynian chain, NW-Spain). Journal of Structural geology, **6**(5): 499-519.

Julivert, M. & Arboleya, M.L. (1986) Areal balancing and estimate of areal reduction in a thin-skinned fold and thrust belt (Cantabrian Zone, NW Spain); constraints on its emplacement mechanism. In: Thrusting and deformation. (Eds. Platt, J.P., Coward, M.P., Deramond, J. & Hossack, J.), Pergamon, **8 (3-4):** 407-414.

Karner, G.D., Steckler, M.S. & Thorne, J. (1983) Long-term mechanical properties of the continental lithosphere. Nature, **304**: 250-253.

Kegel, W. (1929) Das Gotlandium in den Kantabrischen Ketten Nordspaniens. Z. Dt. Gel. Ges., **81**: 35-62.

Keller, M. (1988) Die La-Vid-Gruppe: Fazies, Paläogeographie und synsedimentäre Tektonik im Unterdevon des Kantabrischen Gebirges (NW-Spanien). Erlanger geol. Abh., **115**: 77-154.

Keller, M. & Grötsch, J. (1990) Depositional history and conodont biostratigraphy of the Lower Devonian La Vid Group in the Luna area (Cantabrian Mountains, NW Spain). Neues Jahrbuch fuer Geologie und Palaeontologie, **Monatshefte, 3**: 141-164.

Keller, M. & Krumm, S. (1993) Variscan versus Caledonian and Precambrian Metamorphic Events in the Cantabrian Mountains, Northern Spain. Z. dt. geol. Ges., **144**: 88-103.

Kendall, C.G.S.C., Strobel, J., Cannon, R., Bezdek, J. & Biswas, G. (1991) The simulation of the sedimentary fill of basins. Jour. of Geophys. Research, **96**(B4): 6911-6929.

Kendall, C.G.S.C., Moore, P., Whittle, G. & Cannon, R. (1992) A challenge; is it possible to determine eustasy and does it matter? In: Eustasy; the historical ups and downs of a major geological concept. (Ed. Dott, R.H.Jr.), GSA-Memoir, **180**: 93-107.

Kendall, C.G.S.C. & Sen, A. (1998) Use of sedimentary simulations and measuring the size of eustatic sea level changes: an example from the Neogene of the Bahama. In: Computerized modelling of sedimentary systems. (Eds. Harff, J., Lemke, W. & Stattegger, K.), Springer**:** 291-306.

Kenter, J., Hoeflaken, F., Bahamonde, J.R., Bracco Gartner, G.L., Keim, L. & Besems, R.E. (2002) Anatomy and lithofacies of an intact and seismic-scale Carboniferous carbonate platform (Asturias, NW Spain): analogs of hydrocarbon reservoirs in the Pricaspian basin (Kazakhstan). In: Paleozoic Carbonates of the Commonwealth of Independent States (CIS): Subsurface Reservoirs and Outcrop Analogs. (Eds. Zempolich, W. & Cook, H.), SEPM Spec. Publ., **74:** 185-207.

Kiessling, W., Flügel, E. & Golonka, J. (2000) Fluctuations in the carbonate production of Phanerozoic reefs. In: Carbonate Platform Systems: components and interactions. (Eds. Insalaco, E., Skelton, P.W. & Palmer, T.J.), Geological Society, London, **178:** 191-215.

Klein, G. de V. (1987) Current aspects of basin analysis. Sedimentary Geology, **50**: 95-118.

Kollmeier, J., van der Pluijm, B.A. & Van der Voo, R. (2000) Analysis of Variscan dynamics; early bending of the Cantabria-Asturias Arc, northern Spain. Earth and Planetary Science Letters, **181**: 203-216.

Krans, T.F. (1982) Block-movements and sedimentation in the Upper Silurian and Lower Devonian of the Cantabrian Mountains (NW Spain). In: Subsidenz-Entwicklung im Kantabrischen Variszikum und an passiven Kontinentalraendern der Kreide; Teil 1, Sonderforschungsbereich 53 Tuebingen. (Eds. Kullmann, J., Schoenenberg, R. & Wiedmann, Schweizerbart'sche Verlagsbuchhandlung, **163:** 163-172.

Krebs, W. (1974) Devonian carbonate complexes of central Europe. In: Reefs in Time and Space; Selected Examples from the Recent and Ancient, SEPM Spec. Publ., **18**: 155-208.

Kruse, S. & Royden, L. (1994) Bending and unbending of an elastic lithosphere: the Cenozoic historyof the Appenine and Dinaride foredeep basins. Tectonics, **13**: 278-302.

Kullmann, J. (1985) Relaciones faunísticas de los Ammonoideos Carboníferos de España-Portugal (Península Ibérica). 10. Congr. Internat. Stratigr. Geol. Carbonifère, Madrid 1983,, Madrid, C.R. 2.

Kullmann, J. & Schoenenberg, R. (1979) Das Kantabrische Orogen; ein Modell fuer den Komplex "Geosynkline-Orogen" im europaeischen Variszikum. Geologische Rundschau, **68**(1): 163-171.

Lawrence, D.T., Doyle, M. & Aigner, T. (1990) Stratigraphic simulation of sedimentary basins: concepts and calibration. AAPG Bulletin, **74**(3): 273-295.

Leeder, M.R. (1978) A quantitative stratigraphic model for alluvium, with special reference to channel deposit density and interconnectedness. In: Fluvial Sedimentology. Miall, A.D., Can. Soc. Petrol. Geol. Mem. **5:** 587-596.

Leeder, M.R. (1999) Sedimentology and sedimentary basins. From turbulence to tectonics. Blackwell Science: 592 p.

Lees, A. (1961) The Waulsortian „reefs" of Eire; a carbonate mudbank complex of lower Carboniferous age. Journ. of Geol., **69**, 1: 101-109.

Leprvrier, C. & Martínez García, E. (1990) Fault development and stress evolution of the post-Hercynian Asturian Basin (Asturias and Cantabria, northwestern Spain). Tectonophysics, **184**: 345-356.

Leweke, H.B. (1983) Das Unterdevon im Kantabrischen Gebirge, NW Spanien (La-Vid-Formation)-Der Übergang von siliziklastischer zu karbonatischer Sedimentation. Ph. D. thesis, Tübingen: 151 p.

Leyva, F., Matas, J. & Rodríguez Fernández, L.R. (1984) Memoria del mapa geologico de España, Escala 1:50.000, No.129 (La Robla), 2. Seria (MAGNA). IGME, Madrid: 98 p.

Lin, A. & Watts, A.B. (2002) Origin of the West Taiwan basin by orogenic loeading and flexure of a rifted continental margin. Jour. of Geophys. Research, **107**(B9): 2185.

Linzer, H.G. (1989) Ausgeglichenes Profil und Kinematik der zentralen Lechtal- und Inntaldecke, Tirol. Ph. D. thesis, Karlsruhe:119 p.

Liñán, E., Perejón, A. & Sdzuy, K. (1993) The Lower-Middle Cambrian stages and stratotypes from the Iberian Peninsula: a revision. Geol. Mag., **130**: 817-833.

Liñán, E., Gozalo, R., Palacios, T., Gámez Vintaded, J.A., Ugidos, J.M. & Mayoral, E. (2002) Cambrian. In: The Geology of Spain. (Eds. Gibbons, W. & Moreno, T.), The Geological Society, London**:** 17-29.

Liu, K., Pigram, C.J., Paterson, L. & Kendall, C.G.S.C. (1998) Computer simulation of a Cenozoic carbonate platform, Marion Plateau, north-east Australia. In: Reefs and carbonate platforms in the Pacific and Indian Ocean. (Eds. Camoin, G.F. & Davies, P.J.), IAS Special Publication, **25:** 145-161.

Lobato, L., García-Alcalde, J.L., Sánchez de Posada, L.C. & Truyols, J. (1984) Cartografía del mapa geologico de España, Escala 1:50.000, No.104 (Boñar), IGME, Madrid.

Loevezijn, van G.B.S. (1983) Upper Devonian block movements and sedimentation in the Asturo-Leonese Basin (Cantabrian Mountains, Spain). Leidse Geologische Mededelingen, **52**(2): 185-192.

Loevezijn, van G.B.S. (1986) Stratigraphy and facies of the Nocedo, Fueyo and Ermita formations (Upper Devonian to lowermost Carboniferous) in Leon, N Spain. Scripta Geol., **81**: 1-116.

Loevezijn, van G.B.S. (1988) The Famennian of the Cantabrian Mountains, northwestern Spain. N. Jb. Geol. Paläont. Mh., **5**: 278-292.

Loevezijn, van G.B.S. & Raven, J.G.M. (1983) The Upper Devonian deposits in the northern part of Leon (Cantabrian Mountains, northwestern Spain). Leidse Geologische Mededelingen, **52**(2): 179-183.

Lorenz, V. & Nicholls, I. (1984) Plate and intraplate processes of Hercynian Europe during the Late Palaeozoic. Tectonophysics, **107**: 25-56.

Lotze, F. (1945) Zur Gliederung der Varisziden der Iberischen Meseta (Spanien). Geotekt. Forsch., **6**: 78-92.

Lotze, F. (1956) Das Präkambrium Spaniens. Neues Jb. Geol. Paläont. Mh., **8**: 373-380.

Lotze, F. (1961) Das Kambrium Spaniens. Teil I: Stratigraphie. Akad. Wiss. Lit., Abh. Math. Naturw., **Kl. 6-8**: 411 p.

Lyon-Caen, H. & Molnar, P. (1984) Gravity anomalies and the structure of the western Tibet and the southern Tarim. Geophys. Res. Lett., **11**(1251-1254).

Maggi, A., Jackson, J.A., McKenzie, D. & Priestley, K. (2000) Earthquake focal depths, effective elastic thickness, and the strength of the continental lithosphere. Geology, **28**(6): 495-498.

Marcos, A. (1968) La tectonica de la unidad de la Sobia-Bodon. Trabajos de Geología, **2**: 59-87.

Marcos, A. (1973) Las series del Paleozoico inferior y la estructura herciniana del occidente de Asturias (NW de Espana). The lower Paleozoic series and the Hercynian structure of western Asturias, northwestern Spain. Trabajos de Geologia, **6**: 113 p.

Marcos, A., Kullmann, J. & Schoenenberg, R. (1979) Facies differentiation caused by wrench deformation along a deep-seated fault system (Leon Line, Cantabrian Mountains, North Spain); discussion and reply. Tectonophysics, **60**(3-4): 303-309.

Marcos, A. & Pulgar, J., A. (1982) An approach to the tectonostratigraphic evolution of the Cantabrian foreland thrust and fold belt, Hercynian Cordillera of NW Spain. Neues Jahrbuch fuer Geologie und Palaeontologie.Abhandlungen, **163**(2): 256-260.

Martín Parra, L.M. (1989) Memoria del mapa geológico de España. Escala 1:50.000, No. 128 (Riello), 2. Serie (MAGNA). ITGE, Madrid**:** 119.

Martínez Catalán, J. (1990) A non-cylindrical model for the northwest Iberian allochtonous terranes and their equivalents in the Hercynian belt of Western Europe. Tectonophysics, **179**: 253-272.

Martínez Catalán, J.R., Arenas, R., Díaz García, F. & Abati, J. (1997) Variscan accretionary complex of nortwestern Iberia: Terrane correlation and succession of tectonothermal events. Geology, **25**(12): 1103-1106.

Martínez Chacón, M.L. & Winkler Prins, C.F. (1993) Carboniferous brachiopods and the palaeogeographic position of the Iberian Peninsula. Comptes Rendus XII Congr. Int. Strat. Géol. Carbonifère Permien, Buenos Aires, 1991: 573-580.

Martínez García, E., Wagner, R.H., Lobato, L., Fernández, L. & Alonso, J.L. (1983) El Carbonífero de la Región Oriental (Pisuerga-Carrión). In: Carbonífero y Pérmico de España, IGME**:** 116-132.

Matas, J. & Rodríguez Fernández, L.R. (1984) Cartografía del mapa geologico de España, Escala 1:50.000, No.129 (La Robla). IGME, Madrid.

Matte, P. (1991) Accretionary history and crustal evolution of the Variscan Belt in Western Europe. In: Accretionary tectonics and composite continents. (Eds. Hatcher, R.D., Jr. & Zonenshain, L.), Elsevier, **196 (3-4):** 309-337.

Matte, P. (2001) The Variscan collage and orogeny (480-290 Ma) and the tectonic definition of the Armorica Microplate; a review. Terra Nova, **13**(2): 122-128.

Matte, P. & Ribiero, A. (1975) Forme et orientation de l´episode de déformation dans la virgation hercynienne de Galíce. Rélations avec le plissement et hypothèse sur la génèse de l´arc Ibero-Armoricaine. Académie de Sci. comptes Rendus, **280**: 2825-2828.

Matthews, R.W. (1988) Sea level history. Science, **241**: 597-599.

McClay, K.R. (1992) Glossary of thrust tectonics terms. In: Thrust tectonics. (Ed. Mc Clay, K.R.), Chapman & Hall**:** 419-433.

McKenzie, D. (1978) Some remarks on the development of sedimentary basins. Earth and Planetary Science Letters, **40**: 25-32.

McKenzie, D. & Fairhead, D. (1997) Estimates of the effective elastic thickness of the continental lithosphere from Bouguer and free air gravity anomalies. Jour. of Geophys. Research, **102**(B12): 27523-27552.

McKerrow, W., Dewey, J. & Scotese, C.R. (1991) The Ordovician and Silurian development of the Iapetus Ocean. Palaeontology, **44**: 165-178.

Meer Mohr, van der, C. (1969) The stratigraphy of the Cambrian Lancara Fm. between the Luna River and the Esla River in the Cantabrian Mountains, Spain. Leidse Geologische Mededelingen, **43**.

Meer Mohr, van der, C., Kuijper, R.P., Calsteren, van P. & Tex, de E. (1981) The Hesperian Massif: from Iapetus aulacogen to ensialic orogen. A model for its development. Geol. Rundschau, **70**(2): 459-472.

Méndez-Bedia, I. (1976) Biofacies y litofacies de la Formación Moniello-Santa Lucia (Dévonico de la Cordillera Cantábrica, NW de España). Trabajos Geología Universidad Oviedo, **9**: 1-93.

Méndez-Bedía, I., Soto, F. & Fernández-Martínez, E. (1994) Devonian reef types in the Cantabrian Moun-

tains (NW Spain) and their faunal composition. Cour. Forsch.-Inst. Senckenberg, **172**: 161-183.

Menning, M. (1995) A numerical time scale for the Permian and Triassic periods. An integrated time analysis. In: Permian of the northern continents. (Eds. Scholle, P., Peryt, T.M. & Ulmer-Scholle, D.S.), Springer, **1:** 77-97.

Menning, M., Weyer, D., Drozdzewski, G., Amerom, H.W.J. & Wendt, I. (2000) A Carboniferous time scale 2000: discussion and use of geological parameters as time indicators from Central and Western Europe. Geol. Jb., **A 156**: 3-44.

Menning, M. (2001) A Permian time scale 2000 and correlation of marine and continental sequences using the Illawarra Reversal (265Ma). Natura Bresciana, Ann. Mus. Civ. Sc. Nat.,, **25**: 355-362.

Miall, A.D. (1986) Eustatic sea level changes interpreted from seismic stratigraphy-a critique of the methodology with particular reference to the North Sea Jurrasic record. AAPG Bulletin, **70**(2): 131-137.

Mitchum, R.M.J. & Wagoner, van J.C. (1991) High-frequency sequences and their stacking patterns: sequence-stratigraphic evidence of high-frequency eustatic cycles. Sedimentary Geology, **70**: 131-160.

Mitra, S. (1986) Duplex structures and imbricate thrust systems: geometry structural position and hydrocarbon potential. AAPG Bulletin, **70**: 1087-1112.

Mohanti, M. (1972) The Portilla Formation (Middle Devonian) of the Alba Syncline, Cantabrian Mountains, Prov. Léon, NW Spain. Carbonate facies and Rhynchonellid paleontology. Leidse Geologische Mededelingen, **48**: 135-205.

Muir, I., Wong, P. & Wendte, J. (1985) Devonian Hare Indian-Ramparts (Kee Scarp) evolution, MacKenzie Mountains and subsurface Norman Wells, N.W.T.; basin-fill and platform reef development. In: Rocky Mountain carbonate reservoirs; a core workshop (Eds. Longman, M.W., Shanley, K.W., Lindsay, R.F. & Eby, D.E.), SEPM Core Workshop, **7**: 311-341.

Murphy, J. & Nance, R. (1991) Supercontinent model for the contrasting character of Late Proterozoic orogenic belts. Geology, **19**: 469-472.

Nance, R. & Murphy, J. (1996) Basement isotopic signatures and Neoproterozoic paleogeography of Avalonian-Cadomian and related terranes in the Circum-North Atlantic. In: Avalonian and related Peri-Gondwanan Terranes of the circum-North Atlantic. (Eds. Nance, R. & Thompson, M.), GSA, Spec. Paper, **304:** 109-120.

Nieuwland, D.A., Leuschner, J.H. & Gast, J. (2000) Wedge equilibrium in fold-and-thrust belts: prediction of out-of-sequence thrusting based on sandbox experiments and natural examples. Geologie en Mijnbouw/Netherlands Journal of Geosciences, **79**(1): 81-91.

Nijman, W. & Savage, J.F. (1989) Persistent basement wrenching as controlling mechanism of Variscan thin-skinned thrusting and sedimentation, Cantabrian Mountains, Spain. In: Palaeozoic plate tectonics with emphasis on the European Caledonian and Variscan belts. (Eds. Matte, P. & Zwart, H.J.), Elsevier, **169:** 281-302.

Nordlund, U. (1996) Formalizing geological knowledge - with an example of modeling stratigraphy using fuzzy logic. Jour Sed Res, **66**: 689-698.

Oczlon, M.S. (1992) Gondwana and Laurussia before and during the Variscan Orogeny in Europe and related areas. Heidelberger Geowissenschaftliche Abhandlungen, **53**: 159 p.

Oele, E. (1964) Sedimentological aspects of four lower-paleozoic formations in the northern part of the province of León (Spain). Leidse Geologische Mededelingen, **30**: 1-100.

Pálfy, J., Smith, P.L. & Mortensen, J.K. (2000) U-Pb and 40Ar/39Ar time scale for the Jurassic. Can. J. Earth Sci., **37**(6): 923-944.

Paola, C. (2000) Quantitative models of sedimentary basin filling. Sedimentology, **47** (supplement): 121-179.

Parés, J., Van der Voo, R., Stamatakos, J. & Pérez-Estaún, A. (1994) Remagnetizations and postfolding oroclinal rotations in the Cantabrian/Asturian arc, northern Spain. Tectonics, **13**(6): 1461-1471.

Paris, F. (1998) Early Palaeozoic palaeobiogeography of northern Gondwana regions. Acta Univ. Carolinae-Geol., **42**: 473-483.

Paris, F. & Robardet, M. (1990) Early Paleozoic palaeobiogeography of the Variscan regions. Tectonophysics, **177**: 193-213.

Parker, G. (1978) Self-formed straight rivers with equilibrium banks and mobile bed. Part 1. J. Fluid Mechanics, **89**: 109-125.

Parkinson, D. (1957) Lower Carboniferous reefs of northern England. AAPG Bulletin, **41**, 3: 511-537.

Pérez-Estaún, A. (1978) Estratigrafía y estructura de la rama sur de la Zona Asturoccidental-Leonesa. Mem. Inst. Geol. Min. España, **92**: 149 p.

Pérez-Estaún, A., Bastida, F., Alonso, J.L., Marquinez, J., Aller, J., J, A.-M., Marcos, A. & Pulgar, J.A. (1988) A thin-skinned tectonics model for an arcuate fold and thrust belt; the Cantabrian Zone (Variscan Ibero-Armorican Arc). Tectonics, **7**(3): 517-537.

Pérez Estaún, A. & Bastida, F. (1990) Structure: Cantabrian Zone. In: Pre-Mesozoic geology of Iberia. (eds. Dallmeyer, R.D. & Martínez García, E.), Springer**.**

Pérez-Estaún, A., Bastida, F., Martinez Catalan, J.R., Gutierrez Marco, J.C., Marcos, A. & Playford, P.E. (1980) Devonian "great barrier reef" of Canning Basin, Western Australia. AAPG Bulletin, **64**, 6: 814-840.

Pulgar, J.A. (1990) Stratigraphy. In: Pre-Mesozoic geology of Iberia. (Eds. Dallmeyer, R.D. & Martínez García, E.), Springer.

Pérez-Estaún, A., Martinez-Catalán, J.R. & Bastida, F. (1991) Crustal thickening and deformation sequence in the footwall to the suture of the Variscan belt of northwest Spain. Tectonophysics, **191**: 243-253.

Pérez-Estaún, A., Pulgar, J.A., Banda, E. & Álvarez, M.J. (1994) Crustal structure of the external variscides in northwest Spain from deep seismic reflection profiling. Tectonophysics, **232**: 91-118.

Pérez-Estaún, A., Pulgar, J.A. & Álvarez, M.J. (1995) Crustal structure of the Cantabrian zone; seismic image of a Variscan foreland thrust and fold belt (NW Spain). Revista de la Sociedad Geologica de España, **8**(4): 307-319.

Perroud, H. (1986) Paleomagnetic evidence for tectonic rotations in the Variscan mountain belt. Tectonics, **5**(2): 205-214.

Perroud, H. & Bonhommet, N. (1981) Palaeomagnetism of the Ibero-Armorican arc and the Hercynian orogeny in western Europe. Nature, **292**: 445-447.

Pitman, W. (1978) Relationship between eustacy and stratigraphic sequences of passive margins. GSA Bulletin, **89**: 1389-1403.

Platt, J.P. (1986) Dynamics of orogenic wedges and the uplift of high-pressure metamorphic rocks. GSA Bulletin, **97**: 1037-1053.

Playford, P.E., Hurley, N.F., Kerans, C. & Middleton, M. (1989) Reefal platform development, Devonian of the Canning Basin, Western Australia. In: Controls on carbonate platforms and basin development. (Eds. Crevello, P.D., Wilson, J.T., Sarg, J.F. & Read, J.F.), SEPM Spec. Publ., **44:** 187-202.

Poelchau, H., Baker, D., Hantschel, T., Horsfield, B. & Wygrala, B. (1997) Basin simulation and the design of the conceptual basin model. In: Petroleum and basin evolution; insights from petroleum geochemistry, geology and basin modeling. (Eds. Welte, D.H., Horsfield, B., Baker, D.R.), Springer**:** 3-70.

Posamentier, H.W., Jervey, M.T. & Vail, P.R. (1988) Eustatic controls on clastic deposition; I, Conceptual framework. In: Sea-level changes; an integrated approach. (Eds. Wilgus, C.K., Hastings, B.S., Ross, C.A., Posamentier, H.W., Wagoner, van J.C. & Kendall, C.G.S.C.), SEPM Spec. Publ., **42:** 109-124.

Posamentier, H.W. & Vail, P.R. (1988) Eustatic controls on clastic deposition; II, Sequence and systems tract models. In: Sea-level changes; an integrated approach. (Eds. Wilgus, C.K., Hastings, B.S., Ross, C.A., Posamentier, H.W., Wagoner, van J.C. & Kendall, C.G.S.C.), SEPM Spec. Publ., **42:** 125-154.

Posamentier, H.W. & James, D.P. (1993) An overview of sequence-stratigraphic concepts: uses and abuses. Spec. Publ. Int. Ass. Sediment., **18**: 3-18.

Potent, S. & Reuther, C. (2000) Kinematik der Faltungs- und Überschiebungsprozesse der variszisch angelegten Montuerto-Struktur im südlichen Kantabrischen Gebirge, Nord-Spanien. Mitt. Geol.-Paläont. Inst. Univ. Hamburg, **84**: 83-110.

Priewalder, H. (1997) SEM-Revision of a Chitinozoan Assemblage from the Uppermost San Pedro Fm (Pridoli). Cantabrian Mountains (Spain). Jahrbuch der Geologischen Bundesanstalt, **140**: 73-93.

Prosser, S. (1993) Rift-related linked depositional systems and their seismic expression. In: Tectonics and Seismic Sequence Stratigraphy. (Eds. Williams, G.D. & Dobb, A.), Geological Society, London, **71:** 35-66.

Pulgar, J.A., Pérez, E.A., Gallart, J., Alvarez, M.J., Gallastegui, J. & Alonso, J.L. (1995) The ESCI-N2 deep seismic reflection profile; a traverse across the Cantabrian Mountains and adjacent Duero Basin. Revista de la Sociedad Geologica de Espana, **8**(4): 383-394.

Pulgar, J., Alonso, J., Espina, R. & Marin, J. (1999) La deformacion alpina en el basamento varisco de la Zona Cantabrica. Trabajos de Geologia, **21**: 283-294.

Quesada, C. (1991) Geological constraints on the Paleozoic tectonic evolution of tectonostratigraphic terranes in the Iberian Massif. Tectonophysics, **185**: 225-245.

Radig, F. (1962) Ordovizium und Silur und die Frage prävariskischer Faltungen in Nordspanien. Geologische Rundschau, **52**: 346-357.

Ramsay, J.G. & Huber, M.I. (1987) The techniques of modern structural geology, volume 2: Folds and Fractures, Academic Press: 700 p.

Ranalli, G. (1994) Nonlinear flexure and equivalent mechanical thickness of the lithosphere. Tectonophysics, **240**: 107-114.

Raven, J.G.M. (1983) Conodont biostratigraphy and depositional history of the Middle Devonian to Lower Carboniferous in the Cantabrian Zone (Cantabrian Mountains, Spain). Leidse Geologische Mededelingen, **52**(2): 265-339.

Raven, J.G.M. & Pluijm, van der B.A. (1986) Metamorphic fluids and transtension in the Cantabrian Mountains of northern Spain: an application of the conodont colour alteration index. Geol. Mag., **123**(6): 673-681.

Read, J.F., Grotzinger, J.P., Bone, J.A. & Koerschner, W.F. (1986) Models for generation of carbonate cycles. Geology, **14**: 107-110.

Read, J.F., Osleger, D. & Elrick, M. (1991) Two-dimensional modeling of carbonate ramp sequences and component cycles. In: Sedimentary modeling; computer simulations and methods for improved parameter definition. (Eds. Franseen, E.K., Watney, W.L., Kendall, C.G.S.C. & Ross, W.), Bulletin - Kansas, State Geological Survey, **233:** 473-488.

Reijers, T.J.A. (1972) Facies and diagenesis of he Devonian Portilla Limestone Formation between the river Esla and the Embalse de la Luna, Cantabrian Mountains, Spain. Leidse Geologische Mededelingen, **47**: 163-249.

Reijers, T.J.A. (1973) Stratigraphy, sedimentology and palaeogeography of Eifelian, Givetian and Frasnian strata between the River Porma and the Embalse de la Luna, Cantabrian Mountains, Spain. Geologie en Mijnbouw, **52**(3): 115-124.

Reijers, T.J.A. (1974) Diagenesis in the reefal facies of the Middle to Upper Devonian Portilla Limestone Formation of NW Spain. Breviora Geologica Asturica, **XVIII** (3): 33-48.

Reijers, T.J.A. (1984) The Penolos Structure in the Pena Corada Unit, Cantabrian Mountains (Spain). Boletin Geologico y Minero, **95**(3): 214-224.

Reijers, T.J.A. (1985) Devonian basin-fill histories of the Spanish Cantabrian Mountains and the Belgian Ardennes; a comparison. Geologie en Mijnbouw, **64**(1): 41-62.

Reijers, T.J.A. & Have, ten A.M. (1983) Ooid Zonation as Indication for Environmental Conditions in a Givetian/Frasnian Carbonate Shelf-Slope Transition. In: Coated Grains. (Ed. Peryt, T.M.), Springer.

Reijers, T.J.A., Baan, van der D. & Sluys, van der G. (1984) The Esla Nappe and its implications for the paleogeography of the Givetian-Frasnian Portilla Limestone Formation in the Cantabrian Mountains (N.W. Spain). Boletin Geologico y Minero, **95**(3): 203-213.

Reuther, C.D. (1977) Das Namur im südlichen Kanabrischen Gebirge (Nordspanien), Krustenbewegungen und Faziesdifferenzierung im Übergang Geosynklinale-Orogen. Clausthaler Geol. Abh., **28**: 122 p.

Reynolds, D.J., Steckler, M.S. & Coakley, B.J. (1991) The role of sediment load in sequence stratigraphy: the influence of flexural isostasy and compaction. J. Geophys. Res., **96**(B4): 6931-6949.

Rich, J.L. (1934) Mechanics of low-angle overthrust faulting illustrated by Cumberland thrust block, Virginia, Kentucky and Tennessee. AAPG Bulletin, **18**: 1584-1596.

Richardson, J.B., Rodríguez González, R.M. & Sutherland, S.J.E. (2000) Palynology and recognition of the Silurian/Devonian boundary in some British terrestrial sediments by correlation with Cantabrian and other European marine sequences - a progress report. Courier Forschungsinstitut Senckenberg, **220**: 1-7.

Richardson, J.B., Rodríguez, R.M. & Sutherland, S.J.E. (2001) Palynological zonation of Mid-Paleozoic sequences from the Cantabrian Mountains, NW-Spain: implications for inter-regional and interfacies correlation of the Ludford/Pridoli and Silurian/Devonian boundaries, and plant dispersal patterns. Bull. nat. Hist. Mus. London (Geol.), **57**(2): 115-162.

Riding, R. (1974) Model of the Hercynian fold belt. Earth and Planetary Science Letters, **245**: 125-135.

Riding, R.E. (1979) Donezella bioherms in the Carboniferous of the southern Cantabrian Mountains, Spain. Bull. Centre Rech. Explor. Prod. Elf-Aquitaine, **3**: 787-794.

Robardet, M. (2000) An alternative approach to consider the Variscan belt in SW Europe: The pre-orogenic paleogeograpgical constraints. Basement Tectonics, A Coruña. 23-26.

Robardet, M. (2002) Alternative approach to the Variscan Belt in southwestern Europe: Preorogenic palaeobiogeographical constraints. In: Variscan-Apalachian dynamics: The building of the late Paleozoic basement. (Eds. Martínez Catalán, J.R., Hatcher, R., Arenas, R. & Díaz García, F.), GSA Spec. Paper, **364:** 1-15.

Robardet, M. (2003) The Armorica 'microplate': fact or fiction? Critical review of the concept and contradictory palaeobiogeographical data. Palaeogeography, Palaeoclimatology, Palaeoecology, **195**: 125-148.

Robardet, M., Paris, F. & Racheboeuf, P.R. (1990) Palaeogeographic evolution of southwestern Europe during early Palaeozoic times. In: Palaeozoic palaeogeography and biogeography. (Eds. McKerrow, W.S. & Scotese, C.R.), Geological Society of London Memoir, **12:** 411-419.

Robardet, M., Paris, F. & Plusquellec, Y. (2001) Comment on "New Early Devonian paleomagnetic data from NW France: "Paleogeography and imlpications for the Armorican microplate hypothesis" by J. Tait. Jour. of Geophys. Res, **106**(B7): 13307-13310.

Robardet, M. & Gutiérrez-Marco, J.C. (2002) Silurian. In: The Geology of Spain. (Eds. Gibbons, W. & Moreno, T.), The Geological Society, London**:** 51-66.

Rose, P.R. (1976) Mississippian carbonate shelf margins, western United States. Journ. Res. USGS, **4**, 4: 449-466.

Ross, C.A. & Ross, J.R.P. (1985) Late Paleozoic depositional sequences are synchronous and worldwide. Geology, **13**: 194-197.

Ross, C.A. & Ross, J.R.P. (1988) Late Paleozoic transgressive-regressive deposition. In: Sea-level changes; an integrated approach. (Eds. Wilgus, C., K , Hastings, B., S, Ross, C., A , Posamentier, H., W , Van Wagoner, J. & Kendall, C., St.) SEPM Spec. Publ., **42:** 227-247.

Ross, C.A. & Ross, J.R.P. (1996) Silurian sea-level fluctuations. In: Paleozoic Sequence Stratigraphy: Views from the North American Craton. (Eds. Witzke, B.J., Ludvigson, G.A. & Day, J.), GSA Spec. Paper, **187-192:** 203-211.

Royden, L.H. (1993) The tectonic expression slab pull at continental convergent boundaries. Tectonics, **12**(2): 303-325.

Rupke, J. (1965) The Esla Nappe, Cantabrian Mountains (Spain). Leidse Geologische Mededelingen, **32**: 74 p.

Russo, A. & Bechstädt, T. (1994) Evolución sedimentológica y paleogeográfica de la formación Vegadeo (Cámbrico Inferior-Medio) en la zona entre Visuña y Piedrafita do Caurel (Lugo NO de España). Rev. Soc. Geol. España, **7**: 299-310.

Sachsenhofer, R.F., Lankreijer, A., Cloetingh, S. & Ebner, F. (1997) Subsidence analysis and quantitative basin modelling in the Styrian Basin (Pannonian Basin System, Austria). Tectonophysics, **272**: 175-196.

San Jose, de M.A., Pieren, A.P., Garcia-Hidalgo, J.F., Vilas, L., Herranz, P., Pelaez, J.R. & Perejón, A. (1990) Ante-Ordovician stratigraphy. In: Pre-Mesozoic geology of Iberia. (Eds. Dallmeyer, R.D. & Martínez García, E.), Springer.

Sánchez de la Torre, S., Agueda Villar, J.A., Colmenero Navarro, J.R., Garcia-Ramos, J.C. & Gonzales Lastra, J. (1983) Evolucion sedimentaria y paleogeografica del Carbonifero en la Cordillera Cantabrica. In: Carbonifero y Permico de Espana. IGME, Madrid**:** 133-150.

Sánchez de la Torre, L., Vera de la Puente, C., Suárez de Centi, C. & Agueda Villar, J.A. (1984) Facies y ambientes sedimentarios del Silúrico y Devónico inferior en la región central de Asturias. In: Homenaje a Luis Sánchez de la Torre. Publ. Geol. Univ. Auton. Barcelona, **20:** 57-71.

Sanchez de Posada, L.C., Martínez Chacón, M.L., Méndez Férnandez, C., Menéndez Alvarez, J.R., Truyols, J. & Villa, E. (1990) Carboniferous Pre-Stepha-

nian rocks of the Asturian-Leonese Domain (Cantabrian Zone). In: Pre-Mesozoic Geology of Iberia. (Eds. Dallmeyer, R.D. & Martínez García, E), Springer.

Santanach, P., Ed. (1997) ESCI, Estudios sísmicos de la corteza Ibérica. Revista de la Sociedad Geologica de España, **8**(4).

Sanz-López, J., García-López, S., Montesinos, J. & Arbizu, M. (1998) Biostratigraphy and sedimentation of the Vidrieros Formation (middle Famenian-lower Tournaisian) in the Gildar-Montó unit (northwest Spain). Bollettino della Societa Paleontologica Italiana, **37**(2-3): 393-406.

Sarg, J.F. (1988) Carbonate sequence stratigraphy. In: Sea-level changes; an integrated approach. (Eds. Wilgus, C.K., Hastings, B.S., Ross, C.A., Posamentier, H.W., Wagoner, van J.C. & Kendall, C.G.S.C.), SEPM Spec. Publ., **42:** 155-181.

Sarmiento, G., Mendez, B.I., Aramburu, C., Arbizu, M. & Truyols, J. (1994) Early Silurian conodonts from the Cantabrian Zone, NW Spain. Geobios, **27**(4): 507-522.

Savage, J.F., Boschma, D. (1980) Geological maps of the southern Cantabrian Mountains (Spain). Leidse Geologische Mededelingen, **50**(2): 75-114.

Sawyer, D.S. & Harry, D.L. (1991) Dynamic modelling of divergent margin formation: application to the U.S. Atlantic margin. Marine Geol., **102**: 29-42.

Schlager, W. (1981) The paradox of drowned reefs and carbonate platforms. GSA Bulletin, **Part I, 92**: 197-211.

Schlager, W. (1993) Accommodation and supply - a dual control on stratigraphic sequences. Sedimentary Geology, **86**: 111-136.

Schlager, W. (2000) Sedimentation rates and growth potential of tropical, cool-water and mud-mound carbonate systems. In: Carbonate Platform Systems: components and interactions. (Eds. Insalaco, E., Skelton, P.W. & Palmer, T.J.), Geological Society London, **178:** 217-227.

Schlager, W. (2003) Benthic carbonate factories of the Phanerozoic. International Journal of Earth Sciences, **92**: 445-464.

Scotese, C.R. (2004) **"**Paleomap project." http://www.scotese.com/earth.htm (10.05. 2004).

Scotese, C.R., Bambach, R.K., Barton, C., Van Der Voo, R. & Ziegler, A. (1979) Paleozoic base maps. J. Geol, **87**(3): 217-277.

Scotese, C.R. & Barrett, S. (1990) Gondwana´s movement over the South Pole during the Palaezoic: Evidence from lithological indicators of climate. In: Palaeozoic palaeogeography and biogeography. (Eds. McKerrow, W.S. & Scotese, C.R.), Geological Society of London Memoir, **12:** 75-85.

Scotese, C.R. & McKerrow, W. (1990) Revised world maps and introduction. In: Palaeozoic palaeogeography and biogeography. (Eds. McKerrow, W.S. & Scotese, C.R.), Geological Society of London Memoir, **12:** 1-21.

Sdzuy, K. (1961) Das Kambrium Spaniens. Teil II: Trilobiten. Akad. Wiss. Lit., Abh. Math. Naturw., **Kl. 7-8**: 217-408 (499-690).

Sdzuy, K. (1967) Trilobites del Cámbrico medio de Asturias. Trabajos de Geología, **1**: 77-133.

Sdzuy, K. (1968) Biostratigrafía de la griotte cámbrica de los Barrios de Luna (Léon) y de otras sucesiones comparables. Trabajos de Geología, **2**: 45-57.

Seibert (1986) Fazies und Paläogeographie des Unter-Karbon (Alba Formation) im Kantabrischen Gebirge (Nordspanien). Ph.D. thesis, Tübingen.

Sitter, L.U. (1961) Le Precambrien dans a chaine Cantabrique. C. R. Somm. Soc. Geol. France, **9**: 253-254.

Sitter, L.U. (1962) The structure of the southern slope of the Cantabrian Mountains. Leidse Geologische Mededelingen, **26**: 255-264.

Sjerp, N. (1967) The geology of the San Isidro-Porma area (Cantabrian mountains, Spain). Leidse Geologische Mededelingen, **39**: 55-128.

Sloss, L.L. (1962) Stratigraphic models in exploration. Bull. Am. Assoc. Petrol. Geol., **46**: 1050-1057.

Sloss, L.L. (1963) Sequences in the cratonic interior of North America. Bull. Geol. Soc. Am., **74**: 93-114.

Smits, B.J. (1966) The Caldas Formation, a new Devonian unit in Leon (Spain). Leidse Geologische Mededelingen, **31**: 179-187.

Staalduinen, van C.J. (1973) Geology of the area between the Luna and Torio rivers, southern Cantabrian Mountains, NW Spain. Leidse Geologische Mededelingen, **49**(2): 167-205.

Steckler, M.S. & Watts, A.B. (1978) Subsidence of the Atlantic-type margin of New York. Earth and Planetary Science Letters, **41**: 1-13.

Steckler, M.S., Reynolds, D.J., Coakley, B.J., Swift, B.A. & Jarrard, R. (1993) Modeling passive margin sequence stratigraphy. In: Sequence stratigraphy and facies associations. (Eds. Posamentier, H.W., Summerhayes, C.P., Haq, B.U. & Allen, G.P.), Spec. Publ. Int. Ass. Sediment. **18:** 19-42.

Stewart, J. & Watts, A.B. (1997) Gravity anomalies and spatial variations of flexural rigidity at mountain ranges. Jour. of Geophys. Research, **102**: 5327-5352.

Stewart, S.A. (1995) Paleomagnetic analysis of fold kinematics and implications for geological models of the Cantabrian/Asturias Arc, northern Spain. J. Geophys. Res., **100**: 20079-20094.

Stockmal, G.S., Beaumont, C. & Boutilier, R. (1986) Geodynamic models of convergent margin tectonics: transition from rifted margin to overthrust belt and consequences for foreland-basin development. AAPG Bulletin, **70**(2): 181-190.

Stüwe, K. (2000) Geodynamik der Lithosphäre, Springer. 405 p.

Suárez, A., Barba, P., Heredia, N. & Rodríguez Fernández (1994) Mapa geologico de la provincia de León, Escala 1:200,000. ITGE, Madrid.

Suarez de Centi, C. (1988) Estratigrafía y sedimenentología de la Unidad Fm. Furada/San Pedro (Siluri-

co superior-Devónico inferior), Zona Cantábrica, Cuenca Astur-Leonesa. IGME, Madrid**:** 1-530.

Suarez de Centi, C., Garcia Ramos, J.C. & Valenevela, M. (1989) Icnofosiles del Silurico de la zona cantabrica. Boletin Geologico y Minero, **100**(3): 339-394.

Suárez Rodríguez, N., Heredia, F., López Díaz, J.M., Toyos, L.R., Rodríguez Fernández, L.R. & Gutiérrez, G. (1990) Cartografía del mapa geologico de España, Escala 1:50.000, No.102 (Los Barrios de Luna). ITGE, Madrid.

Suppe, J. (1983) Geometry and kinematics of fault-bend folding. Am. J. Sci., **283**: 684-721.

Suppe, J. (1985) Principles of structural geology. Prentice Hall: 536 p.

Tait, J. (1999) New Early Devonian paleomagnetic data from NW France: Paleogeography and implications for the Armorican microplate hypothesis. Journal of Geophysical research, **104**(B2): 2831-2839.

Tait, J., Bachtadse, V., Franke, W. & Soffel, H. (1997) Geodynamic evolution of the European Variscan fold belt: palaeomagnetic and geological constraints. Geol. Rundschau, **86**: 585-598.

Tait, J., Schätz, M., Bachtadse, V. & Soffel, H. (2000) Palaeomagnetism and Palaeozoic palaeogeography of Gondwana and European terranes. In: Orogenic Processes: Quantification and Modelling in the Variscan Belt. (Eds. Franke, W., Haak, V., Oncken, O. & Tanner, D.), Geological Society, London, **179:** 21-34.

Tarling, D.H. (1985) Carboniferous reconstructions based on palaeomagnetism. Dixieme Congres Int. de Stratigraphie et de Geologie du Carbonifere, Madrid: 153-161.

Terry, C.E. & Williams, J.J. (1969) The Idris 'A' bioherm and oilfield, Sirte Basin, Libya; its commercial development, regional Palaeocene geologic setting and stratigraphy. In: The exploration for petroleum in Europe and north Africa, Inst. Petrol., London.

Tetzlaff, D.M. & Harbough, J.W. (1989) Simulating clastic sedimentation. Van Nostrand: 202 p.

Thorne, J.A. & Swift, D.J.P. (1991) Sedimentation on continental margins, VI: a regime model for depositional sequences, their component systems tracts, and bounding surface. In: Shelf sand and sandstone bodies. (Eds. Swift, D.J.P., Oertel, G.F., Tillman, R.W. & Thorne, J.A.), IAS Spec. Publ., **14:** 189-255.

Tinker, S.W. (1998) Shelf-to-basin facies distributions and sequence stratigraphy of a steep-rimmed carbonate margin: Capitan Depositional System, McKittrick Canyon, New Mexico and Texas. Journal of Sedimentary Research, **68**: 1146-1174.

Torsvik, T., Smethurst, M., Van der Voo, R., Trench, A., Abrahamsen, N. & Halvorsen, E. (1992) BALTICA: a synopsis of Vendian-Permian palaeomagnetic data and their palaeotectonic implications. Earth Sci. Rev., **33**(133-152).

Toth, J., Kusznir, N. & Flint, S. (1996) A flexural isostatic model of lithosphere shortening and foreland basin formation: application to the Eastern Cordillera and Subandean belt of NW Argentina. Tectonics, **15**(1): 213-223.

Trench, A. & Torsvik, T. (1991) A revised Palaeozoic apparent polar wander path for southern Britain (eastern Avalonia). Geophys. J. Int., **104**: 227-233.

Truyols, J. (1969) Un nuevo hito faunístico en el Georgiense de la Cordillera Cantábrica. Com. Serv. Geol. Portugal, **53**: 57-60.

Truyols, J., Philippot, A. & Julivert, M. (1974) Les formations siluriennes de la zone cantabrique et leurs faunes. Bulletin de la Societe Geologique de France, **16**(1): 23-35.

Truyols, J., Arbizu, M., García-Alcalde, J.L., García-López, S., Martínez Chacón, M.L., Mendez-Fernández, C., Menéndez, J.R., Sánchez de Posada, L.C., Soto, F., Truyols-Massoni, M., Villa, E., Marcos, A., Pérez-Estaún, A., Pulgar, J.A., Bastida, F., Aller, J. & Lorenzo, P. (1982) Memoria explicativa de la Hoja Núm. 77 (La Plaza) del Mapa Geológico Nacional E. 1:50.000. IGME, Madrid.

Truyols, J. & Julivert, M. (1983) El Silúrico en el Macizo Ibérico. In: Libro Jubilar J. M. Ríos, Geología de España. (Ed. Comba, J.A.), IGME, Madrid, **1:** 246-2654.

Truyols, J. & Sanchez de Posada, L.C. (1983) El carbonifero inferior y medio de la Región de Pliegues y Mantos. In: Carbonifero y Permico de España. (Ed. Truyols, J.), IGME, Madrid**:** 39-59.

Truyols, J., Arbizu, M., García-Alcalde, J.L., García-López, S., Méndez Bedia, I., Soto, F. & Truyols-Massoni, M. (1990) Cantabrian and Palentian Zones; Stratigraphy: The Asturian-Leonese Domain (Cantabrian Zone). In: Pre-Mesozoic Geology of Iberia. (Eds. Dallmeyer, R.D. & Martínez García, E.), Springer.

Tucker, R.D. & McKerrow, W.S. (1995) Early Paleozoic chronology: a review in light of new U-Pb zircon ages from Newfoundland and Britain. Can. J. Earth Sci., **32**: 68-379.

Turcotte, D.L. & Schubert, G. (1982) Geodynamics-applications of continuum physics to geological problems. Wiley**:** 450 p.

Turcotte, D.L. & Schubert, G. (2002) Geodynamics. Cambridge University Press: 456 p.

Vail, P.R., Mitchum, R.M., Jr., Todd, R.G., Widmier, J.M., Thompson, S., Sangree, J.B., Bubb, J.N. & Hatlelid, W.G., Eds. (1977) Seismic Stratigraphy and Global Changes of Sea Level. In: Seismic Stratigraphy - applications to hydrocarbon exploration. AAPG Memoir, 26: 49-205.

Vail, P.R., Hardenbol, J. & Todd, R.G., Eds. (1984) Jurassic unconformities, chronostratigraphy, and sea-level changes from seismic stratigraphy and biostratigraphy. AAPG Memoir, **36**.

Vail, P.R., Audemard, F., Bowman, S.A., Eisner, P.N. & Pérez-Cruz, C. (1991) The stratigraphic signatures of tectonics, eustasy and sedimentology – an overwiew. In: Cycles and events in stratigraphy (Eds. Einsele, G., Ricken, W. & Seilacher, A.), Springer: 619-659.

Valladares, M.I., Barba, P. & Ugidos, J.M. (2002) Precambrian. In: The Geology of Spain. (Eds. Gibbons, W. & Moreno, T.), The Geological Society London**:** 7-16.

Van Der Voo, R. (1993) Paleomagnetism of the Atlantic, Tethys and Iapetus oceans. Cambridge University Press.

Van Der Voo, R., Stakamatos, J.A. & Parés, J.M. (1997) Kinematic constraints on thrust-belt curvature from syndeformational magnetizations in the Lagos del Valle syncline in the Cantabrian Arc, Spain. Jour. Geophys. Res., **102**: 10105-10119.

Vera de la Puente, C. (1989) Revision litoestratigrafica y correlacion de los grupos Raneces y La Vid (Devonico Inferior de la cuenca Astur-Leonesa). Trabajos de Geologia, **18**: 53-65.

Verhoef, J. & Srivastava, S.P. (1989) Correlation of sedimentary basins across the North Atlantic as obtained from gravity and magnetic data, and its relation to early evolution of the North Atlantic. In: Extensional tectonics and stratigraphy of the North Atlantic margins. (Eds. Tankard, A.J. & Balkwill, H.R.), AAPG Memoir, **46:** 131-147.

Vidal, G., Palacios, T., Moczydlowska, M. & Gubanov, A.P. (1999) Age contraints from small shelly fossils on the early Cambrian terminal Cadomian Phase in iberia. Geologiska Föreningens i Stockholm Förhandlingar, **121**: 137-143.

Vilas Minondo, L. (1971) El Paleozoico Inferior y Medio de la Cordillera Cantabrica entre los ríos Porma y Bernesga (León). Memoria del IGME, **80**: 66-155.

Villegas, H. (1996) Exploracion e investigacion de un nuevo yacimiento de carbon en la cuenca

minera Cinera-Matallana (Leon). Unpubl. Ph.D. Thesis, Universidad Complutense, Madrid: 417 p.

Wagner, R.H., Winkler, P.C.F. & Riding, R.E. (1971) Lithostratigraphic units of the lower part of the Carboniferous in northern Leon, Spain. In: The Carboniferous of Northwest Spain, part II. Universidad de Oviedo, Facultad de Ciencias, **4:** 603-663.

Wagner, R.H. & Winkler Prins, C.F. (1999) Carboniferous stratigraphy of the Sierra del Brezo in northern Palencia: evidence of major uplifts. Trabajos de Geologia: 385-403.

Wagoner, van J.C., Posamentier, H.W., Mitchum, R.M., Jr., Vail, P.R., Sarg, J.F., Loutit, T.S. & Hardenbol, J. (1988) An overview of the fundamentals of sequence stratigraphy and key definitions. In: Sea-level changes; an integrated approach. (Eds. Wilgus, C.K., Hastings, B.S., Ross, C.A., Posamentier, H.W., Wagoner van, J.C. & Kendall, C.G.S.C.), SEPM Spec. Publ., **42:** 39-45.

Wagoner, van J.C., Mitchum, R.M., Campion, K.M. & Rahmanian, V.D. (1990) Siliciclastic sequence stratigraphy in well logs, cores, and outcrops: concepts for high-resolution correlation of time and facies. Amer. Ass. Petrol. Geol., Methods in Explor. Studies, **7**: 53 p.

Walls, R.A., Mountjoy, E & Fritz, P. (1979) Isotopic composition and diagenetic history of carbonate cements in Devonian Golden Spike Reef, Alberta, Canada. GSA Bulletin, **90**, 10: 963-982.

Warr, L.N. (2000) The Variscan Orogeny: the welding of Pangea. In: Geological History of Britain and Ireland. (Eds. Woodcock, N. & Strachan, R.), Blackwell**:** 271-294.

Warrlich, G.M.D., Waltham, D.A. & Bosence, D.W.J. (2002) Quantifying the sequence stratigraphy and drowning mechanisms of atolls using a new 3-D forward stratigraphic modelling program (CARBONATE 3D). Basin Research, **14**: 379-400.

Waschbusch, P.J. & Royden, L.H. (1992) Spatial and temporal evolution of foredeep basins: lateral strength variations and inelastic yielding in continental lithosphere. Basin Research, **4**: 179-196.

Watts, A.B. (1992) The effective elastic thickness of the lithosphere and the evolution of foreland basins. Basin Research, **4**: 169-178.

Watts, A.B. (2001) Isostasy and flexure of the lithosphere. Cambridge Univ. Press: 458 p.

Watts, A.B. & Ryan, W.B.F. (1976) Flexure of the lithosphere and continental margin basins. Tectonophysics, **36**(1-3): 25-44.

Watts, A.B., Karner, G.D. & Steckler, M.S. (1982) Lithosphere flexure and the evolution of sedimentary basins. Philosophical Transactions of the Royal Society of London, **ser. A.** (305): 249-281.

Weddige, K., Ed. (2001) Devon-Bibliographie. http://www.senckenberg.de/publ/Dev-Bibl.htm (10.05. 2004).

Weil, A.B., Van der Voo, R., Van der Pluijm, B.A. & Parés, J. (2000) The formation of an orocline by multiphase deformation: a paleomagnetic investigation of the Cantabria-Asturias Arc (northern Spain). Journal of Structural Geology, **22**: 735-756.

Weil, A.B., Van der Voo, R. & van der Pluijm, B.A. (2001) Oroclinal bending and evidence against the Pangea megashear: the Cantabria-Asturias arc (northern Spain). Geology, **29**: 991-994.

Weil, A.B., Gutiérrez-Alonso, G. & Fernández-Suárez, J. (2003) Orocline triggered lithosphere delamination. GSA - Annual Meeting Abstracts, Seattle: p. 346.

Welte, D.H., Horsfield, B. & Baker, D.R. (1997) Petroleum and basin evolution, Springer: 535 p.

Wendebourg, J. & Harbaugh, J.W. (1997) Simulating oil entrapment in clastic sequences. In: Computer Methods in the Geosciences. **16**: 199 p.

Wendt, J. & Aigner (1985) Facies patterns and depositional environmens of Palaeozoic cephalopod limestones. Sedimentary Geology, **44**: 263-300.

Wheeler, H.E. (1964) Baselevel, lithosphere surface, and time-stratigraphy. GSA Bulletin, **75**: 599-609.

Whitaker, F., Smart, P., Hague, Y., Waltham, D. & Bosence, D. (1999) Structure and function of a coupled two-dimensional diagenetic and sedimentological model of carbonate platform evolution. In: Numerical experiments in stratigraphy; recent advances in stratigraphic and sedimentologic computer simulations. (Eds.

Harbaugh, J.W., Watney, W.L., Rankey, E.C., Slingerland, R., Goldstein, R.H. & Franseen, E.K.), Soc. Sedim. Geol., Spec. Publ., **62:** 337-355.

Winkler Prins, C.F. (1968) Carboniferous Productidina and Chnetidina of the Cantabrian Mountains (NW Spain): Systematics, stratigraphy and paleoecology. Leidse Geologische Mededelingen, **43**(41-155).

Witzke, B.J. (1990) Palaeoclimatic constraints for Palaeozic palaeolatidues of Laurentia and Euramerica. In: Palaeozoic palaeogeography and biogeography. (Eds. McKerrow, W.S. & Scotese, C.R.), Geological Society of London Memoir, **12:** 57-73.

Witzke, B.J. & Bunker, B.J. (1996) Relative sea-level changes during Middle Ordovician through Mississippian deposition in the Iowa area, North American craton. In: Paleozoic Sequence Stratigraphy: Views from the North American Craton. (Eds. Witzke, B.J., Ludvigson, G.A. & Day, J.), GSA Spec. Paper, **307-330:** 203-211.

Witzke, B.J. & Bunker, B.J. (1997) Sedimentation and stratigraphic architecture of a Middle Devonian (late Givetian) transgressive-regressive carbonate-evaporite cycle, Coralville Formation, Iowa area. In: Paleozoic sequence stratigraphy, biostratigraphy, and biogeography; studies in honor of J. Granville ("Jess") Johnson. (Eds. Klapper, G., Murphy, M. A. & Talent, J.), GSA Spec. Paper, **321:** 67-88.

Woodward, N., Boyer, S. & Suppe, J. (1985) An outline of balanced cross-sections. In: Studies in Geology, University of Tennessee, **11**: 166 p.

Woodward, N., Boyer, S. & Suppe, J. (1989) Balanced Geological Cross-Sections: An Essential Technique in Geological Research and Exploration. In: Short Course in Geology (Eds. Crawford, M.L. & Padovani, E.), Am. Geophys. Union, **6**: 132 p.

Zamarreño, I. (1972) Las litofacies carbonatadas del Cámbrico de la Zona Cantábrica (NW España) y su distribución geográfica. Trabajos de Geología, **5**: 3-118.

Zamarreño, I. & Julivert, M. (1967) Estratigrafía del Cámbrico del oriente de Asturias y estudio petrográfico de las facies carbonatadas. Trabajos de Geología, **1**: 135-163.

Zühlke, R., Bouaouda, M.S., Ouajhain, B., Bechstädt, T. & Leinfelder, R. (2004) Quantitative Meso-/Cenozoic Development of the Eastern Central Atlantic Continental Shelf, Western High Atlas, Morocco. Marine and Petroleum Geology, *in press*.

LIST OF FIGURES

Fig.1.2. Workflow of the modelling study 1

Fig. 2.1. Tectonic zonation of the Variscan Belt and subdivision of the Cantabrian Zone 4
Fig. 2.2. Geotectonic and metamorphic evolution of the Iberian Variscan Orogen 5
Fig. 2.3. Diachronic evolution of the main tectonothermal events across the NW Iberian Massif 6
Fig. 2.4. Geological cross-section through the northern part of the Iberian Peninsula 7
Fig. 2.5. Continuous deformation of progressive rotational thrust displacement 9
Fig. 2.6. The Variscan deformation history of the Cantabrian-Asturias Arc 10
Fig. 2.7. Effect of lithospheric bending around a vertical axis 10
Fig. 2.8. Relationship between post-orogenic oroclinal bending and lithospheric delamination 11
Fig. 2.9. Neoproterozoic terrane distribution and Early Palaeozoic plate-tectonic 12
Fig. 2.10. Angular unconformity between the Neoproterozoic Mora Fm. and the Herrería Fm. 13
Fig. 2.11. Geological evolution of NW Iberia during the Proterozoic to Early Palaeozoic 13
Fig. 2.12. Relative movements of North Gondwana, Baltica and Laurentia 14
Fig. 2.13. Palaeogeographical models of the Early Ordovician through Late Carboniferous 15
Fig. 2.14. Global palaeogeographic evolution from the Early Silurian to the Late Carboniferous 17
Fig. 2.15. Tectonic evolution of the NW Iberian Variscan Belt 18
Fig. 2.16. Continuing foreland-directed deformation in the Cantabrian Zone 19
Fig. 2.17. Detailed geological cross-section through the Cantabrian Zone 20
Fig. 2.18. Deep crustal seismic section across the ESCI-N2 transect 21
Fig. 2.19. Typical structural features of the Iberian fold and thrust belt 22
Fig. 2.20. Stratigraphic section through the Cantabrian Zone 23
Fig. 2.21. Stratigraphic chart of the Southern Cantabrian Mountains 24
Fig. 2.22. Polished slab of the Herrería Fm. 27
Fig. 2.23. “Embalse de Luna” north of the village Barrios de Luna with the outcropping Barrios Fm. 27
Fig. 2.24. Efflorescence of pyrite-bearing black shales and siltstones (Formigoso Fm.) 27
Fig. 2.25. Abundant ripple marks in the shallow marine sandstones of the San Pedro Fm. 27
Fig. 2.26. Desiccation polygons in the Mb. A of the San Pedro Fm. 27
Fig. 2.27. Thrust within the San Pedro Fm., displacing shaly sediments onto massive ironstones 27
Fig. 2.28. Type locality of the La Vid Group 31
Fig. 2.29. Symmetric wave ripples in the Dolomite Mb. of the Abelgas Fm. 31
Fig. 2.30. Erosional tempestite-scour in the Abelgas Fm. (La Vid section) 31
Fig. 2.31. Thin section from the upper part of the Abelgas Fm. (Limestone Marlstone Mb.) 31
Fig. 2.32. Coquina composed of brachiopods and crinoidal stems in the shales of the Esla Fm. 31
Fig. 2.33. Type locality of the Santa Lucía Fm. 33
Fig. 2.34. Abundant silicified corals of the Santa Lucía Fm. in the lower part of the Beberino section 33
Fig. 2.35. Desiccation cracks in the lagoonal deposits of the Santa Lucía Fm. (Valporquero section) 33
Fig. 2.36. Thin section of a stromatoporoid boundstone of the Santa Lucía Fm. (Santa Lucía section) 33
Fig. 2.37. Thin section of a mudstone with abundant birds-eye structures, Santa Lucía Fm. 33
Fig. 2.38. Thin section of a crinoidal grainstone at the top of the Santa Lucía Fm. 35
Fig. 2.39. Threefolded section of the Portilla Fm. north of the village of La Pola de Gordón 35
Fig. 2.40. Thin section of the middle Portilla member (fine sandstones with crinoidal debris) 35
Fig. 2.41. Highly fossiliferous limestones of the Portilla Fm. south of Mirantes de Luna 35
Fig. 2.42. Thin section of the middle Portilla member composed of ooidal grainstone 35
Fig. 2.43. Thin section of the lower Portilla Fm. in its type section (south of Matallana de Torio) 35

Fig. 2.44. Thin section of the Nocedo Fm. (uppermost Gordón Mb.) in the Huergas section 37
Fig. 2.45. Nocedo Fm. composed of quartz sandstones with herringbone cross-stratification 37
Fig. 2.46. The top of the Millar Mb. (Nocedo Fm.) with conglomerates composed of exotic clasts 37
Fig. 2.47. Dark shales alternating with well-sorted siltstones; Fueyo Fm. 37
Fig. 2.48. The Ermita Fm. south of Llomberas with large-scale cross-bedded sandstones 37
Fig. 2.49. Multiple crosscutting channels of the Ermita Fm. in the Millaró section 37
Fig. 2.50. Ermita Fm. composed of iron-rich, polymict conglomerates in the Millaró section 41
Fig. 2.51. Well-sorted sandstones with abundant brachiopod moulds of the Ermita Fm. 41
Fig. 2.52. Vegamián Fm. at the Mirador de Vegamián (Porma Lake) 41
Fig. 2.53. Nodular limestones of the Alba Fm. in the section Los Chabanos 41
Fig. 2.54. Thin section of the Alba Fm. with carbonate-rich nodules with dark red clay-streaks 41
Fig. 2.55. Polished slab of the Alba Fm. (Rocalo section) 43
Fig. 2.56. Bedding plane of the Alba Fm. with articulated crinoid stems up to one metre long 43
Fig. 2.57. Intense bioturbation in the upper Alba Fm. (Los Chabanos section) 43
Fig. 2.58. Red bioclastic wacke to packstone with abundant ammonoid shells (Alba Fm.) 43
Fig. 2.59. Large slump folds on top of the Alba Fm. (Piedrasecha section) 43
Fig. 2.60. Barcaliente Fm. at the Carbonera section 43
Fig. 2.61. Poorly sorted, polymict Porma Breccia at the top of the Barcaliente Fm. 45
Fig. 2.62. Turbiditic Olleros Fm. in the Olleros section 45
Fig. 2.63. Valdeteja carbonate platform covered by the shaly/sandy San Emiliano Fm. 45
Fig. 2.64. San Emiliano Fm. composed of dark turbiditic successions 45
Fig. 2.65. Detail of a fining-upward calci-turbiditic bed of the San Emiliano Fm. 45
Fig. 2.66. Stephanian conglomerates erosively overlying the Baleas and Alba formations 45

Fig. 3.1. Deformation of a piggy-back thrust mechanism 48
Fig. 3.2. Different balancing methods for regions affected by thrusting 49
Fig. 3.3. Location of the Bernesga Transect on the southern slope of the Cantabrian Mountains 51
Fig. 3.4. Geological map of the Bernesga region 52
Fig. 3.5. Map of main structural domains (Bodón, Pedrosa and Alba) 54
Fig. 3.6. Alba Syncline from the village Mallo de Luna, facing east 55
Fig. 3.7. South-vergent, asymmetric Montuerto Syncline south of Nocedo de Curueño 56
Fig. 3.8. Large-scale, recumbent folds within the Santa Lucía Fm. NE of the village Corecillas 56
Fig. 3.9. Large-scale folds in the centre of the Alba Syncline 56
Fig. 3.10. Concentric fold south of Llombera within the Portilla Fm. 56
Fig. 3.11. North-vergent kink folds (chevron fold) with flexural slip movement 56
Fig. 3.12. Variable folding in the Alba Fm. caused by flexural flow 56
Fig. 3.13. Growth model for the development of fault-bend folds 57
Fig. 3.14. Geometry of an antiformal stack as a possible model for the Cueto Negro Antiform 58
Fig. 3.15. Structural balancing of the Bernesga Transect; deformed and balanced transect 61

Fig. 4.1. The Beberino section showing the three members of the Portilla Fm. 69

Fig. 5.1. Flexural response of the lithosphere adjacent to wide linear loads 75
Fig. 5.2. Plot of Te against the age of oceanic lithosphere at time of loading 76
Fig. 5.3. Plot of Te against the age of continental lithosphere at time of loading 77
Fig. 5.4. Dependency of Te - thermal age of the lithosphere - Moho-depth/crustal thickness 77
Fig. 5.5. Map of global distribution of effective elastic thickness (Te) 79

Fig. 5.6. Flexural-induced subsidence rates for two time increments (389Ma and 317Ma)_____ 81
Fig. 5.7. Workflow of the PHIL/BASIM™ modelling procedure_____ 84

Fig. 6.1. Genetic components of accommodation-oriented 2D reverse basin modelling_____ 86
Fig. 6.2. Basin architecture along the Bernesga Transect_____ 88
Fig. 6.3. Burial depth of time lines at the time of maximum burial (34Ma)_____ 89
Fig. 6.4. Composed eustatic sea-level curve for the Southern Cantabrian Basin_____ 90
Fig. 6.5. Porosity versus burial depth for the most common lithologies_____ 93
Fig. 6.6. 2D reverse modelling displayed as plots of selected time lines_____ 95
Fig. 6.7. Spectrogram plots of total subsidence rates and its components_____ 96
Fig. 6.8. Specific numbers of subsidence trends and development stages of the basin_____ 99

Fig. 7.1. Siliciclastic depositional profile within the 2D stratigraphic forward modelling_____ 103
Fig. 7.2. Carbonate productivity function for stratigraphic forward modelling_____105
Fig. 7.3. Variables that control erosion processes during stratigraphic modelling_____107
Fig. 7.4. Selected time lines and the predicted lithologic distribution along the Bernesga Transect____112
Fig. 7.5. Depositional depths and chronostratigraphic plot for the time 560Ma to 322Ma_____114
Fig. 7.6. Comparison of outcrop data and synthetic cross-section_____115
Fig. 7.7. Predicted stratigraphic column with lithologic and palaeobathymetric information_____116
Fig. 7.8. Relative sea-level changes, tectonic and total subsidence_____117
Fig. 7.9. Siliciclastic flux, carbonate deposition, stratigraphic gaps and sea-level changes_____ 118
Fig. 7.10. Compacted carbonate accumulation rates for the Devonian, Carboniferous and Cenozoic__ 119
Fig. 7.11. Porosity distribution along the Bernesga Transect for the entire simulation time_____120
Fig. 7.12. Density distribution along the Bernesga Transect for the entire simulation time_____ 120
Fig. 7.13. Modified eustatic curve as a result of multiple stratigraphic forward simulations_____ 121
Fig. 7.14. Palaeobathymetry distribution for three different effective elastic thickness adjustments___ 123
Fig. 7.15. Lithofacies and thickness distribution due to eustatic sea-level fluctuations switched off___ 124
Fig. 7.16. Comparison of the dependency on eustatic sea-level fluctuations_____126
Fig. 7.17. Lithofacies changes due to different time steps (300, 500 and 700ka)_____ 129
Fig. 7.18. Differences in thermo-tectonic subsidence (reverse basin/stratigraphic forward modelling)_ 130

Fig. 8.1. Overview of parameters for the Southern Cantabrian Basin development_____ 132
Fig. 8.2. Palaeogeographic evolution from the Namurian A through Westphalian D_____ 136
Fig. 8.3. Main stages of the foreland basin evolution during the Carboniferous_____137
Fig. 8.4. Phanerozoic continental encroachment cycles_____ 138

LIST OF TABLES

Table 3.1. Values for minimal shortening and displacement widths along the transect_____ 63

Table 6.1. Input parameters for 2D numerical reverse basin modelling_____ 87
Table 6.2. List of lithologies and compaction parameters used in the present study_____ 91
Table 6.3. Trends of total subsidence rates and its specific components_____ 97

Table 7.1. Adjustable variables for siliciclastic depositional environments_____ 103
Table 7.2. Maximum and minimum carbonate production rates_____104

Table 7.3. Adjustable variables for carbonate depositional environments and physical variables_____ 105
Table 7.4. Depositional gradients for the siliciclastic and carbonate environments_____ 106
Table 7.5. Compacted and decompacted accumulation rates_____ 110
Table 7.6. Maximum and minimum carbonate production rates_____ 111

LIST OF ANIMATIONS

Movie_1.mov. Architectural evolution of the Bernesga Transect_____ on CD
Movie_2.mov. Stratigraphic forward model for the Southern Cantabrian Basin_____ on CD

LIST OF CROSS-SECTIONS

Aralla_____ 166
Barrios de Luna-Pantano_____ 168
Beberino_____ 173
Caldas de Luna_____ 175
Carbonera_____ 180
Embalse de Porma_____ 182
Felmin_____ 183
Geras_____ 184
Huergas_____ 187
La Pola de Gordón_____ 189
La Vid_____ 190
Llamazares_____ 194
Llomberas_____ 195
Los Chábanos_____ 198
Matallana_____ 200
Millaró_____ 202
Montuerto_____ 204
Olleros_____ 206
Piedrasecha_____ 207
Redilluera_____ 211
Rocalo_____ 212
Santa Lucía_____ 214
Valporquero_____ 217

APPENDIX

Cross-sections

Selection of cross-sections meassured in the field. For the location within the Southern Cantabrian Basin see Fig. 3.5 in Chapter 3.

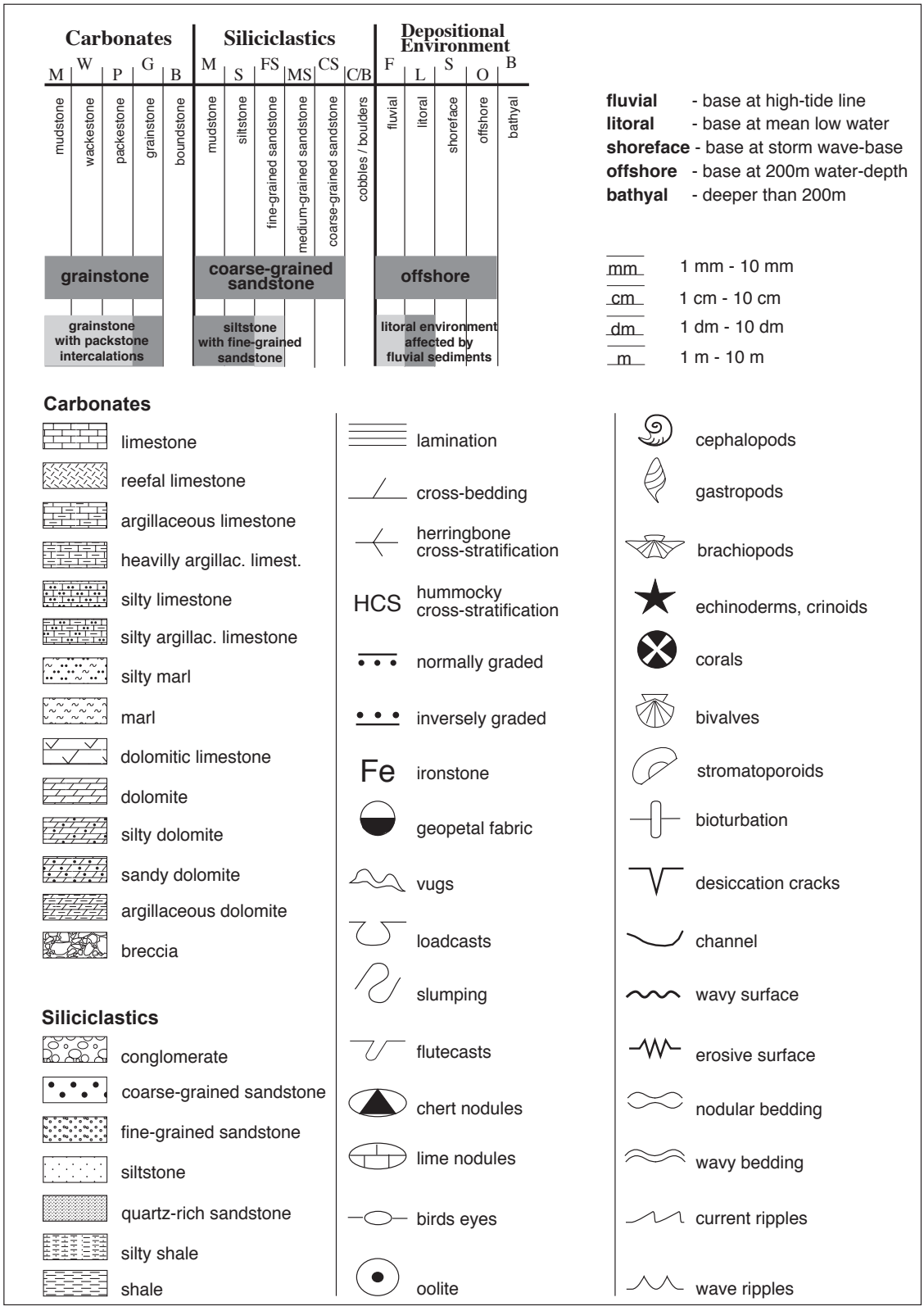

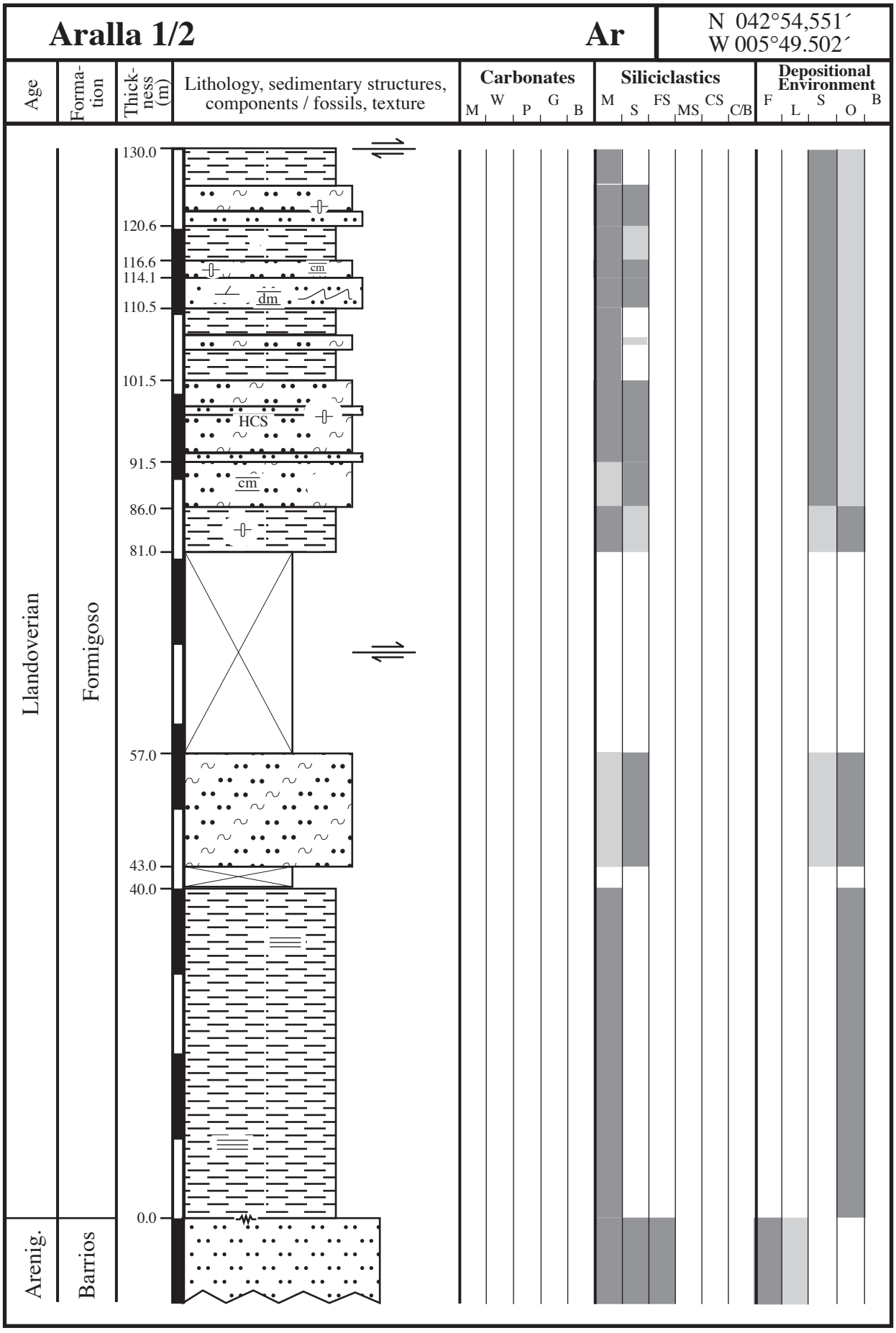
Aralla 1/2
Ar
N 042°54,551´
W 005°49.502´
Age
Forma-tion
Thick-ness (m)
Lithology, sedimentary structures, components / fossils, texture
Carbonates
M W P G B
Siliciclastics
M S FS MS CS C/B
Depositional Environment
F L S O B
Llandoverian
Arenig.
Formigoso
Barrios
130.0
120.6
116.6
114.1
110.5
101.5
91.5
86.0
81.0
57.0
43.0
40.0
0.0
cm
dm
HCS
cm

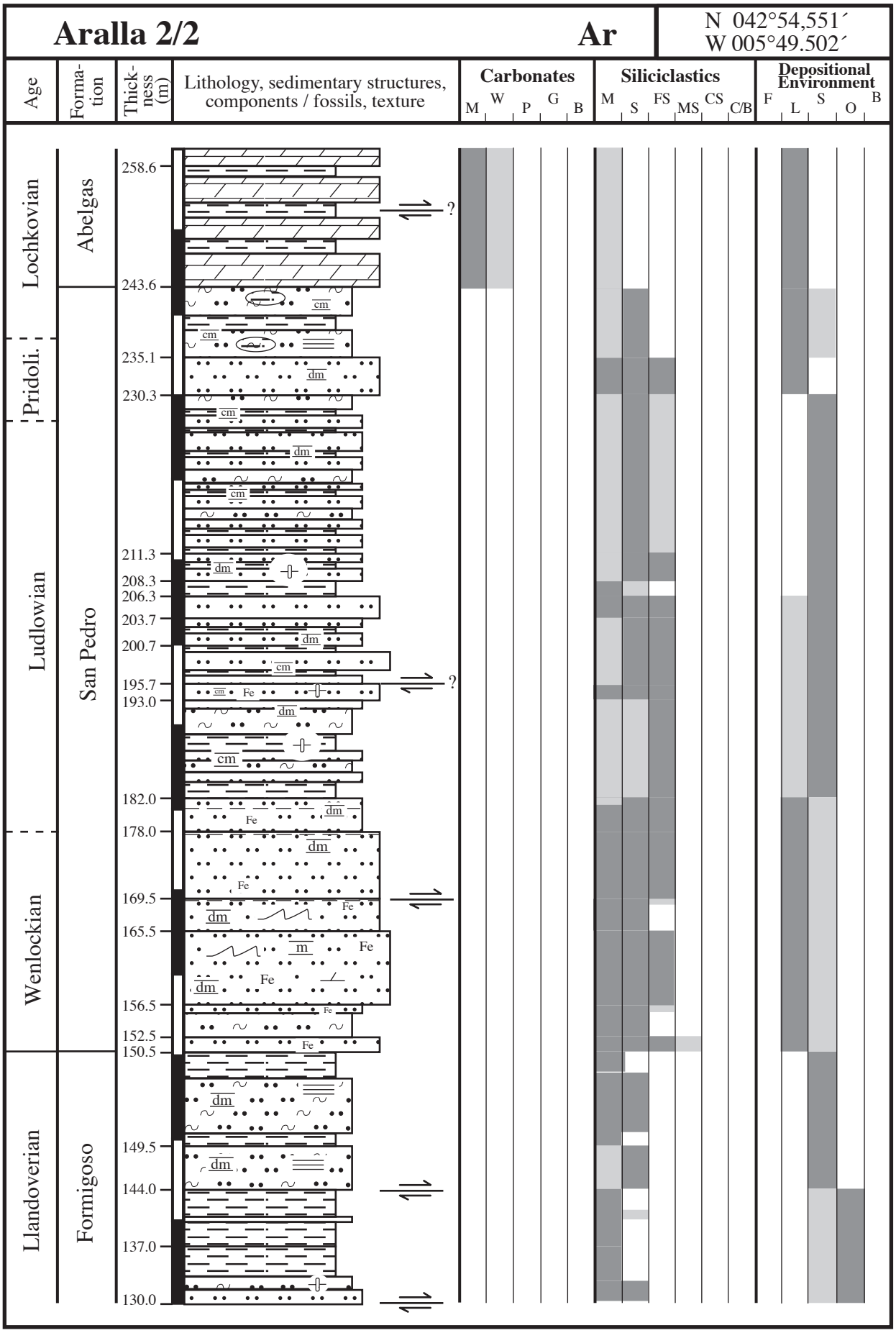
Aralla 2/2
Ar
N 042°54,551´
W 005°49.502´
Age
Formation
Thickness (m)
Lithology, sedimentary structures, components / fossils, texture
Carbonates
M W P G B
Siliciclastics
M S FS MS CS C/B
Depositional Environment
F L S O B
Lochkovian
Pridoli.
Ludlowian
Wenlockian
Llandoverian
Abelgas
San Pedro
Formigoso
258.6
243.6
235.1
230.3
211.3
208.3
206.3
203.7
200.7
195.7
193.0
182.0
178.0
169.5
165.5
156.5
152.5
150.5
149.5
144.0
137.0
130.0
cm
dm
m
Fe
?

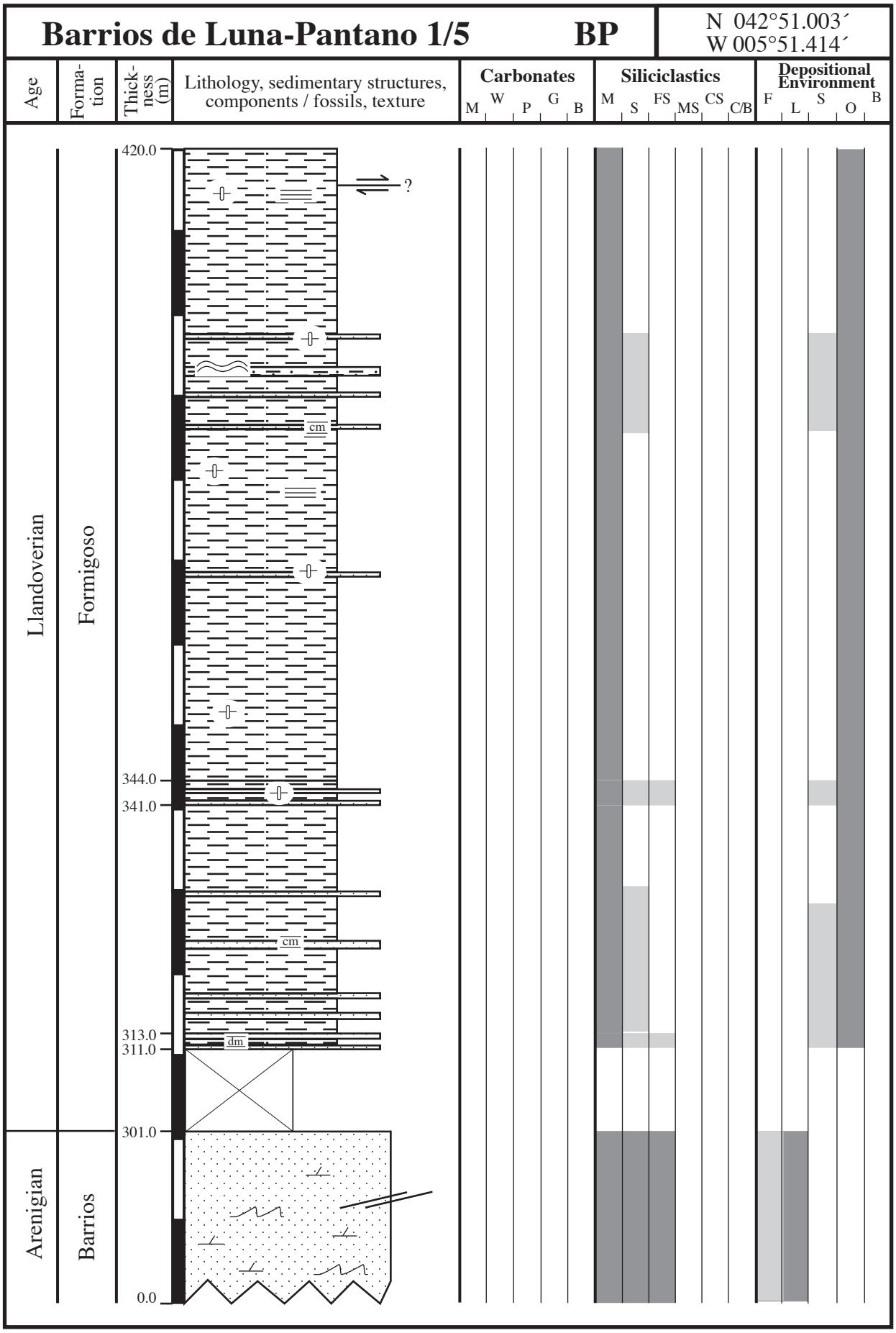
Barrios de Luna-Pantano 1/5
BP
N 042°51.003´
W 005°51.414´
Age
Formation
Thickness (m)
Lithology, sedimentary structures, components / fossils, texture
Carbonates
M W P G B
Siliciclastics
M S FS MS CS C/B
Depositional Environment
F L S O B
Llandoverian
Arenigian
Formigoso
Barrios
420.0
344.0
341.0
313.0
311.0
301.0
0.0
?
cm
cm
dm

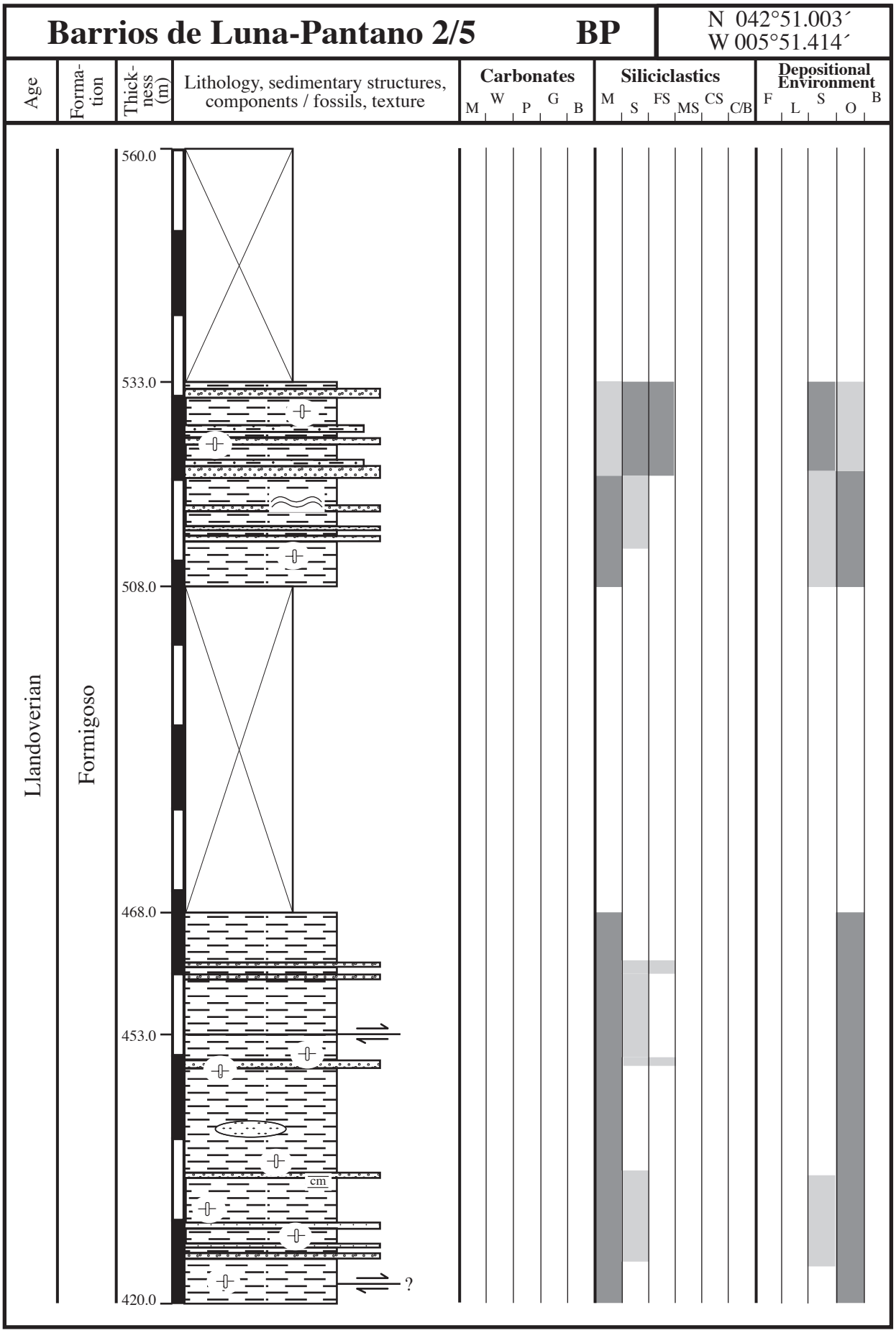
Barrios de Luna-Pantano 2/5
BP
N 042°51.003´
W 005°51.414´
Age
Forma-tion
Thick-ness (m)
Lithology, sedimentary structures, components / fossils, texture
Carbonates
M W P G B
Siliciclastics
M S FS MS CS C/B
Depositional Environment
F L S O B
Llandoverian
Formigoso
560.0
533.0
508.0
468.0
453.0
420.0
cm
?

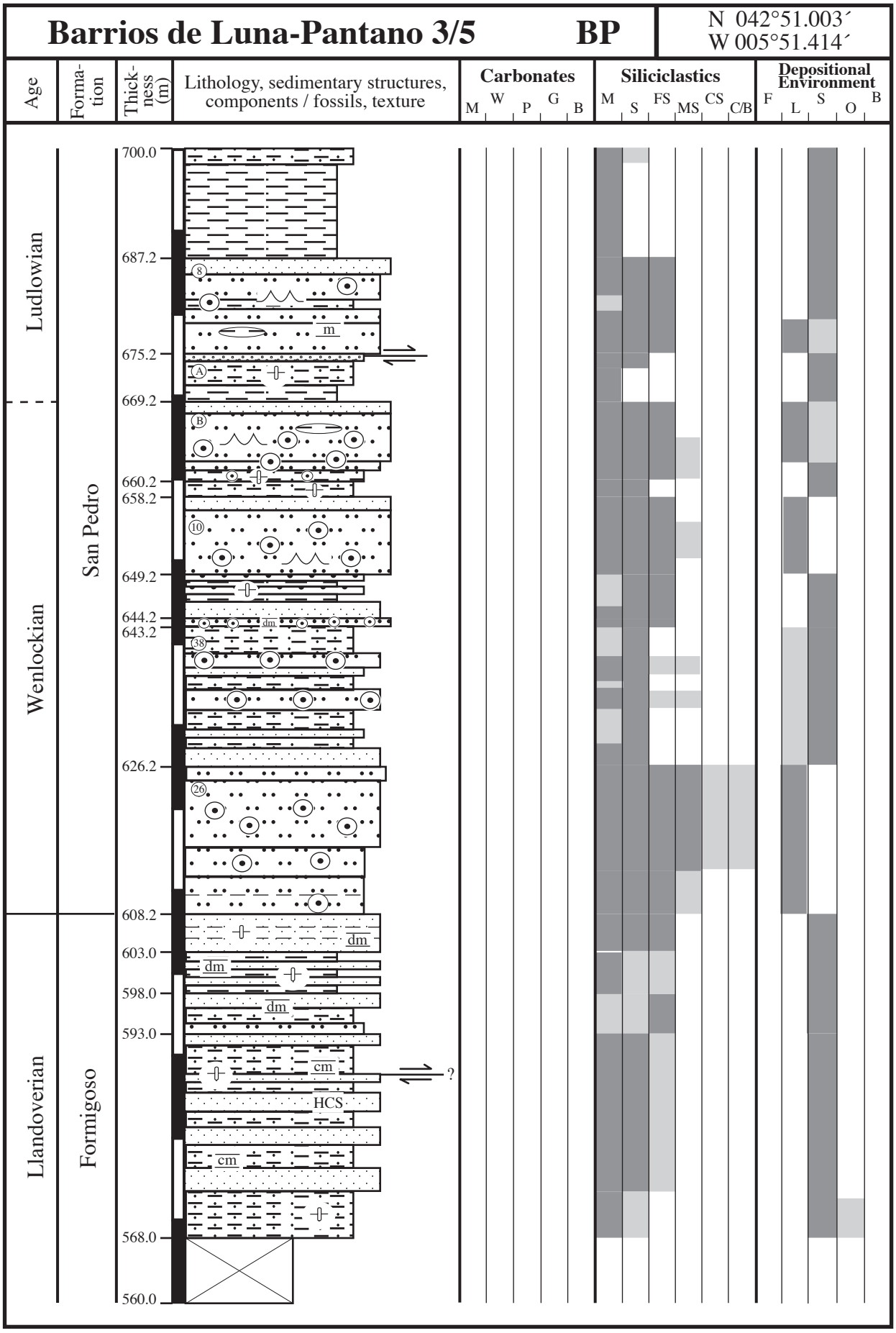
Barrios de Luna-Pantano 3/5
BP
N 042°51.003´
W 005°51.414´
Age
Forma-tion
Thick-ness (m)
Lithology, sedimentary structures, components / fossils, texture
Carbonates
M W P G B
Siliciclastics
M S FS MS CS C/B
Depositional Environment
F L S O B
Ludlowian
Wenlockian
Llandoverian
San Pedro
Formigoso
700.0
687.2
675.2
669.2
660.2
658.2
649.2
644.2
643.2
626.2
608.2
603.0
598.0
593.0
568.0
560.0
m
dm
cm
HCS
?

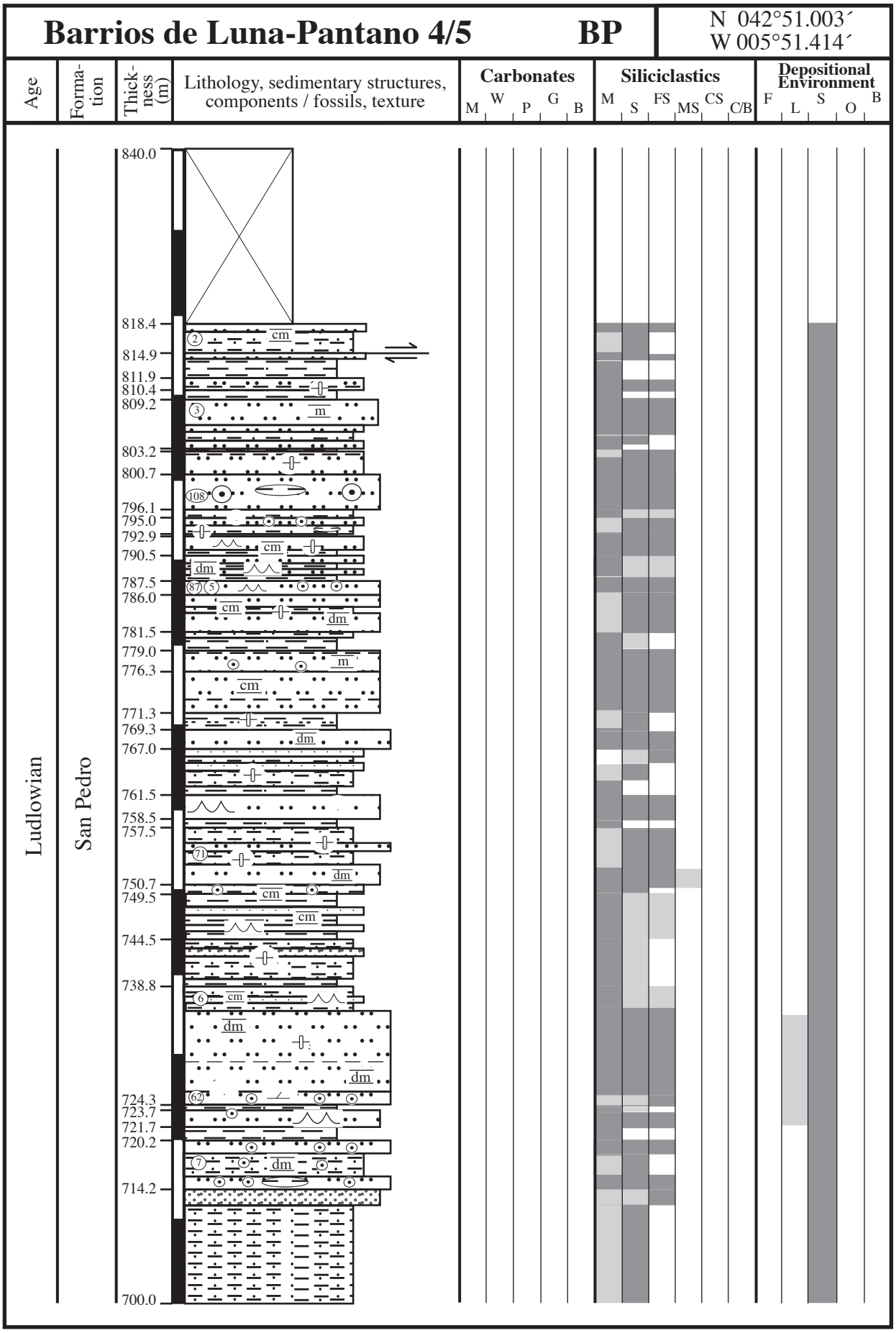
Barrios de Luna-Pantano 4/5
BP
N 042°51.003´
W 005°51.414´
Age
Formation
Thickness (m)
Lithology, sedimentary structures, components / fossils, texture
Carbonates
M W P G B
Siliciclastics
M S FS MS CS C/B
Depositional Environment
F L S O B
Ludlowian
San Pedro
840.0
818.4
814.9
811.9
810.4
809.2
803.2
800.7
796.1
795.0
792.9
790.5
787.5
786.0
781.5
779.0
776.3
771.3
769.3
767.0
761.5
758.5
757.5
750.7
749.5
744.5
738.8
724.3
723.7
721.7
720.2
714.2
700.0
cm
dm
m

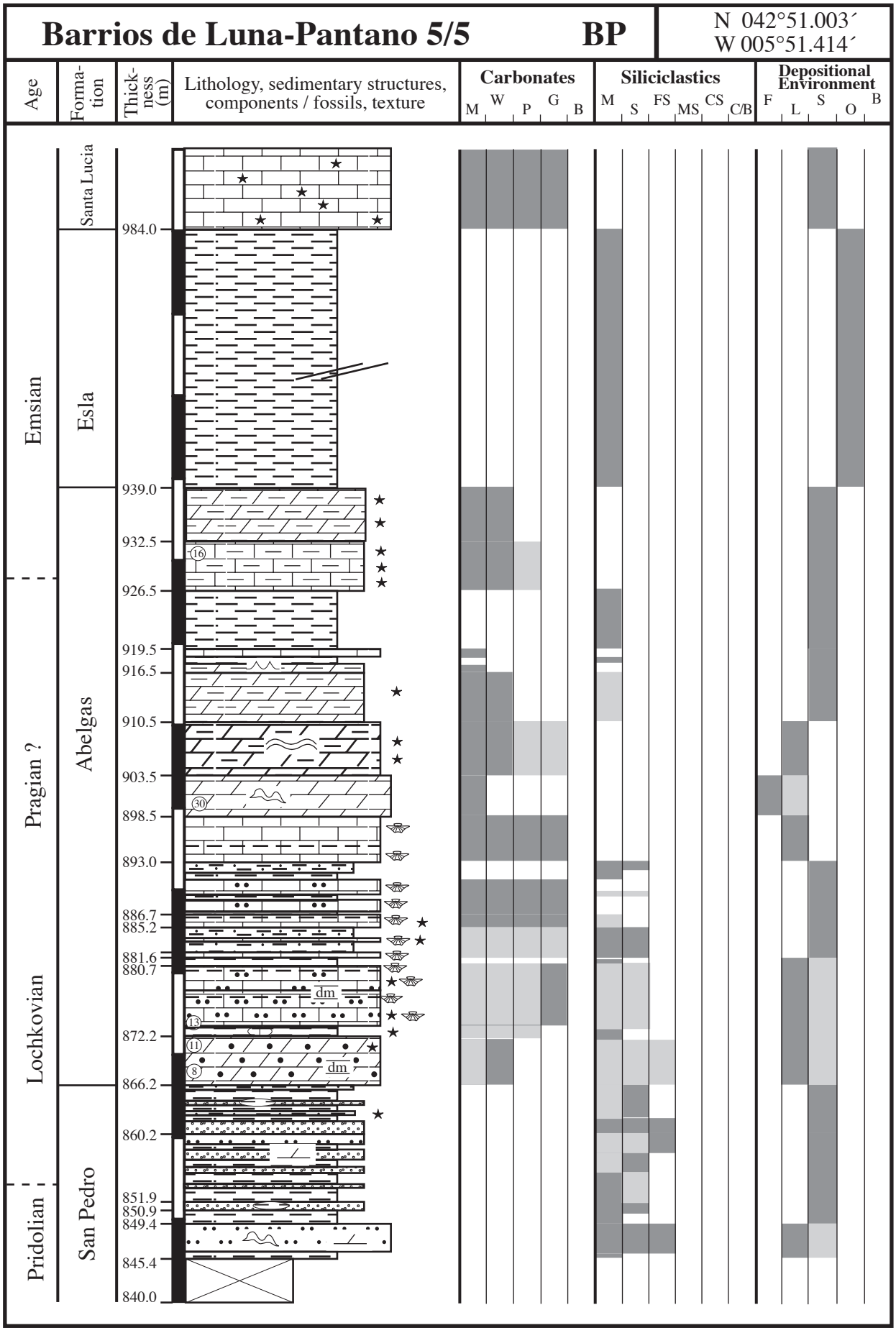
Barrios de Luna-Pantano 5/5
BP
N 042°51.003´
W 005°51.414´
Age
Formation
Thickness (m)
Lithology, sedimentary structures, components / fossils, texture
Carbonates
M W P G B
Siliciclastics
M S FS MS CS C/B
Depositional Environment
F L S O B
Emsian
Pragian ?
Lochkovian
Pridolian
Santa Lucia
Esla
Abelgas
San Pedro
984.0
939.0
932.5
926.5
919.5
916.5
910.5
903.5
898.5
893.0
886.7
885.2
881.6
880.7
872.2
866.2
860.2
851.9
850.9
849.4
845.4
840.0
16
30
13
11
8
dm
dm

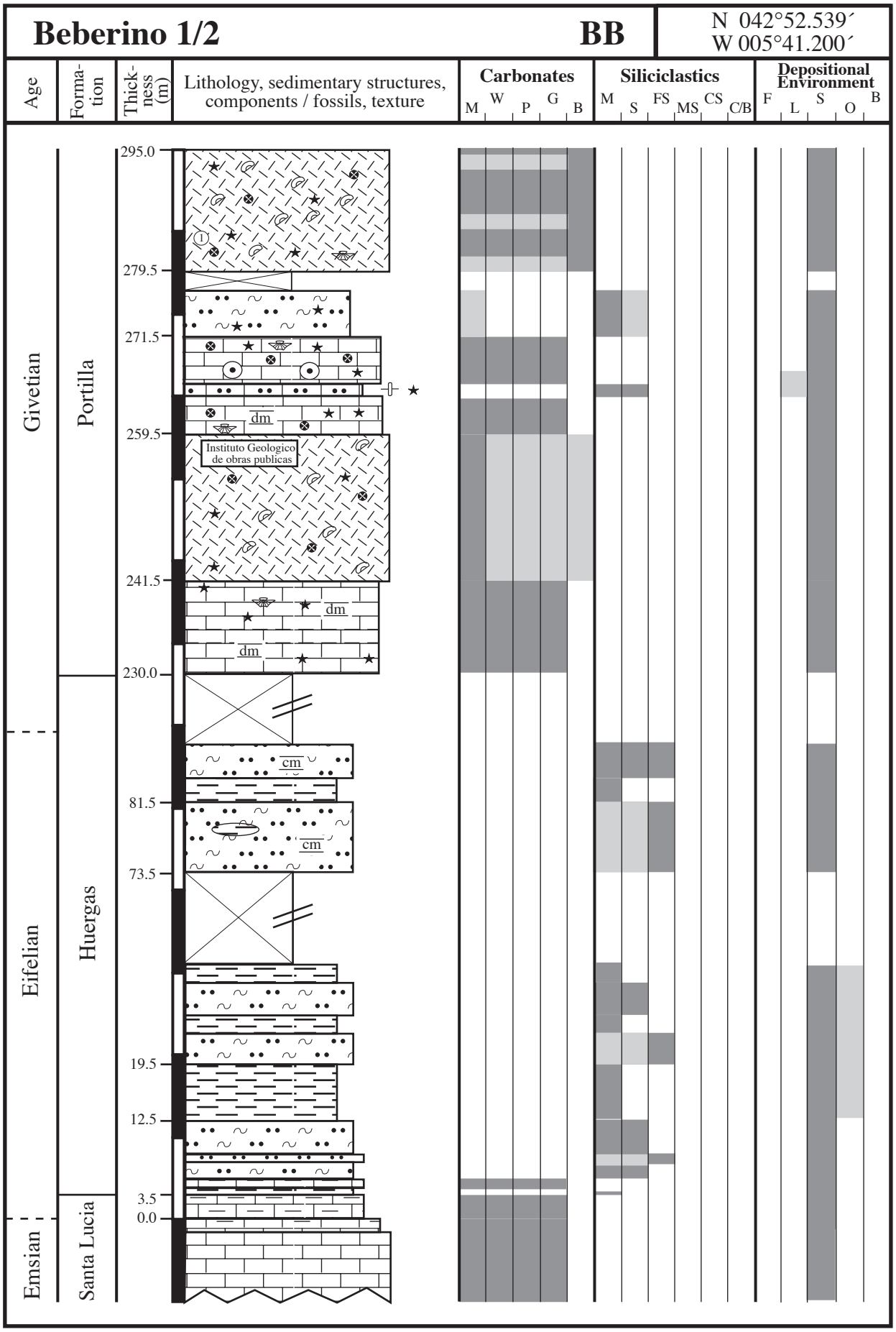
Beberino 1/2
BB
N 042°52.539´
W 005°41.200´
Age
Formation
Thickness (m)
Lithology, sedimentary structures, components / fossils, texture
Carbonates
M W P G B
Siliciclastics
M S FS MS CS C/B
Depositional Environment
F L S O B
Givetian
Eifelian
Emsian
Portilla
Huergas
Santa Lucia
295.0
279.5
271.5
259.5
241.5
230.0
81.5
73.5
19.5
12.5
3.5
0.0
dm
cm
Instituto Geologico de obras publicas

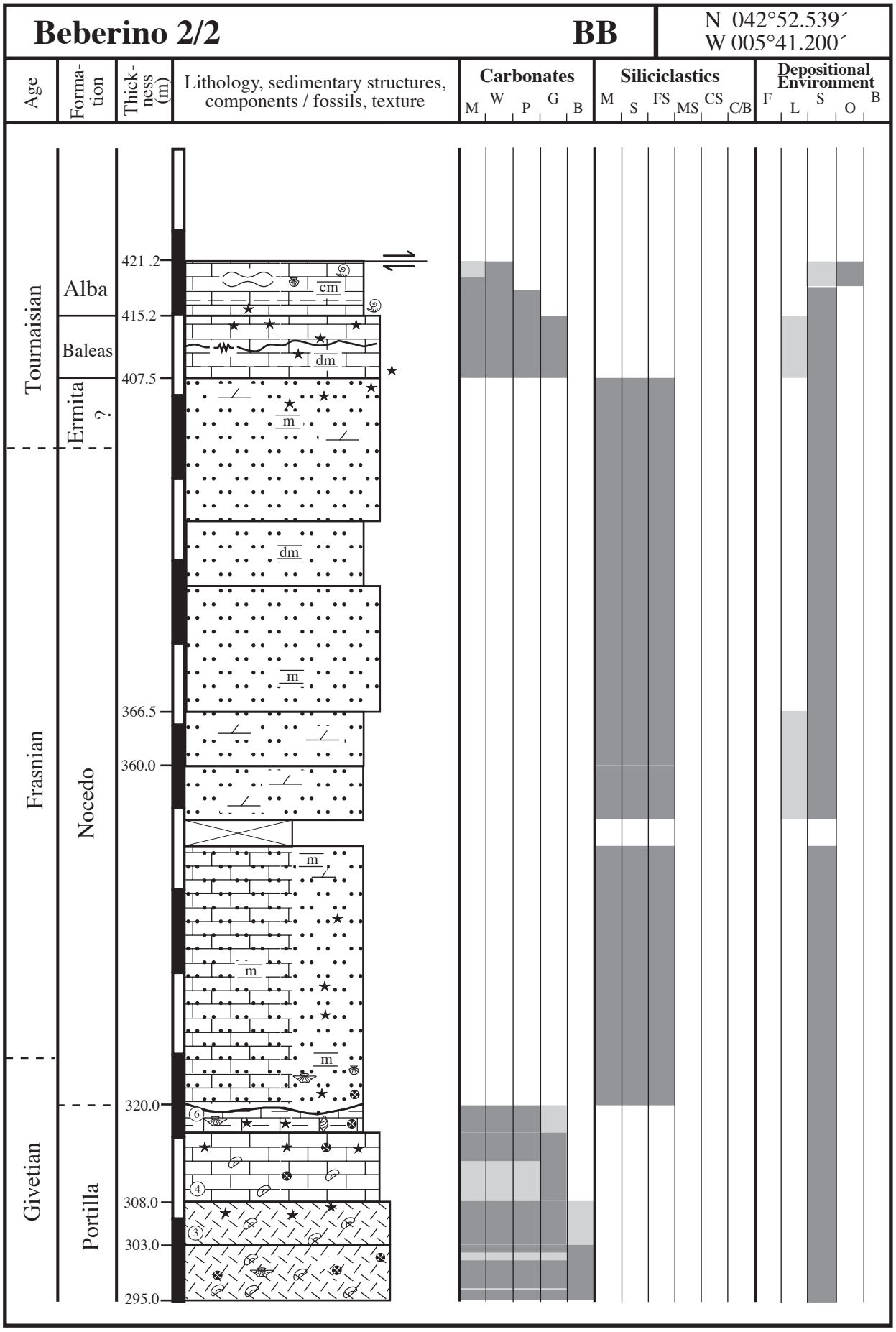
Beberino 2/2
BB
N 042°52.539´
W 005°41.200´
Age
Formation
Thickness (m)
Lithology, sedimentary structures, components / fossils, texture
Carbonates
M W P G B
Siliciclastics
M S FS MS CS C/B
Depositional Environment
F L S O B
Tournaisian
Frasnian
Givetian
Alba
Baleas
Ermita ?
Nocedo
Portilla
421 .2
415.2
407.5
366.5
360.0
320.0
308.0
303.0
295.0
cm
dm
m
6
4
3

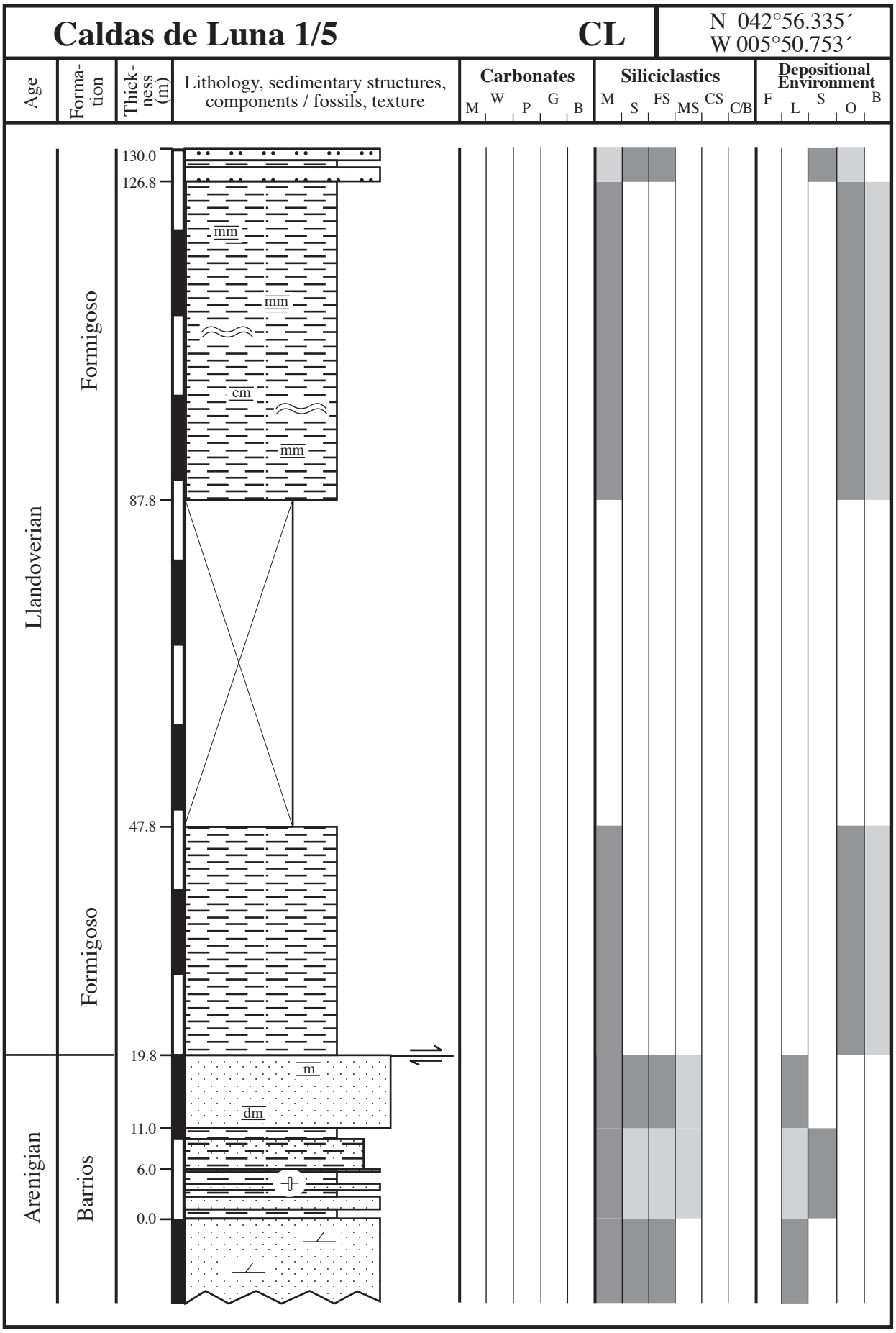
Caldas de Luna 1/5
CL
N 042°56.335´
W 005°50.753´
Age
Formation
Thickness (m)
Lithology, sedimentary structures, components / fossils, texture
Carbonates
M W P G B
Siliciclastics
M S FS MS CS C/B
Depositional Environment
F L S O B
Llandoverian
Arenigian
Formigoso
Formigoso
Barrios
130.0
126.8
87.8
47.8
19.8
11.0
6.0
0.0
mm
mm
cm
mm
m
dm

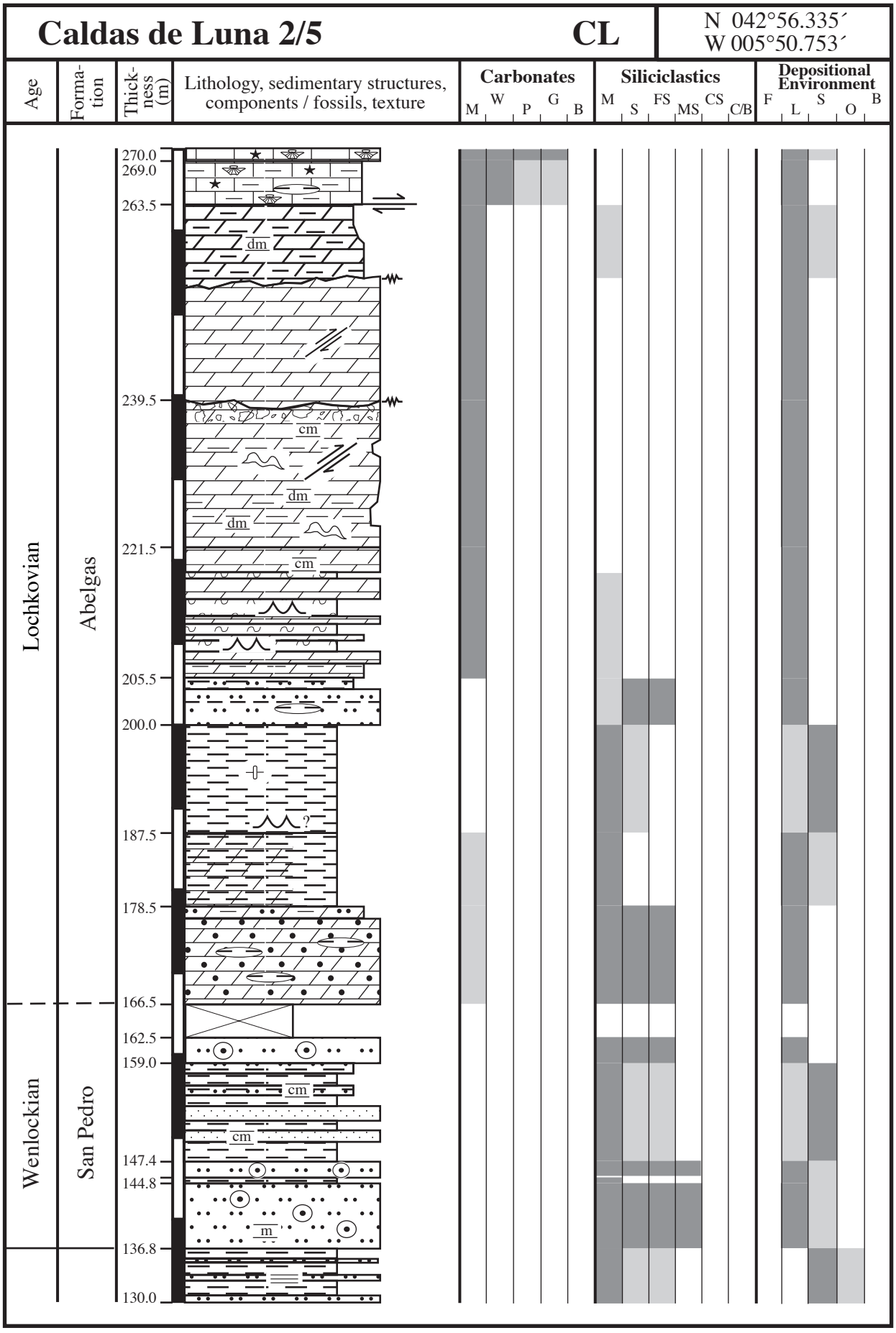
Caldas de Luna 2/5
CL
N 042°56.335´
W 005°50.753´
Age
Formation
Thickness (m)
Lithology, sedimentary structures, components / fossils, texture
Carbonates
M W P G B
Siliciclastics
M S FS MS CS C/B
Depositional Environment
F L S O B
Lochkovian
Wenlockian
Abelgas
San Pedro
270.0
269.0
263.5
239.5
221.5
205.5
200.0
187.5
178.5
166.5
162.5
159.0
147.4
144.8
136.8
130.0
dm
cm
m
?

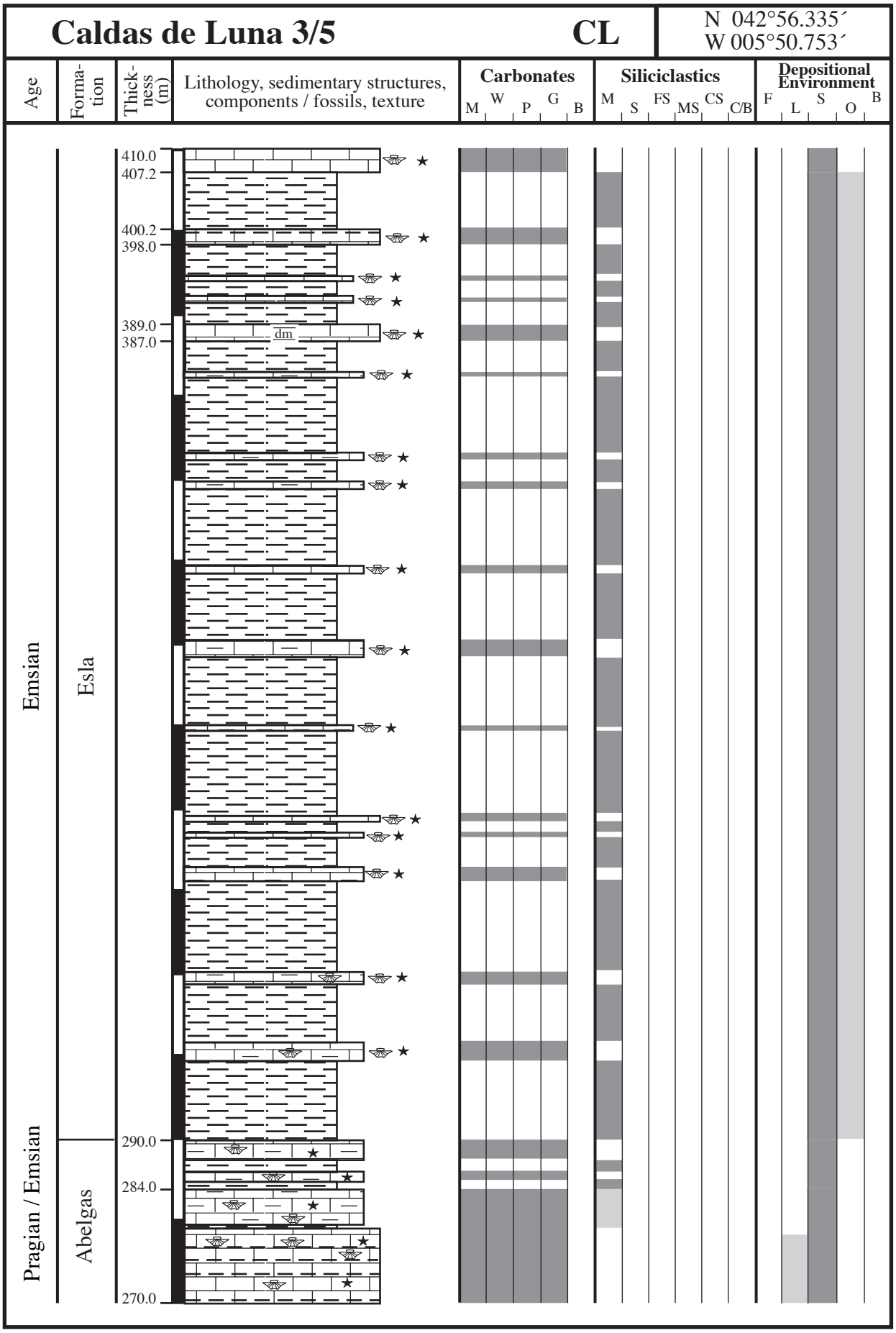
Caldas de Luna 3/5
CL
N 042°56.335´
W 005°50.753´
Age
Formation
Thickness (m)
Lithology, sedimentary structures, components / fossils, texture
Carbonates
M W P G B
Siliciclastics
M S FS MS CS C/B
Depositional Environment
F L S O B
Emsian
Pragian / Emsian
Esla
Abelgas
410.0
407.2
400.2
398.0
389.0
387.0
290.0
284.0
270.0
dm

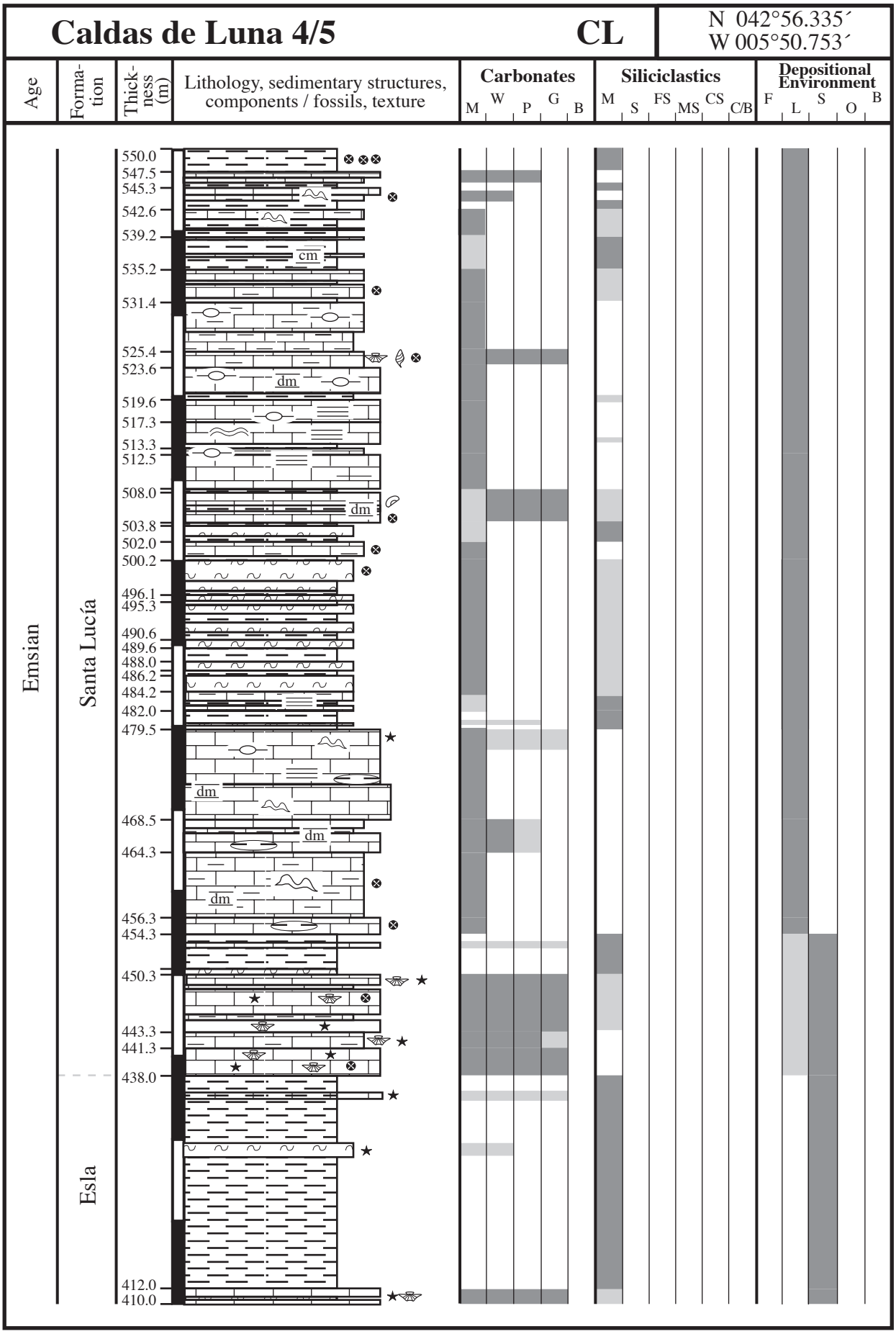
Caldas de Luna 4/5
CL
N 042°56.335´
W 005°50.753´
Age
Forma-tion
Thick-ness (m)
Lithology, sedimentary structures, components / fossils, texture
Carbonates
M W P G B
Siliciclastics
M S FS MS CS C/B
Depositional Environment
F L S O B
Emsian
Santa Lucía
Esla
550.0
547.5
545.3
542.6
539.2
535.2
531.4
525.4
523.6
519.6
517.3
513.3
512.5
508.0
503.8
502.0
500.2
496.1
495.3
490.6
489.6
488.0
486.2
484.2
482.0
479.5
468.5
464.3
456.3
454.3
450.3
443.3
441.3
438.0
412.0
410.0
cm
dm
dm
dm
dm
dm

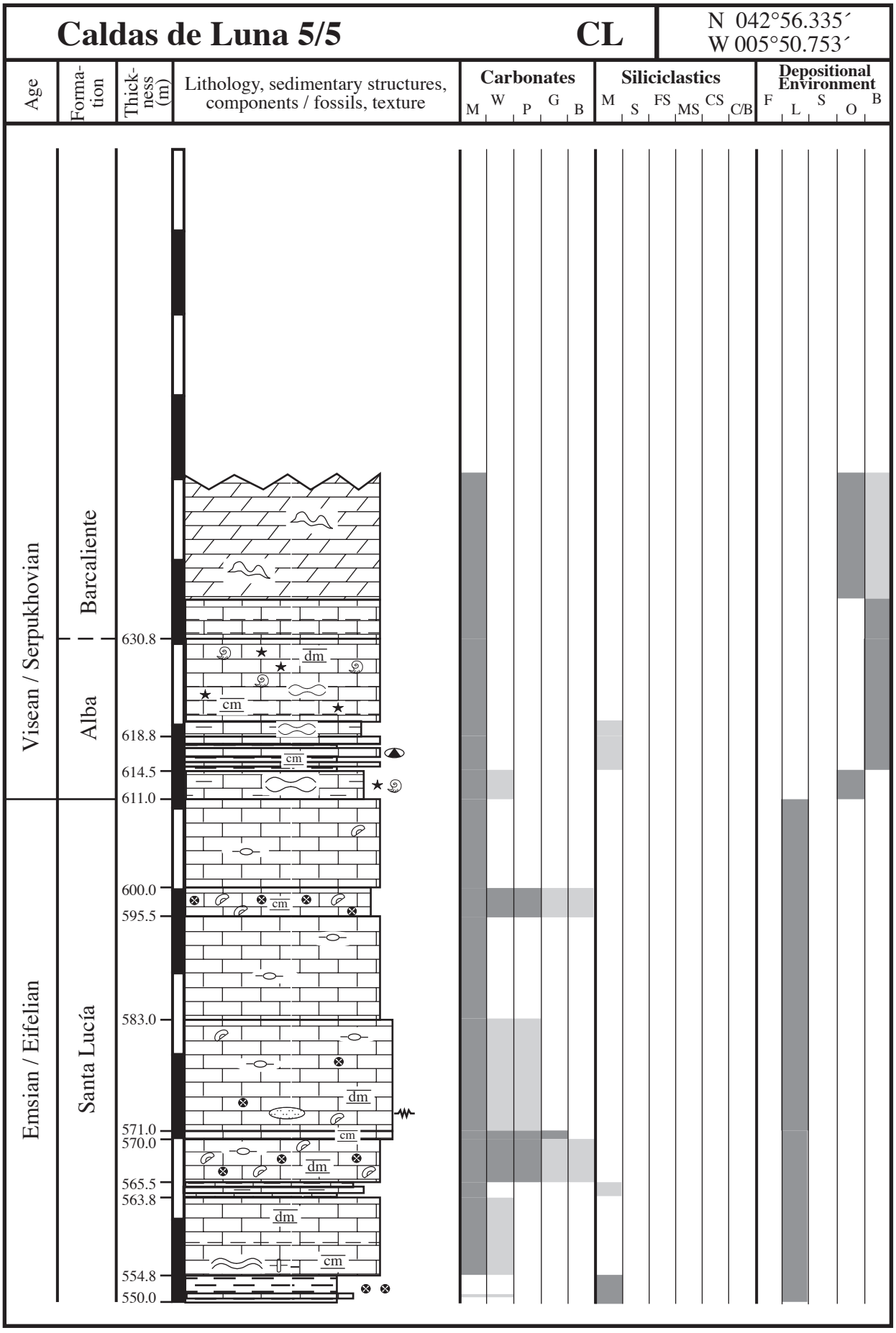
Caldas de Luna 5/5
CL
N 042°56.335´
W 005°50.753´
Age
Formation
Thickness (m)
Lithology, sedimentary structures, components / fossils, texture
Carbonates
M W P G B
Siliciclastics
M S FS MS CS C/B
Depositional Environment
F L S O B
Visean / Serpukhovian
Emsian / Eifelian
Barcaliente
Alba
Santa Lucía
630.8
618.8
614.5
611.0
600.0
595.5
583.0
571.0
570.0
565.5
563.8
554.8
550.0
dm
cm

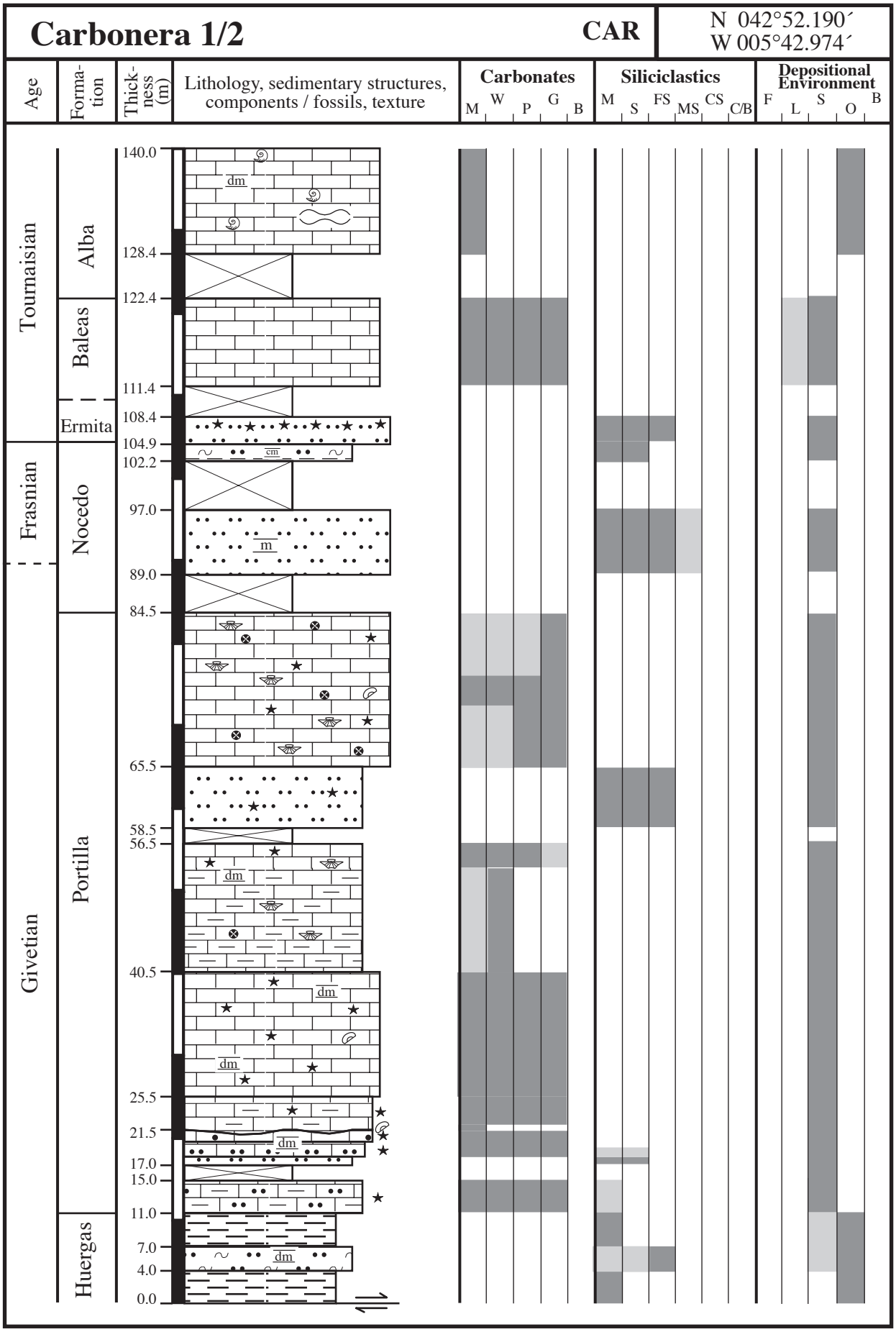
Carbonera 1/2
CAR
N 042°52.190´
W 005°42.974´
Age
Formation
Thickness (m)
Lithology, sedimentary structures, components / fossils, texture
Carbonates
M W P G B
Siliciclastics
M S FS MS CS C/B
Depositional Environment
F L S O B
Tournaisian
Frasnian
Givetian
Alba
Baleas
Ermita
Nocedo
Portilla
Huergas
140.0
128.4
122.4
111.4
108.4
104.9
102.2
97.0
89.0
84.5
65.5
58.5
56.5
40.5
25.5
21.5
17.0
15.0
11.0
7.0
4.0
0.0
dm
cm
m

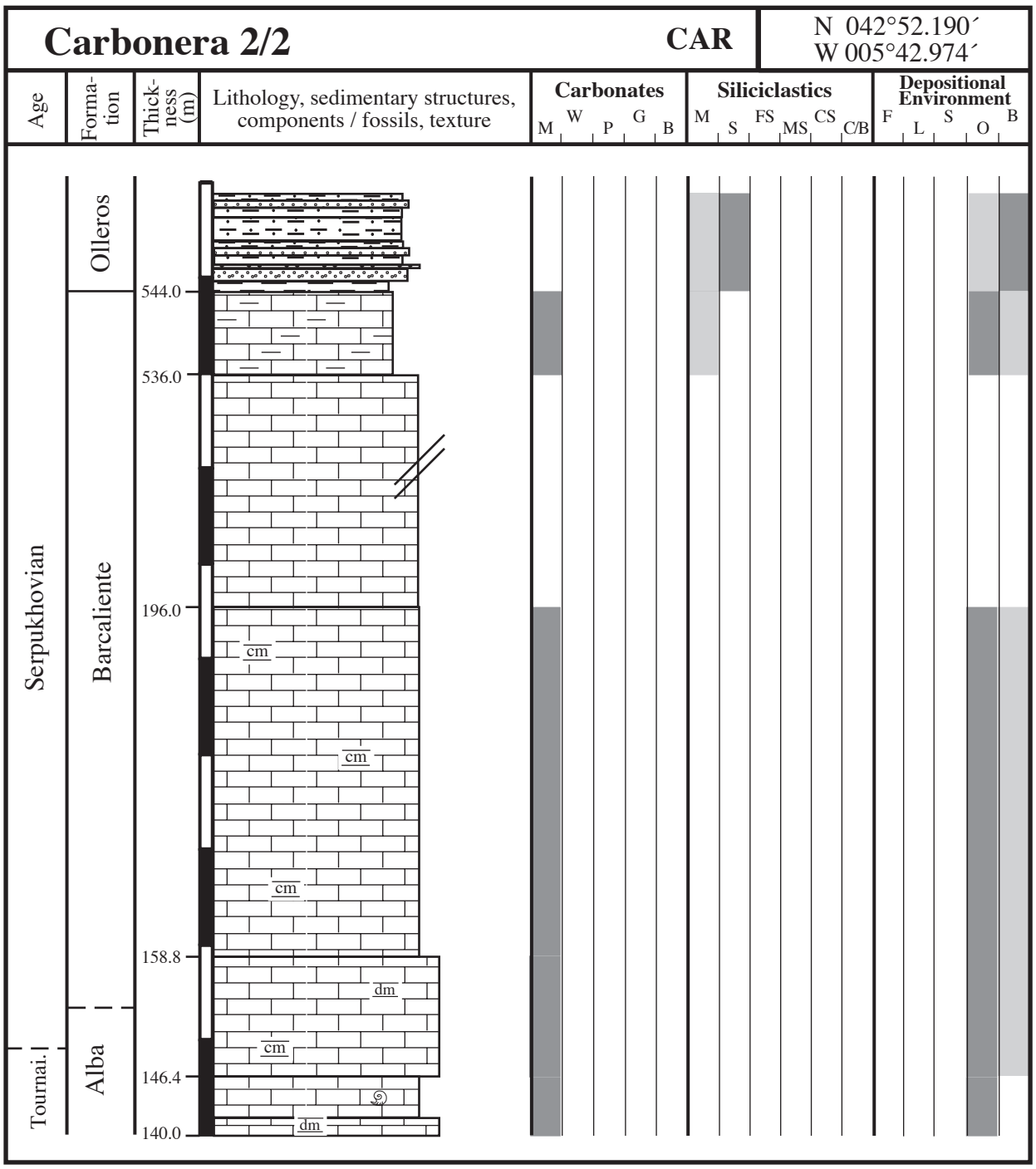
Carbonera 2/2
CAR
N 042°52.190´
W 005°42.974´
Age
Forma-tion
Thick-ness (m)
Lithology, sedimentary structures, components / fossils, texture
Carbonates
M W P G B
Siliciclastics
M S FS MS CS C/B
Depositional Environment
F L S O B
Serpukhovian
Tournai.
Olleros
Barcaliente
Alba
544.0
536.0
196.0
158.8
146.4
140.0
cm
cm
cm
dm
cm
dm

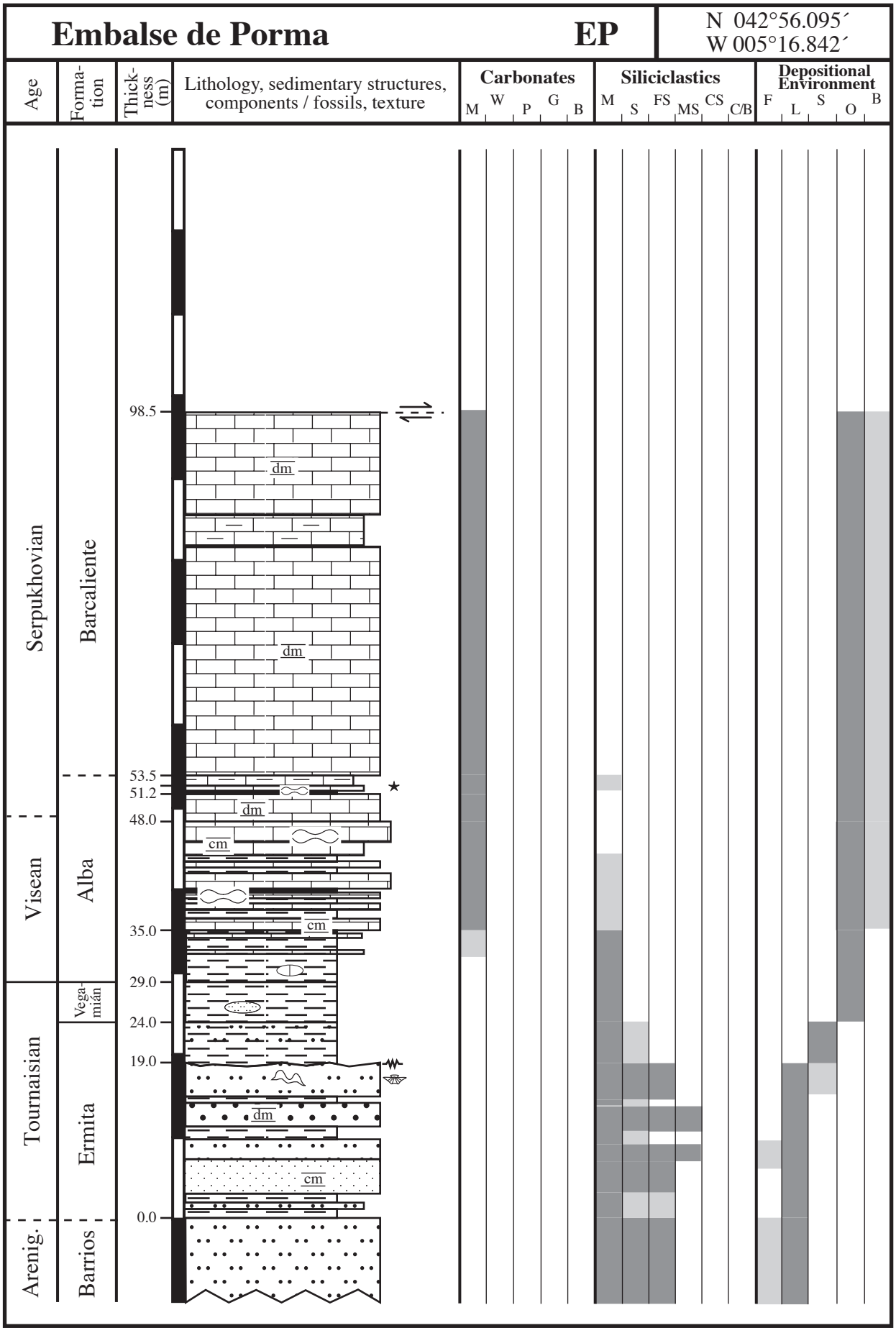
Embalse de Porma
EP
N 042°56.095´
W 005°16.842´
Age
Formation
Thickness (m)
Lithology, sedimentary structures, components / fossils, texture
Carbonates
M W P G B
Siliciclastics
M S FS MS CS C/B
Depositional Environment
F L S O B
Serpukhovian
Visean
Tournaisian
Arenig.
Barcaliente
Alba
Vegamián
Ermita
Barrios
98.5
53.5
51.2
48.0
35.0
29.0
24.0
19.0
0.0
dm
cm

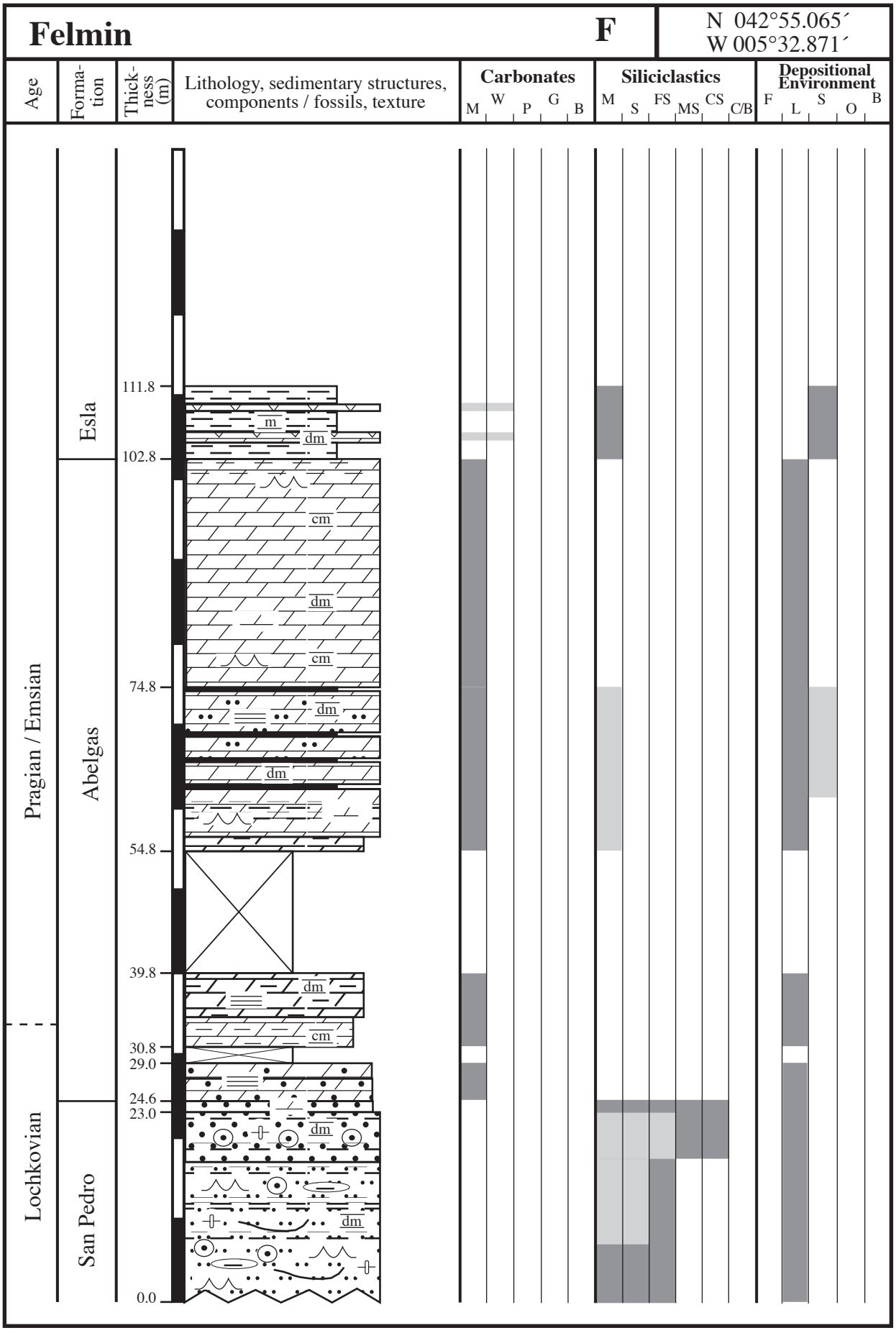
Felmin
F
N 042°55.065´
W 005°32.871´
Age
Formation
Thickness (m)
Lithology, sedimentary structures, components / fossils, texture
Carbonates
M W P G B
Siliciclastics
M S FS MS CS C/B
Depositional Environment
F L S O B
Pragian / Emsian
Lochkovian
Esla
Abelgas
San Pedro
111.8
102.8
74.8
54.8
39.8
30.8
29.0
24.6
23.0
0.0
m
dm
cm

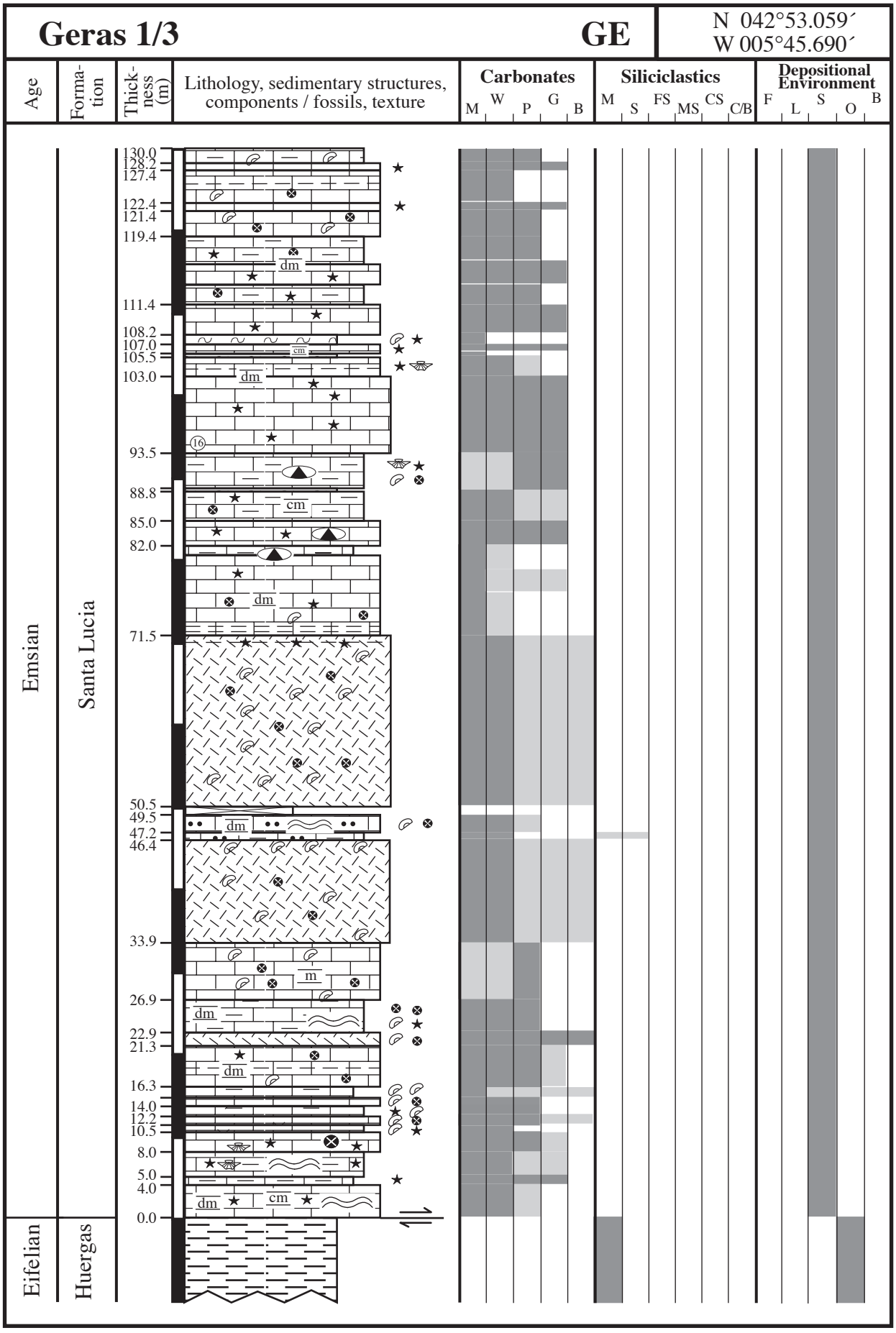
Geras 1/3
GE
N 042°53.059´
W 005°45.690´
Age
Forma-tion
Thick-ness (m)
Lithology, sedimentary structures, components / fossils, texture
Carbonates
M W P G B
Siliciclastics
M S FS MS CS C/B
Depositional Environment
F L S O B
Emsian
Eifelian
Santa Lucia
Huergas
130.0
128.2
127.4
122.4
121.4
119.4
111.4
108.2
107.0
105.5
103.0
93.5
88.8
85.0
82.0
71.5
50.5
49.5
47.2
46.4
33.9
26.9
22.9
21.3
16.3
14.0
12.2
10.5
8.0
5.0
4.0
0.0
dm
cm
m
16

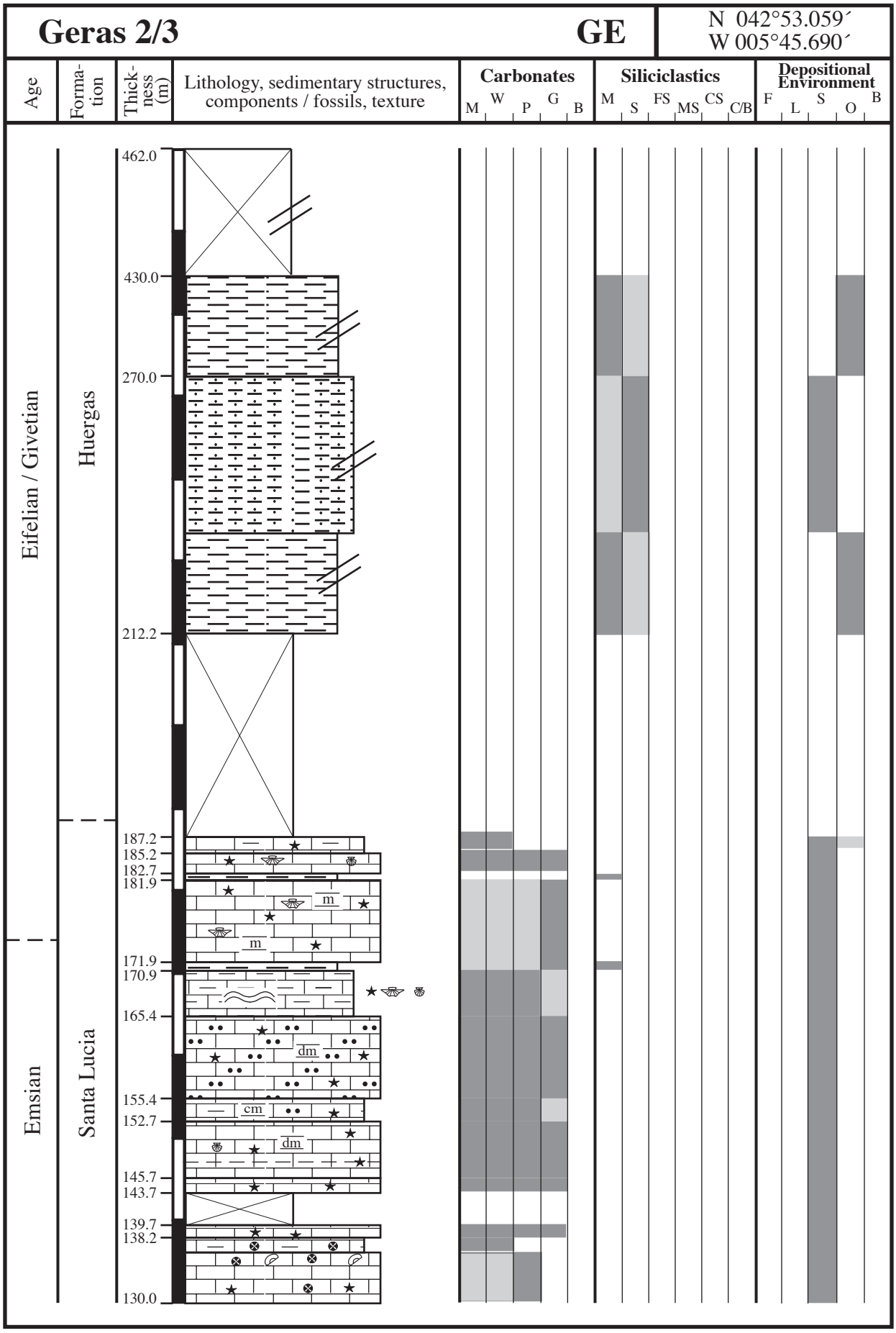
Geras 2/3
GE
N 042°53.059´
W 005°45.690´
Age
Formation
Thickness (m)
Lithology, sedimentary structures, components / fossils, texture
Carbonates
M W P G B
Siliciclastics
M S FS MS CS C/B
Depositional Environment
F L S O B
Eifelian / Givetian
Emsian
Huergas
Santa Lucia
462.0
430.0
270.0
212.2
187.2
185.2
182.7
181.9
171.9
170.9
165.4
155.4
152.7
145.7
143.7
139.7
138.2
130.0
m
m
dm
cm
dm

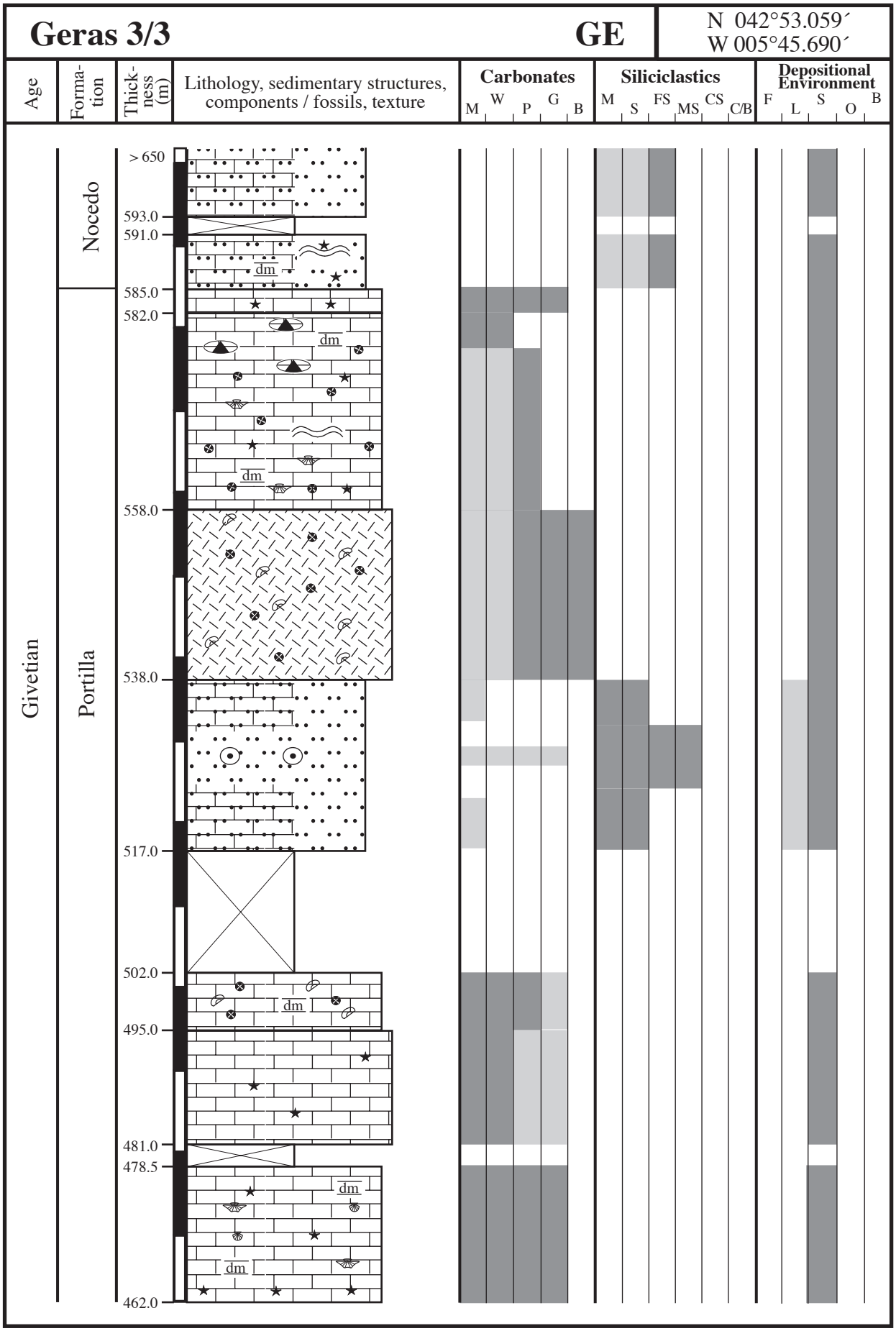
Geras 3/3
GE
N 042°53.059´
W 005°45.690´
Age
Forma-tion
Thick-ness (m)
Lithology, sedimentary structures, components / fossils, texture
Carbonates
M W P G B
Siliciclastics
M S FS MS CS C/B
Depositional Environment
F L S O B
Givetian
Nocedo
Portilla
> 650
593.0
591.0
585.0
582.0
558.0
538.0
517.0
502.0
495.0
481.0
478.5
462.0
dm

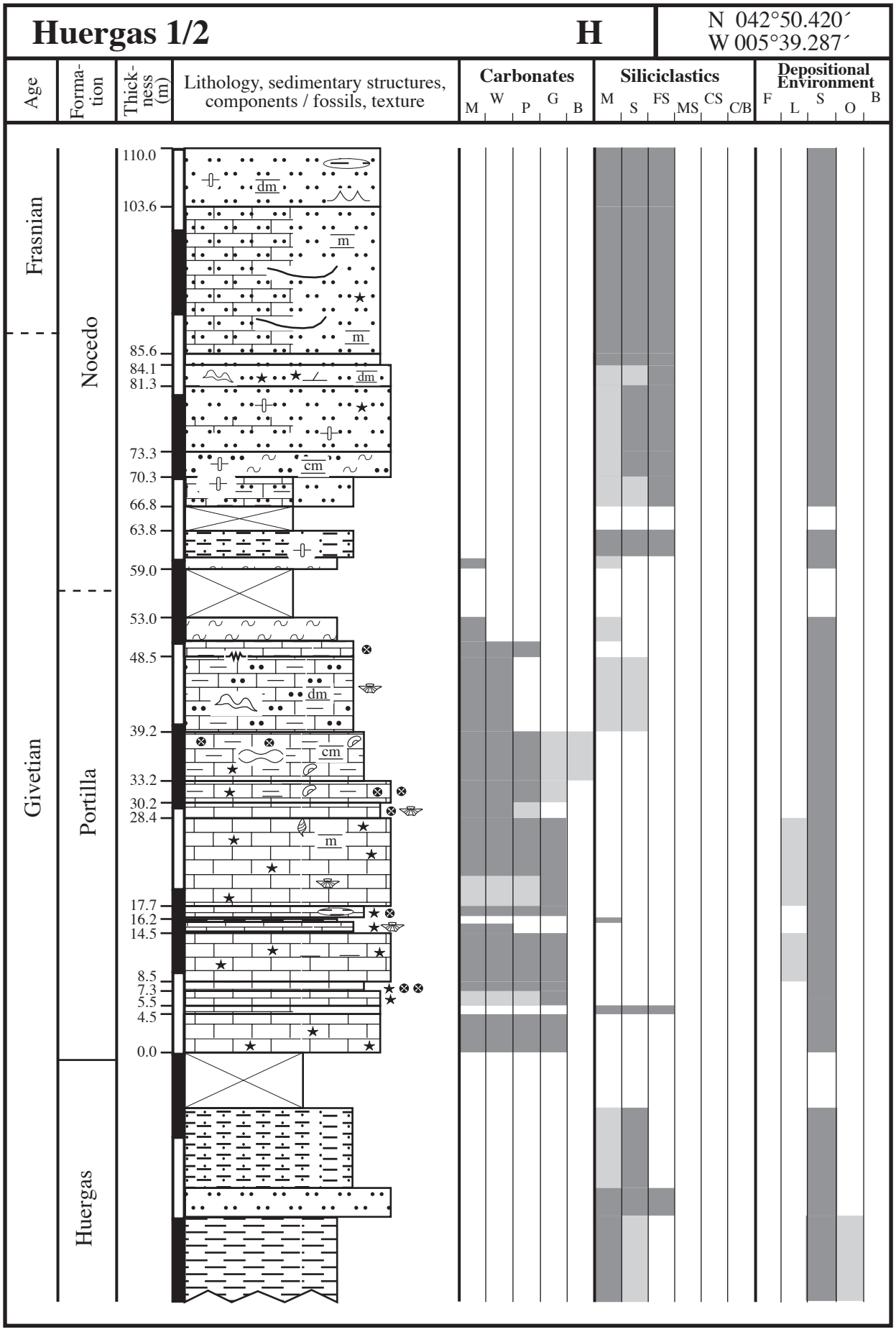
Huergas 1/2
H
N 042°50.420´
W 005°39.287´
Age
Formation
Thickness (m)
Lithology, sedimentary structures, components / fossils, texture
Carbonates
M W P G B
Siliciclastics
M S FS MS CS C/B
Depositional Environment
F L S O B
Frasnian
Givetian
Nocedo
Portilla
Huergas
110.0
103.6
85.6
84.1
81.3
73.3
70.3
66.8
63.8
59.0
53.0
48.5
39.2
33.2
30.2
28.4
17.7
16.2
14.5
8.5
7.3
5.5
4.5
0.0
dm
m
cm

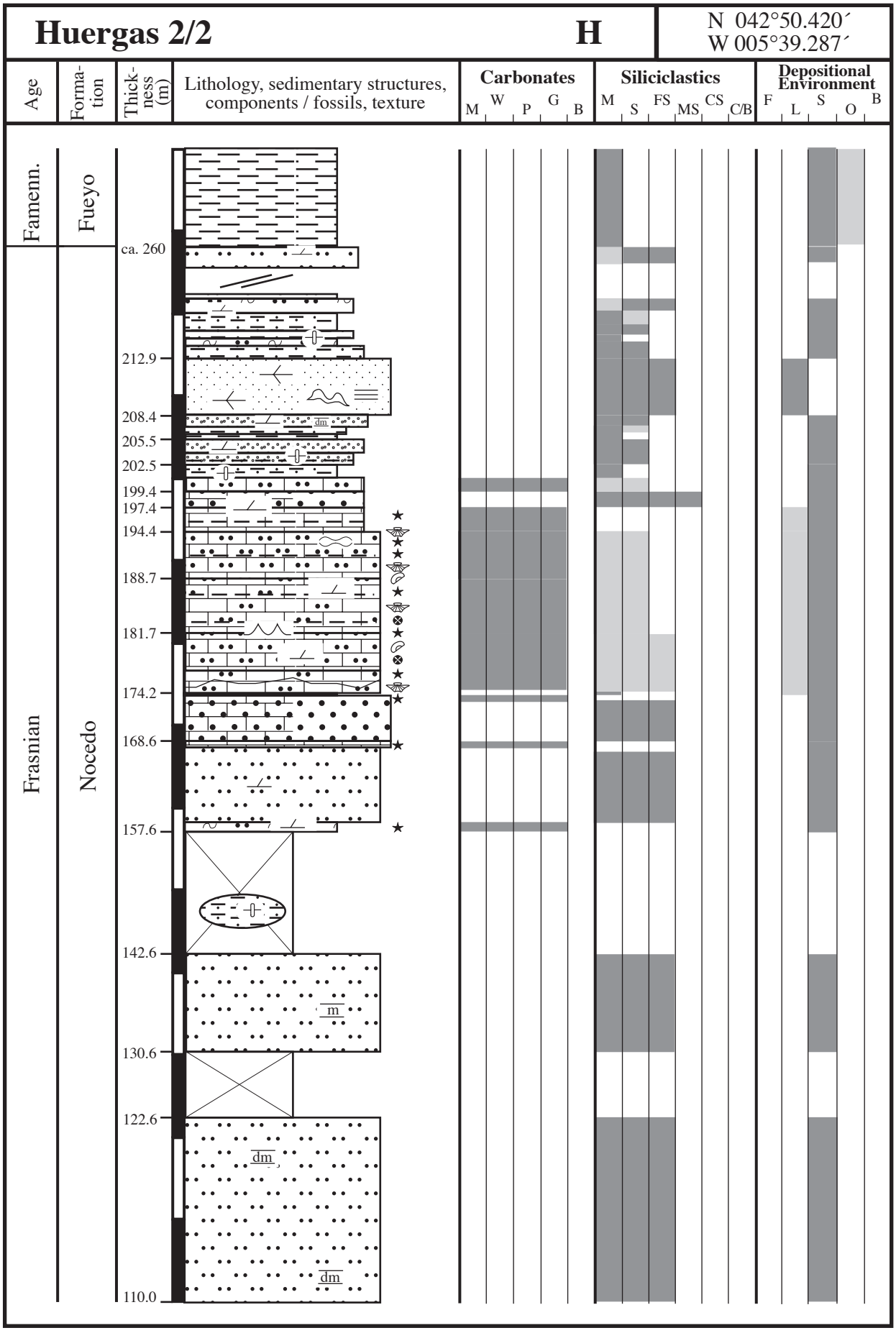
Huergas 2/2
H
N 042°50.420´
W 005°39.287´
Age
Formation
Thickness (m)
Lithology, sedimentary structures, components / fossils, texture
Carbonates
M W P G B
Siliciclastics
M S FS MS CS C/B
Depositional Environment
F L S O B
Famenn.
Frasnian
Fueyo
Nocedo
ca. 260
212.9
208.4
205.5
202.5
199.4
197.4
194.4
188.7
181.7
174.2
168.6
157.6
142.6
130.6
122.6
110.0
dm
m
dm
dm

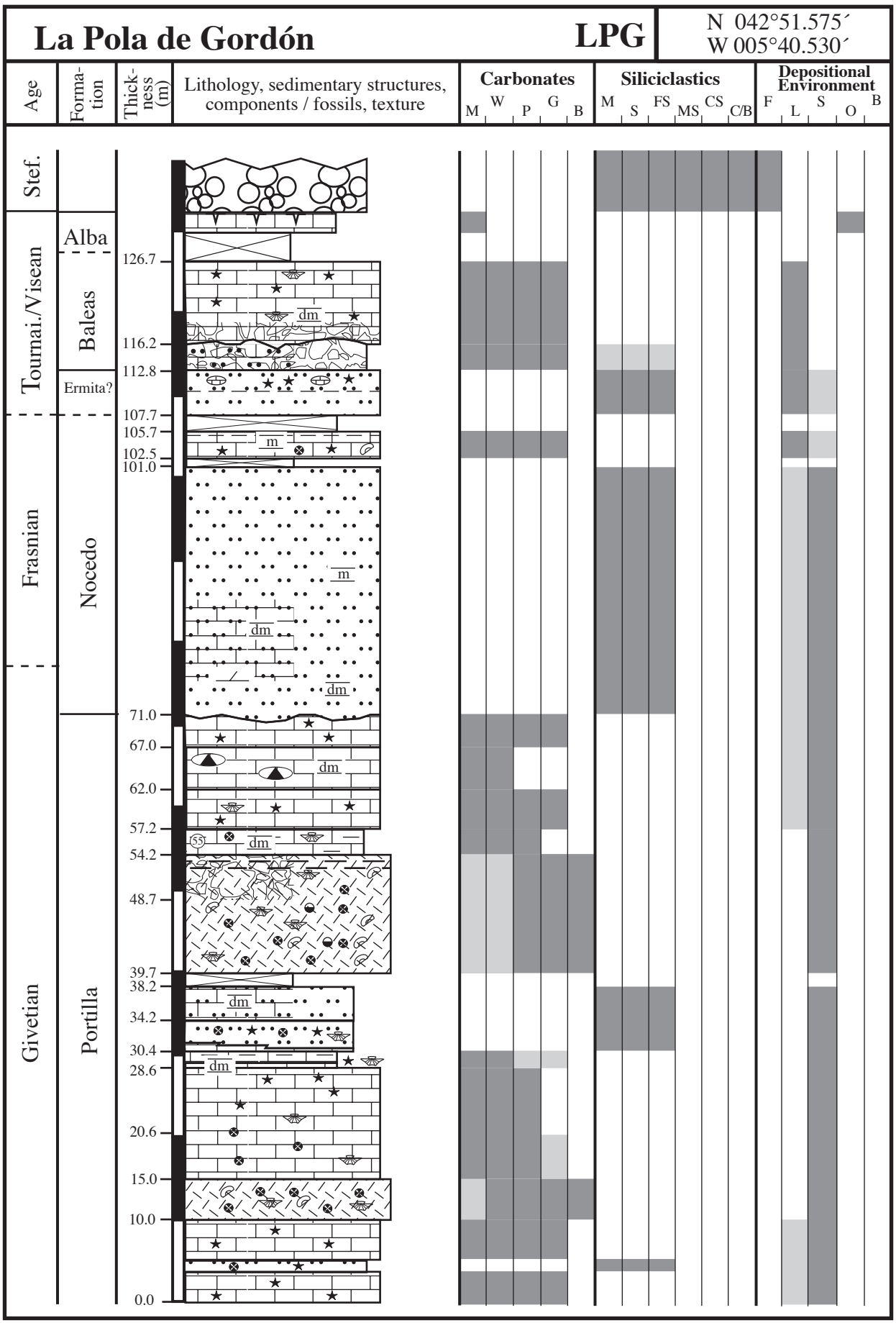
La Pola de Gordón
LPG
N 042°51.575´
W 005°40.530´
Age
Formation
Thickness (m)
Lithology, sedimentary structures, components / fossils, texture
Carbonates
M W P G B
Siliciclastics
M S FS MS CS C/B
Depositional Environment
F L S O B
Stef.
Tournai./Visean
Frasnian
Givetian
Alba
Baleas
Ermita?
Nocedo
Portilla
126.7
116.2
112.8
107.7
105.7
102.5
101.0
71.0
67.0
62.0
57.2
54.2
48.7
39.7
38.2
34.2
30.4
28.6
20.6
15.0
10.0
0.0
dm
m
55

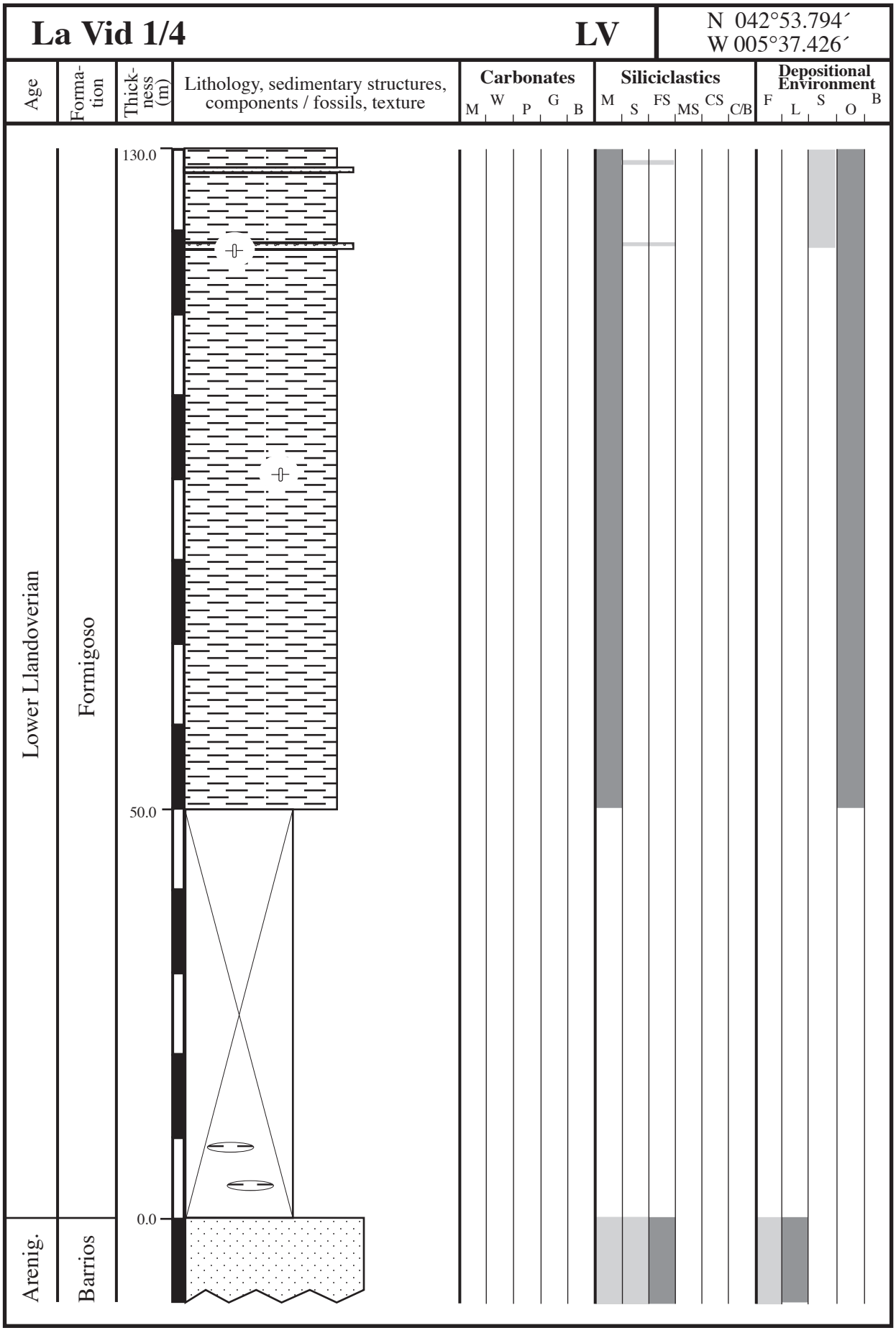
La Vid 1/4
LV
N 042°53.794´
W 005°37.426´
Age
Forma-tion
Thick-ness (m)
Lithology, sedimentary structures, components / fossils, texture
Carbonates
M W P G B
Siliciclastics
M S FS MS CS C/B
Depositional Environment
F L S O B
Lower Llandoverian
Formigoso
Arenig.
Barrios
130.0
50.0
0.0

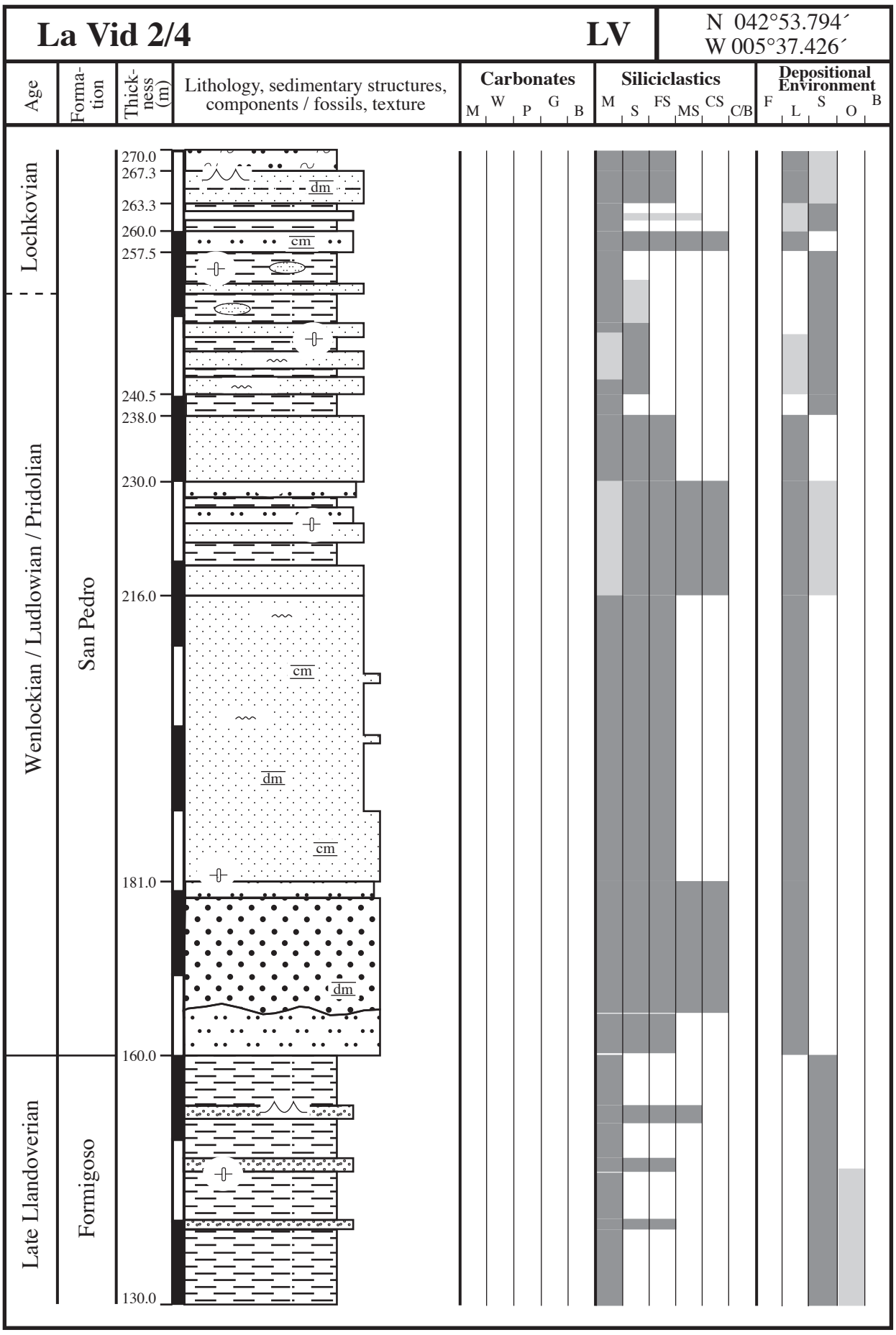
La Vid 2/4
LV
N 042°53.794´
W 005°37.426´
Age
Formation
Thickness (m)
Lithology, sedimentary structures, components / fossils, texture
Carbonates
M W P G B
Siliciclastics
M S FS MS CS C/B
Depositional Environment
F L S O B
Lochkovian
Wenlockian / Ludlowian / Pridolian
Late Llandoverian
San Pedro
Formigoso
270.0
267.3
263.3
260.0
257.5
240.5
238.0
230.0
216.0
181.0
160.0
130.0
dm
cm
dm
cm
dm

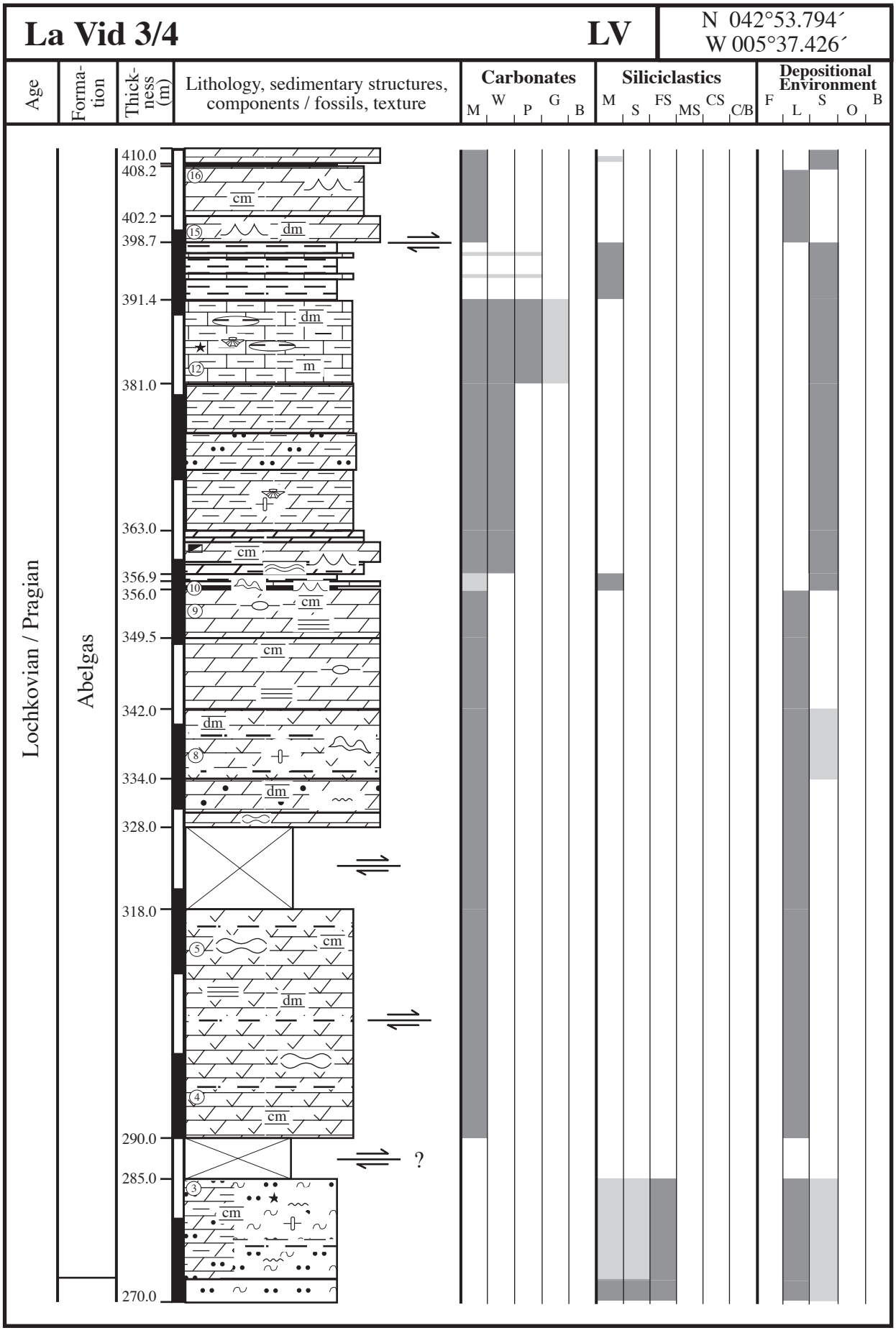
La Vid 3/4
LV
N 042°53.794´
W 005°37.426´
Age
Formation
Thickness (m)
Lithology, sedimentary structures, components / fossils, texture
Carbonates
M W P G B
Siliciclastics
M S FS MS CS C/B
Depositional Environment
F L S O B
Lochkovian / Pragian
Abelgas
410.0
408.2
402.2
398.7
391.4
381.0
363.0
356.9
356.0
349.5
342.0
334.0
328.0
318.0
290.0
285.0
270.0
cm
dm
m
?

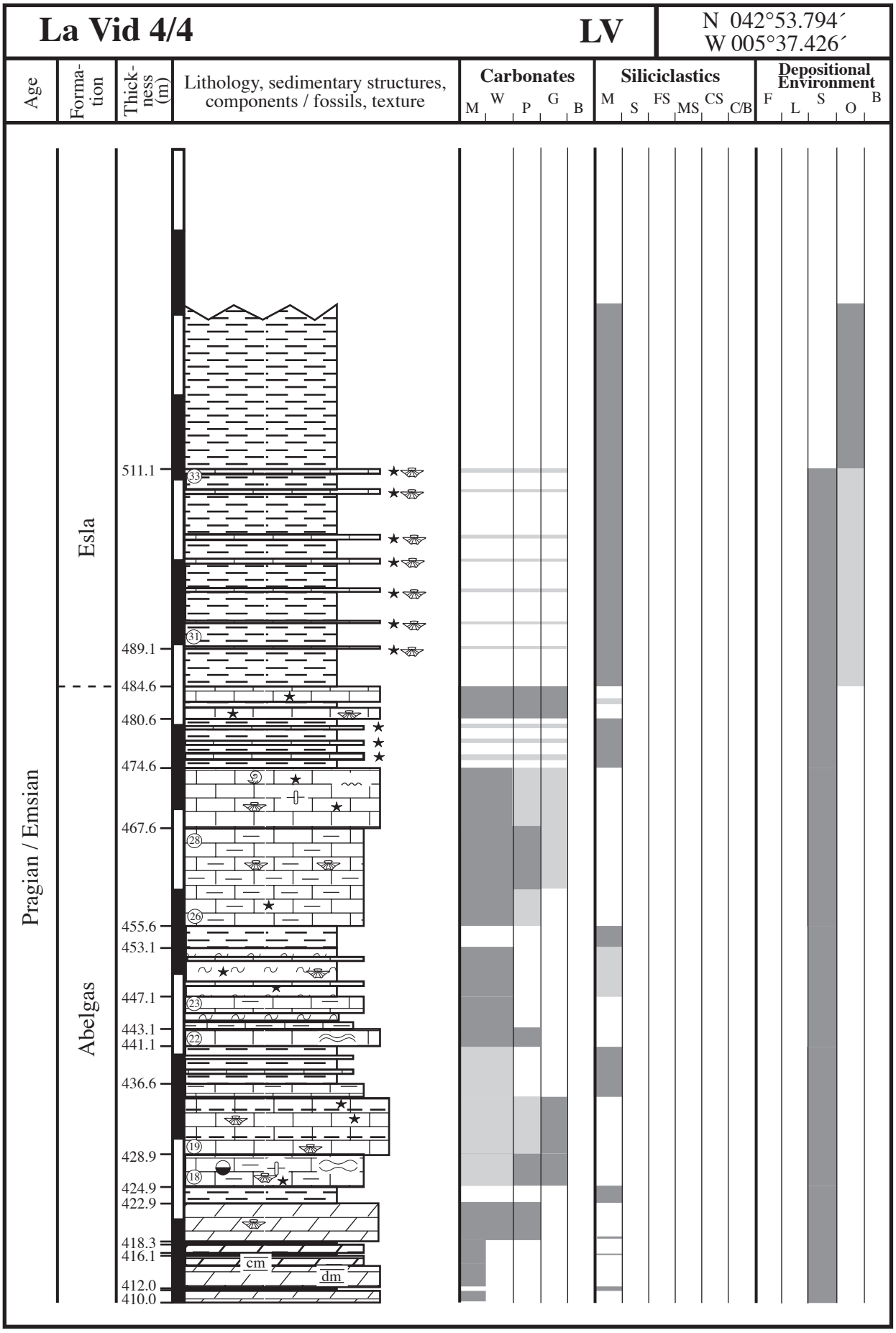
La Vid 4/4
LV
N 042°53.794´
W 005°37.426´
Age
Forma-tion
Thick-ness (m)
Lithology, sedimentary structures, components / fossils, texture
Carbonates
M W P G B
Siliciclastics
M S FS MS CS C/B
Depositional Environment
F L S O B
Pragian / Emsian
Esla
Abelgas
511.1
489.1
484.6
480.6
474.6
467.6
455.6
453.1
447.1
443.1
441.1
436.6
428.9
424.9
422.9
418.3
416.1
412.0
410.0
cm
dm

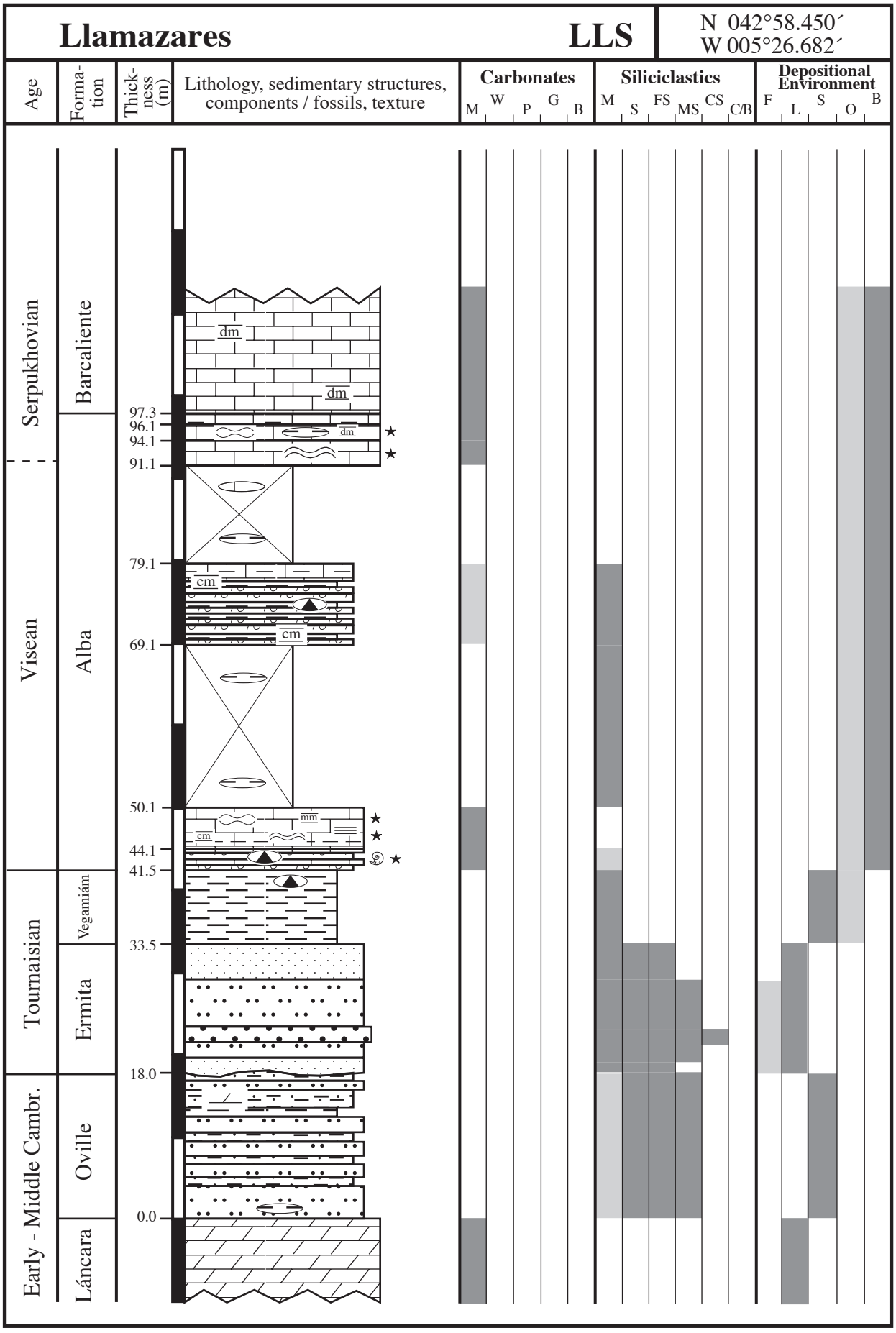
Llamazares
LLS
N 042°58.450´
W 005°26.682´
Age
Formation
Thickness (m)
Lithology, sedimentary structures, components / fossils, texture
Carbonates
M W P G B
Siliciclastics
M S FS MS CS C/B
Depositional Environment
F L S O B
Serpukhovian
Visean
Tournaisian
Early - Middle Cambr.
Barcaliente
Alba
Vegamiám
Ermita
Oville
Láncara
97.3
96.1
94.1
91.1
79.1
69.1
50.1
44.1
41.5
33.5
18.0
0.0
dm
cm
mm

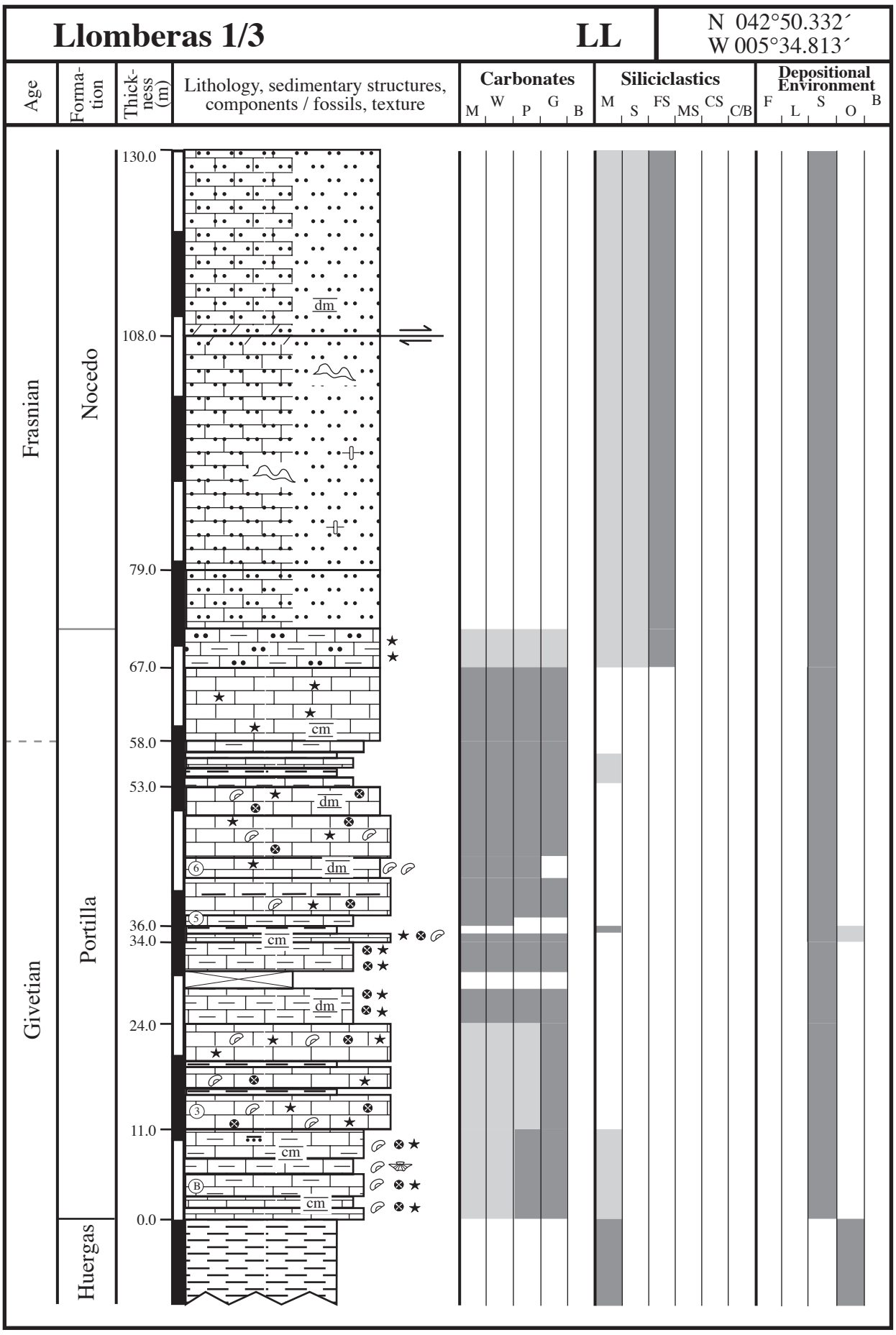
Llomberas 1/3
LL
N 042°50.332´
W 005°34.813´
Age
Forma-tion
Thick-ness (m)
Lithology, sedimentary structures, components / fossils, texture
Carbonates
M W P G B
Siliciclastics
M S FS MS CS C/B
Depositional Environment
F L S O B
Frasnian
Givetian
Nocedo
Portilla
Huergas
130.0
108.0
79.0
67.0
58.0
53.0
36.0
34.0
24.0
11.0
0.0
dm
cm
6
5
3
B

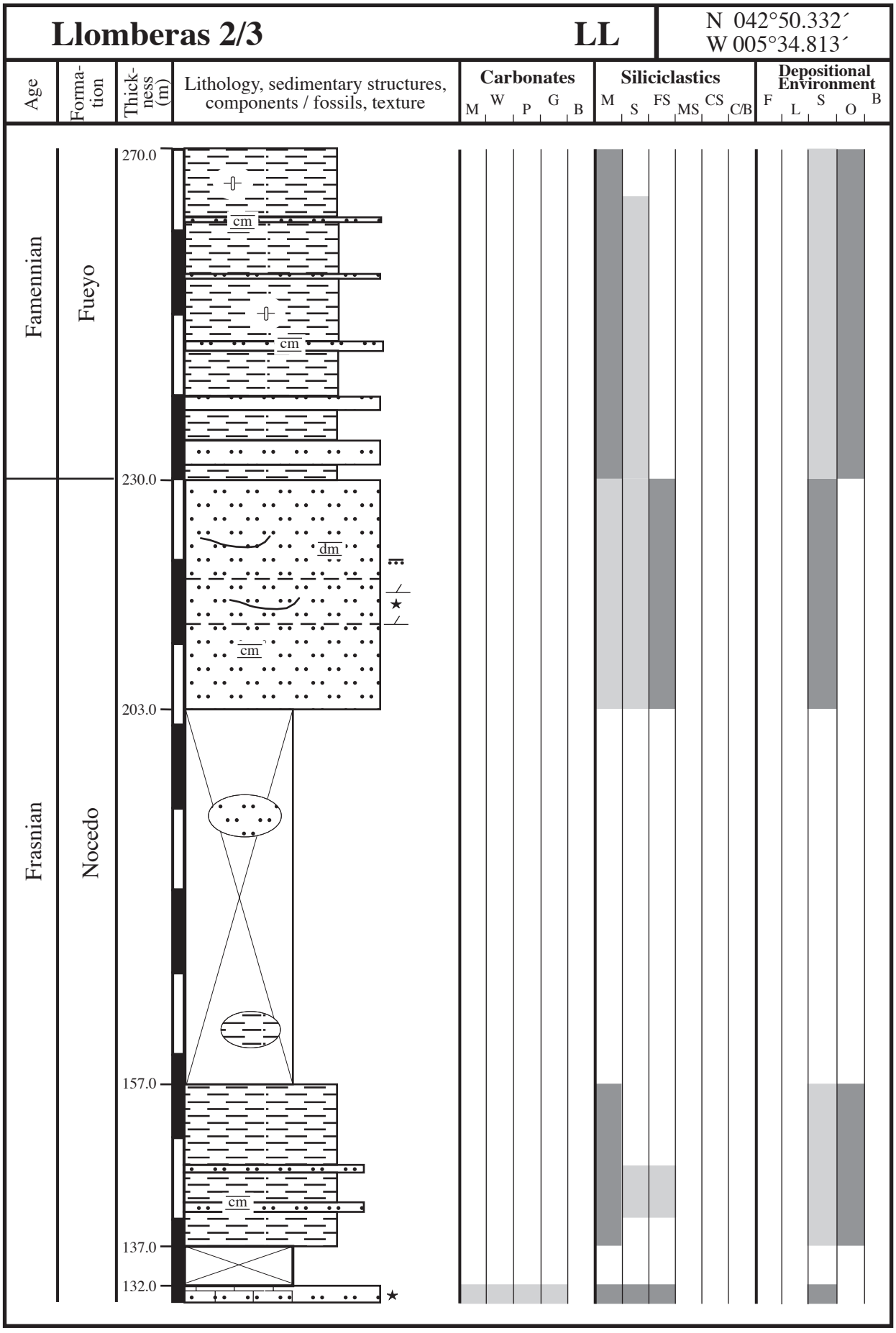
Llomberas 2/3
LL
N 042°50.332´
W 005°34.813´
Age
Formation
Thickness (m)
Lithology, sedimentary structures, components / fossils, texture
Carbonates
M W P G B
Siliciclastics
M S FS MS CS C/B
Depositional Environment
F L S O B
Famennian
Frasnian
Fueyo
Nocedo
270.0
230.0
203.0
157.0
137.0
132.0
cm
dm

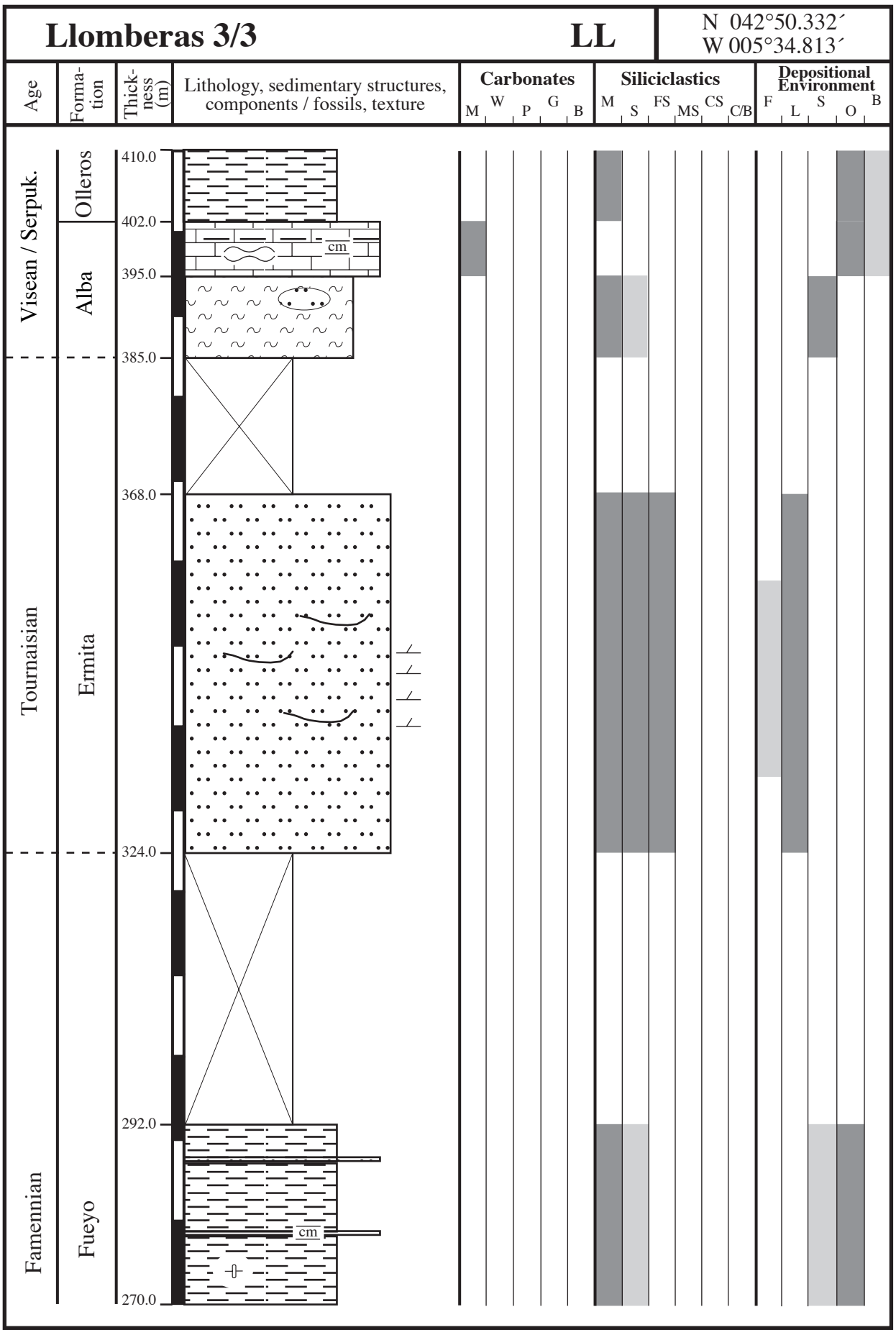
Llomberas 3/3
LL
N 042°50.332´
W 005°34.813´
Age
Formation
Thickness (m)
Lithology, sedimentary structures, components / fossils, texture
Carbonates
M W P G B
Siliciclastics
M S FS MS CS C/B
Depositional Environment
F L S O B
Visean / Serpuk.
Tournaisian
Famennian
Olleros
Alba
Ermita
Fueyo
410.0
402.0
395.0
385.0
368.0
324.0
292.0
270.0
cm
cm

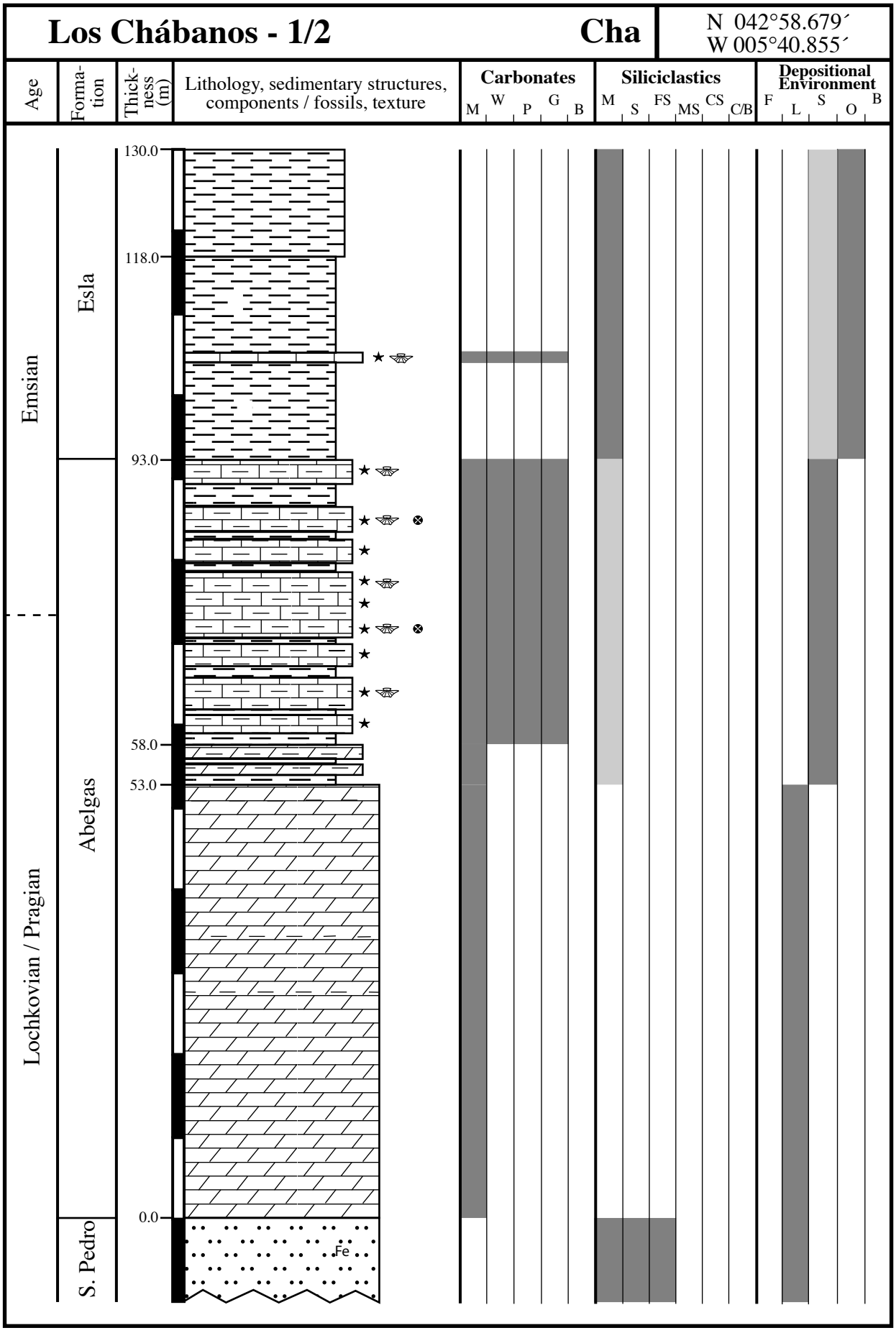
Los Chábanos - 1/2
Cha
N 042°58.679´
W 005°40.855´
Age
Formation
Thickness (m)
Lithology, sedimentary structures, components / fossils, texture
Carbonates
M W P G B
Siliciclastics
M S FS MS CS C/B
Depositional Environment
F L S O B
Emsian
Lochkovian / Pragian
Esla
Abelgas
S. Pedro
130.0
118.0
93.0
58.0
53.0
0.0
Fe

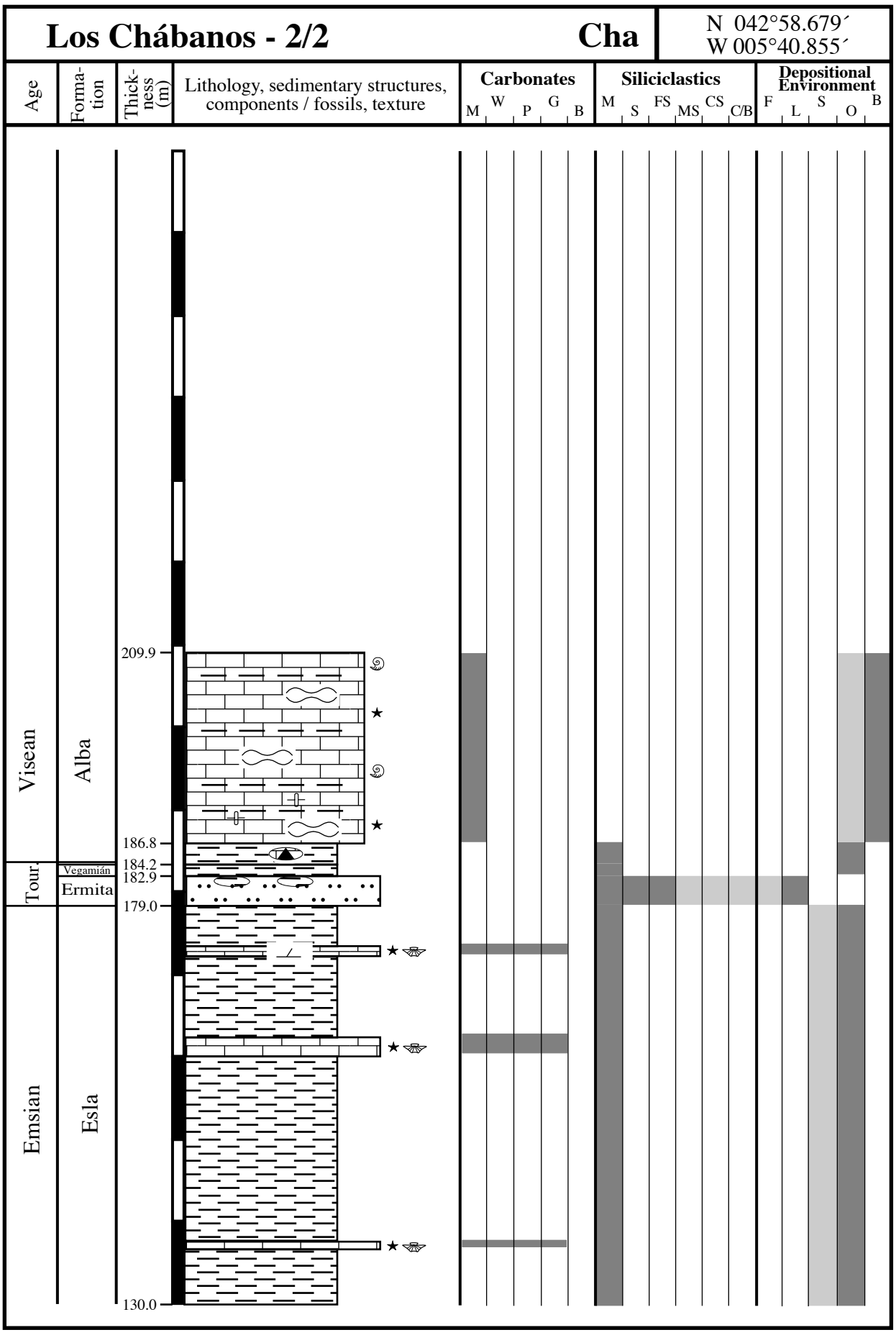
Los Chábanos - 2/2
Cha
N 042°58.679´
W 005°40.855´
Age
Formation
Thickness (m)
Lithology, sedimentary structures, components / fossils, texture
Carbonates
M W P G B
Siliciclastics
M S FS MS CS C/B
Depositional Environment
F L S O B
Visean
Tour.
Emsian
Alba
Vegamián
Ermita
Esla
209.9
186.8
184.2
182.9
179.0
130.0

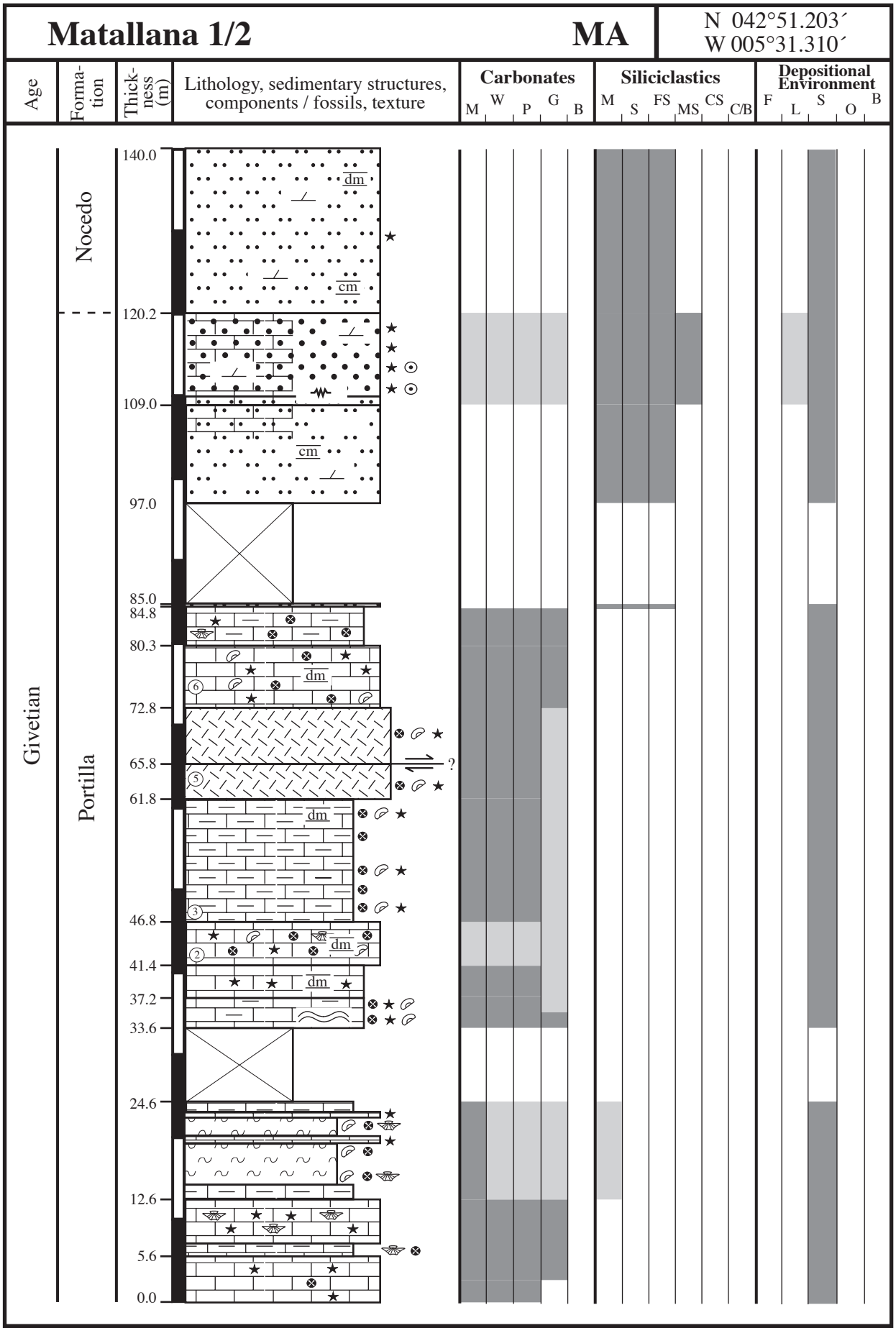
Matallana 1/2
MA
N 042°51.203´
W 005°31.310´
Age
Formation
Thickness (m)
Lithology, sedimentary structures, components / fossils, texture
Carbonates
M W P G B
Siliciclastics
M S FS MS CS C/B
Depositional Environment
F L S O B
Givetian
Nocedo
Portilla
140.0
120.2
109.0
97.0
85.0
84.8
80.3
72.8
65.8
61.8
46.8
41.4
37.2
33.6
24.6
12.6
5.6
0.0
dm
cm
?

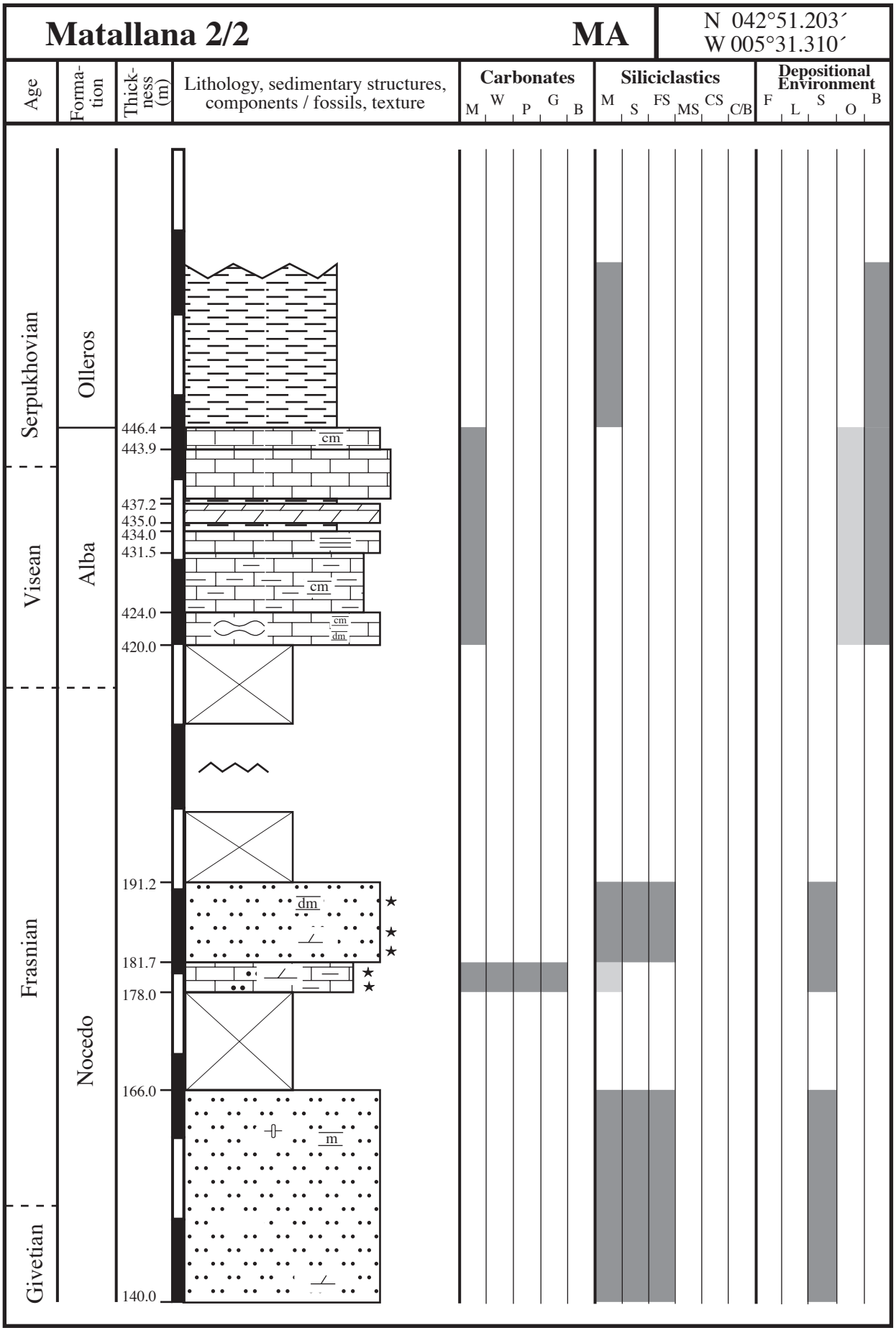
Matallana 2/2
MA
N 042°51.203´
W 005°31.310´
Age
Forma-tion
Thick-ness (m)
Lithology, sedimentary structures, components / fossils, texture
Carbonates
M W P G B
Siliciclastics
M S FS MS CS C/B
Depositional Environment
F L S O B
Serpukhovian
Visean
Frasnian
Givetian
Olleros
Alba
Nocedo
446.4
443.9
437.2
435.0
434.0
431.5
424.0
420.0
191.2
181.7
178.0
166.0
140.0
cm
dm
m

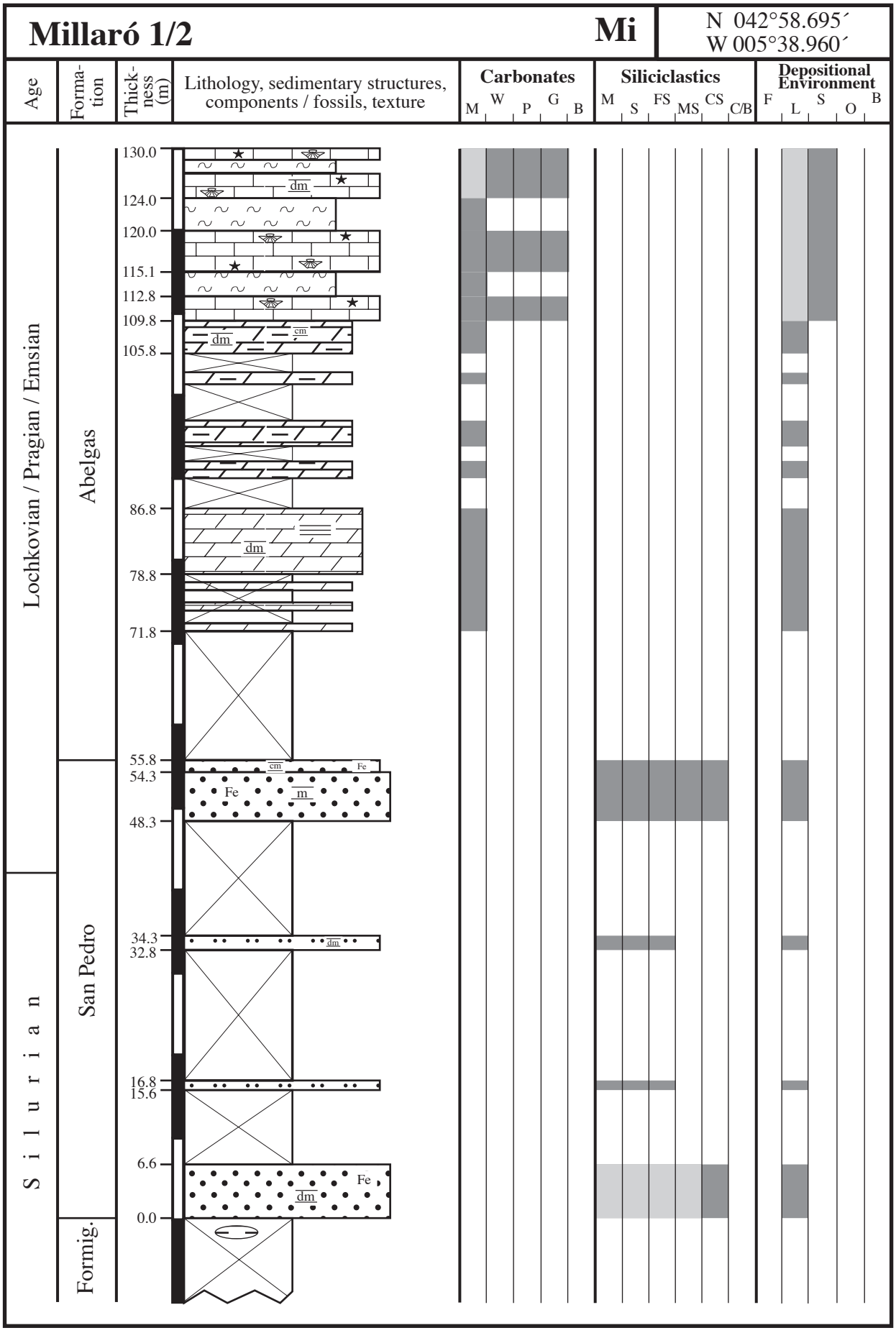
Millaró 1/2
Mi
N 042°58.695´
W 005°38.960´
Age
Formation
Thickness (m)
Lithology, sedimentary structures, components / fossils, texture
Carbonates
M W P G B
Siliciclastics
M S FS MS CS C/B
Depositional Environment
F L S O B
Lochkovian / Pragian / Emsian
Siluriano
Abelgas
San Pedro
Formig.
130.0
124.0
120.0
115.1
112.8
109.8
105.8
86.8
78.8
71.8
55.8
54.3
48.3
34.3
32.8
16.8
15.6
6.6
0.0
dm
cm
Fe
m

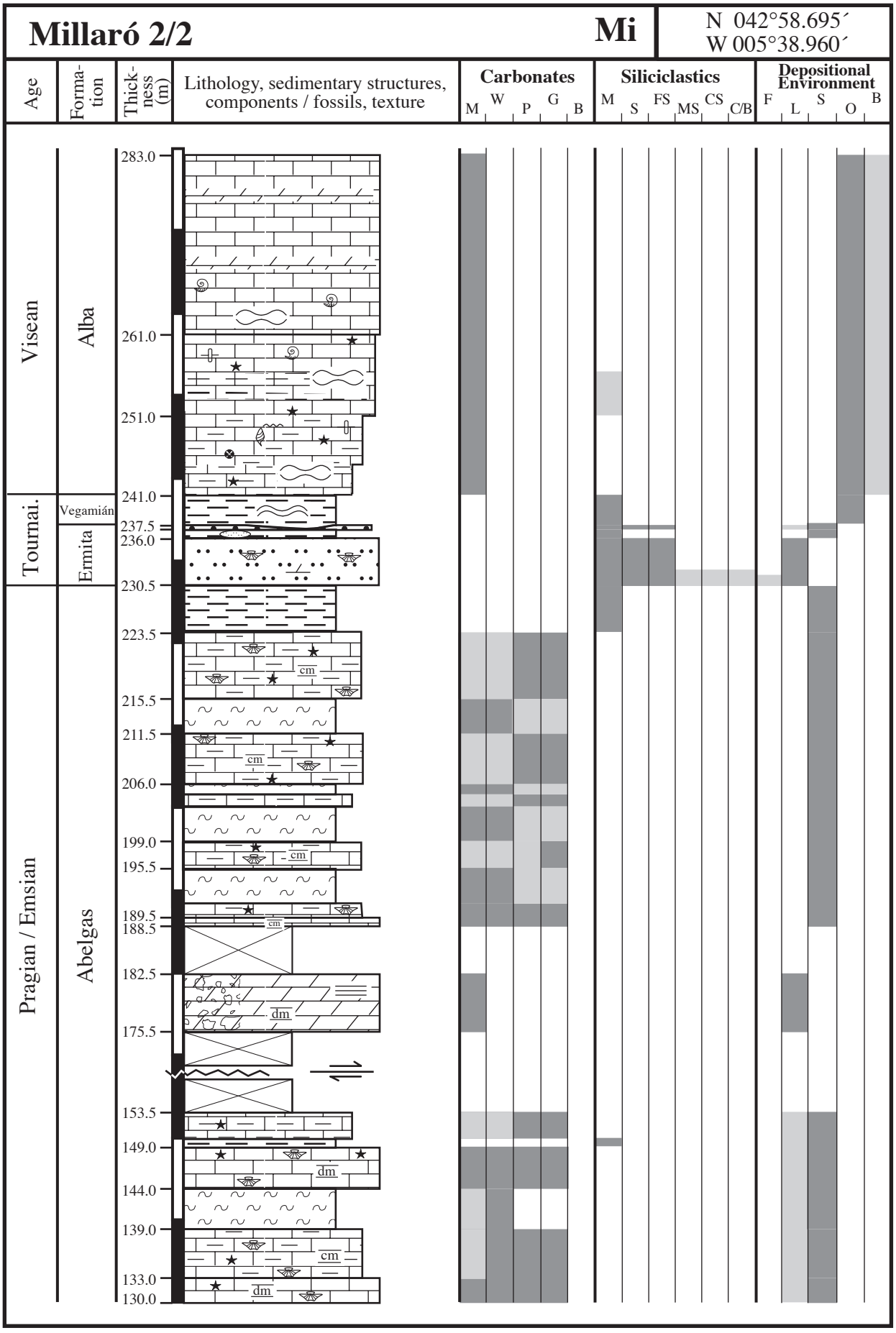
Millaró 2/2
Mi
N 042°58.695´
W 005°38.960´
Age
Formation
Thickness (m)
Lithology, sedimentary structures, components / fossils, texture
Carbonates
M W P G B
Siliciclastics
M S FS MS CS C/B
Depositional Environment
F L S O B
Visean
Tournai.
Pragian / Emsian
Alba
Vegamián
Ermita
Abelgas
283.0
261.0
251.0
241.0
237.5
236.0
230.5
223.5
215.5
211.5
206.0
199.0
195.5
189.5
188.5
182.5
175.5
153.5
149.0
144.0
139.0
133.0
130.0
cm
dm

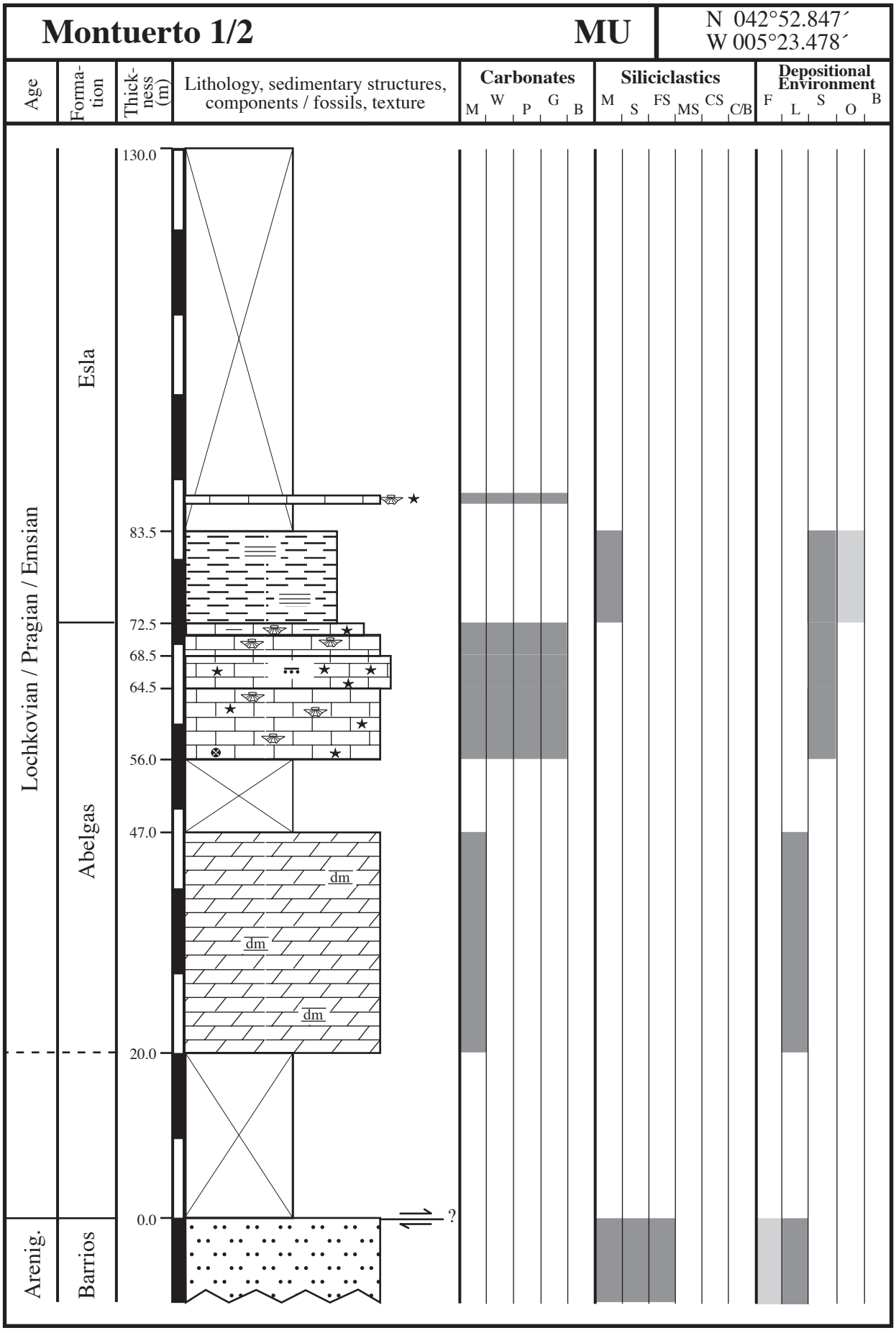
Montuerto 1/2
MU
N 042°52.847´
W 005°23.478´
Age
Formation
Thickness (m)
Lithology, sedimentary structures, components / fossils, texture
Carbonates
M W P G B
Siliciclastics
M S FS MS CS C/B
Depositional Environment
F L S O B
Lochkovian / Pragian / Emsian
Arenig.
Esla
Abelgas
Barrios
130.0
83.5
72.5
68.5
64.5
56.0
47.0
20.0
0.0
dm
dm
dm
?

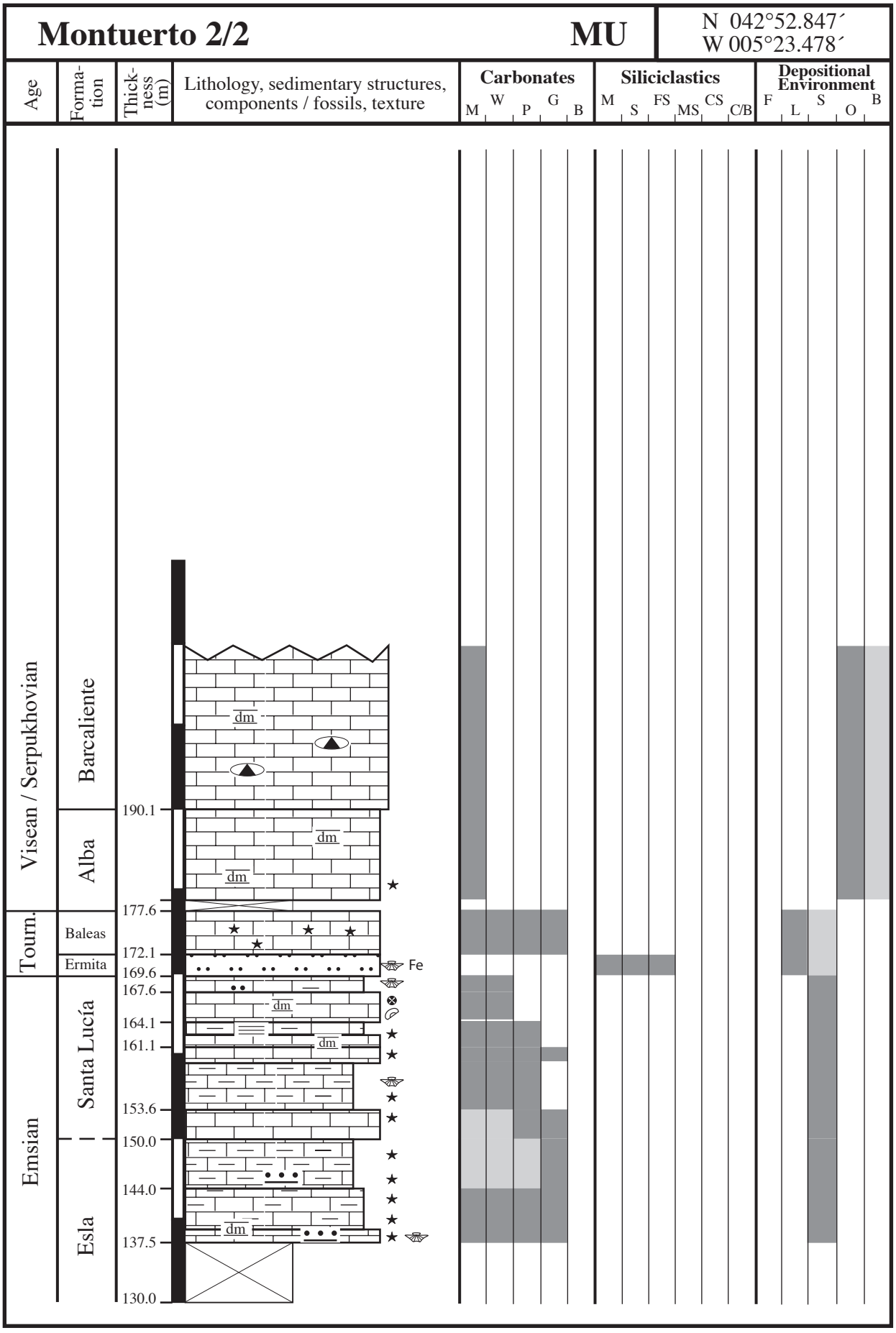
Montuerto 2/2
MU
N 042°52.847´
W 005°23.478´
Age
Formation
Thickness (m)
Lithology, sedimentary structures, components / fossils, texture
Carbonates
M W P G B
Siliciclastics
M S FS MS CS C/B
Depositional Environment
F L S O B
Visean / Serpukhovian
Tourn.
Emsian
Barcaliente
Alba
Baleas
Ermita
Santa Lucía
Esla
dm
Fe
190.1
177.6
172.1
169.6
167.6
164.1
161.1
153.6
150.0
144.0
137.5
130.0

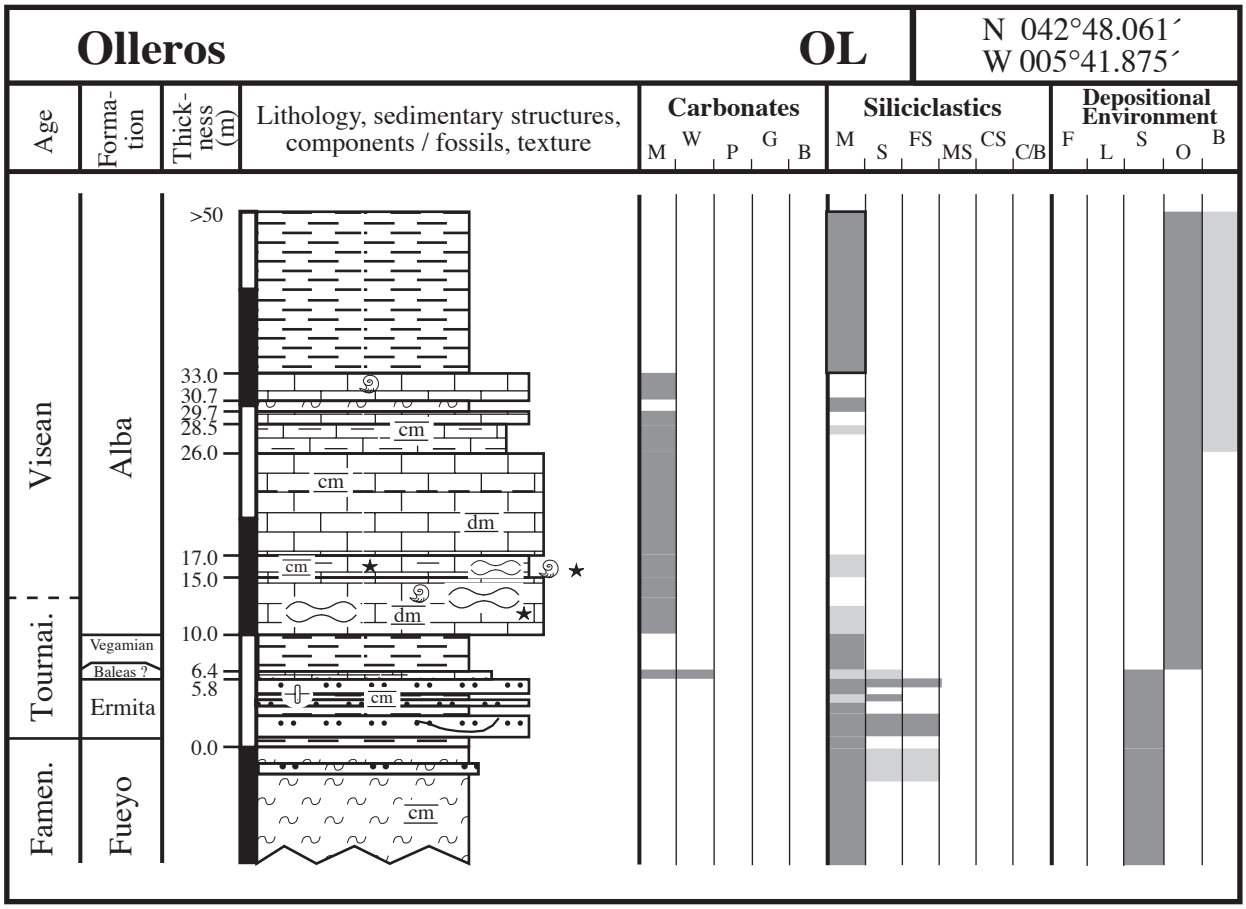
Olleros
OL
N 042°48.061´
W 005°41.875´
Age
Formation
Thickness (m)
Lithology, sedimentary structures, components / fossils, texture
Carbonates
M W P G B
Siliciclastics
M S FS MS CS C/B
Depositional Environment
F L S O B
Visean
Tournai.
Famen.
Alba
Vegamian
Baleas ?
Ermita
Fueyo
>50
33.0
30.7
29.7
28.5
26.0
17.0
15.0
10.0
6.4
5.8
0.0
cm
dm

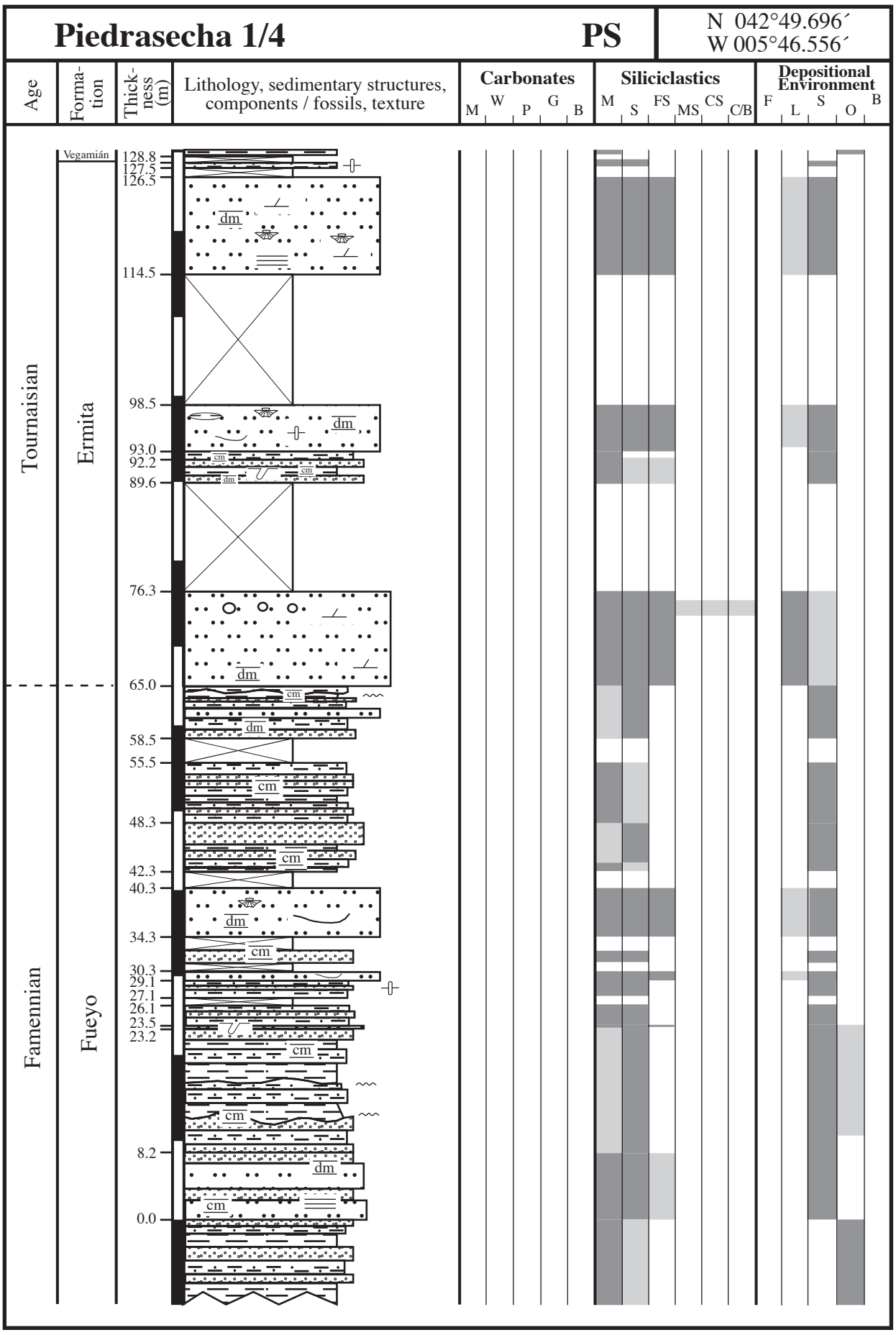
Piedrasecha 1/4
PS
N 042°49.696´
W 005°46.556´
Age
Formation
Thickness (m)
Lithology, sedimentary structures, components / fossils, texture
Carbonates
M W P G B
Siliciclastics
M S FS MS CS C/B
Depositional Environment
F L S O B
Tournaisian
Famennian
Vegamián
Ermita
Fueyo
128.8
127.5
126.5
114.5
98.5
93.0
92.2
89.6
76.3
65.0
58.5
55.5
48.3
42.3
40.3
34.3
30.3
29.1
27.1
26.1
23.5
23.2
8.2
0.0
dm
cm

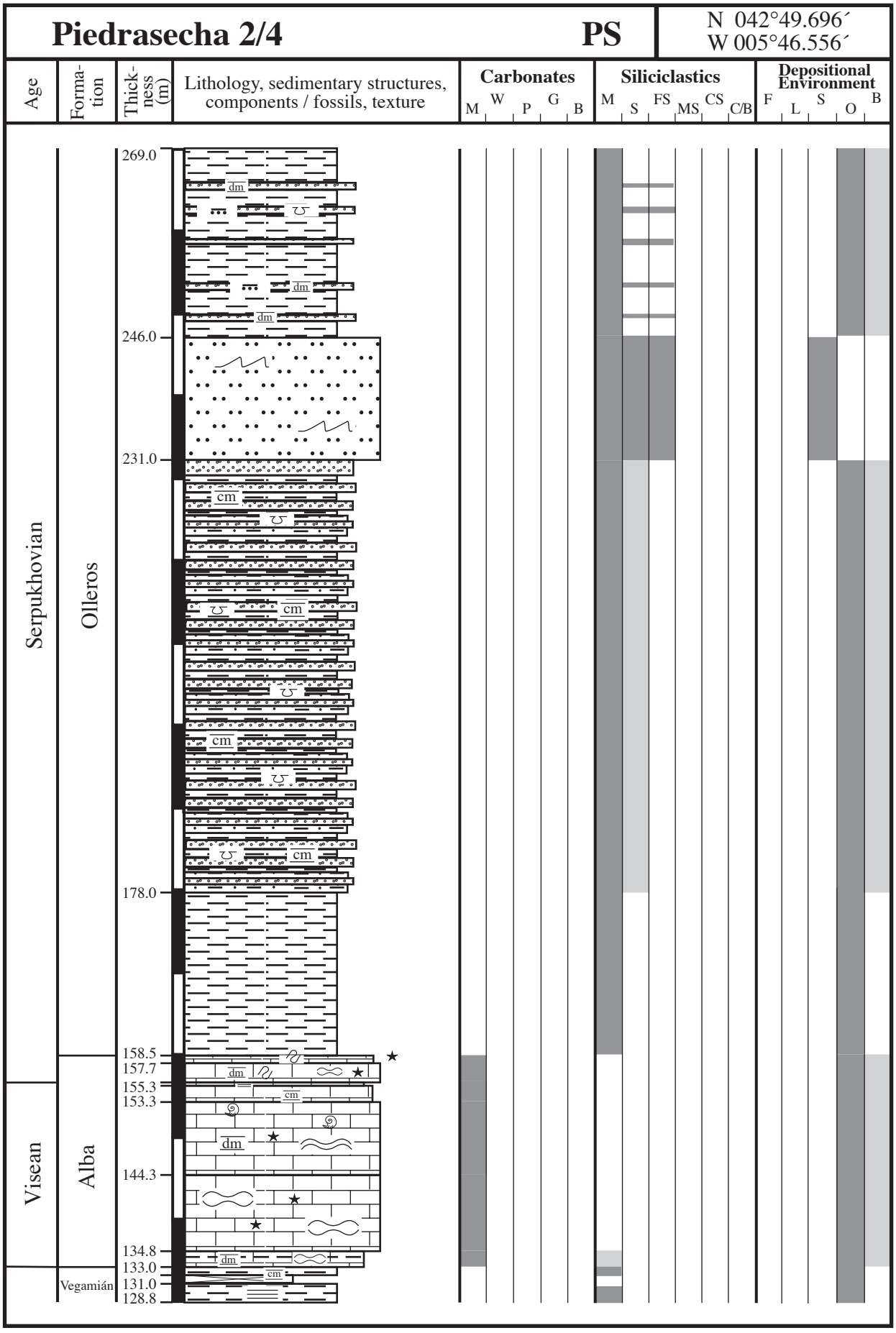
Piedrasecha 2/4
PS
N 042°49.696´
W 005°46.556´
Age
Formation
Thickness (m)
Lithology, sedimentary structures, components / fossils, texture
Carbonates
M W P G B
Siliciclastics
M S FS MS CS C/B
Depositional Environment
F L S O B
Serpukhovian
Visean
Olleros
Alba
Vegamián
269.0
246.0
231.0
178.0
158.5
157.7
155.3
153.3
144.3
134.8
133.0
131.0
128.8
dm
cm

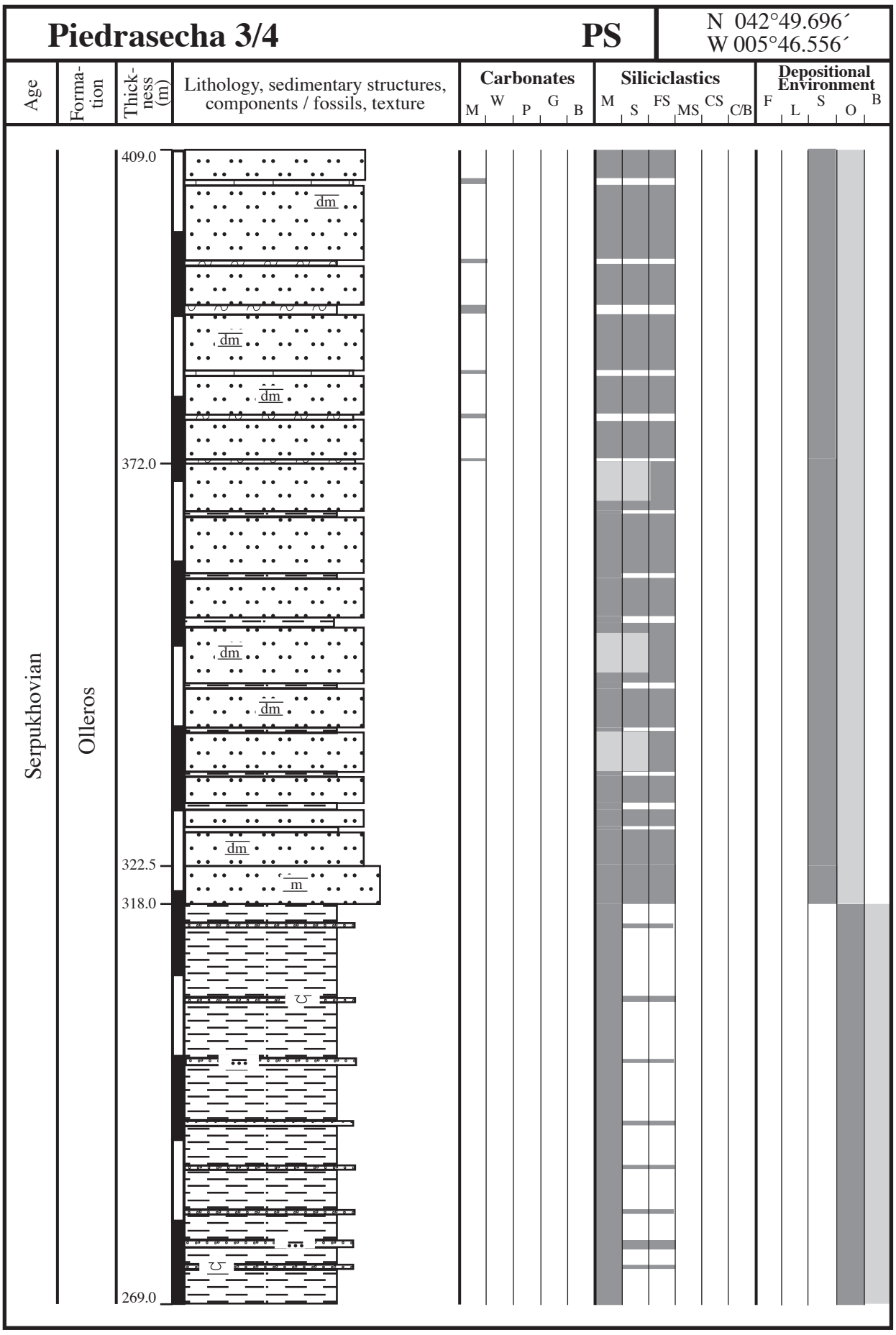
Piedrasecha 3/4
PS
N 042°49.696´
W 005°46.556´
Age
Forma-tion
Thick-ness (m)
Lithology, sedimentary structures, components / fossils, texture
Carbonates
M W P G B
Siliciclastics
M S FS MS CS C/B
Depositional Environment
F L S O B
Serpukhovian
Olleros
409.0
372.0
322.5
318.0
269.0
dm
m

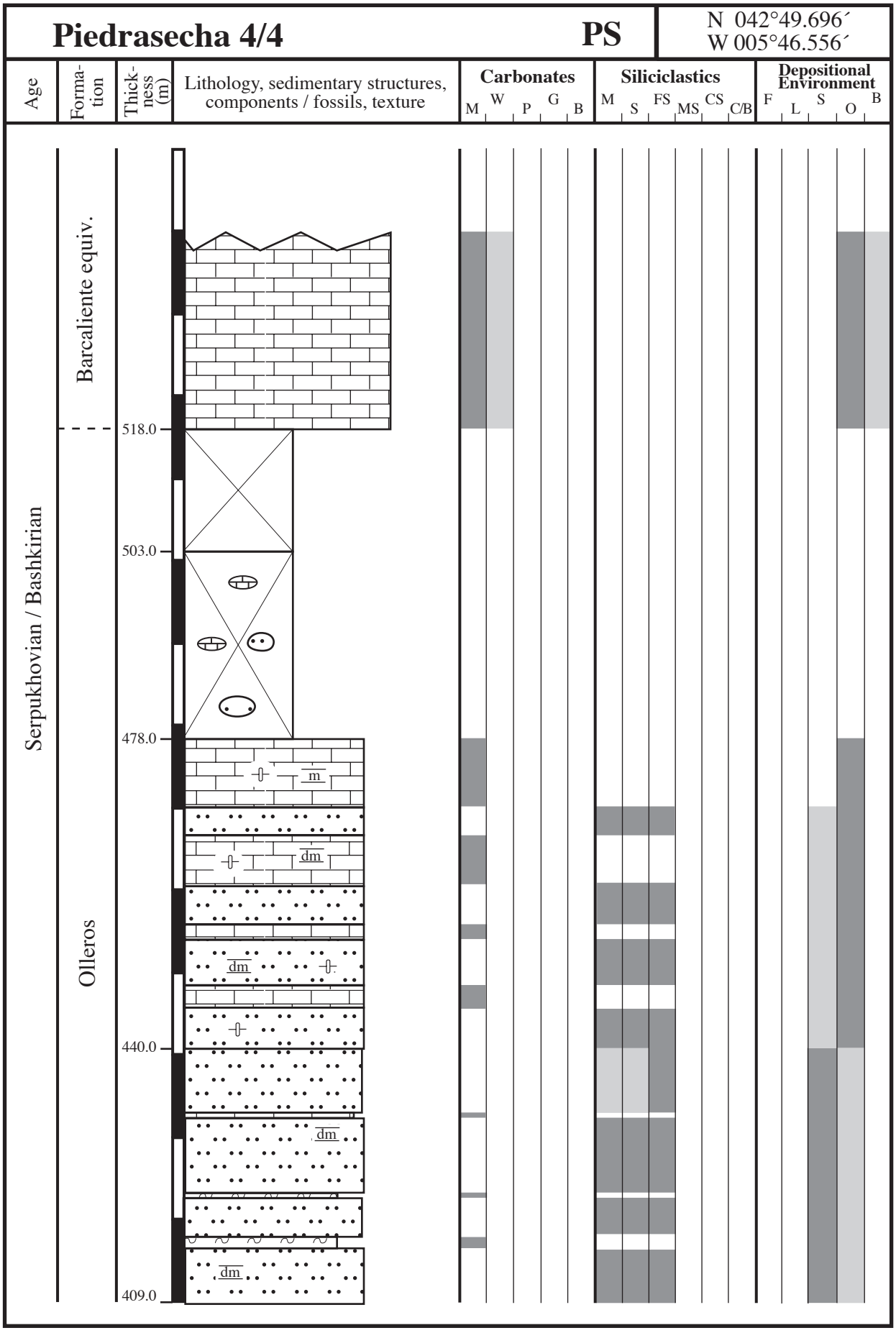
Piedrasecha 4/4
PS
N 042°49.696´
W 005°46.556´
Age
Forma-tion
Thick-ness (m)
Lithology, sedimentary structures, components / fossils, texture
Carbonates
M W P G B
Siliciclastics
M S FS MS CS C/B
Depositional Environment
F L S O B
Serpukhovian / Bashkirian
Barcaliente equiv.
Olleros
518.0
503.0
478.0
440.0
409.0
m
dm
dm
dm
dm

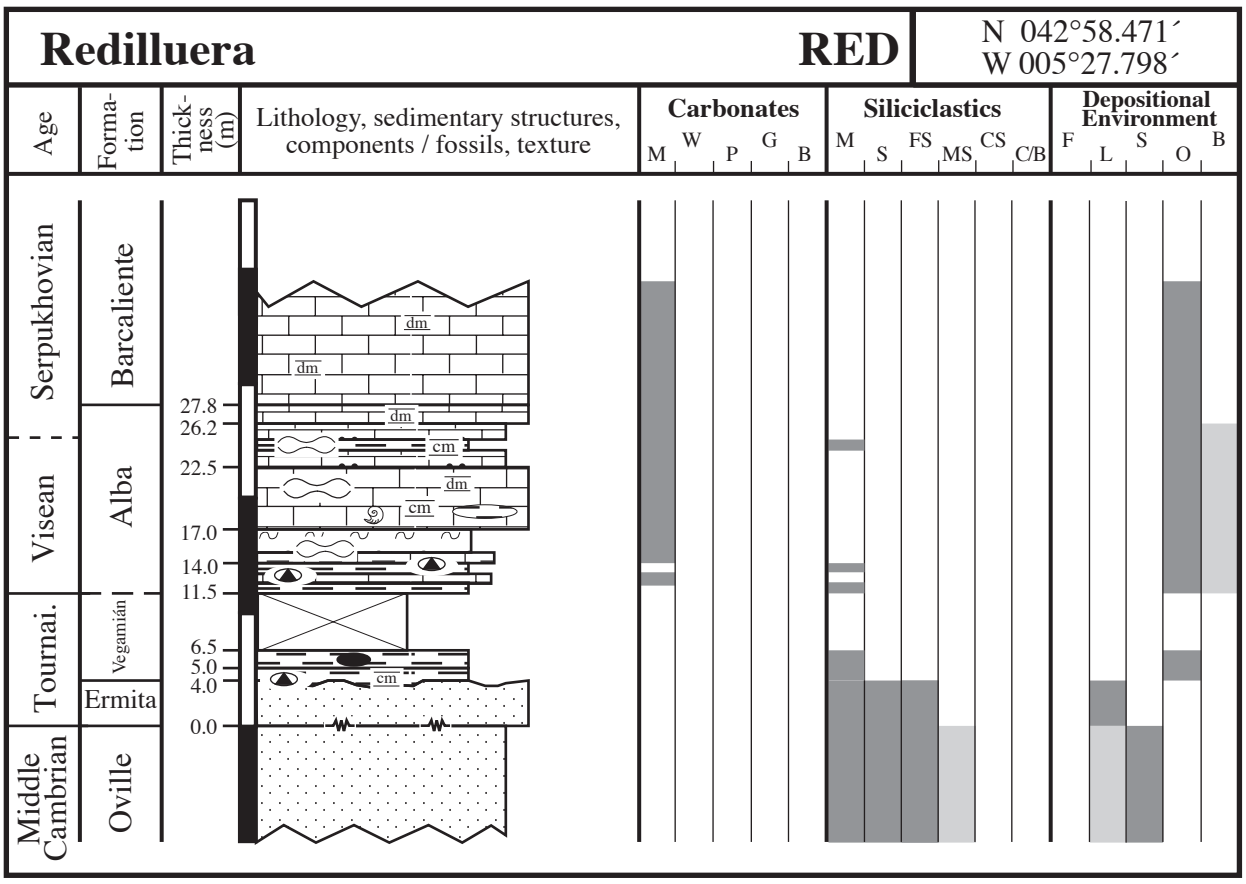
Redilluera
RED
N 042°58.471´
W 005°27.798´
Age
Formation
Thickness (m)
Lithology, sedimentary structures, components / fossils, texture
Carbonates
M W P G B
Siliciclastics
M S FS MS CS C/B
Depositional Environment
F L S O B
Serpukhovian
Visean
Tournai.
Middle Cambrian
Barcaliente
Alba
Vegamián
Ermita
Oville
27.8
26.2
22.5
17.0
14.0
11.5
6.5
5.0
4.0
0.0
dm
cm

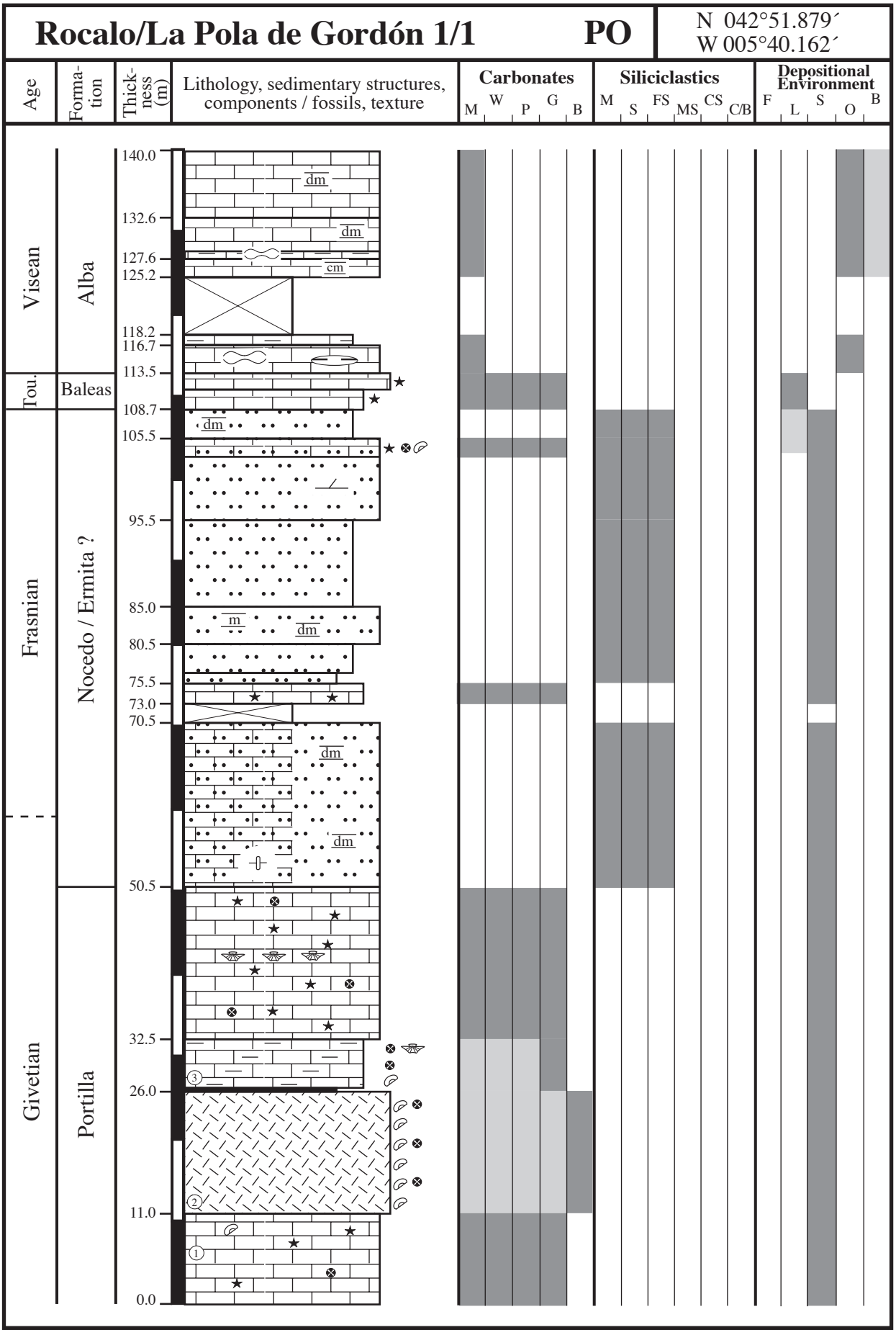
Rocalo/La Pola de Gordón 1/1
PO
N 042°51.879´
W 005°40.162´
Age
Formation
Thickness (m)
Lithology, sedimentary structures, components / fossils, texture
Carbonates
M W P G B
Siliciclastics
M S FS MS CS C/B
Depositional Environment
F L S O B
Visean
Alba
Tou.
Baleas
Frasnian
Nocedo / Ermita ?
Givetian
Portilla
140.0
132.6
127.6
125.2
118.2
116.7
113.5
108.7
105.5
95.5
85.0
80.5
75.5
73.0
70.5
50.5
32.5
26.0
11.0
0.0
dm
cm
m
1
2
3

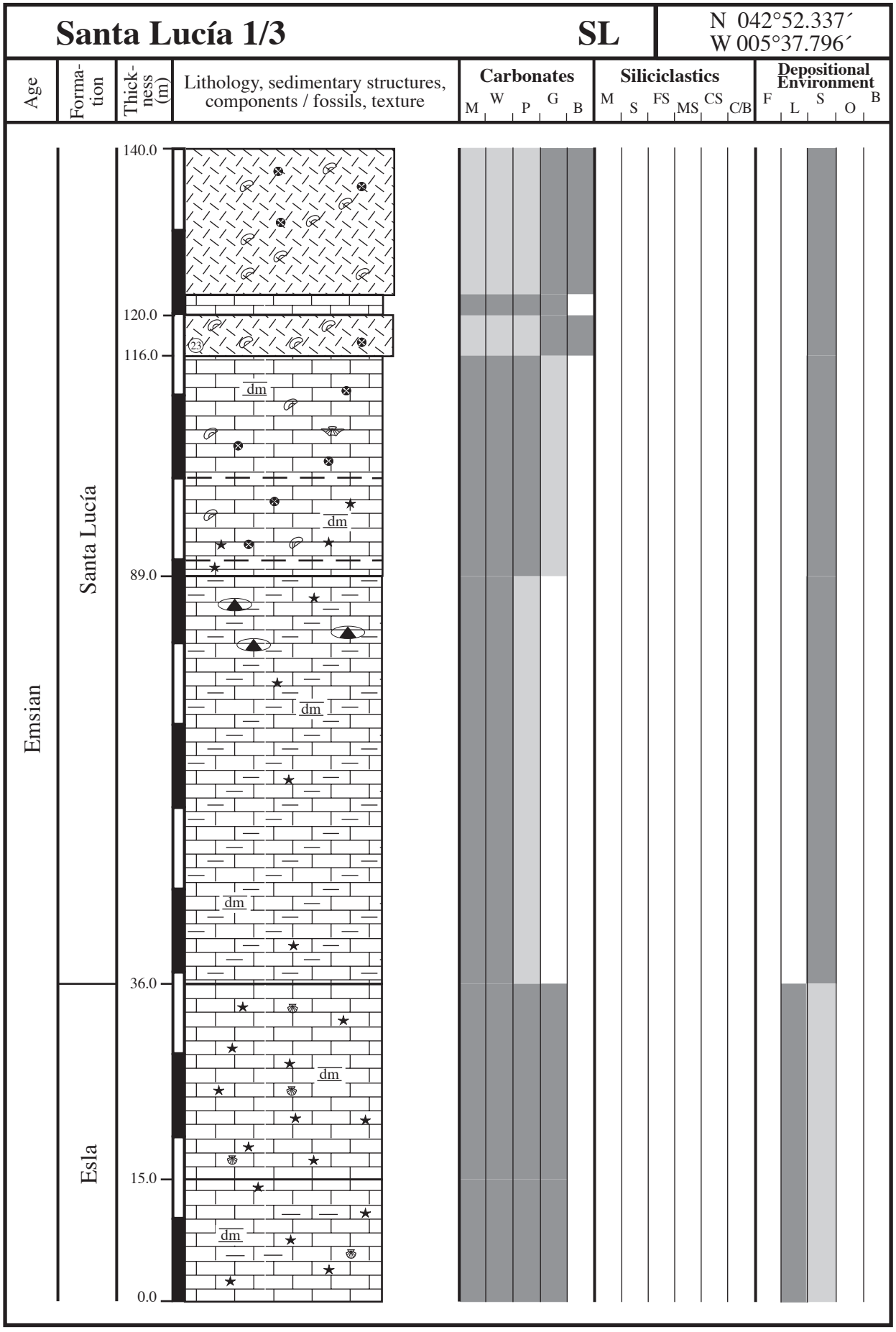
Santa Lucía 1/3
SL
N 042°52.337´
W 005°37.796´
Age
Forma-tion
Thick-ness (m)
Lithology, sedimentary structures, components / fossils, texture
Carbonates
M W P G B
Siliciclastics
M S FS MS CS C/B
Depositional Environment
F L S O B
Emsian
Santa Lucía
Esla
140.0
120.0
116.0
89.0
36.0
15.0
0.0
23
dm

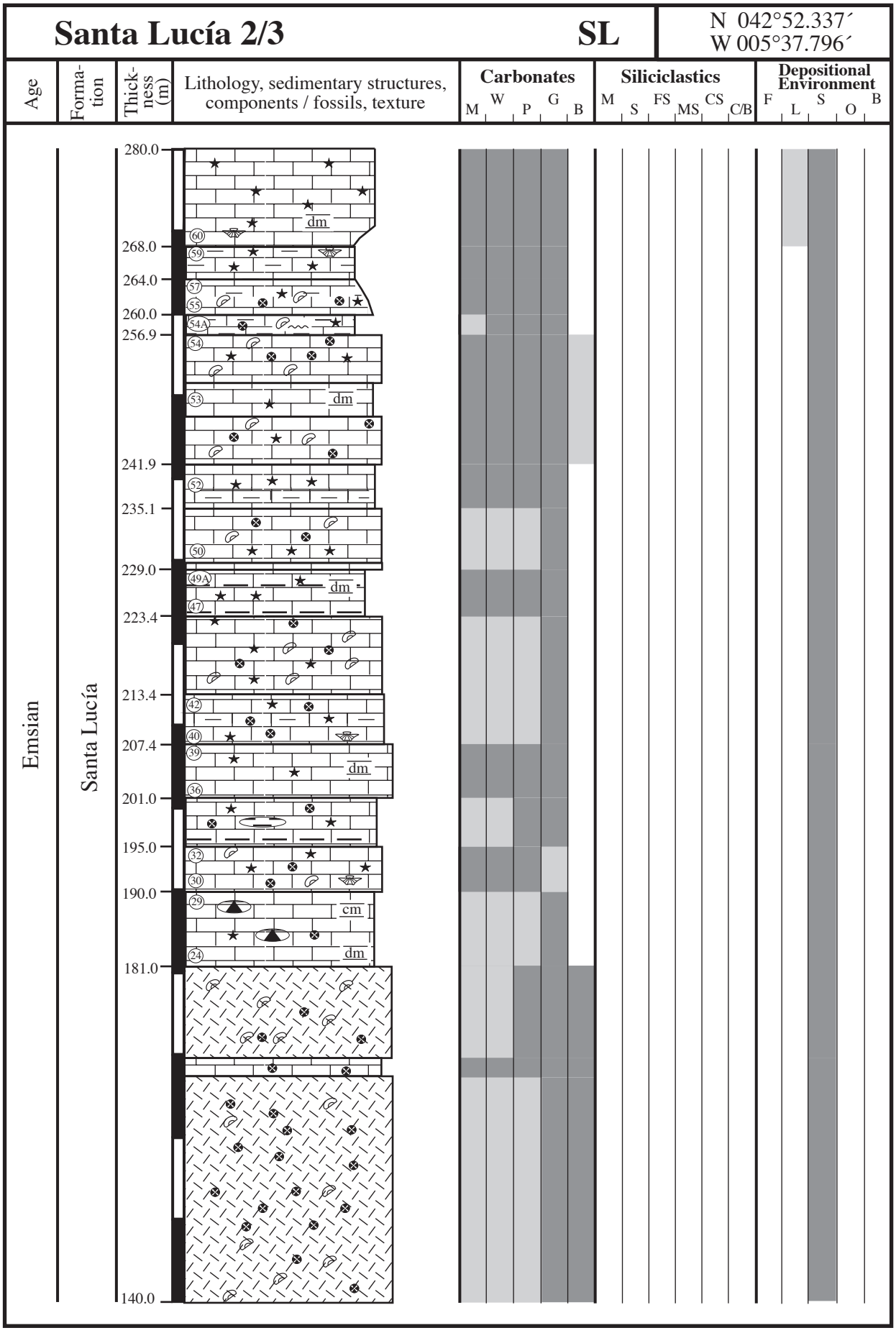
Santa Lucía 2/3
SL
N 042°52.337´
W 005°37.796´
Age
Formation
Thickness (m)
Lithology, sedimentary structures, components / fossils, texture
Carbonates
M W P G B
Siliciclastics
M S FS MS CS C/B
Depositional Environment
F L S O B
Emsian
Santa Lucía
280.0
268.0
264.0
260.0
256.9
241.9
235.1
229.0
223.4
213.4
207.4
201.0
195.0
190.0
181.0
140.0
dm
cm

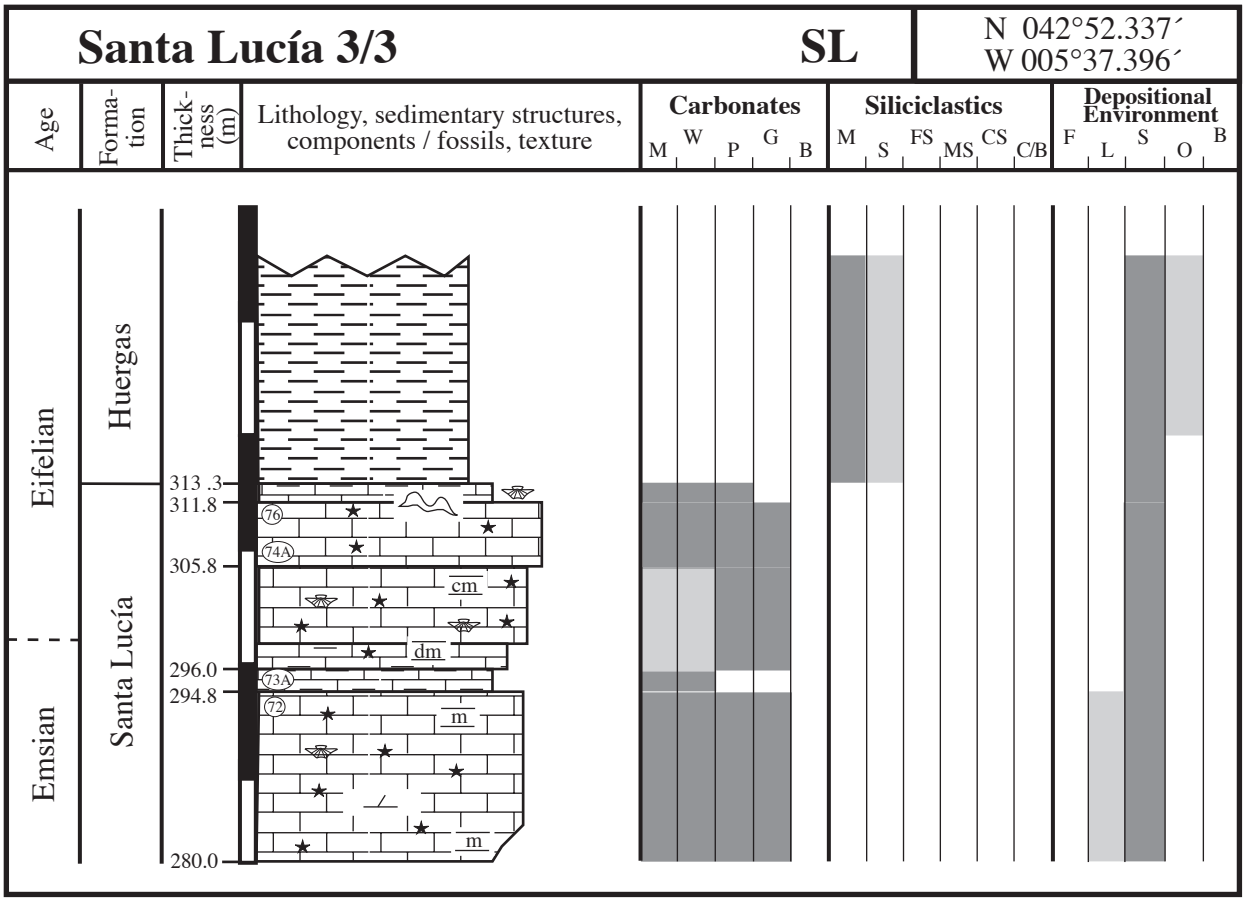
Santa Lucía 3/3
SL
N 042°52.337´
W 005°37.396´
Age
Formation
Thickness (m)
Lithology, sedimentary structures, components / fossils, texture
Carbonates
M W P G B
Siliciclastics
M S FS MS CS C/B
Depositional Environment
F L S O B
Eifelian
Emsian
Huergas
Santa Lucía
313 .3
311.8
305.8
296.0
294.8
280.0
76
74A
73A
72
cm
dm
m
m

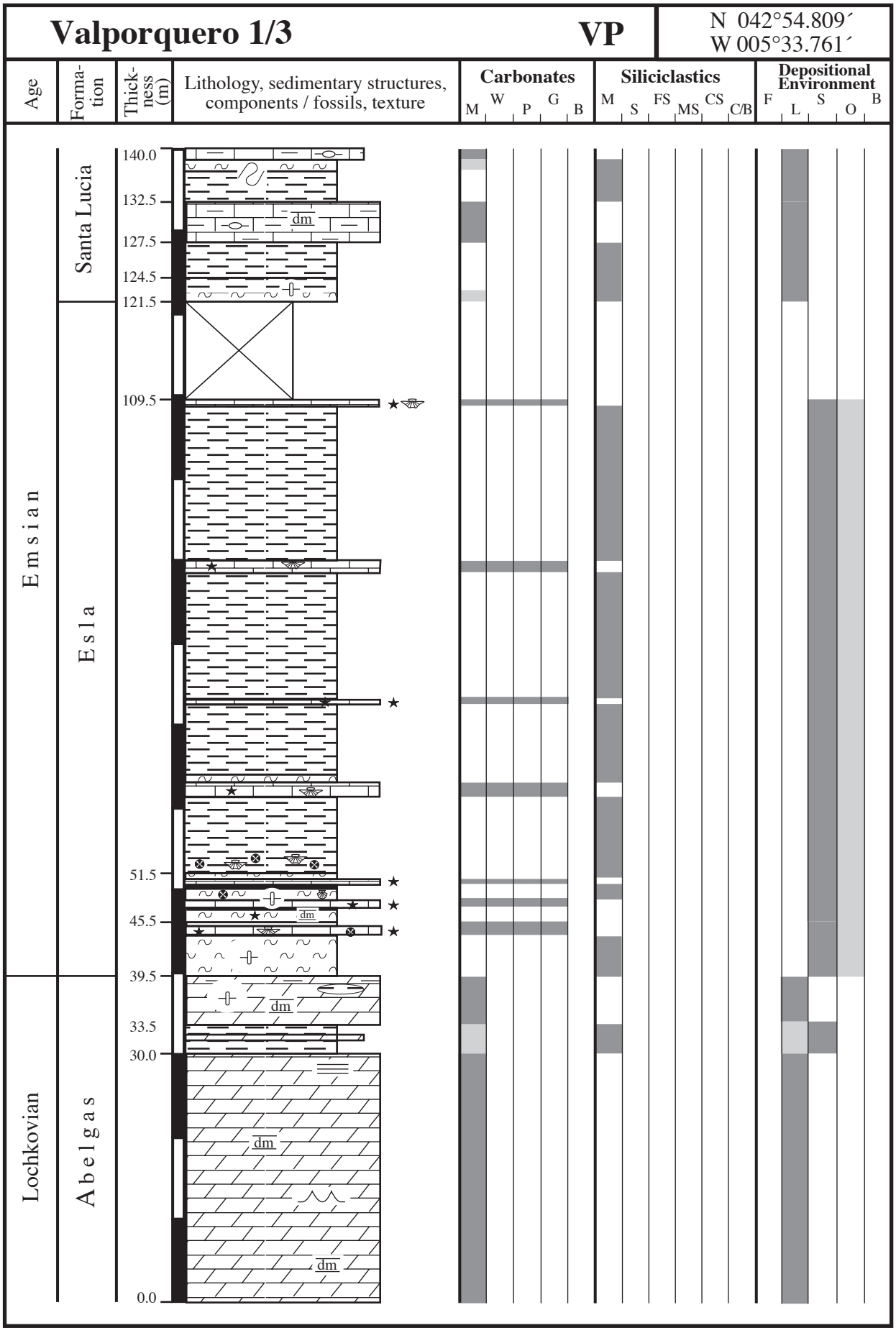
Valporquero 1/3
VP
N 042°54.809´
W 005°33.761´
Age
Forma-tion
Thick-ness (m)
Lithology, sedimentary structures, components / fossils, texture
Carbonates
M W P G B
Siliciclastics
M S FS MS CS C/B
Depositional Environment
F L S O B
Emsian
Lochkovian
Santa Lucia
Esla
Abelgas
140.0
132.5
127.5
124.5
121.5
109.5
51.5
45.5
39.5
33.5
30.0
0.0
dm

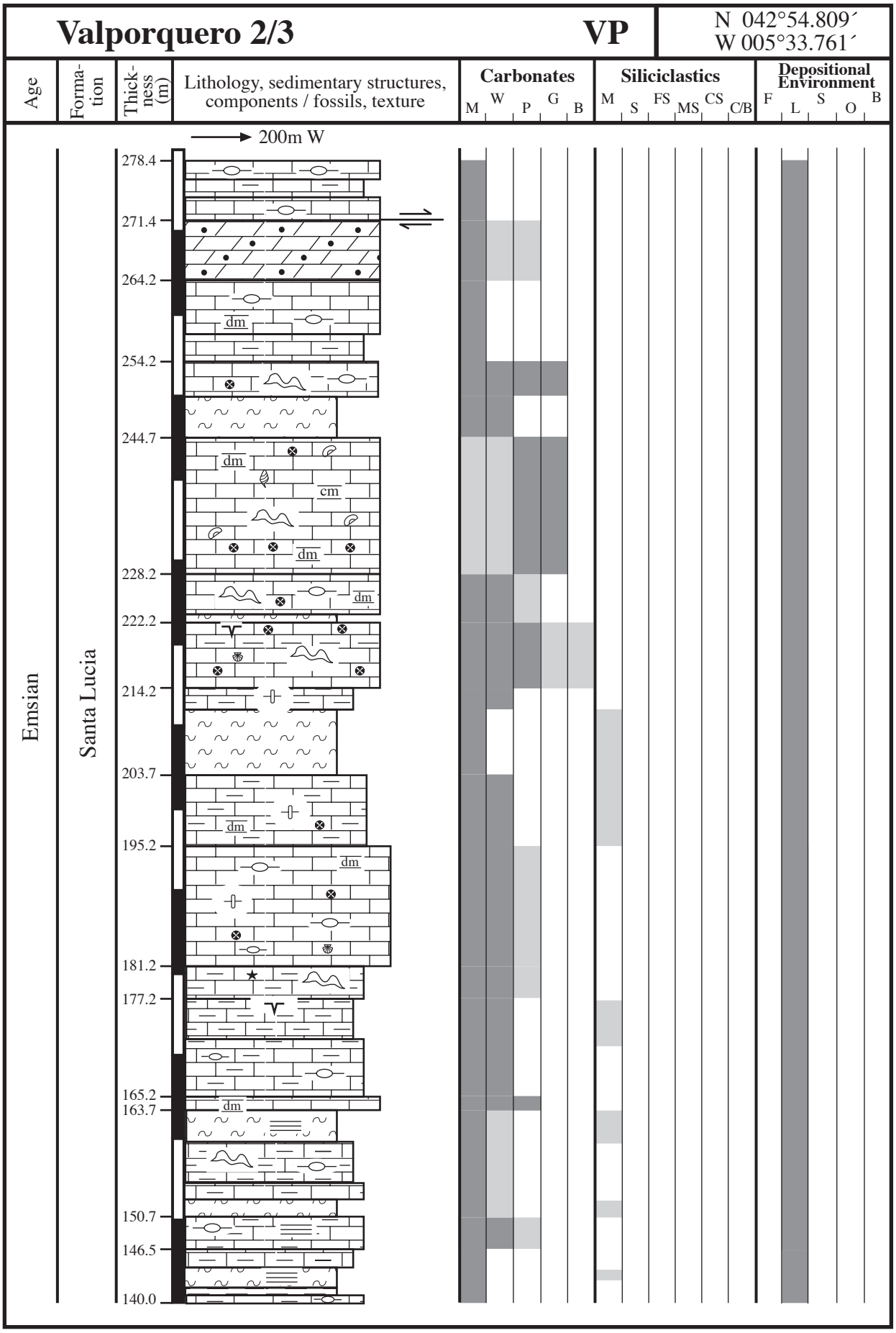
Valporquero 2/3
VP
N 042°54.809´
W 005°33.761´
Age
Formation
Thickness (m)
Lithology, sedimentary structures, components / fossils, texture
Carbonates
M W P G B
Siliciclastics
M S FS MS CS C/B
Depositional Environment
F L S O B
200m W
Emsian
Santa Lucia
278.4
271.4
264.2
254.2
244.7
228.2
222.2
214.2
203.7
195.2
181.2
177.2
165.2
163.7
150.7
146.5
140.0
dm
cm

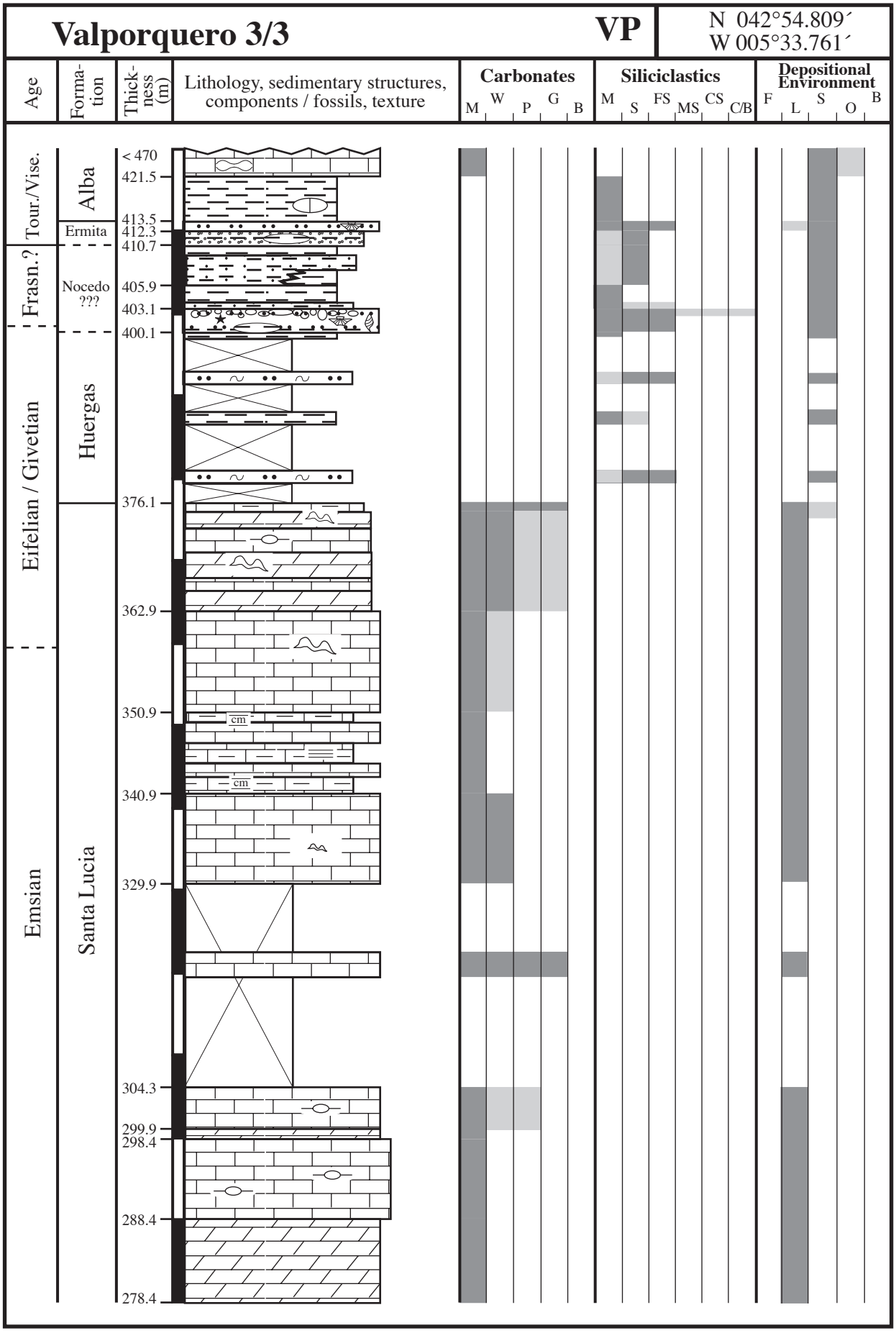
Valporquero 3/3
VP
N 042°54.809´
W 005°33.761´
Age
Formation
Thickness (m)
Lithology, sedimentary structures, components / fossils, texture
Carbonates
M W P G B
Siliciclastics
M S FS MS CS C/B
Depositional Environment
F L S O B
Tour./Vise.
Frasn.?
Eifelian / Givetian
Emsian
Alba
Ermita
Nocedo ???
Huergas
Santa Lucia
< 470
421.5
413.5
412.3
410.7
405.9
403.1
400.1
376.1
362.9
350.9
340.9
329.9
304.3
299.9
298.4
288.4
278.4
cm
cm

Predicted stratigraphic columns

Synthetic stratigraphic columns as an output from 2D stratigraphic forward modelling. The position along transect is given in km. Black triangles represent hiati. They are proportional to the hiatus time span. See Fig.7.4 for 2D sections along the Bernesga Transect. For explanation of the columns see Fig. 7.6 and Chapter 7.

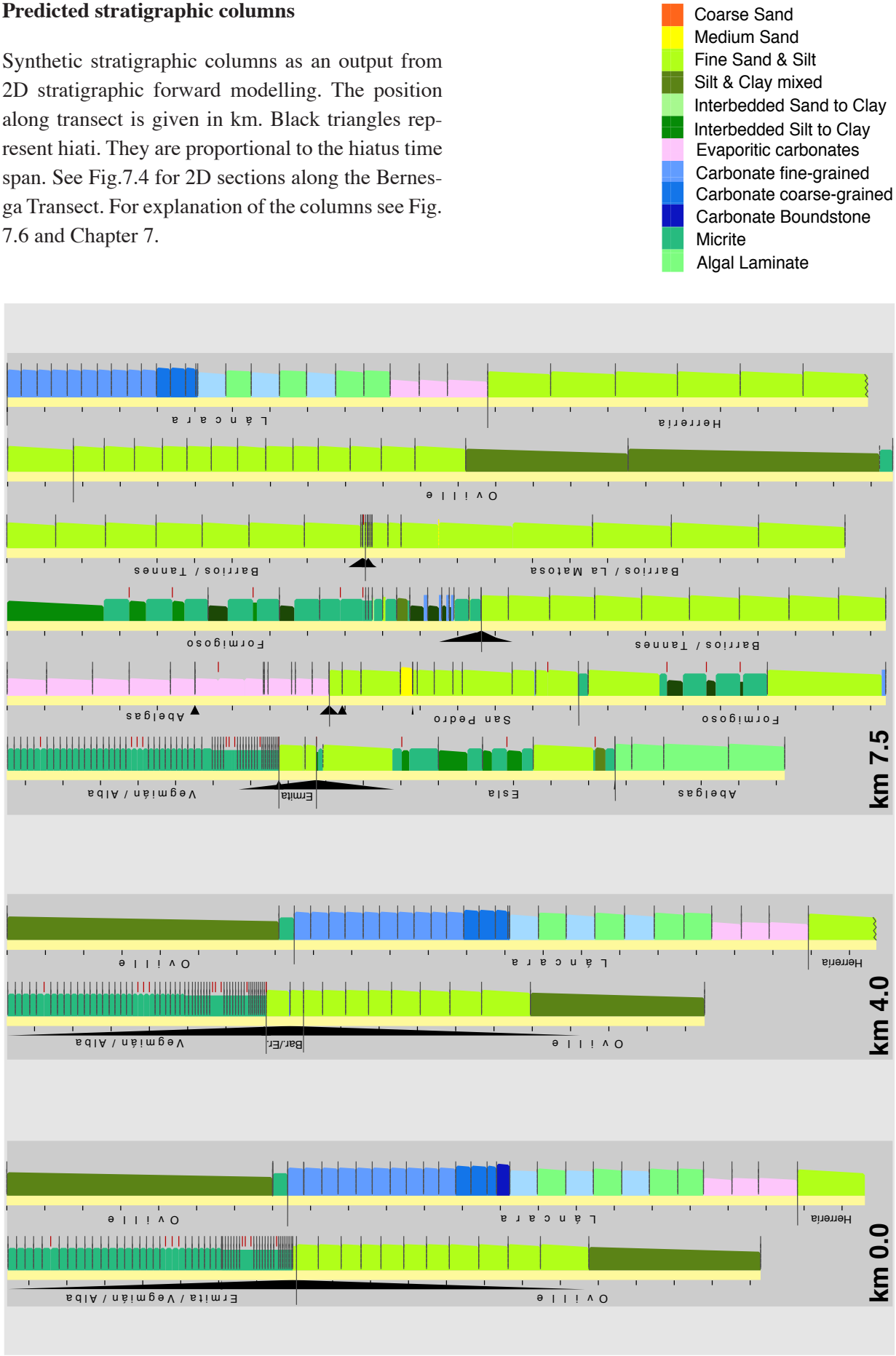

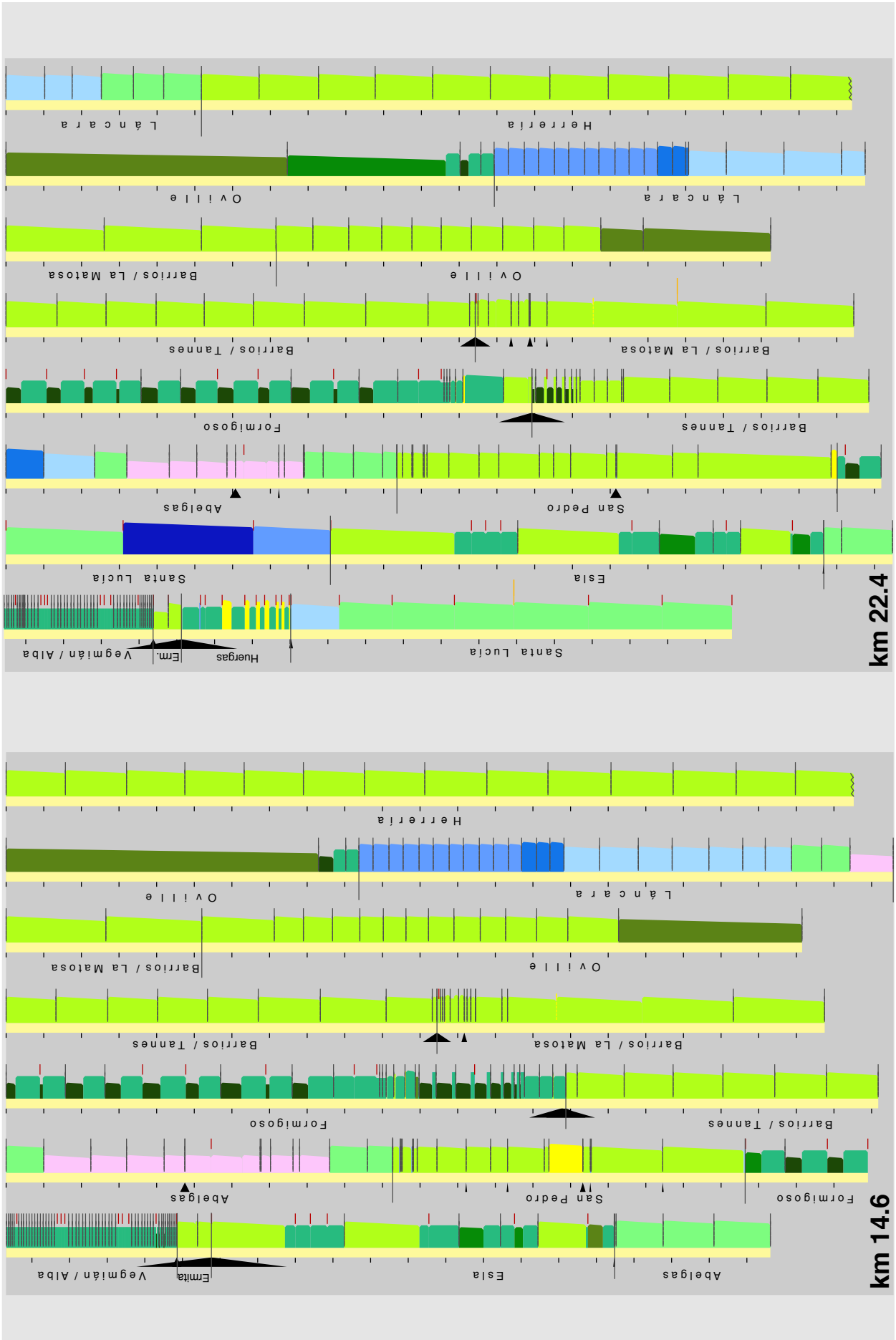
km 22.4
Santa Lucía
Huergas
Erm.
Vegmián / Alba
Esla
Santa Lucía
Abelgas
San Pedro
Formigoso
Barrios / Tanne s
Barrios / La Matosa
Ovi i i e
Herrería
Láncara
km 14.6
Abelgas
Esla
Ermita
Vegmián / Alba
Abelgas
San Pedro
Formigoso
Barrios / Tanne s
Barrios / La Matosa
Ovi i i e
Herrería
Láncara

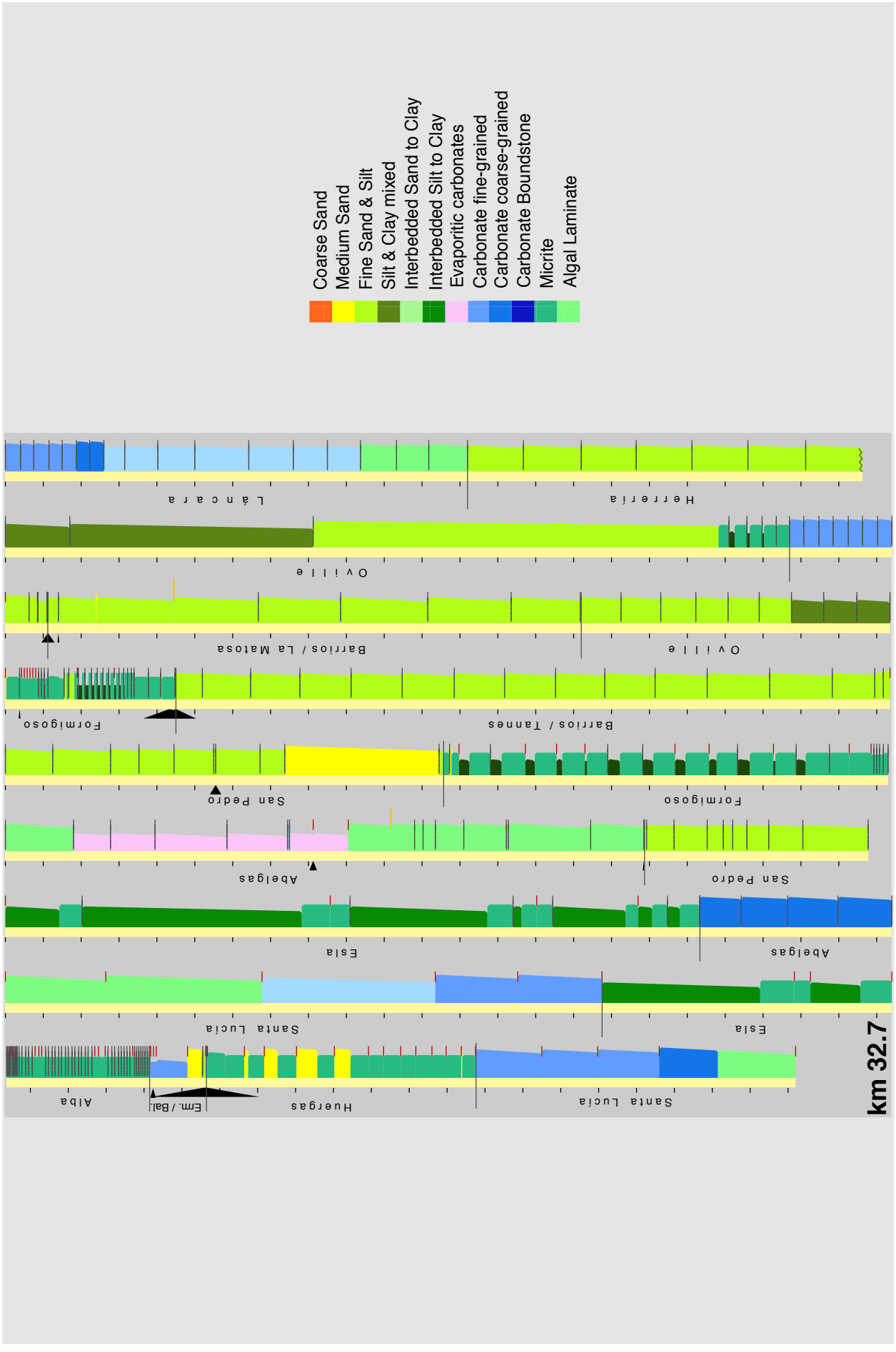
Coarse Sand
Medium Sand
Fine Sand & Silt
Silt & Clay mixed
Interbedded Sand to Clay
Interbedded Silt to Clay
Evaporitic carbonates
Carbonate fine-grained
Carbonate coarse-grained
Carbonate Boundstone
Micrite
Algal Laminate
Láncara
Herrería
Ovíile
Barrios / La Matosa
Ovíile
Formigoso
Barrios / Tannes
San Pedro
Formigoso
Abeigas
San Pedro
Esla
Abeigas
Santa Lucía
Esla
Alba
Em./Bal.
Huergas
Santa Lucía
km 32.7

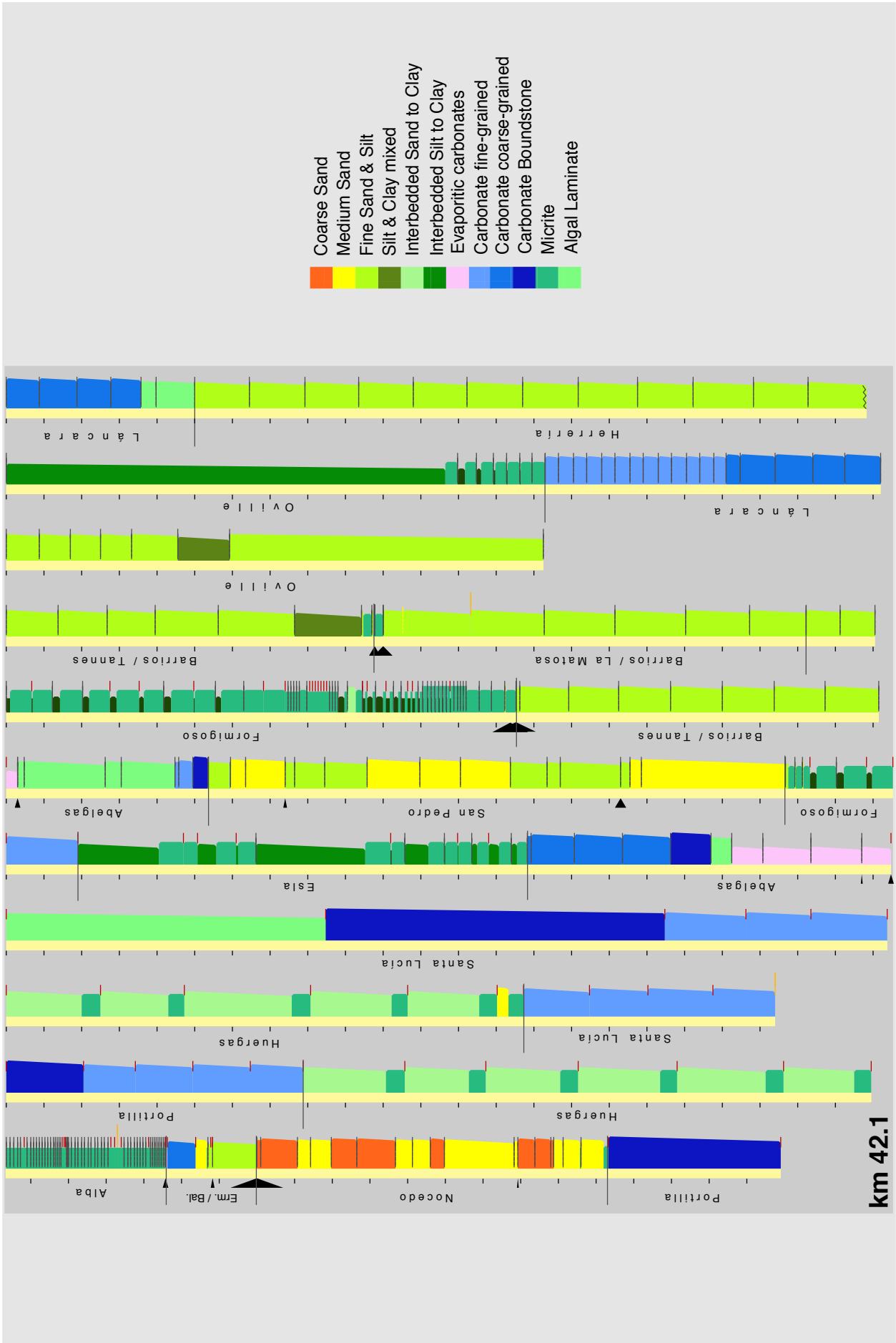
Coarse Sand
Medium Sand
Fine Sand & Silt
Silt & Clay mixed
Interbedded Sand to Clay
Interbedded Silt to Clay
Evaporitic carbonates
Carbonate fine-grained
Carbonate coarse-grained
Carbonate Boundstone
Micrite
Algal Laminate
Lánc ara
Herreria
Lánc ara
Ovi i i e
Ovi i i e
Barrios / Tannes
Barrios / La Matosa
Formigoso
Barrios / Tannes
Abeigas
San Pedro
Formigoso
Abeigas
Esla
Santa Lucia
Huergas
Santa Lucia
Portilla
Huergas
Alba
Em. / Bal.
Nocedo
Portilla
km 42.1

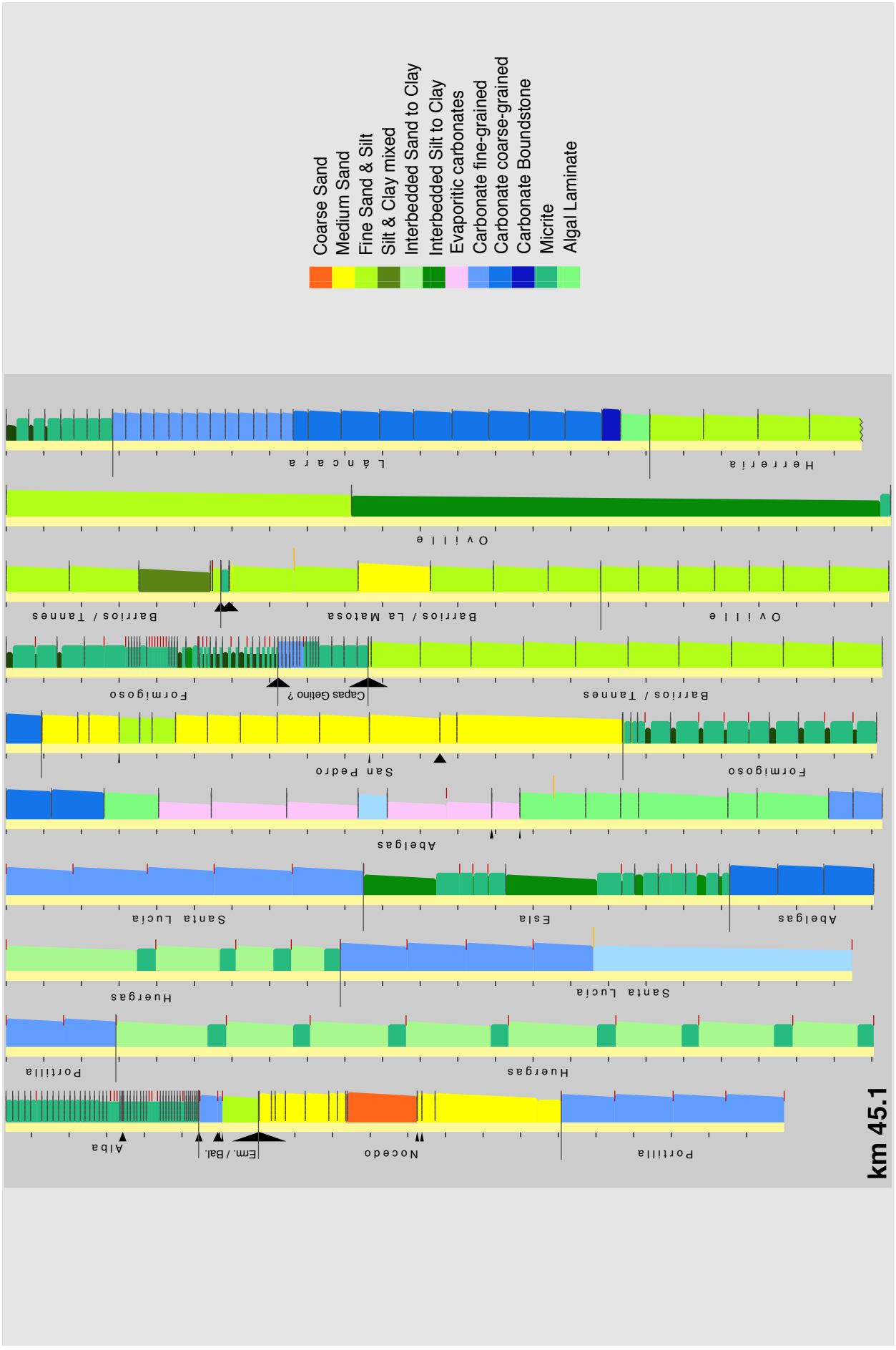
Coarse Sand
Medium Sand
Fine Sand & Silt
Silt & Clay mixed
Interbedded Sand to Clay
Interbedded Silt to Clay
Evaporitic carbonates
Carbonate fine-grained
Carbonate coarse-grained
Carbonate Boundstone
Micrite
Algal Laminate
Herrería
Láncara
Ovilile
Barrios / Tannes
Barrios / La Matosa
Ovilile
Formigoso
Capas Getino ?
Barrios / Tannes
Formigoso
San Pedro
Abelgas
Santa Lucia
Esla
Abelgas
Huergas
Santa Lucia
Portilla
Huergas
Alba
Erm. / Bal.
Nocedo
Portilla
km 45.1

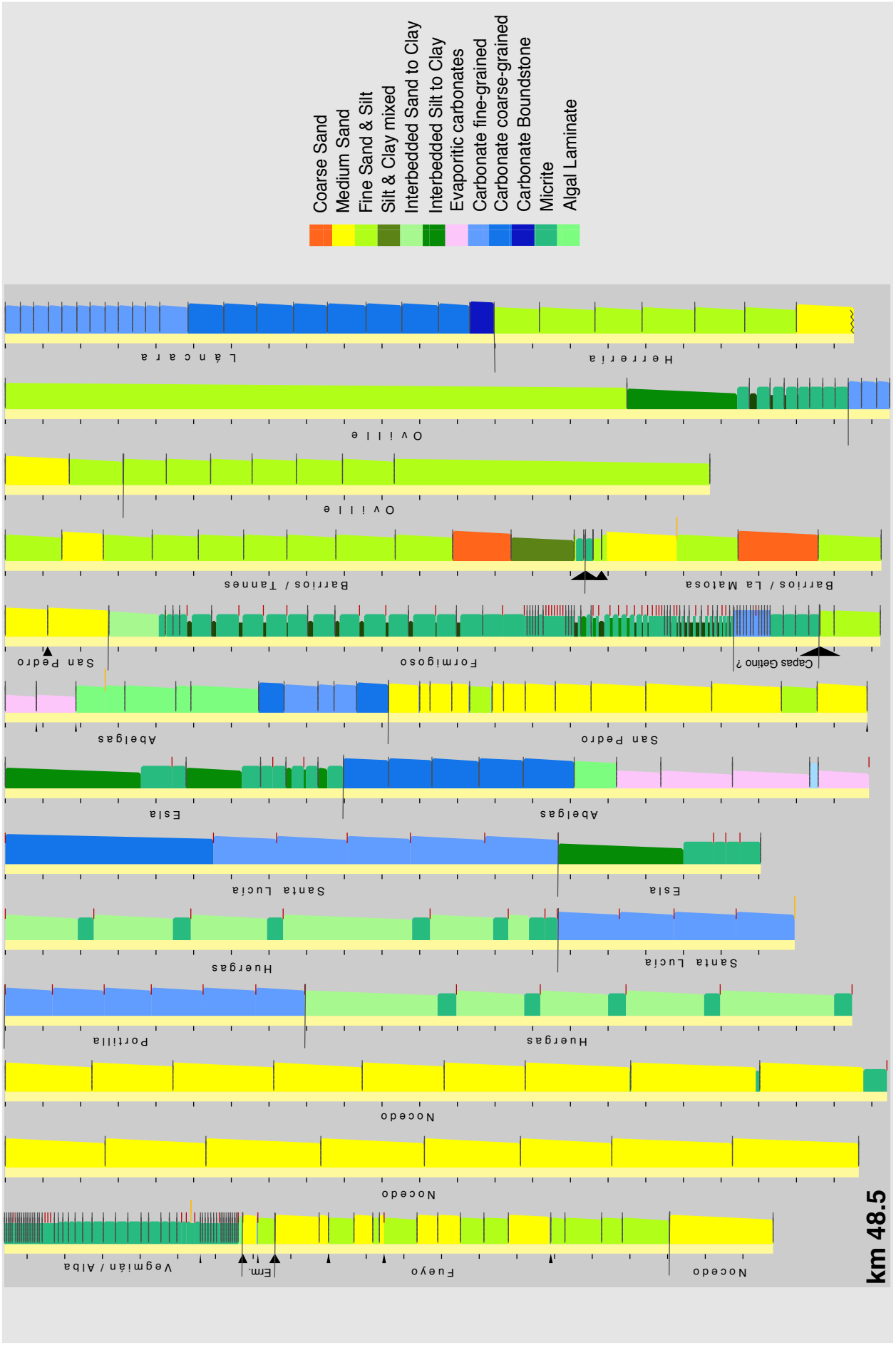
Coarse Sand
Medium Sand
Fine Sand & Silt
Silt & Clay mixed
Interbedded Sand to Clay
Interbedded Silt to Clay
Evaporitic carbonates
Carbonate fine-grained
Carbonate coarse-grained
Carbonate Boundstone
Micrite
Algal Laminate
Láncara
Herrería
Oville
Oville
Barrios / Tannes
Barrios / La Matosa
San Pedro
Formigoso
Capas Getino ?
Abelgas
San Pedro
Esla
Abelgas
Santa Lucía
Esla
Huergas
Santa Lucía
Portilla
Huergas
Nocedo
Nocedo
Vegmian / Alba
Fuejo
Nocedo
km 48.5

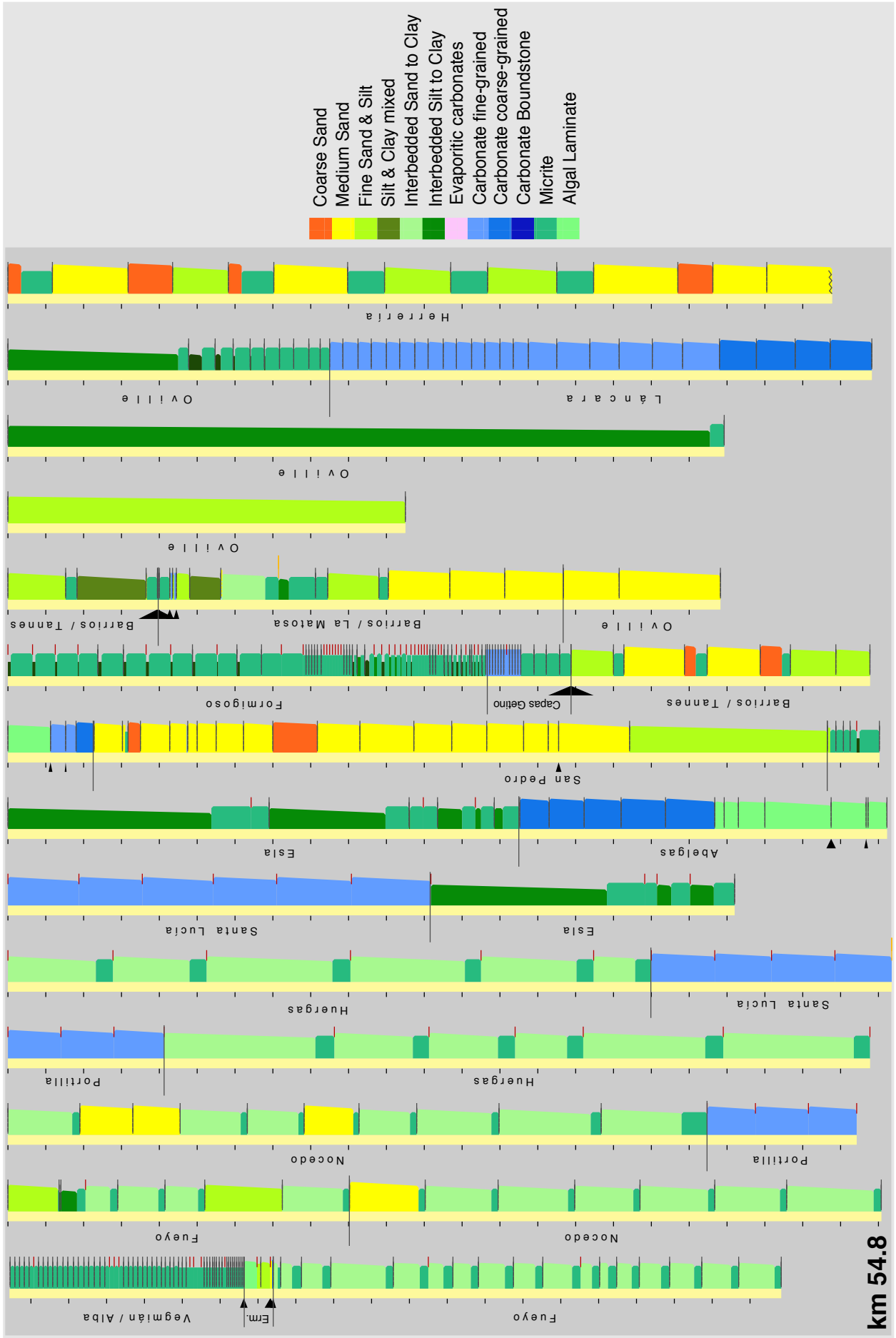
Coarse Sand
Medium Sand
Fine Sand & Silt
Silt & Clay mixed
Interbedded Sand to Clay
Interbedded Silt to Clay
Evaporitic carbonates
Carbonate fine-grained
Carbonate coarse-grained
Carbonate Boundstone
Micrite
Algal Laminate
Herrería
Ovi i l e
Lán c a r a
Ovi i l e
Ovi i l e
Barrios / Tanne s
Barrios / La Matosa
Ovi i l e
Formigoso
Capas Geino
Barrios / Tanne s
San Pedro
Esla
Abelgas
Santa Lucía
Esla
Huergas
Santa Lucía
Huergas
Portilla
Nocedo
Portilla
Fueyo
Nocedo
Vegmián / Alba
Em.
Fueyo
km 54.8

I love deadlines. I like the whooshing sound they make as they fly by.

(Douglas Adams)